APS SCIENCE 2017

RESEARCH AND ENGINEERING HIGHLIGHTS FROM THE ADVANCED PHOTON SOURCE AT ARGONNE NATIONAL LABORATORY

ANL-18/14
ISSN 1931-5007
August 2018

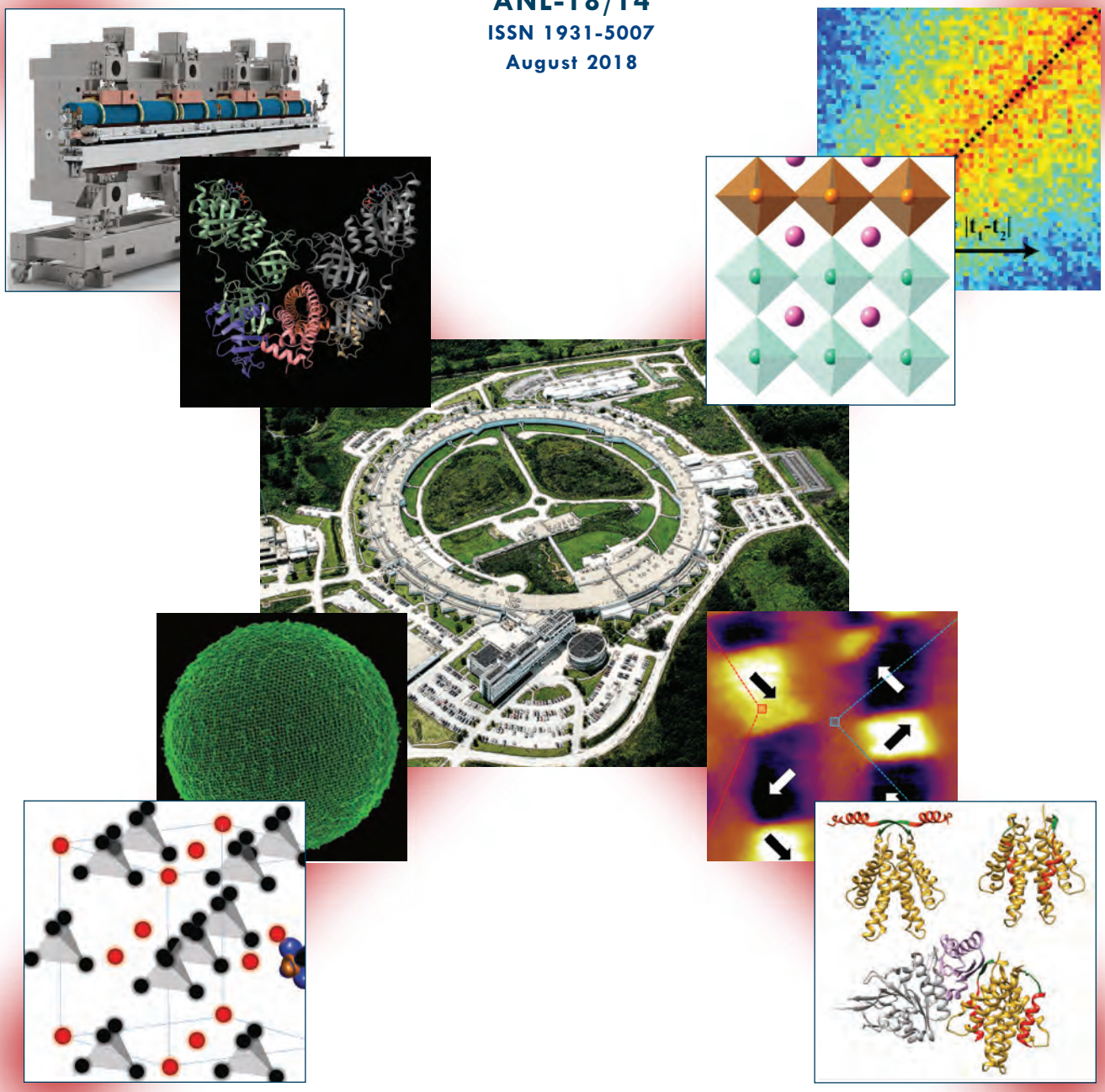

Argonne NATIONAL LABORATORY

ANL-18/14 • SSN 1931-5007 • August 2018

The Advanced Photon Source is a U.S. Department of Energy (DOE) Office of Science User Facility
operated for the DOE Office of Science by Argonne National Laboratory under Contract No. DE-AC02-06CH11357.

About Argonne National Laboratory
Argonne is a U.S. Department of Energy laboratory managed by UChicago Argonne, LLC
under contract DE-AC02-06CH11357. The Laboratory's main facility is outside Chicago,
at 9700 South Cass Avenue, Argonne, Illinois 60439. For information about Argonne
and its pioneering science and technology programs, see www.anl.gov.

Argonne NATIONAL LABORATORY

ANL-18/14
ISSN 1931-5007
August 2018

APS SCIENCE 2017

RESEARCH AND ENGINEERING HIGHLIGHTS FROM THE ADVANCED PHOTON SOURCE AT ARGONNE NATIONAL LABORATORY

Argonne is a U.S. Department of Energy (DOE) laboratory managed by UChicago Argonne, LLC.
The Advanced Photon Source is a DOE Office of Science user facility
operated for the DOE Office of Science by Argonne National Laboratory under Contract No. DE-AC02-06CH11357.

Table of Contents

In Memoriam:
Gopal K. Shenoy, a Founder of the APS

We are truly saddened to note the passing of Dr. Gopal K. Shenoy, world-renowned materials scientist, Argonne Distinguished Fellow, and a driving force, with the late Dr. Yanglai Cho, in bringing the Advanced Photon Source (APS) to Argonne. Throughout his long and illustrious career, Gopal had a profound and lasting impact on synchrotron x-ray science, both in his brilliant research, and in his central role in the creation and evolution of our marvelous APS. But beyond his scientific contributions, and throughout his professional life, Gopal touched many, many lives, as a mentor, as a colleague, and as a friend. Our deepest sympathies go out to Gopal's wife, Ravibala, and his daughters Shami (Anand) and Lakshmi, as well as his grandchildren Maya and Anika. An appreciation of Gopal follows.

Stephen Streiffer, Argonne Associate Laboratory Director for Photon Sciences and Director, Advanced Photon Source

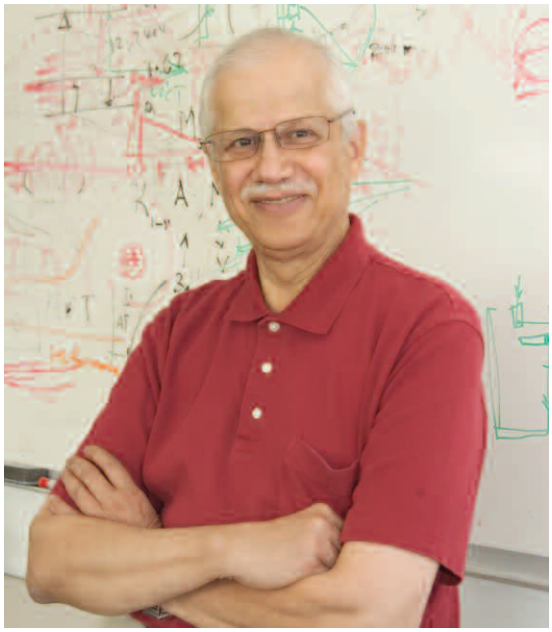

Dr. Gopal K. Shenoy

Dr. Gopal K. Shenoy's career Argonne National Laboratory started in 1967 and spanned 43 years. During this time, he had a major impact, first as a bench scientist in the Mössbauer Spectroscopy Laboratory, then as a group leader for synchrotron radiation research in the Materials Science Division, then as a founding father of the current X-ray Science Division. He played a leading role in formulating the need for an advanced synchrotron radiation source for the nation, and then in raising Argonne's capacity to compete for this light source, culminating in bringing the Advanced Photon Source to Argonne.

Gopal began his career at Argonne in the Solid State Science Division in the Mössbauer Laboratory carrying out fundamental work on actinide and lanthanide chemistry, and physics and pioneering studies on magnetism and superconductivity in uranium, neptunium, ytterbium, gadolinium, erbium, and europium compounds. Argonne's reputation as the premier Mössbauer laboratory in the world was well established, which later helped the Laboratory attract new generations of scientists to develop excellence in nuclear resonant scattering. Gopal was the first researcher to enter the 200+ club of the Mössbauer Effect Data Center. The impact of his studies is quite visible in the development of electronic structure of heavy fermions, ternary superconductors, Chevrel phase compounds, and high-performance magnets.

By the mid-1980's, Gopal's scientific interest moved to nanocluster physics, and working with researchers from Fritz-Haber Institute, he pioneered the use of extended x-ray absorption fine structure (EXAFS) spectroscopy in studying the atomic arrangements in pure-metal nanoclusters embedded in noble-gas matrix. Their work on gold, silver, copper, and iron nanoclusters is still being extensively cited today. With the work on EXAFS coinciding with the development of the Argonne Intense Pulsed Neutron Source, the time was right for Argonne to bid for a major scientific research facility. Shenoy seized on this historic opportunity and as early as 1982, he was in the forefront advocating for an insertion-device-based synchrotron light source. He formed a research group in synchrotron radiation and installed the most advanced computational codes at the time for undulator radiation. His enthusiasm was matched by that of Dr. Yanglai Cho, and working together, they came up with a low-emittance-lattice storage ring design with extensive undulator sources. The entire synchrotron radiation community felt the intensity of his early work, such that 350 participants attended the first User Meeting for an unfunded, unnamed synchrotron source held at Argonne in 1986. This was a turning point for Argonne in its successful bid to build and operate the Advanced Photon Source.

During the 1990's, Gopal's attention, and that of Dr. David Moncton, the first Director of the APS, was given to completion of the APS, as well as to creating a healthy scientific user community.

Gopal played a major role in the science case for the Linac Coherent Light Source at Stanford, and remained actively involved in guiding the early scientific proposals. He served on many scientific advisory committees of major hard x-ray synchrotron radiation facilities in the world, including the Australian Synchrotron, the European Synchrotron Radiation Facility, the European XFEL, and SPring-8 (Japan).

In the 2000s, after leaving his position in top management of the APS, Gopal turned his attention to novel experimental development issues, which led to the first successful demonstration of a fast mechanical chopper in nuclear-resonant scattering studies. His work on microelectromechanical systems–based cantilevers to manipulate the time-structure of light sources promises to be very useful in time-resolved studies at current and future light sources. Gopal always had an eye on the future. As early as 1995, he was active in developing free-electron-laser-based light sources.

Gopal Shenoy proved time and again that he could connect to young researchers, support their work, light their enthusiasm, challenge their ideas, and encourage them to publish their work.

Ercan Alp, Senior Physicist, Argonne X-ray Science Division

The Advanced Photon Source Facility at Argonne National Laboratory

The Advanced Photon Source (APS) occupies an 80-acre site on the Argonne National Laboratory campus, about 25 miles from downtown Chicago, Illinois. It shares the site with the Center for Nanoscale Materials and the Advanced Protein Characterization Facility.

For directions to Argonne, see www.anl.gov/directions-and-visitor-information.

The APS, a national synchrotron radiation research facility operated by Argonne for the U.S. Department of Energy (DOE) ,Office of Science-Basic Energy Sciences, Scientific User Facilities Division provides this nation's brightest high-energy x-ray beams for science. Research by APS users extends from the center of the Earth to outer space, from new information on combustion engines and microcircuits to new drugs and nanotechnologies whose scale is measured in billionths of a meter. The APS helps researchers illuminate answers to the challenges of our high-tech world, from developing new forms of energy, to sustaining our nation's technological and economic competitiveness, to pushing back against the ravages of disease. Research at the APS promises to have far-reaching impact on our technology, our economy, our health, and fundamental knowledge of the materials that make up our world.

Contact us

For more information about the APS send an email to apsinfo@aps.anl.gov or write to APS Info, Bldg. 401, Rm. A4115, Argonne National Laboratory, 9700 S. Cass Ave., Argonne, IL 60439.

To order additional copies of this, or previous, issues of *APS Science* send email to apsinfo@aps.anl.gov.

To download PDF versions of *APS Science* back issues go to www.aps.anl.gov/Science/APS-Science

Visit the APS on the Web at www.aps.anl.gov

Welcome

Stephen Streiffer (right, Argonne Associate Laboratory Director for Photon Sciences and Director of the Advanced Photon Source; and Bob Hettel (left) APS Upgrade Project Director, pass APS storage ring magnets current (background) and future (foreground) on a trike tour of the APS experiment hall.

August 2018

Here at the APS, we find ourselves with a unique opportunity. Thanks to our APS Upgrade (APS-U), we are reinventing our APS facility, and reimagining the science that flows from the APS. As the APS-U picks up speed under the leadership of Bob Hettel (you can read his thoughts on the facing page), we have a great incentive to create a new-model APS that is retooled to deliver even better scientific capabilities to our users, who will use the new APS to make even more important discoveries about our world.

We are positioning the APS to morph seamlessly into the APS-U. Our well-maintained accelerator complex and conventional facilities will assure productive operations for critical components not replaced by the APS-U. We have settled on a suite of new and upgraded beamlines selected through a rigorous vetting process. APS scientists, engineers, and technicians are advancing the frontiers of hard x-ray science and techniques, insertion devices, optics, and detectors to actualize and take advantage of the upgraded APS.

We are leveraging Argonne leadership in computing and applied math to work with our own computational scientists on meeting the challenge of exponential growth in the data from users of the APS-U. And we continue our successful partnership with the outstanding Argonne practitioners of hard x-ray science who are among our most valued users.

In parallel with technical R&D, APS-U leadership (Bob Hettel, Jim Kerby, et al.) meets regularly with our Division Directors (John Connolly of AES, John Byrd of ASD, and Jonathan Lang of XSD) and their teams to coordinate our resources of the human variety (and make sure that APS Operations beamline and accelerator strategies for transition to the APS-U are synchronized with APS-U plans).

We are working closely with our users and with the DOE light-source complex to plan for the "dark time" when we turn off the machine to install the new storage ring, front ends, insertion devices, and all the other technology that comprise the upgraded APS. We are maintaining solid communication with the user community in order to keep them apprised of the dark-time start date, its duration, and planned commissioning activities for the accelerator and beamlines after the dark time. This is a regular topic at our yearly user meetings as well as our quarterly all-hands and Partner User Council/APS Users Organization meetings. Our sister DOE x-ray light sources will be a valuable resource as we find ways to lessen the dark-time impact on our users.

The APS-U also presents us with a set of interesting questions:

How do we maximize the science from our facility in the APS-U era? How do we best take advantage of the existing APS infrastructure and equipment and judiciously apply our resources to the most critical and challenging needs? How do we improve the way we utilize the universities, laboratories, and industries who support our users so that we can continue to succeed together? How do we maintain our sponsor's trust in our ability to carry out our mission?

And most important of all, how do we do all of this safely?

We do not have complete answers to all these questions, but we are well on the way and I know we can and will answer them.

Many of those answers can be found in the "Advanced Photon Source Five-Year Facility Plan," which we update every year at the request of BES, and which is the roadmap to our future. You can find it at https://bit.ly/2w4AwrY. I encourage you to read it.

As always, the safety of our personnel and our users is of paramount importance. Our mantra holds that everyone goes home at the end of the day in the same condition as when they came to work. The PSC Diversity & Inclusion (D&I) Working Group (formed by XSD Associate Division Director Patricia Fernandez and XSD Assistant Physicist Rebecca Bradford) meets monthly. Argonne is updating the charter for its D&I initiative, and we are evaluating next steps in light of results from the 2017 Climate Survey (the second such evaluation of D&I at the Lab).

As you can see from the highlights in this book, our users continue to produce impactful science (23,184 peer-reviewed journal articles as of the date of this writing). We are always mindful of our core mission: "To serve a multifaceted scientific community by providing high-energy x-ray science tools and techniques that allow users to address the most important basic and applied research challenges facing our nation, while maintaining a safe, diverse, and environmentally responsible workplace."

Stephen Streiffer
Associate Laboratory Director for Photon Sciences and Director, Advanced Photon Source

The Advanced Photon Source Upgrade Project

August 2018

Bob Hettel

There are, relatively speaking, a handful of people who have the good fortune to work on large accelerator projects. Those of us who do, know that there are few things more rewarding than developing a plan, joining with a team, and building the next big thing. So, I'm excited to have been asked to serve as Project Director for the Advanced Photon Source Upgrade Project, which we colloquially call the APS-U.

One could not have drawn up a better situation to join. Stuart Henderson, the former APS-U Project Director (and now the Director of the DOE's Thomas Jefferson National Accelerator Facility) did a remarkable job of rounding up an extremely talented team and laying a solid foundation for the Project's success. Jim Kerby, the APS-U's very experienced Project Manager, kept the enterprise on course and moving ahead after Stuart's departure and handed over a smoothly humming operation. Our DOE partners in the Basic Energy Sciences Scientific User Facilities Division provide guidance and encouragement and steadfastly represent the Project's interests. Paul Kearns, Argonne's Director, and all of Argonne's management are fully aware of how important the APS-U is to Argonne, and to our nation, and are committed to giving us the very best support. Of course, APS Director Stephen Streiffer, the APS management group, and the APS Operations personnel have always been fully invested in the Project's success.

When the APS-U is completed, together we will have made the APS a world-leading hard x-ray facility. The upgraded APS will be a member of a select group of countries (Sweden, France, Brazil, and China) that have built or are in the process of building 4th generation storage ring x-ray light sources based on multi-bend achromat arrangements of magnets in the rings Many others are in line with proposals to build 4th generation rings. But our machine will stand out in its ability to deliver highly coherent (tightly focused) hard x-ray beams (in the 20-100-keV range) that will enable our outstanding user community to carry out:

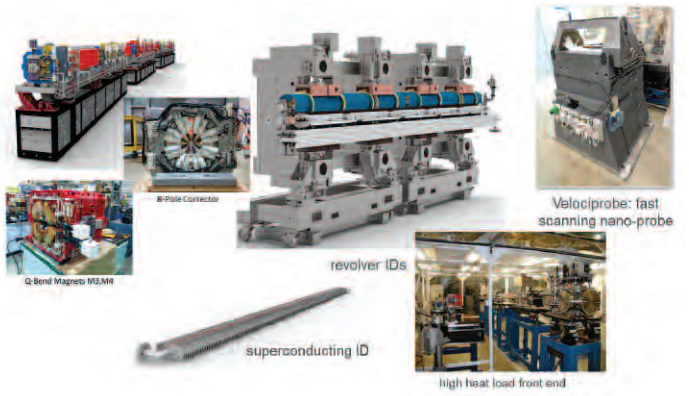

Some examples of APS-U accelerator and beamline technology.

- Small-beam scattering and spectroscopy for nanometer-scale imaging with chemical and structural contrast and few-atom sensitivity; and room-temperature, serial, single-pulse pink beam for macromolecular x-ray crystallography
- Resolution coupled to speed for mapping all of the critical atoms in a cubic millimeter; detecting and following rare events; and multiscale imaging of enormous fields of view with high resolution
- Coherent scattering and imaging with the highest possible spatial resolution for three-dimensional visualization, imaging of materials defects, and study of disordered heterogeneous materials; and x-ray photon correlation spectroscopy to probe continuous processes from nanoseconds onward, opening up 5 orders of magnitude in time inaccessible to today's x-ray synchrotron researchers

The APS Upgrade will enable the United States to maintain a world leadership position in storage ring-based hard x-ray sources.

To do this we are continuing to design the best possible APS-U in order to meet the technical parameters we have promised to DOE and to our users.

The state-of-the-art design for the accelerator is reaching maturity with highly advanced simulation codes, beam physics understanding, high-performance component design, and a novel on-axis injection scheme that enables reaching an electron beam emittance close to or at the diffraction limit for keV photons.

We continue to refine planning for the eight new "feature" beamlines, and for the enhanced existing beamlines included in the APS-U Project scope that will be made "APS-U ready."

The experts in the APS Accelerator Systems Division Magnetic Devices Group have already achieved great success with new superconducting insertion devices for some beamlines.

Designs for new or upgraded front ends that connect insertion devices to beamlines are well along as are critical components such as beam position monitors and improvements to the APS electron-beam injection system.

And this is just a partial list of the work still ahead of us as we progress through a series of detailed reviews by the DOE to an aggressive schedule of long-lead component procurements.

The APS-U offers opportunities for human development, as well. The Project affords opportunities for young engineers and physicists to grow professionally as they take on responsibilities. We are bringing new people to the APS who offer fresh ideas and afford management with an opportunity to carry out efficient succession planning.

All in all, it's a great time at the APS. I'm delighted to be part of it.

Robert Hettel
Project Director,
Advanced Photon Source Upgrade

ARGONNE NATIONAL LABORATORY 400-AREA FACILITIES

ADVANCED PHOTON SOURCE

(Beamlines, Disciplines, and Source Configuration)

ADVANCED PROTEIN CHARACTERIZATION FACILITY

CENTER FOR NANOSCALE MATERIALS

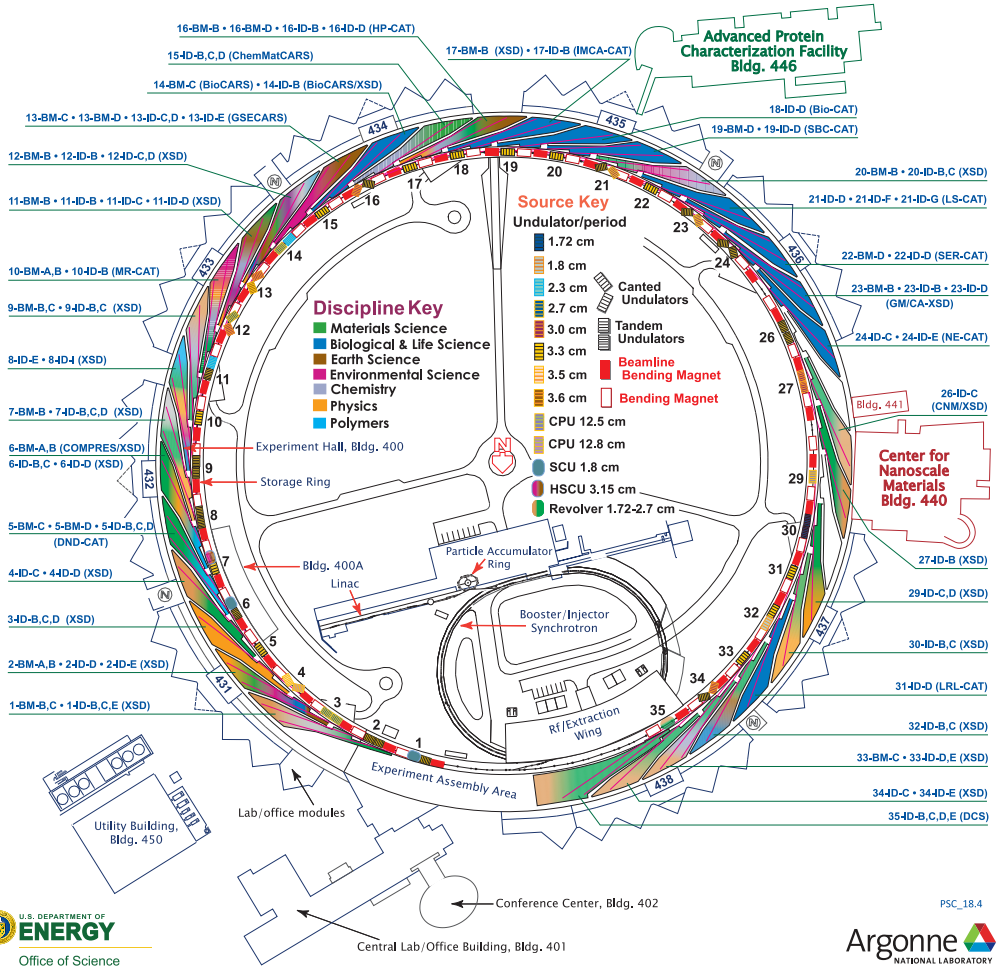

APS SECTORS: At the APS, a "sector" comprises the radiation sources (one bending magnet and nominally one insertion device, although the number of insertion devices in the straight sections of the storage ring can vary), and the beamlines, enclosures, and instrumentation that are associated with a particular storage ring sector. The APS has 35 sectors dedicated to user science and experimental apparatus. **X-ray Science Division (XSD)** sectors comprise those beamlines operated by the APS. **Collaborative access team (CAT)** sectors comprise beamlines operated by independent groups made up of scientists from universities, industry, and/or research laboratories.

Key to the beamline descriptions that accompany science highlights:
Beamline designation • Sector operator • Disciplines • Techniques • Radiation source energy • User access mode(s) • General-user status •

ACRONYMS FOR BEAMLINE OPERATORS USED IN THIS BOOK

BioCARS-CAT • Bio Center for Advanced Radiation Sources Collaborative Access Team

Bio-CAT • Biophysics Collaborative Access Team

ChemMatCARS-CAT • ChemMat Center for Advanced Radiation Sources Collaborative Access Team

CNM/XSD • Center for Nanoscale Materials/X-ray Science Division

DCS • Dynamic Compression Sector

DND-CAT • DuPont-Northwestern-Dow Collaborative Access Team

GM/CA-XSD • National Institute of General Medical Sciences and National Cancer Institute-X-ray Science Division

GSECARS-CAT • GeoSoilEnviro Center for Advanced Radiation Sources Collaborative Access Team

HP-CAT • High Pressure Collaborative Access Team

IMCA-CAT • Industrial Macromolecular Crystallography Association Collaborative Access Team

LRL-CAT • Lilly Research Laboratories Collaborative Access Team

LS-CAT • Life Sciences Collaborative Access Team

MR-CAT • Materials Research Collaborative Access Team

NE-CAT • Northeastern Collaborative Access Team

SBC-CAT • Structural Biology Center Collaborative Access Team

SER-CAT • Southeast Regional Collaborative Access Team

XSD • X-ray Science Division

APS Organization Chart

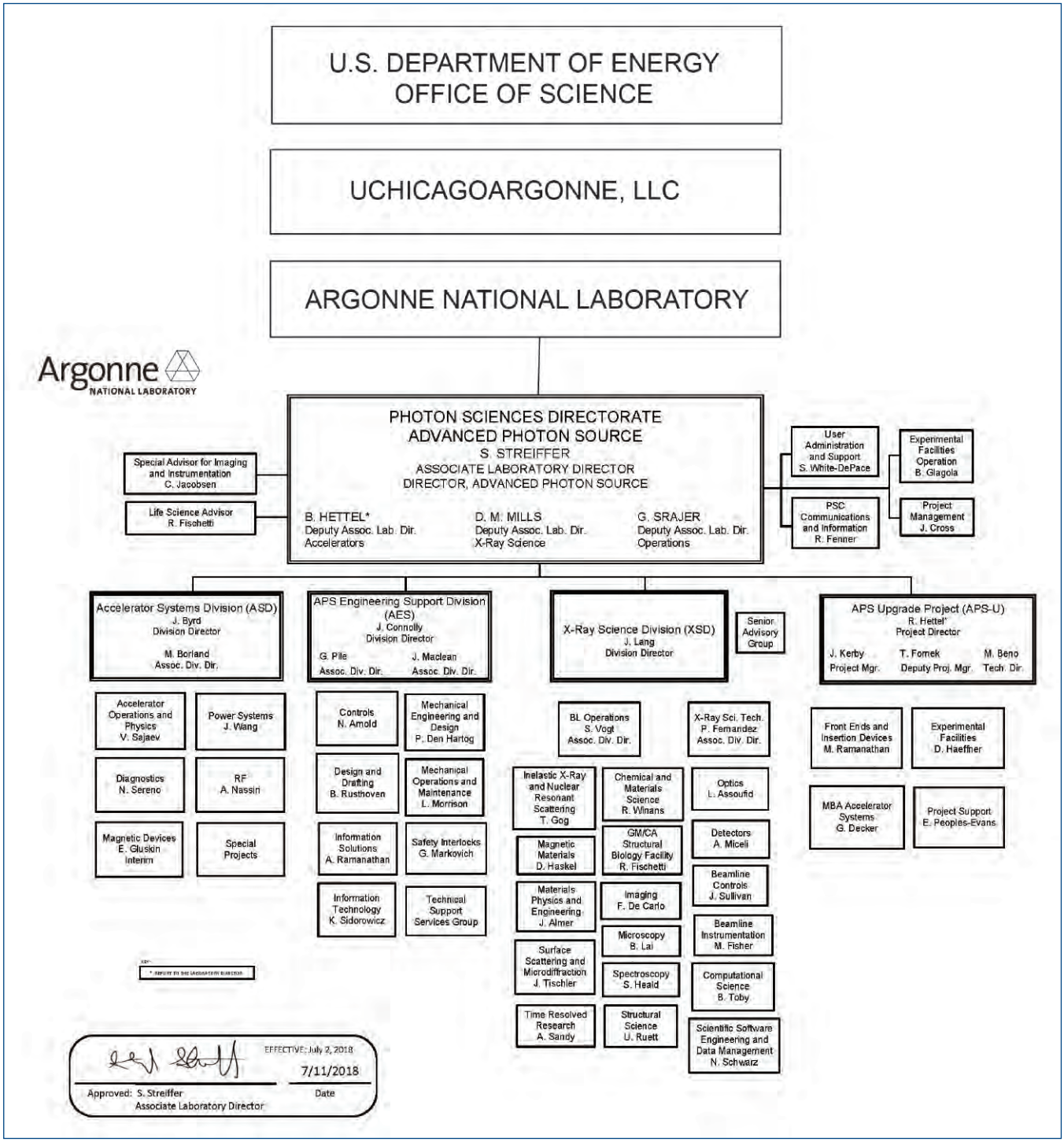

Acronyms for Argonne Organizations used in this book

AES - APS Engineering Support Division
ASD - Accelerator Systems Division
CELS/ALCF - Computing, Environment and Life Sciences/Argonne Leadership Computing Facility
CNM - Center for Nanoscale Materials
MSD - Materials Science Division
XSD - X-ray Science Division

Advanced Photon Source Chronology

March 14, 1984: "Planning Study for Advanced National Synchrotron-Radiation Facilities," sponsored by the U.S. Department of Energy (DOE) Office of Basic Energy Sciences (Peter Eisenberger and Michael L. Knotek, co-chairs), gives first priority to construction of a synchrotron-radiation facility optimized for insertion devices

July 24, 1984: "Major Facilities for Materials Research and Related Disciplines," sponsored by the Major Materials Facilities Committee of the Commission on Physical Sciences, Mathematics, and Resources of the National Research Council (Dean E. Eastman and Frederick Seitz, co-chairs), gives highest priority to construction of a facility with undulator radiation in the hard x-ray region of spectrum

February 1986: "6-GeV Synchrotron X-Ray Source Conceptual Design Report" published by Argonne National Laboratory

April 1987: "7-GeV Advanced Photon Source Conceptual Design Report" published by Argonne National Laboratory

May 1988: DOE approves new-project start

October 1, 1989: First construction funds released by DOE

June 4, 1990: Groundbreaking ceremony and start of Advanced Photon Source (APS) facility construction

October 7, 1993: Begin linac commissioning (50-MeV electron beam)

April 17, 1994: First electron beam stored in particle accumulator ring

July 31, 1994: Linac positron-current performance specifications met

January 22, 1995: First 7-GeV electron beam in booster synchrotron

February 20, 1995: First injection of 7-GeV electron beam from booster synchrotron to storage ring

March 18, 1995: First turn of 7-GeV electron beam in storage ring

March 25, 1995: First stored electron beam (4.5 GeV)

March 26, 1995: First storage ring bending magnet radiation detected in Sector 1 (beamline 1-BM-A)

April 15, 1995: First stored 7-GeV electron beam

August 9, 1995: First x-ray beam from APS undulator in Sector 1 (beamline 1-ID)

October 11, 1995: Attain DOE storage-ring commissioning milestone of 20-mA operation, minimum 10 hours of beam lifetime

January 12, 1996: First 100-mA stored electron beam

January 26, 1996: First undulator operated with 100-mA stored electron beam

May 1, 1996: APS dedication ceremony in APS experiment hall

July 30, 1996: First stored 7-GeV positron beam

July 31, 1996: First stored positron beam at 100-mA current

August 8, 1996: Secretary of Energy signs Key Decision #4 declaring project completion milestone

Electronic & Magnetic Materials

Revealing Ion Migration for Improved Perovskite Solar Cells and LEDs

Optoelectronic devices play an essential role in the modern world by converting an electric current to light (as exemplified by the ubiquitous LED lights), or conversely, by capturing light to produce electricity (as in solar cells). A class of materials offering significant potential for highly cost-effective optoelectronics are the so-called hybrid perovskites. In practice, the use of hybrid perovskites faces several challenges, including rapid changes in output in response to a voltage. Previous experiments were unable to directly observe the chemical origin of these changes. Using nanoprobe x-ray fluorescence (nano-XRF) at the APS, researchers have for the first time directly measured nanoscale changes in the chemical composition of crystals of methylammonium lead (Pb) bromide, a leading hybrid perovskite candidate for optoelectronic devices. The experiments revealed how the presence of an applied voltage depleted the bromine (Br) within regions of the material, degrading its optoelectronic performance. The researchers contend that limiting bromine migration within methylammonium lead bromide, and in similar hybrid perovskites, should stabilize these compounds, thereby enhancing their outstanding optoelectronic properties and promoting their use for inexpensive, yet highly-efficient, solar cells, photonic lasers, photodetectors, and light-emitting diodes (LEDs).

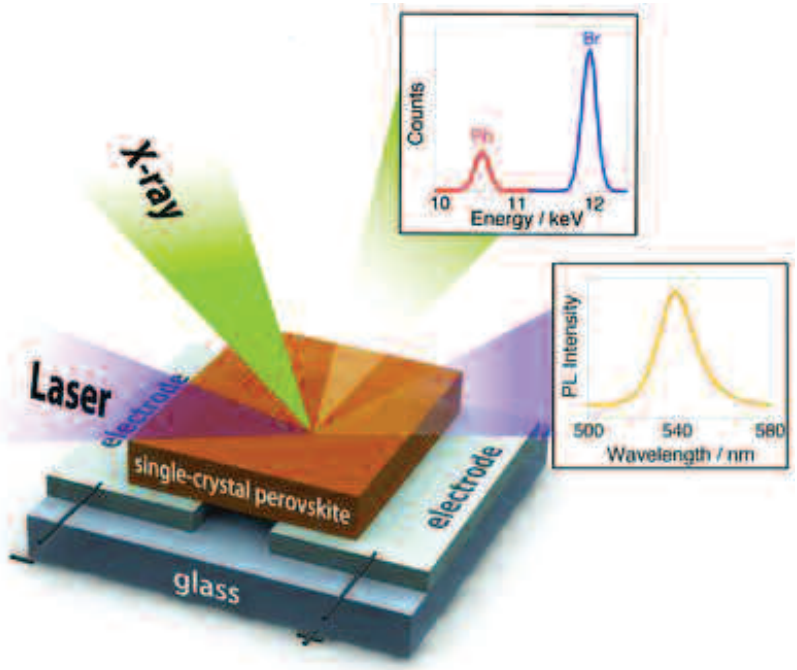

Fig. 1. Schematic of the experimental setup. A thin-film crystal of methylammonium lead bromide is mounted atop two electrodes and an insulating glass base. Nano-XRF measurements probed the crystal's bromine and lead elements. Upper-right inset shows that under zero voltage, nano-XRF detected around three times more bromine than lead in the crystal (as expected). The x-ray data also revealed how this ratio changed as the bromine migrated under voltage. Following the x-ray measurements, a violet laser excited the crystal, inducing light emission (photoluminescence) at a longer wavelength (~ 540 nm). The laser measurements showed that optoelectronic quality increased with higher bromine concentrations.

To increase the practicality of solar-generated electricity, the cost of fabricating photovoltaic cells must be reduced while simultaneously boosting their power-conversion efficiency. These cost and efficiency goals have drawn researchers to study hybrid perovskites for solar cells. The methylammonium lead halide compounds exhibit exceptional optoelectronic characteristics, yet are inexpensive to manufacture. Moreover, solar conversion efficiencies of over 22% have been demonstrated in the lab using hybrid perovskite thin films.

Traditional perovskites are inorganic, oxygen-bearing minerals with distinctive octahedral within a cubic crystalline structure. Methylammonium lead bromide (chemical formula $CH_3NH_3PbBr_3$) possesses the same perovskite structure with its distinctive octahedral arrangement, but differs from oxide perovskites in a couple of ways. First, the oxygen anion is replaced by bromine, one of the halogen elements (the others being iodine, chlorine, fluorine, and astatine). Second, it is an organic-inorganic compound wherein inorganic lead bromide ($PbBr_6$) octahedra are joined with organic methylammonium cations (CH_3NH_{3+}). This organic-inorganic mixture gives the compound its excellent optoelectronic properties and leads to its designation as a “hybrid” perovskite.

Theoretical calculations indicate that hybrid perovskites possess a large number of vacancies, or missing atoms, in their crystalline structure. Theoretical considerations also indicate that certain elements within the hybrid perovskites can readily move within these vacancies when subjected to an electric potential (voltage). In the case of methylammonium lead bromide, bromine ions are by far the most likely to move in response to an applied voltage.

The techniques used in previous studies to measure halide migration exhibited various drawbacks, such as sample destruction, or imaging limited

to near-surface depths. In contrast, the nano-XRF used for this study by researchers from the University of California, San Diego, AMOLF (Netherlands), and Argonne National Laboratory penetrated through the entire sample depth, while limiting damage to its crystalline structure.

The nano-XRF measurements were made at the XSD x-ray beamline 2-ID-D at the APS. Several high-quality, thin-film crystals of methylammonium lead bromide were grown. Each rectangular crystal measured around 20 to 30 µm per side. Figure 1 depicts the basic experimental setup. A highly collimated x-ray beam mapped each sample's heavier elements (bromine and lead) with a parts-per-million sensitivity, in 250-nm steps. Following the x-ray measurements, a laser probed the same microscopic area to determine its optoelectronic response via photoluminescence. (Photoluminescence involves the absorption and reemission of light of differing wavelengths. Higher-intensity photoluminescence indicates better optoelectronic properties.) A series of x-ray and laser measurements was made while the crystal was subjected to voltages of 0, -2, and +2 V.

Figure 2 illustrates the migration of bromine within the sample region as the voltage is varied. The images show that bromide ions move from the negative region of the sample towards the positive side. The laser-induced photoluminescence measurements demonstrated that better optoelectronic quality was associated with higher concentrations of bromine.

These findings quantitatively characterize bromine migration in methylammonium lead bromide under an applied voltage at room temperature. The findings also demonstrate that higher local bromine concentration is correlated with improved optoelectronic performance. In order to achieve the highest optoelectronic performance, the researchers suggest techniques for limiting bromine depletion in methylammonium lead bromide, such as growing the crystals in a bromine-excess environment to lower the number of crystalline vacancies following growth of the crystal. These important findings are applicable to other hybrid perovskites, such as methylammonium lead iodide wherein iodine supplants bromine. *— Philip Koth*

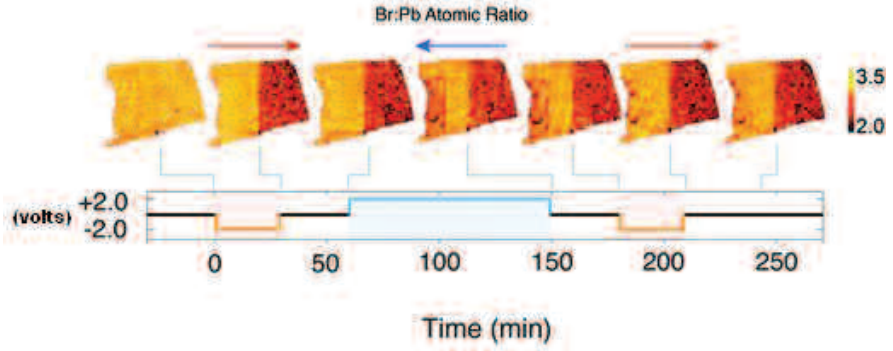

Fig. 2. Nano-XRF fluorescence maps depicting the ratio of Br to Pb in the crystal. Each map is 20-30-µm per side. Left-most map shows an evenly-distributed Br/Pb ratio prior to applying any voltage, as indicated by the uniform color. The next six maps clearly show the line dividing the two underlying electrodes, and a change in the bromine distribution (and Br/Pb ratio). Time is indicated below the maps, while current direction is shown by upper arrows. Left-hand electrode is grounded (0 V), while right-hand electrode is either 0, +2, or -2 V. Starting with the second map from left, after 30 min of exposure to a -2-V bias, bromine has migrated to the left. The darker color indicates that bromine concentration is depleted above the right-hand negative (-2-V) electrode, while lighter color indicates more bromine above the left-hand positive electrode (0 V). Subsequent cycling of the voltage bias from -2 V, to zero, to +2 V shows bromine migration is only partially reversible, leading to a permanent degradation in the optoelectronic quality of the crystal.

See: Yanqi Luo[1], Parisa Khoram[2], Sarah Brittman[2], Zhuoying Zhu[1], Barry Lai[3], Shyue Ping Ong[1], Erik C. Garnett[2], and David P. Fenning[1]*, "Direct Observation of Halide Migration and its Effect on the Photoluminescence of Methylammonium Lead Bromide Perovskite Single Crystals," Adv. Mater., early view publication, 1703451 (29 September 2017).
DOI: 10.1002/adma.201703451
Author affiliations: [1]University of California, San Diego, [2]AMOLF, [3]Argonne National Laboratory
Correspondence:
* dfenning@eng.ucsd.edu

Y.L. acknowledges the support of the University of California (UC) Carbon Neutrality Initiative. D.P.F. acknowledges UC San Diego startup funds and the support of the Hellman Foundation. This work is part of the research program in The Netherlands Organization for Scientific Research. P.K. and E.C.G. acknowledge financial support from the European Research Council (ERC) under the European Union's Seventh Framework Programme (FP/2007-2013)/ERC Grant Agreement No. 337328, "NanoEnabledPV." S.B. acknowledges the grant from an industrial partnership between Philips and FOM. Z.Z. and S.P.O. acknowledge funding support from the U.S. Department of Energy (DOE) Office of Science, Basic Energy Sciences under Award No. DE-SC0012118 for the computational portion of the work as well as computing resources provided by Triton Shared Computing Cluster at the UC San Diego, the National Energy Research Scientific Computing Center, and the Extreme Science and Engineering Discovery Environment supported by the National Science Foundation under Grant No. ACI-1053575. This research used resources of the Advanced Photon Source, a U.S. DOE Office of Science user facility operated for the DOE Office of Science by Argonne National Laboratory under Contract No. DE-AC02-06CH11357.

2-ID-D • XSD • Life sciences, materials science, environmental science • Microfluorescence (hard x-ray), micro x-ray absorption fine structure, nanoimaging • 5-30 keV • On-site • Accepting general users

The Anomalous Behavior of Rh-doped Sr_2IrO_4 Clarified

High-temperature superconductivity continues to mature as a technology even though the underlying mechanisms responsible for it in cuprates (copper oxides) remain unclear, despite decades of research. Today, the iridium oxide Sr_2IrO_4 is attracting intensive study because of its many parallels with La_2CuO_4, the parent compound of some cuprate superconductors. The hope is that when modifications of Sr_2IrO_4 are discovered that make it superconducting, these will yield insights into the root cause of superconductivity in cuprates as well. To advance this quest, an international group of researchers carried out spectroscopic x-ray measurements on rhodium (Rh)-doped $Sr_2Ir_{1-x}Rh_xO_4$ samples at the APS.

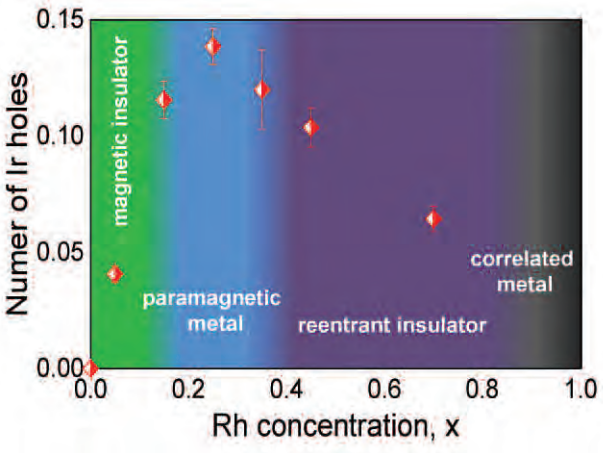

Fig. 1. Anomalous hole doping in Rh-doped Sr2IrO4 shown superimposed on the electronic phase diagram.

There are theoretical and experimental reasons to believe that superconductivity may be possible in Sr_2IrO_4 through electron or hole doping, which can be achieved by replacing either strontium (Sr) or iridium (Ir) cations with a non-isovalent ion. One approach involves doping with Rh ions to create $Sr_2Ir_{1-x}Rh_xO_4$; however, several fundamental issues regarding the doping process remain to be resolved. Among these are the oxidation state of Rh when it enters the $Sr_2Ir_{1-x}Rh_xO_4$ lattice, the impact of the disparate strength of spin-orbit interactions in 4d (Rh) and 5d (Ir) ions, and how increasing Rh content causes $Sr_2Ir_{1-x}Rh_xO_4$ to switch from an insulator to a metal. Equally mysterious is the reversion of the metallic state to an insulating condition as the Rh doping level continues to increase (Fig. 1).

Contrary to earlier reports of Rh being in either an Rh^{4+} or Rh^{3+} oxidation state across the compositional range, the researchers in this study, carrying out experiments at the XSD 4-ID-D beamline at the APS, found a smooth evolution from Rh^{3+} at doping levels below x = 0.05 toward Rh^{4+} at doping levels above x = 0.70, with the average Rh valence eventually reaching the Rh^{4+} value in the end compound Sr_2IrO_4.

At low Rh concentrations, Rh assumes a predominant 3+ state which dopes holes into nearest-neighbor Ir ions, which assume a 5+ oxidation state. This explains the rapid decrease in the system's resistivity leading to a metallic state at $x \sim 0.16$, since doped holes at Ir sites reduce the on-site Couloumb repulsion at these sites enabling hopping of charge from site to site (Sr_2IrO_4 is a Mott insulator). As x continues to increase, and with it the probability of finding Rh-O-Rh bonds, the number of doped holes decreases systematically as the average Rh valence moves toward 4+ (and so does the Ir valence), causing a reentrant insulating phase to emerge at $x \sim 0.35$. Only a small fraction of Ir ions (less than 25%) assume a 5+ oxidation state across the doping-dependent Rh/Ir charge partitioning.

Although the decrease in the number of charge carriers at high doping level is the most likely explanation for the reentrant insulating phase, the researchers note that doping-induced disorder is also likely to be at play. These findings should prove key to informing ongoing searches for novel electronic phases, including superconductivity, in (5d) Iridium-oxide compounds doped with 4d (or 3d) elements where charge disproportionation is expected.

— Vic Comello

See: S. Chikara[1,2], G. Fabbris[1,3,4], J. Terzic[5], G. Cao[5], D. Khomskii[6], and D. Haskel[1]*, "Charge partitioning and anomalous hole doping in Rh-doped Sr_2IrO_4," Phys. Rev. B **95**, 060407 (15 February 2017); manuscript selected by Phys. Rev. B editors as an Editors' Suggestion.

Author affiliations: [1]Argonne National Laboratory, [2]Los Alamos National Laboratory, [3]Washington University, [4]Brookhaven National Laboratory, [5]University of Colorado-Boulder, [6]Universität zu Köln

Correspondence: * haskel@aps.anl.gov

The work at the APS is supported by the U.S. Department of Energy (DOE) Office of Science under Grant No. DEAC02-06CH11357. Work at Los Alamos National Laboratory is supported by the Laboratory-Directed Research and Development program. The NHMFL Pulsed-Field Facility is funded by the U.S. National Science Foundation through cooperative Grant No. DMR-1157490, the State of Florida, and the DOE. Work at Brookhaven National Laboratory is supported by the DOE Office of Basic Sciences under Contract No. DE-SC00112704 and the Early Career Award Program under Award Number 1047478. G.C. acknowledges support of U.S. National Science Foundation grants DMR-1265162 and DMR-1712101. The work of D.Kh. was supported by DFG via the project SFB 1238 and by Köln University via the German Excellence Initiative.

Tipping the Balance to a Quantum Spin Liquid

Sometimes a little frustration and disorder can be a good thing, at least in the quest for the elusive and exotic state of matter known as a quantum spin liquid (QSL). In such systems, the electrons are strongly "entangled," a quantum phenomenon that is the basis of quantum computing but has proven extremely difficult to recreate except under tightly controlled laboratory environments. But QSLs naturally form such states, arising from their strong interactions (or correlations) that also serve to protect their entanglement from environmental influences. One class of these systems is the Kitaev quantum spin liquid, which takes advantage of anisotropic magnetic interactions on a honeycomb lattice. In the actual materials, the electron spins relieve their frustration and align themselves in one of two ways: a honeycomb "zig-zag" pattern or a "spiral" (technically an incommensurate) order. A group of researchers carrying out studies at the APS found that in the recently discovered Kitaev candidate compound β-Li_2IrO_3, a single material can be driven from the incommensurate state to a strongly correlated state with zig-zag broken symmetry upon the application of a small magnetic field, indicating the fragility of the material ground state.

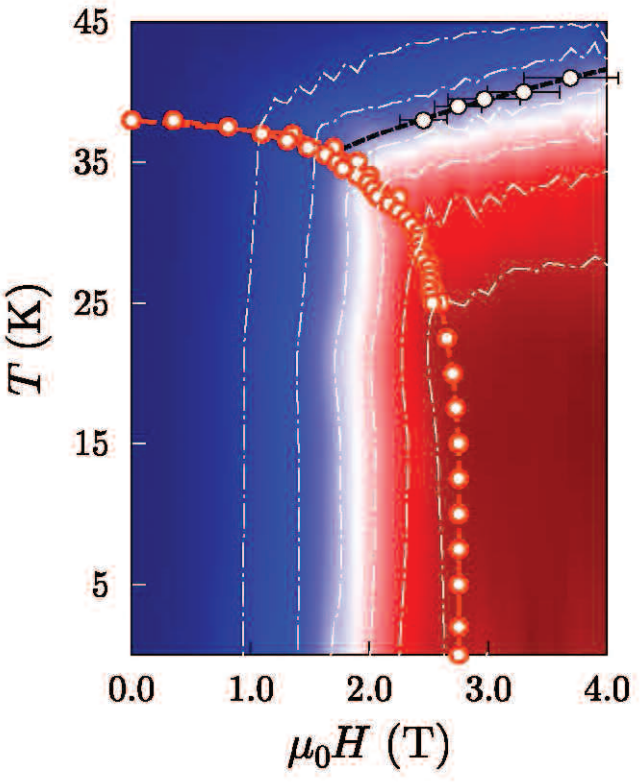

Fig. 1. T-H phase diagram determined using resonant x-ray magnetic scattering at the APS. The diagram was constructed by combining the normalized scattering intensity of a commensurate peak (blue-red scale contours), with the ***H**** and TI extracted from magnetization and heat capacity measurements (red/white circles), and a cusp observed in the field dependence of Cp (white dots).

Although the material β-Li_2IrO_3 is not quite a true Kitaev spin liquid, this study provides some new and tantalizing hints about possible ways to realize that elusive state of matter. The demonstration that this particular system could be induced to transition from an incommensurate to a field-induced zig-zag (FIZZ) state with the application of a small magnetic field shows that the exchange interactions in these magnetic honeycomb iridates are delicately balanced and ready to tip from one state to another with a properly placed nudge. At this point, the key to a quantum spin liquid appears to be merely a matter of a little fine tuning.

The β-Li_2IrO_3 compound structure (Fig. 2) is the simplest of the three-dimensional Kitaev systems. Due to its crystal symmetry, one of the Kitaev interactions favors b-axis spin coupling, likely the reason that the system's ground state is so susceptible to magnetic fields in this direction. To examine the thermodynamic behavior of the system, the researchers, from Lawrence Berkeley National Laboratory, the University of California, Berkeley, the Massachusetts Institute of Technology, the University of Texas at Dallas, and Argonne studied the iridium (Ir) L_3 edge with field-dependent magnetic resonance x-ray scattering (MRXS) at the XSD 6-ID-B,C beamline of the APS.

The field-induced change in the quantum state is manifested in the magnetization as an abrupt kink at $\mu_0 H^* = 2.8$ T. Studying the magnetic peak at propagation vector **q** = (-0.574, 0, 16) to examine the incommensurate state, the research team found that scattering intensity rapidly diminishes but with unchanging wavevector, indicating suppression of the incommensurate order vanishing completely at ***H****.

Beyond ***H****, thermodynamic data show a smooth crossover from one phase to another, but without a sharp phase boundary. However, the experimenters observed changes in the MRXS intensity at some reciprocal lattice vectors, corresponding to both structurally allowed and structurally forbidden peaks. The presence of the

"Tipping" cont'd. on page 13

Striped Nanodomains Creeping in Nominal Atomic Layers of Ferroelectrics

Ferroelectrics refers to materials with spontaneous electric polarization that can be switched by external electric fields. They are very similar to magnets but with electric instead of magnetic polarization. Besides their widespread applications in piezoelectric nanopositioners and ferroelectric random-access memorys that make use of the net ferroelectric polarization, the spatial arrangements of polarization domains in nominal atomic layers of ferroelectrics are also considered for high-density information storage due to their well-defined spatial structures with characteristic lengths as small as a few nanometers, so the stability of the domain structures is key to the design of nonvolatile memories. But tracking the domain motion in real time is extremely challenging as it requires detecting sub-angstrom atomic fluctuation on a nanometer spatial scale at elevated temperature. Researchers utilizing the APS overcame this obstacle with their study of serpentine striped ferroelectric nanodomains in a ferroelectric/dielectric superlattice. Ferroelectric polarization ordering is a promising candidate for self-assembly growth next-generation information storage, so these results provide a quantitative approach for measuring the stability of these structures, providing essential information for both modeling and application of complex ferroelectric oxides in a variety of technologies.

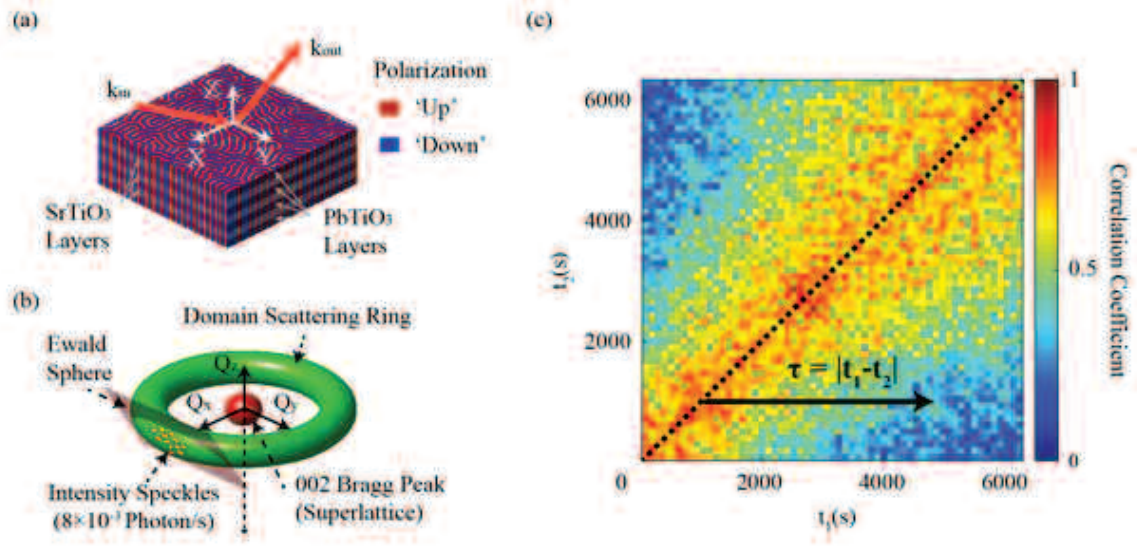

Fig. 1. (a) Ferroelectric/dielectric multilayer sample with domain pattern and diffraction geometry. (b) Domain pattern (c) A two-time intensity-intensity correlation function at elevated temperature.

The group of researchers from Argonne, the University of Wisconsin-Madison, Stony Brook University, and the University of Science and Technology of China investigated the temperature dependence of the equilibrium dynamics of ferroelectric nanodomains in a ferroelectric/dielectric $PbTiO_3/SrTiO_3$ superlattice using wide-angle x-ray photon correlation spectroscopy (XPCS) at the XSD 8-ID-E beamline at the APS. With the XPCS technique set to resolve atomic scale wave-vectors, the domain motion was recorded in a movie of coherent x-ray scattering patterns from the domains. The temporal decorrelation of the intensity speckles in the coherent scattering patterns revealed the time-scale of the domain dynamics. Fig. 1c shows the two-time correlation function of speckle patterns collected at time t_1 and t_2. Speckle patterns decorrelate as a function of time delay $|t_1 - t_2|$, and the process is in equilibrium as this decorrelation time is constant along the dashed line $t_1 = t_2$. This decorrelation time was measured from correlation functions performed at increasing temperatures.

Alternating atomic layers of $PbTiO_3$ and $SrTiO_3$ preserved the nanoscale spatial order of ferroelectric domains and provided additional robustness for the domain structures. The characteristic length scales are 6 nm for the domain periodicity and 30 nm for the in-plane coherence of the domain pattern. Spatial disorder in the domain pattern yields coherent hard x-ray scattering patterns exhibiting intensity speckles.

Variable-temperature Bragg-geometry XPCS reveals that x-ray scattering patterns from the disordered domains exhibit a continuous temporal decorrelation due to spontaneous domain fluctuations. The temporal decorrelation can be described using a compressed exponential function, consistent with what has been observed in other systems with arrested dynamics. The fluctuation speeds up at higher temperatures and the thermal activation energy estimated from the Arrhenius model is $> < 0.35 \pm 0.21$ eV. This energy barrier is smaller than both the activation energy for the migration of oxygen ion vacancies (a common domain wall pinning mechanism in ferroelectric perovskites) and the energy

Cont'd. on the next page

required to change the directions of domain walls as predicted from first-principle simulations.

The team suggests that the complicated energy landscape of the domain structure is induced by pinning mechanisms, and domain patterns fluctuate via the generation and annihilation of topological defects, a mechanism that requires little change of the system free energy and is commonly seen in soft materials such as block copolymers. The future APS Upgrade will enable such studies with much higher time and spatial resolution, probing these fluctuations on submillisecond time scales with beams smaller than 500 nm.

See: Qingteng Zhang[1], Eric M. Dufresne[1], Pice Chen[1], Joonkyu Park[2], Margaret P. Cosgriff[2], Mohammed Yusuf[3], Yongqi Dong[1,4], Dillon D. Fong[1], Hua Zhou[1], Zhonghou Cai[1], Ross J. Harder[1], Sara J. Callori[3], Matthew Dawber[3], Paul G. Evans[2], and Alec R. Sandy[1]*, "Thermal Fluctuations of Ferroelectric Nanodomains in a Ferroelectric-Dielectric $PbTiO_3/SrTiO_3$ Superlattice," Phys. Rev. Lett. **118**, 097601 (2017).
DOI: 10.1103/PhysRevLett.118.097601
Author affiliations: [1]Argonne National Laboratory, [2]University of Wisconsin-Madison, [3]Stony Brook University, [4]University of Science and Technology of China
Correspondence: * asandy@anl.gov

Work on the reference sample for the calibration of the setup stability was supported by U.S. Department of Energy (DOE) Office of Science-Basic Energy Sciences, Materials Sciences and Engineering Division. Work at the University of Wisconsin-Madison was supported under Grant No. DE-FG02-10ER46147 (P. E.). Work at Stony Brook University was supported by the U.S. National Science Foundation, Division of Materials Research under Grant No. 1055413 (M. D.). This research used resources of the Advanced Photon Source, a U.S. DOE Office of Science user facility operated for the DOE Office of Science by Argonne National Laboratory under Contract No. DE-AC02-06CH11357.

8-ID-E • XSD • Materials science, polymer science, physics • Grazing incidence small-angle scattering, x-ray photon correlation spectroscopy • 7.35-7.35 keV, 11-11 keV • On-site • Accepting general users •

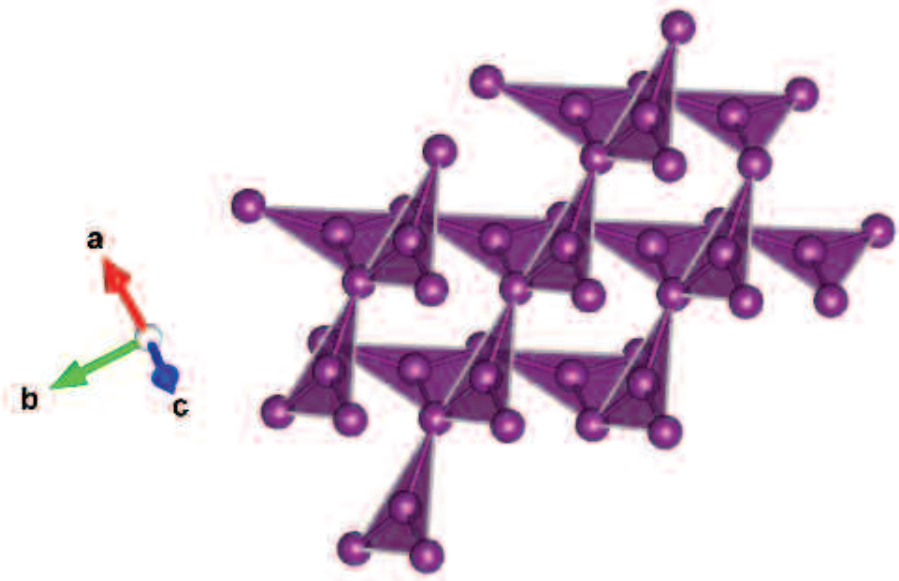

Fig. 2. An image of the compound crystal structure.

"Tipping" cont'd. from page 11

latter indicates an additional **q** = 0 broken symmetry induced by the applied magnetic field. Also, the structurally forbidden peaks show enhancement at the Ir L_3 edge with the magnetic field applied, suggesting that this broken symmetry state is electronic in origin.

The experimenters note that the observed behavior is quite different from the typically seen first-order phase transitions, such an antiferromagnetic to spin-polarized state. In this case, all broken symmetry states are seen simultaneously, yet retain intrinsic periodicity as a function of the applied field, showing a near-degenerate state.

Two types of symmetries are consistent with the data, one with zig-zag symmetry and the second ferromagnetic character, each of which explains different aspects of the observations. The research team suggests that the best interpretation is a high temperature transition from a trivial paramagnet to a low-temperature quantum correlated state. Even a small magnetic field is seen to drive β-Li_2IrO_3 from a zero-field incommensurate spiral order into a FIZZ state. This provides further evidence of the link between lithium-based iridates such as β-Li_2IrO_3 and other compounds such as α-$RuCl_3$/Na_2IrO_3 that also display a commensurate zigzag phase. *— Mark Wolverton*

See: Alejandro Ruiz[1,2]*, Alex Frano[1,2], Nicholas P. Breznay[1,2], Itamar Kimchi[1,3], Toni Helm[1,2], Iain Oswald[4], Julia Y. Chan[4], R.J. Birgeneau[1,2], Zahirul Islam[5], and James G. Analytis[1,2]**, "Correlated states in β-Li_2IrO_3 driven by applied magnetic fields," Nat. Commun. **8**, 961 (16 October 2017).
DOI: 10.1038/s41467-017-01071-9
Author affiliations: [1]University of California, Berkeley, [2]Lawrence Berkeley National Laboratory, [3]Massachusetts Institute of Technology, [4]The University of Texas at Dallas, [5]Argonne National Laboratory
Correspondence:
* alejandro@berkeley.edu,
** analytis@berkeley.edu

This work was supported the U.S. Department of Energy (DOE Office of Science-Basic Energy Sciences, Materials Sciences and Engineering Division, under the Early Career program, Contract No. DE-SC0014039. A.R. acknowledges support from the National Science Foundation (NSF) Graduate Research Fellowship under Grant No. DGE 1106400. I.A. and J.Y.C. acknowledge the support of NSF DMR-1360863. N.P.B. and T.H. were supported by the Gordon and Betty Moore Foundations EPiQS Initiative through Grant GBMF4374. This research used resources of the Advanced Photon Source, a U.S. DOE Office of Science user facility operated for the DOE Office of Science by Argonne National Laboratory under Contract No. DE-AC02-06CH11357.

6-ID-B,C • XSD • Physics, materials science • Magnetic x-ray scattering, anomalous and resonant scattering (hard x-ray), general diffraction, grazing incidence diffraction • 3.2-38 keV • On-site • Accepting general users •

A New Twist on Phases of Matter

Putting certain materials under the right conditions, such as applying an electrical field or changing their temperature, can lead to emergent properties that do not normally exist in the parent material; supercooling aluminum, for instance, turns it into a superconductor. A group of researchers using the APS has discovered a new state of matter in which whirlpools of polarization, known as "vortices," can arise. What's more, the scientists can control these vortices by changing the structure or temperature of the materials or by applying electrical fields. The work gives scientists the capability of creating new material properties that haven't been seen before, potentially creating new applications as well as opening new areas of inquiry in physics.

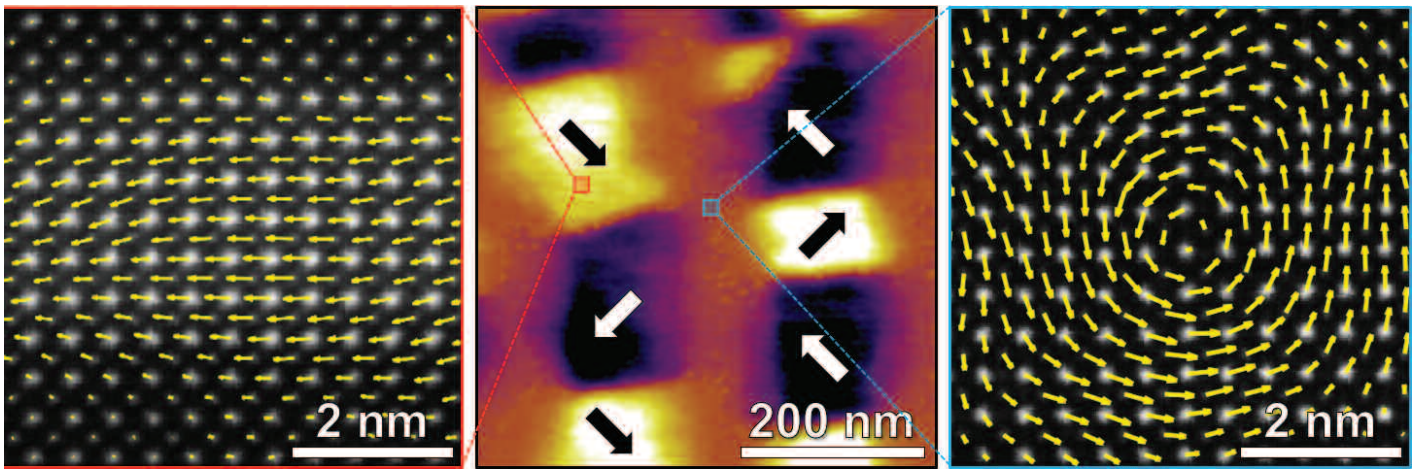

Fig. 1. Superlattices of lead titanate and strontium titanate self-assemble their dipoles into classical ferroelectric phases with alternating polarization (bright and dark areas) between emergent toroidal phases (brown). All the moments, indicated by arrows, point in one direction in a ferroelectric area (left), while they form vortices in the toroidal areas (right).

The materials the researchers worked with are perovskites, which have a particular crystalline structure, arranged in superlattices, which are periodic structures built from layers of different materials. In this case, they used lead titanate ($PbTiO_3$) and strontium titanate ($SrTiO_3$), grown on a dysprosium scandium oxide substrate. The lead titanate contains ferroelectric dipoles, electrical polarization that is analogous to the north-south polarization of ferromagnetic dipoles, while the strontium titanate has no electrical polarization. When just 10 to 20 layers of the two materials are stacked on top of one another in the right way, the dipoles within the lead titanate undergo an unexpected change. Because the dipoles have different polarizations, the lead titanate must rearrange them in order to settle into a new lowest-energy state. In the end, a handful of competing forces causes the formation of polarization vortices, whirlpool-like arrangements that spin clockwise or counterclockwise in alternating rows.

The researchers, from the University of California, Berkeley; Lawrence Berkeley National Laboratory; The Pennsylvania State University; Argonne; the University of Colorado Boulder, Universidad del País Vasco (Spain); Donostia International Physics Center (Spain); Universidad de Cantabria (Spain); and the Luxembourg Institute of Science and Technology (LIST) wanted to understand how the vortices would change as they changed the structure, altered the temperature of the material, or applied an electrical field. It turns out that changing the number of layers in the superlattice also changed the arrangement of the two types of phases within the material, the vortex phase and the more familiar ferroelectric phase, which exist next to each other in alternating stripes. The vortices existed in the material at room temperature, but researchers found that as they raised the temperature the material became entirely ferroelectric. They also used a technique called piezoresponse force microscopy (PFM), touching a conductive tip to the material to apply an electrical field to switch it between the vortex phase and the classical ferroelectric phase.

The switching was non-volatile, suggesting it could be used for some form of memory. The fact that the material responds to such manipulations means researchers might be able to induce, for example new effects, such as pyrotoroidic or piezotoroidic effects, analogous to the pyroelectric and piezoelectric effects found in some classical materials.

To analyze the material, the researchers performed synchrotron x-ray diffraction at the XSD 33-BM-C beamline of the APS. The brightness of the beam allowed them to obtain detailed information about the arrangement of the atoms and the periodicity of the lay-

"Twist" cont'd. on page 16

Control of Magnetic Coupling and Dimensionality by Chemical Substitution

All sorts of interesting properties, including Mott insulating states, antiferromagnetism, and insulator-to-metal transitions can sometimes manifest within a single compound. Enhancing or suppressing such properties presents both a theoretical and practical challenge. For this study, the strontium-iridium-oxide $Sr_3Ir_2O_7$ was explored. This compound has a bilayer crystalline structure formed by linked iridium-oxygen (IrO_6) octahedra. It exhibits an antiferromagnetic insulating state that lies very close to an insulator-to-metal transition. A research team altered (doped) a series of $Sr_3Ir_2O_7$ samples by replacing tiny amounts of strontium (Sr) with lanthanum (La), thereby varying the samples' electronic and magnetic behavior. X-ray scattering experiments carried out by the team at the APS and at the European Synchrotron Radiation Facility (ESRF) revealed that La doping in $Sr_3Ir_2O_7$ decreased the range of the compound's three-dimensional antiferromagnetic ordering, culminating in a short-range two-dimensional ordering and a metallic state. The researchers posit that this metallic state, which hosts strong antiferromagnetic fluctuations, could provide a new platform for manipulating novel magnetic/electronic states by the controlled application of perturbations. More generally, these findings should advance our fundamental understanding of the magnetic and electronic behavior of similarly doped compounds.

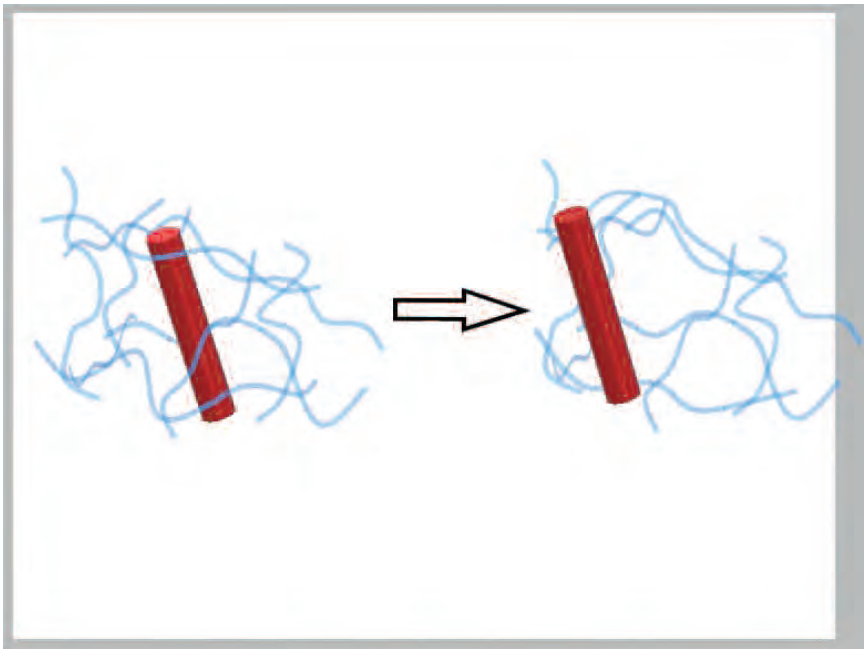

Fig. 1. Phases of $(Sr_{1-x}La_x)_3Ir_2O_7$ resulting from distinct doping levels of lanthanum. The red dots near the bottom indicate the five actual doping levels used for this study. Starting with a completely un-doped compound (x = 0), on up to a doping level of x = 0.03, $(Sr_{1-x}La_x)_3Ir_2O_7$ exhibits an insulating phase due to a long-range antiferromagnetic ordering. By contrast, higher La doping levels (x = 0.05 and 0.065) cause the compound to exhibit a conducting (metallic) phase due to a short-range antiferromagnetic ordering. The transition from the insulating phase to the metallic phase is indicated by the narrow vertical band at center; the actual IMT occurs at a doping level around x = 0.04 (red dashed line).

The $Sr_3Ir_2O_7$ compound was chosen for this study largely because of the unusual combination of novel properties it exhibits: small insulating band gap; strong interlayer couplings (i.e., correlations between electrons in different layers); magnetic excitations; and spin-orbit-coupling-induced antiferromagnetic Mott insulating behavior. Previous research has shown that doping of $Sr_3Ir_2O_7$ can drive the system into a metallic state. However, in spite of the previous investigations, the nature of the doped $Sr_3Ir_2O_7$ metallic state, in particular its magnetic properties, has remained largely elusive.

The researchers from the Paul Scherrer Institut, the ESRF, the University of Kentucky, the University of Colorado Boulder, and Argonne devised two strategies to help resolve these mysteries. First, a wider range of doping levels was employed. And, secondly, powerful synchrotron radiation from the APS and the ESRF was used to probe the magnetic ordering and electronic excitations in the samples via elastic and inelastic x-ray scattering.

The doping agent used was the metallic element lanthanum. The resulting modified chemical formula, $(Sr_{1-x}La_x)_3Ir_2O_7$, indicates the tiny quantity of lanthanum added. For instance, since the maximum doping level was x = 0.065, then at most 6.5% of the strontium (Sr) was replaced by lanthanum. At XSD beamline 27-ID-B at the APS, inelastic x-ray scattering measurements were performed on samples with no doping present (x = 0), and for x = 0.03. Doping levels for the ESRF measurements were x = 0.02, 0.05, and 0.065.

$Sr_3Ir_2O_7$ is a Mott insulator, which means it is electrically insulating below a certain temperature. However, unlike common insulators like glass, a Mott insulator's behavior is determined by repulsive interactions between certain electrons in the material. Doping can

"Control" cont'd. on page 16

"Twist" cont'd. from page 14

ers within the superlattice. The vortex phases caused interference with the x-rays, producing signatures that showed their distribution.

They also performed synchrotron x-ray nanodiffraction at the XSD 2-ID-D beamline, where they were able to focus the x-ray beam down to an area of approximately 200 nm and scan it across the sample to make a map of the structure. They made nanodiffraction measurements of the material, then used PFM to switch the phase, and made new measurements to observe that the phase had indeed changed.

— Neil Savage

See: A.R. Damodaran[1,2], J.D. Clarkson[1,2], Z. Hong[3], H. Liu[4], A.K. Yadav[1,2], C.T. Nelson[1,2], S.-L. Hsu[1,2], M.R. McCarter[1], K.-D. Park[5], V. Kravtsov[5], A. Farhan[2], Y. Dong[4], Z. Cai[4], H. Zhou[4], P. Aguado-Puente[6,7], P. García-Fernández[8], J. Íñiguez[9], J. Junquera[8], A. Scholl[2], M. B. Raschke[5], L.-Q. Chen[3], D.D. Fong[4], R. Ramesh[1,2], and L.W. Martin[1,2]*, "Phase coexistence and electric-field control of toroidal order in oxide superlattices," Nat. Mater. **16** 1003 (October 2017).
DOI: 10.1038/NMAT4951

Author affiliations: [1]University of California, Berkeley, [2]Lawrence Berkeley National Laboratory, [3]The Pennsylvania State University, [4]Argonne National Laboratory, [5]University of Colorado, Boulder, [6]Universidad del País Vasco, [7]Donostia International Physics Center, [8]Universidad de Cantabria, [9]Luxembourg Institute of Science and Technology (LIST)
Correspondence:
* lwmartin@berkeley.edu

A.R.D. acknowledges support from the Army Research O□ce under grant W911NF-14-1-0104 and the U.S. Department of Energy (DOE) O□ce of Science-Basic Energy Sciences (BES) under grant no. DE-SC0012375 for synthesis and structural study of the materials. Z.H. acknowledges support from NSF-MRSEC grant number DMR-1420620 and NSF-MWN grant number DMR-1210588. A.K.Y. acknowledges support from the U.S. DOE-BES under DE-AC02-05CH11231. C.T.N. acknowledge support from the U.S. DOE-BES DE-AC02-05CH11231. S.L.H. acknowledges support from the National Science Foundation (NSF) under the MRSEC program (DMR-1420620). M.R.M. acknowledges support from the NSF Graduate Research Fellowship under grant number DGE-1106400. K.-D.P., V.K., and M.B.R. acknowledge support from the U.S. DOE-BES, Division of Material Sciences and Engineering, under Award No. DE-SC0008807. A.F. acknowledges support from the Swiss National Science Foundation. P.G.-F. and J.J. acknowledge financial support from the Spanish Ministry of Economy and Competitiveness through grant number FIS2015-64886-C5-2-P.J.Í. is supported by the Luxembourg National Research Fund (Grant FNR/C15/MS/10458889 NEWALLS). L.-Q.C. is supported by the U.S. DOE-BES under Award FG02-07ER46417. R.R. and L.W.M. acknowledge support from the Gordon and Betty Moore Foundation's EPiQS Initiative, under grant GBMF5307. Nanodi□raction measurements were supported by the U.S. DOE-BES, Materials Sciences and Engineering Division. Electron microscopy of superlattice structures was performed at the Molecular Foundry at Lawrence Berkeley National Laboratory, supported by the U.S. DOE-BES (DE-AC02-05CH11231). This research used resources of the Advanced Photon Source, a U.S. DOE Office of Science user facility operated for the DOE Office of Science by Argonne National Laboratory under Contract No. DE-AC02-06CH11357.

"Control" cont'd. from page 15

sometimes force a Mott insulator to become conducting, producing a so-called insulator-to-metal transition (IMT). In this study, various levels of doping forced $Sr_3Ir_2O_7$ samples to cross the insulator-to-metal transition at lower-than-normal temperatures. Magnetic order and electronic/magnetic excitations were probed using x-ray measurements in the insulating and metallic phases of $Sr_3Ir_2O_7$.

The two doped samples examined at the APS, namely $(Sr_{1-x}Lax)_3Ir_2O_7$ with x = 0 and x = 0.03, were found to have long-range antiferromagnetic ordering. A similar sample probed at the ESRF (x = 0.02) displayed the same long-range antiferromagnetic ordering. (In antiferromagnetism, the spins of certain outer electrons orient in alternating directions: if one electron spin points upward, a neighboring electron points downward.) For the two higher doping levels of x = 0.05 and x = 0.065, the compound exhibited a conducting metallic phase that was associated with a short-range antiferromagnetic order (Fig. 1).

The entanglement of spin (the intrinsic angular momentum of the electrons) and orbit (angular momentum due to cyclic movement of the electrons), is known as spin-orbit coupling (SOC). SOC plays a central role in the novel Mott insulating states appearing in doped $Sr_3Ir_2O_7$. This study sorts out how the spin-orbit-coupled magnetic moments develop in response to the electron doping of $Sr_3Ir_2O_7$, from the insulating to the metallic state. (The phrase "electron doping" refers to the fact that lanthanum donates electrons to $Sr_3Ir_2O_7$.)

The $Sr_3Ir_2O_7$ compound is but one of a sequence of iridium-based compounds known as the Ruddlesden-Popper series. Like $Sr_3Ir_2O_7$, these related compounds also generally possess a layered structure and hold out promise for fine-tuning of their novel electronic and magnetic states via doping. The impact that doping had on the magnetic and electronic interactions observed in $Sr_3Ir_2O_7$ will directly benefit future studies on similar iridium compounds.

— William Atkins and Philip Koth

See: Xingye Lu[1]*, D.E. McNally[1], M. Moretti Sala[2], J. Terzic[3,4], M.H. Upton[5], D. Casa[5], G. Ingold[1], G. Cao[3,4], and T. Schmitt[1]**, "Doping Evolution of Magnetic Order and Magnetic Excitations in ðSr1−xLaxÞ3Ir2O7," Phys. Rev. Lett. **118**, 027202 (2017).
DOI: 10.1103/PhysRevLett.118.027202

Author affiliations: [1]Paul Scherrer Institut, [2]European Synchrotron Radiation Facility, [3]University of Kentucky, [4]University of Colorado at Boulder, [5]Argonne National Laboratory,
Correspondence: * xingye.lu@psi.ch,
** thorsten.schmitt@psi.ch

The work at the Paul Scherrer Institut is supported by the Swiss National Science Foundation through its Sinergia network Mott Physics Beyond the Heisenberg Model and the NCCRMARVEL. Xingye Lu acknowledges financial support from the European Community's Seventh Framework Programme (FP7/2007–2013) under Grant agreement No. 290605 (COFUND: PSI-FELLOW). G. Cao acknowledges support by the US National Science Foundation via Grants No. DMR-1265162 and No. DMR-1712101. This research used resources of the Advanced Photon Source, a U.S. Department of Energy (DOE) Office of Science user facility operated for the DOE Office of Science by Argonne National Laboratory under Contract No. DE-AC02- 06CH11357.

27-ID-B • XSD • Physics • Resonant inelastic x-ray scattering • 5-14 keV, 5-30 keV • On-site • Accepting general users •

Confirming the J_{EFF}=3/2 Ground State in a Lacunar Spinel

The phenomenon of spin-orbit coupling (SOC) in certain degenerate molecular systems can lead to unusual quantum phases, topological Mott states, and other interesting phenomena, some of which may even be important for spintronics and related applications. One such state arising from spin-orbit coupling is the molecular J_{eff}=3/2 ground state, which has been predicted by theory and modeling to be particularly exotic. A group of researchers working at the APS has achieved the first experimental verification of this state in the lacunar spinel $GaTa_4Se_8$ through resonant inelastic x-ray scattering (RIXS).

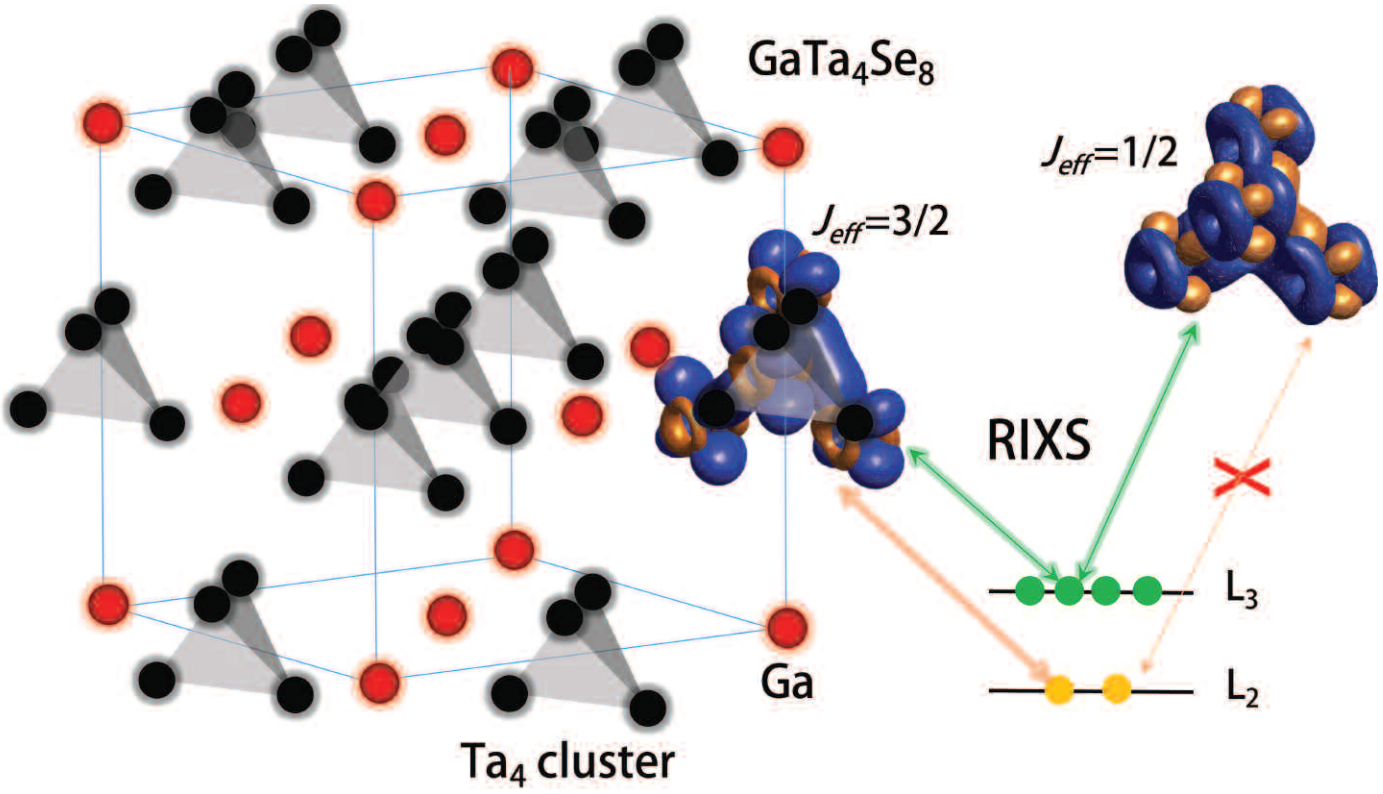

Fig. 1. Crystal structure and RIXS process in $GaTa_4Se_8$. The Ta_4 tetrahedron clusters form a face-centered-cubic lattice. The low-energy allowed L_2- and L_3-edge RIXS processes are indicated by green and orange arrows, respectively. The destructive interference at the L_2 edge RIXS of the J_{eff}= 1/2 establishes the J_{eff}=3/2 ground state in $GaTa_4Se_8$.

In 5*d* transition-metal systems, the J_{eff}=3/2 ground state exists near the Fermi energy, governing many-body behavior. Various materials have been proposed as candidates and studied with magnetic resonant x-ray scattering (MRXS), but this technique cannot be used for non-magnetically-ordered structures. Among non-magnetic systems, the lacunar spinel $GaTa_4Se_8$ is a 5*d* transition-metal compound that has been proposed as an especially good possibility for the J_{eff}=3/2 ground state. Its Ta_4Se_4 tetramerized crystal structure is split by spin-orbit coupling into a Kramers doublet of J_{eff}=1/2 and quartet of J_{eff}=3/2 molecular orbital (MO) states. To confirm this, the experimenters from KAIST (South Korea), Chung-Ang University (South Korea), the Computational Condensed Matter Physics Laboratory (Japan), the Interdisciplinary Theoretical Science Research Group (Japan), Argonne, Université de Nantes (France), the RIKEN Center for Emergent Matter Science (Japan), and the RIKEN Advanced Institute for Computational Science (Japan) performed high-resolution RIXS at the

"Confirming" cont'd. on page 19

Determining the Absorption Bandgap Inhomogeneity of PbSe Quantum Dots

Scientists using the APS have developed a novel means of determining the absorption bandgap inhomogeneity of colloidal lead selenide (PbSe) quantum dots (QDs) using femtosecond two-dimensional (2-D) Fourier transform spectroscopy. The simple analysis promises to be applicable to solutions and arrays of many other quantum-confined materials as well.

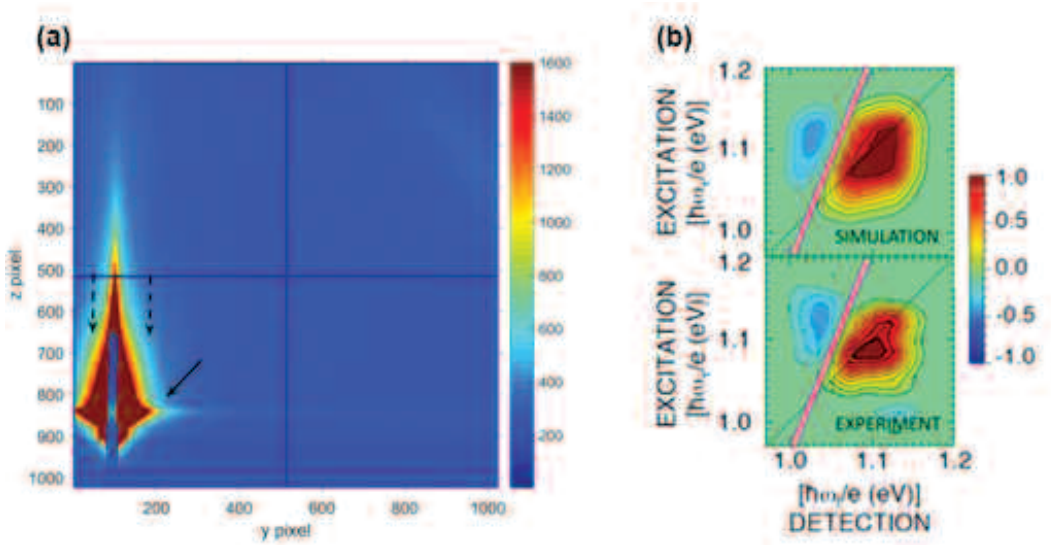

Fig. 1. (a) GISAXS image obtained on an ensemble of PbSe nanoparticles dispersed on SiO_2 support. The arrows indicate scattering from nanosized objects. (b) After optical excitation, 2-D spectra show transient changes in sample transmission as a function of both excitation and detection frequencies. The 2-D spectrum shows contours like a topographic map. The solid contours are at 10% intervals of the maximum positive signal (green to red fill colors). Dashed 10% contours show negative signals (blue fill colors). The dotted black line is the diagonal, with equal excitation and detection frequencies. The nodal line that separates positive and negative is shown in pink. The slope of the nodal line determines the optical bandgap inhomogeneity, which is important for many applications of quantum dots. Adapted with permission from S. D. Park et al., Nano Lett. **17**, 762 (2017). ©Copyright 2017 American Chemical Society.

For instance, due to their size-tunable optical and electronic properties, quantum-confined semiconductor nanocrystals have shown great potential in many emerging optoelectronic applications including light-emitting diodes, lasers, solar cells, and photodetectors. However, these and other applications require very stringent control over the line width of the first exciton (electron-hole) transition of the QDs.

Line width broadening has contributions from dynamic broadening mechanisms arising within each nanocrystal and static inhomogeneous broadening arising from differences between nanocrystals in an ensemble, such as size and shape dispersion. These two broadening mechanisms have different impacts on transport in nanocrystal arrays. In particular, it is the energetic disorder from the static inhomogeneity of the first quantum-confined exciton bandgap that must be tightly controlled for optimal transport.

Initial attempts to compare the absorption bandgap inhomogeneity of the QDs obtained from 2-D spectroscopy to the value calculated from the size and shape distribution of the QDs led to inconsistencies when standard methods based on transmission electron microscopy (TEM) were used to determine the sizes and shapes. The researchers from the University of Colorado, Boulder, and Argonne resolved the conflicts in part by using new 2-D histograms that correlate major and minor TEM image projections, revealing the elongated structure of the nanocrystals, a result that was supported by measurements using high-resolution TEM and grazing incidence small-angle x-ray scattering (GISAXS), the latter at XSD beamline 12-ID-C,D of the APS. Because the band-gap inhomogeneity calculated from the size and shape distribution didn't include impacts from surface effects, but that measured from 2-D spectroscopy did, the comparison revealed that no more than ~ 41-meV of the broadening came from surface contributions.

In 2-D spectroscopy, a sample is excited by light, and transient changes in its spectrum are measured as a function of two frequency dimensions. These 2-D spectra have positive signals from reduced ground state absorption, positive signals from excited state stimulated emission, and negative signals from excited state absorption. The researchers showed that the absorption bandgap inhomogeneity of the ensemble was robustly determined by the slope of the nodal line separating the positive and negative peaks in the 2-D spectrum around the bandgap transition (Fig. 1b). That is, it was shown that the slope of the nodal line provides a robust, single-parameter determination of the absorption bandgap inhomogeneity for the entire quantum dot ensemble, which was shown to reveal the dynamic absorption line shape as well.

This was the first application of 2-D spectroscopy to the determination of nanoparticle size distributions. Since

Cont'd. on the next page

the 2-D spectra indicated a new analysis of TEM images was needed, the researchers wanted to connect to an established determination of nanoparticle size and shape. Like 2-D spectroscopy, GISAXS would also probe more of the ensemble than the thousands of nanoparticles that could be analyzed by TEM. Using the GISAXS technique, a large area (100-mm × 0.55-mm strip) of the sample surface with many millions of nanoparticles could be probed. The GISAXS technique has the advantage of determining both the lateral size and the height of the nanoparticles. The analysis of the 2-D GISAXS images, as shown in Fig. 1a, revealed prolate particles with axes 4.4 nm and 3.4 nm long (within an accuracy of ± 0.2 nm), lying on the surface along their longer axis and validated the new TEM analysis techniques. *— Vic Comello*

See: Samuel D. Park[1], Dmitry Baranov[1], Jisu Ryu[1], Byungmoon Cho[1], Avik Halder[2], Sönke Seifert[2], Stefan Vajda[2], and David M. Jonas[1]*, "Bandgap Inhomogeneity of a PbSe Quantum Dot Ensemble from Two-Dimensional Spectroscopy and Comparison to Size Inhomogeneity from Electron Microscopy," Nano Lett. **17**, 762 (2017).
DOI: 10.1021/acs.nanolett.6b03874
Author affiliations: [1]University of Colorado, [2]Argonne National Laboratory
Correspondence:
* david.jonas@colorado.edu

The work of S.D.P., D.B., J.R., B.C., and D.M.J. was supported by the U.S. Department of Energy (DOE) Office of Science-Basic Energy Sciences, Division of Chemical Sciences, Geosciences, and Biosciences, under Award Number DE-FG02-07ER15912. A.H. and S.V. acknowledge the support by DOE-Basic Energy Sciences, Materials Science and Engineering, under Contract DE-AC02-06CH11357 with UChicago Argonne, LLC, the operator of Argonne National Laboratory. This research used resources of the Advanced Photon Source, a U.S. DOE Office of Science user facility operated for the DOE Office of Science by Argonne National Laboratory under Contract No. DE-AC02-06CH11357.

12-ID-C,D • XSD • Chemistry, physics, materials science • Small-angle x-ray scattering, grazing incidence small-angle scattering, wide-angle x-ray scattering, surface diffraction • 4.5-40 keV • On-site • Accepting general users •

"Confirming" cont'd. from page 17

Ta L_2 and L_3 edges using the RIXS spectrometer at the XSD 27-ID-B beamline of the APS, along with x-ray absorption spectroscopy (XAS).

The excitation spectra from both the RIXS and XAS studies show the structure of the unoccupied states and a wide energy range density of states, with many unoccupied states above the 2-eV level with both t_{2g} and e_g symmetry. Near the Fermi energy, however (±2 eV), t_{2g} symmetry is dominant. Three narrow peaks are seen with RIXS at the L_3 edge at 0.27, 0.7, and 1.3 eV, yet the 1.3-eV peak is not present at the L_2 edge. Based on their analyses of momentum transfer measurements and band structure and cluster model calculations, the experimenters attribute this to destructive interference of the J_{eff}=1/2 state at the L_2 edge.

Examining band structure near the Fermi energy, the researchers observe that without a large degree of spin-orbit coupling, only strong electron correlation can split the t_2 molecular orbital band into a narrow lower band and broad upper band, which would result in no differences between the spectra of the L_2 and L_3 edges. In this lacunar spinel, however, there is clear separation between the J_{eff}=3/2 and J_{eff}=1/2 molecular orbitals, leaving out the J_{eff}=3/2 MO band near the Fermi energy in which a moderate U opens a gap, making it a molecular J_{eff}=3/2 Mott insulator. The absence of the 1.3-eV peak at the Ta L_2 edge on RIXS is due to destructive interference which thus confirms a J_{eff}=3/2 ground state. In addition, the research team suggests that the phase transition from Mott insulator to superconductor displayed by $GaTa_4Se_8$ under high pressure may result from a frustrated magnetic phase emerging from the non-trivial interactions among relativistic J_{eff}=3/2 moments.

This first experimental verification of the J_{eff}=3/2 ground state with RIXS demonstrates the utility of this particular technique even in the many systems without long-range magnetic order, and can serve as a general solution for establishing Jeff states. Such studies require only moderate energy resolution of around 100 meV, easily achievable in all 5*d* transition-metal l edges with current instruments.

As a next step, the team plans to investigate other likely candidates for the J_{eff}=3/2 ground state using RIXS measurements. The work promises to reveal fresh insights into exotic new quantum phases in materials that may eventually find application in future generations of microelectronic, superconducting, and spintronic technologies.

— Mark Wolverton

See: Min Yong Jeong[1], Seo Hyoung Chang[2], Beom Hyun Kim[3,4], Jae-Hoon Sim[1], Ayman Said[5], Diego Casa[5], Thomas Gog[5], Etienne Janod[6], Laurent Cario[6], Seiji Yunoki[3,4,7,8], Myung Joon Han[1]*, and Jungho Kim[5]**, "Direct experimental observation of the molecular J_{eff} = 3/2 ground state in the lacunar spinel $GaTa_4Se_8$," Nat. Commun. **8**, 782 (2017).
DOI: 10.1038/s41467-017-00841-9
Author affiliations: [1]Korea Advanced Institute of Science and Technology [2]Chung-Ang University, [3]Computational Condensed Matter Physics Laboratory, [4]Interdisciplinary Theoretical Science Research Group, [5]Argonne National Laboratory, [6]Université de Nantes, [7]RIKEN Center for Emergent Matter Science, [8]RIKEN Advanced Institute for Computational Science
Correspondence: * mj.han@kaist.ac.kr, ** jhkim@aps.anl.gov

M.Y.J., J.-H.S., and M.J.H. were supported by the Basic Science Research Program through NRF (2014R1A1A2057202). The computing resource was supported by KISTI (KSC-2014-C2-046) and the RIKEN supercomputer system (HOKUSAI GreatWave). S.H.C. was supported by the Basic Science Research Program through NRF (2016K1A3A7A09005337). B.H.K. was supported by the RIKEN iTHES Project. S.Y. was supported by a Grant-in-Aid for Scientific Research from MEXT Japan under the Grant No. 25287096. This research used resources of the Advanced Photon Source, a U.S. DOE Office of Science user facility operated for the DOE Office of Science by Argonne National Laboratory under Contract No. DE-AC02- 06CH11357.

27-ID-B • XSD • Physics • Resonant inelastic x-ray scattering • 5-14 keV, 5-30 keV • On-site • Accepting general users •

Precise Layer Growth in a Superlattice Controls Electron Coupling and Magnetism

Two-dimensional (2-D) crystalline films often exhibit interesting physical characteristics, such as unusual magnetic or electric properties. By layering together distinct crystalline thin films, a so-called "superlattice" is formed. Due to their close proximity, the distinct layers of a superlattice may significantly affect the properties of other layers. In this research, single 2-D layers of strontium iridium oxide were sandwiched between either one, two, or three layers of strontium titanium oxide to form three distinct superlattices. Researchers then used x-ray scattering at the APS to probe the magnetic structure of each superlattice. The x-ray data revealed that the number of layers of the titanium-based material produced a dramatic difference in the magnetic behavior of the iridium-based layer. These findings are especially significant because the iridium compound is one of the perovskites, a class of materials known for their unique electric, magnetic, optical, and other properties that have proven useful in sensors and energy-related devices, and which are being intensively investigated for their application towards improved electronics and other technologies.

The original perovskite mineral, $CaTiO_3$, was discovered in the mid-1800s. Many similar compounds have been found over the years, featuring two metal elements combined with oxygen in the chemical ratio ABO_3 (where A and B are the metals). The experimental research described here involved artificially-grown stacks, or superlattices, of $SrIrO_3$ and $SrTiO_3$, both of which have a perovskite-like structure. Figure 1b depicts the alternating layers that make up the superlattice. The artificially-grown $SrIrO_3/SrTiO_3$ superlattice used for this research is similar to the widely-studied bulk $Sr2IrO_4$ and Perovskite ABO_3 crystals that can form a similar superlattice. However, unlike the better-known $Sr2IrO_4$ system, the magnetic interactions of the $SrIrO_3/SrTiO_3$ superlattice are highly tunable.

$SrIrO_3/SrTiO_3$ superlattices also exhibit antiferromagnetism. Both ferromagnetism and antiferromagnetism constitute magnetically-ordered states. In ferromagnetism, the spins of certain outer electrons in a material (e.g., iron) all tend to point in one direction, producing a magnet. In antiferromagnetism, the spins stack in alternating directions (one electron spin points "right," while its neighbor's spin points "left"). As a result of this alternating spin arrangement, antiferromagnetic ordering produces a negligible overall net magnetic field quite different from the better-known ferromagnets.

Researchers have previously used the well-known $Sr2IrO_4$ crystalline system to investigate Mott insulating behavior and antiferromagnetism. The $Sr2IrO_4$ system can naturally grow into an alternating $SrIrO_3/SrO/SrIrO_3/SrO/...$ layering scheme (Fig. 1a). In the superlattice derived from $Sr2IrO_4$ crystals, the $SrIrO_3$ layers are antiferromagnetic and Mott-insulating perovskites, while the SrO layers are relatively inert. Interestingly, the Mott insulating behavior and antiferromagnetism of the superlattice are believed to be affected by both intralayer (within the layer) and interlayer (between layers) exchanges.

Unfortunately, the $SrIrO_3/SrO$ crystal system poses certain limitations. For instance, the thicknesses of its layers cannot be readily adjusted. For this study, the researchers from the University of Tennessee, Knoxville, Brookhaven National Laboratory, Charles University (Czech Republic), Academy of Sciences of the Czech Republic, Argonne, and Dublin City University (Ireland) instead used the recently-developed superlattice in which the inert SrO layers are replaced with layers of the similarly-inert titanium compound $SrTiO_3$. Using a laser deposition technique, superlattices composed of atomically thin layers of $SrIrO_3/SrTiO_3$ were created.

The superlattices were made with 1, 2, or 3 $SrTiO_3$ layers between each $SrIrO_3$ layer, as shown in Fig. 1b. Each superlattice was probed to compare the effects of their different layering arrangements. Magnetic ordering was determined using x-ray scattering techniques specifically designed to detect magnetic structure, carried out at XSD x-ray beamlines 4-ID-D and 6-ID-B,C at the APS. The x-ray data revealed that the highest magnetic ordering, attributed to greater interlayer exchange coupling, occurred in the $SrIrO_3$ layers separated by just a single $SrTiO_3$ inert layer. On the other hand, greater intralayer electron correlation occurred (i.e., correlation of electrons within each $SrIrO_3$ layer) in superlattices with two or three inert $SrTiO_3$ layers.

This study demonstrated that superlattices can be created with precisely-tuned layer thicknesses and sequences of perovskite $SrIrO_3$ and inert $SrTiO_3$. In turn, this capability allows re-

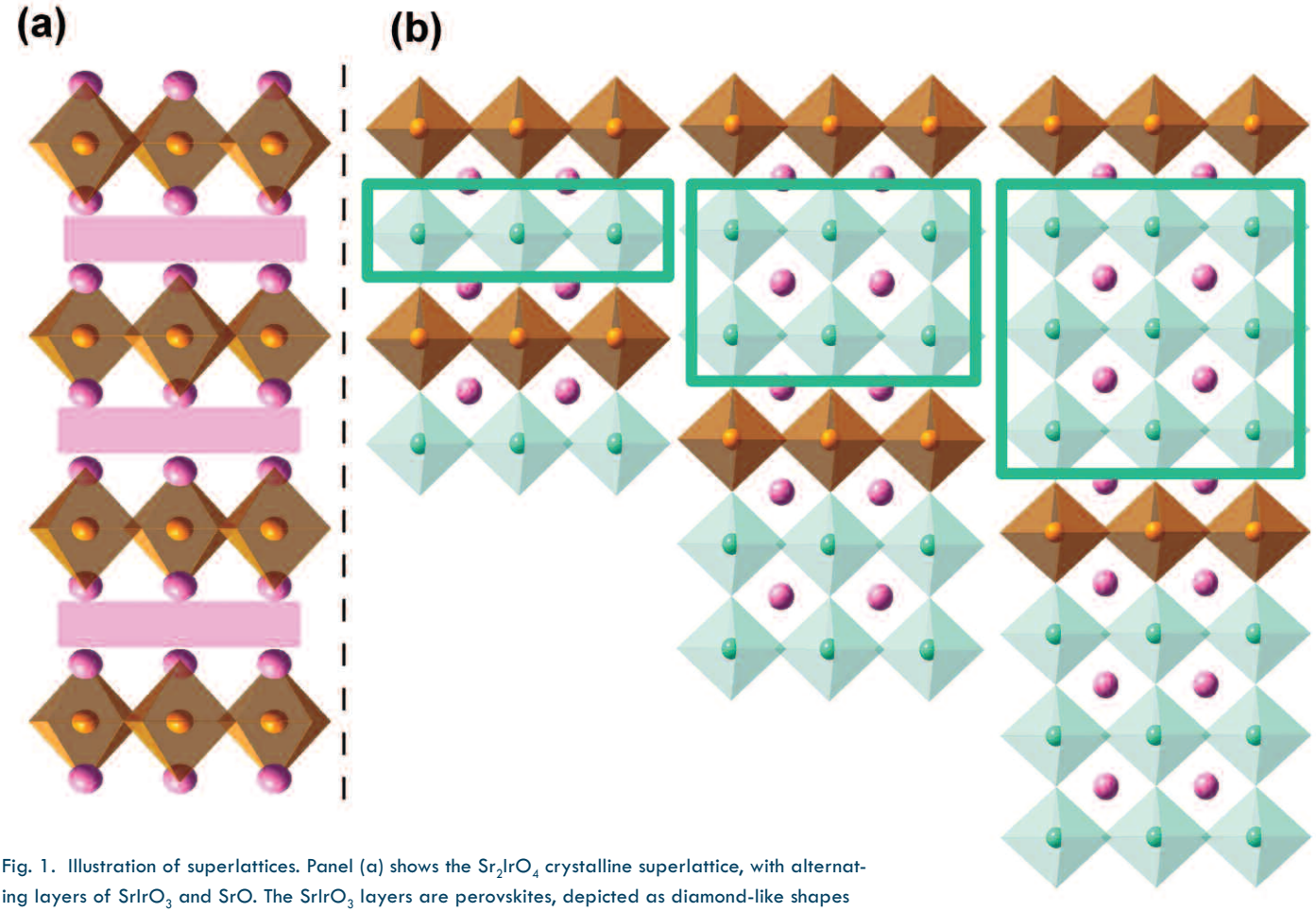

Fig. 1. Illustration of superlattices. Panel (a) shows the Sr_2IrO_4 crystalline superlattice, with alternating layers of $SrIrO_3$ and SrO. The $SrIrO_3$ layers are perovskites, depicted as diamond-like shapes formed by six oxygen atoms; inside each diamond is a gold-colored iridium ion (cation), while pink strontium ions lay near the diamond's ends. The $SrIrO_3$ layers are separated by non-perovskite (inert) SrO layers, depicted as pink bars. Panel (b) shows the more-recently developed $SrIrO_3/SrTiO_3$ superlattice used for this research. Three distinct $SrIrO_3/SrTiO_3$ superlattices were created, having 1, 2, or 3 layers of inert $SrTiO_3$ layers (colored green) separating the active $SrIrO_3$ layers. Bold green boxes highlight the number of inert $SrTiO_3$ layers in the three distinct lattices. While both $SrIrO_3$ (gold diamonds) and $SrTiO_3$ (green diamonds) are perovskites, the green-colored $SrTiO_3$ layers buffer the active $SrIrO_3$ layers.

searchers to tailor electron correlations within and/or between the perovskite $SrIrO_3$ layers. Quite interestingly, the researchers also found that the sign (i.e., direction) of the magnetic coupling between the neighboring $SrIrO_3$ layers could be controlled by adjusting the number of buffering $SrTiO_3$ layers.

— Philip Koth

See: Lin Hao[1]*, D. Meyers[2], Clayton Frederick[1], Gilberto Fabbris[2], Junyi Yang[1], Nathan Traynor[1], Lukas Horak[3], Dominik Kriegner[3,4], Yongseong Choi[5], Jong-Woo Kim[5], Daniel Haskel[5], Phil J. Ryan[5,6], M.P.M. Dean[2]**, and Jian Liu[1]***, "Two-Dimensional J_{eff} =1=2 Antiferromagnetic Insulator Unraveled from Interlayer Exchange Coupling in Artificial Perovskite Iridate Superlattices," Phys. Rev. Lett. **119**, 027204 (14 July 2017).
DOI: 10.1103/PhysRevLett.119.027204
Author affiliations: [1]University of Tennessee, Knoxville, [2]Brookhaven National Laboratory, [3]Charles University, [4]Academy of Sciences of the Czech Republic, [5]Argonne National Laboratory, [6]Dublin City University
Correspondence:
* lhao3@utk.edu,** mdean@bnl.gov,
*** jianliu@utk.edu

The authors acknowledge experimental assistance from H.D. Zhou, C. Rouleau, Z. Gai, J.K. Keum, and H. Suriya. J.L. acknowledges support from the Science Alliance Joint Directed Research & Development Program and the Transdisciplinary Academy Program at the University of Tennessee. J. L. also acknowledges support by the DOD-DARPA under Grant No. HR0011-16-1-0005. M.P.M.D. is supported by the U.S. Department of Energy (DOE) Office of Science-Basic Energy Sciences Early Career Award Program under Award No. 1047478. Work at Brookhaven National Laboratory was supported by the U.S. DOE Office of Science-Basic Energy Sciences, under Contract No. DESC00112704. D. K. and L. H. acknowledge support from the ERDF (Project No. CZ.02.1.01/0.0/0.0/15_003/ 0000485) and the Grant Agency of the Czech Republic Grant No. (14-37427G). A portion of the fabrication and characterization was conducted at the Center for Nanophase Materials Sciences, which is a DOE Office of Science user facility. This research used resources of the Advanced Photon Source, a U.S. DOE Office of Science user facility operated for the DOE Office of Science by Argonne National Laboratory under Contract No. DE-AC02-06CH11357.

4-ID-D • XSD • Physics, materials science • Anomalous and resonant scattering (hard x-ray), magnetic x-ray scattering, magnetic circular dichroism (hard x-ray) • 2.7-40 keV • On-site • Accepting general users •

6-ID-B,C • XSD • Physics, materials science • Magnetic x-ray scattering, anomalous and resonant scattering (hard x-ray), general diffraction, grazing incidence diffraction • 3.2-38 keV • On-site • Accepting general users •

Using Electric Fields to Efficiently Control Memory

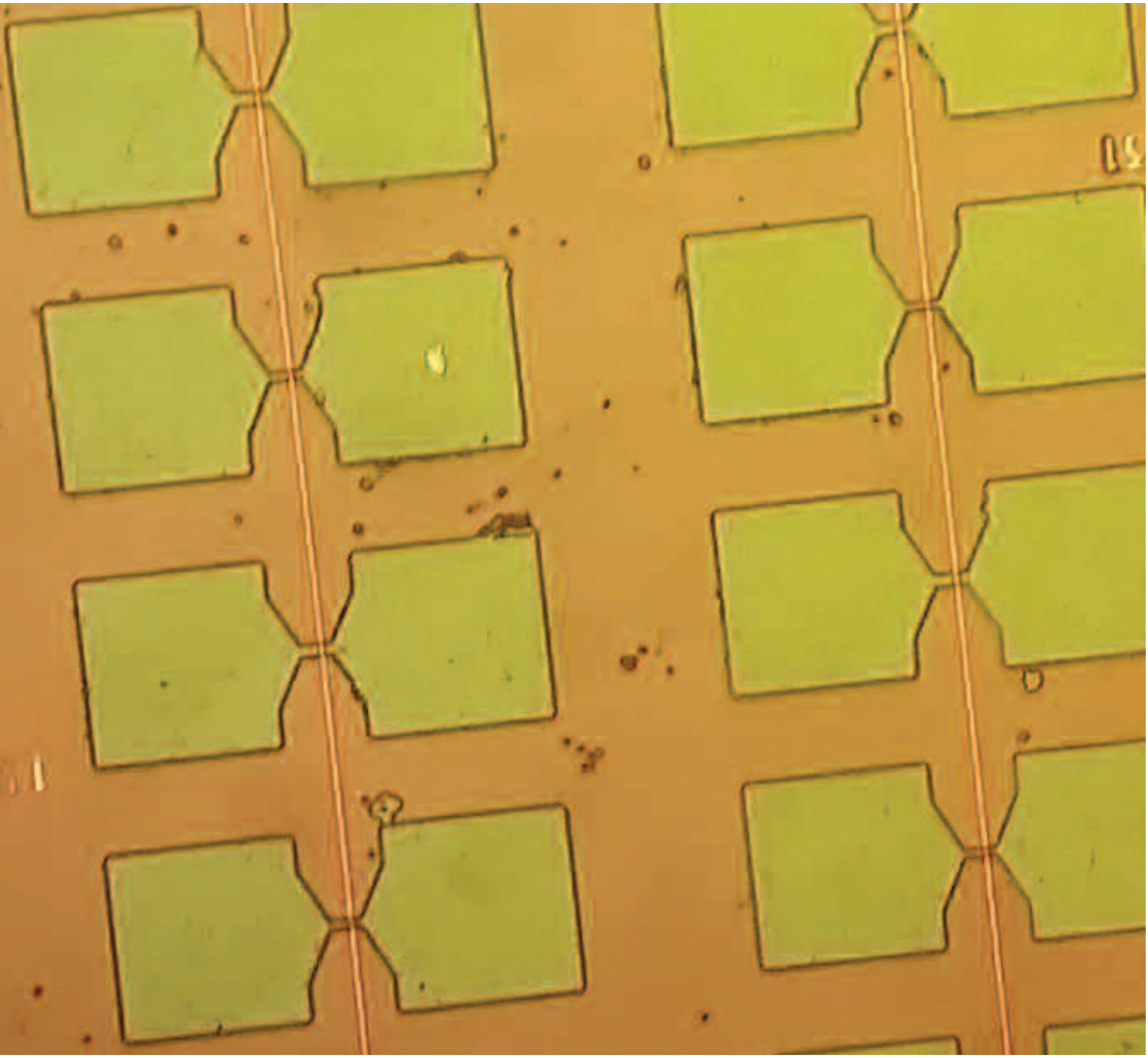

Fig. 1. Magnetic tunnel junctions with GdO_x barriers where the interlayer coupling between the soft and hard magnetic layers can be controlled by voltage

4-ID-C • XSD • Physics, materials science • Magnetic circular dichroism (soft x-ray), x-ray magnetic linear dichroism, x-ray photoemission spectroscopy, x-ray photoemission electron microscopy, anomalous and resonant scattering (soft x-ray) • 500-2800 eV • On-site • Accepting general users ••

While modern hard drives use magnetic fields to control the magnetization of memory elements, memory storage by electric fields is desirable because that method would be much more energy efficient. In this work, carried out at the APS, researchers discovered an efficient technique for using electric fields to control magnetic thin films at room temperature. This work demonstrated that electric fields can transport oxygen, and perhaps other anions, across an interface using very little energy. In addition to memories and logic units, this advancement of nonvolatile control of tunneling magnetoresistance may lead to new applications such as microwave devices and magnetic field sensors with variable sensitivity and range. Voltage-controlled spintronic devices would use much less power and so be made smaller or could last longer between charges. Additional research may lead to a better understanding of the material combinations that require the application of voltages for shorter times at room temperature. With these advances, nanomagnets could be the next generation of memory and transistor.

Spintronics researchers create new memory devices by switching the spin orientations of nanomagnets. While they typically control the spin using magnetic fields or spin-polarized currents, these methods are energy hogs. The challenge is to use electric fields, which are far more energy efficient, to lower the nanomagnet switching energy in magnetic tunnel junctions. Until recently, this had only been accomplished at very low temperatures. To be really useful, of course, the process must take place at room temperature and the spin-orientation switching must be nonvolatile, meaning that the effect must persist even when the voltage is removed.

In this experiment, an ultra-thin cobalt film was sandwiched between a heavy ferromagnesian metal layer and a gate oxide layer (GdO_x). The researchers, from the University of Arizona, Oak Ridge National Laboratory, the University of Minnesota, Bryn Mawr College, and Argonne controlled the magnetic properties of interlayer coupling in the magnetic tunnel using small applied voltages (Fig. 1). Indeed, they changed the magnetic state of the thin film by inducing oxygen ions to migrate through an oxide layer and change the oxidation state of the ferromagnetic CoFeB layer. Even just a few volts resulted in a reversible and non-volatile anisotropy change that was over 2 orders of magnitude larger than found by previous studies. The researchers were successful at getting this to work at room temperature. The control of spin by voltage is due to the interfacial nature of the magnetism, the ability to move oxygen vacancies within the GdO_x tunnel barrier, and a large induced net magnetic moment of Gd ions.

At the APS, tunneling magnetoresistance, x-ray absorption spectroscopy, and x-ray magnetic circular dichroism were measured simultaneously at XSD beamline 4-ID-C. The researchers determined the oxidation states of the CoFeB films, quantified the saturation magnetization, and provided evidence that applying the voltage results in reversible diffusion of O^{2-} ions between Gd_2O_3 and Co.

Their measurements confirmed the hypothesis of voltage-driven oxidation-reduction in the GdO_x and proximity-induced moment of the Gd ions by the Co film. Through the unique combination of strong interfacial perpendicular magnetic anisotropy, efficient manipulation of oxygen vacancies and a large induced net moment of GdO_x, not only the magnitude but also the sign of the interlayer coupling can be effectively manipulated by applied voltage.

— Dana Desonie

See: T. Newhouse-Illige[1], Yaohua Liu[2], M. Xu[1], D. Reifsnyder Hickey[3], A. Kundu[1], H. Almasi[1], Chong Bi[1], X. Wang[4], J.W. Freeland[5], D.J. Keavney[5], C.J. Sun[5], Y.H. Xu[1], M. Rosales[1], X.M. Cheng[4], Shufeng Zhang[1], K.A. Mkhoyan[3], and W.G. Wang[1]*, "Voltage-controlled interlayer coupling in perpendicularly magnetized magnetic tunnel junctions," Nat. Commun. **8**,15232 (16 May 2017).
DOI: 10.1038/ncomms15232
Author affiliations: [1]University of Arizona, [2]Oak Ridge National Laboratory, [3]University of Minnesota, [4]Bryn Mawr College, [5]Argonne National Laboratory
Correspondence:
* wgwang@physics.arizona.edu

We thank Richard Rosenberg and Yu Le for assistance during the synchrotron experiments. This work was supported in part by C-SPIN, one of six centres of STARnet; a Semiconductor Research Corporation programme, sponsored by MARCO and DARPA; and by the National Science Foundation (NSF) through ECCS-1554011. Work at ORNL was supported by the Division of Scientific User Facilities-Basic Energy Sciences, U.S. Department of Energy (DOE) Office of Science. This research used resources of the Advanced Photon Source, a U.S. DOE Office of Science user facility operated for the DOE Office of Science by Argonne National Laboratory under Contract No. DE-AC02- 06CH11357. This work also utilized the College of Science and Engineering (CSE) Characterization Facility, University of Minnesota (UMN), supported in part by the NSF through the UMN MRSEC program (No. DMR-1420013); and the CSE Minnesota Nano Center, UMN, supported in part by NSF through the NNIN program. This research used resources of the Advanced Photon Source, a U.S. DOE Office of Science user facility operated for the DOE Office of Science by Argonne National Laboratory under Contract No. DE-AC02-06CH11357.

High-Speed Shocks Induce a Phase Change in Calcium Fluoride Crystals

Placing a crystal under extreme pressure can sometimes change its structure from one form, or phase, to another. Determining exactly how crystals change phase under compression is an important area of materials physics research and the availability of x-ray diffraction at synchrotron facilities has allowed scientists to observe compression-driven phase changes in unprecedented detail. Most of the research in this field has focused on pressure-induced phase changes using slow (static) compression over a timescale of minutes. Now, utilizing x-ray diffraction (XRD) at the APS, a multi-institution research team has observed microstructural phase changes over nanosecond timescales within a two-element (calcium fluoride) crystal subjected to extreme pressures. The high pressures were achieved both through high-velocity instantaneous shock compression and by statically squeezing the samples. The researchers expect that their real-time observations of phase transitions within calcium fluoride will provide a template for the phase transitions of similarly-structured compounds. More generally, it is anticipated that the experimental methods and results of this study will lead to improved modeling of phase transitions over nanosecond timescales, within a wide range of complex materials.

Calcium fluoride (CaF_2) is a naturally-occurring mineral with a greenish hue. Its common crystalline form is called fluorite. Under high pressure, the crystalline structure of CaF_2 can change from fluorite, which possesses a cubic crystal lattice, to cotunnite, which exhibits an orthorhombic lattice. Previous static high-pressure experiments had demonstrated the presence of the fluorite-to-cotunnite phase transition. Shock compression studies on CaF_2 crystals have also previously been performed, but these studies were not able to probe the structure of the crystals at the microscopic scale.

The experiments in this study carried out by researchers from Sandia National Laboratories: Washington State University: The University of Nevada, Las Vegas: and the Carnegie Institution of Washington focused on high-velocity impacts with calcium fluoride samples. Speeds of 6 km/s were achieved utilizing a two-stage light gas gun. This specialized gun type is regularly used to attain hypervelocity speeds, which can range as high as the speeds of orbiting spacecraft. A conventional single-barrel gun was also used for lower-speed impacts down to 2 km/s. All the impact experiments were carried out at the DCS beamline 35-ID-E at the APS. This sector houses both the high-speed guns and the specialized equipment neces-

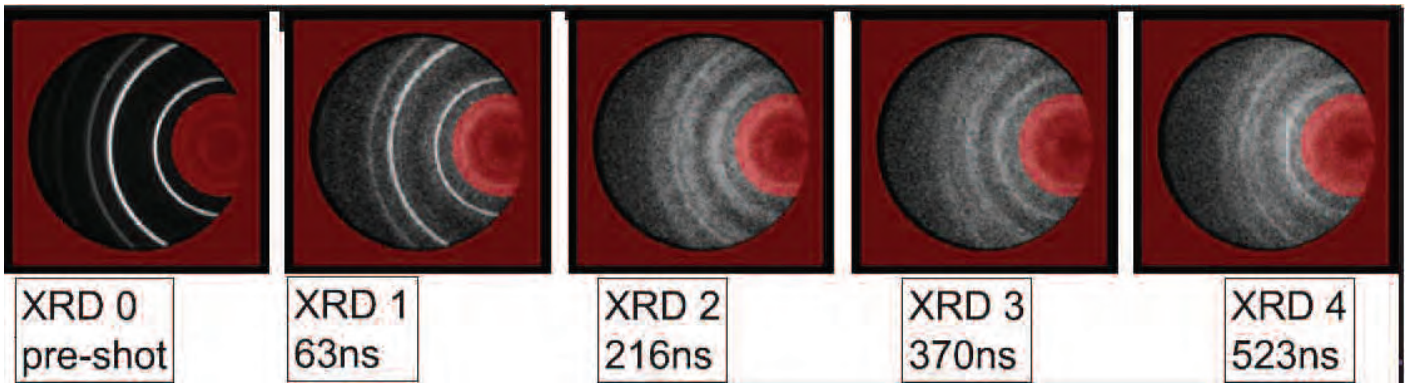

Fig. 1. A sequence of XRD patterns of a CaF_2 sample. The circular arcs in each image form part of a Debye-Scherrer ring, a type of diffraction pattern caused by powdered materials. The images show the effects of the impact-induced shock wave as it moves through the sample. The leftmost diffraction pattern is recorded just before impact. The next image (63 ns) shows the effects of the shock wave midway through the sample. Middle image (216 ns) shows shock-wave effects as the wave approaches the sample's far end. The pronounced diffusion of the Debye-Scherrer arcs in the two rightmost images arises from multiple stress states due to reflected shock waves. Adapted from P. Kalita et al., Phys. Rev. Lett. **119,** 255701 (2017). © 2017 American Physical Society

16-ID-B • HP-CAT • Materials science, geoscience, chemistry, physics • Microdiffraction, single-crystal diffraction, high-pressure diamond anvil cell • 18-60 keV • On-site • Accepting general users •

35-ID-B,C,D,E • DCS • Physics, materials science, geoscience • Time-resolved x-ray scattering, phase contrast imaging, radiography • 7-35 keV, 7-100 keV, 24-24 keV • On-site• Accepting general users •

sary for gathering x-ray diffraction data on samples during impacts.

A high-speed impact creates a shock wave within a material that spikes its pressure and temperature as the wave propagates. These extreme impact conditions caused the fluorite-to-cotunnite phase transition in CaF_2 samples. Figure 1 shows the changing x-ray diffraction patterns caused by a propagating shock wave within one of the samples. Figure 2 is a schematic of the experimental setup for the projectile/sample impact, including the orientation of the impinging x-ray beam.

Real-time x-ray measurements of the unfolding impact event were recorded with nanosecond precision. The high spatial resolution attained by the x-ray diffraction revealed how the spacing between atoms within the crystalline lattice shifted in response to the passing shock wave. This information corresponded to a fluorite-to-cotunnite phase change in the crystalline CaF_2. After passing through the sample, the shock wave bounced off the transparent viewing window and travelled back through the sample. Several such shock-wave reverberations occurred, resulting in a complex configuration of pressure and temperature states. Sorting through this complex data set indicated that the shock stress required for the fluorite-to-cotunnite phase transition lies between 7.8 and 22.6 GPa.

As a comparison to the impact experiments, diamond anvil cell compression tests were performed at the HP-CAT beamline 16-ID-B, also at the APS. The researchers found that at similar pressure and stress states, the lattice unit cell volumes of the shocked samples were between 0.5% and 2% larger than the cell volumes of the statically-compressed samples. This difference in lattice unit cell size is attributed to heating of the shocked samples, which increases in magnitude as the stress state increases.

These atomic-scale x-ray observations, performed with nanosecond precision, allowed the researchers to observe the unfolding phase changes during high-speed impact events. Such results go well beyond revealing the fluorite-to-cotunnite phase transition in

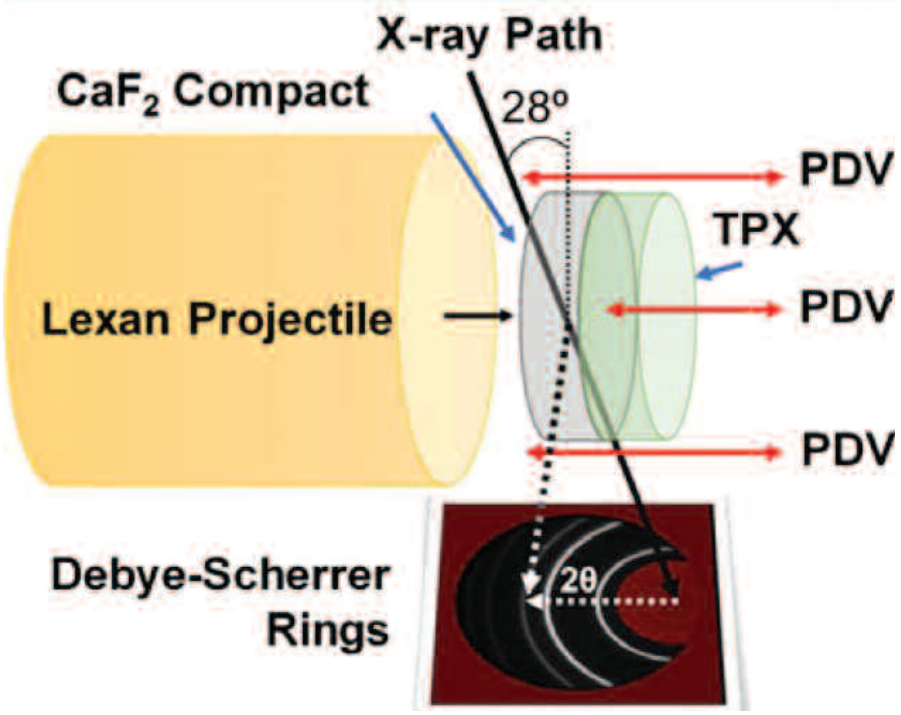

Fig. 2. Schematic of the basic experimental setup. The powdered sample is labeled "CaF_2 Compact" and is identified by the blue arrow. The sample is mounted to a TPX window that is transparent to x-rays. The high-speed Lexan™ projectile approaches from the left. The synchrotron x-ray beam is shown offset 28° from vertical. The horizontal red lines on the right side of the schematic indicate photonic Doppler velocimetry (PDV) measurements of the impact event and particle velocities within the sample. Bottom inset shows orientation of the Debye-Scherrer ring diffraction pattern. Adapted from P. Kalita et al., Phys. Rev. Lett. **119,** 255701 (2017). © 2017 American Physical Society

CaF_2; they help push the state-of-the-art for exploring and interpreting the dynamics of complex phase transitions in a wide array of solids. *— Philip Koth*

See: Patricia Kalita[1]*, Paul Specht[1], Seth Root[1], Nicholas Sinclair[2], Adam Schuman[2], Melanie White[3], Andrew L. Cornelius[3], Jesse Smith[4], and Stanislav Sinogeikin[4], "Direct Observations of a Dynamically Driven Phase Transition with *in situ* X-Ray Diffraction in a Simple Ionic Crystal," Phys. Rev. Lett. **119**, 255701 (2017).
DOI: 10.1103/PhysRevLett.119.255701
Author affiliations: [1]Sandia National Laboratories, [2]Washington State University, [3]University of Nevada, Las Vegas, [4]Carnegie Institution of Washington
Correspondence: * pekalit@sandia.gov

The authors thank P. Rigg and the DCS team, N. Cofer, J. Usher, K. Hodge and R. Hickman of SNL, S. Payne of NSTEC, as well as E. Rod and the HP-CAT team. Sandia National Laboratories is a multi-mission laboratory managed and operated by National Technology and Engineering Solutions of Sandia, LLC., a wholly owned subsidiary of Honeywell International, Inc., for the U.S. Department of Energy's (DOE'S) National Nuclear Security Administration (NNSA) under Contract No. DE-NA-0003525. A portion of this publication is based upon work performed at the DCS, which is operated by Washington State University under the U.S. DOE/NNSA Award No. DE-NA0002442. Portions of this work were performed at HP-CAT whose operations are supported by DOE-NNSA under Award No. DE-NA0001974, with partial instrumentation funding by National Science Foundation. J. S. and S. S. acknowledge the support of DOE-Basic Energy Sciences/ Materials Sciences and Engineering Division under Award No. DE-FG02-99ER45775. Work at HiPSEC is supported by the DOE NNSA under the Stewardship Science Academic Alliances program through DOE Cooperative Agreement No. DE-NA0001982.

Studying Strain

The recently discovered hexagonal $LuFeO_3$ ($hLuFeO_3$) is a multiferroic material that exhibits spontaneous electric and magnetic polarizations simultaneously. Structurally distorting materials such as $hLuFeO_3$ is known to alter their ferroelectricity. One way to modify structural distortion in a material is through elastic strain. The conventional methods for inducing elastic strain, applying high pressure and epitaxial strain, are not applicable to $hLuFeO_3$. So, researchers used a lesser known technique called "restrained thermal expansion" and assessed changes to the film sample's structure with x-ray diffraction measurements carried out at the APS. The researchers found that biaxial (or two-dimensional) strain can significantly alter the structural distortion in $hLuFeO_3$ (especially at high temperatures), which ultimately impacts the material's electrical and magnetic properties. These findings may provide clues about fine-tuning the ferroelectric properties of materials like $hLuFeO_3$ that can play important roles in data storage devices.

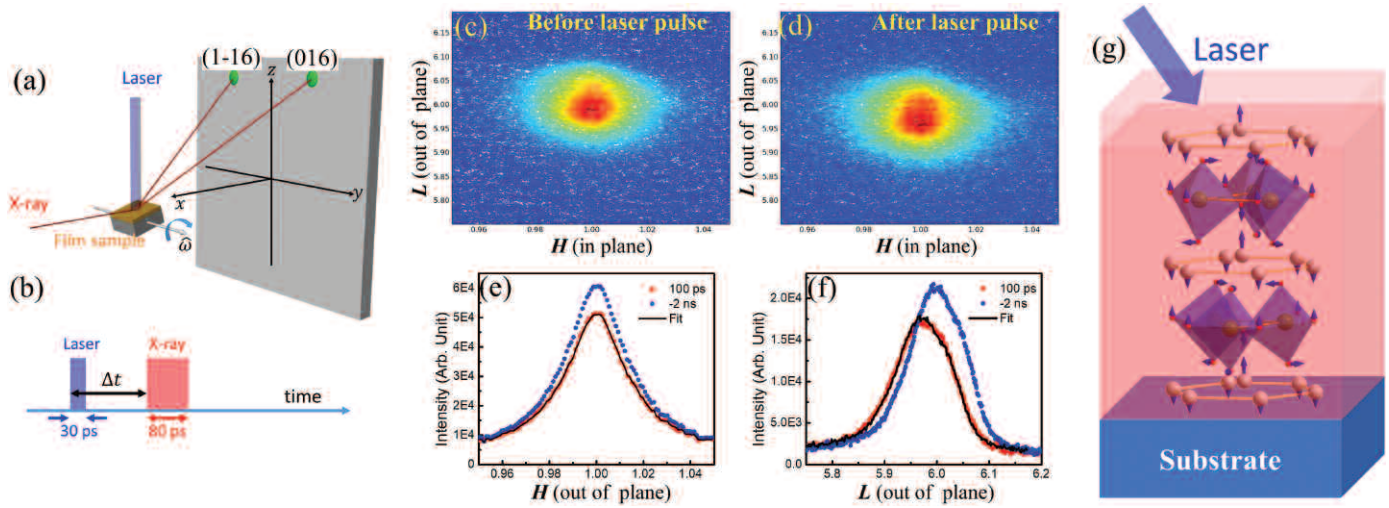

Fig. 1. (a) Schematic of the experimental setup of for the time-resolved x-ray diffraction after laser illumination; the time sequence is depicted in (b). (c) and (d) are two-dimensional diffraction patterns of the (106) peak before and after the laser pulse, respectively. (e) and (f) are the comparisons of the diffraction intensities as a function of in-plane and out-of-plane reciprocal indices, respectively. (g) schematic of the restrained thermal expansion process in which the film is heated but can only expand along the out-of-plane direction; the structural model indicates the enhanced lattice distortion under the effective compressive strain.

The combination of ferroelectricity and ferromagnetism, or "multiferroicity," is believed to have great importance for future technologies, such as energy efficient information storage and processing. But very few materials are known to be ferroelectric and ferromagnetic at the same time. The recently discovered hexagonal $LuFeO_3$ ($hLuFeO_3$) is a multiferroic material that exhibits spontaneous electric and magnetic polarizations simultaneously. By fine-tuning its crystal structure, the physical properties of materials such as $hLuFeO_3$ may be modified. Elastic strain, a form of strain in which a distorted sample returns to its original shape and size when the deforming force is removed, is a promising tool for tuning $hLuFeO_3$'s properties—including ferroelectricity and magnetism—owing to the coupling between the material's crystal structure and its electronic structure.

The primary means of inducing elastic strain have been applying high pressure or epitaxial strain. The latter is the strain that occurs when thin-film materials are grown epitaxially on the substrates and the materials' lattices are mismatched. But it can be difficult to apply high enough pressure to brittle material such as $hLuFeO_3$ to induce the desired level of strain. Also, the lack of structurally compatible substrates makes the growth of defect-free films

"Strain" cont'd. on page 28

A Tantalizing Study of Lithium Tantalate

Lithium tantalate plays an essential role in modern telecommunications devices that use light to transmit signals: fiber optic cables, photonic computers, and robotics, to name just a few. It is very effective at controlling light with electricity, and electricity with light. This allows lithium tantalate to convert signals sent as light down a fiber optic cable into electronic signals that a computer understands as the text images and video of the internet, for example. Lithium tantalate's reaction to ultraviolet, infrared, and visible light is well understood, but its reaction to x-rays has never been probed before, so researchers used the APS to observe the electrical fields lithium tantalate generates in response to x-rays. The researchers found the electrical fields were large and easy to detect, and responded to changes in the x-rays almost instantaneously. This could allow researchers to use lithium tantalate to observe materials with x-rays at ultrafast timescales that have not been previously possible.

Lithium tantalate ($LiTaO_3$) is a perovskite, part of a family of crystalline materials that are industrially useful and optically active; they are now used in solar cells, for example, and their structures have been well characterized, and their responses to optical, ultraviolet and infrared light are well known. Scientists shine lasers onto the material and use x-rays to detect the tiny structural changes that happen when the atoms are energized by the light.

But researchers from Purdue University and Argonne wanted to look at the opposite phenomenon. Instead of using x-rays to detect structural changes caused by lasers, they wanted to use lasers to detect electrical fields caused by x-rays. They used the APS to shine very bright x-ray pulses at a crystal of lithium tantalate. They chose the BioCARS/XSD 14-ID-B beamline because it has one of the strongest x-ray pulses in the world, with the rare ability to control the time between x-ray pulses; the unique time-resolved capabilities of the XSD 7-ID-B,C,D beamline were also important for this work.

As x-ray pulses hit the lithium tantalate, the researchers simultaneously shone a polarized laser beam at the crystal in such a way that it split, so that half was vertical and half horizontal. When x-rays caused electric fields to build up in the crystal, some of vertically polarized light switched into the horizontally polarized light. By measuring changes in the polarized beams emerging from the other side, the researchers could figure out the size and orientation of the electrical fields inside the lithium tantalate, and how these changed with crystal direction (Fig. 1).

These electrical fields were huge. And they changed almost simultaneously with the x-ray pulse. At the beginning of the pulse, the electric fields were small, and they grew along with the pulse. As far as the researchers could tell, the size of the fields mirrored the intensity of the x-ray pulse precisely, down to the picosecond.

Picosecond timing is exciting, because that is the speed at which atoms move and chemical reactions occur. Existing techniques cannot use x-rays to make picosecond measurements at x-ray synchrotrons; only ultrafast x-ray lasers can do that. But x-ray lasers tend to be less stable, and the results of x-ray laser experiments can be harder to reliably reproduce than x-ray synchrotron work. These lithium tantalate results show a promising direction for extending x-ray synchrotron studies down to picosecond time scales.

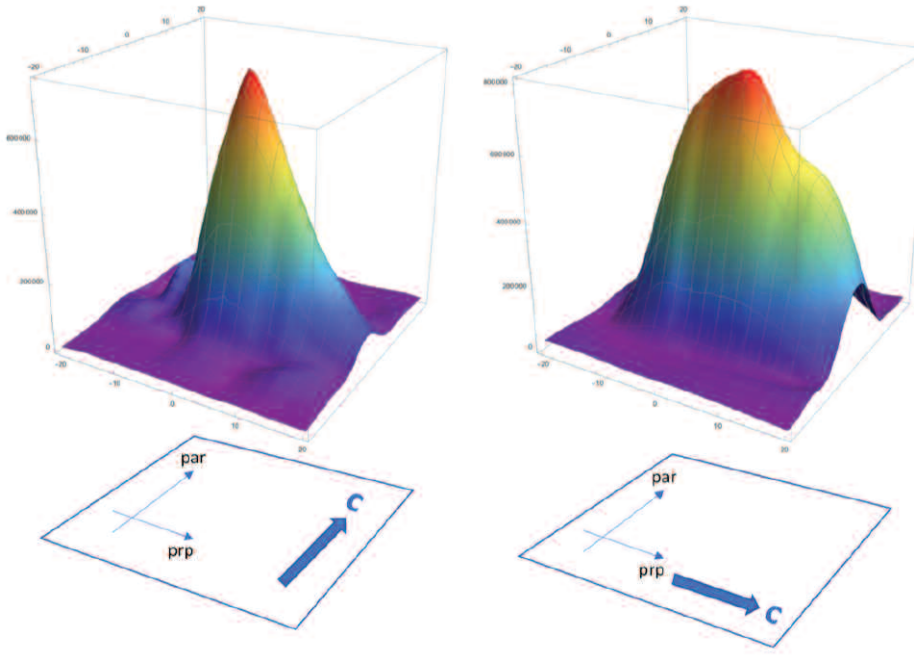

Fig. 1. These three-dimensional plots reveal the strong intensity and high spatial resolution of the transmitted laser polarization signal as it is scanned across the x-ray spot on the lithium tantalate sample in micron-size steps. The change in the two peaks was caused by simply rotating the lithium tantalate sample by 90°, showing how the fine details of the x-ray induced electric field can be mapped out by this method.

"Tantalizing" cont'd. on page 28

"Strain" cont'd. from page 26
impossible and makes epitaxial strain difficult to control. As a result, investigations on the elastic strain effect in $hLuFeO_3$ have been rare.

The researchers from the University of Nebraska, Lincoln; Temple University; Bryn Mawr College; Xi'an Jiaotong University (China); Argonne; and Los Alamos National Laboratory employed the restrained thermal expansion technique, in which elastic strain is generated in a film sample by heating the film with short laser pulses that cannot be absorbed by the substrate. Normally, thermal strain can be generated in a material in all crystalline dimensions in an isobaric (i.e., constant pressure) thermal expansion. Alternatively, for a thin film on a substrate, if the film is heated and the substrate remains the same temperature, the out-of-plane dimension of the film is free to expand while the in-plane dimensions of the film can be restrained by the substrate (restrained thermal expansion). By comparing the material properties in the isobaric thermal expansion and restrained thermal expansion conditions, the effect of isothermal compressive strain at a higher temperature can be obtained.

The researchers used time-resolved x-ray diffraction measurements at the BioCARS 14-ID-B beamline of the APS to measure the lattice constants and the structural distortions within $hLuFeO_3$ (Fig. 1). In this technique, the sample is heated with 30 psec laser pulse. To learn how the laser impacts the sample, a very short time later, the sample is probed with x-rays that scatter onto a two-dimensional detector, revealing the material's structure. The team also carried out x-ray diffractions at a variety of temperatures to measure the isobaric thermal expansion using XSD beamline 6-ID-B.

The researchers demonstrated the usefulness of the restrained thermal expansion method with their observations that the compressive biaxial strain in the basal plane of $hLuFeO_3$ significantly enhances structural distortion, a parameter that in part dictates the material's ferroelectricity. They found this effect to be enhanced at high temperatures. In addition, the team's computational models suggest that the compressive strain combined with enhanced structural distortion increases the spontaneous electric polarizations but reduces the weak ferromagnetic moments.

These findings are important for understanding the effect of elastic strain on $hLuFeO_3$ as well as the coupling between the lattice structure and the improper multiferroicity in the material. The experimental measurement of the strain effect in $hLuFeO_3$ films also suggests that the restrained thermal expansion can be a viable method to unravel the strain effect in many other thin-film materials. In the future, the team will focus on extending the restrained thermal expansion method to measure a material's electronic and magnetic properties, when probes such as soft (low-energy) x-ray are included. Ultimately, the knowledge gained about how to tune $hLuFeO_3$ and similar materials could lead to a novel use for the materials in data storage technologies.

— Chris Palmer

See: Kishan Sinha[1], Yubo Zhang[2], Xuanyuan Jiang[1], Hongwei Wang[2], Xiao Wang[3], Xiaozhe Zhang[1,4], Philip J. Ryan[5], Jong-Woo Kim[5], John Bowlan[6], Dmitry A. Yarotski[6], Yuelin Li[5], Anthony D. DiChiara[5], Xuemei Cheng[3], Xifan Wu[2]*, and Xiaoshan Xu[1,7]**, "Effects of biaxial strain on the improper multiferroicity in h-$LuFeO_3$ films studied using the restrained thermal expansion method ," Phys. Rev. B **95**, 094110 (2017).
DOI: 10.1103/PhysRevB.95.094110
Author affiliations: [1]University of Nebraska, Lincoln, [2]Temple University, [3]Bryn Mawr College, [4]Xi'an Jiaotong University
Correspondence:
* xifanwu@temple.edu
** xiaoshan.xu@unl.edu

This research was mainly supported by National Science Foundation (NSF), Division of Materials Research (DMR) Award No. DMR-1454618. X.M.C. acknowledges partial support from NSF Grant No. DMR-1053854. This research used resources of the Advanced Photon Source, a U.S. Department of Energy (DOE) Office of Science user facility operated for the DOE Office of Science by Argonne National Laboratory under Contract No. DE-AC02-06CH11357. Use of BioCARS was supported by the National Institute of General Medical Sciences of the National Institutes of Health under Grant No. R24GM111072. Time-resolved setup at Sector 14 was funded in part through a collaboration with Philip Anfinrud (NIH/National Institute of Diabetes and Digestive and Kidney Diseases).

"Tantalizing" cont'd. from page 27
Since each x-ray pulse at the APS is about 80 psec long, using the electric field response in lithium tantalate might allow researchers to take picosecond-by-picosecond measurements of a phenomenon such as a chemical reaction that is triggered by a laser flash during the x-ray pulse. It could also allow researchers to bridge work done at a synchrotron with experiments done with x-ray lasers. This type of ultrafast x-ray research would lead to better understanding of advanced solar cells, light-sensitive catalysts, and light-activated chemistry. Current efforts are focused on improving the techniques and exploring other materials similar to lithium tantalate to achieve much higher sensitivity so that picosecond x-ray studies can be applied to a wide range of materials research. *— Kim Krieger*

See: S. M. Durbin[1]*, A. Landcastle[1], A. DiChiara[2], Haidan Wen[2], D. Walko[2], and B. Adams[2‡], "Optical birefringence imaging of x-ray excited lithium tantalate," APL Phototonics **2**, 086102 (2017). DOI: 10.1063/1.4997414
Author affiliations: [1]Purdue University, [2]Argonne National Laboratory ‡Present address: Incom, Inc.
Correspondence: * durbin@purdue.edu

The authors thank R. Henning for crucial assistance with measurements at Sector 14. This work was supported by the U.S. Department of Energy (DOE)-Basic Energy Science (Grant No. DE-SC0004078), and utilized resources of the Advanced Photon Source, a U.S. DOE Office of Science user facility operated for the DOE Office of Science by Argonne National Laboratory (Contract No. DE-AC02-06CH11357). Use of BioCARS was also supported by the National Institute of General Medical Sciences of the National Institutes of Health (Grant No. R24GM111072). The time-resolved setup at Sector 14 was funded in part through a collaboration with Philip Anfinrud (NIH/NIDDK).

7-ID-B,C,D • XSD • Materials science, atomic physics, chemistry • Time-resolved x-ray scattering, time-resolved x-ray absorption fine structure, phase contrast imaging • 6-21 keV • On-site • Accepting general users •

14-ID-B • BioCARS • Life sciences, materials science, physics, chemistry • Time-resolved crystallography, time-resolved x-ray scattering, Laue crystallography, wide-angle x-ray scattering, biohazards at the BSL2/3 level, macromolecular crystallography • 7-19 keV • On site • Accepting general users •

Engineering Materials & Applications

Unraveling the Electronic Properties of Actinide Compounds

Actinides are a series of chemical elements that form the basis of nuclear fission technology, finding applications in strategic areas such as power generation, space exploration, diagnostics and medical treatments, and also in some special glass. Thorium (Th) and Uranium (U) are the most abundant actinides in the Earth's crust. A deeper understanding of the properties of uranium and other actinides is necessary not only for their more efficient use in existing applications but also for proposing new applications. Several open questions remain; progress in this area is usually limited in part by the difficulty in handling these materials safely. An international research collaboration demonstrated that x-ray magnetic circular dichroism (XMCD) in the L-absorption edge of uranium and relatively high-energy x-rays (17 keV) can be utilized to investigate 5*f* and 6*d* orbitals, as well as their hybridization, directly and selectively. The studies were carried out at the Brazilian Synchrotron Light Laboratory (LNLS) and at the APS.

The distribution of electrons in the outer orbital of atoms that make up a given material is what defines whether they are electrical insulators, conductors, or semiconductors, as well as whether they are hard or malleable. Other structural, electronic and magnetic properties are also defined by these valence electrons which may undergo electronic hybridization with other orbitals. Such mixture of orbitals modifies material properties influencing oxidation states, the way bonding between atoms takes place, and hence the geometrical arrangement formed in crystals and molecules with actinide elements.

In the actinide elements, the 5*f* and 6*d* orbitals have the tendency to hybridize especially in atoms of this series that have a small number of electrons in the 5*f* orbitals, as is the case of uranium. In compounds with this element, it is recognized that the degree of localization of electrons in the *f*-orbitals, affected by electronic hybridization, is a determining factor in their properties. However, experimental methods for direct and selective investigation of 5*f* state and their hybridization with other valence electronic states do not exist.

The ability to obtain this information is crucial for understanding a plethora of open questions in actinide compounds, which may promote an increase in the potential of applications of these materials.

Uranium L_3 XMCD measurements were performed by researchers from the Brazilian Center for Research in Energy and Materials, Universidade Estadual de Campinas, Argonne, the University Grenoble Alpes (France), and Institut NÉEL (France) at the D04-DXAS beamline of the Brazilian LNLS, while the uranium M4-edge XMCD measurements were performed at the XSD 4-ID-D beamline of the APS (Fig. 1).

This seems to be the first report of the high-energy XMCD technique being used to probe the electronic properties of compounds based on actinide elements. For this, it was necessary to overcome challenges of measuring small XMCD signals in addition to difficulties of manipulating these types of compounds.

The development of this new technique was carried out with the aim of opening new possibilities for the study of actinide materials by the scientific community.

The proposed APS Upgrade will be a game changer for these types of studies. The implementation of novel superconducting undulators will produce arbitrarily polarized x-rays directly at the source. Such devices will deliver a high degree of circular polarization at the L-edge resonances of actinide materials in the 17 keV-25 keV range. Such capability does not exist today. The reported L-edge measurements were done at a bending magnet beamline that produced an acceptable degree of circular polarization only by paying a high price in flux. To measure efficiently, and to extend these measurements to extreme condition environments such as high pressure, brilliant beams with a high degree of circular polarization are required, which will be delivered by the APS Upgrade.

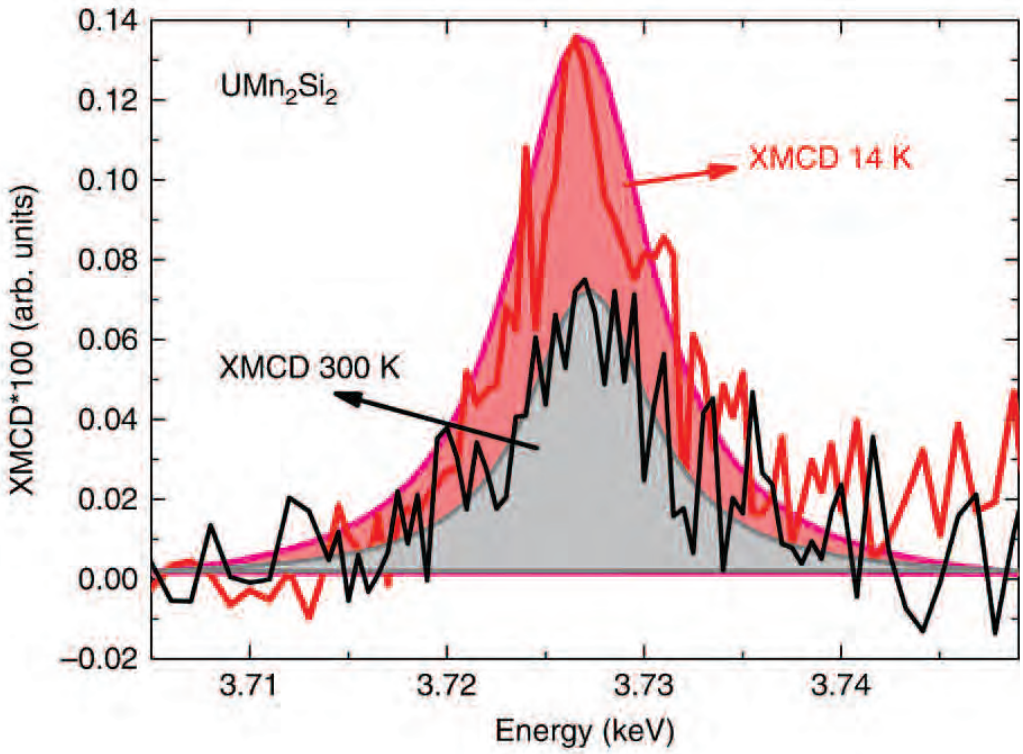

Fig. 1. Isolated probe of the 5*f* contribution. Uranium M_4-edge XMCD spectra measured for the UMn_2Si_2 compound at temperatures of 14 K and 300 K.

See: R.D. dos Reis[1,2], L.S.I. Veiga[1,2], C.A. Escanhoela, Jr.[1], J.C. Lang[3], Y. Joly[4,5], F.G. Gandra[2], D. Haskel[3], and N.M. Souza-Neto[1,3]*, "Unraveling 5*f*-6*d* hybridization in uranium compounds via spin-resolved L-edge spectroscopy," Nat. Commun. **8**, 1203 (2017). DOI: 10.1038/s41467-017-01524-1

Author affiliations: [1]Brazilian Center for Research in Energy and Materials, [2]Universidade Estadual de Campinas, [3]Argonne National Laboratory, [4]University Grenoble Alpes, [5]Institut NÉEL

Correspondence:

* narcizo.souza@lnls.br

This research was supported by FAPESP grants 2013/22436-5, 2014/05480-3, 10/19979-9, and 2014/26620-8. R.D.d.R. thanks the funding for his Ph.D. fellowship from CAPES Brazilian agency. This research used resources of the Advanced Photon Source, a U.S. DOE Office of Science user facility operated for the DOE Office of Science by Argonne National Laboratory under Contract No. DE-AC02- 06CH11357.

4-ID-D • XSD • Physics, materials science • Anomalous and resonant scattering (hard x-ray), magnetic x-ray scattering, magnetic circular dichroism (hard x-ray) • 2.7-40 keV • On-site • Accepting general users •

Keeping Li-Ion Batteries from Fading Away

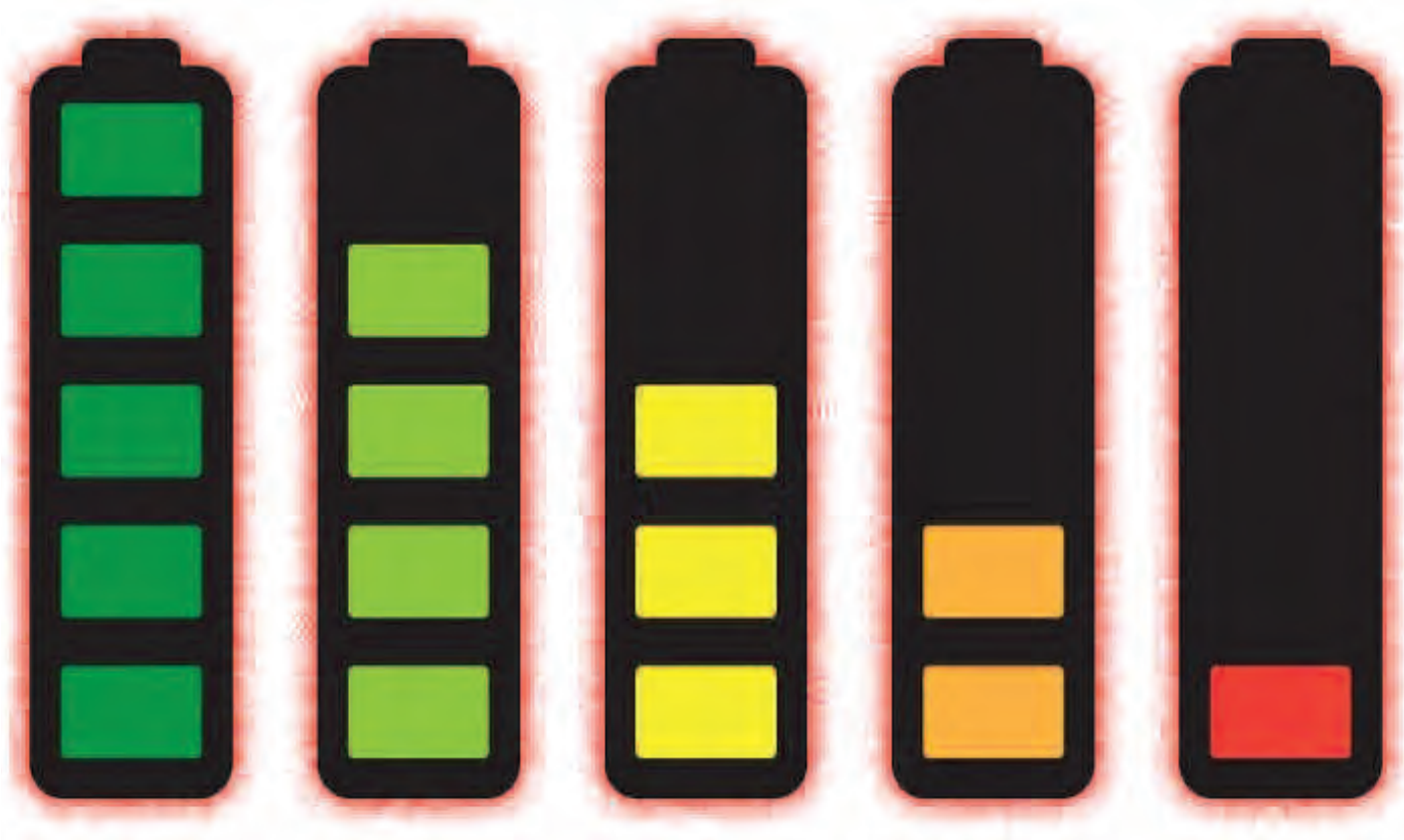

The rechargeable lithium-ion (Li-ion) batteries in our smartphones, laptops, and various other personal electronic devices make them completely portable, allowing us to unplug so long as the batteries are charged. But rechargeable batteries don't last forever, and the more times they're recharged, the less energy they store. The question is: Why? A team of researchers used x-ray beams from two U.S. DOE Office of Science national user facilities, including the APS, to reveal a major cause of charging capacity fading in Li-ion batteries: inter-granular cracking in the interface between the electrode granules.

Rechargeable battery performance always involves a compromise between charge capacity and lifetime: a higher initial charge capacity usually results in a more rapid fade in capacity. By limiting the capacity of currently available Li-ion batteries to only about 70% of their theoretical potential capacity, we can ensure they retain their capacity for longer. Studying the processes that lead to this capacity fade provides a roadmap to mitigate performance loss and to increase battery efficiency and lifetimes.

But such work is complicated by the challenge in extrapolating from a few days of laboratory studies to the many months over which capacity fades under normal operating conditions.

The experiment team from Argonne, the University of Illinois at Chicago, Brookhaven National Laboratory, and Lawrence Berkeley National Laboratory set out to overcome this challenge using long-duration *operando* x-ray diffraction (XRD) experiments at the XSD 11-ID-B beamline at the APS to observe charge-discharge cycles spanning approximately three months. They studied the mechanism of capacity fade in a commonly-used electrode material NCA ($LiNi_{0.8}Co_{0.15}Al_{0.05}O_2$), which allowed them to see how the charge reaction changed following capacity fade. They also used transmission x-ray microscopy techniques to see the associated microstructural changes.

In studying an NCA electrode through more than 90 charge-discharge cycles, the researchers saw that capacity fade was solely due to the part of the electrode in which the charge lagged behind the rest of the electrode and never fully recharged. As revealed by tomography studies carried out by this group at the DOE Stanford Synchrotron Radiation Lightsource, this sluggish charging is linked to the formation of inter-granular cracking at particle boundaries, which degrades connectivity and increases impedance, leading to the slower charging.

Cycling the electrode at 14 mA/g from 2.7 to 4.5 V, the team found a 20% drop in discharge capacity from the first to the 93rd cycle, with no significant change in the atomic structure of the

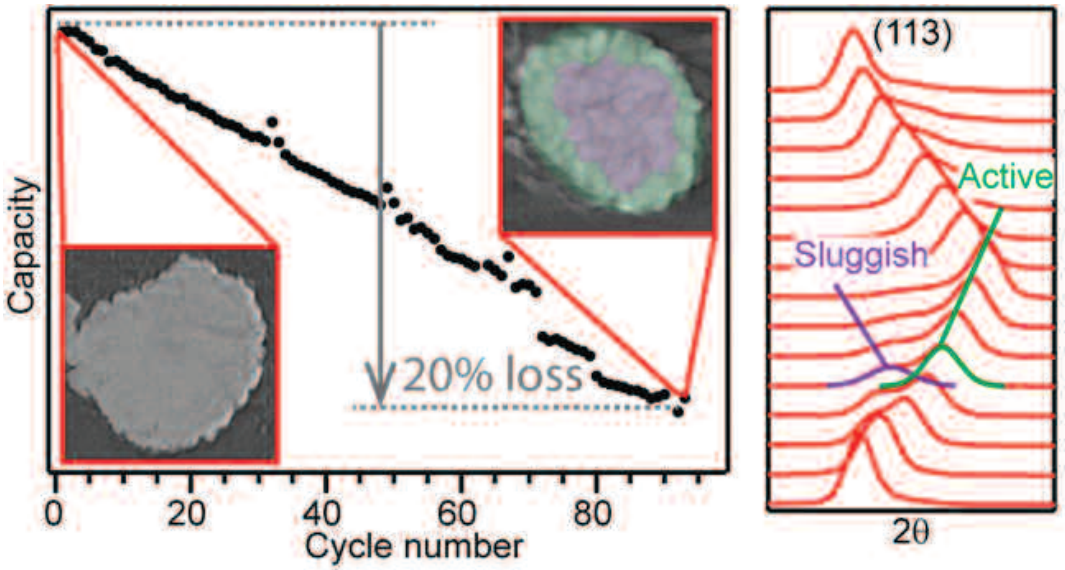

Operando x-ray diffraction reveals two populations of NCA ("sluggish" and "active") after capacity fade that charge at different rates. Intergranular cracking compromises the ionic and electrical conductivity of grains inside a secondary particle and leads to the active and the sluggish NCA grains at the surface and core of a secondary particle, respectively.

NCA, but a change in the charge-discharge process.

Operando XRD conducted during the 92nd and 93rd cycles revealed the development of two separate Li populations, one with a charge-discharge response similar to pristine NCA and a second with a more sluggish response (Fig. 1). This divergence in Li composition appears only after extended cycling.

Such heterogeneous Li distribution, causing loss of conductivity between NCA particles and degradation of charge capacity, results from the formation of cracks at the boundaries of primary particles. The inter-granular cracking occurs because the primary particles expand and contract as Li goes in and out during charge and discharge. This difference in the expansion and contraction at the interface between particles causes them to break apart in a process analogous to thermal fatigue in ceramics.

By reducing the surface area available for electronic transport between neighboring particles, this cracking increases impedance and, thus, compromises electronic conductance at a microstructural level.

The researchers found that other known causes for battery capacity fading, particularly the formation of Ni-rich compounds at particle surfaces after repeated cycling, play a lesser role in the observed capacity fading. They distinguished chemical from mechanical factors in capacity fading by cycling NCA electrodes to the same upper cut-off voltage (4.5 V) but different lower cut-off voltages (4.25, 4.05, and 2.5 V), comparing effects on the NCA lattice. The electrodes subjected to broader cycling ranges displayed markedly lower capacity than those undergoing a narrower voltage range, indicating that the mechanical phenomenon of cracking was more significant to capacity loss than chemical changes.

The research team notes that while previous studies generally used accelerated cycling rates, which can induce inter-granular cracking and capacity loss for different reasons, the present study was conducted solely at slow rates over a normal operating period of approximately three months. This indicates that the inter-granular cracking observed here is an inevitable result of the cycling of commercially-available Li-ion batteries. Lower cycling rates may preserve capacity for somewhat longer periods, but ultimately the significant loss of capacity is unavoidable.

The confirmation of the primary cause of capacity fading identified in this work also points to possible solutions, or at least mitigation of the effect. The experimenters suggest several possible approaches, including eliminating secondary particles in the aggregate structure, limiting their size, or coating them, as well as optimizing voltage ranges to ensure minimal lattice structural changes. While immortal batteries may never be possible, understanding the phenomena that lead to their fading and ultimate failure is the first step in extending their lifetimes and utility.

— Mark Wolverton

See: Hao Liu[1], Mark Wolf[2], Khim Karki[3], Young-Sang Yu[2,4], Eric A. Stach[3], Jordi Cabana[2], Karena W. Chapman[1]*, and Peter J. Chupas[1]**, "Intergranular Cracking as a Major Cause of Long-Term Capacity Fading of Layered Cathodes," Nano Lett. **17**, 3452 (2017). DOI: 10.1021/acs.nanolett.7b00379

Author affiliations: [1]Argonne National Laboratory, [2]University of Illinois at Chicago, [3]Brookhaven National Laboratory, [4]Lawrence Berkeley National Laboratory

Correspondence:

* chapmank@aps.anl.gov, ** chupas@aps.anl.gov

This research is supported as part of the NorthEast Center for Chemical Energy Storage, an Energy Frontier Research Center funded by the U.S. DOE Office of Science-Basic Energy Sciences under Award Number DE-SC0012583. Y.S.Y. also acknowledges support from an Advanced Light Source Collaborative Postdoctoral Fellowship. Use of the Stanford Synchrotron Radiation Lightsource, SLAC National Accelerator Laboratory, is supported by the U.S. DOE Office of Science-Basic Energy Sciences under Contract No. DE-AC02-76SF00515. Scanning electron microscopy was performed at the Center for Functional Nanomaterials, which is a U.S. DOE Office of Science Facility, at Brookhaven National Laboratory under Contract No. DE-SC0012704. This research used resources of the Advanced Photon Source, a U.S. DOE Office of Science user facility operated for the DOE Office of Science by Argonne National Laboratory under Contract No. DEAC02- 06CH11357.

11-ID-B • XSD • Chemistry, environmental science, materials science • Pair distribution function, high-energy x-ray diffraction • 58.66 keV, 86.7 keV • On-site • Accepting general users •

Magnesium Rechargeable Batteries Advance

Rechargeable magnesium (Mg) batteries have been attracting increasing attention recently because of their high-energy density, relatively low price, and good safety characteristics. However, development of a suitable high-capacity cathode material for such batteries that can quickly store and release intercalated Mg^{2+} ions remains problematic. One factor is that $MgCl^{+}$ ions, the electroactive species most used in Mg-battery electrolytes, must be broken up into their constituents before they can serve as sources of Mg^{2+} ions, and these scissions require high activation energies. Also, most Mg-ion cathodes suffer from sluggish Mg^{2+} diffusion because of a high-energy barrier for divalent Mg^{2+} migration inside host materials. To overcome these problems, researchers developed an innovative battery chemistry based on $MgCl^{+}$ instead of Mg^{2+} ions. The battery consisted of an Mg anode, a standard chlorine-based electrolyte containing $MgCl^{+}$ ions, and an interlayer-expanded form of titanium disulfide (TiS^2) as the cathode material. The resultant battery demonstrated excellent rate and cycling performances even at room temperature and capacities up to 400 mAh g^{-1} based on the mass of TiS^2. Because of the possible general applicability of the new approach, the researchers thoroughly investigated the intercalation process utilizing a combination of theoretical calculations and various electrochemical and spectroscopic studies, including x-ray investigations at the APS and the Advanced Light Source (ALS, Lawrence Berkeley National Laboratory).

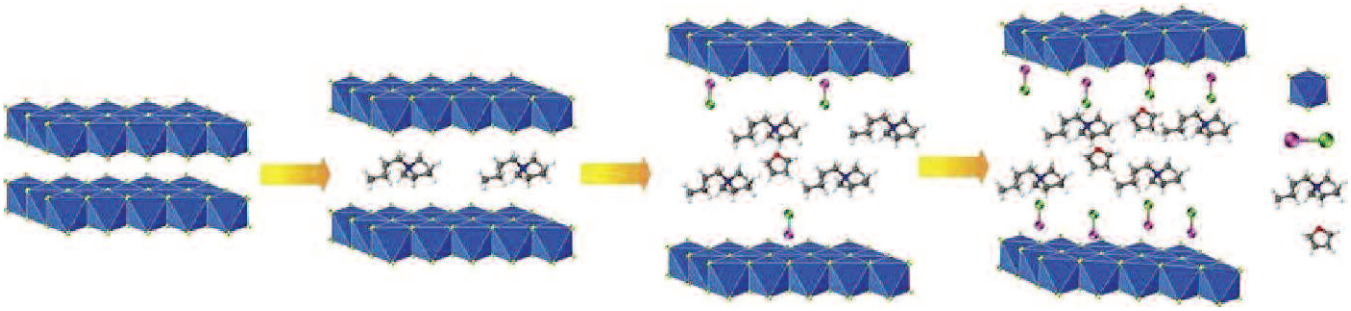

Fig. 1. Schematic shows the structural evolution of titanium disulfide at different stages of intercalation. Interlayers are expanded or distorted as different amounts of pillaring molecules, complex cations, and solvents are intercalated into the van der Waals gaps of the host material at each stage.

The x-ray studies were crucial because the TiS^2 interlayer expansion could not be accomplished normally through mechanical or chemical means before the TiS^2 cathode material was placed into the battery. Instead, the researchers from the University of Houston; Vanderbilt University; Texas A&M University; and the Oak Ridge, Lawrence Berkley, and Argonne national laboratories took an *in situ* approach in which 1-butyl-1-methylpyrrolidinium ($PY14^{+}$) ions were added to the battery's electrolyte before the battery was charged for the first time. Discharging the battery caused the $PY14^{+}$ ions to enter the interlayer spaces of the TiS^2, increasing the interlayer spacing as they did so and also buttressing the expansions in the manner of organic "pillars." Eventually, they created spaces that were large enough for the $MgCl^{+}$ ions to fit inside as well.

The battery was discharged to 0 V in stages, with the interlayer spacing of the TiS^2 first expanding from 5.69 Å (stage 0) to 10.87 Å (stage 1) and then to 18.63 Å (stages 2 and 3), with lattice distortions appearing at stage 3. High-energy x-ray diffraction (HE-XRD) measurements at XSD x-ray beamline 11-ID-C of the APS determined the interlayer distances at high resolution and showed that the intralayer structure of TiS^2 was preserved during the expansions despite the distortions at stage 3. From stage 1 to 2, the interlayer distance increased sufficiently to allow $MgCl^{+}$ ions to begin entering the expanded spaces. Then at stage 3, the $MgCl^{+}$ ions entered in large numbers, giving rise to mechanical stresses that resulted in the structural distortions. After completion of the first discharge process, the interlayer-expanded TiS^2 cathode showed a reversible capacity as high as 239 mAh g^{-1} at room temperature, as the highly mobile $MgCl^{+}$ ions intercalated and deintercalated reversibly while the $PY14^{+}$ ions stayed in place. Completing stage 3 was essential in realizing such a large reversible capacity, as stopping at stage 2 led to a lower reversible capacity of about 60 mAh g^{-1} even though TiS^2 was expanded to the same interlayer distance for both stages 2 and 3.

Near-edge x-ray absorption fine structure (NEXAFS) measurement of the Mg *K*-edge at beamline 6.3.1.2 of the ALS revealed that Mg atoms of the inserted $MgCl^{+}$ ions maintained tetra-coordination with 1 chlorine and 3 sulphur atoms. To probe the coordina-

"Magnesium" cont'd. on page 36

Detecting Nanoscale Intermediates in Li-Ion Battery Materials

Lithium-ion (Li-ion) batteries are often the go-to power source for electronic devices and electric vehicles because they can durably store a lot of energy and deliver it in short times. But battery life can be cut short by high mechanical stress that builds up within the crystal structures of the battery electrodes. Certain battery materials minimize this potentially damaging stress by forming intermediate crystalline phases during the electrode charging reactions. The prevailing wisdom has been that these intermediate phases are metastable, meaning that they only last a short time, but a new study has revealed the presence of intermediate phases in battery materials long after the reactions are stopped. This surprising finding — realized at the APS — suggests batteries could be made more resilient by designing components that favor low-stress intermediate phases.

The typical Li-ion battery cathode contains small crystals of lithium transition metal compounds that release lithium ions during charge and recuperate them later when the battery is discharged. A well-known example is lithium iron phosphate ($LiFePO_4$), which can be found in power tools and energy storage facilities. As lithium ions vacate a lithium iron phosphate crystal, certain domains in the material transform into iron phosphate ($FePO_4$). This lithium-free crystalline phase is more compact (takes up less volume) than the lithium-full phase, which implies that stress will develop at boundaries between $FePO_4$ and $LiFePO_4$ domains. If the stress gets high enough, the crystal will fracture and no longer perform its battery functions properly. However, in practice, electrodes based on lithium iron phosphate rank among the most resilient on the market.

Over the past decade, many studies have tried to understand this unexpected resiliency, and the results have shown that lithium iron phosphate can transform following a "solid solution pathway." Along such a pathway, the electrode reactions proceed through single phases with intermediate levels of lithium content. An example would be $Li_{0.6}FePO_4$, which has only 60% of its potential lithium ion sites full. This one-phase solution is distinct from a two-phase mixture containing 60% $LiFePO_4$ and 40% $FePO_4$. The main difference is that the volume change in going from $LiFePO_4$ to $Li_{0.6}FePO_4$ is more gradual than going to the two-phase mixture, which means battery materials can avoid high-stress phase boundaries by forming intermediate phases.

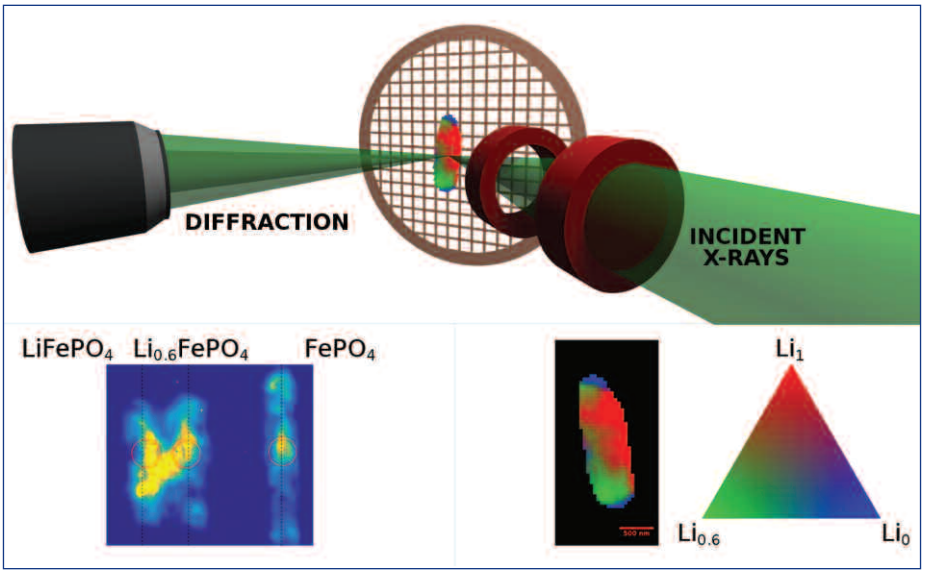

Fig. 1. To study crystal structure changes in lithium-ion batteries, researchers have employed scanning x-ray diffraction microscopy. The graphic (top image) shows a beam of x-rays focused onto a $LiFePO_4$ crystal that has been partially delithiated. The diffracted light is collected by a detector and analyzed. Peaks in the diffraction signal (bottom left image) allow different crystalline phases to be identified, including an intermediate phase referred to as $Li_{0.6}FePO_4$. From this data, a map (bottom right image) is generated showing where the different phases are located in the crystal. Credit: Brain May, adapted from Nano Lett. **17,** 7364 (2017). © 2017 American Chemical Society

Theoretical models of lithium iron phosphate have generally assumed that the intermediate phases are not stable. Most researchers believed that — once electrode reactions stop — a phase like $Li_{0.6}FePO_4$ should evolve into the corresponding two-phase mixture. But new

"Detecting" cont'd. on page 36

"Magnesium" cont'd. from page 34
tion environment change of the sulfur in the TiS^2 upon $MgCl^+$ intercalation, a NEXAFS measurement of the sulphur *K*-edge was performed at XSD beamline 9-BM-B,C of the APS. The observed spectral changes showed the structural distortion upon $MgCl^+$ intercalation and that the coordination number of sulphiur changed from 3 in unexpanded form of TiS^2 to 6 after interlayer expansion had occurred (Fig. 1).

The research demonstrated a new direction toward overcoming the challenge of the high-migration energy barrier and kinetically sluggish dissociation processes in magnesium rechargeable batteries. The battery chemistry used can be extended to the intercalation of a wide range of multivalent ions (e.g., Zn^{2+}, Ca^{2+}, Al^{3+}) into various two-dimensional materials, highlighting the importance of an unexploited route of materials design for multivalent-ion batteries.

— Vic Comello

See: Hyun Deog Yoo[1], Yanliang Liang[1], Hui Dong[1], Junhao Lin[2,3], Hua Wang[4], Yisheng Liu[5], Lu Ma[6], Tianpin Wu[6], Yifei Li[1], Qiang Ru[1], Yan Jing[1], Qinyou An[1], Wu Zhou[3], Jinghua Guo[5], Jun Lu[6], Sokrates T. Pantelides[2,3], Xiaofeng Qian[4], and Yan Yao[1]*, "Fast kinetics of magnesium monochloride cations in interlayer-expanded titanium disulfide for magnesium rechargeable batteries," Nat. Commun. **8**, 339 (2017).
DOI: 10.1038/s41467-017-00431-9
Author affiliations: [1]University of Houston, [2]Vanderbilt University, [3]Oak Ridge National Laboratory, [4]Texas A&M University, [5]Lawrence Berkeley National Laboratory, [6]Argonne National Laboratory
Correspondence: * yyao4@uh.edu

Y.Y. acknowledged financial support from the Office of Naval Research Young Investigator Award (No. N00014-13-1-0543), the National Science Foundation (CMMI-1400261), the TcSUH core funding, and the University of Houston Start-up Fund. J.L. and S.T.P. acknowledged support from the U.S. Department of Energy (DOE) (No. DE-FG02-09ER46554). S.T.P. also acknowledged support from the Gas Subcommittee Research and Development under Abu Dhabi National Oil Company (ADNOC). X.Q. and H.W. acknowledged the start-up funds from Texas A&M University, and portions of this research were conducted with the advanced computing resources provided by Texas A&M High Performance Research Computing. W.Z. acknowledged support by the DOE Office of Science, Basic Energy Sciences, Materials Science and Engineering Directorate. The STEM characterization was supported in part through a user project supported by Oak Ridge National Laboratory's Center for Nanophase Materials Sciences, which is sponsored by the Scientific User Facilities Division, Office of Basic Energy Sciences, of the DOE. The Advanced Light Source is supported by the Director, Office of Science, Office of Basic Energy Sciences, of the DOE under Contract No. DE-AC02-05CH11231. Use of the Advanced Photon Source (9-BM and 11-ID) was supported by the DOE Office of Science-Basic Energy Sciences, under Contract No. DE-AC0206CH11357.

9-BM-B,C • XSD • Materials science, chemistry, environmental science • X-ray absorption fine structure, x-ray absorption near-edge structure • 2.1-25.2 keV • On-site • Accepting general users •

11-ID-C • XSD • Materials science, chemistry, physics • High-energy x-ray diffraction, diffuse x-ray scattering, pair distribution function • 105.6 keV • On-site • Accepting general users •

"Detecting" cont'd. from page 35
work has shown that this assumption is not entirely correct. A scientific team from the University of Illinois at Chicago, Lawrence Berkeley National Laboratory, Argonne, and the University of Cambridge (UK) pinpointed intermediate phases in micron-wide lithium iron phosphate crystals that were delithiated to different levels and then allowed to "rest" for months. The results showed that intermediate phases can be long-lived.

Unlike previous experiments, which relied on spectroscopy to indirectly infer which phases were present inside a battery material, the research team utilized scanning x-ray diffraction microscopy (SXDM). SXDM allows phases to be directly identified by the spacing between crystal planes. The Hard X-Ray Nanoprobe at CNM/APS beamline 26-ID-C provided the necessary nanometer resolution for mapping out the micron-sized crystals. In one case, the examined crystal was delithiated to a level where only half of the lithium ions were remaining. The data showed a few lithium-full ($LiFePO_4$) and lithium-free ($FePO_4$) domains, but the majority of the crystal was in an intermediate phase. In addition, full-field transmission x-ray microscopy coupled with x-ray absorption near-edge spectroscopy data was collected at beamline 6−2 at the Stanford Synchrotron Radiation Lightsource at SLAC National Accelerator Laboratory

The team explained their results by considering the way that the lithium ions diffuse in $LiFePO_4$. In the plate-shaped crystals that the researchers used, lithium ions preferentially travelled along the direction perpendicular to the face of the plates. This directionality introduced strain relationships inside the material that stabilized the formation of intermediate phases. Because electrodes operating through solid solution pathways are less susceptible to fracture, battery designers may want to engineer crystals whose geometry promotes the long-term stability of intermediate phases.

— Michael Schirber

See: Brian M. May[1], Young-Sang Yu[1,2], Martin V. Holt[3], Fiona C. Strobridge[4], Ulrike Boesenberg[2], Clare P. Grey[4], and Jordi Cabana[1]*, "Nanoscale Detection of Intermediate Solid Solutions in Equilibrated Li_xFePO_4 Microcrystals," Nano Lett. **17**, 7364 (2017).
DOI: 10.1021/acs.nanolett.7b03086
Author affiliations: [1]University of Illinois at Chicago, [2]Lawrence Berkeley National Laboratory, [3]Argonne National Laboratory, [4]University of Cambridge
Correspondence: * jcabana@uic.edu

This material is based upon work supported as part of the NorthEast Center for Chemical Energy Storage (NECCES), an Energy Frontier Research Center funded by the U.S. Department of Energy (DOE) Office of Science-Basic Energy Sciences (BES) under Award Number DE-SC0012583. Use of the Stanford Synchrotron Radiation Lightsource, SLAC National Accelerator Laboratory, is supported by the U.S. DOE Office of Science-BES under Contract No. DE-AC02-76SF00515. This research used resources of the Advanced Photon Source, a U.S. DOE Office of Science user facility operated for the DOE Office of Science by Argonne National Laboratory under Contract No. DEAC02- 06CH11357.

A Nanocomposite Anode for Better Batteries?

One of the most promising pathways to the goal of more efficient rechargeable lithium-ion (Li-ion) battery technology is finding and developing new materials with better capacity and cycling performance. Anode materials such as tin phosphide (Sn_4P_3) have demonstrated far greater performance capacity than conventional graphite anodes but also a high fading rate. Researchers from the Illinois Institute of Technology and Ohio University have developed a novel nanocomposite anode combining the high capacity of Sn_4P_3 and the high electrical conductivity of graphite. Employing APS high-brightness x-ray beams, they performed *in situ* extended x-ray absorption fine structure (EXAFS) studies of the new composite, showing the resulting local structural changes in an operating cell and allowing detailed modeling of the lithiation/delithiation mechanism. The composite demonstrated a reversible capacity of 651 mA h g^{-1} after 100 cycles, unlike pure Sn_4P_3 anode, which rapidly fades after about 20 cycles.

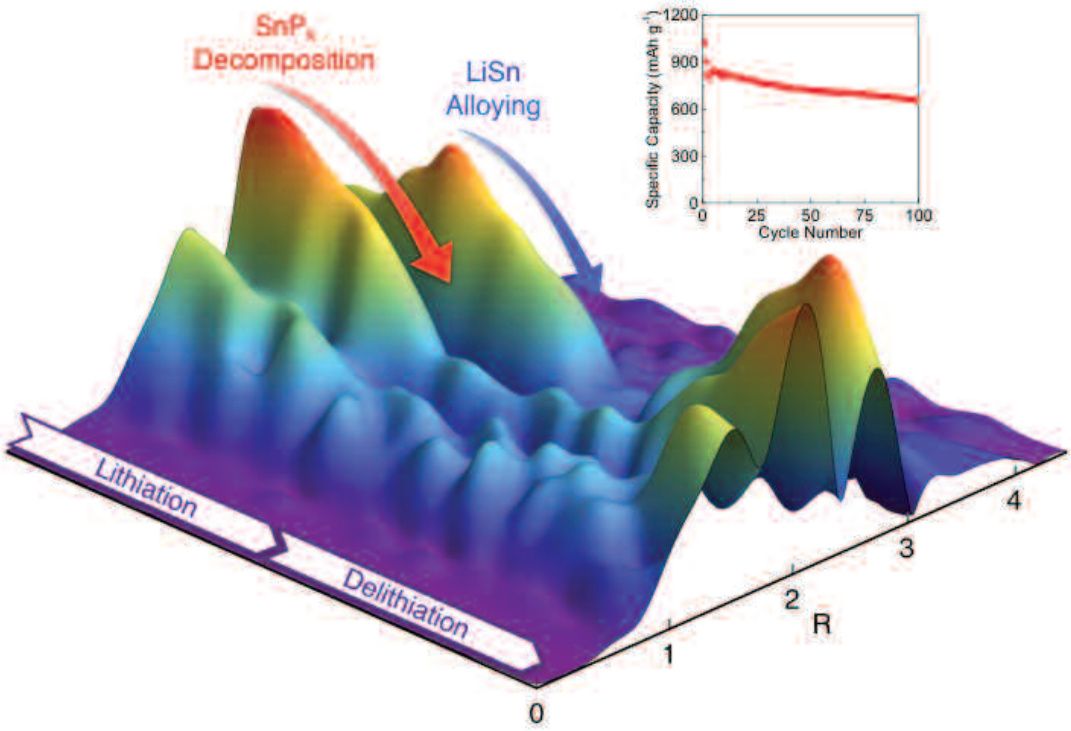

Fig 1. Three-dimensional surface plot of $|\chi(R)|$ as a function of cell capacity for the entire third *in situ* cycle of the Sn_4P_3/graphite composite anode. The initial loss of the SnP_x phase (red arrow) is followed by growth and then loss of Sn metal clusters (blue arrow) as full lithiation is achieved. The inset shows the 100-cycle capacity of a Sn_4P_3/graphite composite coin cell charged at a rate of 100 mA g^{-1}.

Previous attempts to study Sn_4P_3 using x-ray diffraction (XRD) showed that its crystal structure was quickly lost with lithiation, becoming amorphous and rendering further XRD measurements essentially useless. Other *ex situ* studies of Sn_4P_3 electrodes using x-ray absorption fine structure (XAFS) and XRD revealed an apparently irreversible conversion reaction after several cycles. The present work sought an understanding of the highly reversible lithiation/delithiation mechanism observed in the new composite anode material through *in situ* EXAFS, performed at the MR-CAT 10-ID-B beamline at the APS.

Initial XRD characterization of the synthesized Sn_4P_3/graphite composite showed peaks matching the usual Sn_4P_3 crystalline structure. The EXAFS analysis takes into account some difficulties inherent in examining operating coin cells, particularly the need for faster cycling in order to reproduce a number of repeated full cycles in the limited time available under experimental conditions. To overcome this, the researchers used the data from the first four cycles for their analysis and modeling and included the measurements from an *ex situ* electrode sample after 100 cycles. They observed that after the first two cycles, an amorphous SnP_x phase develops, completely replacing the crystalline Sn_4P_3. This amorphous phase structure contributes to highly reversible conversion and alloying processes in subsequent cycles, with amorphous SnP_x initially converting to metallic Sn clusters and Li_3P, followed by alloying of metallic Sn with Li-ions.

This amorphous SnP_x phase is the main reason for the marked superiority in reversibility and capacity in the

"Anode" cont'd. on page 39

Understanding Sodium-Ion Batteries' Sluggish Performance

In the past few decades, lithium (Li)-ion batteries' (LIBs') high-energy density has made them into the rechargeable power source of choice for a variety of portable electronic devices, such as cell phones, laptop computers, and some electric vehicles. However, because lithium is relatively rare on Earth, and thus costly, these batteries aren't suitable for larger-scale stationary energy storage. For these applications, researchers have been exploring less expensive sodium (Na)-ion batteries (SIBs) instead. But compared to LIBs, SIBs are an inferior energy storage medium, with lower capacities (the discharge current the battery delivers over time) and worse rate capabilities (the speed of charge and discharge). The reason for SIBs' lower performance has been unclear. Some studies have attributed this inferior functioning to the larger radius of the Na^+ ion compared to the Li^+ ion, which could lead to slower diffusion during charge and discharge, and damage electrode materials by causing larger volumetric changes. However, no research had strongly supported either possibility. To explore reasons behind SIBs' poor performance, a team of researchers examined LIB and SIB anodes at the APS. They found less overall structural change after charge and discharge cycles with SIBs compared to LIBs, suggesting a lower interaction of Na^+ with the electrode material rather than damage caused by the size of this ion.

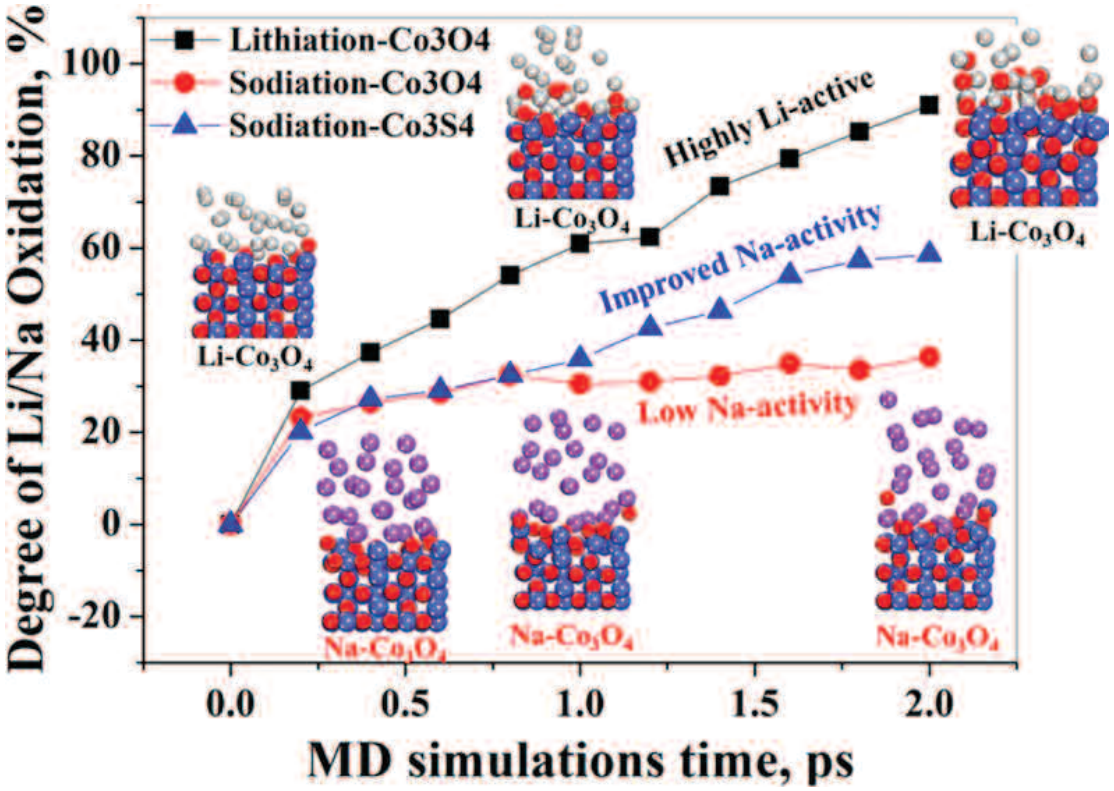

Fig 1. Degree of oxidation of Li/Na as a function of molecular dynamics simulation time for lithiated Co_3O_4, sodiated Co_3O_4 and sodiated Co_3S_4. The gray and purple atoms represent Li and Na, respectively. The red atoms represent oxygen, the blue atoms represent cobalt, and the yellow atoms represent sulfur.

For the electrode in this study, the researchers from Argonne, Xiamen University (China), and the University of Rochester used porous cobalt oxide (PCO), which has been investigated as a potential new electrode material for LIBs. After crafting batteries with PCO anodes, they compared the performance of lithium and sodium as counter electrodes. Results showed that the batteries with sodium counter electrodes performed significantly worse than those with lithium counter electrodes, with lower initial discharge capacity, worse rate capability, and continuous capacity degradation over multiple cycles.

To better understand the differences between these

Cont'd. on the next page

electrochemical performances, the researchers performed a variety of experiments with different synchrotron x-ray techniques.

They utilized the XSD x-ray beamlines 11-ID-C (high-energy synchrotron x-ray diffraction), 11-ID-D (*in operando* synchrotron x-ray diffraction), 12-ID-B (*in operando* small-angle x-ray diffraction), and 20-BM-B (*in operando* x-ray absorption fine structure) at the APS to look for structural changes, and to examine its structure again after charge and discharge cycles. Their findings showed that compared to batteries with lithium as the counter electrode, those with sodium actually underwent lower levels of changes to the pore structure, changes to the local and overall crystalline structure, and changes to the oxidation state (gain or loss of electrons). These were surprising findings given that the larger size of Na^+ should cause more changes if this ion was interacting with PCO in the same way as Li^+.

Thus, the researchers suspected that the lower performance of the SIBs stemmed from less electrochemical reactions between Na^+ and PCO. To investigate this possibility, the researchers performed computer modeling experiments known as ab initio molecular dynamics simulations. Their findings (Fig. 1) revealed a lower level of atomic distortion when Na^+ reacts with Co_3O_4, one of the molecular species that makes up PCO, compared to when Li^+ reacts with this species — a result consistent with their experimental findings.

However, when they ran similar simulations using metal sulfides rather than metal oxides as anode materials, they found higher levels of atomic distortion. These results suggest that metal sulfides might make better anode materials for SIBs.

The researchers note that future studies aimed at discovering the underlying mechanism of SIBs compared to LIBs are crucial to developing a better understanding of these potential new rechargeable power sources and a key step to the rational design of better and more affordable batteries.

— Christen Brownlee

See: Gui-Liang Xu[1], Tian Sheng[2], Lina Chong[1], Tianyuan Ma[3], Cheng-Jun Sun[1], Xiaobing Zuo[1], Di-Jia Liu[1], Yang Ren[1], Xiaoyi Zhang[1], Yuzi Liu[1], Steve M. Heald[1], Shi-Gang Sun[2], Zonghai Chen[1]*, and Khalil Amine[1]**, "Insights into the Distinct Lithiation/Sodiation of Porous Cobalt Oxide by *in Operando* Synchrotron X-ray Techniques and Ab Initio Molecular Dynamics Simulations," Nano Lett. **17**, 953 (2017).
DOI: 10.1021/acs.nanolett.6b04294
Author affiliations: [1]Argonne National Laboratory, [2]State Key Laboratory Physical Chemistry of Solid Surfaces, [3]University of Rochester
Correspondence:
* zonghai.chen@anl.gov,
** amine@anl.gov

Research at Argonne National Laboratory was funded by U.S. Department of Energy (DOE), Vehicle Technologies Office. Support from Tien Duong of the U.S. DOE Office of Vehicle Technologies Program is gratefully acknowledged. Sector 20 facilities at the Advanced Photon Source and research at these facilities are supported by the U.S. DOE-Basic Energy Sciences, and the Canadian Light Source and its funding partners. Research at State Key lab of Xiamen University was funded by the National Natural Science Foundation of China (Grant 21321062). This research used resources of the Advanced Photon Source, a U.S. DOE Office of Science user facility operated for the DOE Office of Science by Argonne National Laboratory under Contract No. DE-AC02-06CH11357.

11-ID-C • XSD • Materials science, chemistry, physics • High-energy x-ray diffraction, diffuse x-ray scattering, pair distribution function • 105.6 keV • On-site • Accepting general users •

11-ID-D • XSD • Chemistry, environmental science, materials science • Time-resolved x-ray absorption fine structure, time-resolved x-ray scattering • 6-25 keV • On-site • Accepting general users •

12-ID-B • XSD • Chemistry, materials science, life sciences, polymer science, physics • Small-angle x-ray scattering, grazing incidence small-angle scattering, wide-angle x-ray scattering, grazing incidence diffraction • 7.9-14 keV • On-site • Accepting general users •

20-BM-B • XSD • Materials science, environmental science, chemistry • X-ray absorption fine structure, microfluorescence (hard x-ray) • 2.7-32 keV, 2.7-35 keV • On-site • Accepting general users •

"Anode" cont'd. from page 37
Sn_4P_3/graphite composite material compared with pure crystalline Sn_4P_3. The experimenters propose that this is best explained by the presence of the graphite matrix forming after high-energy ball milling, which allows electrical conductivity among the widely dispersed SnP_x clusters throughout the material. The graphite matrix also prevents aggregation of Sn clusters during lithiation/delithiation, thus preserving greater capacity for longer periods. The researchers attribute the eventual capacity fading to the slow increase in metallic Sn-Sn cluster sizes observed with EXAFS over cycling.

The detailed picture of the conversion and alloying mechanisms at work in these tin phosphide anode materials seems to indicate that the use of graphite provides one possibility for enhancing their capacity and cycle life. Use of the *in situ* XAFS technique enables detailed understanding of factors affecting reversibility of redox processes in battery materials, which will be instrumental for further performance improvement. *— Mark Wolverton*

See: Yujia Ding[1], Zhe-Fei Li[2], Elena V. Timofeeva[1], and Carlo U. Segre[1]*, "In Situ EXAFS-Derived Mechanism of Highly Reversible Tin Phosphide/Graphite Composite Anode for Li-Ion Batteries," Adv. Energy Mater. **8**, 1702134 (2018,).
DOI: 10.1002/aenm.201702134
Author affiliations: [1]Illinois Institute of Technology, [2]Ohio University
Correspondence: * segre@iit.edu

This research was funded in part by U.S. Department of Energy, Advanced Research Funding Agency-Energy (ARPA-E) (Award # AR000387). MR-CAT operations were supported by the Department of Energy and the MRCAT member institutions. This research used resources of the Advanced Photon Source, a U.S. DOE Office of Science user facility operated for the DOE Office of Science by Argonne National Laboratory under Contract No. DE-AC02-06CH11357.

10-ID-B • MR-CAT • Materials science, environmental science, chemistry • X-ray absorption fine structure, time-resolved x-ray absorption fine structure, microfluorescence (hard x-ray) • 4.3-27 keV, 4.8-32 keV, 15-65 keV • On-site • Accepting general users •

Peering Inside Batteries with X-ray Vision

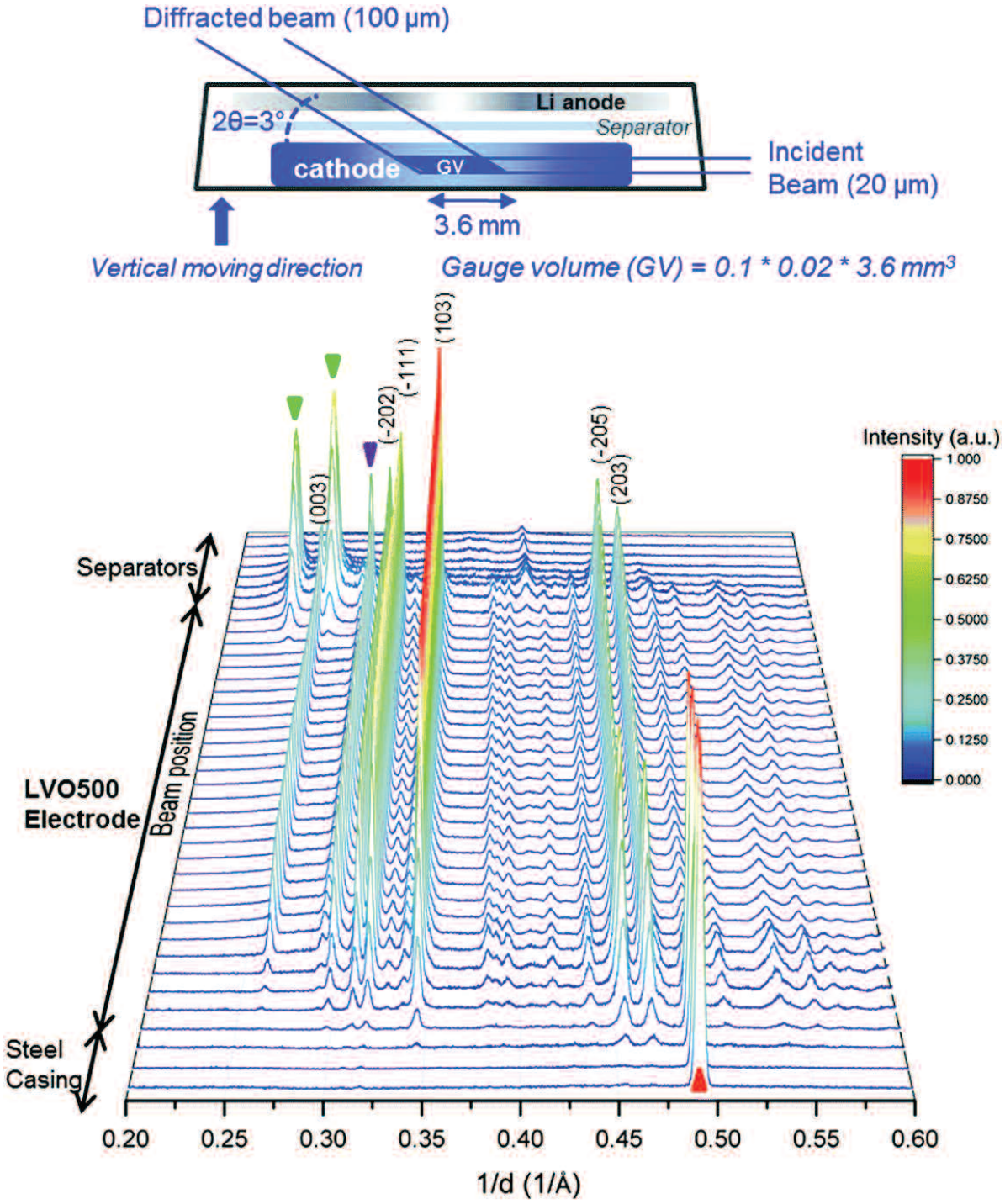

To create a future where electric cars and renewable energy sources are inexpensive and pervasive, scientists need to develop more powerful and longer lasting batteries. In lithium ion (Li-ion) batteries, which are common in portable electronics, the lithium ions move from the negatively charged anode to the positively charged cathode during discharge and back again while charging. One approach to making a Li-ion battery with more oomph is to improve the cathode. Vanadium materials have several appealing qualities in this regard, such as the capacity to hold a lot of lithium ions, boosting energy density, as well as the ability to charge and discharge rapidly. To interrogate the potential of one promising vanadium cathode compound, $Li_{1.1}V_3O_8$ (LVO), researchers studied the material using synchrotron-based energy-dispersive x-ray diffraction (EDXRD) at the APS. EDXRD utilizes high-energy photons to obtain diffraction patterns as a function of spatial location, providing a functional map. The researchers conducted the EDXRD experiments on LVO in its original state and during operation, leading to a better understating of the mechanism of lithiation and delithiation. These insights may facilitate the development of next-generation lithium ion batteries.

The process for generating LVO involves several variables that affect the material's ultimate properties. For example, different annealing temperatures produce electrode materials with unique structures, which seems to influence cycling stability. This suggests that the underlying structure is important in the development of optimal cathodes. The structure of LVO is like a many-layered peanut butter sandwich, with the V_3O_8 sheets acting as bread and the lithium ions serving as the peanut butter holding it all together. During the charging and discharging process, LVO shifts from an alpha phase to a beta phase, depending in part on the amount of lithium in the material; a lithium-poor scenario favors the alpha phase and the lithium-rich state favors the beta phase.

To understand the structural changes accompanying the phase transition, the researchers from Stony Brook University, Rensselaer Polytechnic University, and Brookhaven National Laboratory wanted to observe the material in an actual battery during operation, as lithium ions flowed into and out of the cathode. EDXRD allowed them to observe the changes going on inside the battery in real time because it utilizes high-energy x-rays that penetrate a battery's metallic coating.

As a first step, the researchers generated two different versions of LVO, one annealed at a temperature of 300° C (LVO300) and the other at 500° C (LVO500). Then, they built the batteries, creating coin-type cells with LVO electrodes, Li metal anodes, and polypropylene separators, with 1 M LiPF6 in ethylene carbonate/dimethyl carbonate as an electrolyte.

The *in situ* EDXRD experiments carried out at COMPRES/XSD beamline 6-BM-A,B of the APS indicated that LVO500 material was more crystalline than the LVO300, which translated into a more uniform distribution of lithium ions, while the lithium ions favored localization on two sides of the LVO300 material (Fig. 1). Mapping out the location of lithium ions during the delithiation of the LVO500 material revealed the origin and direction of the lithiation reaction. In addition, the data suggest that the structural changes that occur during the charging reaction are not simply the opposite of the discharging reaction: each direction is unique.

The researchers also observed, for the first time, the coexistence of three states during charging, as the Li-poor alpha state emerged before the disappearance of the Li-rich alpha and Li-rich beta phases. Thus, using EDXRD measurements, the researchers were able to map the LVO electrode inside the battery during electrochemical operation, providing mechanistic insights into the lithiation reaction. These insights can help to develop electrode materials that are stable over the course of many cycles of charging and discharging. *— Erika Gebel Berg*

< Fig. 1. EDXRD experimental setup (top) and EDXRD patterns (bottom) with respect to the beam position of the LVO500 coin cell. Peaks which are associated with polypropylene separators, graphite and stainless steel casing are indicated by green, purple and red triangles, respectively. From Q. Zhang et al., Phys. Chem. Chem. Phys. **19**, 14160 (2017). © the Owner Societies 2017

See: Qing Zhang[1], Andrea M. Bruck[1], David C. Bock[2], Jing Li[1], Varun Sarbada[3], Robert Hull[3], Eric A. Stach[2], Kenneth J. Takeuchi[1]*, Esther S. Takeuchi[1,2]**, and Amy C. Marschilok[1]***, "Visualization of structural evolution and phase distribution of a lithium vanadium oxide ($Li_{1.1}V_3O_8$) electrode *via* an *operando* and *in situ* energy dispersive X-ray diffraction technique," Phys. Chem. Chem. Phys. **19**, 14160 (2017).
DOI: 10.1039/c7cp02239e
Author affiliations: [1]Stony Brook University, [2]Brookhaven National Laboratory, [3]Rensselaer Polytechnic Institute
Correspondence:
* kenneth.takeuchi.1@stonybrook.edu,
** esther.takeuchi@stonybrook.edu,
*** amy.marschilok@stonybrook.edu

This work was supported by the Center for Mesoscale Transport Properties, an Energy Frontier Research Center supported by the U.S. Department of Energy (DOE) Office of Science-Basic Energy Sciences (BES), under Award #DE-SC0012673. Transmission electron microscopy experiments were performed using facilities at the Center for Functional Nanomaterials at Brookhaven National Laboratory, which was supported by the DOE-BES User Facility Division, under Contract No. DE-SC0012704 and the facilities in the Center for Materials, Devices and Integrated Systems (cMDIS) at Rensselaer Polytechnic Institute. This research used resources of the Advanced Photon Source, a U.S. DOE Office of Science user facility operated for the DOE Office of Science by Argonne National Laboratory under Contract No. DE-AC02-06CH113.

6-BM-A,B • COMPRES/XSD • Materials science, geoscience • Energy dispersive x-ray diffraction, high-pressure multi-anvil press • 20-100 keV • On-site • Accepting general users •

Getting Into 3-D Printing

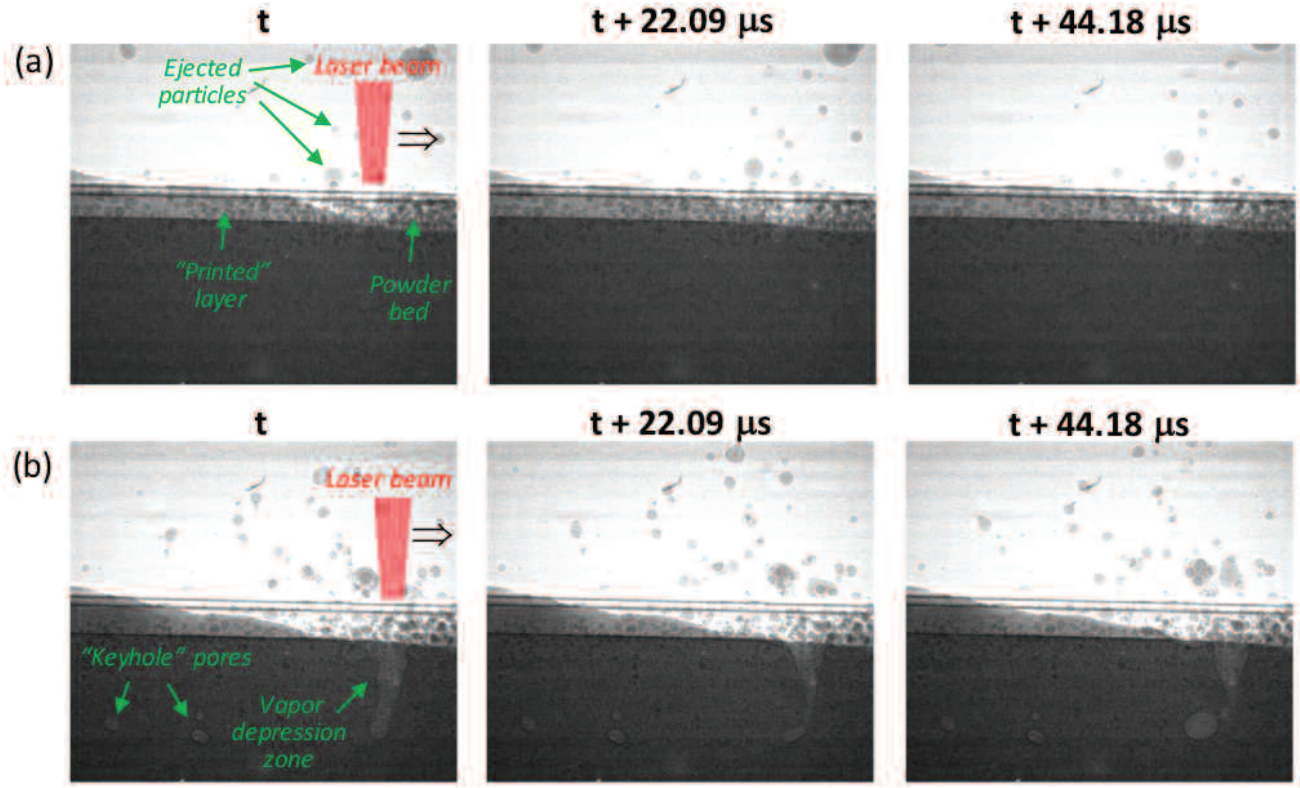

Fig. 1. X-ray imaging shows how a metal line is printed as a laser beam scans across the powder bed over several microseconds in a conduction heating mode (row a). With higher laser power, rapid heating causes deep vapor pressure zones, which lead to the formation of keyhole pores (row b).

Additive manufacturing, also known as three-dimensional (3-D) printing, has long been employed to create prototypes and is increasingly being utilized to build commercial items, from sneakers to aircraft parts. Most 3-D printing with metal works by scanning a laser across a thin layer of metallic powder, then melting to join with the layer below until a structure has been built up. Many such parts, however, suffer from mechanical weaknesses caused by defects in the layers, such as rough surfaces and large numbers of pores. It has been difficult to measure exactly how the defects form, in part because the process happens so quickly. Now scientists have developed a technique using the APS to capture defects as they form.

Most previous studies of the process known as "laser powder-bed fusion" had relied on high-speed photography in visible light, but that can only capture what's happening at the surface. So the researchers from Argonne, Carnegie Mellon University, and the Missouri University of Science and Technology built a setup that allowed them to probe below the surface with a hard x-ray beam from the XSD 32-ID-B,C beamline of the APS. They designed and built a miniature powder bed where a laser beam from above treated the metal and they sent an x-ray beam through the molten powder bed to both an imaging and a diffraction detector.

The researchers were able to watch and measure many of the dynamics involved in the rapid heating and cooling of the metal powder, a titanium-aluminum-vanadium alloy. For instance, they observed the formation of keyhole pores, which are significant defects within the structure. When the

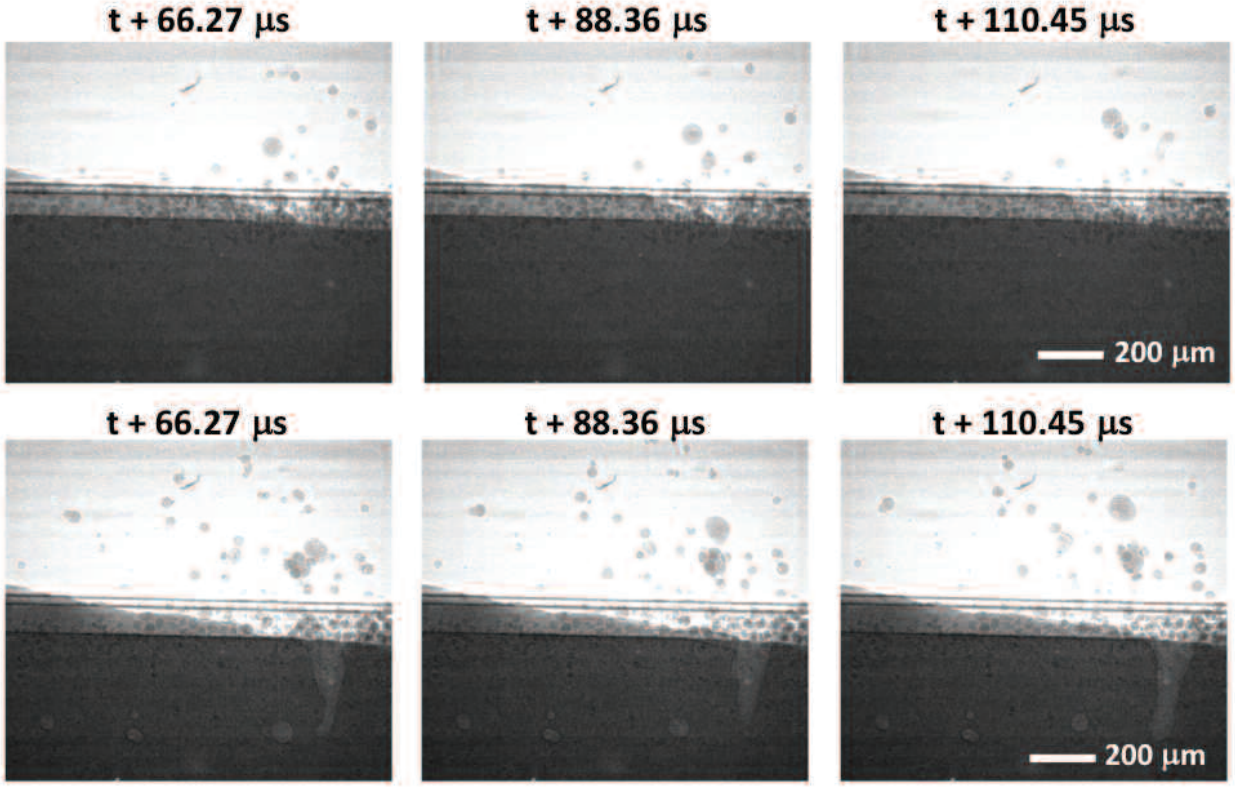

laser struck the powder, the metal melted, and both the molten metal and the heat flowed away from the center of the zone heated by the laser (Fig. 1). When the laser was scanned away, the sample started to cool down and the metal flowed back toward the center of the melted area, but the material on the top moved more quickly than that below, resulting in a cavity in the hardened structure. The researchers measured the closure of the keyhole for the first time, and found it could be faster than 50 µm, too quick for trapped gas to escape before the surface closed over it.

The study also showed how the metal behaved differently at different laser power levels. When the powder was subjected to 340 W of laser power for 1 µsec, first the powder then the hardened metal beneath it melted and a depression was created. Eventually, a dome-shaped metal structure formed without any notable defects. But when they set the laser to 520 W, the powder and base melted much faster, and some of the molten material was ejected, while the cavity formed was deeper. This process too produced a dome, but this one had a pore about 150 µm in diameter underneath it.

The researchers also measured such factors as the ejection rate of the material, which at high powers could be as fast as 15 m/sec. Under these conditions, the solidification rate of the molten alloy was about .5 m/sec.

The researchers hope these kinds of measurements will improve their understanding of the processes involved in laser-bed powder fusion so that they will be able to adjust parameters such as laser power and scan speed to achieve the best microstructures. They say the technique will likely become critical in additive manufacturing, particularly as new materials and new printing processes are developed.

— Neil Savage

See: Cang Zhao[1], Kamel Fezzaa[1], Ross W. Cunningham[2], Haidan Wen[1], Francesco De Carlo[1], Lianyi Chen[3], Anthony D. Rollett[2], and Tao Sun[1]*, "Real-time monitoring of laser powder bed fusion process using high-speed X-ray imaging and diffraction," Sci. Rep. **7**, 3602 (2017). DOI:10.1038/s41598-017-03761-2

Author affiliations: [1]Argonne National Laboratory, [2]Carnegie Mellon University, [3]Missouri University of Science and Technology

Correspondence:

* taosun@aps.anl.gov

This work is supported by Laboratory Directed Research and Development funding from Argonne, provided by the Director, Office of Science, U.S. Department of Energy (DOE) under Contract No. DE-AC02-06CH11357. R.C. is grateful for support from the Northrop Grumman Corporation. A.D.R. is grateful for support of the National Nuclear Security Agency under grant DE-NA0002918. L.C. appreciates the support from University of Missouri Research Board. This research used resources of the Advanced Photon Source, a U.S. DOE Office of Science user facility operated for the DOE Office of Science by Argonne National Laboratory under Contract No. DE-AC02-06CH11357.

32-ID-B,C • Materials science, life sciences, geoscience • Phase contrast imaging, radiography, transmission x-ray microscopy, tomography • 7-40 keV • On-site • Accepting general users •

Materials That Shrink When Heated

Most materials expand as temperature rises to accommodate the increased motion of the molecules within. Engineers are now identifying and developing materials that contract when heated, offering interesting possibilities. Mixing materials that expand with those that contract when heated could produce objects that stay the same size at different temperatures or change size predictably. One possible application is fillings that expand and contract at the same rate as teeth, leading to fewer toothaches. To develop tunable negative thermal expansion materials for engineering and other applications, researchers performed experiments at the APS and the POWGEN beamline at the Spallation Neutron Source (SNS) at Oak Ridge National Laboratory on substituted metal fluorides, analyzing thermal properties and structure at different temperatures and pressures.

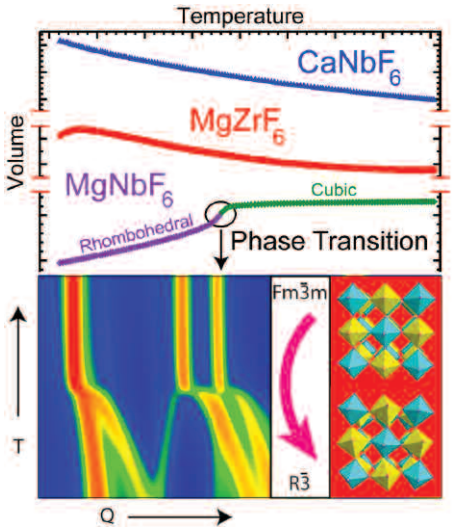

Fig. 1. Top: Volume per formula unit as temperature increases for three materials with Re-O_3-related structures, $CaNbF_6$(blue), $MgZrF_6$ (Red), and $MgNbF_6$(purple). A change from cubic to rhombohedral symmetry occurs for $MgNbF_6$ at ~280 K. Bottom, left: Synchrotron x-ray data for $MgNbF_6$ showing a discontinuous phase transition at ~280 K. Right, bottom: Structural changes associated with the phase transition as $MgNbF_6$ goes from *Fm*3*m* (cubic) to *R*3 (rhomohedral).

Mixing negative thermal expansion materials with positive thermal expansion materials to achieve neutrality is tricky. If the expansion and contraction occur at different rates, the material can come under significant stress, leading to a host of undesirable outcomes, such as phase transitions. Furthermore, negative thermal expansion materials display a wide range of properties, with some that soften under pressure (become more compressible) and others that have structural instabilities. Researchers need a firmer understanding of these behaviors and how to modify them to fully take advantage of negative thermal expansion materials.

Following recent work exploring metal fluorides with ReO_3-type structures, a research team from the Georgia Institute of Technology focused on $CaZrF_6$, which shows strong negative thermal expansion over a wide temperature range (10-1000 K). Plus, $CaZrF_6$ displays optical transparency from mid-infrared to ultraviolet ranges, an optical property with multiple applications. To explore the effect of composition on the materials' properties, the researchers swapped out the calcium for magnesium and the zirconium for niobium and studied the physical properties of the substances at different temperatures and pressures.

As a first step, the team collected x-ray powder diffraction data at the XSD 17-BM-B beamline of the APS on $CaNbF_6$, $MgZrF_6$, and $MgNbF_6$ at temperatures ranging from 100 to 1000 K. They measured high-resolution synchotron powder diffraction data for $MgZrF_6$ at the XSD 11-BM-B beamline at low temperature, down to 10 K. For additional structural information, they took neutron powder differaction measurements from 10-300 K at the POWGEN beamline at the SNS. To evaluate the effects of pressure on the substituted materials, high-pressure x-ray powder diffraction data were collected for $CaNbF_6$ and $MgZrF_6$ — also at beamline 17-BM-B — at P<8.6 GPa, and for $MgZrF_6$ at XSD beamline 11-ID-B, at P < 310 MPa.

Collectively, the experiments suggested that the substitution of zirconium with niobium had less of an impact on the materials' properties than the substitution of calcium by magnesium. For example, $CaZrF_6$ and $CaNbF_6$ both maintain cubic ReO_3-type structures down to 10 K, while also displaying negative thermal expansion at tempertures as high as 900 K. They also both display pressure-induced softening. The calcium substitution material began to introduce some significant differences. $MgNbF_6$ has a cubic structure at room temperature, but undergoes a octahedral tilting transition at 280 K and does not show negative thermal expansion at any temperature the researchers looked at 100-950 K. Thus, the replacement of calcium by magnesium led to significant changes in phase behavior and thermal expansion, potentially because magnesium is smaller and more polarizing than calcium. — *Erika Gebel Berg*

See: Brett R. Hester[1], Justin C. Hancock[1‡], Saul H. Lapidus[2],and Angus P. Wilkinson[1]*, "Composition, Response to Pressure, and Negative Thermal Expansion in $M^{II}B^{IV}F_6$ (M = Ca, Mg; B = Zr, Nb)," Chem. Mater. **29**, 823 (2017). DOI: 10.1021/acs.chemmater.6b04809

Author affiliations: [1]Georgia Institute of Technology, [2]Argonne National Laboratory ‡Present address: Northwestern University

Correspondence:

* angus.wilkinson@chemistry.gatech.edu

The researchers acknowkledge experimental assistance from the beamline staff of POWGEN at the SNS and at the APS. The work at Georgia Tech was partially supported under National Science Foundation DMR-1607316. A portion of this research used resources at the Spallation Neutron Source, a U.S. Department of Energy (DOE) O□ce of Science user facility operated by the Oak Ridge National Laboratory, and of the Advanced Photon Source, a U.S. DOE O□ce of Science user facility operated for the DOE O□ce of Science by Argonne National Laboratory under Contract No. DE-AC02−06CH11357.

Measuring Melting Points under Pressure

Understanding the properties of a material, particularly a property as crucial as its melting point, is important to predicting the material's performance. A metal such as molybdenum, for instance, can be subjected to extreme conditions in a power plant or a deep-sea drill, so scientists need to know at what combination of temperature and pressure it will turn from solid to liquid. Unfortunately, the answer is not known with any certainty; theory and some recent experiments point to melting temperatures for molybdenum almost 3000 K higher than other experiments at 1 million atmosphere pressure, a vast discrepancy. Scientists utilized the APS to get results that more closely match theory, and in the process demonstrated what may be a better method for pressure-temperature melting studies.

One possible reason for the previous discrepancy is the difficulty of making the measurements. The method chosen by these researchers from the Carnegie Institution of Washington employed a laser-heated diamond anvil cell (DAC). The sample of metal was placed between two tiny diamonds, which were then pressed together to exert pressure on the sample. At the same time, short pulses of laser light heated the metal. Utilizing synchrotron x-ray diffraction, which can detect liquid by the differences in how it scatters the x-rays compared to crystal, researchers can increase the pressure and heat by steps and should be able to see at what combination of temperature and pressure the liquid appears.

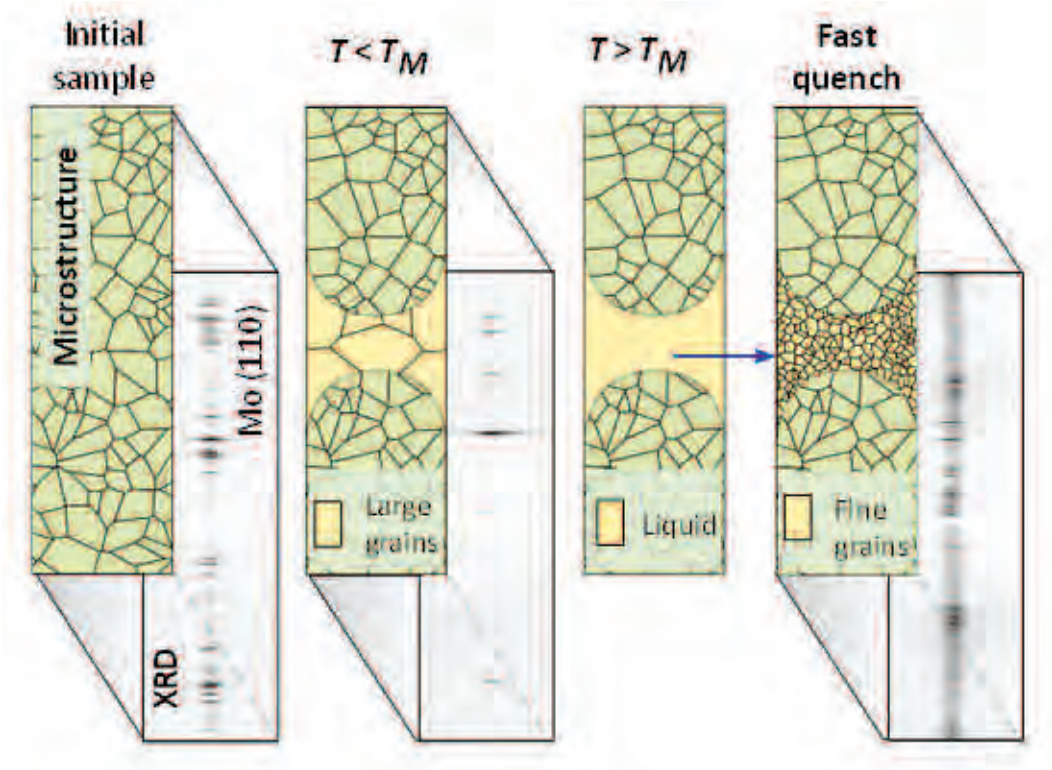

Fig. 1. Cross-sectional schematics showing the Mo sample. Grain growth is promoted in the central region when temperature is below T_M; fine-grained microstructure emerges from the quenched molten region. Microstructure evolution seen in a sequence of azimuthally unwrapped XRD images of Mo (110) reflection.

Unfortunately, this method creates only a small volume of liquid, which produces a very weak signal from the x-rays and therefore requires collecting x-rays for 100 times as long as the duration of the heating pulse, making it hard to use. Heating has to be brief, because a longer duration may cause chemical contamination or material diffusion. The researchers got around this limitation by using a "cook and look" approach, first pulse heating the sample, then performing x-ray diffraction (XRD) to look for any changes after rapid quenching.

This works, they found, because the grain structure of the crystal changed as it was heated. Their expectation was that, as the sample got hotter, the grains in the crystal would grow until the melting point, and that when it was rapidly cooled from the melt, the solidifying material would form a fine-grained structure. By heating then quenching the sample, then looking at it with x-ray diffraction, they could see if it had melted and reformed (Fig. 1).

It turned out, though, that there was a third crystalline microstructure. The researchers had placed single-crystal magnesium oxide next to the molybdenum as an insulating layer. At a high temperature, but below melting, the crystal abruptly changed from a

"Measuring" cont'd. on page 47

Strong, Stiff, and Inexpensive: Carbon Fibers Built with Boron

Whether the future includes ultralight low-emission automobiles made from carbon fiber may come down to a question of cost. The current standard carbon fiber goes for around $10/lb, a price tag that limits its use in industrial and automotive settings. The high cost is largely due to the expense of the fiber's precursor, polyacrylonitrile. To lower the cost, scientists are exploring alternate precursor materials, including polyethylene. Carbon fibers developed from polyethylene, while less expensive, aren't as strong or stiff as those made from polyacrylonitrile, limiting their application. Graphitization at high temperatures improves the fiber properties, but the extra heat is expensive. The key, it turned out, to developing an economically friendly polyethylene-based carbon fiber at low cost was boron. By doping the polyethylene with boron, the researchers found they could catalyze the graphitization process and produce high-quality fibers at much lower temperatures. A research team from The Dow Chemical Company, in collaboration with staff of the DND-CAT beamline at the APS, designed and built an apparatus that enabled them to take wide-angle x-ray diffraction (WAXD) measurements of the fibers as they were carbonized under tension, revealing the secrets of how boron boosts carbon fiber strength and stiffness on a microstructural level.

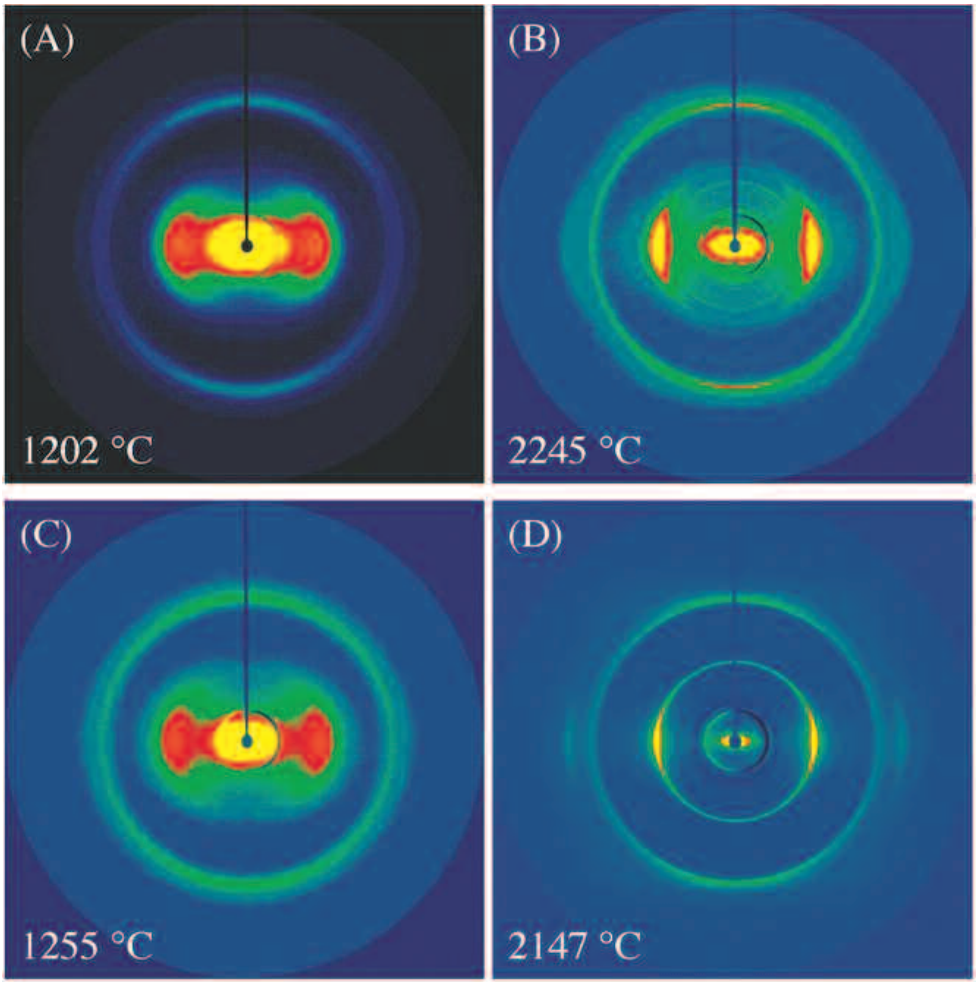

Carbon fibers are thread-like materials that can be woven together to form a carbon cloth; combined with a polymeric hardening agent, the woven molded fibers can act as a stronger, lighter replacement for metal. Two critical properties that engineers use to assess the quality of a carbon fiber are tensile modulus, a measure of stiffness, with higher values indicating greater rigidity, and tensile strength, a measure of how much force is required to permanently deform the material. Standard polyacrylonitrile carbon fibers have a tensile strength of between about 3 to 5 GPa and a tensile modulus of around 230 GPa.

The threshold for an industrially useful fiber is a tensile modulus of about 200 GPa, according to the researchers. Polyethylene-based carbon fibers typically have a tensile modulus of around 100-150 GPa. The researchers found they could increase the tensile modulus to 200 GPa when the fibers are graphitized at temperatures of ~ 2400° C, but such high temperatures come at a high cost. To bring the graphitization temperature down to less than 1800° C, the threshold for meeting the team's economic goals, the researchers explored the addition of boron to the polyethylene precursor. Boron is known to improve the tensile modulus of carbon fibers, but researchers have previously only observed this benefit at temperatures exceeding 2400° C. To incorporate boron into the fibers, the researchers bathed the precursor materials in boric acid, ending up with a compos-

Cont'd. on the next page

< Fig. 1. WAXD patterns of control SPE-CFs heated *in situ* under 0.5-N tension to 1202° C (A) and 2245° C (B), compared to 0.5-m boron-doped SPE-CFs heated to 1255° C (C) and 2147° C (D). From B.E. Barton et al., small **13,** 1701926 (2017). © 2017 Wiley-VCH Verlag GmbH & Co. KGaA, Weinheim

ite including 2.8% boron. At 1800° C, fibers created from undoped polyethylene had a tensile modulus of 116 GPa and a tensile strength of 1.21 GPa, while the fibers produced from doped polyethylene reached a tensile modulus of 201 GPa and a tensile strength of 2.4 GPa.

To figure out how boron was improving the polyethylene carbon fibers, the researchers turned to the DND-CAT 5-ID-D beamline at the APS to collect WAXD data. WAXD reports on the graphitic microstructure. The researchers collected data on the doped and undoped versions of the carbon fibers while they were being heated to elevated temperatures in the custom-made high-temperature fiber tensile device. The results suggested that the presence of boron catalyzes graphitization, leading to a more highly-oriented microstructure, with more stacked layers in the fiber and larger two-dimensional sheets, all of which are believed to contribute to an increase in the tensile modulus and the tensile strength. Carbon fibers produced via this process represent a new class of carbon fiber, which may be commercially viable due to lower cost and a high modulus.

— Erika Gebel Berg

See: Bryan E. Barton[1]*, Michael J. Behr[1]**, Jasson T. Patton[1], Eric J. Hukkanen[1], Brian G. Landes[1], Weijun Wang[1], Nicholas Horstman[1], James E. Rix[2], Denis Keane[2], Steven Weigand[2], Mark Spalding[1], and Chris Derstine[1], "High-Modulus Low-Cost Carbon Fibers from Polyethylene Enabled by Boron Catalyzed Graphitization," small **13**, 1701926 (2017).
DOI: 10.1002/smll.201701926
Author affiliations: [1]The Dow Chemical Company, [2]Northwestern University
Correspondence:
* bebarton@dow.com,
** mjbehr@dow.com

This work received funding support from the 21st Century Jobs Trust Fund received through the Michigan Strategic Fund from the State of Michigan (Grant No. DOC-2868). DND-CAT is supported by Northwestern University, E.I. DuPont de Nemours & Co., and The Dow Chemical Company. This research used resources of the Advanced Photon Source, a U.S. Department of Energy (DOE) Office of Science user facility operated for the DOE Office of Science by Argonne National Laboratory under Contract No. DE-AC02-06CH11357.

The research team including Rostislav Hrubiak (right), Yue Meng (middle), and Guoyin Shen (left) worked together at the HP-CAT experimental station 16-ID-B, where a double-sided, pulsed-laser heating system is installed for *in situ* x-ray diffraction measurements. The laser heating system is optimized for diamond anvil cell high-pressure devices, thus providing a powerful structural probe for studying materials at extremely high-pressure (>300 GPa) and high-temperature (>5000 K) conditions.

"Measuring" cont'd. from page 45
coarse-grained structure to a fine-grained structure in which the grains were aligned with the MgO crystal. That may be, they said, because the crystal lattice of the MgO matches well with that of the molybdenum. When they tried the same thing with aluminum oxide, which has a lattice mismatch with molybdenum, they did not observe the alignment. Failing to account for that phenomenon may lead to inaccurate results, they said. The experiment was carried out using *in situ* microfocused x-ray diffraction at HP-CAT beamline 16-ID-B of the APS, which allows the combination of the DAC and the laser pulse with the x-ray beam.

In the end, the researchers produced a pressure-temperature melting curve — which they extrapolated out beyond their experimental measurements — that more closely matched the theoretical predictions. It also was a closer fit with more recent experiments that used shockwave compression to produce high pressures. This method could be used to determine the melting profiles of other materials where there is poor agreement between theory and experiment, including iron, lead, and tantalum. *— Neil Savage*

See: Rostislav Hrubiak, Yue Meng, and Guoyin Shen*, "Microstructures define melting of molybdenum at high pressures," Nat. Commun. **8**, 14562 (1 March 2017).
DOI: 10.1038/ncomms14562
Author affiliation: Carnegie Institution of Washington
Correspondence: * gshen@ciw.edu

This research was supported by the U.S. Department of Energy (DOE) Office of Science-Basic Energy Sciences (BES), Division of Materials Sciences and Engineering under Award DE-FG02-99ER45775. HP-CAT operations are supported by DOE-National Nuclear Security Administration under Award No. DE-NA0001974, with partial instrumentation funding by the National Science Foundation. This research used resources of the Advanced Photon Source, a U.S. DOE Office of Science user facility operated for the DOE Office of Science by Argonne National Laboratory under Contract No. DEAC02-06CH11357.

16-ID-B • HP-CAT • Materials science, geoscience, chemistry, physics • Microdiffraction, single-crystal diffraction, high-pressure diamond anvil cell • 18-60 keV • On-site • Accepting general users •

Stressing Over New Materials

Alloyed with small amounts of aluminum and vanadium, titanium is used in aircraft, premium sports equipment, race cars, spacecraft, high-end bicycles, and medical devices because of its light weight, ability to withstand extreme temperatures, and excellent corrosion resistance. But it is also expensive. Metallurgists want to understand what makes it so strong so that they can design other materials with similarly desirable properties out of more common, less expensive elements. Researchers utilizing the APS used high-intensity x-rays to show how titanium alloy responds to stress in its hidden interior. Eventually, the researchers believe they will be able to predict how strong a titanium part such as an aircraft engine will be, just by knowing how the crystals are arranged inside of it. Materials scientists may be able to use such a computational model to swap in atoms from different metals to see how their crystalline structures compare to that of titanium.

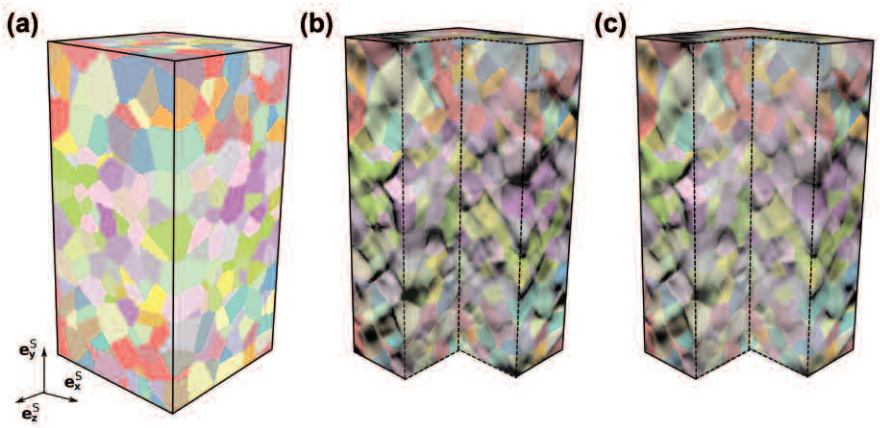

Fig. 1. (a) A computational model of crystals inside a block of titanium, (b) includes effects noticed during the experiment to place permanent deformations (the darkened areas,) while (c) models permanent deformations without incorporating the diversity of load seen in the experiment.

Previous work on titanium's physical qualities meant growing a macroscopic crystal large enough to see. But researchers from Lawrence Livermore National Laboratory, Carnegie Mellon University, and the U.S. Air Force Research Laboratory wanted to see how a typical titanium alloy made up of crystals of realistic size — tens of microns or so across — reacted to stress in its natural environment inside a larger block of titanium, just as a titanium crystal inside a bicycle frame or artificial hip might react. They took a chunk of titanium alloyed with 7% aluminum and, working with colleagues from Argonne, exposed it to high-energy x-rays at the XSD 1-ID-B,C,E beamline at the APS. The titanium-aluminum alloy is similar to titanium-aluminum-vanadium but simpler to model. The 1-ID-B,C,E beamline delivers a high flux of x-rays energetic enough to penetrate a full centimeter into solid metal. There are only five facilities in the world capable of producing bright, coherent x-rays of energy high enough to do that.

The researchers carefully aligned a titanium testing specimen inside an apparatus that exerts various forces on it — pulling or squeezing, for example. The rays penetrated about a millimeter through the specimen with minimal resistance. Then, the x-rays began to bounce off microcrystal faces inside the metal and interfere with each other. This interference made a tell-tale diffraction pattern the researchers could interpret. As they pulled on the titanium block, the crystals inside were stressed and their atoms shifted slightly, changing the lengths of the bonds between them. The changes in the bond lengths reflected the stress the bonds were under. The x-ray diffraction patterns changed as the atoms shifted, revealing how stress on the atoms increased as the load on the titanium block grew.

Surprisingly, as the load grew so large that the crystals began to permanently deform, the stress on some of the individual atomic bonds and even on entire crystal faces began to drop; in other places the stress grew to compensate (Fig. 1). The researchers did not expect this, and it puts a wrinkle into their theories as to why the titanium alloy is as strong as it is. Permanently deformed areas are where cracks and other damage can start.

The researchers utilized data gathered at the APS to build a new computational model of titanium at the molecular level. In future experiments, they hope to gather more data in more complex environments closer to real life situations, including very high or low temperatures as well as repeatedly stressing and then relaxing the metal to simulate fatigue that happens during actual use. *— Kim Krieger*

See: Darren C. Pagan[1*‡], Paul A. Shade[2], Nathan R. Barton[1], Jun-Sang Park[3], Peter Kenesei[3], David B. Menasche[4], and Joel V. Bernier[1], "Modeling slip system strength evolution in Ti-7Al informed by in-situ grain stress measurements," Acta Mater. **128**, 406 (2017).
DOI: 10.1016/j.actamat.2017.02.042
Author affiliations: [1]Lawrence Livermore National Laboratory, [2]Air Force Research Laboratory, [3]Argonne National Laboratory, [4]Carnegie Mellon University ‡Present address: Cornell University
Correspondence: * dcp99@cornell.edu

The work of D.C.P., N.R.B., and J.V.B. was performed under the auspices of the U.S. Department of Energy (DOE) by Lawrence Livermore National Laboratory under contract DE-AC52-07NA27344 (LLNL-JRNL-703660). Support from the Materials and Manufacturing Directorate of the U.S. Air Force Research Laboratory is acknowledged. This research used resources of the APS, a U.S. DOE Office of Science user facility operated for the DOE Office of Science by Argonne National Laboratory under Contract No. DE-AC02-06CH11357.

Nearest Neighbor Behavior behind Non-Cubic Scaling Law for Metallic Glasses

The excellent mechanical and electrical properties of metallic glasses make them useful in a wide range of applications: they are utilized as the magnetic cores of efficient transformers in electrical grids and are also formed into screws and pins implanted in bone to help heal fractures. However, our understanding of their glassy characteristics, including the way in which atoms order themselves in this quasi-liquid state, is still evolving. Previous experiments have shown an unanticipated relationship between the density of the material and the average interatomic distance. Recently, researchers employed synchrotron x-ray experiments at the APS and the Shanghai Synchrotron Radiation Facility (SSRF) to investigate the hypothesis that these materials exhibit fractal ordering at medium ranges, but they instead found evidence that the relationship between density and average interatomic distance is determined by the behavior of nearest neighbors at short range.

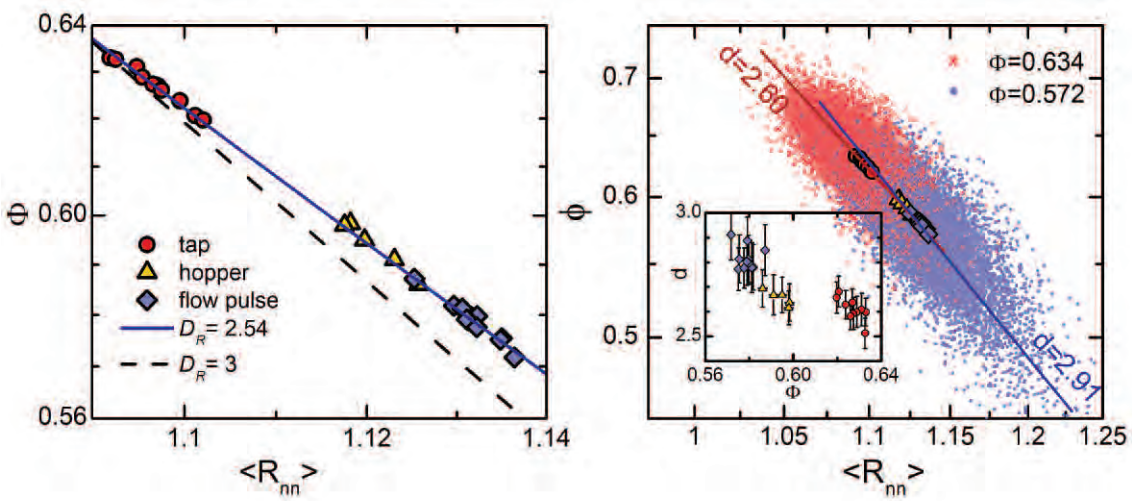

Fig. 1. Left: Noncubic scaling law of packing fraction and average nearest neighbor distance. Right: The exponent d of noncubic scaling is not universal and instead is changing with packing fraction.

In crystalline and liquid systems, the relationship between density and average interatomic distance is cubic and understood to result from the three-dimensional nature of the bulk density. Yet previously-published experiments working with metallic glasses have shown a noncubic scaling relationship between the two. To explain this difference, scientists have theorized a fractal nature for the packing structures of metallic glasses. This fractal theory raises additional questions, motivating researchers from Shanghai Jiao Tong University (China), Argonne, the Chinese Academy of Sciences, and the University of Montpellier and CNRS (France) to further examine the packing structures of metallic glasses.

The researchers used synchrotron x-ray computerized tomography at the XSD 2-BM-A,B beamline of the APS and the BL13W1 beamline of the SSRF to measure the packing structures of metallic glass material analogues. This technique allowed them to conduct real-space measurements of disordered granular packing structure, providing more information than metallic glass scattering experiments. They varied the packing fraction — the amount of spherical particles in a standard amount of space — to produce a variety of packing structures.

The researchers looked at structure factor and pair correlation function peaks as they varied packing fraction but found contradictory results. Because this structural information is complex and indirect, they chose to define a length scale per given number of packed particles and then calculate the scaling relation between this length scale and the packing fraction. To determine the length scale, they ordered all neighbors by distance and calculated the average nearest neighbor distance for a given number of neighbors.

They found that the average nearest neighbor distance scales with the packing fraction (for a given number of nearest neighbors). They also found that the exponent which relates the packing fraction and the length scale depends on the number of nearest neighbors chosen. For a choice of

"Neighbor" cont'd. on page 51

What Hath Iron (and Other Ions) Wrought?

Nearly all structural lumber in the Northern Hemisphere is composed of softwoods, also referred to as conifers or gymnosperms. These wood species are susceptible to attack from brown rot fungi, which account for approximately 6% of the known species of wood rotting fungi. Brown rot fungi degrade the structural components of wood and assimilate the nutrients via extracellular processes using both enzymatic and non-enzymatic mechanisms. Ion movement and translocation is an important aspect of brown rot and is implicated in both enzymatic and non-enzymatic modes of decay. While scientists know that many ion species play important roles in fungal decay mechanisms, little is known about how abundant each species is, exactly where they accumulate within fungi, the wood they attack, and their movements throughout the decay process. Researchers used the APS to map and quantify physiologically relevant ions in wood being decayed by the brown rot fungus *Serpula lacrymans Wulfen* (P. Karst). The results show that the fungus actively transports some ions, such as iron (Fe), into the wood and controls the distribution of ions at both the bulk wood and cell wall length scales. In addition to having important implications for building materials, a better understanding of the role of ions in the fungal decay process of wood and other lignocellulose biomaterials has significance for fields ranging from plant pathology and forest ecology to carbon sequestration and sustainable biorefinery applications.

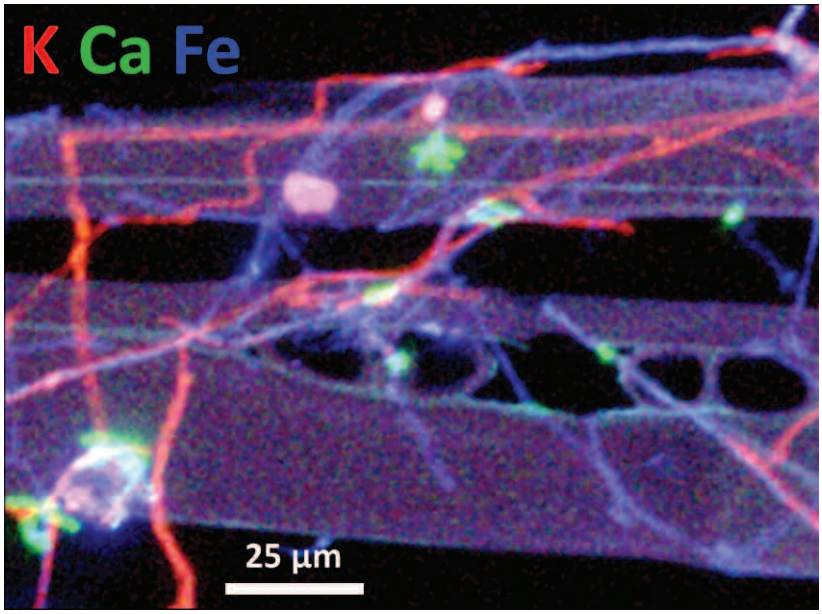

Fig. 1. This XFM co-localization map of fungal hyphae on a two-micron-thick section of wood shows the amounts of potassium (K, red), calcium (Ca, green), and iron (Fe blue) ions in individual cell wall layers and hyphae.

Wood is the primary building material in the vast majority of homes in the northern hemisphere. And for a good reason: it is abundant, easy to work with, durable, and strong. But as anyone who works with wood — or has spent a reasonable amount of time walking through the forest — knows, when wood gets wet, it rots. In fact, around 10% of the lumber harvested each year is used to replace in-service wood that has been attacked by decay-inducing fungi, such as the fairly common brown rot fungus.

Brown rot is typically initiated when the long, branching strands of the fungi called “hyphae” come into contact with the cell lumen of the wood in the presence of adequate moisture. The cell matrix pores of sound wood are typically too small for the diffusion of larger cellulolytic enzymes, but brown rot fungi initiate the breakdown process via a mediated-Fenton chemistry diffusion that can effectively penetrate the cell wall. The process involves the production of H_2O_2 outside the fungal hyphae to facilitate production of hydroxide radicals that permeate the lignocellulose cell wall and ultimately weaken the cellulose matrix. While the mechanisms of brown rot are not fully understood, the chemical reactions involved rely on the actions of numerous ions, including potassium, calcium, manganese, zinc, and the aforementioned iron.

Knowing where, and in what amounts, these ion species accumulate and are transported during the decay process can give scientists clues about the degradation mechanisms. An improved understanding of the mechanisms would benefit researchers developing improved wood protection treatments, as well as those developing biomimetic processes to improve the efficiency of biorefineries utilizing biomass to make sustainable fuels and chemicals. However, the tools that researchers have used to investigate the distribution of ions within fungi and rotting wood have not provided enough spatial resolution and sensitivity to distinguish between the localization of ions within the cell wall versus within the fungal hyphae. In addition,

Cont’d. on the next page

most previous studies have involved grinding or other disruption of wood, which also disrupts localized concentrations of the ions and prevents mapping ion distributions.

Researchers from the USDA Forest Products Laboratory, the University of Massachusetts-Amherst, Northwestern University, Universidade de São Paulo (Brazil), CMPC Celulosa (Chile),and Argonne have shown that synchrotron-based x-ray fluorescence microscopy (XFM) can map out trace amounts of elements in decaying wood across multiple length scales down to the sub-micron spatial resolution needed to probe individual wood cell walls, fungal hyphae, and calcium oxalate crystals that often grow around the hyphae. X-ray fluorescence microscopy is an imaging technique where a beam of x-rays is directed at a specimen and the intensities of the x-rays emitted back are detected as a function of wavelength and position. Because these energies are ion-specific, raster scanning the focused x-ray beam over the sample allows the researchers to make maps of numerous ions simultaneously.

Large-field XFM was performed on the XSD 8-BM-B beamline at the APS to map ions across the cleaved face of 10-mm wood cubes exposed to the decay fungi. Submicron-resolution XFM using the XSD beamline 2-ID-E was performed on three different types of samples to map and measure ions in the fungal hyphae and wood cell wall layers before and after decay (Fig. 1).

The XFM maps allowed the scientists to observe a substantial increase in Fe concentration in both the wood block and wood cell walls, which was consistent with the theory that brown rot progression is mediated by iron redox reactions. The XFM results also showed that calcium moves out of the wood cell walls during decay and is likely being deposited into oxalate crystals created by the fungus.

The results of this study demonstrate that synchrotron-based XFM can be a powerful, multiscale tool for simultaneously mapping numerous ions in complex substrates, such as decaying wood. Future studies will focus on studying additional species of fungi, improving these methods, and using decayed samples within a humidity-controlled environment to permit imaging of a living fungus as it colonizes wood cell walls and initiates degradation.

— Chris Palmer

See: Grant Kirker[1], Sam Zelinka[1], Sophie-Charlotte Gleber[2], David Vine[2], Lydia Finney[2], Si Chen[2], Young Pyo Hong[3], Omar Uyarte[4,5], Stefan Vogt[2], Jody Jellison[6], Barry Goodell[6], and Joseph E. Jakes[1]*, "Synchrotron-based X-ray fluorescence microscopy enables multiscale spatial visualization of ions involved in fungal lignocellulose deconstruction," Sci. Rep. **7**, 41798 (31 January 2017). DOI: 10.1038/srep41798
Author affiliations: [1]USDA Forest Service, [2]Argonne National Laboratory, [3]Northwestern University, [4]Universidade de São Paulo, [5]CMPC Celulosa, [6]University of Massachusetts-Amherst
Correspondence: * jjakes@fs.fed.us

J.E.J. acknowledge funding from 2011 USDA PECASE awards. B.G. acknowledges support from USDA Hatch Multistate Project S-1041 VA-136288. O.U. acknowledge support from FAPESP/BEPE Project N° 2013-04481-3. This research used resources of the Advanced Photon Source, a U.S. Department of Energy (DOE) Office of Science user facility operated for the U.S. DOE Office of Science by Argonne National Laboratory under Contract No. DE-AC02-06CH11357.

"Neighbor" cont'd. from page 49
many neighbors, the value of the exponent deviates from 3, the cubic relationship expected for a bulk material (Fig. 1).

To further assess the relationship between nearest neighbors and the exponent scaling law, the researchers examined how neighbors at different distances are displaced as a function of packing fraction. They found that changing the packing fraction most affects neighbors in the first shell. Separating the first shell neighbors into quasicontact neighbors (the six nearest neighbors) and noncontact neighbors, they found that these groups displaced differently as a function of packing fraction, creating a structural arrangement that was non-uniform. This non-uniform structural arrangement results from the geometric constraints of hard spherical particles. The researchers concluded there was a link between the non-uniform structural arrangement of all the nearest neighbors and the exponent scaling law.

The researchers also calculated three-point correlation functions using the angle between the central particle and each set of any two of its nearest neighbors. They found that the quasi-contact neighbors ordered into regular triangles and eventually quasiregular tetrahedral structures, while the non-contact neighbors did not obviously order. The non-uniform structural arrangement of particles in the first shell led the researchers to conclude three things: (a) The noncubic relationship between atom density and average interatomic distance is related to the number of contact neighbors; (b) The exponent in the scaling law results from packing structure at the particle contact length scale instead of the much longer medium-range scale as originally expected; and (c) The noncubic scaling relationship is a function of jamming rather than fractal glass order. The researchers additionally posited that the scaling exponent may be universal at the jamming transition point for spherical particles. *— Mary Alexandra Agner*

See: Chengjie Xia[1], Jindong Li[1], Binquan Kou[1], Yixin Cao[1], Zhifeng Li[1], Xianghui Xiao[2], Yanan Fu[3], Tiqiao Xiao[3], Liang Hong[1], Jie Zhang[1], Walter Kob[4], and Yujie Wang[1]*, "Origin of Noncubic Scaling Law in Disordered Granular Packing," Phys. Rev. Lett. **118**, 238002 (2017).
DOI: 10.1103/PhysRevLett.118.238002
Author affiliations: [1]Shanghai Jiao Tong University, [2]Argonne National Laboratory, [3]Chinese Academy of Sciences, [4]University of Montpellier and CNRS
Correspondence:
* yujiewang@sjtu.edu.cn

The work is supported by the National Natural Science Foundation of China (No. 11175121, 11675110 and U1432111), Specialized Research Fund for the Doctoral Program of Higher Education of China (Grant No. 20110073120073). This research used resources of the Advanced Photon Source, a U.S. Department of Energy (DOE) Office of Science user facility operated for the U.S. DOE Office of Science by Argonne National Laboratory under Contract No. DE-AC02-06CH11357.

How Heat Moves

For tiny electronic devices, heat is the enemy; If they get too hot, they malfunction. The need to keep the semiconductor brains of our devices cool has led to some impressive advances in the engineering of fans and airflow. But there's a limit to the cooling power of airflow, especially as computer processors grow tinier. Now that processors are being made on the nanoscale — meaning individual components can be made from just a few atoms — we need to think differently about how to keep them cool. At its most basic, heat is movement. When atoms get hot, they jiggle, and the hotter they get, the more they jiggle. Researchers employed the APS to track how far a single wave of jiggle, formally called a "phonon," could move through a material without bumping into a different phonon. Being able to visualize phonon movement so clearly will help researchers understand how heat moves through nanoscale computer processors, and lead to processors that can work faster without melting. *Cont'd. on the next page*

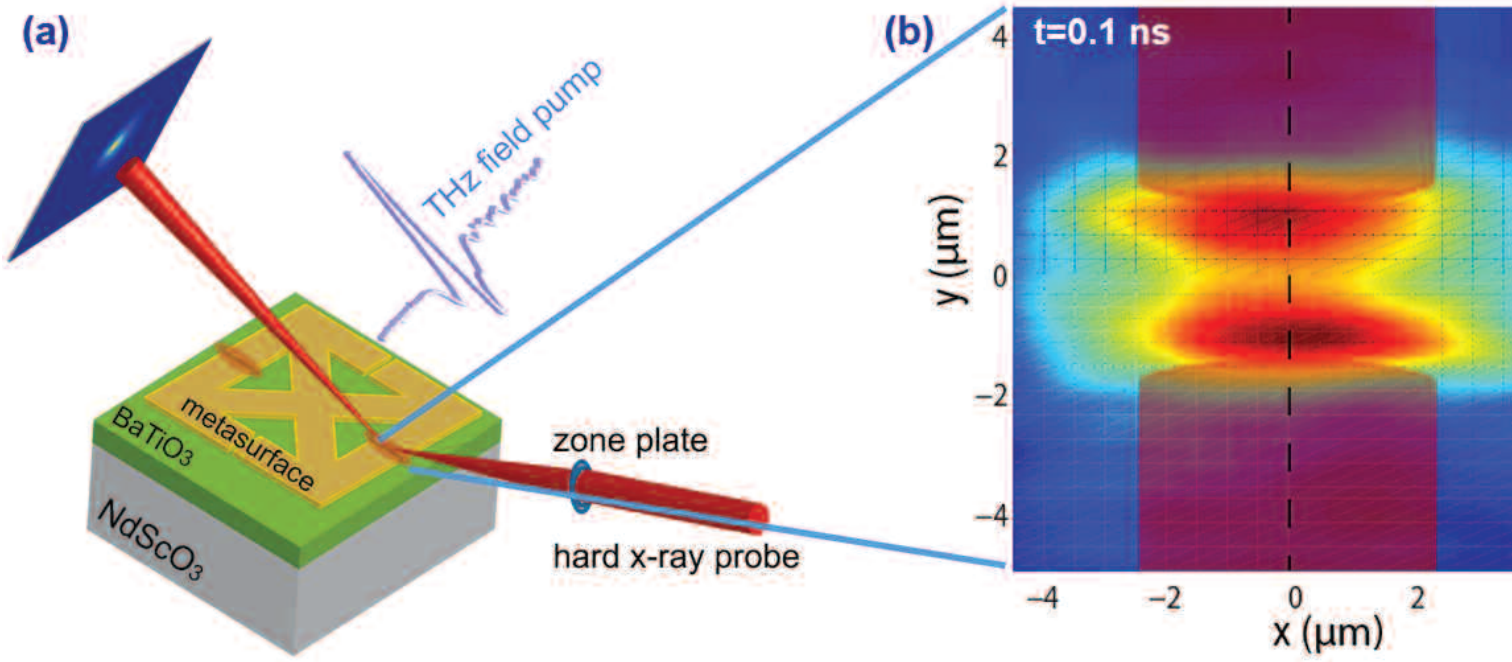

Fig. 1. A schematic of the experiment is shown in (a) with the gold split-ring resonator concentrating terahertz light onto a thin film of barium titanium oxide. A hard x-ray probes a small spot on that thin film (b) and shows the map of the strain induced by the terahertz waves; the redder the area, the more it was displaced by terahertz-induced phonons. The cylindrical magenta overlays show the gold metamaterial. (c) A plot of the strain versus position of the material; the data match the predicted pattern of a ballistic phonon (green) far better than that of a diffusive one (red).

7-ID-B,C,D • XSD • Materials science, atomic physics, chemistry • Time-resolved x-ray scattering, time-resolved x-ray absorption fine structure, phase contrast imaging • 6-21 keV • On-site • Accepting general users •

Researchers from Argonne; Stanford University; SLAC National Accelerator Laboratory; the University of Wisconsin-Madison; the University of California, Berkeley; and Lawrence Berkeley National Laboratory carried out an experiment that used metamaterial-enhanced terahertz excitation to heat barium titanium oxide ($BaTiO_3$), a ferroelectric material with built-in polarization that can couple to incoming terahertz light. The metamaterial, a split-ring resonator made of gold, concentrated the terahertz pulses to a very localized and high-strength electric field. This focused terahertz light generated low-energy phonons that are more dramatic and easier to see in the $BaTiO_3$. The researchers used time-resolved hard x-ray diffraction microscopy to measure the phonons, tracking how much they jiggled the atoms of $BaTiO_3$ as they passed, and how far each phonon traveled before it bumped into another wave like itself (Fig. 1).

Time-resolved x-ray imaging allowed the scientists to see how the phonons moved though the material with much finer detail than is possible with microscopy and visible light, because optical waves are too long to resolve objects as small as atoms. X-ray wavelengths are much shorter, and so can provide detailed images of nanoscale features.

The group used the XSD 7-ID-B,C,D beamline at the APS because it is the only beamline in the world able to perform terahertz-field-pump and hard x-ray diffraction microscopy probe measurements. This new capability allowed the researchers to see structural dynamics upon terahertz field excitation with a spatial and temporal resolution of 400 nm and 100 psec.

The researchers found that the terahertz-induced phonons began as very localized jiggles in the $BaTiO_3$ that gradually broadened out by a few hundred nanometers over 100 psec. This broadening out of the phonon wave doesn't fit the standard model of heat diffusion that works in materials at larger scales. Instead, it fits a different model, one in which the phonons are moving ballistically, that is, the phonons are moving in straight lines without bumping into other phonons. This is the first time researchers have imaged this in real time. The phonons seemed to move ballistically for no more than 500 nm. Along farther distances, they began to move in the standard, diffusive way.

The measurements of phonon movement captured at the APS illuminate a fundamental shift in how heat moves through materials at the nanoscale. The technique is a gateway direct imaging of transient structural changes caused by heat in electronic and semiconductor materials. Management of thermal properties is a key issue in real-world applications. New tools to visualize the movement of heat through materials at the nanoscale will open up new opportunities to design smaller, faster, more efficient computers that can operate at high speeds without melting. Understanding how material gets hot should help us keep it cool.

— Kim Krieger

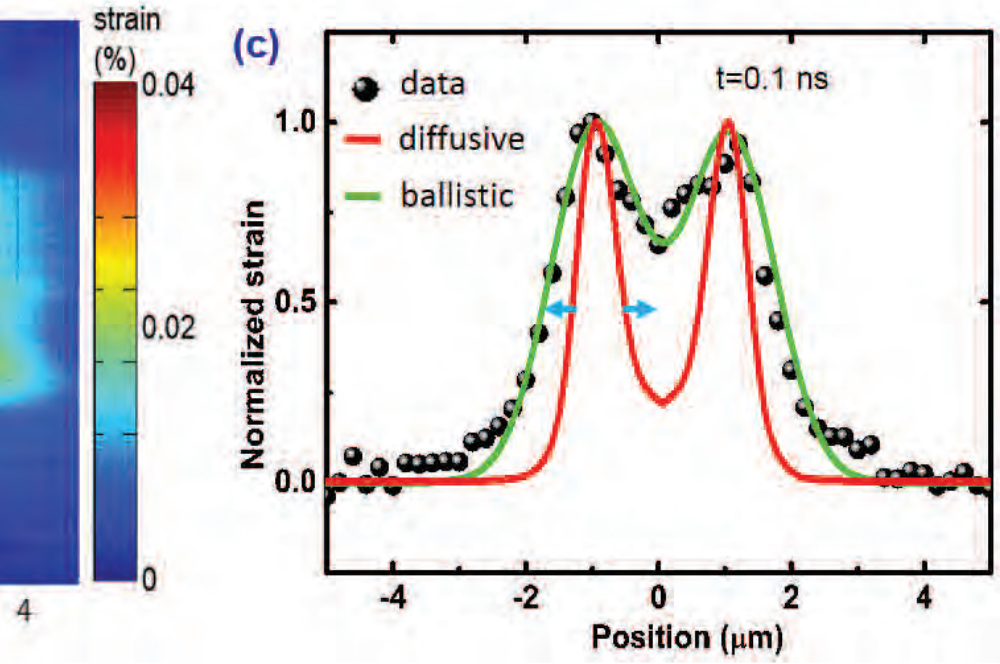

See: Yi Zhu[1], Frank Chen[2,3], Joonkyu Park[4], Kiran Sasikumar[1], Bin Hu[1], Anoop R. Damodaran[5,6], Woong Jung[1], Matthew J. Highland[1], Zhonghou Cai[1], I-Cheng Tung[1], Donald A. Walko[1], John W. Freeland[1], Lane W. Martin[5,6], Subramanian K.R.S. Sankaranarayanan[1], Paul G. Evans[4], Aaron M. Lindenberg[3,2], and Haidan Wen[1]*, "Structural imaging of nanoscale phonon transport in ferroelectrics excited by metamaterial-enhanced terahertz fields," Phys. Rev. Mater. **1**, 060601(R) (2017). DOI: 10.1103/PhysRevMaterials.1.060601

Author affiliations: [1]Argonne National Laboratory, [2]Stanford University, [3]SLAC National Accelerator Laboratory, [4]University of Wisconsin-Madison, [5]University of California, Berkeley, [6]Lawrence Berkeley National Laboratory

Correspondence: * wen@aps.anl.gov

This work was supported by the U.S. Department of Energy (DOE) Office of Science-Basic Energy Sciences (BES), Materials Sciences and Engineering Division. H.W., L.W.M., and J.F. acknowledge support from the U.S. DOE under Grant No. DE-SC0012375. This research used computational resources of the National Energy Research Scientific Computing Center, a DOE Office of Science user facility supported by the Office of Science of the U.S. DOE under Contract No. DE-AC02-05CH11231. A.M.L. and F.C. acknowledge support from the DOE Office of Science-BES, Materials Science and Engineering under Contract No. DE-AC02-76SF00515. P.G.E. and J.P. were supported by the U.S. DOE Office of Science-BES through Contract No. DE-FG02-04ER46147. A.R.D. acknowledges support from the Army Research Office under Grant No. W911NF-14-1-0104. The use of Advanced Photon Source and Center for Nanoscale Materials is supported by the U.S. DOE Office of Science-BES under Contract No. DE-AC02-06CH11357.

Imaging Polycrystalline Defect Dynamics under Working Conditions

Most materials used in everyday life, such as almost all metals or ceramics, are polycrystalline — they are composed of many small crystals arranged in different orientations with boundaries just a few atoms thick in between. Each crystal tends to hold multiple defects, such as dislocations between rows of atoms. The size and shape of crystals that make up these materials, as well as their defects, strongly affect the material's bulk properties. This micro-scale structure, and in turn the material's associated macro-level properties, can change under working conditions such as exposure to high heat, high pressure, and chemicals. To understand how these factors affect the material's behavior, it's important to be able to nondestructively view this microstructure and how it changes under working conditions. However, accomplishing this feat at the atomic level has remained a challenge. In this study, researchers showed the utility of a technique that they call "grain Bragg coherent diffractive imaging" (gBCDI) to follow dynamic changes in polycrystalline materials over time. In experiments at the APS, the researchers utilized scattering of coherent x-ray beams to reveal a variety of different types of shifts in structure as crystals were gradually heated. The researchers suggest that this technique could be promising for gaining a better understanding of a material's response under sometimes harsh external stimuli, findings that could be used to engineer polycrystalline materials with more resilient designs.

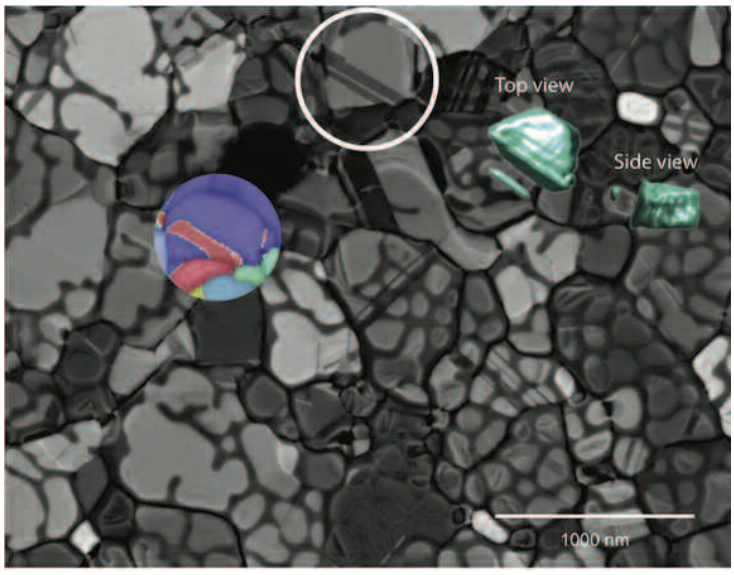

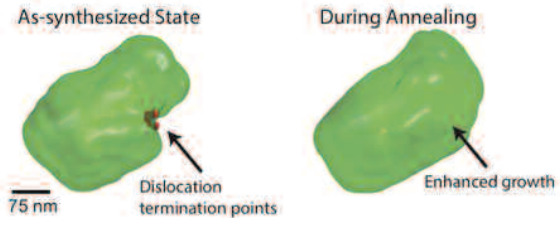

Fig. 1. An x-ray beam non-destructively tracked atomic-scale details in three dimensions. Top view is a scanning electron micrograph two-dimensional image of a textured film composed of many nanoscale gold particles. The white circle identifies a particle that has been imaged in three dimensions with a new coherent x-ray scattering technique that can be used in harsh environments. Top and side views of the imaged particle are shown (green overlays). A two-dimensional electron scattering orientation map of the same region (overlay in purple and red) shows the crystallographic texture of the film. The extracted three-dimensional images (bottom, green isolated particle views) show a similar but different particle from the film, before and after heating. Heat-induced changes include a filled cavity and removal of an atomic-scale "dislocation" defect.

34-ID-C • XSD • Materials science, physics • Coherent x-ray scattering • 5-15 keV • On-site • Accepting general users •

Bragg coherent diffractive imaging, in which researchers use computer algorithms to translate coherent x-ray scattering patterns into real-space images, can give both the three-dimensional shape and the internal deformation distribution of a sub-micron sized crystal, BCDI has been used to image the behavior of isolated nanoparticles. This study was the first demonstration of BCDI to capture dynamics of a crystal grain within a polycrystalline material, providing a new view of grain growth, grain boundary dynamics, and dislocation dynamics with a resolution of about 10 nm.

These researchers from Stanford University and Argonne performed their initial experiments at XSD beamline

"Imaging" cont'd. on page 56

Coping with Strain in Metal Hydrides

Hydrogen fuel cells can be utilized for portable technologies that must function for long periods without recharging. Such fuel cells often employ metal hydrides to store hydrogen, and work much the same way as lithium-ion battery cathodes that store lithium. They have the same problems, too: Charging and draining the metal hydride stresses the material and causes tiny defects to form, defects that degrade the material's ability to store hydrogen. Eventually, the storage material can only hold a fraction of the hydrogen it could originally, much like an old lithium battery in a cell phone that ceases to hold a charge. Materials scientists have known that the strain on the storage material is the primary reason for degradation, but they didn't know the details. Now, for the first time, researchers working at the APS have obtained detailed images of strain defects caused by repeated charge/discharge cycles in hydrogen. Their work shows the optimal size for a particle of metal hydride in a palladium-hydride storage system, and it could ultimately help engineer storage materials that take strain in controlled ways that do not damage, but rather improve them.

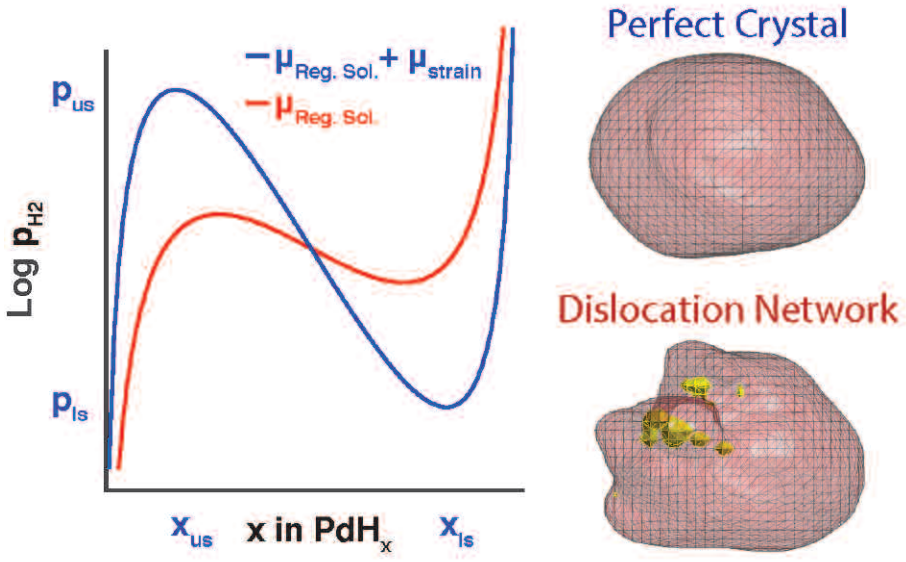

Fig. 1. Left: The graph shows the log of the hydrogen partial pressure on the y-axis versus the amount of hydrogen in the palladium hydride on the x-axis. The red line represents the graph of an unstrained crystal; the blue is a strained crystal. Right: The pink shapes are crystals of palladium hydride; the gold patches in the lower are defect locations.

12-ID-C,D • XSD • Chemistry, physics, materials science • Small-angle x-ray scattering, grazing incidence small-angle scattering, wide-angle x-ray scattering, surface diffraction • 4.5-40 keV • On-site • Accepting general users •

34-ID-C • XSD • Materials science, physics • Coherent x-ray scattering • 5-15 keV • On-site • Accepting general users •

When a metal hydride is "charged," hydrogen gas physically flows into the storage material. The hydrogen does not just fill up empty space—it actually sticks to binding sites within the metal and exerts force on the nearby metal atoms. When the hydride discharges, the hydrogen has to physically pull away from the material. The forces exerted by the hydrogen stress the storage material and cause it to deform.

Researchers from Argonne National Laboratory, the Canadian Nuclear Laboratories, and the DOE's SLAC National Accelerator Laboratory used the APS to image these defects as they formed in real time. They took a sample of palladium, a model storage material for hydrogen storage, and forced hydrogen through it. At the same time, they illuminated the palladium with x-rays from the XSD 34-ID-C beamline at the APS. Utilizing Bragg coherent diffractive (BCDI) imaging, they recorded the manner in which the x-rays scattered; changes in the x-ray scattering pattern allowed the researchers to see structural changes and defects that formed within the metal.

This is only the second time ever that this technique — BCDI — has been utilized to catch defects in the act

"Coping" cont'd. on page 56

"Imaging" cont'd. from page 54
34-ID-C of the APS with gBCDI on gold films with a thickness of about 200 nm grown on boron-doped diamond substrates. They first acquired baseline images of individual grains, then gradually heated the sample up to 500° C, tracking the scattering from the grains to image them multiple times as the temperature rose.

Using this technique, the team saw clear atomic mobility in the crystal structure and found that heat caused bordering crystal grains to grow non-uniformly and facets to sharpen. In one instance, much of the growth seemed to center around a previously identified defect in the crystal structure. As the temperature increased to around 400° C, that defect disappeared.

In the same crystal, the researchers used gBCDI to map a dislocation line in three dimensions. They found that it followed a horseshoe path—originating near a grain boundary, curving about 40 nm inside the crystal, and then terminating at the grain surface at a different location about 35 nm away. This dislocation line also faded with heating, disappearing completely at 400° C.

To investigate a different type of crystal defect known as coherent twin boundaries (CTBs) — in which the atomic stacking order mirrors itself on different sides of a crystal grain boundary — the researchers performed another set of experiments using a thin gold film grown on a SiO_2 substrate. This condition created gold crystals that were more highly textured than those on the boron-doped diamond substrate, with more CTBs.

Initially, gBCDI images of one part of this sample showed several distinct sections joined by CTBs. As this sample was heated, subsequent images revealed the largest sections growing and becoming sharper, while the smaller ones shrank. However, at higher temperatures, this situation reversed. Changes continued to occur as the temperature approached 500° C, unlike in the gold film on the boron-doped diamond substrate, which stabilized around 400° C.

Together, the authors suggest, these findings show the utility of gBCDI for imaging grains and defects in polycrystalline materials in reactive environments to reveal the mechanisms that can dramatically affect material properties. They add that this method can provide atomic-scale understanding of the mechanisms important to many applications, including corrosion-resistant materials for chemical processing, high-strength and fatigue-resistant structural materials, and improved catalysts and solar cells. *— Christen Brownlee*

See: Allison Yau[1], Wonsuk Cha[2], Matthew W. Kanan[1], G. Brian Stephenson[2]*, and Andrew Ulvestad[2], "Bragg coherent diffractive imaging of single-grain defect dynamics in polycrystalline films," Science **356**, 739 (19 May 2017). DOI: 10.1126/science.aam6168
Author affiliations: [1]Stanford University, [2]Argonne National Laboratory
Correspondence: * gbs@anl.gov

This work was supported by the U.S. Department of Energy (DOE) Office of Science-Basic Energy Sciences, Materials Sciences and Engineering Division (gBCDI technique and analysis), and by the National Science Foundation CHE-1565945 (sample synthesis, electron microscopy). This research used resources of the Advanced Photon Source, a U.S. DOE Office of Science user facility operated for the DOE Office of Science by Argonne National Laboratory under Contract DE-AC02-06CH11357.

"Coping" cont'd. from page 55
of forming. Advances in algorithms and beamline optics at the APS were what enabled the researchers to succeed. The 34-ID-C beamline is optimized for coherent x-ray flux that can be focused down to a spot just 1-μm across, or 1000 nm. This is small enough to use Bragg coherent x-ray diffraction imaging to watch the nanoscale defects form step-by-step. *In situ* x-ray scattering measurements were carried out at the XSD 12-ID-C,D beamline to see if the observed BCDI effects were present in the ensemble scattering of many Pd nanoparticles of different shapes and sizes..

With APS x-rays, the researchers could now see not only where the defects formed, but also how the defects altered the pressure at which the palladium could bind and release the hydrogen (Fig. 1). They also discovered that the best size for the palladium particles is 300 nm or smaller. Particles in this size range take the least strain and suffer far fewer defects when absorbing and releasing hydrogen than do larger particles. Previously, hydride manufacturers hadn't considered particle size an important parameter; they often use metal powders that contain many different sizes. Grading the powders and using only particles 300 nm across or smaller should make a hydrogen storage device, or a lithium ion battery cathode, that will cycle and last quite a bit longer than current technologies.

The researchers are also excited about using the APS to study how defects in metal hydrides could be used in a controlled way to actually improve the qualities of the material, much the way semiconductors are doped with impurities that introduce defects to change their electronic properties. The 34-ID-C beamline optics are optimal for using Bragg coherent x-ray diffraction imaging, and this technique could potentially be used to investigate similar strain defects in solar cells of any other crystalline material that gets repeated nanoscale strain damage.

— Kim Krieger

See: A. Ulvestad[1]*, M.J. Welland[2], W. Cha[1], Y. Liu[1], J.W. Kim[1], R. Harder[1], E. Maxey[1], J.N. Clark[3], M.J. Highland[1], H. You[1], P. Zapol[1], S.O. Hruszkewycz[1], and G.B. Stephenson[1], "Three-dimensional imaging of dislocation dynamics during the hydriding phase transformation," Nat. Mater. **16**, 565 (May 2017). DOI: 10.1038/NMAT4842
Author affiliations: [1]Argonne National Laboratory, [2]Canadian Nuclear Laboratories, [3]SLAC National Accelerator Laboratory
Correspondence: * aulvestad@anl.gov

Design of the hydriding phase transformation experiment and image analysis was supported by the U.S. Department of Energy (DOE) Office of Science-Basic Energy Sciences, Division of Materials Sciences and Engineering. We thank the staff at the Advanced Photon Source for their support. This research used resources of the Advanced Photon Source, a U.S. DOE Office of Science user facility operated for the U.S. DOE Office of Science by Argonne National Laboratory under Contract No. DE-AC02-06CH11357.

Carbon Clusters and the Detonation of High Explosives

The detonation of high explosives is complex and difficult to understand. What is known is that a fast shockwave decomposes energetic material to produce carbon clusters, including graphite and nanodiamonds. This study is the first in the United States to measure the formation and evolution of carbon clusters during the detonation of a plastic explosive containing the widely used insensitive high-explosive triaminotrinitrobenzene (TATB). Time-resolved small-angle x-ray scattering (TR-SAXS) after detonation carried out at the APS revealed the time scales of carbon cluster formation and provided insights into the chemical and physical transformations that occurred. A better understanding of high-explosive detonation improves our scientific models underpinning the physics involved in detonation process relevant to the U.S. nuclear deterrent.

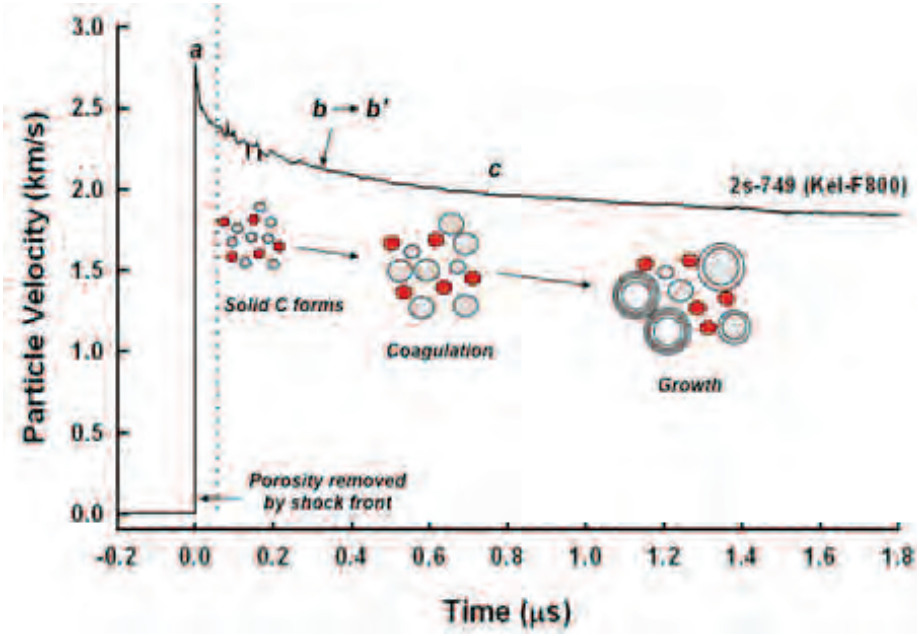

Fig. 1. Carbon clustering and aggregation with the arrival of the shock front at t=0. PBX 9502 detonation wave profile measured at a Kel-F 800 window (from Dattelbaum et al., Proc. 15th Int. Detonation Symposium, 2014).

High-performance explosives initiate a chemical reaction that serves as the trigger to drives the nuclear primary to critical mass. Understanding their performance is important for physics-based models that serve as part of our nation's predictive capabilities in the absence of nuclear testing. As the detonation reaction propagates, the explosive is transformed from reactant to products in the chemical reaction zone behind the shock front. For many high-performance explosives, these chemical reactions are so rapid that the shock wave front and the subsequent chemical reactions are contemporaneous. Insensitive high explosives provide a safer option for the nuclear arsenal because their reactions are much more difficult to initiate. Despite their importance, researchers have not known the exact chemical process of energy transfer in insensitive high explosives.

In this study, researchers from Los Alamos National Laboratory, Lawrence Livermore National Laboratory, Washington State University, and Argonne detonated small samples (3 gm) of plastic bonded explosive (PBX) 9502. This widely used, carbon-rich, insensitive high explosive is composed of 95% TATB with 5% fluoropolymer binder. To study the detonation products, these experiments were performed utilizing TR-SAXS at the DCS special-purpose 35-ID-B beamline at the APS.

The solid carbon detonation products form over 0.1 to 2.0 μsec behind the detonation front (Fig. 1). X-ray scattering reveals carbon clusters at nano- to mesoscales, indicating particle size and composition (Fig. 2). The chemical reactions take place in two stages. In the fast reaction zone, small carbon clusters and dense fluids (H_2O, N_2, CO, CO_2) are produced; these clusters coalesce into larger carbon clusters to create graphite, amorphous carbon, and nanodiamonds.

A quantitative understanding of the dynamics of carbon clustering — including the size, shape, composition and evolution — provide evidence of how the explosives deliver energy. This evidence is important because it: (1) reveals information on the conditions of detonation, such as the type of high explosive used; (2) yields explosive synthesized carbon materials, such as nanodiamonds and other useful materials; and (3) facilitates accurate modeling of the detonation. For example, the researchers have learned that as carbon clusters grow during detonation, the surface area-to-volume of carbon decreases, and the formation of carbon-carbon bonds release energy, which shifts the locus of the detonation. This information improves computer models of explosive performance.

The SAXS studies revealed several important insights. Carbon clusters grow more rapidly than previously thought, within 200 nsec behind the shockwave front. Late-time carbon clusters match the particle sizes of recovered products. Simulations are in

"Carbon" cont'd. on page 59

The Mechanical Properties of 3-D-printed Polymer Matrices during Failure

Additive manufacturing (AM), or three-dimensional (3-D) printing, is of particular interest because it allows for direct fabrication, reduced material waste, and production of components with complex geometries. In spite of these positive features, the polymers used in AM require further development, as they are currently structurally inferior to more traditionally manufactured material. To better understand the microstructure of AM materials and how the print orientation and thermal history of recycled material impacts the toughness and strength of fabricated specimens, researchers collected x-ray computed microtomography (CT) data at the APS. By collecting images of dog-bone–shaped specimens, the exact nature of the material's failure was visualized. This level of detail is important for linking manufacturing processes to material performance, providing a roadmap for how to tailor and improve the strength of AM materials.

When evaluating the strength of a given material, tensile response, failure, and strain evolution are important measures. In this study, the 3-D-printed, dog-bone–shaped specimen the researchers from Los Alamos National Laboratory, Argonne, and Arizona State University evaluated was generated through a common mode of manufacturing called selective laser sintering (SLS), in which a laser is used for focused polymerization of loose thermoplastic material held within a vat. One set of specimens was designed to assess the impact of using several percentages of recycled material: recycled material is material that was present in the vat during a previous SLS session, and therefore has thermal history from being previously heated but not polymerized. In addition, the researchers assessed the variability in strength of polymerized material in different printing directions along the specimen (X, Y, and Z direction): this difference in strength, termed anisotropy, is of central importance when evaluating the overall strength of an additively manufactured item.

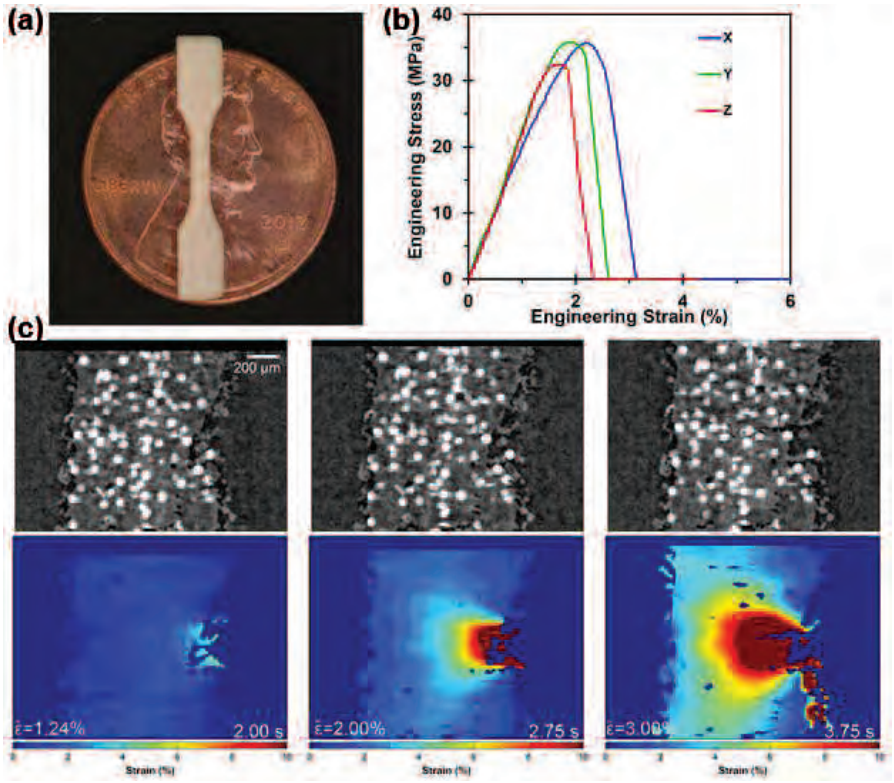

Fig. 1. a) Photograph of the 3-D printed specimen (dog-bone), b) the stress strain curve generated during the tension experiment, and c) 3-D reconstructed slices (grey) and digital volume correlation strain heat maps that show changes as a specimen is pulled apart (left to right). The crack in the dog bone is visible mid-way down the slices, and propagates horizontally.

Using the high x-ray flux available at the XSD 2-BM-A,B beamline at the APS, full 3-D images of the printed specimens were continuously collected at the rate of four per second as the specimen was pulled apart over a few seconds. Computed microtomography imaging documented the deformation and damage process on a microscopic level (Fig. 1).The data showed a significant decrease in specimen strength and elasticity that was further diminished with increasing percentages of recycled material used, especially in the direction of printing. Importantly, the ability to observe changes in microstructure and specimen volume as crack propagation through the polymer.

Cont'd. on the next page

Cont'd. on the next page

and delamination of the polymer from the glass beads in the composite allowed researchers to make the observation that while glass particles within the nylon polymer may enhance wear resistance, the weak adhesion between the particles does not help tensile strength.

In future work, improvements to experimental methods will include assessing additional samples and using a load cell that can rotate faster in the synchrotron's x-ray beam for faster acquisition of data. This faster acquisition will permit a more detailed study of strain rate effects and allow for the study of materials with more complex geometries such as microlattices.

— Emma Nichols

See: J.C.E. Mertens[1], K. Henderson[1], N.L. Cordes[1], R. Pacheco[1], X. Xiao[2], J.J. Williams[3], N. Chawla[3], and B.M. Patterson[1]*, "Analysis of thermal history effects on mechanical anisotropy of 3D-printed polymer matrix composites via in situ X-ray tomography," J. Mater. Sci. **52**, 12185 (2017).
DOI: 10.1007/s10853-017-1339-4
Author affiliations: [1]Los Alamos National Laboratory, [2]Argonne National Laboratory, [3]Arizona State University
Correspondence:
* bpatterson@lanl.gov

Note: This paper was also featured on the cover of the October 2017 issue of the *Journal of Materials Science*, and was the October nominee for the journal's annual Cahn prize.

Funding for this research was provided by the Enhanced Surveillance Campaign, Tom Zocco, Program Manager, and the Engineering Campaign, Antranik Siranosian, Program Manager. Los Alamos National Laboratory is operated by Los Alamos National Security, LLC, under Contract Number DE-AC52-06NA25396 for the U.S. Department of Energy (DOE). This research used resources of the Advanced Photon Source, a U.S. DOE Office of Science user facility operated for the DOE Office of Science by Argonne National Laboratory under Contract No. DE-AC02- 06CH11357.

2-BM-A,B • XSD • Physics, life sciences, geoscience, materials science • Tomography, phase contrast imaging • 10-170 keV, 11-35 keV • On-site • Accepting general users •

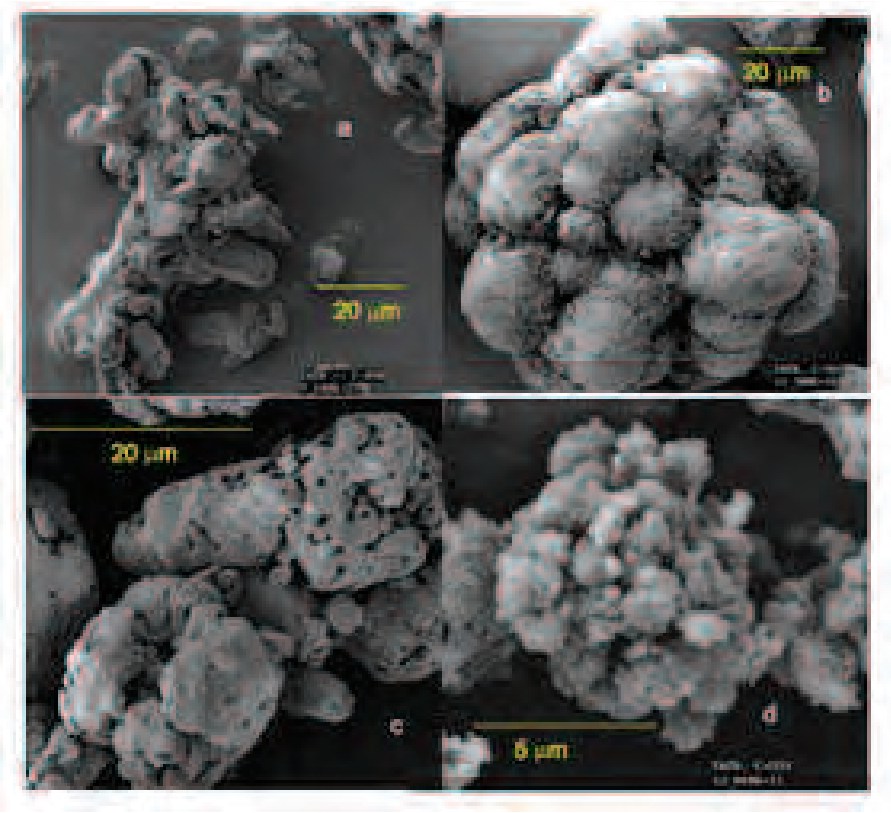

Fig. 2. TATB/PBX 9502 microstructures.

"Carbon" cont'd. from page 57

good agreement with the experimental measurements of cluster growth with a freeze-out temperature and temporal shift associated with the initial precipitation of solid carbon. Surprisingly, the measured ratio of graphite to diamond carbon forms is 80:20; researchers expected to see much more carbon in highly ordered diamond form at the detonation conditions.

This work will help researchers understand the detonation process over time to better predict the velocity and energy delivered by an explosive. The results will inform future product equation-of-state models for solid carbon in PBS 9502 detonation mixtures. Indeed, better modeling leads to better predictions regarding safety, security, and effectiveness of the U.S. nuclear deterrent. *— Dana Desonie*

See: Erik B. Watkins[1], Kirill A. Velizhanin[1], Dana M. Dattelbaum[1]*, Richard L. Gustavsen[1], Tariq D. Aslam[1], David W. Podlesak[1], Rachel C. Huber[1], Millicent A. Firestone[1], Bryan S. Ringstrand[1], Trevor M. Willey[2], Michael Bagge-Hansen[2], Ralph Hodgin[2], Lisa Lauderbach[2], Tony van Buuren[2], Nicholas Sinclair[3], Paulo A. Rigg[3], Soenke Seifert[4], and Thomas Gog[4], "Evolution of Carbon Clusters in the Detonation Products of the Tri-aminotrinitrobenzene (TATB)-Based Explosive PBX 9502," J. Phys. Chem. C **121**, 23129 (2017).
DOI: 10.1021/acs.jpcc.7b05637
Author affiliations: [1]Los Alamos National Laboratory, [2]Lawrence Livermore National Laboratory, [3]Washington State University, [4]Argonne National Laboratory
Correspondence: * danadat@lanl.gov

The authors acknowledge support from the U.S. Department of Energy (DOE) National Nuclear Security Administration (NNSA) and the Dynamic Material Properties program. The DCS is operated by Washington State University with support from the U.S. DOE-NNSA under Award Number DE-NA0002442. This work was performed, in part, at the Center for Integrated Nanotechnologies (CINT). CINT is funded by the DOE-Basic Energy Sciences. This research used resources of the Advanced Photon Source, a U.S. DOE Office of Science User facility operated for the DOE Office of Science by Argonne National Laboratory under Contract No. DE-AC02-06CH11357.

35-ID-B,C,D,E • DCS • Physics, materials science, geoscience • Time-resolved x-ray scattering, phase contrast imaging, radiography • 7-35 keV, 7-100 keV, 24-24 keV • On-site• Accepting general users •

Probing Nanoscale Microstructural Evolution Mechanisms in Aluminum Alloys by 4-D X-ray Nanotomography

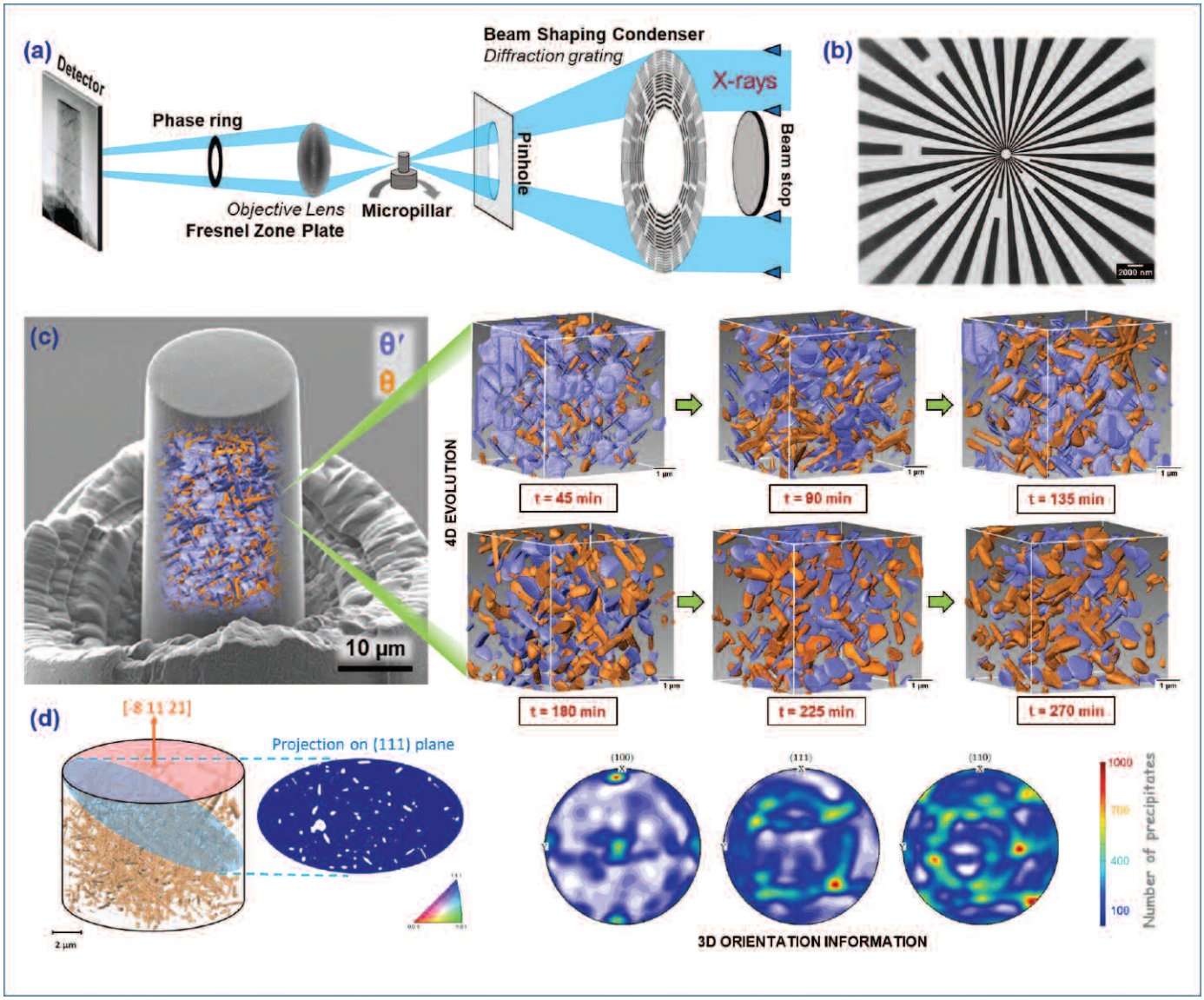

Fig. 1. (a) Schematic of the TXM setup showing its principle of operation. (b) Absorption radiograph of 100 nm Siemens star imaged using a 60-nm FZP objective lens. (c) Nanoscale 3-D rendering of microstructural evolution of θ' (Al_2Cu) and θ at T = 350° C in an Al-4%Cu alloy. (d) Schematic showing re-sectioning of the virtual microstructure to obtain inter-particle spacing (λ) from the (111) slip plane, and pole figure maps representing the 3-D crystallographic orientation of the maximum Feret diameter of the θ precipitates.

When a single-phase solid solution of aluminum (Al) and copper (Cu) is rapidly quenched, a supersaturated solid solution of Cu in Al forms that, on subsequent "aging" at elevated temperatures, yields the precipitation of various metastable, intermediate, second-phase particles. As the aging process continues, these particles undergo complex transitions in morphology and crystallographic structure and in their interfacial relationships with the aluminum matrix. The final outcome of this process is an alloy containing a three-dimensional (3-D) array of particles of various sizes, shapes, and compositions that play an important role in determining the strength of the material. The particles harden the alloy largely by impeding the movement of crystallographic dislocations, which are important sources of plasticity. Although understanding particle evolution is critical to modeling an alloy's mechanical and thermodynamic responses, much debate persists about the mechanisms driving the process. High-temperature studies carried out using transmission electron microscopy have been hampered by the fact that specimens need to be ultra-thin, thus giving essentially two-dimensional information about a 3-D process. Several models and theories have attempted to explain the interaction of dislocations with different kinds of particles, but lack experimental verification. A comprehensive model that accounts in 3-D for dislocation interactions with multimodal distributions of varying precipitate sizes remains lacking. Capitalizing on the capabilities of a new transmission x-ray microscope (TXM) at beamline 32-ID-B,C of the APS, researchers implemented synchrotron-based, absorption, full-field hard x-ray nanotomography, and answered some of the most fundamental metallurgical questions pertaining to precipitation-strengthened systems.

This instrument represents a new generation of full-field x-ray microscopes has emerged that allow 3-D analyses of large volumes of materials at unprecedented length scales, enabling the dawn of "four-dimensional (4-D) characterization" (time being the fourth dimension) and it is pushing the global frontiers of hard x-ray nanotomography, in that it is capable of imaging at energies up to 15 keV, with spatial resolutions of 20 and 60 nm. The researchers in this study, from Arizona State University, the Indian Institute of Technology Kanpur, and Argonne were able to measure the evolution kinetics of different nanoscale phases of Al-Cu alloys in 3-D for the first time, revealing insights into several observed novel phase transformation reactions. Their experimental results lent support to particle coarsening models from the Lifshitz-Slyozov-Wagner (LSW) theory to an unprecedented extent, thereby establishing a new paradigm for thermodynamic analysis of precipitate assemblies. The study also shed light on the possibilities for establishing new theories for dislocation–particle interactions. Another important advancement in this work was the correlation of nanotomography and electron backscatter diffraction (EBSD) data to obtain 3-D crystallographic orientation information.

Al-4wt%Cu samples were aged at 350° C and 400° C. Imaging was performed using a monochromatic beam at 9.1 keV, just above the Cu K-edge, to maximize contrast between the Al_2Cu and Al phases. Tomograms were obtained at all aging conditions, making it possible for the first time to track 3-D microstructural changes in bulk at the 60-nm length scale. Aging the samples at 350° C revealed complex transformation reactions that were occurring in the alloys, most of which are nearly impossible to capture using other characterization techniques.

The Al-4wt%Cu alloy was aged at 400° C to closely monitor the coarsening of the θ phase alone. The experiments rendered a more thorough understanding of the coarsening behavior of the θ phase through the 3-D measurements. A transition from interface-controlled to volume diffusion-controlled growth in thickness was captured from scaled precipitate size distribution curves, and a validation of the LSW theory was carried out. The study utilized a unique correlative approach, bridging tomography data with EBSD, allowing experimental estimation of Orowan strengthening as well as quantification of the preferred orientation of the θ phase in 3-D.

The experiments demonstrated the ability to virtually probe the 3-D microstructure at the nanoscale and nondestructively quantify parameters such as the critical precipitate shearing stress, Orowan looping stress, and inter-precipitate dislocation cell size, which is a colossal step that can have seminal implications in predicting the mechanical responses of many high-performance materials. — *Vic Comello*

See: C. Shashank Kaira[1], V. De Andrade[2], Sudhanshu S. Singh[1,3], C. Kantzos[1], Antony Kirubanandham[1], F. De Carlo[2], and Nikhilesh Chawla[1]*, "Probing Novel Microstructural Evolution Mechanisms in Aluminum Alloys Using 4D Nanoscale Characterization," Adv. Mater. **29**, 1703482 (2017). DOI: 10.1002/adma.201703482
Author affiliations: [1]Arizona State University, [2]Argonne National Laboratory, [3]Indian Institute of Technology Kanpur
Correspondence: * nchawla@asu.edu

The authors are grateful for financial support from the Army Research Office (ARO) under Contract No. W911NF1410550. This research used resources of the Advanced Photon Source, a U.S. Department of Energy (DOE) Office of Science user facility operated for the U.S. DOE Office of Science by Argonne National Laboratory under Contract No. DE-AC02-06CH11357.

32-ID-B,C • Materials science, life sciences, geoscience • Phase contrast imaging, radiography, transmission x-ray microscopy, tomography • 7-40 keV • On-site • Accepting general users •

How Far Can Thin Films Stretch?

Researchers are interested in using piezoelectric materials, which change shape in response to an applied voltage, for a variety of applications, including a new type of transistor that could be faster and less power-hungry than existing silicon transistors. To build such devices, they have to understand exactly how much the piezoelectric deforms under voltage, and how they can design the material to get the desired results. A group of scientists has used the APS to measure just how much a piezoelectric thin film moves under particular conditions.

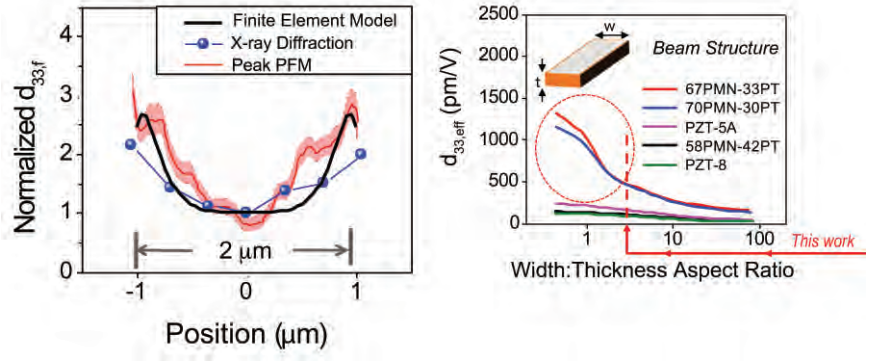

Fig. 1. The normalized piezoelectric response of the thin film, measured in pm V^{-1}, over the width of the feature from the clamped center to the declamped sidewalls was in good agreement between the model and two experimental measurements (left). The aspect ratio of the film affects its response for a variety of materials (right).

Engineers would like to use piezoelectric thin films to build devices such as piezoelectronic transistors (PETs). In a PET, applying a voltage causes the film to push against a piezoresistive element, closing a circuit and switching it on. Such a transistor might have 10 times the switching speed of a silicon transistor but operate on a tenth of the power. Thin films, however, are limited in how much they can deform by the fact that they're attached to a substrate. To stretch in one direction — to get thicker — they have to contract in another, a movement that's inhibited by being stuck on their base. The researchers from The Pennsylvania State University, the University of Connecticut, North Carolina State University, and Auburn University wanted to determine how much deformation they could achieve, a quantity known as the piezoelectric coefficient, if they detached portions of the film from the substrate.

They started by growing a 300-nm-thick thin film 70% lead magnesium niobate and 30% lead titanate on a platinum-coated silicon substrate. They then used reactive ion etching to pattern the film into strips that ranged from 0.75- to 9-μm wide with sidewalls that were unattached to anything, a process called "declamping." They knew from the literature that the ratio of the strip's width to its thickness affects the degree of declamping, with lower ratios leading to better functional properties.

The researchers assessed the piezoelectric coefficient by three methods. One was a numerical modeling approach, finite element modeling (FEM), which provided a theoretical measurement. The other two were experimental. They utilized piezoresponse force microscopy, a type of atomic force microscopy that measures the out-of-plane displacement when a voltage is applied. The probe's tip is so small that it provides good lateral resolution, but its absolute vertical accuracy is poor.

To make quantitative measurements of the vertical movement, the team performed synchrotron x-ray diffraction at the XSD 2-ID-D beamline of the APS. This nanoprobe beamline can focus the x-ray beam down to a spot size of 240 nm (the full width at half the maximum of the beam's intensity), providing good resolution. They also moved the spot across the sample in sub-micron steps, allowing them to map the thin film and its displacement.

The three methods all found that the film showed a piezoelectric coefficient of 40 to 50 pm V^{-1}, under an excitation of 200 kV cm^{-1}, where they were most strongly attached to the substrate, but rose to approximately 160 pm V^{-1} at the sidewalls, where they were declamped (Fig. 1). The freedom at the sidewalls caused the material to behave as if it were partially declamped over a distance of about 500 to 600 nm into the structure. The researchers also found that the coefficient increased as the ratio of width to thickness got smaller. The experiment was limited to the 240-nm spot size of the x-ray beam, but the FEM results predict that the average response will get better with smaller aspect ratios. *— Neil Savage*

See: Ryan Keech[1], Linghan Ye[2], James L. Bosse[2], Giovanni Esteves[3], Jonathon Guerrier[3], Jacob L. Jones[3], Marcelo A. Kuroda[4], Bryan D. Huey[2], and Susan Trolier-McKinstry[1]*, "Declamped Piezoelectric Coefficients in Patterned 70/30 Lead Magnesium Niobate-Lead Titanate Thin Films," Adv. Funct. Mater. **27**, 1605014 (2017).
DOI: 10.1002/adfm.201605014
Author affiliations: [1]The Pennsylvania State University, [2]University of Connecticut, [3]North Carolina State University, [4]Auburn University
Correspondence:
* STMcKinstry@psu.edu

The authors gratefully acknowledge the assistance of Zhonghou Cai at beamline 2-ID-D of the APS. This work was funded by Pennsylania State University MRSEC (NSF DMR-1420620) and National Science Foundation (NSF) DMR-1410907, NSF-IMR-0817263, and DOE-BES-ESPM project DE-SC0005037 (UConn), and NSF DMR-1409399 (NC State). Initiative through Grant GBMF4374. This research used resources of the Advanced Photon Source, a U.S. Department of Energy (DOE) Office of Science user facility operated for the DOE Office of Science by Argonne National Laboratory under Contract No. DE-AC02- 06CH11357.

Soft Materials & Liquids

Roll Up, Roll Up Your Amphiphiles

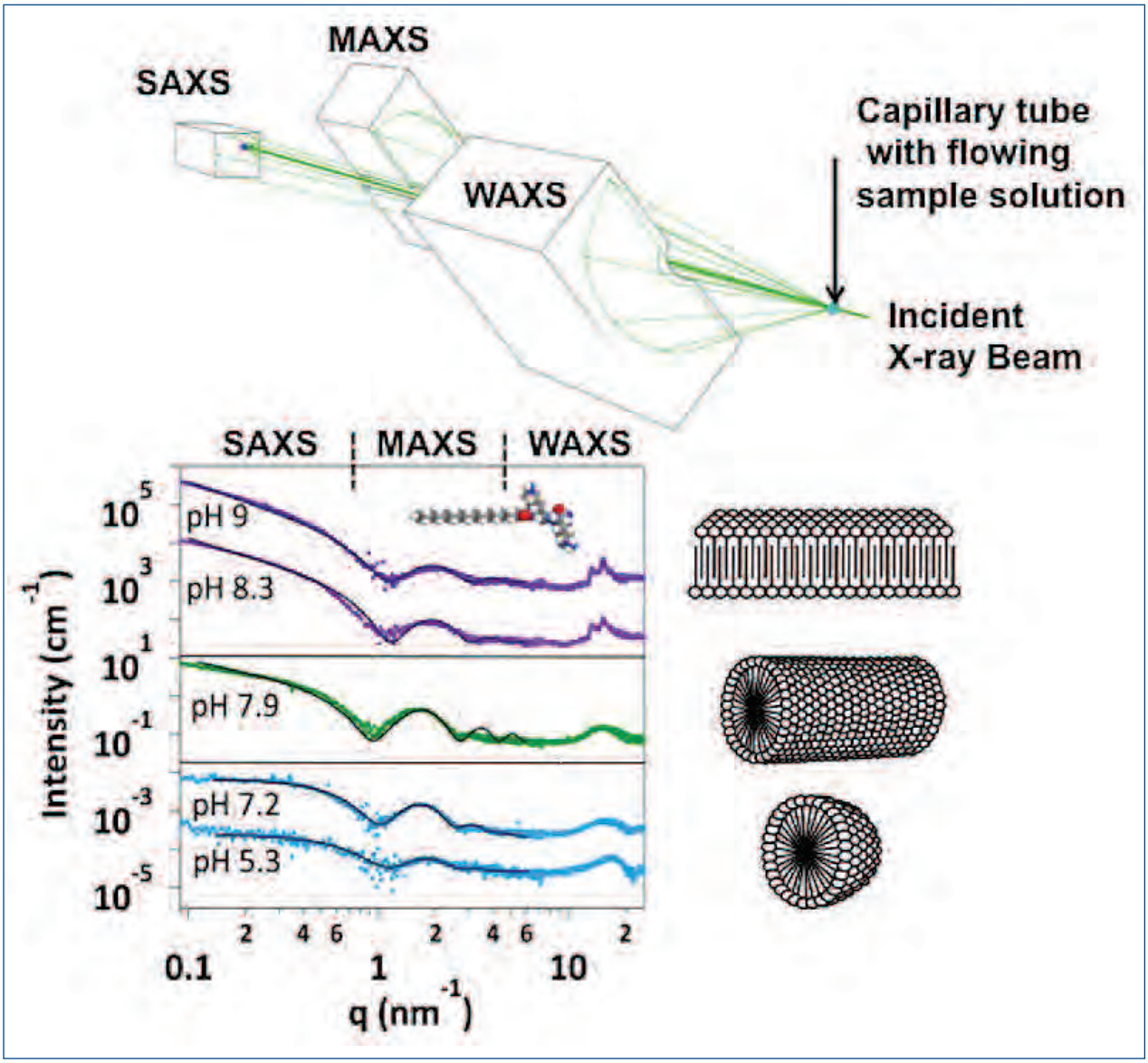

Fig. 1. SAXS/MAXS/WAXS combine forces at the APS to provide detailed information about how amphiphilic molecules form spherical micelles, roll up into tubes or can be laid out as flat bilayer sheets.

5-ID-B,C,D • DND-CAT • Materials science, polymer science, chemistry • Powder diffraction, x-ray standing waves, x-ray optics development/ techniques, small-angle x-ray scattering, surface diffraction, x-ray reflectivity, wide-angle x-ray scattering • 6-17.5 keV • On-site • Accepting general users •

12-ID-B • XSD • Chemistry, materials science, life sciences, polymer science, physics • Small-angle x-ray scattering, grazing incidence small-angle scattering, wide-angle x-ray scattering, grazing incidence diffraction • 7.9-14 keV • On-site • Accepting general users •

Researchers working at the APS investigated the transformation of assemblies of amphiphiles, molecules having a polar water-soluble group attached to a water-insoluble hydrocarbon chain. The amphiphiles under study were those that form micelles, microscopic molecular bubbles that can utilized to model the structure of a cell membrane and help us improve our understanding of the way the body works. Micelles can also mimic some of the properties of the cell membranes in a laboratory or even industrial context, filtering out toxic chemicals from water, detecting trace elements and drugs in environmental and medical samples, and even cleaning up contaminated wasteland. The study provides a facile method for manipulating the assembly structures of charged molecules as required for given applications.

This research, involving *in situ* small, medium, and wide-angle x-ray scattering (SAXS/MAXS/WAXS) at the DND-CAT 5-ID-B,C,D and XSD 12-ID-B beamlines at the APS, observed for the first time the corresponding cylindrical micelles and bilayer sheets. The results show precisely how tuning the molecular charge and intermolecular interactions via the pH (the potential of hydrogen, a logarithmic scale used to specify the acidity or basicity of an aqueous solution) gives rise to different micellar structures. Of particular interest is the bilayer structure, which is typically not expected for molecules with a head group much larger than the tail. The x-ray experiments reveal that such molecules can assemble into bilayers if the tails of the two leaflets interdigitate.

Soap, or surfactant, molecules are two-faced, or double ended. At the head they are water loving, hydrophilic, at the tail end they repel water, they are hydrophobic, or put another way oil-loving (lipophilic). It is this chemical ambivalence that allows them to break up oily compounds in water, such as the grease on your dishwashing or the dirt and stains on your laundry. Surfactant molecules are thus known as amphiphilic, they have two characteristics in one. Add a surfactant to water and the molecules will form aggregates in which their lipophilic tails all congregate together within a bubble like structure with the hydrophilic heads looking out at the water molecules in which they find themselves. A larger version of the micelle is the liposome in which there is a hydrophilic hollow within the "bubble," Similarly, if there are constraints that preclude formation of a sphere a cylindrical micelle can be formed. Also, spread out as a layer on a watery surface or a polar layer, and the amphiphilic molecules will form a bilayer in which the tails are sandwiched in between two layers of hydrophilic heads.

The micelle, liposome and bilayer sheets formed by surfactants are well studied because of their resemblance to the membranes of cells in our bodies. They can be used to hold other small molecules, have holes punched in them and be used to model the physical and chemical properties of membranes. A realistic model of an object can, of course, carry out some of the functions of that object, albeit imperfectly. But, conversely imperfect does not necessarily mean inappropriate, the simplicity of a micelle compared to a real cell membrane makes them easier to manipulate and they might, nevertheless, offer useful functionality in a wide range of situations from the biomedical laboratory to industrial cleanup.

There are a vast number of amphiphilic molecules any one of which might generate micelles and bilayers with specific properties for a particular application. One class of amphiphiles of growing interest is those in which the tail is an alkyl hydrocarbon group, not dissimilar to the molecular structure of different oil molecules. The head of those amphiphiles comprises a short sequence of amino acids, the building blocks of peptides and proteins. The oily tail is lipophilic, while the acidic heads are charged and thus hydrophilic and so can dissolve in water while the water repels the tails.

Of particular interest is the presence of different charged amino acids in the same head. For such molecules, adjusting the acidity or alkalinity, the pH, of the solution can change the charge state of the head group and the intermolecular electrostatic interactions. Thus, the aggregation state of the molecules (micelles, liposomes etc.) may be reconfigured by changing the pH.

— David Bradley

See: Changrui Gao, Honghao Li, Yue Li, Sumit Kewalramani, Liam C. Palmer, Vinayak P. Dravid, Samuel I. Stupp, Monica Olvera de la Cruz*, and Michael J. Bedzyk**, "Electrostatic Control of Polymorphism in Charged Amphiphile Assemblies," J. Phys. Chem. B **121**, 1623 (2017).
DOI: 10.1021/acs.jpcb.6b11602
Author affiliation:
Northwestern University
Correspondence:
* m-olvera@northwestern.edu,
** bedzyk@northwestern.edu

This research was primarily supported by the U.S. Department of Energy (DOE) Office of Basic Energy Sciences under Contract DE-FG02-08ER46539. Additional support to L.C.P and S.I.S. for peptide synthesis was provided by the National Science Foundation (Grant DMR-1006713). DND-CAT is supported by Northwestern University, E.I. DuPont de Nemours & Co., and The Dow Chemical Company. The APS, an Office of Science user facility operated for the DOE by Argonne National Laboratory, is supported by the DOE under Contract DE-AC02-06CH11357. The authors thank S. Weigand (DND-CAT) and B. Lee (APS, Sector 12) for assistance with the x-ray scattering measurements. This research used resources of the Advanced Photon Source, a U.S. DOE Office of Science user facility operated for the U.S. DOE Office of Science by Argonne National Laboratory under Contract No. DE-AC02-06CH11357.

Gel Formation Revealed

Knowledge about colloidal gel formation and dissolution has implications for understanding the preparation and stability of many consumer goods such as milk and yogurt, and personal care products such as cosmetics. At the same time, more fundamentally, colloidal gels exhibit physical behavior that can help address challenging scientific problems such as the formation, stability, and dynamics of glasses. Studies by a research team utilizing high-brightness x-rays from the APS provides important insight into a key question that has long puzzled scientists in the field, namely, why do nanoparticle gels take so long to form after a quench even though the constituent nanoparticles are rapidly diffusing through the suspension?

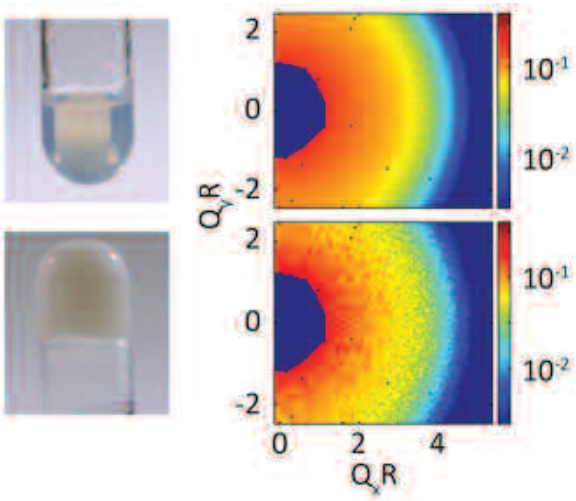

Fig. 1. Left panels: Pictures of a colloidal nanoparticle suspension in its fluid state (top) and gel state (bottom). Right panels: time-average coherent x-ray scattering patterns for a colloidal suspension just after (top) and well after (bottom) it has been quenched into the gel-forming regime. The irregular shape centered at 0,0 is the shadow of a beam stop that protects the detector from the damaging direct x-ray beam while the isolated blue dots in the images are defective sensor elements. Both are excluded from the data processing.

A gel is formed when particles suspended in solution become unstable to aggregation, ultimately forming a system spanning network that imparts mechanical rigidity to the system. The time required for this process can vary from a fraction of a second to many hours depending on the concentration of the particles and the strength of their attraction for one another. This sensitivity creates a scientific challenge that is central to the field of soft matter but also an opportunity for designing suspensions with properties tailored for specific applications, such as those noted above. The researchers studied this transformation from fluid to gel in aqueous suspensions of nanometer-scale silica particles. Taking advantage of newly developed x-ray scattering capabilities and the ability to precisely tune the strength of the particle attractions, the scientists were able to track the evolution in the microscopic organization and mobility of the particles and correlate these properties with the time-dependent macroscopic mechanical behavior of the suspensions. They found that the rate of gel formation is surprisingly sensitive to the strength of attraction, but that the suspensions proceed through identical intermediate states of microscopic and macroscopic behavior even as the time needed to form a gel varies by orders of magnitude. To explain these observations, they propose a model of gel formation in the regime of weak attraction in which network formation is a hierarchical process whose initiation depends on the creation and stability of small clusters in which the particles arrange in particularly favorable configurations.

The intermediate concentration gels that the researchers from Argonne , FAMU-FSU College of Engineering, AGH University of Science and Technology (Poland), and Johns Hopkins University chose to study are particularly intriguing because there remain many unanswered questions about the mechanisms by which such gels form from a suspension of rapidly diffusing constituent nanoparticles. The left panels of Fig. 1 are pictures of a colloidal nanoparticle suspension like the one the researchers studied. The upper left picture is the suspension in its fluid state while the lower left is it in its gelled state. The gelled suspension appears milky and does not fall out of the test tube because of the formation of a large-scale mechanically rigid structure in the gel.

For the reasons outlined above, gels have been studied for many years utilizing a variety of experimental techniques such as confocal microscopy and light, neutron, and x-ray scattering, as well as via simulation tools such as molecular dynamics. In particular, previous x-ray photon correlation (XPCS) studies performed at the APS [H. Guo et al., J. Chem. Phys. **135**, 154903 (2011)], were able to examine slower formation and aging behavior of gels, but were unable to reveal how the colloids in suspension transitioned from a fluidized state at higher temperatures to an almost fully immobile state in the gel. XPCS measures fluctuating coherent scattering patterns to provide information about motion in materials at the nanoscale. To date, a key shortcoming of the technique has been limited detector speed that restricts the range of fluctuations that can be measured.

To address this shortcoming, the current experiment team worked closely with pixel-array x-ray detector developers at the AGH University of Science and Technology to commission and then deploy the world's first XPCS-suitable (ultrafast, x-ray-photon-counting, pixel-array detector, or UFXC) area detector for measurements at the XSD 8-ID-I beamline at the APS. The detector is nearly ten times faster than any device available on the commercial market and pro-

vided the researchers with an unprecedented view of the early stages of gel formation.

To obtain information about the formation of the gel, the researchers started with the nanoparticle suspension at a higher temperature, when it is in its fluidized state, and then rapidly quenched it to temperatures at which a gel forms. The UFXC detector was then used to repeatedly measure "video clips" of the gel formation as a function of time after the quench to lower temperature was complete. The right panels of Fig. 1 show the time-average coherent scattering patterns measured just after (upper right) and well after (lower right) a quench. The upper-right pattern is smooth or blurred because the constituent nanoparticles were moving rapidly during the data collection period while the lower-right pattern is speckled or grainy, because the nanoparticles are now mostly frozen in position.

The coherent scattering patterns collected by the UFXC can be used to measure the dynamic properties (the so-called time autocorrelation decay functions) of the nanoparticle suspension as a function of time after it has been quenched into the gel-forming regime. Fig. 2 shows autocorrelation functions for three such quenches. Squares are the correlation points for a 1.5-K quench below the gel temperature while the circles and diamonds are for 1.25-K and 1.0-K quenches. The curve labelled A was obtained soonest after the quench, while that labelled G was obtained latest. The time scale of the decay from the maximum amplitude of the traces on the left to the minimum on the right provides a measure of how dynamic the nanoparticles are. Soon after the quench (A curves), the decay is rapid, indicating motion of small clusters of nanoparticles while long after the quench (G curves), the decay is incomplete indicating that the nanoparticle motion has largely been arrested and that the gel is nearly fully formed. The illustrations in the lower left and upper right of Fig. 2 are schematic illustrations of the microscopic state of the suspension at these two extremes of observed behavior.

The most intriguing part of the research performed by the team was the finding that the shapes that the correlation decays exhibit as the gel forms after the quench are identical irrespective of the quench temperature, i.e., each curve (A–G) is comprised of points from different quenches that lie atop one another. The only difference observed between the behavior of different quench temperatures was how long after the quench the scientists had to wait to observe an overlapping correlation function. For instance, curve D in Fig. 2 was measured 658 s after the quench to 1.5 K below the gel temperature (squares), while curve D was also measured after 1156 s and 1856 s, respectively, for 1.25-K and 1.0-K quenches. Similar observations were also made using a rheometer that measures the solid-like nature of the suspension and also by carefully examining the time-average scattering patterns like those presented in the right panels of Fig. 1.

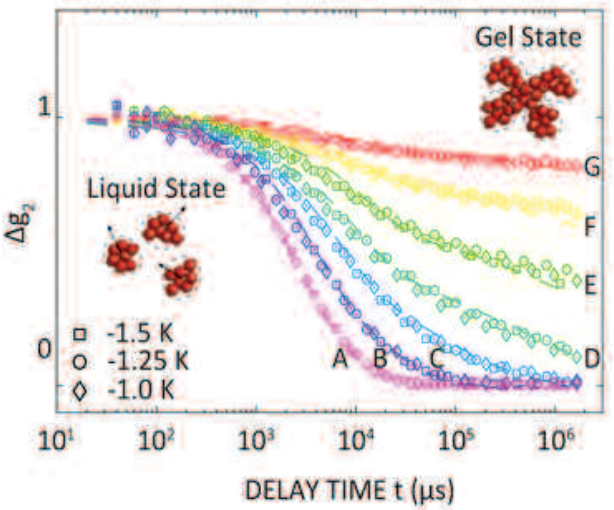

Fig. 2: Time autocorrelation decay functions indicating the dynamic state of the nanoparticle suspension after three different quenches into the gel-forming regime. Each of the curves (A–G) is comprised of data points obtained from the three quenches listed in the legend with the only difference being how long after the quench the same decay functions were measured. The lines through the data points are guides-to-the-eye. The microscopic structures of the gel in its liquid and gelled states are shown schematically in the figure.

This work suggests that gel formation occurs via the formation of highly favored small clusters of nanoparticles like those illustrated schematically in the lower left of Fig. 2, and via relatively slow diffusion; the clusters interact and form a space-spanning gel structure like that shown schematically in the upper right of Fig. 2. The work provides important insight into a key question that has long puzzled scientists in the field, namely, why do nanoparticle gels take so long to form after a quench even though the constituent nanoparticles are rapidly diffusing through the suspension? The UFXC detector provided the team with a unique opportunity to observe the early formation process of a gel and demonstrated that with the right tools, XPCS at markedly faster time scales will be possible with the dramatic gains in coherent flux that proposed APS Upgrade will provide.

See: Qingteng Zhang[1], Divya Bahadur[2], Eric M. Dufresne[1], Pawel Grybos[3], Piotr Kmon[3], Robert L. Leheny[4], Piotr Maj[3], Suresh Narayanan[1], Robert Szczygiel[3], Subramanian Ramakrishnan[2], and Alec Sandy[1]*, "Dynamic Scaling of Colloidal Gel Formation at Intermediate Concentrations," Phys. Rev. Lett. **119**, 178006 (25 October 2017). DOI: 10.1103/PhysRevLett.119.178006

Author affiliations: [1]Argonne National Laboratory, [2]FAMU-FSU College of Engineering, [3]AGH University of Science and Technology, [4]Johns Hopkins University

Correspondence: * asandy@anl.gov

S.R. thanks the Argonne National Laboratory XSD Visiting Scientist program for support. S.R. and R.L. acknowledge support from the NSF through CBET-1336166. This material is based upon work supported by Laboratory Directed Research and Development (LDRD) funding from Argonne National Laboratory, provided by the Director, Office of Science, of the U.S. Department of Energy under Contract No. DE-AC02-06CH11357. AGH University of Science and Technology was supported by the National Center for Research and Development, Poland, PBS1/A3/ 12/2012. This research used resources of the Advanced Photon Source, a U.S. DOE Office of Science user facility operated for the DOE Office of Science by Argonne National Laboratory under Contract No. DE-AC02- 06CH11357.

Diblock Copolymer Melts Mimic Metallic Alloys When Thermally Processed

Understanding how atoms and molecules fill space to form solids and liquids has challenged mathematicians, scientists, and technologists since antiquity. While the self-assembly of "soft" materials — including surfactants and lipids, supramolecular assemblies, and block polymers — has long been thought to be governed by very different molecular packing phenomena than those of "hard" materials, such as metals and alloys, evidence of some similarities between the two has recently emerged. Accordingly, a team of scientists sought to build on this body of new data by exploring how thermal processing influences the nucleation and growth of order in compositionally asymmetric low-molar-mass 1,4-poly(isoprene)-b-poly(±lactide) (PI-PLA) diblock copolymer melts by cooling them from the disordered state to temperatures below the order-disorder transition (TO_{DT}) temperature. The two-pronged study involved self-consistent field theory (SCFT) calculations and small-angle x-ray scattering (SAXS) experiments conducted at the APS. The resulting observations suggested enticing analogies between the underlying mechanisms responsible for symmetry-breaking in hard and soft matter. *Cont'd. on the next page*

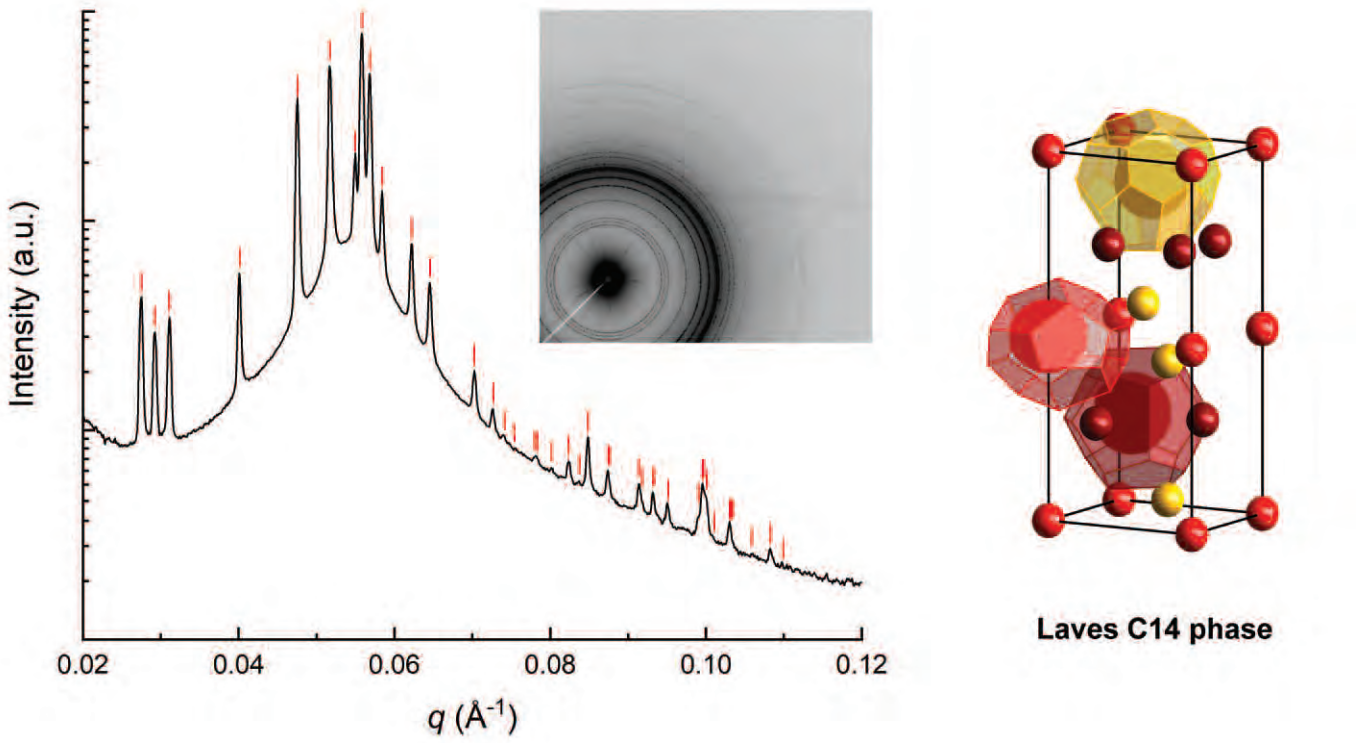

Fig. 1. Small-angle x-ray scattering pattern of the C14 Laves phase obtained from a 1,4-poly(isoprene)-b-poly(±lactide) (PI-PLA) diblock copolymer after rapidly cooling the disordered melt in liquid nitrogen and reheating to just below the order-disorder transition. The unit cell of the C14 Laves phase contains 12 micelles with 3 different polyhedral shapes as determined using self-consistent field theory.

Block polymers are uniquely tunable self-assembling soft materials, making them ideal model materials for fundamental inquiries into the formation and stability of soft quasicrystals. In most asymmetric variants, diblock copolymers form point particles, nominally spherical in shape. When packed together in the absence of a diluent, these "soft" micelles are forced to assume polyhedral shapes such that space is filled without voids while maintaining the uniform density dictated by short-range liquid-like packing of chain segments. Until recently, theory and experiments supported the notion that the universal equilibrium state is a body centered cubic (bcc) arrangement of such particles.

The SCFT calculations showed that Laves and Frank-Kasper phases commonly found in alloys have nearly degenerate free energies, suggesting that processing history would drive the materials into long-lived metastable states defined by populations of self-assembled particles having different volumes and polyhedral shapes. Guided by these calculations, the researchers from the University of Minnesota subjected two PI-PLA diblock copolymer melts to two different thermal treatments. The melts were either cooled directly to $T < T_{ODT}$ (at about 2° C/sec) or immediately submerged into liquid nitrogen ($T = -196$°C) then reheated to $T < T_{ODT}$ and held at final target temperatures for up to 20 days.

The SAXS studies carried out at the DND-CAT 5-ID-B,C,D and XSD 12-ID-B beamlines at the APS revealed that a sample containing a PLA block component at 15 volume percent became ordered as bcc and the Frank-Kasper σ phases upon being cooled directly to 70° C and 55° C, respectively. On the other hand, such a sample that was rapidly quenched to –196° C and reheated to 25° C developed a liquid-like packing (LLP) configuration. At 35° C, a SAXS pattern associated with the dodecagonal quasicrystalline phase emerged after several days, whereas heating to 85° C produced a Laves C14 phase (Fig. 1). Increasing the PLA block volume from 15 to 20% at about the same molar mass resulted in a different complement of ordered structures during thermal processing. When cooled directly to 80° C, the sample transformed rapidly to the hexagonally packed cylinder phase, while quenching the sample from –196° C to 25° C again resulted in the LLP state, with the Laves σ phase emerging at 85° C and a SAXS pattern consistent with the Laves C15 phase fully forming after several days at 100° C. This unprecedented set of results reinforces the conclusion drawn from the SCFT calculations that processing history can lead to multiple metastable particle packing arrangements.

The researchers explain these results by pointing out that the spatial arrangement of self-assembled diblock copolymer micelles depends on the distribution of particle sizes and short-range repulsive interactions. However, unlike individual atoms, each micelle can spontaneously adjust its size by shedding or absorbing diblock copolymer chains, leading to a distribution of particle volumes. At equilibrium, the average particle diameter increases with decreasing temperature, so rapidly supercooling the disordered melt to $T < T_{ODT}$ (e.g., by immersion in liquid nitrogen) drives the material far out of equilibrium. As the quenched material is heated above the glass transition temperature, rearrangement of the particle sizes through fusion, fission, and chain diffusion stabilizes a state of local packing that guides nucleation and growth of long-range order along a path on the free-energy surface that funnels into a local minimum associated with one of the low-symmetry phases. Once formed, free-energy barriers trap the various Frank-Kasper and quasicrystalline phases for long times. Cooling the disordered melt directly to temperatures where block copolymer diffusion remains rapid allows the system to continuously adjust the distribution of particle sizes, accessing alternative paths on the free-energy surface leading to the development of different states of order.

These results reinforce fundamental analogies between the way metals and self-assembled soft materials break symmetry when subjected to changes in thermodynamic state variables that drive phase transitions. Competition between lattice symmetry and the drive to minimize system free energy through tailoring the overall size and shape of the polyhedral micelles in real space has intriguing analogies with the competition between the packing configurations of metal atoms, where the tendency for the electronic configuration to support a nearly spherical Fermi surface can induce transitions to low-symmetry reciprocal-space lattices. The exquisite control over block polymer molecular structure afforded by controlled polymerization offers opportunities to unravel the basic principles that define order and disorder in condensed matter. *— Vic Comello*

See: Kyungtae Kim, Morgan W. Schulze‡, Akash Arora, Ronald M. Lewis III, Marc A. Hillmyer, Kevin D. Dorfman,** and Frank S. Bates*, "Thermal Processing of Diblock Copolymer Melts Mimics Metallurgy, Science **356**, 520 (2017).
DOI: 10.1126/science.aam7212
Author affiliation: University of Minnesota ‡Present address: University of California, Santa Barbara
Correspondence:
** dorfman@umn.edu,
* bates001@umn.edu

This work was supported by the National Science Foundation under grants DMR-1104368 and DMR-1333669. DND-CAT is supported by E. I. DuPont de Nemours and Co., The Dow Chemical Company, and Northwestern University. This research used resources of the Advanced Photon Source, a U.S. DOE Office of Science user facility operated for the U.S. DOE Office of Science by Argonne National Laboratory under Contract No. DE-AC02-06CH11357.

5-ID-B,C,D • DND-CAT • Materials science, polymer science, chemistry • Powder diffraction, x-ray standing waves, x-ray optics development/ techniques, small-angle x-ray scattering, surface diffraction, x-ray reflectivity, wide-angle x-ray scattering • 6-17.5 keV • On-site • Accepting general users •cepting general users •

12-ID-B • XSD • Chemistry, materials science, life sciences, polymer science, physics • Small-angle x-ray scattering, grazing incidence small-angle scattering, wide-angle x-ray scattering, grazing incidence diffraction • 7.9-14 keV • On-site • Accepting general users •

Unravelling the Mystery of Nanoparticle-Reinforced Polymers

A transformative discovery was that the addition of nano-sized particles can mechanically reinforce a polymeric matrix. The resulting flexible composite forms a lightweight, yet strong material that is of considerable commercial interest. Examples over the last century include the clay-reinforced resin used in common household goods ("bakelite"), nanoparticle-toughened rubber for automobiles, and mica-reinforced nylon with a 5-fold increase in yield and tensile strength. The growing availability of nanoparticles with precise size and shape and properties, combined with the development of high-resolution characterization techniques, has spurred even greater interest in nanoparticle-polymer composites, which have potential applications in aerospace, defense, transportation, biomaterials, and energy storage and conversion. A team of researchers exploited the power of the APS as a means of tracking, for the first time, the motion of a high concentration of silica nanoparticles in polymer melts relevant to commercial polymer nanocomposite applications. Motion of nanoparticles in polymeric melts has so far been investigated only in the dilute nanoparticle regime due to the challenges in dispersing nanoparticles in polymer melts at high volume fractions and the sensitivity of the particle dynamics to the morphology of the resulting aggregates.

At present, development of polymer melt materials is hampered by a lack of understanding of the reinforcement mechanism, which is much debated. Most of the previously proposed reinforcement mechanisms focus on polymer mobility in the presence of nanoparticles. However, since the reinforcement is a combined effect of polymer, particle, and the interphases in between, understanding how particle motion is affected as the nanocomposite gets stronger is equally important.

To begin, the team of researchers from the National Institute of Standards and Technology, the University of Maryland, and Argonne took advantage of the favorable interaction between polymer and nanoparticles to prepare a uniform dispersion of silica nanoparticles in a polyethylene oxide melt with a particle volume fraction up to 42%. In preparing this material, they dissolved the polyethylene oxide in acetonitrile solvent and added silica nanoparticles into the polymer solution. The mixtures were then sonicated and vigorously stirred. Finally, the samples were dried under a fume hood, annealed above the melting temperature of the polymer for solvent removal, and molded to sizes of 1-mm diameter and 0.8-mm thickness. The resulting composite samples had particle volume fractions of 2.5% to 42%. Using x-ray photon correlation spectroscopy (XPCS) at XSD beamline 8-ID-I of the APS, the team was able to follow the slow nanoscale motion of the nanoparticles ("relaxation") in the polymer composites over a length scale of 20-200 nm and time scale of 10 msec to 2000 sec.

At the lowest concentrations of 2.5%, the nanoparticles were well separated; thus, the isolated nanoparticles exhibited simple diffusion, unhindered by the presence of other nanoparticles. At the highest concentration of 42%, all polymer chains were practically in direct contact with the nanoparticles; thus, the response was solely from nanoparticles with overlapping bound chains. The composite with 28% nanoparticles presented a rather "hyperdiffusive" (faster than diffusion) behavior but with faster nanoparticle relaxation times. The samples with intermediate concentrations of 8% and 17% presented the features of both dilute and concentrated polymer-nanoparticle composites.

At high concentrations, the nanoparticles served as both fillers for the resulting polymer nanocomposites and probes for the viscoelasticity of the surrounding polymer medium. The slow particle motion allowed the observation of reinforcement in the nanocomposites from the "eyes" of the nanoparticles. The results from XPCS as well as rheological measurements showed that the nanoparticles unexpectedly remain mobile at high concentrations whereas the elastic modulus of the composites increases by three orders of magnitude. Such decoupling of polymer and nanoparticle dynamics has not been reported before and should lead to new experiments and simulations with potentially novel findings. These results call for revising the current thinking on both the reinforcement mechanism in polymer nanocomposites and nanoparticle motion in reinforced polymers.

— Joseph E. Harmon

See: Erkan Senses[1,2*‡], Suresh Narayanan[3], Yimin Mao[1,2], and Antonio Faraone[1**], "Nanoscale Particle Motion in Attractive Polymer Nanocomposites," Phys. Rev. Lett. **119**, 237801 (2017). DOI: 10.1103/PhysRevLett.119.237801
Author affiliations: [1]National Institute of Standards and Technology, [2]University of Maryland, [3]Argonne National Laboratory ‡Present address: Koc University
Correspondence: * esenses@ku.edu.tr, ** antonio.faraone@nist.gov

This work used resources of the Advanced Photon Source, a U.S. DOE Office of Science user facility operated for the DOE Office of Science by Argonne National Laboratory under Contract No. DE-AC02-06CH11357.

Melting a Solid Below the Freezing Point

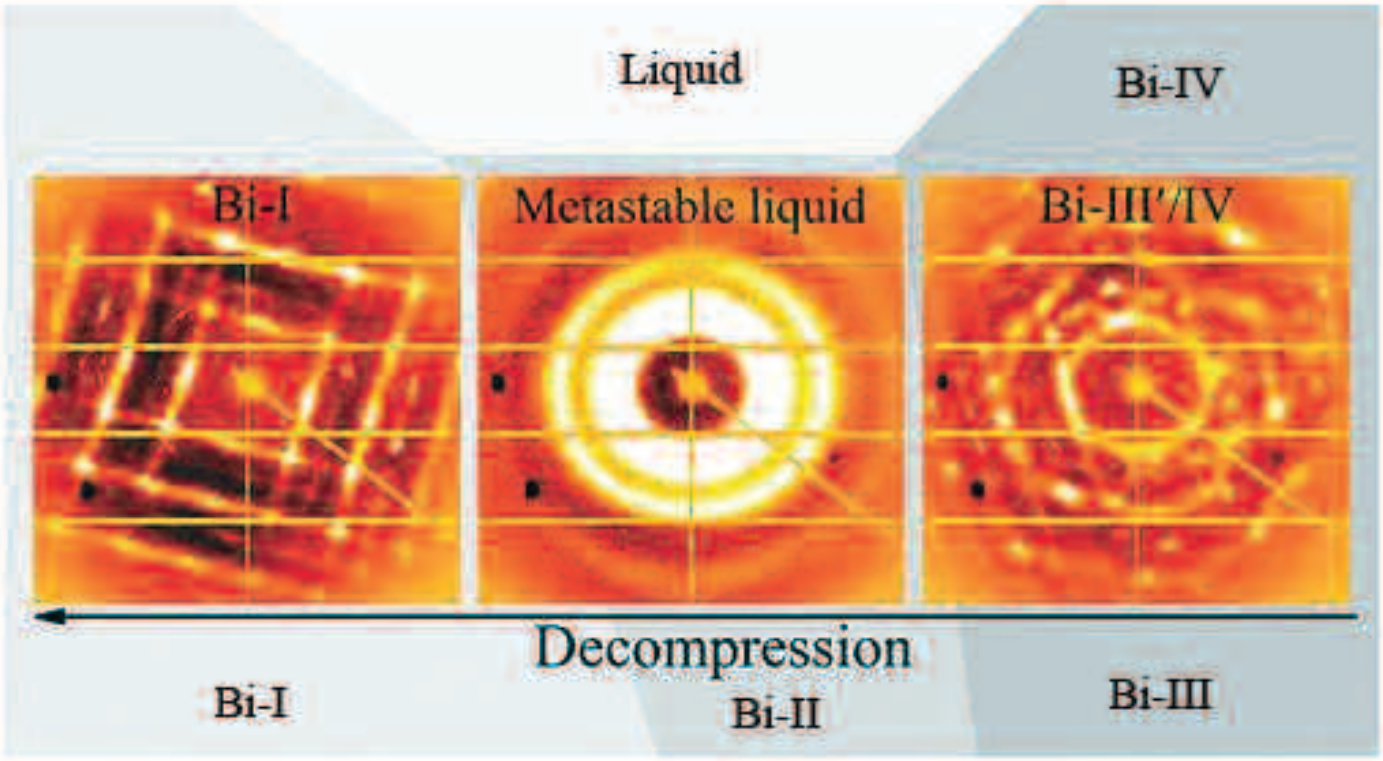

When a crystal structure of bismuth (right) is decompressed from 32,000 atmospheres (3.2 GPa) to 12,000 atmospheres (1.2 GPa) it melts into a liquid at about 23,000 atmospheres (2.3 GPa) (middle). It then recrystallizes at 12,000 atmospheres (left). The so-called metastable liquid produced by this decompression occurs in a pressure-temperature range similar to where the supercooled bismuth is produced; supercooled liquids are cooled below the freezing point without turning into a solid or a crystal. Image courtesy Chuanlong Lin and Guoyin Shen

The original Carnegie Institution for Science press release can be read at: https://carnegiescience.edu/node/2128

Phase transitions surround us — for instance, liquid water changes to ice when frozen and to steam when boiled. Now, researchers at the Carnegie Institution for Science utilized the APS in their discovery of a new phenomenon of so-called metastability in a liquid phase. A metastable liquid is not quite stable. This state is common in supercooled liquids, which are liquids that cool below the freezing point without turning into a solid or a crystal. These scientists report the first experimental evidence of creating a metastable liquid directly by the opposite approach: melting a high-pressure solid crystal of the metal bismuth via a decompression process below its melting point. The results could be important for developing new materials and for understanding the dynamics of planetary interiors, such as earthquakes, because a metastable liquid could act as a lubricant strongly affecting the dynamics of the Earth's interior.

Phase transitions come in two basic "flavors." In one type, the chemical bonds do not break as the material goes from one phase to another. But they do alter in orientation and length in an orderly manner. The other, called reconstructive phase transition, is more chaotic, but the most prevalent in nature and the focus of this study. In these transitions, parts of the chemical bonds are broken and the structure changes significantly when it enters a new phase,

Pressure can be utilized to change the phase of a material, in addition to heating and cooling. The scientists in this study put a form of crystalline bismuth in a pressure-inducing diamond anvil cell at the HP-CAT x-ray beamline at the APS, and subjected it to pressures and decompression ranging from 32,000 times atmospheric pressure (3.2 GPa) to 12,000 atmospheres (1.2 GPa) at a temperature of 420° F (489 K). Under decompression only, at about 23,000 atmospheres, bismuth melted into a liquid. Then at 12,000 atmospheres it recrystallized.

The richness in crystalline structure of bismuth is particularly useful for witnessing changes in the structure of a material.

The researchers imaged the changes using a technique called x-ray diffraction, which uses much higher energy x-rays than those used for medical imaging and can therefore discern structure at the atomic level. They con-

"Melthing" cont'd. on page 73

An Unusual Packing Arrangement of Soft Spheres

Soft particles, including colloidal particles and various types of polymers and liquid crystals, can self-assemble into useful materials that serve as catalysts, microscale materials for manipulating light, and therapeutic drug delivery vehicles among myriad other applications. Learning how to manipulate their microscopic arrangements, which in turn influences their macroscopic properties, requires a fundamental understanding of the interplay between the structures and symmetries of the particles and how they interact. In water, surfactant molecules — key components of soaps — self-assemble into soft spherical particles that have long been thought to assume the same close-packed configurations as hard spheres, such as stacks of oranges at a grocery store. However, a new study by a team of researchers from the University of Minnesota and the University of Wisconsin–Madison demonstrates that the situation can be far more complex. Utilizing information collected at the APS, the researchers found that mixing a particular surfactant known as bis(tetramethylammonium) decylphosphonate (DPA-TMA_2) with precise amounts of water drives its self-assembly into intricate structured solids involving packings of spheres of up to five different sizes that interact through inherent electrical charges. The findings suggest that other charged spherical particles might also self-assemble in water into unusual configurations, all of which could have potentially useful applications.

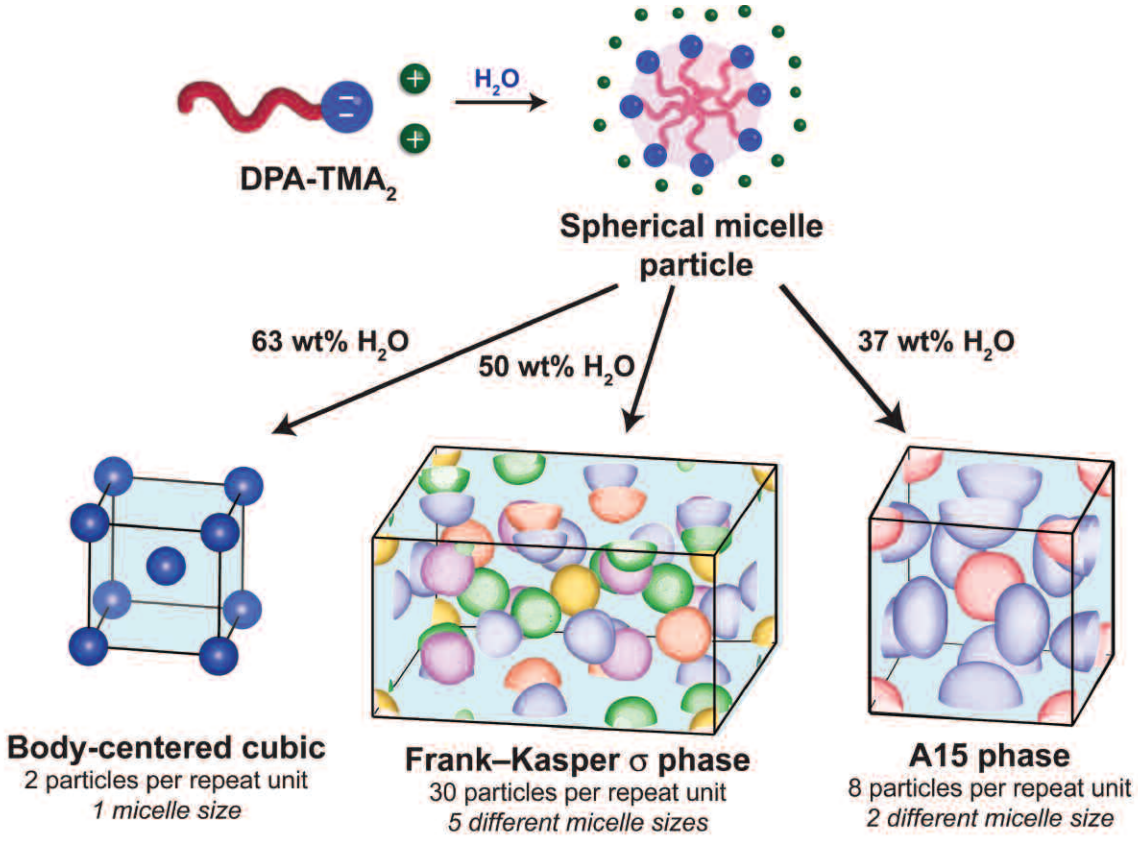

The researchers started by synthesizing pure samples of DPA-TMA_2. Mixing defined ratios of this surfactant and ultrapure water gives rise to soft solids in which the surfactant molecules spontaneously form spherical particles called micelles that pack into periodic three-dimensional (3-D) structures. The researchers then employed the DND-CAT 5-ID-D and XSD 12-ID-B beamlines at the APS to carry out synchrotron small-angle x-ray scattering (SAXS) experiments to investigate the exact packing arrangements of the micelles.

Their findings revealed a zoo of unexpected structures that depend on the relative amounts of water and surfactant that are mixed. When small amounts of DPA-TMA_2 are mixed with a large amount of water, the micelles do not pack into any organized structure but instead form freely flowing fluids. Decreasing the amount of water mixed with surfactant leads to a body-centered cubic packing of micelles, in which the repeating unit is a cube containing a central micelle surrounded by eight nearest neighbors situated at the cube corners. At medium water concentrations, SAXS analyses surprisingly showed that the surfactant micelles organized into a tetrahedral close packing with a giant, repeating unit cell containing 30 deformed spherical micelles. This arrangement fits the pattern of a Frank-Kasper sigma phase, a crystal structure taken on by certain heavy metals (e.g., uranium and tantalum) and intermetallic alloys (e.g., FeCr). A curious feature of this unusual structure is that its repeating pattern contains micelles of five discrete sizes, rather than a single uniform micelle as anticipated by conventional wisdom. The surfactant micelles adopt another periodic crystal structure known as the A15 phase at even lower water concentrations. This micellar A15 structure is also an analog of a known intermetallic structure.

< Fig. 1. Mixing precise amounts of water with the surfactant DPA-TMA2 generates spherical micelle particles that spontaneously assemble into various unexpected configurations that mimic those of hard metal alloys, such as body-centered cubic, Frank-Kasper sigma phase, and A15 phase.

Using computer simulations, the researchers demonstrated that the formation of these complex structures arises from a competition between the spherical symmetry of the micelle particles and the overall symmetry of the packing that they adopt. Packing soft micelles into a regular structure distorts their shape through interactions between micelles that are mediated by clouds of charged particles, or ions, that surround each sphere. However, the ion cloud around each sphere prefers to maintain a spherical shape. To accommodate these competing effects, the particles spontaneously exchange surfactant chains to reconfigure into multiple spheres of different sizes that pack into more complex crystal structures with large unit cells.

The authors note that the structurally periodic arrangements of these soft surfactant micelles are direct analogs of structures of hard metal alloys. Since the properties that appear to be responsible for these surprising crystal structures are present in other types of spherical, ionic particles in solution, the researchers suggest that further investigations of these and related materials could drive the discovery of other soft particle packings with unusual properties that could offer novel ways to manipulate light and other forms of energy. *— Christen Brownlee*

See: Sung A. Kim[1], Kyeong-Jun Jeong[2], Arun Yethiraj[2], and Mahesh K. Mahanthappa[1]*, "Low-symmetry sphere packings of simple surfactant micelles induced by ionic sphericity," Proc. Natl. Acad. Sci. USA **114**(16), 4072 (April 18, 2017). DOI: 10.1073/pnas.1701608114
Author affiliations: [1]University of Minnesota, [2]University of Wisconsin–Madison
Correspondence: *maheshkm@UMN.edu

This work was supported by the U.S. Department of Energy (DOE)-Basic Energy Sciences, Contract No. DE-SC0010328. DND-CAT is supported by E. I. DuPont de Nemours & Co., The Dow Chemical Company, and Northwestern University. This research used resources of the Advanced Photon Source, a U.S. DOE Office of Science user facility operated for the DOE Office of Science by Argonne National Laboratory under Contract No. DE-AC02-06CH11357.

"Melthing" cont'd. from page 71
ducted five compression/decompression rounds of experiments at HP-CAT beamlines 16-ID-B and 16-BM-D.

The bismuth displayed a metastable liquid in the process of solid-solid phase transitions under decompression at about 23,000 to 15,000 atmospheres. The scientists also found that the metastable state can endure for hours below the melting point under static conditions. Interestingly, the metastable liquid produced by decompression occurred in a pressure-temperature range that is similar to where supercooled bismuth is produced.

Because reconstructive phase transitions are the most fundamental type, this research provides a brand new way for understanding how different materials change,. It's possible that other materials could display a similar meta-stable liquid when they undergo reconstructive transitions and that this phenomenon is more prevalent than we thought. The results will no doubt lead to countless surprises in both materials science and planetary science in the coming years.

See: Chuanlong Lin, Jesse S. Smith, Stanislav V. Sinogeikin, Yoshio Kono, Changyong Park, Curtis Kenney-Benson, and Guoyin Shen*, "A metastable liquid melted from a crystalline solid under decompression," Nat. Commun. **8**, 14260 (2016).
DOI: 10.1038/ncomms14260
Author affiliation: Carnegie Institution of Washington
Correspondence: * gshen@ciw.edu

This research was supported by U.S. Department of Energy (DOE)-Basic Energy Sciences (BES), Division of Materials Sciences and Engineering under Award DE-FG02-99ER45775, and DOE-National Nuclear Security Administration (NNSA) Stewardship Science Academic Programs under Award DE-NA0001974. HP-CAT operations are supported by DOE-NNSA under Award No. DE-NA0001974, with partial instrumentation funding by the National Science Foundation (NSF). Use of the COMPRES-GSECARS gas-loading system was supported by COMPRES under NSF Cooperative Agreement EAR 11–57758 and by GSECARS through NSF grant EAR-1128799 and DOE grant DE-FG02-94ER14466. This research used resources of the Advanced Photon Source, a DOE Office of Science user facility operated for the DOE Office of Science by Argonne National Laboratory under Contract No. DE-AC02-06CH11357.

Repulsion Breeds Fragility in Metallic Liquids

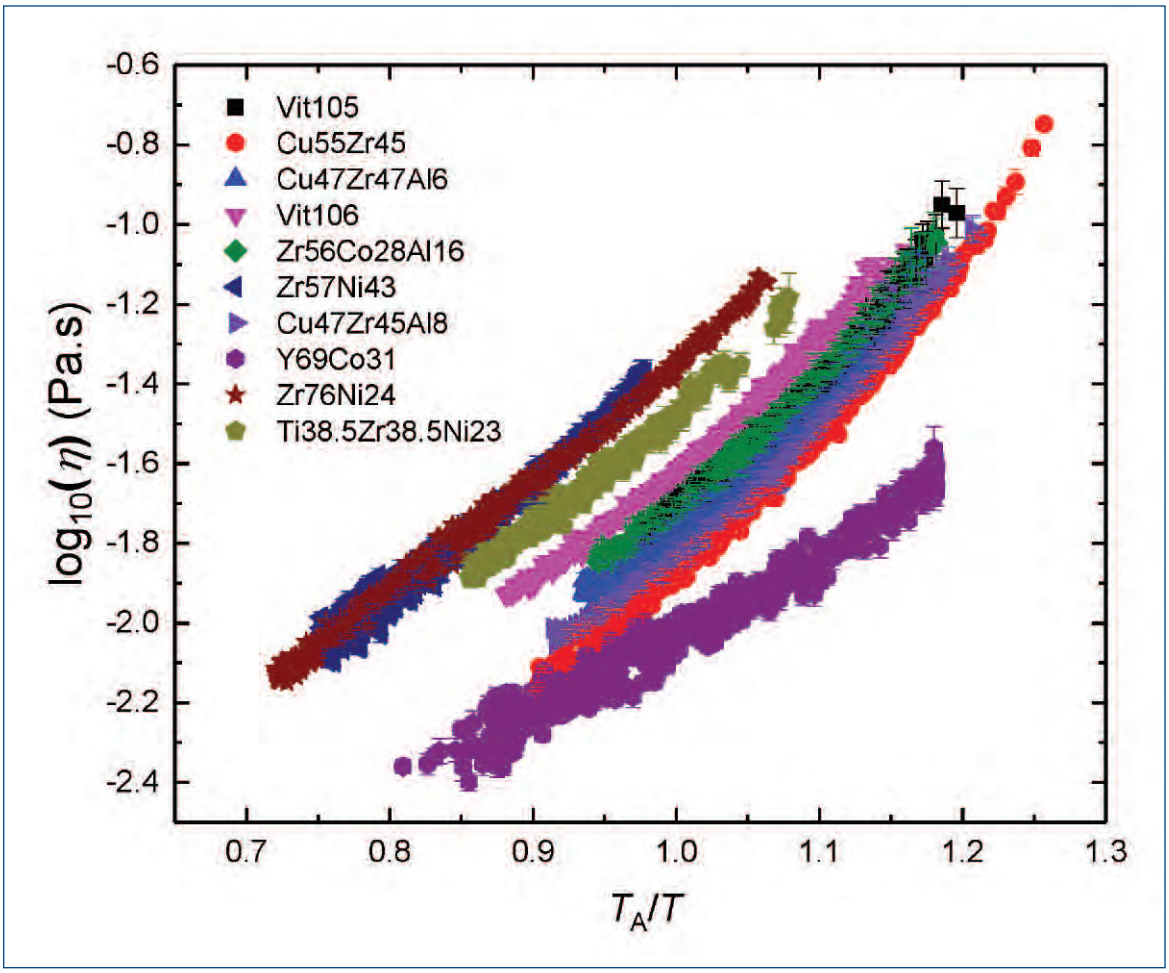

Fig. 1. Comparison of viscosities of all ten metallic liquids examined in this study. Each liquid metal is color-coded, with its chemical formula displayed at upper left. This type of graph is a modified Angell plot, named for Australian-born chemist Charles Austen Angell. In a typical Angell plot the vertical axis is the logarithm of the viscosity, while the horizontal axis is the temperature ratio T_g/T, where T_g is the glass transition temperature. An Angell plot is used to depict the fragility of liquid metals as they approach the glass transition phase. For this modified Angell plot, T_A replaces T_g, thereby allowing this diverse group of liquids to be characterized, including one that did not form a metallic glass ($Ti_{38.5}Zr_{38.5}Ni_{23}$).

The dynamics of metallic liquids, meaning how these liquids move in response to applied forces, is an ongoing area of theoretical and experimental research. The "fragility" of a liquid indicates how quickly its dynamic behavior slows as it cools. This property is believed to be important in the formation of metallic glasses, a class of technologically-important materials that often display extreme strength, elasticity, and wear resistance, and even unusual electric and magnetic properties. While the fragility of a liquid metal can be measured, the microscopic origin of this property has remained somewhat mysterious. However, new research reveals that the magnitude of the repulsion between the atoms of a liquid metal determines the degree of its fragility. These findings were deduced from x-ray scattering experiments carried out at the APS. This new insight into the fundamental mechanisms driving fragility should help materials scientists predict glass formation for a range of metallic liquids and spur the development of new types of metallic glasses with enhanced properties, including improved durability, toughness, and strength.

The term '"glass" conjures up the transparent materials used for windows and jars. These common glasses are typically silica-based ceramics exhibiting a disordered (amorphous) structure that are strong in compression but very brittle. For a materials scientist, the definition of glass is much broader. In that world, any substance that can be cooled from a gooey or viscous liquid into an amorphous solid by entering a glass transition phase can be considered a type of glass.

A surprising variety of metal alloys have been coaxed through the glass transition. Under ordinary cooling conditions these liquids form crystalline structures. However, if cooled rapidly, some metallic liquids can be frozen into a glassy state. When metallic glasses were first created, the required cooling rates were millions of degrees per second, which greatly limited their practicality. Eventually, scientists discovered liquid alloys that formed glasses when cooled at rates comparable to those of silica-based glasses.

Revealing the factors responsible for the glass transition of liquid metals has presented a long-standing challenge in condensed matter physics. As a metallic liquid approaches the glass transition temperature T_g, the movement, or dynamics, of its molecules slows. In some liquid metals, molecular movement drops precipitously approaching T_g, while for others this movement reduces more smoothly. Determining the underlying source of these dynamic behaviors was the aim of this research.

Nearly 50 years ago, materials scientists David Turnbull and Donald Polk hypothesized that the dynamics of liquid metals is directly connected to their interatomic repulsion. The potential energy between atoms or molecules is a function of the distance between them. Further apart there is an attractive force, but closer in there is a mutual repulsion. The greater the repulsion between the atoms of a liquid, the stronger the liquid and the more viscous (more resistant to flow) it is.

To test the Polk-Turnbull hypothesis, researchers from Washington University in St Louis and Harbin Normal University (China) probed 10 metallic liquid alloys via x-ray diffraction carried out at the XSD beamline 6-ID-D of the APS. Seven of these metallic liquids readily formed metallic glasses; two were marginal glass-formers; and one did not form a glass. The x-ray scattering measurements revealed the repulsive portion of each liquid's potential. This was subsequently compared with the measured viscosity of the liquid as its temperature was lowered, thereby indicating the liquid's fragility.

The researchers could have made this comparison as each liquid neared its glass transition temperature T_g. However, T_g was unknown for the liquid that did not form a glass. Instead, a related temperature, TA, was used. Recent experimental and theoretical findings indicate that this is the temperature at which the atoms of a metallic liquid begin to interact cooperatively, which eventually leads to the glass transition (Fig. 1).

Using these parameters to evaluate the x-ray data, the researchers found that stronger metallic liquids (those displaying higher interatomic repulsion) display greater viscosity at higher temperatures, ordering more rapidly near TA than do more fragile liquids. These findings confirm the hypothesis of Polk and Turnbull while refuting models of metallic liquid behavior based on experiments involving colloidal suspensions. This last conclusion is especially pertinent since colloidal suspensions are frequently used as analogues for metallic liquid systems.

The researchers hope that future x-ray experiments can more fully characterize the interplay between fragility and glass formation. An even loftier goal is to determine whether these findings apply to all liquids. *— Philip Koth*

See: Christopher E. Pueblo[1], Minhua Sun[2], and K.F. Kelton[1]*, "Strength of the repulsive part of the interatomic potential determines fragility in metallic liquids," Nat. Mater. **16**, 792 (August 2017). DOI: 10.1038/NMAT4935
Author affiliations: [1]Washington University in St Louis, [2]Harbin Normal University

Correspondence:
* kfk@physics.wustl.edu

We thank D. Robinson for his assistance with the high-energy X-ray diffraction studies at the APS. K.F.K. and C.E.P. gratefully acknowledge support by NASA under Grant No. NNX16AB52G and the National Science Foundation under Grant No. DMR 15-06553. M.S. gratefully acknowledges support by the Foundation for the Science and Technological Innovation Talent of Harbin (No. 2010RFQXG028). This research used resources of the Advanced Photon Source, a U.S. Department of Energy (DOE) Office of Science user facility operated for the DOE Office of Science by Argonne National Laboratory under Contract No. DE-AC02-06CH11357.

6-ID-D • XSD • Physics, materials science • Magnetic x-ray scattering, high-energy x-ray diffraction, powder diffraction, pair distribution function • 50-100 keV, 70-130 keV • On-site • Accepting general users •

KESGIN OF ASD EARNS THE FIRST JAN EVETTS AWARD

The first Jan Evetts Award for the best paper by a young researcher published in the journal *Superconductor Science and Technology* was awarded to **Ibrahim Kesgin** of the ASD Magnetic Devices Group. First-author Kesgin's paper is entitled, "High-temperature superconducting undulator magnets." His co-authors are Matthew Kasa and Yury Ivanyushenkov, also of the ASD Magnetic Devices Group, and Ulrich Welp of the Argonne Materials Science Division.

LEE OF XSD RECEIVES THE APSUO AWARD FOR EXCELLENCE IN BEAMLINE SCIENCE

Byeongdu Lee of the XSD Chemical & Materials Science Group received the APSUO Award for Excellence in Beamline Science, which recognizes beamline scientists who have made significant scientific contributions in their area of research or instrumentation development and have promoted the user community in this area. Lee was named for his leadership and innovations in nanomaterials and contributions to x-ray scattering including theory, application, and development of analytical methods and state-of-the-art instrumentation. He was also selected to acknowledge his demonstrated and sustained commitment to the APS user community by the education, training, and mentoring of young scientists.

RONDINELLI OF NORTHWESTERN U. IS AN MRS OUTSTANDING YOUNG INVESTIGATOR

James Rondinelli (Northwestern University) an APS user and Associate

Professor in Materials Science and Engineering, received a 2017 Materials Research Society Outstanding Young Investigator Award "for pioneering advances in the theoretical understanding of atomic structure-electronic property relations of complex inorganic oxides in bulk, thin film, and superlattice geometries." The Outstanding Young Investigator Award recognizes outstanding, interdisciplinary scientific work in materials research by a young scientist or engineer. The award recipient must show exceptional promise as a developing leader in the materials area.

NORTHWESTERN U.'S ROSENZWEIG ELECTED TO THE NATIONAL ACADEMY OF SCIENCE

Amy Rosenzweig, APS user and the Weinberg Family Distinguished Professor of Life Sciences in the Departments of Molecular Biosciences and of Chemistry at Northwestern University, was elected to the prestigious National Academy of Sciences for distinguished achievements in original research.

SUTTON OF MCGILL U. AWARDED CAP MEDAL FOR LIFETIME ACHIEVEMENT IN PHYSICS

Mark Sutton (McGill U.), APS user and Chair of the APS Scientific Advisory Committee, was awarded the 2017 CAP Medal for Lifetime Achievement in Physics by the Canadian Association of Physicists "for pioneering the development of coherent and time-resolved x-ray scattering techniques for the study of materials, and his resulting contributions to our understanding of materials and phase transitions." The CAP Medal for Lifetime Achievement in Physics is awarded on the basis of distinguished service to physics over an extended period of time, and/or recent outstanding achievement.

TOBY OF XSD ELECTED TO AMERICAN CRYSTALLOGRAPHIC ASSOCIATION FELLOWSHIP

Brian Toby, XSD Computational X-ray Science Group Leader, was elected a Fellow of the American Crystallographic Association (ACA). Fellowship recognizes a high level of excellence in scientific research, teaching, and professional duties, but also service, leadership, and personal engagement in the ACA and the broader world of crystallography and science.

ZHOLENTS OF ASD IS AN ARGONNE DISTINGUISHED FELLOW

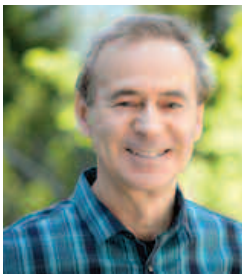

Alexander (Sasha) Zholents, ASD Senior Scientist, was named an Argonne Distinguished Fellow, the Laboratory's highest scientific and engineering rank. To be named an Argonne Distinguished Fellow is an achievement on par with receiving an endowed chair at a top-ranked university. Approximately 3% of the Argonne research staff share this title, which requires sustained outstanding scientific and engineering research and can also be associated with outstanding technical leadership of major, complex, high-priority projects.

Chemical Science

Converting Methane Gas to Liquid Methanol the Bacteria Way

Methanotrophic bacteria found in oceans and lakes are capable of performing a challenging and industrially relevant reaction — converting methane gas to the liquid fuel methanol — with relative ease. Synthetic chemists have aspired to replicate nature's success, but attempts to understand the enzymatic process have been thwarted by its biological complexity. Now, using time-resolved x-ray absorption spectroscopy at the APS and a photocatalytic model system, researchers have revealed a detailed picture of the initial step of the process. These insights may help scientists design artificial catalytic systems for the sustainable generation of methane-based fuels.

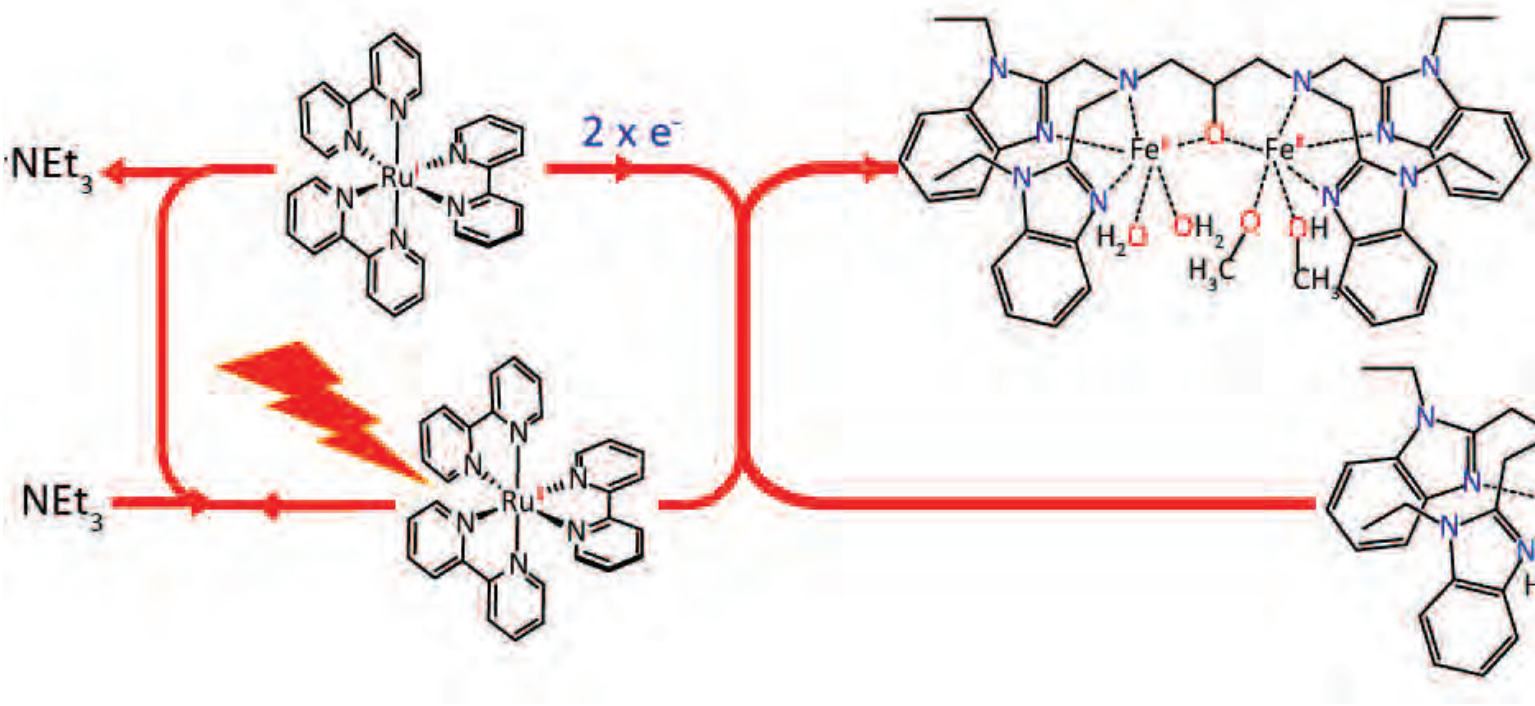

Fig. 1. Photocatalytic system consisting of the diiron(III, III) complex analog of methane monooxygenase enzymes, $[Ru(bpy)_3]^{2+}$ photosensitizer and triethylamine electron donor (NEt_3). The parts highlighted in red represent the activation part of the catalytic module studied in this work, and the grey parts represent the further to be analyzed catalytic route involving the oxidation of a methane analog.

The oxidation of methane to methanol is quite a feat considering methane's strong C-H bonds. Current industrial approaches entail an energy intensive and multi-step process, while the bacterial production of methanol presents an attractive alternative carried out by methane monooxygenase (MMO) enzymes at ambient conditions.

These enzymes exist in an intricate protein environment. To simplify their studies, researchers from Argonne, the Institute of Chemical Research of Catalonia, the Institut de Chimie Moléculaire et des Matériaux d'Orsay (France), and the Institut de Biologie Intégrative de la Cellule (France) used a compound with two bridging iron metal centers previously developed to model the enzymatic core, abbreviated here as diiron(III,III).

The researchers set out to investigate the first step of the reaction, in which the diiron(III,III) species gains two electrons to become a diiron(II,II) species — the key intermediate that can react with oxygen to form the highly reactive species responsible for the oxidation of methane to methanol.

The research team chose a mild photosensitizer called $[Ru(bpy)_3]^{2+}$ instead of the harsh chemical oxidants typically employed. $[Ru(bpy)_3]^{2+}$ absorbs light energy to transfer an electron to the iron catalyst, so studying its role in energy transfer could also be beneficial for artificial photosynthesis, an area that has garnered great research interest.

Using time-resolved x-ray absorp-

tion spectroscopy, the researchers could capture snapshots of the fast electron transfer between $[Ru(bpy)_3]^{2+}$ and the diiron(III,III) core which happens on the nanosecond timescale. By adding a sacrificial electron donor compound called triethylamine to prolong the lifetime of $[Ru(bpy)_3]^{2+}$, the researchers were able to induce a two-electron transfer process and generate the reduced diiron(II,II) species (Fig.1).

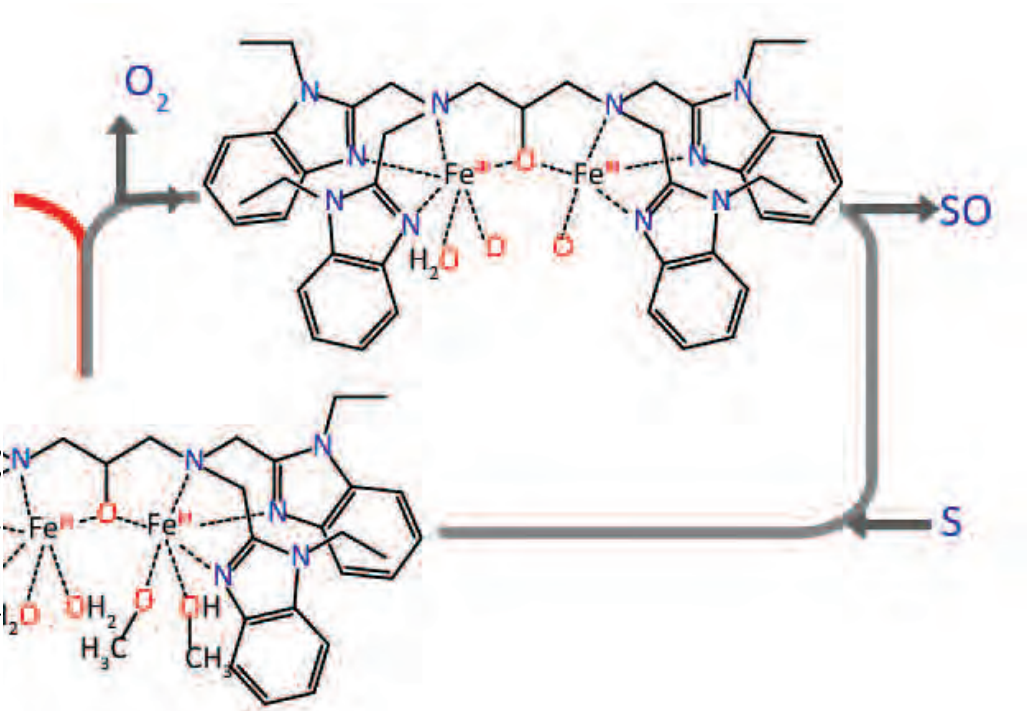

The electronic and structural configurations of the reduced diiron(II,II) core have been uniquely difficult to elucidate by two conventional spectroscopy methods. In ultraviolet-visible light spectroscopy, iron's absorption signal would be overwhelmed by the photosensitizer's absorption while in electron paramagnetic resonance spectroscopy, iron's high-spin character renders it essentially invisible. X-ray absorption spectroscopy sidesteps these limitations and has the advantage of being element specific, meaning that the beam's energy range is tuned to iron and won't pick up interference from other elements in the solution.

In this so-called pump-probe experiment, scientists shot a laser at the solution mixture, inducing an optical response that is then interrogated at ~ 150-ns intervals with incident x-rays to give spectral information. X-ray absorption data were collected at XSD beamline 11-ID-D at the APS. The researchers collected data at every time point enabling them to track the electron transfer and measure minute structural changes to the iron species, such as the elongation of bonds and shifting of the bond angles upon reduction, which is important for understanding the next steps in the reaction.

The team also modeled the structural configuration of the diiron(III,III) and diiron(II,II) species using density functional theory calculations and found that the experimental data matched well with their predictions.

These new insights into the reaction mechanism provide valuable guidance for the rational design of future catalysts capable of transforming methane to methanol. Next, the researchers plan to take the reduced iron species and begin introducing an easily oxidized methane analog, extending their understanding of the reaction one step further. *— Tien Nguyen*

See: Dooshaye Moonshiram[1]*, Antonio Picon[1], Alvaro Vazquez-Mayagoitia[1], Xiaoyi Zhang[1], Ming-Feng Tu[1], Pablo Garrido-Barros[2], Jean-Pierre Mahy[3], Frederic Avenier[3], and Ally Aukauloo[3,4], "Elucidating the light-induced charge accumulation in an artificial analogue of methane monooxygenase enzymes using time-resolved x-ray absorption spectroscopy," Chem. Comm. **53**, 2725 (2017). DOI: 10.1039/C6CC08748E
Author affiliations: [1]Argonne National Laboratory, [2]Institute of Chemical Research of Catalonia (ICIQ), [3]Université Paris-Sud, Orsay, [4]Institut de Biologie Intégrative de la Cellule
Correspondence:
* dmoonshi@gmail.com

This work was supported by the U.S. Department of Energy (DOE) Office of Science-Basic Energy Sciences, Chemical Sciences, Geosciences and Biosciences Division (contract no. DE-AC02-06CH11357), and by LABEX CHARMMAT. This research used the resources of the Advanced Photon Source, a U.S. DOE Office of Science user facility, at Argonne National Laboratory. P.G.B thanks "La Caixa" foundation for a Ph.D. grant. This research used resources of the Advanced Photon Source, a U.S. DOE Office of Science user facility operated for the DOE Office of Science by Argonne National Laboratory under Contract No. DE-AC02-06CH11357.

11-ID-D • XSD • Chemistry, environmental science, materials science • Time-resolved x-ray absorption fine structure, time-resolved x-ray scattering • 6-25 keV • On-site • Accepting general users •

Modifying Methane Quick and Easy

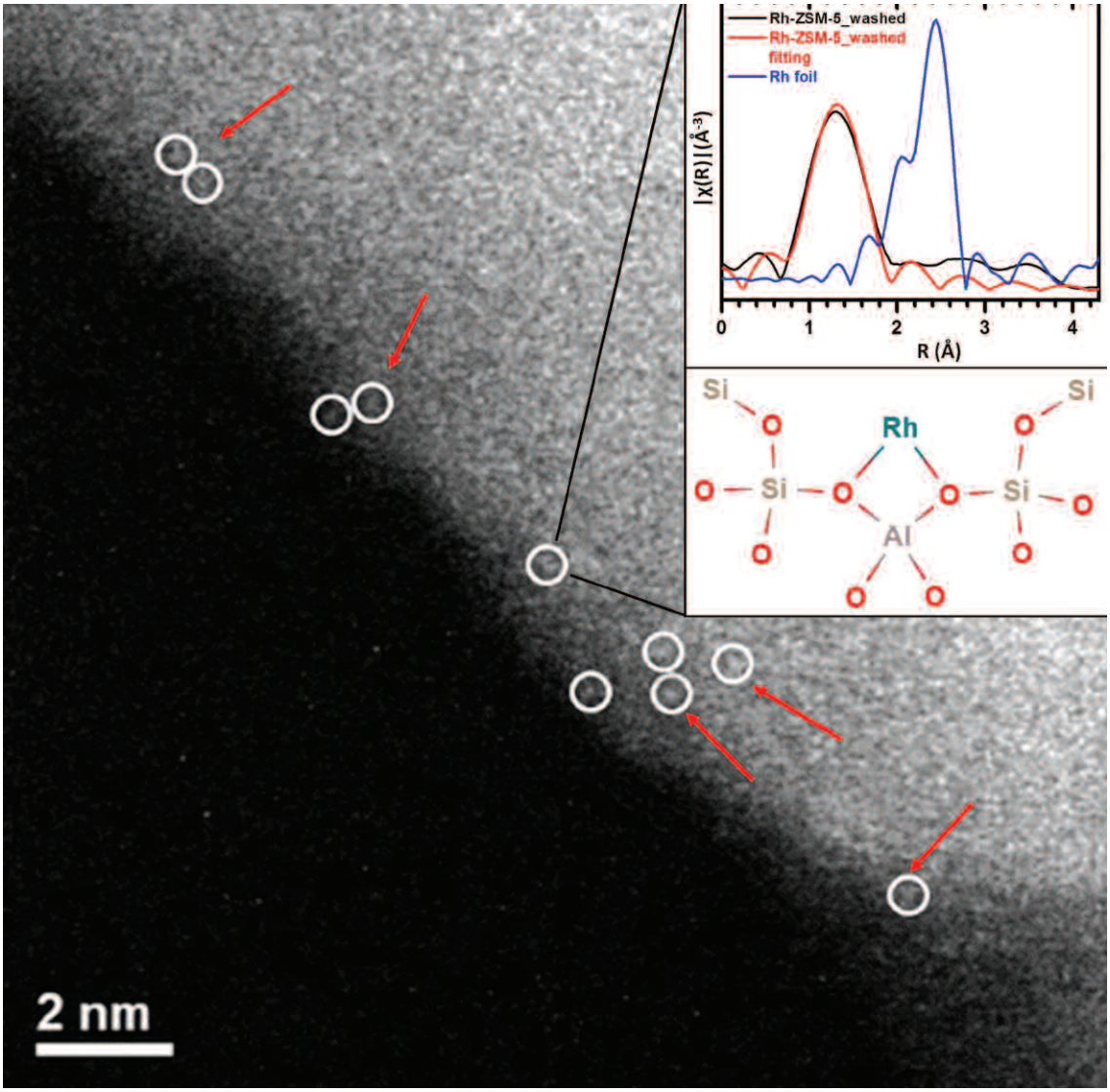

Fig. 1. STEM image of Rh-ZSM-5 showing Rh single cations in white circles (Figure: Lawrence F. Allard, ORNL); Inset upper: EXAFS data and fitting of Rh-ZSM-5; lower: Proposed structure of Rh single cation anchored on the zeolite pore walls.

A quick and simple way to convert the abundant natural gas methane into more complex chemicals such as methanol, which can then be converted into pharmaceuticals, agrochemicals, and plastics, has been demonstrated by U.S. scientists and studied with a variety of experimental tools, including high-brightness x-rays from the APS. Their approach utilizes a single isolated metal atom catalyst to make the conversion proceed rapidly at mild temperatures and pressures. Moreover, it is a truly catalytic conversion, making a lot of the desired product without the time-consuming extraction steps needed with other approaches.

Methane is a relatively abundant gas that can be extracted from gas fields and oil wells, but also exists under pressure in the deep ocean and frozen in Arctic ice fields. It is a simple molecule: a single carbon atom with four attendant hydrogen atoms bonded to it in a tetrahedral shape. Its primary use is as a fuel for heating, cooking, and electricity generation. However, when sources of petrochemicals, (primarily crude oil, on which the chemical and vehicular fuel industries rely for their starting materials) become less abundant and less accessible, methane could represent an alternative feedstock. It would also provide a commercially viable alternative to the flaring of methane from oil wells.

The first step to making methane useful, beyond simply burning it, is the hardest. Catalysts and harsh reaction conditions can add oxygen atoms to the simple molecule and rearrange its atoms to make more complex and chemically active compounds, such as methanol, formaldehyde (methanal), formic acid (methanoic acid), acetic acid and other oxygenated chemicals. The presence of the reactive oxygen in these various molecules means that subsequent reactions can more quickly add other chemical groups containing additional carbon atoms, nitrogen atoms, even sulfur atoms to these compounds. This builds up the requisite complexity for life-saving drugs, agrochemicals such as the pesticides and herbicides essential to large-scale modern agriculture, and the monomer building blocks for making plastics.

The researchers from Tufts University made, tested, and, together with colleagues from Oak Ridge National Laboratory and Argonne, characterized the catalyst for the direct conversion of methane to oxygenate liquids. This catalyst has a single rhodium atom at its heart. The catalyst can be anchored to a porous mineral such as zeolite or onto a titanium dioxide support. The team used the XSD beamline 12-BM-B at the APS to carry out x-ray absorption near edge structure (XANES) and extended x-ray absorption fine structure (EXAFS) spectroscopy on their catalyst. The data from those studies combined with other techniques provided details of the shape and form of the catalyst, which would then help in understanding how it works and in the putative design of a next-generation catalysts (Fig. 1).

The supported catalyst can be suspended in water while methane, oxygen, and carbon monoxide are bubbled through the suspension. The rhodium species facilitates direct conversion of methane to methanol and acetic acid. The reaction proceeds under mild conditions, just 150° C and at pressures below 25-30 bar. This temperature is much cooler than the 500-600° C many catalytic reactions need. Indeed, at temperatures above 170° C, the reaction began to falter and to generate useless carbon dioxide gas rather than the oxygenated methane products.

The researchers have shown that the two products are formed through two different chemical reaction pathways. Radioisotope labeling of the carbon dioxide showed that the carbon atom in the methanol is derived from the methane and that one carbon atom in the acetic acid is from the methane and the other from carbonylation insertion of the carbon monoxide, as might be expected.

This mechanistic understanding, the team explains, allows them to tune the methane conversion depending on which product they desire, methanol or acetic acid. The selectivity is very high, at least 60%, and when they optimize the catalyst composition they can even achieve almost 100% selectivity of methane to oxygenated product at approximately 5% conversion of methane. Another advantage of the new catalyst and process, they discovered, is that it operates with readily available and cheap gaseous oxygen, not a liquid oxidant, such as hydrogen peroxide, which is expensive and not practical for natural gas capture from remote wells.

The team concedes that at present the catalyst activity falls short of commercialization, but they should now be able to optimize the rhodium atom distribution and also the type of support material to make it more practical, scalable, and industrially viable.

— David Bradley

See: Junjun Shan[1‡], Mengwei Li[1], Lawrence F. Allard[2], Sungsik Lee[3], and Maria Flytzani-Stephanopoulos[1*], "Mild oxidation of methane to methanol or acetic acid on supported isolated rhodium catalysts," Nature **551**, 605 (30 November 2017).
DOI: 10.1038/nature24640
Author affiliations: [1]Tufts University, [2]Oak Ridge National Laboratory, [3]Argonne National Laboratory ‡Present address: NICE America Research, Inc.
Correspondence: * maria.flyzani-stephanopoulos@tufts.edu

The financial support of this work by the Department of Energy (DOE/ARPA-e grant DE-AR0000433, under subcontract from MIT), is gratefully acknowledged. Aberration-corrected electron microscopy research at Oak Ridge National Laboratory was sponsored by the U.S. DOE Office of Energy Efficiency and Renewable Energy, Vehicle Technologies Office, Propulsion Materials Program. This research used resources of the Advanced Photon Source, a U.S. DOE Office of Science user facility operated for the U.S. DOE Office of Science by Argonne National Laboratory under Contract No. DE-AC02-06CH11357.

12-BM-B • XSD • Materials science, polymer science, chemistry, physics, environmental science • X-ray absorption fine structure,, x-ray reflectivity,, small-angle x-ray scattering, wide-angle x-ray scattering • 4.5-30 keV, 10-40 keV • On-site • Accepting general users •

Why Zinc Makes Platinum a Better Catalyst

Many industrial processes rely on chemical catalysts to increase the rate of a desired reaction and inhibit the formation of unwanted products. But how catalysts work and how they can be improved are often somewhat mysterious questions. Working at three x-ray beamlines at the APS, researchers have identified two distinct mechanisms by which the addition of a zinc "promoter" to a platinum catalyst increases both the selectivity of a catalytic reaction and the rate at which it works. The findings, backed up by theoretical calculations, should make it easier to design and refine catalysts in rational ways rather than relying on trial and error, which could pave the way for rational design of still better catalysts that would increase the economic value of ethane, propane, and other light alkanes in shale gas.

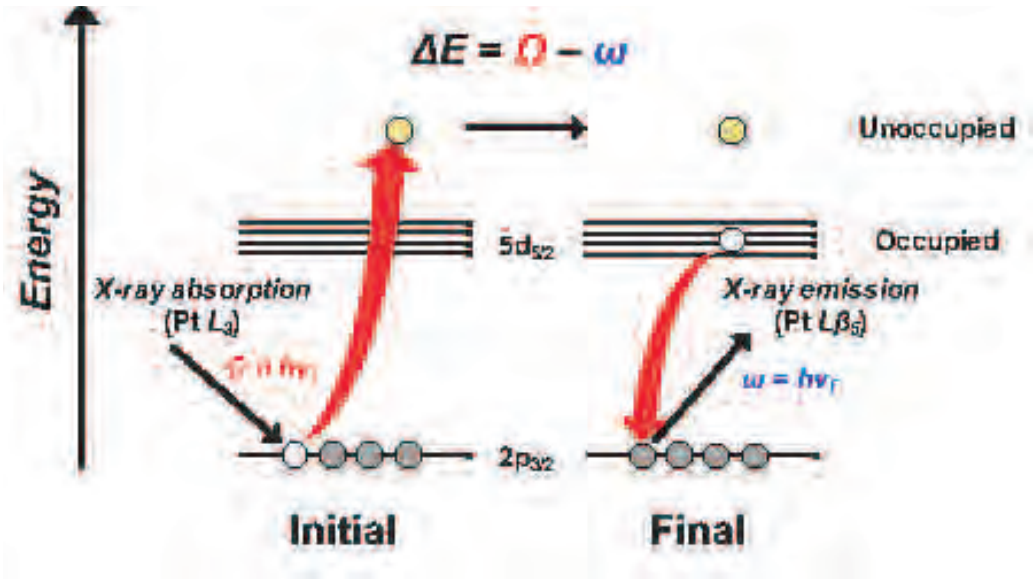

Fig 1. These RIXS planes for Pt and PtZn catalysts plot the incoming x ray energy against the corresponding energy transfer – the difference between the incoming and outgoing x ray energies, which measures the energy gap between occupied and unoccupied 5d valence states. That gap is larger for PtZn than for Pt alone, a crucial factor in its superior performance as a catalyst.

The development of horizontal drilling and hydraulic fracturing ("fracking") in recent years has greatly enhanced the production of natural gas in the United States from shale reserves. The major component of natural gas is methane, but significant amounts of ethane, propane, and heavier hydrocarbons are also produced. Ethane and propane can be converted, by catalyzed dehydrogenation, into ethylene and propylene, which are important feedstocks for polymer production. The quantity of these heavier hydrocarbons promises to exceed what the chemical industry requires, however, raising the possibility that further processing, also requiring catalysis, could convert ethylene and related compounds into still larger molecules that would serve as useful fuels.

Realizing these gains begins with simple reactions, notably the conversion of ethane (C_2H_6) into ethylene (C_2H_4). A team from Purdue University, Argonne National Laboratory, and the National Institute for Standards and Technology combined x-ray studies with theoretical calculations to understand how the atomic and electronic structure of zinc-promoted platinum catalysts influences their performance.

Platinum alone has an affinity for activating single C-H bonds that enables it to catalyze the ethane-ethylene reaction, but it can also convert ethane to unwanted smaller molecules. Adding zinc to platinum catalysts improves their selectivity (the propensity to create ethylene, but not other products) and their turnover rate (the rate of catalyzed reactions per surface platinum atom). How this promotion works has been unclear.

The researchers made Pt and PtZn catalysts on silica (SiO_2) substrates and characterized them in reactors under catalytic conditions at three different APS beamlines (the APS is an Office of Science user facility at Argonne). The team recorded initial selectivities for ethylene of 74% with the Pt-only catalyst and 100% for PtZn at about 40%

Cont'd. on the next page

conversion; the turnover rate for ethane-to-ethylene conversion was also six times higher for PtZn than Pt.

By means of x-ray absorption measurements at the MR-CAT beamline 10-BM-A,B, and x-ray diffraction at XSD beamline 11-ID-C, the researchers determined that in the Pt-only catalysts, the platinum atoms formed metallic nanoparticles, with a structure similar to that of bulk platinum. In the PtZn catalysts, the two metals combined in an ordered Pt_1Zn_1 intermetallic alloy to form nanoparticles with a 1:1 composition. Significantly, the surface platinum atoms on these nanoparticles were isolated, each with about seven zinc nearest neighbors on average, so that the closest Pt-Pt distance was much greater than for the pure platinum nanoparticles.

Next, the researchers turned to resonant inelastic x-ray spectroscopy (RIXS) studies, performed at MR-CAT beamline 10-ID-B. Incoming x-rays excite electrons from the 2p level of platinum to an unoccupied 5d valence state; the empty 2p state is then filled by an electron falling from an occupied 5d valence state, accompanied by the emission of a lower energy x-ray photon . Through a comparison of the absorbed and emitted x rays, RIXS revealed the energy structure of the valence states (Fig. 1). The researchers found that in the isolated platinum atoms of the PtZn nanoparticles, the gap between occupied and unoccupied 5d states increased by about 2 eV.

Researchers have suspected that the catalytic function of platinum derives from the interaction of these filled valence states with molecular species such as ethane. One proposed explanation for zinc's effect as a promoter is that it donates electrons to the unoccupied states of platinum. However, by analyzing the RIXS results with the help of density functional theory calculations that capture the interaction of the occupied 5d levels, the researchers concluded that it is the energy shift of those levels, as opposed to electron transfer, that amplifies their interaction with C-H bonds and thus increases the catalytic turnover rate. Moreover, the isolation of platinum atoms on the surface of the PtZn nanoparticles inhibits, for geometrical reasons, the interaction of the catalyst with C=C double bonds, thus inhibiting carbon deposition on the catalyst surface and improving the selectivity of PtZn to ethylene over side products.

Thus, the understanding of these two factors explain why PtZn is a better catalyst than Pt alone. *— David Lindley*

See: Viktor J. Cybulskis[1], Brandon C. Bukowski[1], Han-Ting Tseng[1], James R. Gallagher[2], Zhenwei Wu[1], Evan Wegener[1], A. Jeremy Kropf[2], Bruce Ravel[3], Fabio H. Ribeiro[1], Jeffrey Greeley[1]*, and Jeffrey T. Miller[1]**, "Zinc Promotion of Platinum for Catalytic Light Alkane Dehydrogenation: Insights into Geometric and Electronic Effects," ACS Catal. **7**, 4173 (2017).
DOI: 10.1021/acscatal.6b03603
Author affiliations: [1]Purdue University, [2]Argonne National Laboratory, [3]National Institute of Standards and Technology
Correspondence:
* jgreeley@purdue.edu,
** mill1194@purdue.edu

Materials Research Collaborative Access Team operations are supported by the U.S. Department of Energy (DOE) and the Materials Research Collaborative Access Team member institutions. Support for V.J.C. and H.-T.T. was provided by Qatar National Research Fund No. 13121024. J.G. and B.C.B. acknowledge support from the Designing Materials to Revolutionize and Engineer our Future program of the National Science Foundation (CBET1437219). This research used resources of the Advanced Photon Source, a U.S. DOE Office of Science user facility operated for the DOE Office of Science by Argonne National Laboratory under Contract No. DE-AC02-06CH11357.

10-BM-A,B • MR-CAT • Materials science, chemistry, environmental science, physics • X-ray absorption fine structure • 4-32 keV • On-site • Accepting general users •

10-ID-B • MR-CAT • Materials science, environmental science, chemistry • X-ray absorption fine structure, time-resolved x-ray absorption fine structure, microfluorescence (hard x-ray) • 4.3-27 keV, 4.8-32 keV, 15-65 keV • On-site • Accepting general users •

11-ID-C • XSD • Materials science, chemistry, physics • High-energy x-ray diffraction, diffuse x-ray scattering, pair distribution function • 105.6 keV • On-site • Accepting general users •

A Word (or Two) about Platinum

Platinum is known as a "transition metal" because it is ductile, malleable, able to conduct electricity and heat, has a high freezing point, and expands upon heating. It is a part of the platinum group of metals, which all share similar properties. Other metals in this group are: ruthenium, rhodium, palladium, osmium, and iridium. Platinum does not oxidize in air and is often combined with other metals.

Originally called "platina," derived from plata, which is Spanish for silver, platinum has been found in ancient Egypt; specifically, the Casket of Thebes was found to be adorned with platinum, along with gold and silver. Platinum was a nuisance for Spanish conquistadors, as little platinum nuggets were mixed with the nuggets of gold they were finding, and were difficult to separate.

Platinum's credited discoverer was Antonio de Ulloa, who returned to Spain in 1746 with platinum samples. Platinum was not recognized as its own element until 1751, when it was successfully melted down. Until the 1820's, Colombia was the only major producer of platinum in the world, Platinum was discovered in the Ural Mountain gold fields in Russia, and in 1924, platinum was discovered in a riverbed in South Africa.

A cylindrical hunk of platinum and platinum alloy is used as the international standard for measuring a kilogram. In the 1880s, about 40 of these cylinders, which weigh about 2.2 lbs. or 1 kilogram, were distributed around the world.

Platinum is used in jewelry, catalytic converters, petroleum, the medical field, spark plugs, gasoline, hard-disk drives, anti-cancer drugs, fibre-optic cables, LCD displays, eyeglasses, paints, and pacemakers. Platinum is also the key catalyst in fuel cells.

It is estimated that today one-fifth of everything we use either contains platinum or requires platinum in its making. 50% of the platinum produced annually in all mines is used for industrial applications.

Source: http://eochemistry.wikispaces.com/Platinum

How a Catalyst Makes Room for Hydrogen

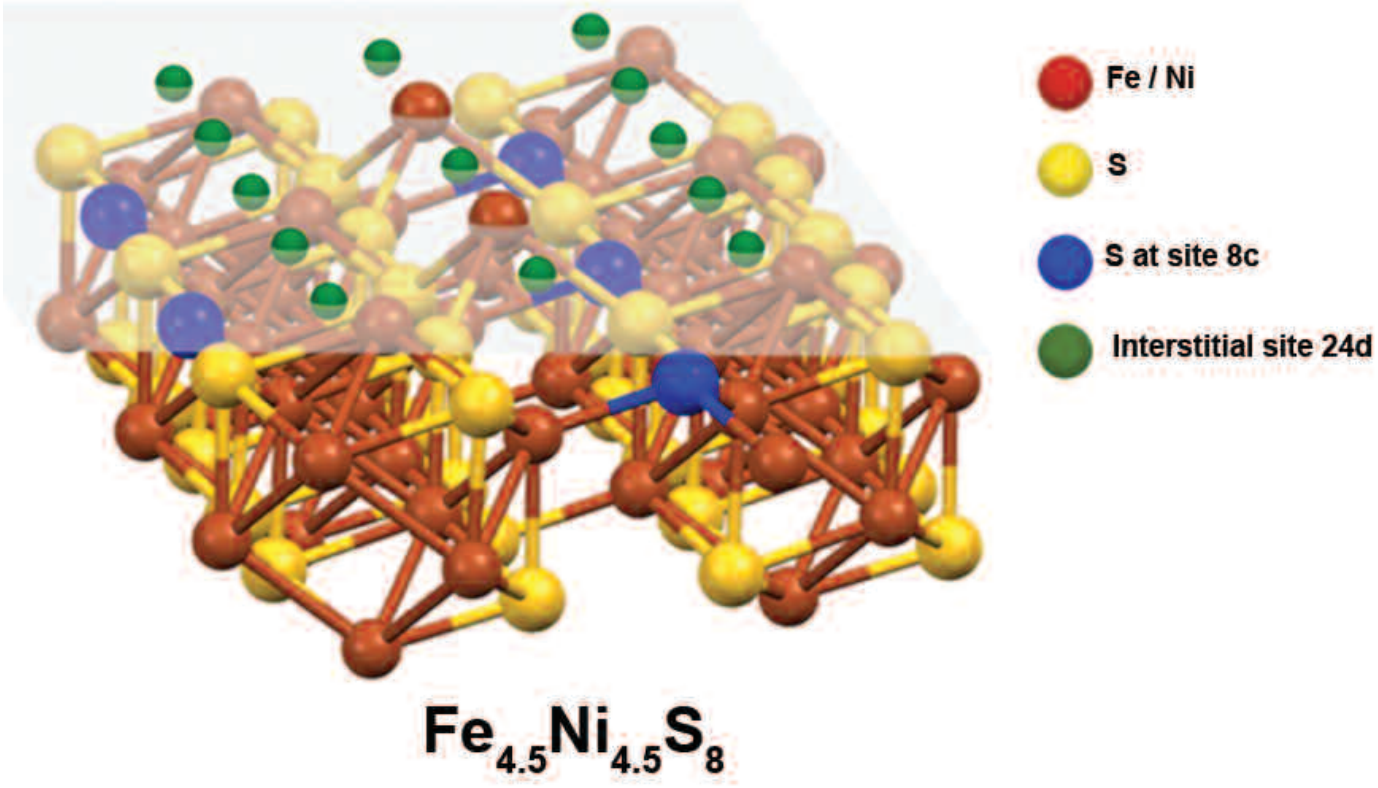

Fig. 1. Lattice structure of pentlandite. At moderately negative applied potentials, some of the S sites are unoccupied (vacancies) and preferentially contribute to the hydrogen uptake. Once all vacancies are filled, at more negative potentials, hydrogen atoms can only be adsorbed at interstitial sites.

3-ID-B,C,D • XSD • Physics, geoscience, life sciences, chemistry, materials science • Nuclear resonant scattering, inelastic x-ray scattering, high-pressure diamond anvil cell • 7-27 keV, 14.41-14.42 keV • On-site • Accepting general users •

Catalysts for the electrolysis of water are crucial to the development of cost-effective hydrogen generation systems for energy storage. Synthetic pentlandite ($Fe_{4.5}Ni_{4.5}S_8$) shows considerable promise as a suitable catalyst, but the mechanism underlying its effectiveness has not been fully understood. Working at the APS, researchers utilized nuclear resonance inelastic x-ray scattering (NRIXS) to demonstrate that hydrogen atoms are efficiently captured into lattice sulfur vacancies at the surface of the mineral. The findings should be of value in effort to refine pentlandite's performance.

Platinum-based catalysts for hydrogen evolution reactions (HER) are highly effective, but the metal is costly and relatively rare. Transition metal dichalcogenides (compounds of transition metals with sulfur, selenium, or tellurium) form a cheaper class of HER catalysts, but they generally need careful preparation, such as nanostructuring or specialized surface modification, to perform well. Three years ago, however, researchers found that the mineral pentlandite, synthesized in unmodified bulk form, has useful catalytic properties. It can sustain high current densities, corresponding to productive electrolytic reactions, and is stable in aqueous acidic conditions.

An oddity of this material is that its overpotential (the voltage required to initiate electrolysis) decreases from 280 mV to 190 mV over the first four days of use. As with related materials, pentlandite's catalytic effect is thought to come about because it readily takes up hydrogen atoms in its lattice. Studies have suggested that the decrease in overpotential is related to a loss of sulfur atoms from the material's surface during the electrochemical reaction, opening up vacancies, but this conclusion has been somewhat tentative, and its connection to the performance of the catalyst is unclear.

Researchers from Ruhr University Bochum, the Max Planck Institut für Eisenforschung, and the Fritz-Haber Institute (all Germany), and from the University of Central Florida and Argonne investigated the atomic structure of pentlandite during catalytic operation in aqueous sulfuric acid. They synthesized pentlandite and made customized electrolytic cells that they could place in the beamline. Using an x-ray beam from XSD beamline 3-ID-B,C,D tuned to a nuclear resonance frequency of iron-57 and striking the samples at a grazing angle, they conducted inelastic scattering measurements to probe the lattice vibrations (phonon spectrum) within about 500 nm of the sample surface (Fig. 1). The measurements were done at two potentials, -0.59 V and -0.79 V versus a common reference (reversible hydrogen electrode).

To interpret the measured phonon spectra, the researchers performed density functional theory (DFT) calculations to explore the spectra expected from the pentlandite lattice, with a variety of modifications. They first established that the iron-projected phonon spectrum of pentlandite in air (that is, under non-electrolysis conditions) agreed well with model predictions for the perfect lattice structure. The team then calculated the expected phonon spectrum of the lattice with two distinct changes: in one case, a hydrogen atom was added interstitially to the perfect lattice; in the other, a hydrogen atom was substituted for sulfur at a specific lattice position. Only the second scenario agreed with the measured nonresonant inelastic x-ray scattering data for an electrolytic cell operating at the least negative applied potential, -0.59 V.

X-ray measurements at the more negative potential, -0.79 V, showed a number of markedly different features. Under these conditions, with a greater current density through the electrodes, the researchers expected a larger number of hydrogen atoms to get into the lattice. The question was where they would go. As before, the calculated spectra from a perfect lattice with hydrogens added only at interstitial positions did not produce a good match to the experimental data. But the team was able to find a good fit with a model in which all available sulfur vacancies were filled with hydrogen atoms and then additional hydrogens took up interstitial positions. This change of the hydrogen uptake mechanism from substitutional to interstitial slows down the electrolysis, because the energy required to occupy interstitial positions is higher.

The researchers conclude that the combination of NRIXS measurements with DFT calculations makes a powerful tool to explore the performance of this and other HER catalysts, and provides new insight on how the structure of these materials might be modified to enhance their catalytic effect.

— David Lindley

See: Ioannis Zegkinoglou[1], Ali Zendegani[2], Ilya Sinev[1], Sebastian Kunze[1], Hemma Mistry[1,3], Hyo Sang Jeon[1], Jiyong Zhao[4], Michael Y. Hu[4], E. Ercan Alp[4], Stefan Piontek[1], Mathias Smialkowski[1], Ulf-Peter Apfel[1], Fritz Körmann[2], Jörg Neugebauer[2], Tilmann Hickel[2]*, and Beatriz Roldan Cuenya[1,5]**, "Operando Phonon Studies of the Protonation Mechanism in Highly Active Hydrogen Evolution Reaction Pentlandite Catalysts," J. Am. Chem. Soc. **139**, 14360 (2017). DOI: 10.1021/jacs.7b07902

Author affiliations: [1]Ruhr-University Bochum, [2]Max-Planck-Institut für Eisenforschung, [3]University of Central Florida, [4]Argonne National Laboratory, [5]Fritz-Haber Institute of the Max Planck Society

Correspondence:

** Beatriz.Roldan@rub.de

* t.hickel@mpie.de

This work was funded by the U.S. National Science Foundation (NSF-Chemistry 1213182, NSF-DMR 1207065) and the Deutsche Forschungsgemeinschaft (DFG) through the Cluster of Excellence RESOLV at RUB (EXC 1069). U.-P.A. thanks the Fonds der Chemischen Industrie (FCI) (Liebig grant), and the DFG (Emmy Noether grant AP242/2-1) for financial support. This research used resources of the Advanced Photon Source, a U.S. Department of Energy (DOE) Office of Science user facility operated by Argonne National Laboratory under Contract No. DE-AC02-06CH11357.

A Catalyst for Sustainable Power

In order to exploit solar energy fully, we need large-scale energy storage. In nature, the process of photosynthesis uses solar power to convert carbon dioxide and water into sugars that the plant can store and use later to release energy. One critical step in the process involves splitting the water into its oxygen and hydrogen equivalents. Recent research at the APS has focused on an artificial catalyst that can do the same job and generate oxygen from water when light shines on it. The water-splitting catalyst uses an Earth-abundant metal, cobalt, at its core, and works in water solution under everyday conditions. This latest work reveals information about the kinetic behavior of such catalysts in terms of how they accelerate reactions, provides detailed information about how light-induced electron transfer changes the nature of the bonds between pairs of oxygen atoms in the catalytic compound the team studied, and how an oxygen-evolving catalyst works through their model compound.

A catalyst that can split water into active oxygen and hydrogen units could be exploited in an artificial photosynthesis system for capturing the energy from sunlight and converting water into its elemental components that can be stored for future use. Recombining these constituents will generate an electric current in a suitable electrochemical cell or could be used in a zero-carbon combustion process. The catalyst studied on XSD beamline 12-BM-B at the APS is a cobalt oxide cubane compound, Co_4O_4 cubane. The "cubane" component of its name refers to the compound having a cube shape formed by pyridyl and acyl chemical groups that corner the metal ions in three dimensions. The cobalt metal ions at its core are in the III and the IV oxidation state, Its structure and stability were probed by spectroelectrochemical experiments and *in situ* x-ray absorption spectroscopy.

Understanding the structure of a catalytic system and how this relates to the properties of such compounds will take us forward another step toward systems that are analogous to the leaves of green plants in that they use sunlight to create chemical energy, which can then be stored and used later to generate electricity. Interestingly, however, the science is not hoping to simply mimic green plants, but to out-perform them in terms of the amount of "sustainable" energy that might be captured from the sun over unit area of the earth's surface. The cobalt catalysts known more generally as a Co-OEC (oxygen-evolving catalyst) are among the main leads in searching for OEC materials for such an endeavor. The production of oxygen as fuel oxidizing agent and the reduced fuel source, hydrogen (or an organic compound such as methanol or methane), could then be used to close the circuit in a carbon neutral manner.

The team has gained an important clue about precisely how the Co-OECs work through their model compound, Co_4O_4 cubane. The researchers explain that the metal ion being in a high-valent IV oxidation state is critical to catalysis and that their experiments on beamline 12-BM-B were essential for extracting this information. Earlier spectroscopic studies could not get to the heart of this because of the greater presence of less oxidized, lower valency cobalt(III) species in the system. The team's model catalyst bears a doubly oxidized $Co(III)_2(IV)_2$, and the Co(IV) in that unit is penetrable using *in situ* x-ray absorption spectroscopy. *— David Bradley*

See: Casey N. Brodsky[1], Ryan G. Hadt[2], Dugan Hayes[2], Benjamin J. Reinhart[2], Nancy Li[1], Lin X. Chen[2,3], and Daniel G. Nocera[1]*, "In situ characterization of cofacial Co(IV) centers in Co_4O_4 cubane: Modeling the high-valent active site in oxygen-evolving catalysts," Proc. Natl. Acad. Sci. USA **114**(15), 3855 (April 11, 2017). DOI: 10.1073/pnas.1701816114

Author affiliations: [1]Harvard University, [2]Argonne National Laboratory, [3]Northwestern University
Correspondence:
* dnocera@fas.harvard.edu

This material is based upon work supported under the Solar Photochemistry Program of the Chemical Sciences, Geosciences and Biosciences Division, U.S. Department of Energy (DOE) Office of Science-Basic Energy Sciences (D.G.N.) and the Solar Energy Conversion program in Chemical Sciences and Engineering Division at Argonne under Contract DE-AC02-06CH11357. R.G.H. is an Enrico Fermi Fellow at Argonne and D.H. is a Joseph J. Katz Postdoctoral Fellow at Argonne. C.N.B. is a National Science Foundation Graduate Research Fellow at Harvard University. This research used resources of the Advanced Photon Source, a U.S. DOE Office of Science user facility operated by Argonne National Laboratory under Contract No. DE-AC02-06CH11357.

12-BM-B • XSD • Materials science, polymer science, chemistry, physics, environmental science • X-ray absorption fine structure,, x-ray reflectivity,, small-angle x-ray scattering, wide-angle x-ray scattering • 4.5-30 keV, 10-40 keV • On-site • Accepting general users •

Life Science

Slow-Motion Unwrapping of DNA Gives a Peek into Nucleosome Disassembly

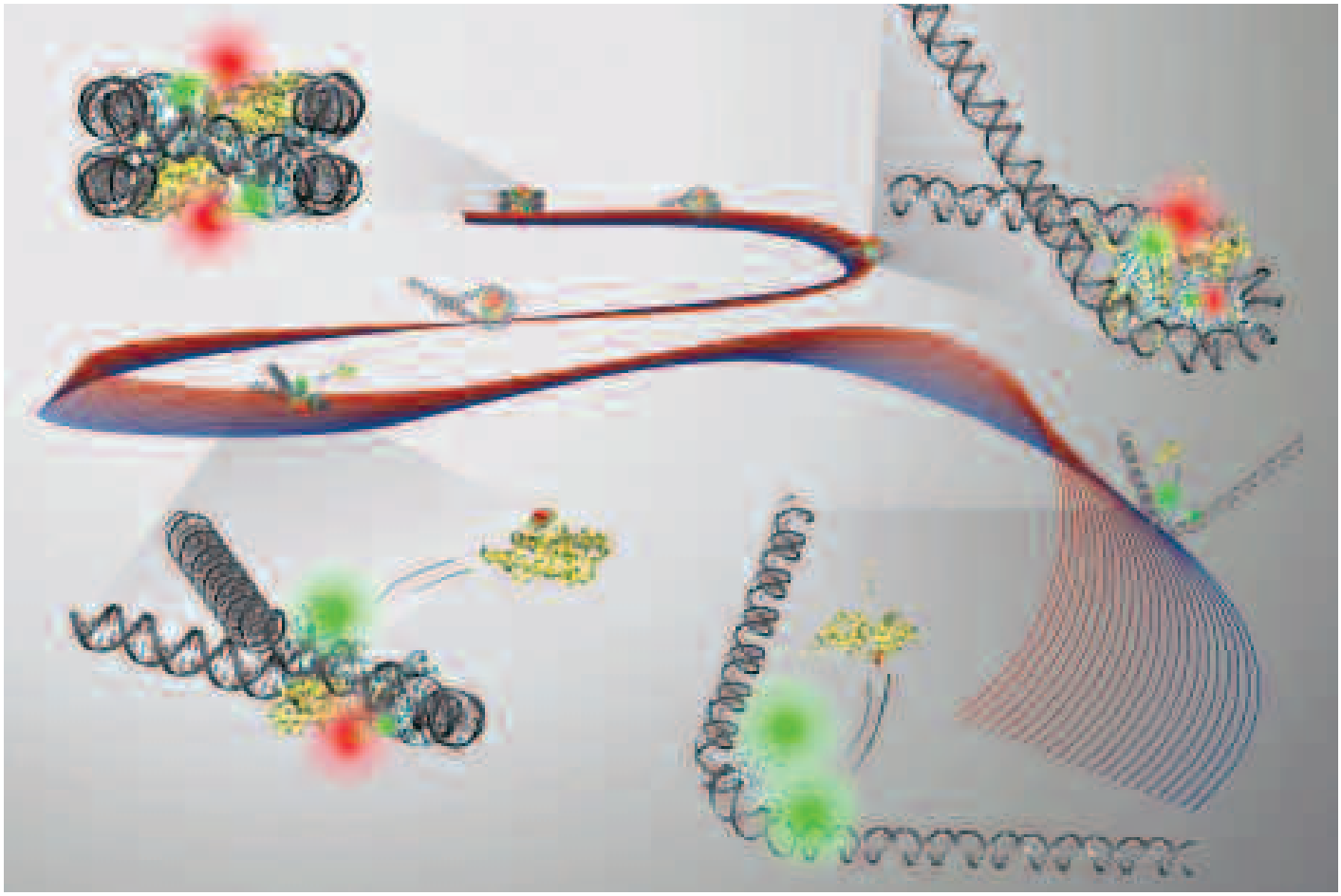

Fig 1. The NCP consists of DNA wound around a core of eight histone proteins. A team of researchers used SAXS to visualize DNA (dark gray) as it unwrapped and took on a variety of shapes. At the same time, the researchers used FRET fluorescence imaging to monitor the histone proteins (yellow and cyan), some of which are released as the NCP disassembles.

Nucleosomes are tightly packed bundles of DNA and protein which, when linked together as chromatin, form the 46 chromosomes found in human cells. The nucleosome core particle (NCP) consists of DNA wound around a core of eight histone proteins. Nucleosomes need to be disassembled to permit a variety of gene regulatory functions — including repair, replication, and transcription — then reassembled afterwards. Therefore, a critical component of gene regulation is nucleosome disassembly. A team of researchers used time-resolved small-angle x-ray scattering (SAXS) at the APS and time-resolved Förster resonance energy transfer (FRET) to study changes in the conformation of DNA and the composition of the histone core, respectively, during different stages of nucleosome disassembly. Using a method for slowing down the unfurling of DNA, the investigators found that components of the nucleosome are released sequentially with an octasome-to-hexasome (8 to 6 histone proteins) transition that is correlated with an asymmetric unwrapping of the DNA. This finding suggests changes to DNA conformation may facilitate the reconfiguration of the histone core. The dynamic structures captured by the researchers provide new insights into the regulation of DNA access during repair, replication, and transcription, and may have important implications for treating a variety of diseases.

46 chromosomes of the human genome in a straight line and it could stretch about 6 feet. All of that genetic material needs to be crammed into the nucleus of every cell in the body. Nature's solution is tightly winding DNA around nucleosomes, which are comprised of eight histone proteins (referred to as the octasome). This assembly is known as a nucleosome core particle (NCP). But DNA in the NCP does not remain forever packed away. Regular access is required for repairing DNA, replicating DNA, and transcribing DNA into mRNA, which can then be translated into proteins needed for routine cellular functions.

Access to DNA can be modulated through the disassembly of the histone core, a process that either facilitates or may be facilitated by DNA unwrapping. The static structure of the NCP is known from molecular x-ray crystallography, but this technique cannot capture large-scale movements within the NCP. However, NCP dynamics can be observed with imaging techniques such as time-resolved FRET and time-resolved SAXS. The trick is initiating the unwrapping. In the body, unwrapping of the DNA structure is elicited by proteins, such as histone chaperones and chromatin remodeling complexes. But it is known from previous studies that unwrapping can also be triggered by bathing the DNA in a solution of salt, which weakens the interactions between the DNA and proteins. In the current experiment, the researchers from Cornell University and Washington State University used different concentrations of added salt solutions to adjust the unwrapping process in order to take notice of each of the intervening steps.

The team utilized SAXS at the BioCAT beamline 18-ID-D at APS to observe the DNA slowly unwrapping over time (Fig. 1). With the SAXS technique, a sample is bombarded with a beam of x-rays, some of which scatter and strike a detector, forming a pattern that contains information on the structure of the sample. The team then used FRET, an imaging technique for observing the transfer of energy between donor and acceptor groups on closely positioned molecules, to monitor interactions among the histone proteins (Fig. 1).

The scientists found that different DNA shapes were produced during the unwrapping process, most notably an asymmetric "teardrop" shape that seemed to induce the histone core to transition from 8 protein molecules to 6 (Fig. 1). This change acts as a signal for disassembly of the histone core and suggests a readily accessible DNA shape that might serve as a good target for proteins in the cell.

The team's findings provide a step toward better understanding of DNA access during transcription, replication and repair. Misregulation of nucleosome assembly is also implicated in many human diseases, from neuro-development and degenerative disorders to immunodeficiency syndromes and cancer. Being able to view a slow-motion, up-close version of this process may provide insight that will aid in the development of new therapeutic strategies for these diseases.

— Chis Palmer

See: Yujie Chen[1], Joshua M. Tokuda[1], Traci Topping[2], Steve P. Meisburger[1], Suzette A. Pabit[1], Lisa M. Gloss[2]**, and Lois Pollack[1]*, "Asymmetric unwrapping of nucleosomal DNA propagates asymmetric opening and dissociation of the histone core," Proc. Natl. Acad. Sci USA **114**(2), 334 (January 10, 2017). DOI: 10.1073/pnas.1611118114
Author affiliations: [1]Cornell University, [2]Washington State University
Correspondence: * LP26@cornell.edu, ** lmgloss@wsu.edu

We thank Srinivas Chakravarthy, Weifeng Shang, and Richard Heurich for experimental and technical assistance at BioCAT (Sector 18-ID) Advanced Photon Source. SAXS research was supported by National Institutes of Health (NIH) Grants EUREKA R01-GM088645 and R01-GM085062 (to L.P.). Bio-CAT is supported by Grant 9 P41 GM103622 from the National Institute of General Medical Sciences (NIGMS) of the NIH. This research used resources of the Advanced Photon Source, a U.S. Department of Energy (DOE) Office of Science User Facilities operated for the DOE Office of Science by Argonne National Laboratory under Contract No. DE-AC02-06CH11357.

18-ID-D • Bio-CAT • Life sciences • Fiber diffraction, microdiffraction, small-angle x-ray scattering, time-resolved x-ray scattering • 3.5-35 keV • On-site • Accepting general users •

Packing and Unpacking Our DNA Suitcase

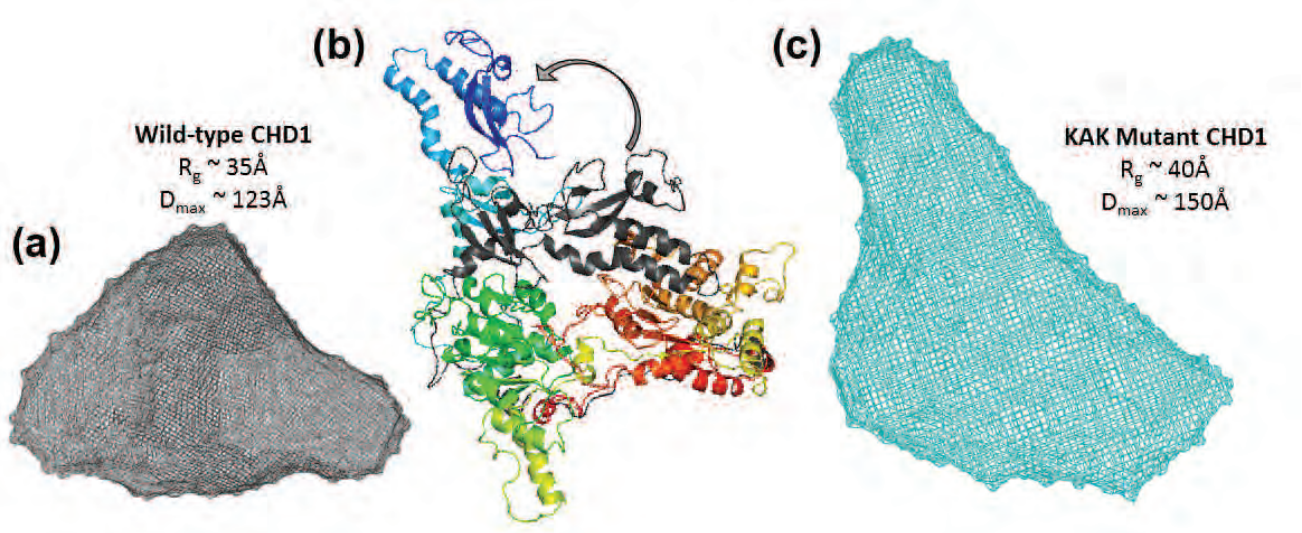

Fig. 1. Low-resolution envelopes calculated from small-angle x-ray scattering data acquired at Bio-CAT for the ATPase and chromo-domains of CHD1 (A = wildtype, C = KAK-mutant) show a more extended structure for the KAK(E265K/D266A/E268K) mutant as a result of disruption of the interface stabilizing the chromo-domain interaction with the ATPase domains (In B, chromo-domains in the wildtype position shown in gray – pdb ID 3mwy and in the speculated KAK-mutant position shown in blue). This important structural insight was used to explain the apparent higher affinity the KAK-mutant showed towards naked dsDNA and therefore a reduced auto-regulatory function of the chromo-domains.

One of the wonders of the biological world is the way our cells package DNA. The human genome consists of 3 billion base pairs and each cell has a full copy. That means each one of our cells has 6 ft of DNA packaged into the nucleus of a cell that is so small we cannot even see it. Take all of one's cells together and that is 10 billion miles of DNA! The cell performs this amazing feat by coiling the DNA and then wrapping it around histone proteins, which then pack into nucleosomes, to eventually form chromosomes. But there is one problem: We don't want to store our DNA like our old high school paraphernalia in the attic, forever and ever; we need to get it out and use it and then pack it away again, neatly, more like our suitcase on vacation. DNA packing is done by remarkable proteins called "DNA remodelers" that are responsible for assembling and disassembling nucleosomes and then sliding them along the DNA to position them evenly. In work that has implications for a variety of biomedical applications, including cancer research and immune diseases, researchers utilizing the APS have found a way to probe the sliding and packing activity of a remodeling protein called "Chd1."

A collaboration of investigators from Johns Hopkins University, the University of Illinois at Urbana-Champaign, the Illinois Institute of Technology, and the Indian Institute of Technology Delhi have developed a method for probing the details of the DNA/nucleosome/Chd1 remodeler interaction. Their method uses a fluorescence resonance energy transfer (FRET) system that generates a fluorescence signal based on the proximity of two different fluorescently-labeled molecules. When the molecules move together or apart, the signal changes.

In this case, the researchers used a labeled nucleosome and a labeled piece of DNA that was tethered to an immobile surface. When the remodeler protein, Chd1, was added, nothing happened. However, when Chd1 was added with ATP (adenosine triphosphate, an energy-carrying molecule found in the cells of all living things) the signal changed, indicating sliding activity associated with Chd1 action on the nucleosome. This ATP-dependent activity is consistent with previous work that has shown that Chd1 consists of an ATPase domain, a DNA binding domain, and two regulatory domains. Experiments with different concentrations of ATP showed that the sliding activity of Chd1 proceeds in "steps" along the DNA. The remodeler appears to move the nucleosome along the DNA in bursts that span multiple base pairs at one time.

Next, the team observed an interesting phenomenon in the FRET data. It appeared that some of the FRET traces showed a repositioning of the nucleosome back to its original position on the DNA. They found that this activity was ATP independent and further experiments suggested that Chd1 forms unstable intermediates that must be maintained by continued energy input. Testing with different lengths of DNA showed that the position is determined based on sequence rather than simply the length of the DNA and that one molecule of Chd1 can mediate movement in both directions.

This finding led to investigation of how the remodeler moves the nucleosome in both directions without losing contact with the DNA it is bound to. The answer seems to lie in the flexibility of the linker between the ATPase domain and the DNA binding domain. When investigators shortened the linker, reducing the flexibility of motion of the protein, they were only able to observe movement in a single direction. Finally, experiments utilizing the FRET system and small-angle x-ray scattering data generated at the Bio-CAT beamline 18-ID-D of the APS to probe the function of the regulatory domains of Chd1 suggest that their job is to make sure the whole package is ready before it is put into storage. If the nucleosome is not complete, the regulatory domains of Chd1 put a hold on the sliding action (Fig. 1).

The investigators hope that this detailed understanding of chromosome remodeling will provide important information for understanding DNA transcriptional activities that are key to many areas of biomedical research.

— Sandy Field

See: Yupeng Qiu[1,2], Rob Levendosky[1], Srinivas Chakravarthy[3], Ashok Patel[4], Gregory Bowman[1]**, and Sua Myong[1,2]*, "The Chd1 chromatin remodeler shifts nucleosomal DNA bidirectionally as a monomer," Mol. Cell **68**(1), 76 (2017).
DOI: 10.1016/j.molcel.2017.08.018
Author affiliations: [1]Johns Hopkins University, [2]University of Illinois at Urbana-Champaign, [3]Illinois Institute of Technology, [4]Indian Institute of Technology Delhi
Correspondence: * smyong@jhu.edu, ** gdbowman@jhu.edu

This work was supported by the Human Frontier Science Program (RGP0007/2012), American Cancer Society RSG-12-066-01-DMC, NIH 1DP2GM105453, National Science Foundation and Physics Frontiers Center Program (0822613) through the Center for the Physics of Living Cells to P.Q. and S.M., and NIH R01-GM084192 to G.D.B. Bio-CAT is supported by Grant 9 P41 GM103622 from the National Institute of General Medical Sciences of the National Institutes of Health. This research used resources of the Advanced Photon Source, a U.S. Department of Energy (DOE) Office of Science user facility operated for the DOE Office of Science by Argonne National Laboratory under Contract No. DE-AC02-06CH11357.

18-ID-D • Bio-CAT • Life sciences • Fiber diffraction, microdiffraction, small-angle x-ray scattering, time-resolved x-ray scattering • 3.5-35 keV • On-site • Accepting general users •

How Some Proteins Function on a Molecular Level

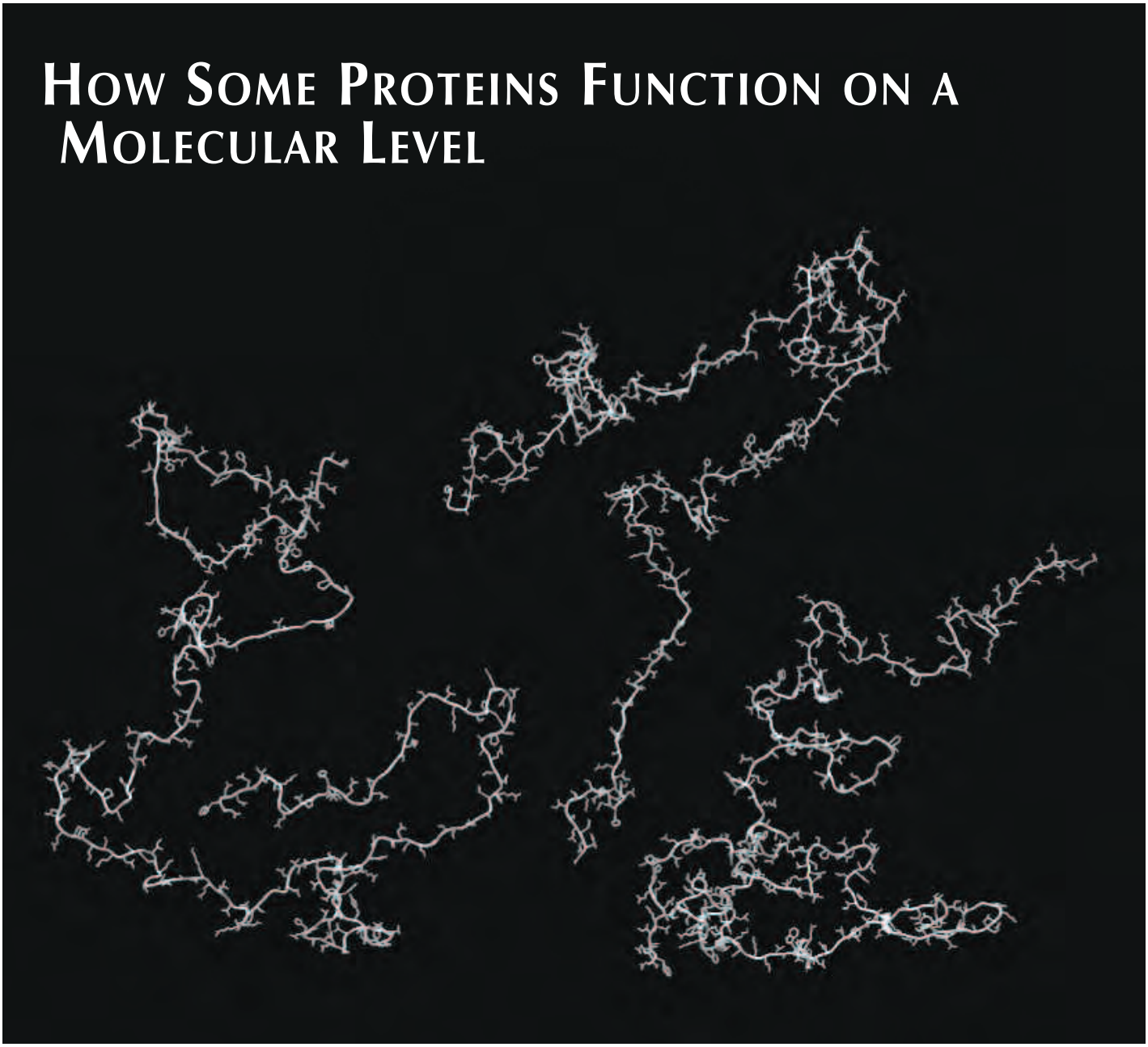

Fig. 1. An unfolded protein adopts expanded conformations according to recent SAXS measurements, as illustrated with these three conformations.

Understanding how proteins work on a molecular level has important implications for understanding a broad range of diseases. A recent study has advanced our knowledge of intrinsically disordered proteins (IDPs), many of which are essential components of key cellular processes. Although these proteins must be unfolded to function properly, controversy has persisted about how disordered these proteins are. Researchers collected data at the APS, and developed a new analysis procedure to assess what happens to IDPs under physiological conditions. The results showed that IDPs are even more disordered than scientists had initially suspected, remaining expanded, not collapsed, under physiological conditions. The researchers propose that this is an evolutionary adaptation to avoid misfolding and aggregation in cells. The results of this study could ultimately help scientists develop new strategies to prevent diseases related to protein misfolding.

Scientists traditionally believed that proteins functioned only when correctly folded into complex three-dimensional shapes. However, in recent decades, studies have challenged this concept, showing that some proteins, the IDPs, including those involved in key cellular processes, need to be completely or partially unfolded to properly function. It is estimated that about 30% of all human proteins are disordered. A characteristic feature of these proteins is that they contain more polar and charged amino acids compared to foldable proteins. This allows IDPs to favorably interact with water.

Many questions about IDPs remain unanswered including the extent of their disorder. For example, under physiological conditions in the cell, are they expanded like a rope or collapsed into a ball? Increased understanding of the conformational changes of IDPs is not only important to realizing how these proteins carry out their different functions, but is also key to better understanding the pathogenesis of protein misfolding-related diseases. So, in the quest for more information, scientists have performed studies using small-angle x-ray scattering (SAXS) and have compared the results to those from fluorescence resonance energy transfer (FRET), to determine the dimensions of IDPs and how they interact with themselves.

According to the researchers, SAXS allows scientists to analyze the conformation of IDPs in solution. In this method, a solution of the protein sample is illuminated by an x-ray beam, causing the beam to scatter in a pattern that relates to the specific shape and size of the protein under investigation. In contrast, in FRET, scientists attach fluorescent molecules to the IDP and determine the size and shape of the IDP by calculating the distance between the fluorescent molecules. Yet, the results using these different techniques have been conflicting. FRET studies have suggested that certain IDPs collapse in water, while most SAXS studies have not observed this collapse.

With this in mind, researchers from The University of Chicago and the University of Notre Dame conducted studies to better characterize IDPs. With data collected at the Bio-CAT beamline 18-ID-D at the APS, they developed a new SAXS approach in order to examine the structure of IDPs under physiological conditions. Their technique involved examining more of the x-ray scattering profile than has been previously analyzed for SAXS, and matching the profiles to models of variably-disordered IDPs that were generated by computer simulations.

In their study, the researchers applied this method to numerous IDPs, and found that most were more disordered than previously realized. The results showed that even IDPs with high hydrophobicity remained expanded in water. These findings therefore suggest that the unfolded state of most foldable protein sequences is expanded (Fig. 1). The researchers hypothesize that this helps to prevent IDPs from unproductively interacting with themselves or with other proteins and resulting in protein dysfunction or misfolding-related diseases.

This more detailed understanding of IDPs can help guide further studies of protein folding and misfolding mechanisms, and could also help identify new ways to prevent protein misfolding diseases. *— Nicola Parry*

See: Joshua A. Riback[1], Micayla A. Bowman[2], Adam M. Zmyslowski[1], Catherine R. Knoverek[2], John M. Jumper[1], James R. Hinshaw[1], Emily B. Kaye[2], Karl F. Freed[1], Patricia L. Clark[2]*, and Tobin R. Sosnick[1]**, "Innovative scattering analysis shows that hydrophobic disordered proteins are expanded in water," Science **358**, 238 (13 October 2017).
DOI: 10.1126/science.aan5774
Author affiliations: [1]The University of Chicago, [2]University of Notre Dame
Correspondence: * pclark1@nd.edu, * trsosnic@uchicago.edu

This research was supported by National Institutes of Health grants GM055694 (T.R.S., K.F.F.), GM097573 (P.L.C.), GM103622 and 1S10OD018090-01 (T. C. Irving), T32 EB009412 (T.R.S.), T32 GM007183 (B. Glick), and T32 GM008720 (J. Picirrilli) and by National Science Foundation grants GRF DGE-1144082 (J.A.R.) and MCB 1516959 (C. R. Matthews). Bioi-CAT is supported by grant 9 P41 GM103622 from the National Institute of General Medical Sciences of the National Institutes of Health. This research used resources of the Advanced Photon Source, a U.S. Department of Energy (DOE) Office of Science user facility operated for the DOE Office of Science by Argonne National Laboratory under Contract No. DE-AC02-06CH11357.

18-ID-D • Bio-CAT • Life sciences • Fiber diffraction, microdiffraction, small-angle x-ray scattering, time-resolved x-ray scattering • 3.5-35 keV • On-site • Accepting general users •

Structural Characterization of the Growth-Ring Layers in Teeth

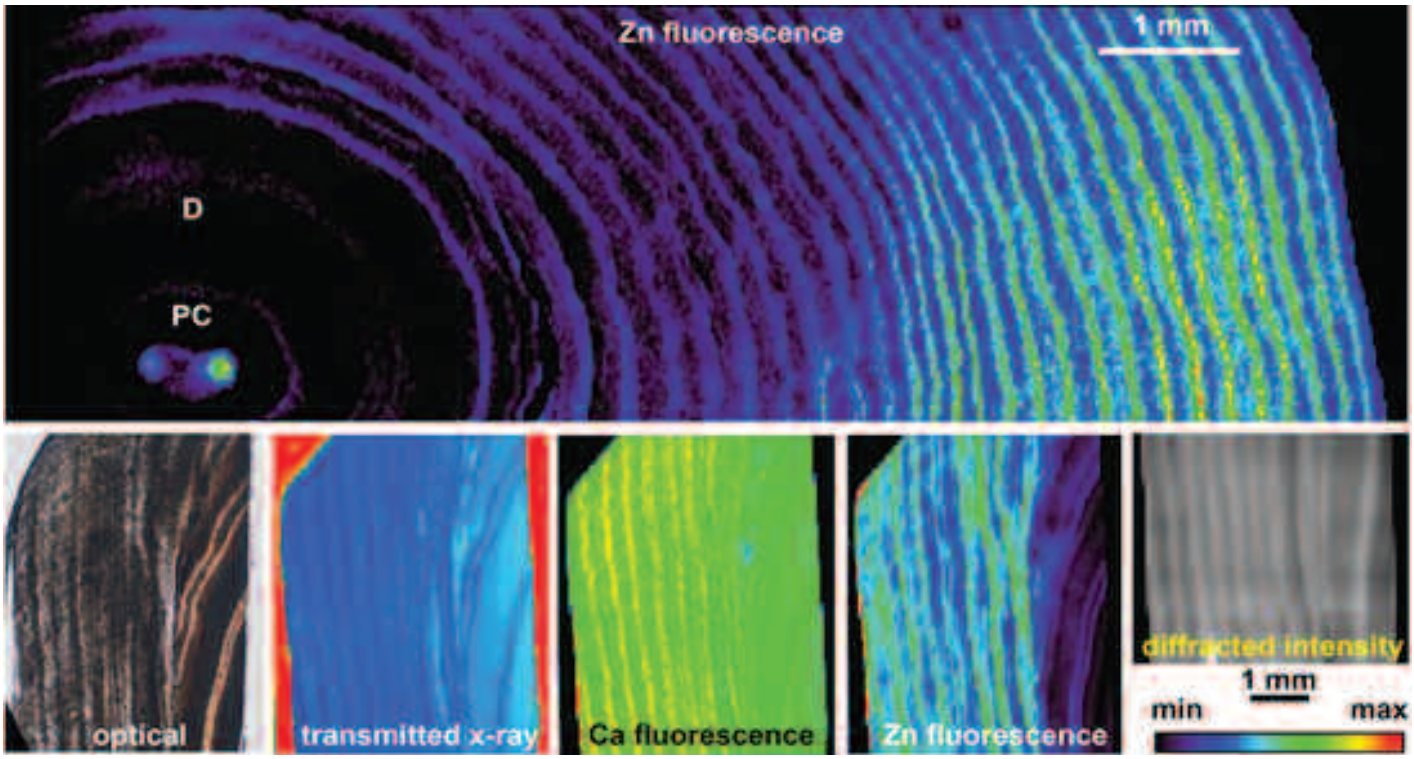

Fig. 1. Top: Zinc fluorescence intensity map of the transverse cross-section of a tooth. Pulp cavity is labeled "PC" and dentin surrounding the pulp cavity is labeled "D." Bottom: Longitudinal tooth sections under the imaging techniques used in this study. The cementum band structure is shown clearly in each one. The transmitted x-ray intensity, calcium (Ca) fluorescence intensity and zinc (Zn) fluorescence intensity maps were recorded simultaneously. The other two maps were recorded separately.

If one counts the rings in a cross-section of a Redwood tree, one for every year of the tree's life, one might lose track. But trees aren't the only species that make annual layered structures. The teeth of vertebrate animals also have rings in an outer layer. By examining these tiny layered structures in beluga whale teeth at the APS, researchers found that calcium and zinc content defines each layer from its neighbor. Their work could make dating of human teeth easier and more accurate.

The outermost layer of teeth roots consist of cementum, a dynamic mineralized tissue made of collagen, proteoglycans and hydroxyapatite. Cementum connects teeth to ligaments in the mouth, securing them in place. Ever noticed the yellow layer on roots of extracted teeth? That's cementum. Under a light microscope, alternating light and dark layers of cementum can be observed in polished cross-sections of teeth. But the layers of human teeth are so thin that they are difficult to count.

An alternative approach to ring-counting that depends instead on structural differences between layers of cementum is offered by the team of researchers from Northwestern University and Argonne. Differences between layers has been hard to pin down — some research shows orientation of collagen or variation in mineral content defines the bands, others find no variation in these materials. But by mapping elements present in beluga whale teeth with x-ray fluorescence, the team found that variation of intensity emitted by zinc atoms is a reliable way to track layers of cementum.

To study cementum layers in depth, the researchers used small x-ray beams, tens of micromicrons in diameter, to map x-ray fluorescence emission and x-ray diffraction from samples of beluga whale teeth. While the thickness of cementum layers in human teeth is 5 to 10 μm, beluga whales have much more widely spaced layers, about 200-μm thick. Thus, the x-ray beams used in this study, 30 to 50 μm in diameter, could easily resolve layers in beluga whale cementum.

The teeth were prepared to give researchers two different viewpoints. When cut in the transverse direction, making 15-mm-wide discs, cementum layers showed as concentric rings. But if cut in the longitudinal direction — down the center of the tooth from top to bottom, following the root and pulp — cementum layers appeared as long, parallel columns.

Researchers took full x-ray fluorescence spectra at every point in a raster scan of the samples using the XSD 8-BM-B beamline at the APS. In a separate experiment, diffraction patterns of the longitudinal samples were taken at the XSD 17-BM-B beamline at the APS.

In the x-ray fluorescence experiment, the appreciable intensities from both zinc and calcium were mapped and compared to optical density and x-ray transmission from the same part of the sample. Researchers found that the alternating dark and light layers of cementum observed optically corresponded to changes in zinc and calcium fluorescent intensity. In the dark layers, emission was higher, while in the light layers, emission decreased. The intensity of x-rays transmitted through the specimen followed the opposite trend; decreasing in dark layers and increasing in light layers.

Not only did the signal intensities correlate, the peaks and valleys matched exactly. The x-ray fluorescence emission from zinc and calcium, and thus concentrations of zinc and calcium in the cementum, are therefore an indicator of the layered structure. A matching periodic variation in signal intensity was observed in x-ray diffraction peaks of the longitudinal samples. These peaks arise from the crystalline hydroxyapatite, the calcium-based mineral within cementum.

No matter the method — x-ray fluorescence or diffraction — the period in both transverse and longitudinal samples gave the same value of 200 to 250 μm for the cementum layer thickness.

In all, 28 cementum layers were counted in the samples. Just like counting tree rings, this means that the beluga whale the teeth came from an individual at least 28 years old at death, which is consistent with previous measurements of these samples and the lifespan of beluga whales.

The beam diameters in this study are too large to resolve cementum layers in the teeth of many other mammals like humans, cows and reindeer. But the researchers note that ~ 250-nm x-ray beams have been used to map fluorescence from calcium and zinc in around micrometer wide tubules in dentin and could be used to resolve more finely spaced tooth samples. If smaller beams are used, this method could give physical anthropologists much better age estimates for almost any mammal.

— Amanda Grennell

See: S.R. Stock[1]*, L.A. Finney[2], A. Telser[1], E. Maxey[2], S. Vogt[2], and J.S. Okasinski[2], "Cementum structure in Beluga whale teeth," Acta Biomater. **48**, 289 (2017).
DOI: 10.1016/j.actbio.2016.11.015
Author affiliations: [1]Northwestern University, [2]Argonne National Laboratory
Correspondence:
* s-stock@northwestern.edu

The authors thank Greg Halder (APS) for support in data collection at 17-BM-B. The research was supported by National Institute of Dental and Craniofacial Research grant DE001374. This research used resources of the Advanced Photon Source, a U.S. Department of Energy (DOE) Office of Science user facility operated for the DOE Office of Science by Argonne National Laboratory under Contract No. DE-AC02-06CH11357.

8-BM-B • XSD • Chemistry, life sciences, environmental science, materials science • Microfluorescence (hard x-ray) • 5.5-20 keV, 9-18 keV • On-site • Accepting general users •

17-BM-B • XSD • Chemistry, materials science • Powder diffraction, pair distribution function • 27-51 keV • On-site • Accepting general users •

DATA

Numberof experiments at the APS (FY 1998-2017)

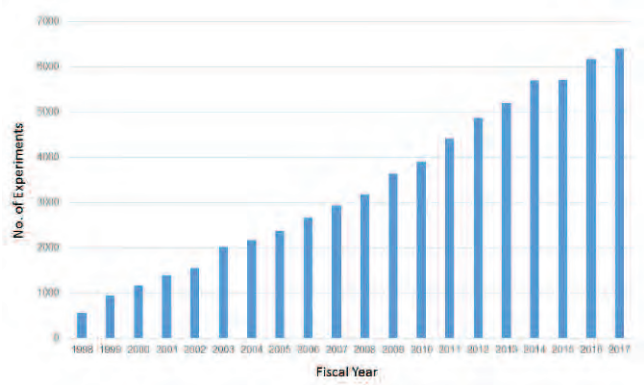

APS users by on-site and remote (FY 1998-2017)

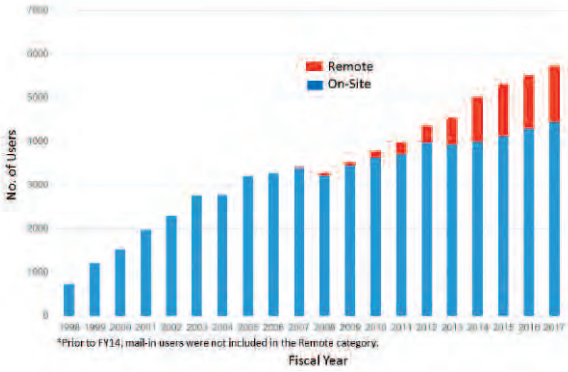

APS users by experiment subject (FY 2017)

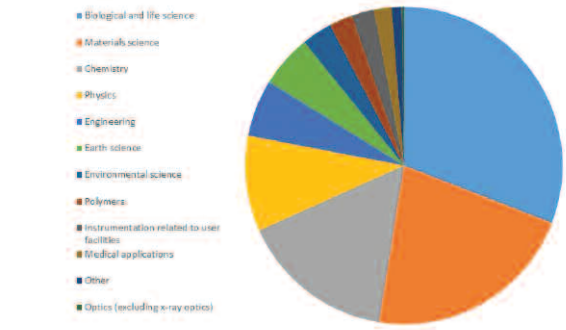

APS users by user type (FY 2017)

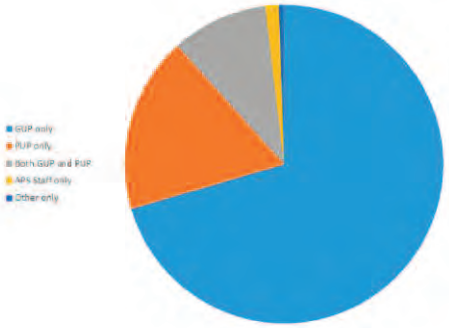

APS users by employer (FY 2017)

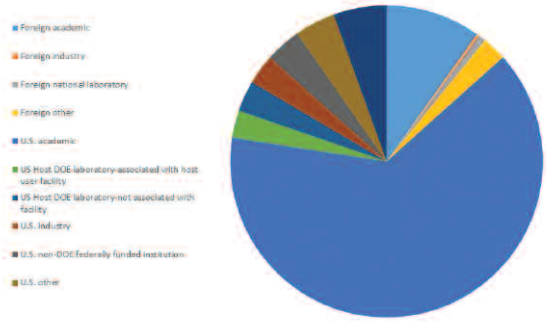

APS users by source of support (FY 2017)

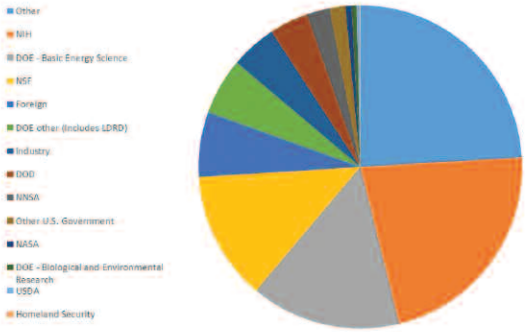

APS users: proprietary/non-proprietary (FY 2017)

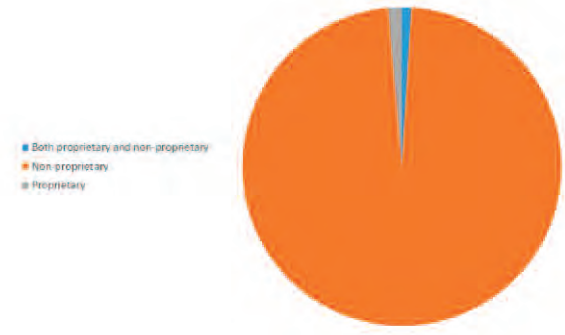

APS users by institutional geographic distribution (FY 2017)

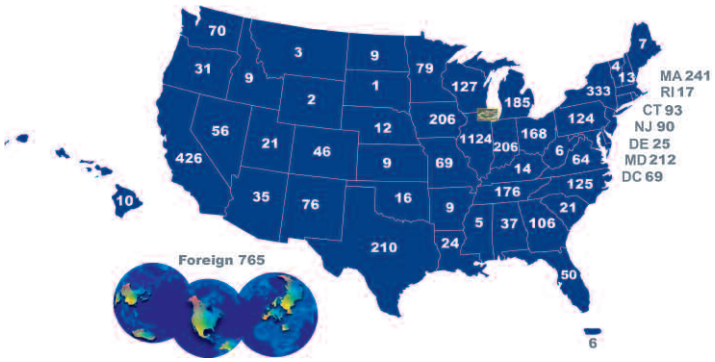

Structural Biology

Designing an Alternative to Opioids

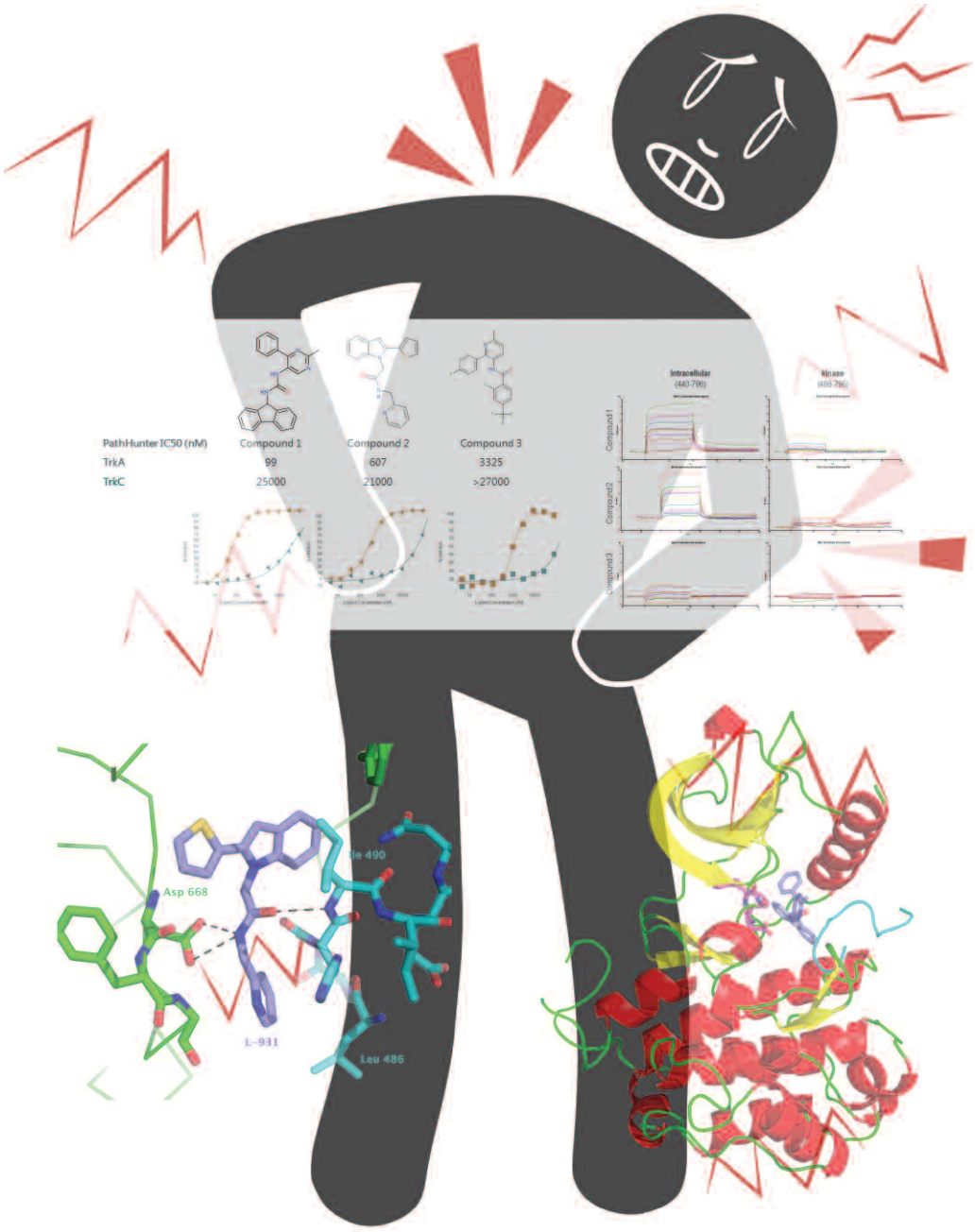

Fig. 1. Using structure information to design a new therapy to treat chronic pain. The researchers in this study utilized an affinity ligand screening technique and structure-based investigations to identify three compounds that specifically inhibit the TrkA kinase, a potential new target for treatment of chronic pain. Image courtesy of Hua-Poo Su.

17-ID-B • IMCA-CAT • Life sciences • Macromolecular crystallography, multi-wavelength anomalous dispersion, microbeam, single-wavelength anomalous dispersion, large unit cell crystallography • Subatomic (<0.85 Å) resolution • 6-20 keV • On-site, remote • Accepting general users •

Managing chronic pain is of critical importance in medicine, but current treatment options, from anti-inflammatory drugs to opioids, don't work for all patients, many of whom are challenged by inadequate pain relief, intolerable side effects, or the risks associated with addiction. New options for pain relief are clearly needed. One area that shows promise has arisen from recent research that has uncovered a new role for neurotrophic growth factor (NGF) and its receptor, the tropomyosin-related kinase (TrkA). NGF signaling through TrkA, well-known for its importance in neuronal growth and survival, has now been shown to regulate pain signaling pathways as well. The pathway activates expression of pain receptors on the cell surface and release of peptides that transmit the pain signal. These molecular data are supported by clinical data, which show that an antibody that blocks the interaction between NGF and TrkA can reduce pain in patients with osteoarthritis, chronic lower back pain, diabetic neuropathy, and cancer. However, antibodies are biologic treatments that are expensive and have side effects of their own; a small-molecule inhibitor of the TrkA kinase would be preferable. A team of researchers has taken on this challenge and, with an assist from APS x-rays, developed a system for screening and evaluating candidate small-molecule inhibitors for the TrkA receptor.

The trick with developing an inhibitor for the TrkA kinase is that it is a member of a conserved family of 518 kinases in the human genome and the desired medicine should only hit the kinase of interest. Off-target binding can cause side effects and reduce efficacy. TrkA resides on the inside of the plasma membrane of cells and responds to NGF interactions with a receptor domain on the cell surface. The intracellular kinase domain and the receptor are linked by a transmembrane domain that stretches across the cell membrane and an unstructured juxtamembrane (JM) domain that tethers the kinase to the rest of the protein and is involved in some downstream signaling events. The structure of the TrkA kinase domain is known and resembles that of other kinases.

Kinase inhibitors either bind to the catalytic active site, a "back pocket" behind the active site, or a combination of these plus other sites on the protein. Binding to other sites provides specificity that allows for inhibition of just the kinase in question. Reasoning that the ideal inhibitor for TrkA would bind to both the kinase domain and other sites on the protein, the team from Merck & Co, Inc., designed an affinity ligand identification system to screen for inhibitors that bound to the TrkA kinase plus the JM region. From the screen, they triaged candidates in a cell-based assay to find inhibitors that were selective for TrkA but did not bind close family members TrkB and TrkC. The specificity of the candidates was confirmed by challenging them against a broader kinase panel of 93 kinases, including TrkB and TrkC. The findings from the screening were confirmed and three candidate compounds that specifically inhibited TrkA were identified (Fig. 1).

The next challenge was crystallography. When the team tried to crystallize their three inhibitors with just the kinase domain of TrkA, they could not get crystals to form. They decided that the inhibitors must also require some contacts with the JM because that was present in the screening but not in the protein they used for crystallography. They had left the JM out of the crystallography step because the disordered structure of the JM can potentially disrupt crystal formation. To overcome this problem, the team designed six constructs with the full kinase domain and various lengths of the JM. They chose the shortest one that bound all of the inhibitors for crystallization, calling it JM-kinase.

Solution of the structure, using data collected at the IMCA-CAT 17-ID-B beamline at the APS, showed that the inhibitors bound in different "modes." The team identified a mode that bound to the back pocket of the kinase plus some of the JM and another that bound the back pocket and a longer piece of the JM. These differences are important because the JM is not well-conserved between Trk family members and could confer specificity on inhibitors. The team has shown that they can change qualities based on the modes they have discovered and can design inhibitors against just TrkA or the whole family of Trk proteins. This knowledge will guide the team in designing an inhibitor with all of the qualities they want.

— Sandy Field

See: Hua-Poo Su*, Keith Rickert‡, Christine Burlein, Kartik Narayan‡‡, Marina Bukhtiyarova, Danielle M. Hurzy, Craig A. Stump, Xufang Zhang‡‡‡, John Reid, Alicja Krasowska-Zoladek, Srivanya Tummala, Jennifer M. Shipman, Maria Kornienko, Peter A. Lemaire‡‡‡‡, Daniel Krosky‡‡‡‡‡, Amanda Heller‡‡‡‡‡‡, Abdelghani Achab, Chad Chamberlin, Peter Saradjian, Berengere Sauvagnat, Xianshu Yang, Michael R. Ziebell‡‡‡‡‡‡‡, Elliott Nickbarg, John M. Sanders, Mark T. Bilodeau‡‡‡‡‡‡‡‡, Steven S. Carroll, Kevin J. Lumb, Stephen M. Soisson, Darrell A. Henze, and Andrew J. Cooke, "Structural characterization of nonactive site, TrkA-selective kinase inhibitors," Proc. Natl. Acad. Sci. USA **114**(3), E297 (January 17, 2017).
DOI: 10.1073/pnas.1611577114
All authors' affiliation: Merck & Co., Inc.

Present addresses: ‡MedImmune, ‡‡Sanofi Pasteur, ‡‡‡Spectrix Analytic Services, LLC., ‡‡‡‡Bristol-Myers Squibb, ‡‡‡‡‡Janssen R&D LLC., ‡‡‡‡‡‡LabConnect, LLC., ‡‡‡‡‡‡‡Novartis Institutes of BioMedical Research, ‡‡‡‡‡‡‡Tarveda Therapeutics

Correspondence:
* hua-poo_su@merck.com

Use of the IMCA-CAT beamline was supported by the companies of the Industrial Macromolecular Crystallography Association through a contract with Hauptman-Woodward Medical Research Institute. This research used resources of the Advanced Photon Source, a U.S. Department of Energy (DOE) Office of Science user facility operated for the U.S. DOE Office of Science by Argonne National Laboratory under Contract DE-AC02-06CH11357.

Structure-based Cattle Vaccine Could Point to a Human RSV Vaccine

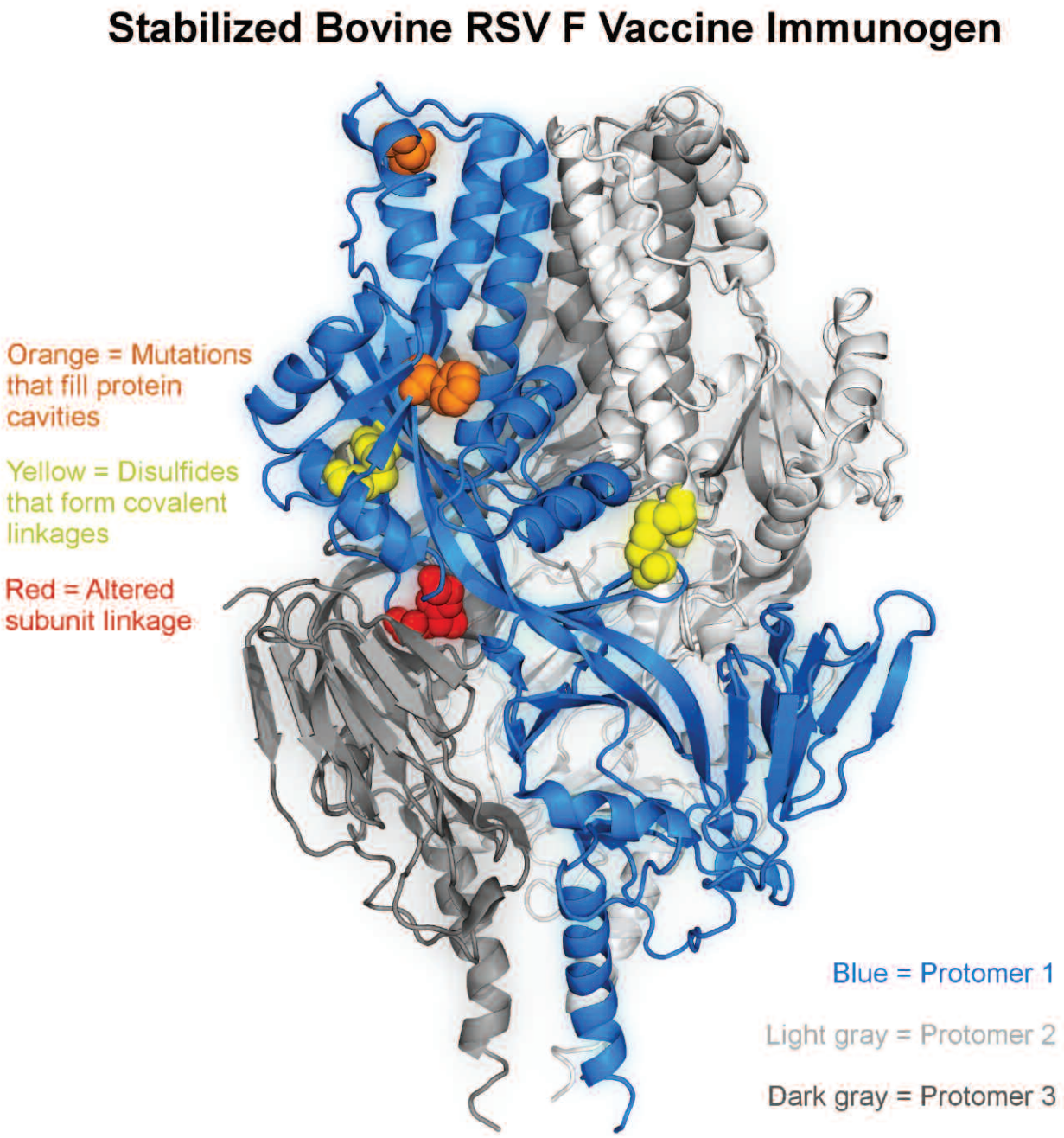

Fig. 1. X-ray crystallography structure of the DS2-stabilized immunogen (blue, light gray, dark gray) is displayed in ribbon representation with stabilizing mutations (orange, yellow, red).

Respiratory syncytial virus (RSV) is the dominant cause of severe respiratory infections in children and calves. However, no licensed human RSV (hRSV) vaccine is available, and bovine RSV (bRSV) vaccines suffer from issues of effectiveness. Researchers, therefore, set out to design, develop, and evaluate an investigational structure-based fusion (F) glycoprotein bRSV vaccine called "DS2," testing it in calves aged 3 to 6 weeks. They collected data at the APS to validate the structure-based design and showed that the novel vaccine generated high titers (concentrations), of neutralizing antibodies, protecting calves from bRSV infection. The results of this study could help to reduce the incidence of bRSV, and — by using a similar vaccine construct for hRSV — could also help scientists develop an efficacious hRSV vaccine.

bRSV is an important cause of respiratory disease in calves, causing high morbidity and mortality, leading to economic losses estimated at more than $1 billion per year. The virus is closely related to hRSV, which results in more than three million hospitalizations for severe respiratory illness annually in children and elderly people, and also presents a significant burden on healthcare resource use and costs.

Currently, no hRSV vaccine is licensed for use, and — although licensed bRSV vaccines are available — none are very effective. For both calves and infants, vaccines must overcome difficulties associated with activation of still-developing immune systems. Another hurdle is the need to vaccinate early, when maternal RSV-directed antibodies are still present and could inhibit the RSV-directed vaccine response.

Development of safe and effective RSV vaccines for cattle and humans remains a priority, and research is ongoing. So far, scientists have found that the most potently neutralizing RSV antibodies target the pre-fusion form of the RSV fusion (F) glycoprotein. Unfortunately, the metastable pre-fusion RSV F changes to the less effective post-fusion form of the protein in a matter of hours. Therefore, a way had to be found to stabilize RSV F in the pre-fusion form for use in vaccines.

A collaboration was formed by researchers from the National Institutes of Health, Università della Svizzera italiana (Switzerland), The Pirbright Institute (UK), the Frederick National Laboratory for Cancer Research, Humabs BioMed SA (Switzerland), and ETH Zurich (Switzerland) to develop and test such a vaccine. In their study, the researchers used the known structures of pre-fusion hRSV F to embark on an iterative, structure-based design process to stabilize bRSV F into its pre-fusion form and to obtain a vaccine immunogen that elicits highly protective immune responses against bRSV.

Using 2.64-Å and 3.6-Å x-ray diffraction data collected at the SER-CAT beamlines 22-BM-D and 22-ID-D at the APS, the researchers performed crystallographic analysis of two bRSV F vaccine immunogen variants, DS-Cav1 and DS2. The best immune responses were generated with the DS2 variant, which contained two additional disulfide bonds (Fig. 1).

The researchers tested the novel DS2 vaccine immunogen in five calves aged 3 to 6 weeks. They also immunized another five calves with a post-fusion F glycoprotein immunogen in its fully triggered conformation. They gave the calves two injections of the respective immunogens, four weeks apart. Four weeks after the second injection, they infected all calves with bRSV.

They found the investigational DS2 vaccine to induce high titers, of neutralizing antibodies, which protected the immunized calves from bRSV infection. The titers were more than 100-fold higher than those generated by the post-fusion conformation of bRSV F.

The results of this study have implications for both cattle and humans. In particular, the effectiveness of the investigational vaccine bodes well for the prevention of bRSV infection in calves. And because bRSV provides a good model for hRSV, vaccination with an equivalent hRSV vaccine is therefore likely to generate high levels of protection. A similar approach with hRSV might therefore allow scientists to produce an effective vaccine to protect people from infection by hRSV. Indeed, imilar approaches are already underway with hRSV, with clinical results expected soon. *— Nicola Parry*

See: Baoshan Zhang[1], Lei Chen[1], Chiara Silacci[2], Michelle Thom[3], Jeffrey C. Boyington[1], Aliaksandr Druz[1], M. Gordon Joyce[1], Efrain Guzman[3], Wing-Pui Kong[1], Yen-Ting Lai[1], Guillaume B.E. Stewart-Jones[1], Yaroslav Tsybovsky[4], Yongping Yang[1], Tongqing Zhou[1], Ulrich Baxa[4], John R. Mascola[1], Davide Corti[2,5], Antonio Lanzavecchia[2,6]*, Geraldine Taylor[3]**, and Peter D. Kwong[1]***, "Protection of calves by a prefusion-stabilized bovine RSV F vaccine," Vaccine **7**, 1 (2017). DOI: 10.1038/s41541-017-0005-9

Author affiliations: [1]National Institutes of Health, [2]Università della Svizzera italiana, [3]The Pirbright Institute, [4]Frederick National Laboratory for Cancer Research, [5]Humabs BioMed SA, [6]ETH Zurich

Correspondence:
* lanzavecchia@irb.usi.ch,
** geraldine.taylor@pirbright.ac.uk,
*** pdkwong@nih.gov

This work was supported by the Intramural Research Program of the Vaccine Research Center, National Institute of Allergy and Infectious Diseases, National Institutes of Health (NIH); Frederick National Laboratory for Cancer Research, NIH under contract with Leidos Biomedical Research, Inc.; the Helmut Horten Foundation; and the BBSRC Institute Strategic Programme on Livestock Viral Diseases at The Pirbright Institute, where G.T. is a Jenner Investigator. The Southeast Regional Collaborative Access Team supporting institutions may be found at www.ser-cat.org/members.html. This research used resources of the Advanced Photon Source, a U.S. DOE O□ce of Science user facility operated for the DOE O□ce of Science by Argonne National Laboratory under Contract No. DE-AC02-06CH11357.

22-BM-D • SER-CAT • Life sciences • Macromolecular crystallography, single-wavelength anomalous dispersion, multi-wavelength anomalous dispersion • 8-20 keV • On-site, remote • Accepting general users •

22-ID-D • SER-CAT • Life sciences • Macromolecular crystallography, multi-wavelength anomalous dispersion, single-wavelength anomalous dispersion, microbeam • 6-20 keV • On-site, remote • Accepting general users •

A Molecular Mechanism for Activity Important in Cell Division and Cancer Development

When human cells replicate, duplicated cellular DNA, packaged as chromosomes, is evenly divided or "segregated" into daughter cells. Before duplicated chromosomes can be segregated and pulled apart into daughter cells by the cellular replication machinery, the cohesion holding sister chromatids together must be dissolved. The protein separase is an enzyme responsible for cleaving the cohesion protein once chromatids are properly aligned and ready for cell division. The timing of this cleavage is critically important, and excessive separase activity is known to occur in the abnormally dividing cells within human tumors. To understand the molecular basis for separase activity and its inhibition by securin — a protein responsible for ensuring that separase remains inactive until it is required — researchers determined the crystal structures of the yeast separase-securin complex up to a resolution of 2.6Å, using the APS. The structures not only reveal the domain organization and overall architecture of separase, but provide a mechanism by which securin inhibits separase. These data provide the structure of a protein important in cell division and detail the molecular mechanism by which securin regulates separase activity at an atomic level. The findings shed light on the basic functions of these two proteins, and pave the way for additional studies on the atomic structure and regulation of human separase, a direct target for potential drug discovery against cancer.

Like the activities of many other cellular proteins, it is important that separase only be active at the right time. Dysregulation of separase activity results in aberrant cell division and uneven distribution of genetic material, an outcome that can ultimately lead to cancer.

In order to control separase activity, the protein securin forms a tight complex with separase, which stabilizes the protease and inhibits its activity. Prior to the publication of this work, the atomic structure of the full-length separase in complex with securin was unknown, and the mechanism by which securin regulates separase was unclear and understood only through biochemical experiments. High-resolution x-ray diffraction data from crystallized separase-securin complex obtained at the NE-CAT x-ray beamlines 24-ID-E and 24-ID-C at the APS permitted researchers to build a model of the complex and illuminate the mechanism of separase inhibition by securin (Fig. 1).

The structures revealed that separase assumes a highly elongated shape and that the overall architecture of the protein includes six protein domains, I, II, III, IV, SD (substrate-binding domain) and CD (catalytic domain). In contact with each of the separase domains is the separase interaction segment (SIS) of securin, located at the C-terminal portion of the protein. This degree of contact is consistent with previous experimental observations that securin can serve as a chaperone, or structural stabilizer, for separase. Most importantly, the N-terminal residues of the securin SIS are located in the separase active site, where cohesion proteins are cleaved, thereby blocking the binding of this substrate. However, securin SIS itself is not cleaved because it assumes a conformation incompatible with proteolysis.

— Emma Nichols

See: Shukun Luo and Liang Tong*, "Molecular mechanism for the regulation of yeast separase by securin," Nature **542**, 255 (9 February 2017). DOI: 10.1038/nature21061

Author affiliation: Columbia University
Correspondence:
* ltong@columbia.edu

We thank S. Banerjee, K. Perry, R. Rajashankar, J. Schuermann, and N. Sukumar for access to NE-CAT 24-C and 24-E beamlines at the Advanced Photon Source. This research is supported by grants R35GM118093 and S10OD012018 from the National Institutes of Health (NIH) to L.T. This work is based upon research conducted at the NE-CAT beamlines, funded by the NIH (P41 GM103403). The Pilatus 6M detector on 24-ID-C beam line is funded by an NIH-ORIP HEI grant (S10 RR029205). This research used resources of the Advanced Photon Source, a U.S. Department of Energy (DOE) Office of Science user facility operated by Argonne National Laboratory under Contract no. DE-AC02-06CH11357.

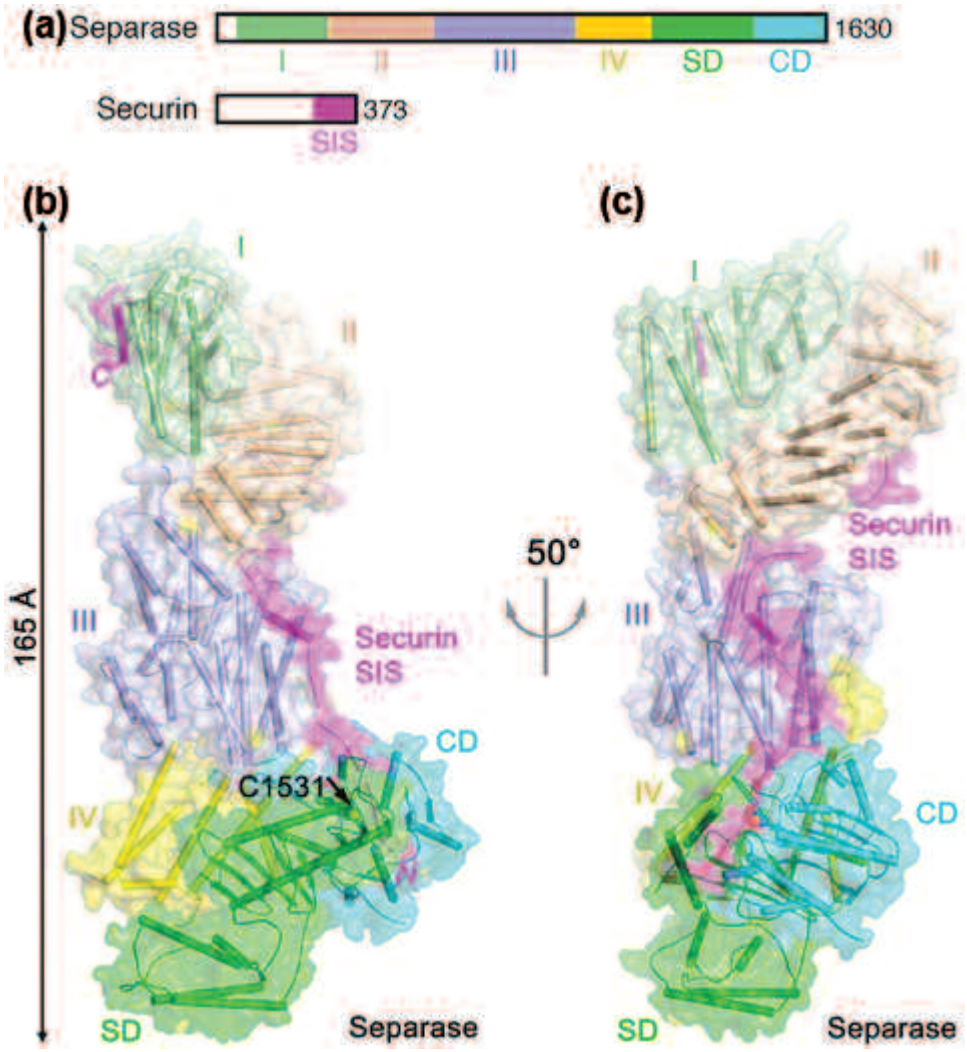

Fig. 1. Crystal structure of the yeast separase-securin complex. (a) The S. cerevisiae separase and securin structural domains. Each domain is labeled and assigned a different color to facilitate identification of domains in the three-dimensional structure shown in panels b and c. (b) The three-dimensional structure of the yeast separase-securin complex. The side chain of the separase catalytic Cys1531 residue (yellow sphere) within the active site is indicated by an arrow. (c) The three-dimensional structure of the complex viewed after a 50° rotation around the vertical axis.

24-ID-C • NE-CAT • Life sciences • Macromolecular crystallography, microdiffraction, single-wavelength anomalous dispersion, single-crystal diffraction, microbeam, multi-wavelength anomalous dispersion, subatomic (<0.85 Å) resolution • 6.5-20 keV • On-site, remote • Accepting general users •

24-ID-E • NE-CAT • Life sciences • Macromolecular crystallography, microbeam, microdiffraction, single-wavelength anomalous dispersion, single-crystal diffraction • 12.68 keV • On-site, remote • Accepting general users •

A Potential New Target for Cancer Therapy

Polycomb repressive complex 2 (PRC2) is a multi-protein complex that is important not only in embryonic development, but also in the pathogenesis of some human cancers. PRC2 functions as a repressor of gene expression, binding to areas in the genome known as "CpG islands" that are implicated in the regulation of gene expression. However, the mechanism by which PRC2 is recruited to CpG islands has remained unclear, especially because no CpG-specific binding protein has been identified in PRC2. Researchers in this study set out to determine how PRC2 is recruited to CpG islands, focusing in particular on polycomb-like (PCL) proteins, which have been considered to play a role in this interaction. They used data collected at the APS and characterized the crystal structure of conserved domains of certain PCL proteins. The results not only revealed an important function of PCL proteins, but also identified a new type of CpG-binding domain. These findings could also help guide discovery of new therapeutic targets for certain cancers.

Studies have shown that PRC2 localizes with DNA sequences in the mammalian genome known as CpG-islands, most of which are associated with important regulatory genes during development. These islands are rich in unmethylated CpG sites. By virtue of this association, PRC2 plays key roles in many normal cellular processes. In contrast, deregulation of its components has been shown to be associated with various types of cancer in humans.

In their study, these researchers from Beijing Normal University (China), the Boston Children's Hospital, the Harvard Medical School, the Brigham and Women's Hospital and Harvard Medical School, and the Memorial Sloan-Kettering Cancer Center investigated PRC2-associated PCL proteins. These form sub-complexes with PRC2, and are believed to regulate the activity of PRC2 or its recruitment to specific regions of the genome. Although these proteins are functionally important, some questions remain about their structures. In particular, the researchers focused on the PCL proteins MTF2, PHF1, and PHF19, all of which directly interact with PRC2. In mouse embryonic stem cells, MTF2 is the main PCL that recruits PRC2 to the CpG-islands.

These three PCL proteins have similar structural features known as conserved domains: a Tudor domain, two plant homeodomain (PHD) fingers, an extended homologous (EH) region at the N-terminal part of the proteins, and a chromo-like domain at the C-terminal part.

The Tudor domain of PHF1 and PHF19 has been reported to bind to methylated at lysine 36 of histone H3. However, the structure and function of the other structural regions of the PCL proteins are unknown. To better understand the molecular structure of PCL proteins and to identify other functions of their conserved domains, the researchers set out to investigate the crystal structure of the Tudor-PHD1-PHD2-EH domains of PHF1 and MTF2. Using data collected at the SBC-CAT 19-ID-D beamline at the APS, the researchers found that the N-terminal domains of both PHF1 and MTF2 associate closely with each other. Unexpectedly, they also found that the EH domain folds into a winged-helix structure, which is a typical DNA-binding motif. Inspired by the structural findings, the researchers first identified that the EH domains prefer to bind unmethylated CpG-containing DNA sequences. They also showed that the EH domains of PHF1 and MTF2 bind DNA in a way that completely differs from that of other winged-helix motifs. According to the researchers, CpG-specific recognition occurs mainly through the winged-like loop 1 (W1) of the EH domain.

These findings have helped to explain how PRC2 is recruited to CpG islands, providing direct evidence that PCL proteins are essential to form the link between the two (Fig. 1). Because both deregulation of PRC2 components and mutant PCLs have been associated with various types of cancer, PRC2 has become a hot target of drug discovery. Because the results of this study may help provide an explanation for PCL-related cancer, PCL proteins could also now serve as new drug targets for such cancers. *— Nicola Parry*

See: Haojie Li[1], Robert Liefke[2,3], Junyi Jiang[1], Jesse Vigoda Kurland[4], Wei Tian[1], Pujuan Deng[1], Weidi Zhang[1], Qian He[1], Dinshaw J. Patel[5], Martha L. Bulyk[4], Yang Shi[2,3], and Zhanxin Wang[1]*, "Polycomb-like proteins link

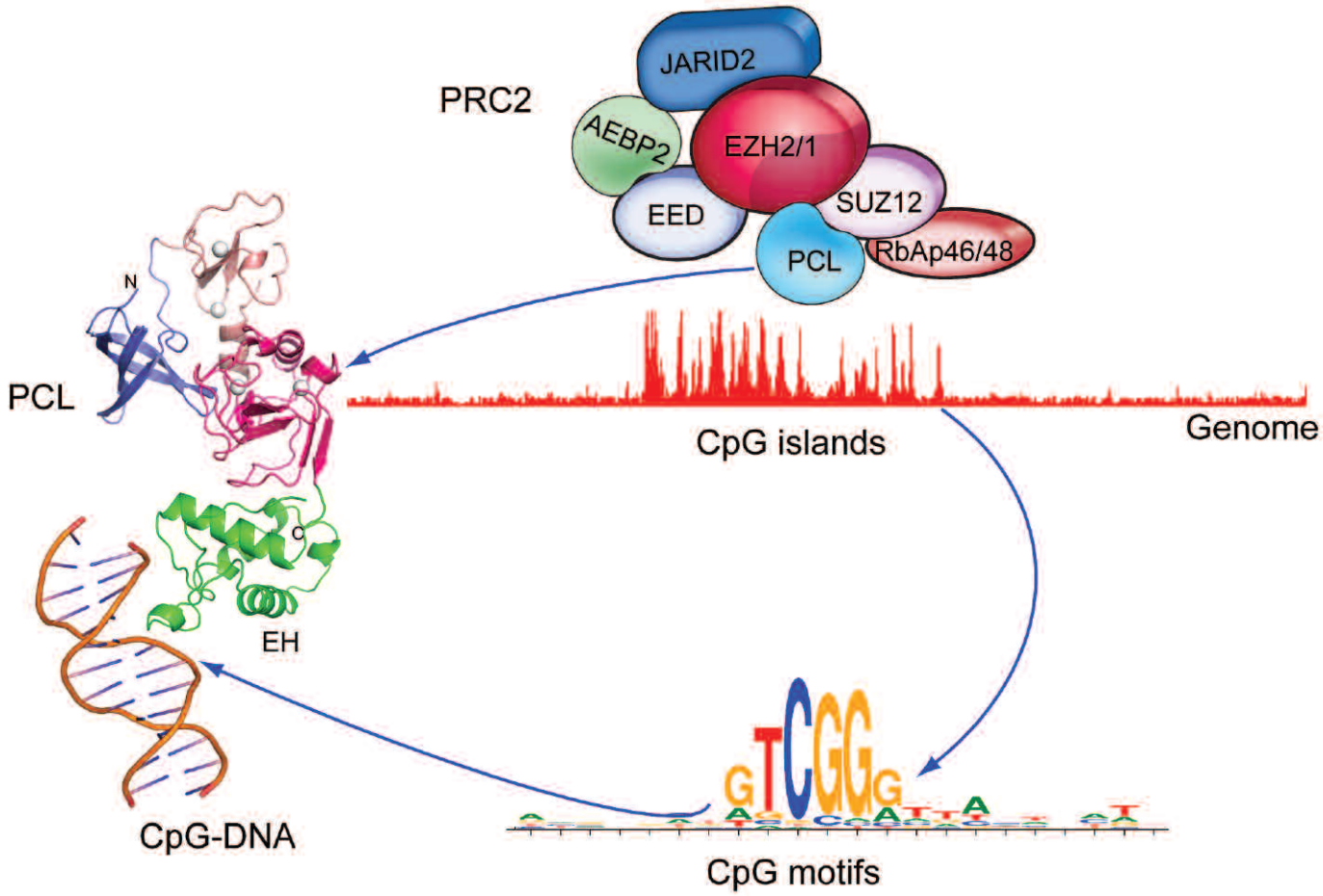

Fig. 1. PCL proteins bind CpG-containing DNA motifs, which help recruit the PRC2 complex to the CpG-islands in the genome.

the PRC2 complex to CpG islands," Nature **549**, 287 (14 September 2017). DOI: 10.1038/nature23881

Author affiliations: [1]Beijing Normal University, [2]Boston Children's Hospital, [3]Harvard Medical School, [4]Brigham and Women's Hospital and Harvard Medical School, [5]Memorial Sloan-Kettering Cancer Center

Correspondence: * wangz@bnu.edu.cn

This work was supported by the National Natural Science Foundation of China (31370719 and 31570729), Beijing Natural Science Foundation (5152015) and the Fundamental Research Funds for the Central Universities (2014KJJCA09 and 2017EYT19) to Z.W. Early research on PCL protein expression undertaken by Z.W. in the laboratory of D.J.P. was supported by the Leukemia and Lymphoma Society and by the Memorial Sloan-Kettering Cancer Center Core Grant (P30 CA008748). Research on PCL proteins was supported by the German Research Foundation (DFG, LI 2057/1-1) to R.L, NIH/NHGRI R01 grant HG003985 to M.L.B., and the National Cancer Institute (R01 CA118487) and funds from Boston Children's Hospital to Y.S. Y.S. is an American Cancer Society Research Professor. SBC-CAT is operated by UChicago Argonne, LLC, for the U.S. Department of Energy (DOE) Office of Biological and Environmental Research under Contract No. DE-AC02-6CH11357. This research used resources of the Advanced Photon Source, a U.S. DOE Office of Science user facility operated for the U.S. DOE Office of Science by Argonne National Laboratory under Contract No. DE-AC02-06CH11357.

19-ID-D • SBC-CAT • Life sciences • Macromolecular crystallography, multi-wavelength anomalous dispersion, subatomic (<0.85 Å) resolution, large unit cell crystallography, single-wavelength anomalous dispersion • 6.5-19.5 keV • On-site, remote, mail-in • Accepting general users •

Paving the Way to Development of New Anti-Cancer Therapies

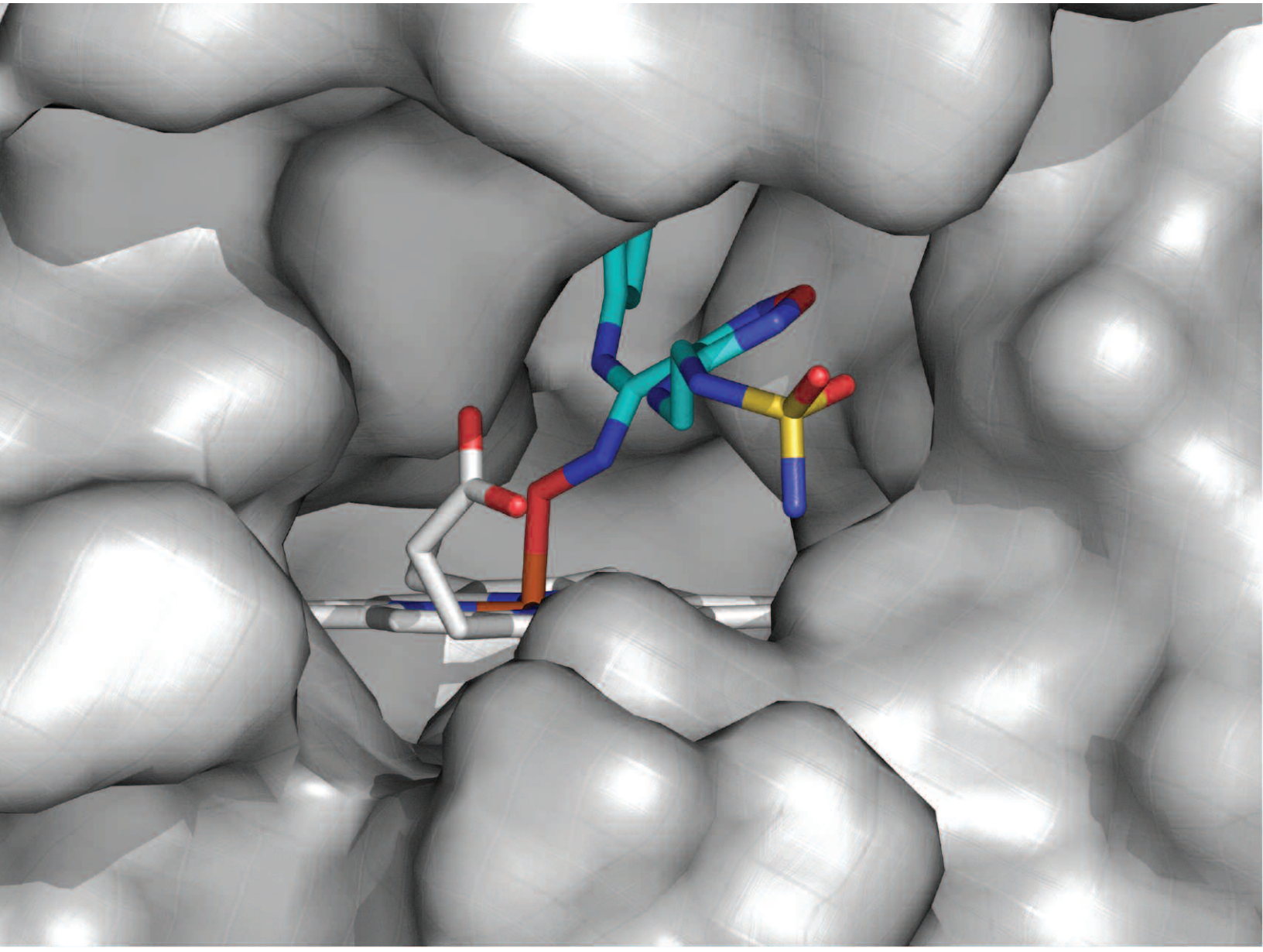

The human indoleamine 2,3-dioxygenase 1 (hIDO1) protein is responsible for the first step in a cellular pathway that metabolizes the essential amino acid tryptophan to yield an immunosuppressive molecule called "kynurenine." Because hIDO1 is over-expressed in several cancers, and is linked to poor disease prognosis, it is an important drug target for cancer therapies. To support structure-based design of new generations of hIDO1 inhibitors, a research team determined, for the first time, the structures of hIDO1 in complex with its substrate (tryptophan), an effector (indole ethanol) or an inhibitor currently in clinical trials (epacadostat). Diffraction data of the complexes were collected at the APS, and the structures of the complexes were solved to a resolution of 2.5 Å. The structural data offer invaluable insight into the mechanism of action for epacadostat and provide new guidelines for development of novel hIDO1 inhibitors.

The hIDO1 protein is over-expressed in a number of cancers and is associated with poor prognosis and shortened survival times. hIDO1 promotes cancer cell escape from recognition and destruction by the immune system, a feature that makes it an attractive drug target for cancer immunotherapies. To design effective inhibitors targeting hIDO1, it is critical that the three-dimensional structure of the protein, in particular the architecture of its active site, is well understood. Prior to this study, the available structures of hIDO1 were limited to the substrate-free forms of the protein. So far, all reported hIDO1 inhibitors are intended to block the activity of the enzyme by binding to the active site, making the lack of active site structural information problematic. Furthermore, the structure of the active site is highly flexible and inhibitors in the active site can coordinate to a resident iron atom of hIDO1, complicating computer modeling, thus highlighting the need for more structural information. Together, these challenges had prevented a clear understanding of how currently available inhibitors work, and how new molecules could be designed to better inhibit hIDO1.

In the current study, all hIDO1 complexes, except the epacadostat complex, were collected remotely using the Stanford Synchrotron Radiation Lightsource (SSRL) beamline 9-2. The high-resolution crystal structure of hIDO1 in complex with epacadostat was determined by LRL-CAT staff at beamline 31-ID-D of the APS. These structures allowed the researchers from the Albert Einstein College of Medicine and the University of California, Irvine, to identify structural elements that are critical for function of the enzyme and specific inhibition by epacadostat (Fig. 1). Additional structural data collected with an hIDO1 effector 3-indole ethanol as a structural probe revealed a new inhibitor binding site that was previously unknown.

These new structural data offer invaluable insight into the mechanism of action for epacadostat, the most advanced hIDO1 inhibitor in clinical trials. In addition, these data provide a springboard for the structure-based development of new cancer therapies that can interrupt the ability of hIDO1 to allow cancer cells to escape from the immune system. *— Emma Nichols*

< Fig. 1. Surface view of the hIDO1 structure (gray) with the inhibitor epacadostat (multicolored stick model) bound to the active site.

See: Ariel Lewis-Ballester[1], Khoa N. Pham[1], Dipanwita Batabyal[2], Shay Karkashon[1], Jeffrey B. Bonanno[1], Thomas L. Poulos[2], and Syun-Ru Yeh[1]*, "Structural insights into substrate and inhibitor binding sites in human indoleamine 2,3-dioxygenase 1," Nat. Commun. **8**, 1693 (22 November 2017).

DOI: 10.1038/s41467-017-01725-8
Author affiliations: [1]Albert Einstein College of Medicine, [2]University of California, Irvine
Correspondence:
* syun-ru.yeh@einstein.yu.edu

This work was supported by NIH Grant GM115773 and National Science Foundation Grant CHE-1404929 (to S.-R.Y.) and NIH Grant GM57353 (to T.L.P.). SSRL is a national user facility operated by Stanford University on behalf of the U.S. Department of Energy (DOE) Office of Science-Basic Energy Sciences. The SSRL Structural Molecular Biology Program is supported by the U.S. DOE Office of Biological and Environmental Research and by the National Center for Research Resources, Biomedical Technology Program, and NIGMS of the National Institutes of Health (NIH). This research used resources of the Advanced Photon Source, a U.S. (DOE) Office of Science user facility operated for the DOE Office of Science by Argonne National Laboratory under contract no. DE-AC02-06CH11357. Use of the LRL-CAT beamline was provided by Eli Lilly Company, which operates the facility. This research used resources of the Advanced Photon Source, a U.S. Department of Energy (DOE) Office of Science user facility operated for the U.S. DOE Office of Science by Argonne National Laboratory under Contract No. DE-AC02-06CH11357.

31-ID-D • LRL-CAT • Life sciences • Macromolecular crystallography, single-wavelength anomalous dispersion • 9-13.5 keV • Mail-in • Accepting general users •

Genome Mining in a Coal Mine

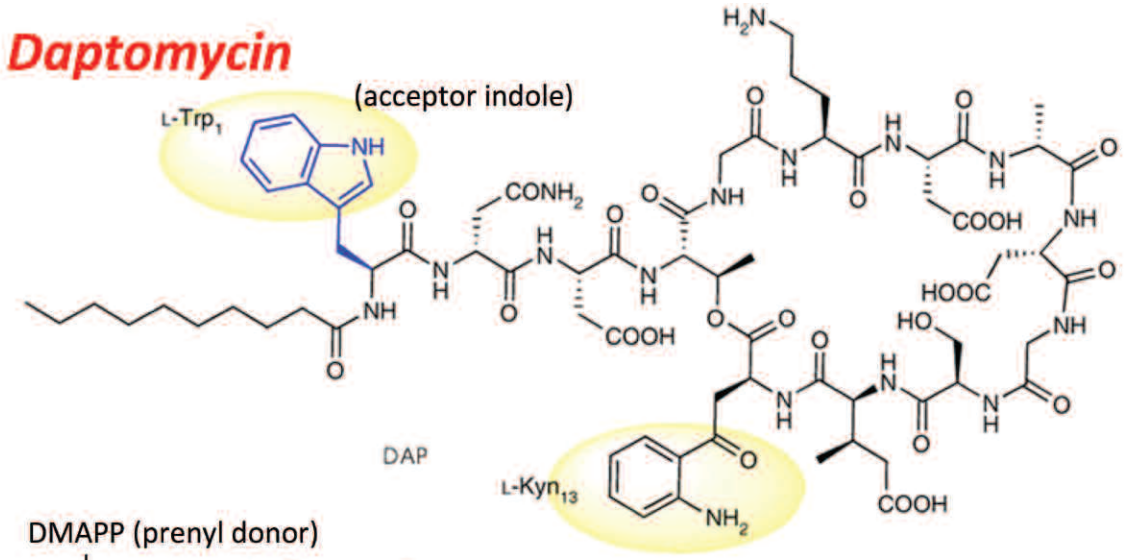

DMAPP (prenyl donor)

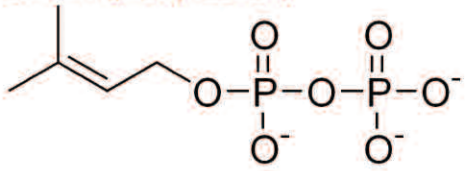

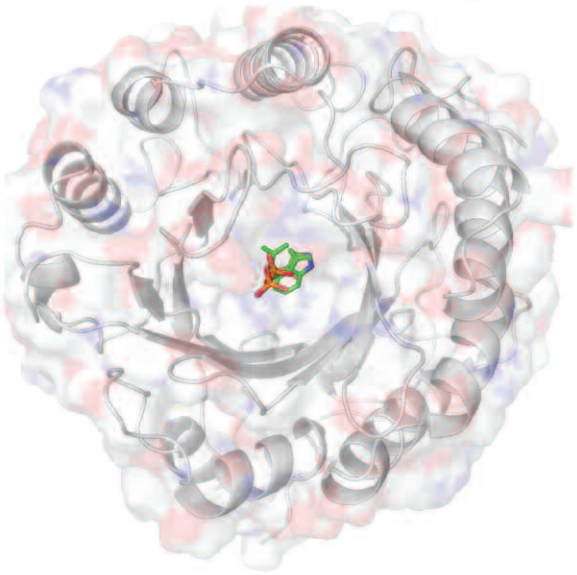

PriB, a permissive C-prenyltransferase

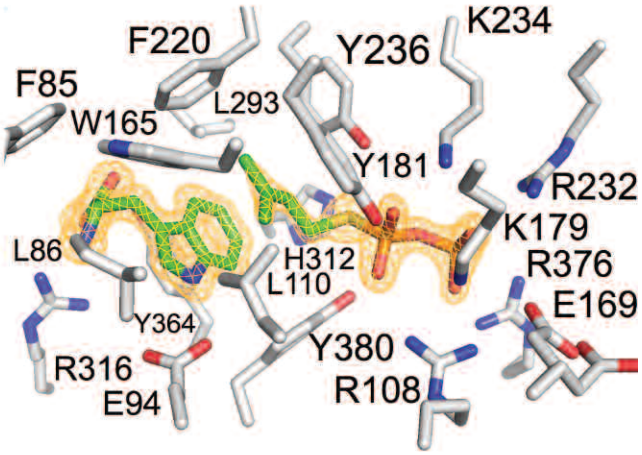

Novel prenylated daptomycin with improved antibacterial activities over the parent drug

Biosynthetic engineering of novel molecules to create new potential medical treatments often involves tinkering with existing natural molecules, such as antibiotics or peptides, to make them better. This can be done with standard synthetic chemical reactions in the laboratory, but sometimes it is easier to find an enzyme to do the work. The search for such an enzyme has led a group of researchers down an unlikely path. By employing high-brightness x-rays from the APS to study a strain of bacteria isolated from a coal mine fire in Appalachia, the team has identified an enzyme that catalyzes a rare reaction and applied it to making a new, improved antibiotic.

The research was based on the observation that a bacterial strain isolated from an underground coal mine fire in Kentucky was able to synthesize two distinct classes of a rare unsaturated hexuronic acid metabolite, suggesting that the bacterium expresses an enzyme that catalyzes a reaction that has presented a challenge to synthetic chemists. In order to identify the enzyme, the team from the University of Kentucky and Rice University sequenced the entire genome of the bacterial strain and performed a bioinformatics analysis on the data to identify the genes. This analysis identified a potential candidate, a single prenyl transferase gene, PriB, that clusters with other biosynthetic genes responsible for making the unusual metabolite.

In order to test whether the enzyme was indeed responsible for the reaction they were interested in, they synthesized the protein in a bacterial expression system and purified it for enzymatic testing. The enzyme assays revealed that PriB was the gene they were seeking and that it is a particularly permissive prenyl transferase that is able to act on a wider variety of substrates than other prenyl transferases in the family, with a wide range of active pH and temperature conditions, and no dependence on metals. Interestingly, the enzyme works on both D- and L-tryptophan, a first for this family of enzymes.

The ability of PriB to work on a wide range of substrates under a wide range of conditions suggested to the researchers that it could be a very useful tool for synthesizing new and interesting molecules from existing natural products. To test one of these possibilities, they tried modifying daptomycin, an antibiotic that contains the right chemical structure to be modified by PriB. It worked! PriB was able to modify daptomycin to make two new products that work 6-10 times better than daptomycin (Fig. 1).

To investigate the structural basis for the permissiveness of PriB, the team solved x-ray crystal structures of PriB with and without ligands. Analysis of data collected at the LRL-CAT 31-ID-D x-ray beamline at the APS revealed a central barrel structure around a solvent-filled core surrounded by a ring of solvent-exposed alpha helices (Fig. 1). The structure undergoes significant conformational changes upon substrate binding and researchers were able to identify differences in PriB that explain why its catalytic action is not dependent on metals the way other prenyl transferases in the family are. PriB also has a unique substrate orientation and binding pocket dynamics that explain its substrate permissiveness compared to other members of the family.

The discovery and characterization of PriB opens doors to new possibilities for biosynthetic tailoring of natural products to make new, more effective products and treatments. The modification of daptomycin in this study is sufficient proof that new tools can be found in the most unlikely locations, even underground in a coal mine fire.

— Sandy Field

< Fig. 1. Engineering a new antibiotic. The structure of daptomycin is shown in the top panel with the recognition elements for PriB highlighted. A ribbon and space-filling representation of the PriB structure is shown on the lower left panel with the substrate shown in the active site as sticks. The active site is shown in more detail in the lower right panel.

See: Sherif I. Elshahawi[1], Hongnan Cao[2], Khaled A. Shaaban[1], Larissa V. Ponomareva[1], Thangaiah Subramanian[1], Mark L. Farman[1], H. Peter Spielmann[1], George N. Phillips, Jr.[2]*, Jon S. Thorson[1],** and Shanteri Singh[1]***‡, " Structure and specificity of a permissive bacterial C-prenyltransferase," Nat. Chem. Biol. **13**, 366 (April 2017). DOI: 10.1038/nchembio.2285

Author affiliations: [1]University of Kentucky, [2]Rice University ‡Present address: University of Oklahoma

Correspondence:

* shanteri.singh@ou.edu,

** jsthorson@uky.edu,

*** georgep@rice.edu

This work was supported by National Institutes of Health grants R37 AI52188 and R01 CA203257 (J.S.T.), U01 GM098248 (G.N.P.) and NCATS (UL1TR001998). Use of the Lilly Research Laboratories Collaborative Access Team (LRL-CAT) beamline at Sector 31 of the Advanced Photon Source was provided by Eli Lilly and Company. This research used resources of the Advanced Photon Source, a U.S. Department of Energy (DOE) Office of Science user facility operated by Argonne National Laboratory (DE-AC02-06CH11357).

31-ID-D • LRL-CAT • Life sciences • Macromolecular crystallography, single-wavelength anomalous dispersion • 9-13.5 keV • Mail-in • Accepting general users •

It's Been a Long, Strange Trip for LSD

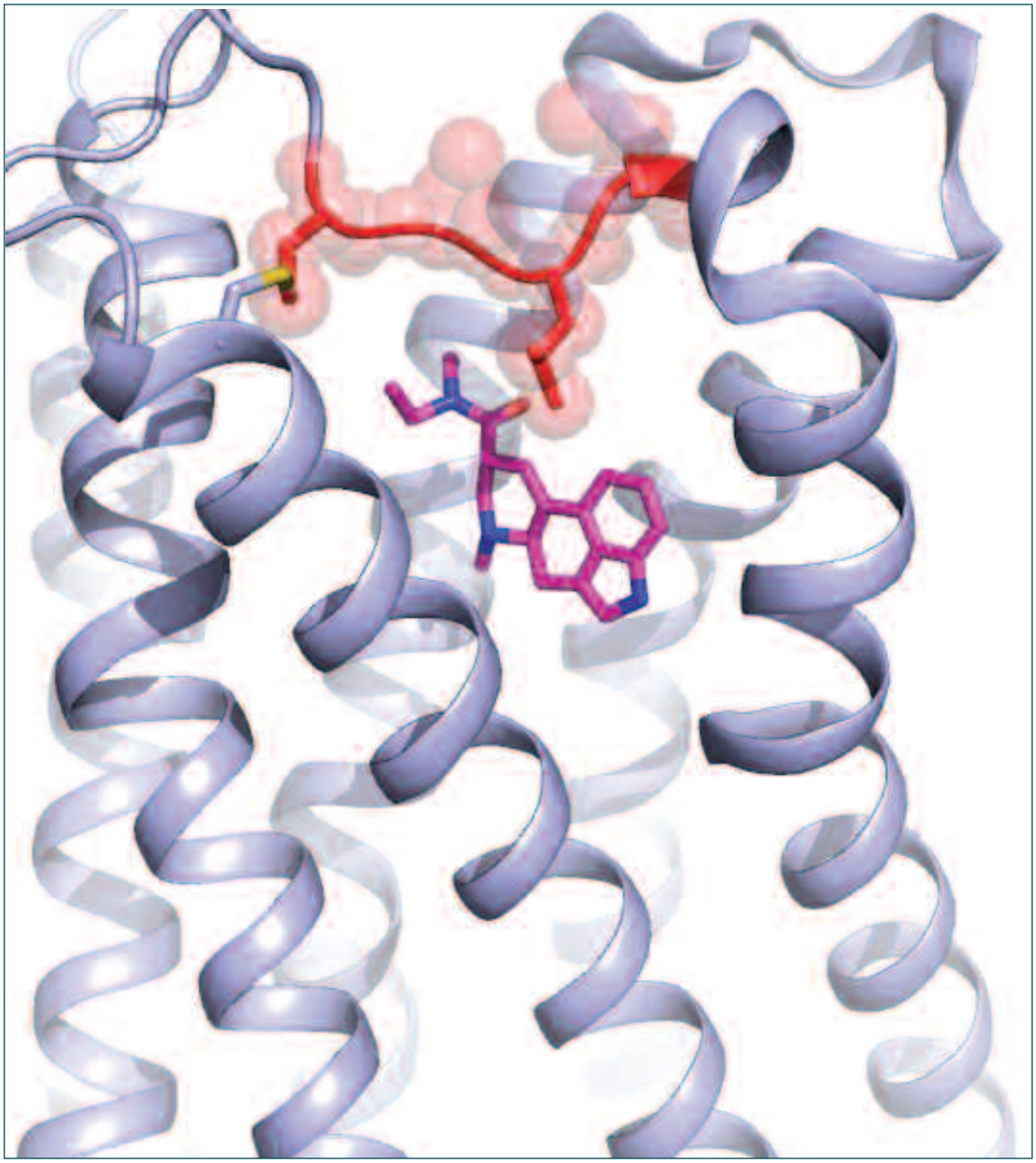

Fig. 1. LSD's long lasting psychedelic effects are caused by a lid that traps LSD in its receptor. The 5-HT2B serotonin receptor is shown in light blue, with LSD (magenta) bound to its ligand binding site within the helical bundle of the receptor. The lid (red) is formed by an extracellular loop that stretches across the receptor and prevents LSD from dissociating into the extracellular space. A leucine within the lid reaches down towards LSD, thereby serving as a latch that helps LSD seal itself inside the receptor.

23-ID-B • GM/CA-XSD • Life sciences • Macromolecular crystallography, microbeam, large unit cell crystallography, subatomic (<0.85 Å) resolution, multi-wavelength anomalous dispersion, single-wavelength anomalous dispersion • 3.5-20 keV • On-site, remote • Accepting general users •

23-ID-D • GM/CA-XSD • Life sciences • Macromolecular crystallography, microbeam, large unit cell crystallography, subatomic (<0.85 Å) resolution, multi-wavelength anomalous dispersion, single-wavelength anomalous dispersion • 5-20 keV • On-site, remote • Accepting general users •

Most of us are familiar with the reputation of the potent hallucinogen lysergic acid diethylamide or, as it's more commonly known, LSD. A synthetic compound created in the 1930s, LSD became a popular recreational drug in the '60s (think "Lucy in the Sky with Diamonds") and was classified as a Schedule I substance soon after that. What is not necessarily known is that researchers have used drugs similar to LSD to treat migraine headaches, post-partum hemorrhage, and Parkinson's disease for years and hope that LSD may be similarly useful in treating substance abuse, cluster headaches, and some types of anxiety. There are difficulties in doing research on a Schedule I drug, of course, but researchers hope that understanding the structure of LSD bound to its target in the body (the serotonin receptor), as determined at the APS (Fig. 1) will provide valuable insights into its unique and potent actions on the human brain.

LSD has been shown to target G-protein-coupled serotonin receptors (5-HT-Rs) that modulate a wide variety of actions in the body from blood vessel constriction to anxiety to sexual behavior. It is thought to interact most potently with the 5-HT2A receptor, and the research team chose to crystallize serotonin receptor 5-HT2B-R in complex with LSD because 5-HT2B-R is a good model for 5-HT2A-R. This also allowed them to make comparisons to a previously described structure for a related molecule, the anti-migraine drug ergotamine (ERG), in complex with 5-HT2B-R.

X-ray diffraction data for LSD in complex with 5-HT2B-R was collected at the GM/CA-XSD 23 ID-B and 23 ID-D beamlines at the APS by the researchers from the University of North Carolina at Chapel Hill School of Medicine; Stanford University; the Stanford University School of Medicine; and the University of California, San Francisco. Comparison of the structures showed that LSD binds to the receptor similar to ERG but in a shallower cleft with important changes in the conformation of key side chains that differ between the two compounds. These differences highlight the remarkable plasticity of these receptors for accommodating similar but distinct molecules to generate potentially subtle differences in receptor response.

The structure of the complex also showed that LSD bound to the receptor adopts a conformation that is totally distinct from that observed for the structure of LSD alone. In fact, molecular dynamics simulations of LSD bound to 5-HT2B-R show that it never adopts the structure seen with LSD alone. This observation led the team to test different versions of LSD that are modified to constrain the structure from adopting different conformations. Both in vitro assays and computer simulations support the observation that LSD must be in the structure observed in the complex with the receptor to exert its action. Even more interesting, these studies provide new information about a phenomenon of G-protein-coupled receptor signaling called "bias." This refers to the way G-protein-coupled receptors work through two different activities – interaction with a G protein that activates other downstream events and interaction with a protein called β-arrestin that causes either receptor desensitization or downstream events distinct from those of G proteins. Bias occurs when a molecule favors one or the other of these interactions. In the case of ERG and LSD, they are biased towards the β-arrestin pathway. In the experiments with different conformationally constrained versions of LSD, the ones that adopted the "free" conformation were unable to activate the β-arrestin pathway as well as the versions that adopted the bound conformation seen in the structure. This provides evidence that this difference could be related to the unique properties of LSD.

Finally, it has been observed that LSD has a very slow rate of dissociation from its receptor, another factor that may explain its potency as a hallucinogen. The structure provides insights into why. There appears to be a lid over the LSD binding site that is not present when ERG is bound (Fig. 1). Simulations showed that the lid only very rarely shifts out of the way to allow LSD in or out, and mutation of a key amino acid that mediates contact between the lid and LSD reduced the dissociation rate of LSD from 44 min. to 4.3 min. And, to put a lid on it, the mutation also greatly affects the bias of LSD for β-arrestin.

The team hopes to use this information, the first structure-based insights into any hallucinogen, to separate the beneficial activities of these molecules from their hallucinogenic properties.

— Sandy Field

See: Daniel Wacker[1]*, Sheng Wang[1], John D. McCorvy[1], Robin M. Betz[2,3], A.J. Venkatakrishnan[2,3], Anat Levit[3], Katherine Lansu[1], Zachary L. Schools[1], Tao Che[1], David E. Nichols[4], Brian K. Shoichet[6], Ron O. Dror[2,3]**, and Bryan L. Roth[1,4]***, "Crystal Structure of an LSD-Bound Human Serotonin Receptor," Cell **168**, 377 (January 26, 2017). DOI: 10.1016/j.cell.2016.12.033

Author affiliations: [1]University of North Carolina at Chapel Hill School of Medicine, [2]Stanford University, [3]Stanford University School of Medicine, [3]University of California, San Francisco, [4]University of North Carolina at Chapel Hill

Correspondence:

* dwacker@email.unc.edu,
** ron.dror@stanford.edu,
*** bryan_roth@med.unc.edu

This work was supported by National Institutes of Health (NIH) grants RO1MH61887 and U19MH82441, the National Institute of Mental Health Psychoactive Drug Screening Program Contract (all to B.L.R.), GM59957 (to B.K.S.), a Terman Faculty Fellowship (R.O.D.), and the Michael Hooker Distinguished Chair of Pharmacology (B.L.R.). We also gratefully acknowledge J. Smith, R. Fischetti, and the staff of GM/CA-XSD, which has been funded with federal funds from the National Cancer Institute (ACB-12002) and the National Institute of General Medical Sciences (AGM-12006). This research used resources of the Advanced Photon Source, a U.S. Department of Energy (DOE) Office of Science user facility operated for the DOE Office of Science by Argonne National Laboratory under contract no. DE-AC02-06CH11357.

How Bacterial Circadian Clocks Tick

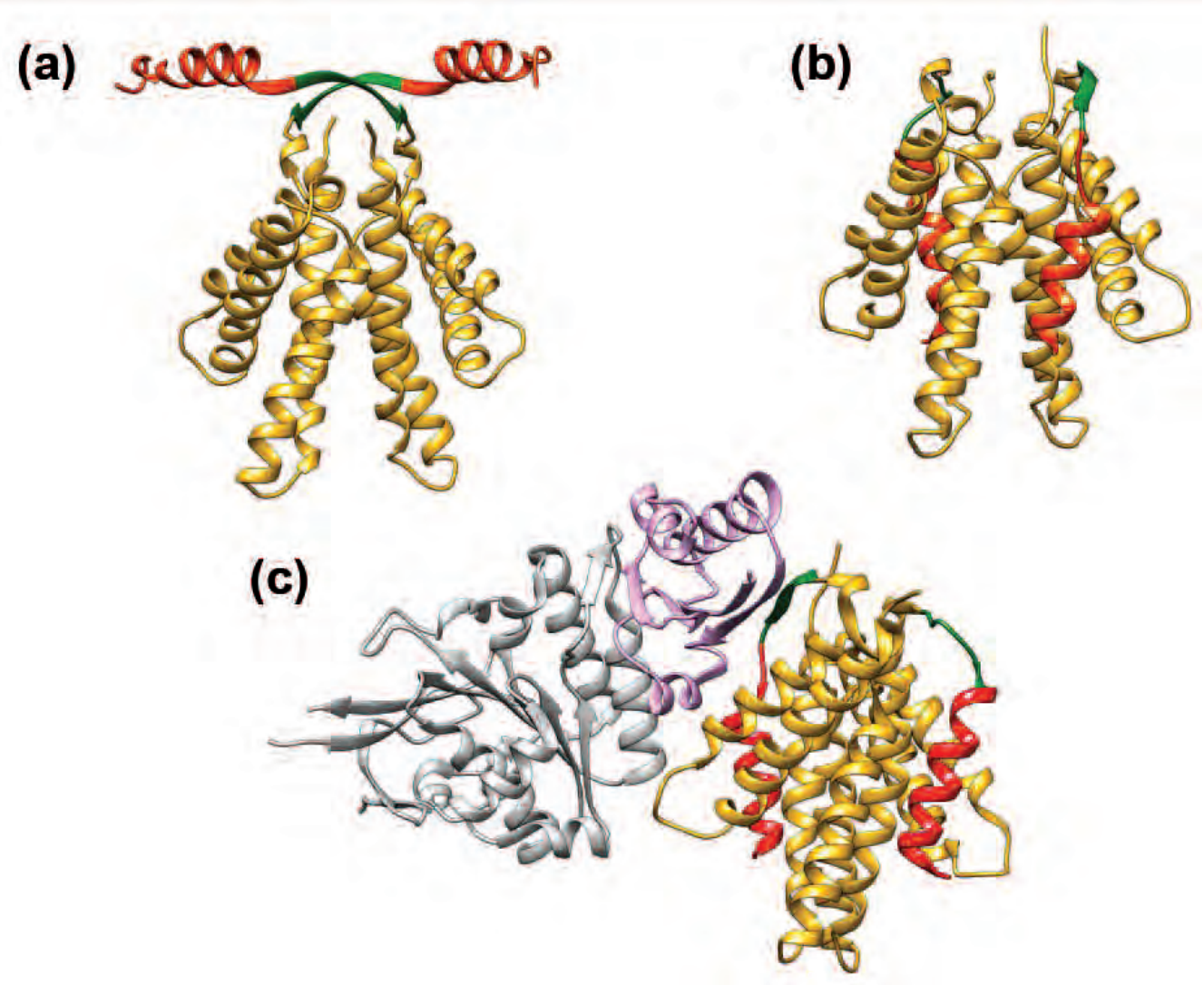

Fig. 1. The active state of KaiA is when the α-helix shown in red is located away from the α-helices shown in gold (image a). In contrast, image (b) shows its inactive conformation, in which these different α-helices are positioned close to each other. Image (c) shows the KaiA-KaiB-KaiC complex. (Grey depicts part of the KaiC protein, and purple depicts KaiB.)

23-ID-B • GM/CA-XSD • Life sciences • Macromolecular crystallography, microbeam, large unit cell crystallography, subatomic (<0.85 Å) resolution, multi-wavelength anomalous dispersion, single-wavelength anomalous dispersion • 3.5-20 keV • On-site, remote • Accepting general users •

Life evolved on a rotating planet, and has adapted to daily changes in ambient light and temperature. As part of this adaptation, an internal biological, i.e., circadian, clock controls metabolism and behavior in anticipation of sunrise and sunset, and this has profound consequences on health and disease. However, a mechanistic understanding has been far from complete for any circadian clock system, mostly because of a lack of structural information at high resolution about these clocks. The circadian clock in cyanobacteria, or blue-green algae, is driven by only three proteins and is the simplest one known. These proteins are KaiA, KaiB, and KaiC, and they take on different arrangements during day and night. Questions have persisted about the molecular structure of these proteins, and especially about how they interact and transition from day to night. Using x-ray diffraction data collected at both the APS and the Advanced Light Source (ALS) at Lawrence Berkeley National Laboratory, researchers investigated the structure of KaiA-KaiB-KaiC complexes. They determined how the active state of KaiB binds KaiC, and how KaiC then changes its structure. They also identified the manner in which KaiA is forced to take on an inactive state within the complex. In addition to closing significant knowledge gaps about the cyanobacterial circadian clock, these findings are guiding deeper studies in this research area.

In the morning, KaiC marks itself with phosphorylation under stimulation by KaiA. At night, though, KaiC removes these marks when KaiB blocks the activity of KaiA within a large KaiA-KaiB-KaiC complex. Major questions that have long gone unanswered have centered on how KaiB binds to KaiC at night, and how KaiB inactivates KaiA within this complex. When the structures of these individual proteins were solved more than a decade ago, the race was on to solve the structure of the KaiA-KaiB-KaiC complex, because this would reveal how this simplest clock works. Yet, the major problem holding back the field was obtaining crystals of the KaiA-KaiB-KaiC complex. Scientists could not form complexes stable enough for crystallization, confounding efforts for more than ten years. However, in 2015, groundbreaking research showed that the originally published crystal structures of KaiB back in 2005 were actually of its inactive state, and that its active state, in which it binds KaiC, had been overlooked.

In order to become active, KaiB had to dramatically change its topology from the inactive fold to the active one. This reversible fold-switching, or metamorphic behavior, is exceedingly rare and has only been shown to occur in a few proteins. This active fold of KaiB is unstable, which explains why previous efforts to crystallize KaiA-KaiB-KaiC complexes had failed.

With this in mind, a collaboration of scientists, from the University of California, Merced; the University of California, Santa Cruz; and the University of California, San Diego conducted a study to further investigate the molecular basis of this cyanobacterial circadian clock, with data collected at GM/CA-XSD beamline 23-ID-B at the APS, as well as at the 8.3.1 beamline at the ALS. The team engineered KaiB so that it was locked into its active state. This key step was missing in previous efforts. Next, they combined this altered KaiB with the other two proteins to form stable KaiA-KaiB-KaiC complexes. According to the researchers, crystals formed within 24 hours of combining the three proteins, from which the team collected high-quality x-ray diffraction data.

Their first major finding was determining how this rare active state of KaiB engages KaiC, and how KaiC, in turn, changes its structure. The second enlightening discovery was discovering how KaiA is forced to take on an inactive conformation within the KaiBC complex (Fig. 1). The researchers found that, in contrast to when KaiA is active with one particular α-helix positioned far away from the remaining α-helices, in its inactive state this α-helix is packed closely with the others (Fig. 1).

The mechanistic insights revealed from the crystal structures obtained in this study have filled several major gaps in knowledge, and have created a new platform for advancing further investigations into the operation of the cyanobacterial circadian clock.

— Nicola Parry

See: Roger Tseng[1], Nicolette F. Goularte[2], Archana Chavan[1], Jansen Luu[2], Susan E. Cohen[3], Yong-Gang Chang[1], Joel Heisler[1], Sheng Li[3], Alicia K. Michael[2], Sarvind Tripathi[2], Susan S. Golden[3], Andy LiWang[1,3]*, and Carrie L. Partch[2,3]**, "Structural basis of the day-night transition in a bacterial circadian clock," Science **355**,1174 (17 March 2017).
DOI: 10.1126/science.aag2516
Author affiliations: [1]University of California, Merced, [2]University of California, Santa Cruz, [3]University of California, San Diego
Correspondence:
* aliwang@ucmerced.edu,
** cpartch@ucsc.edu

We thank the staff at the 23-ID-B beamline at the APS and at the 8.3.1 beamline at the ALS for help with data collection. Access to the 8.3.1 beamline was provided by the University of California Office of the President Multicampus Research Programs and Initiatives grant MR-15-328599 and the Program for Breakthrough Biomedical Research, which is partly funded by the Sandler Foundation. The Advanced Light Source (contract DE-AC02-05CH11231) and Advanced Photon Source (contract DE-AC02-06CH11357) are supported by the U.S. Department of Energy. This work was supported by grants from the Air Force Office of Scientific Research (FA9550-13-1-0154 to A.L.), U.S. National Institutes of Health (NIH) (R01GM107521 to A.L., R01GM107069 to C.L.P., F31CA189660 to A.K.M., and R35GM118290 to S.S.G.). R.T. was supported by the National Science Foundation Graduate Research Fellowship, and S.E.C. was supported by the American Cancer Society Postdoctoral Fellowship PF-12-262-01-MPC. S.L. and the Biomolecular/Proteomics Mass Spectrometry Facility are supported by the NIH (1U19AI117905, R01GM020501, and R01AI101436).

Bacterial Assassins with Poisoned Lances

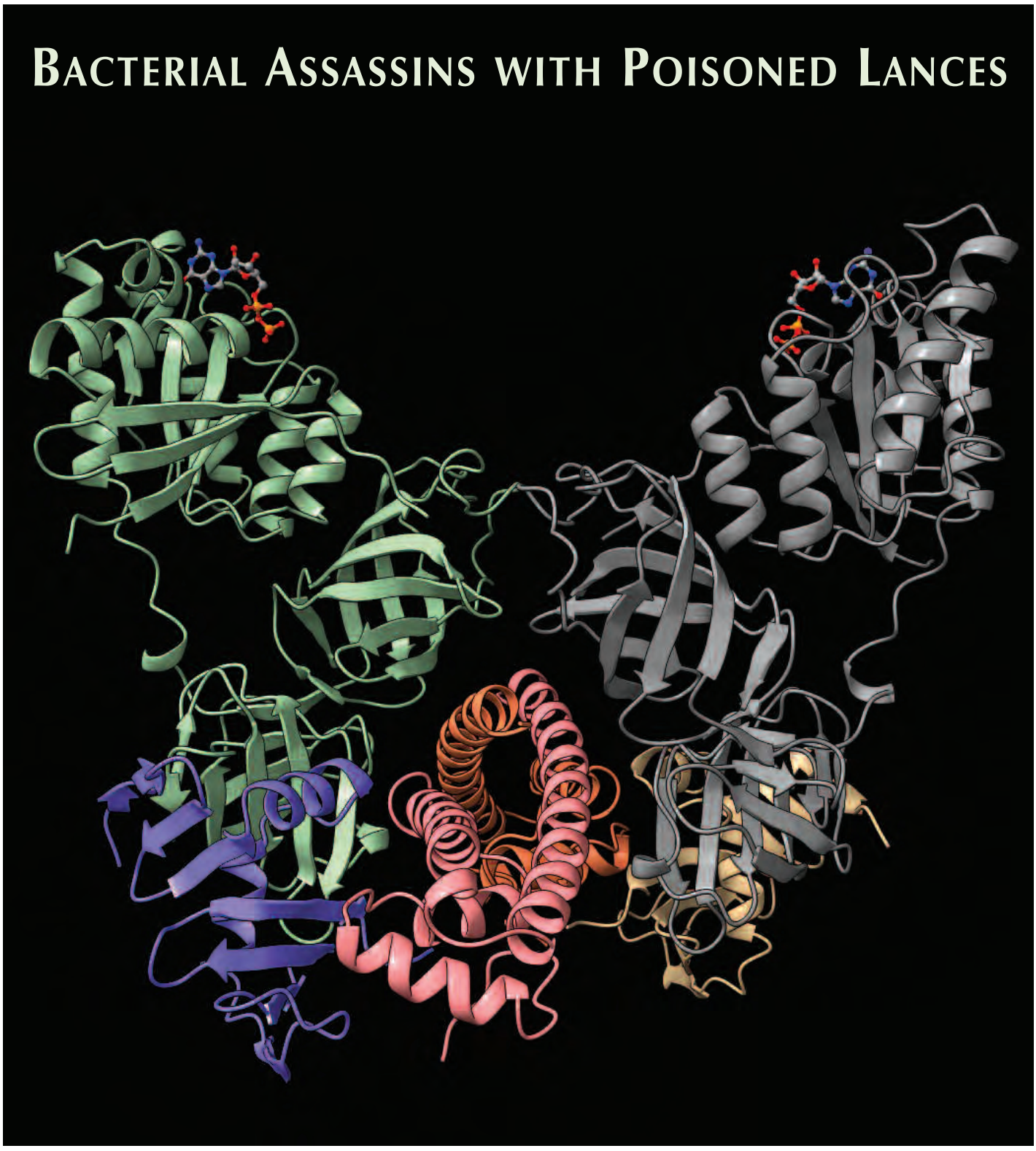

Fig. 1. Structure of EF-Tu•CdiA-CT•CdiI. Ribbon diagram of secondary structures of proteins in the dimeric complex with EF-Tu shown in gray and green (top, left and right) with bound GDP shown as ball and stick model, CdiA-CT shown in purple and brown (lower, left and right) and CdiI shown in pink and orange (lower, center).

Competition in the microbial world is fierce. To stay competitive, bacteria have developed a variety of molecular tools in the form of antibiotics and bacterial toxins that are released into the environment to attack the other microbes around them. Recently, investigators have learned about even more sophisticated systems that bacteria use to inject toxins into neighboring cells upon contact. This phenomenon is called "contact-dependent growth inhibition" (CDI) and involves extension of a protein lance that pokes the neighboring cell and delivers a toxin that inhibits its growth. Of course, just like us, bacteria don't want to harm their relatives, so closely related bacteria all express an immunity protein that binds and neutralizes the toxin. Research in this area has provided many insights into the various activities of CDI toxins, but there are still surprising discoveries that are revealed only through detailed structural and biochemical analysis. Based upon crystallographic structures obtained at the APS, investigators now report that a novel CDI toxin from *Escherichia coli* strain NC101 hijacks an abundant cellular protein — elongation factor Tu (EF-Tu) — to exert its toxic effects. Detailed understanding of this system will broaden our knowledge of this newly uncovered bacterial arms race and may provide ideas for designing toxic lances of our own.

The effort was a collaboration between investigators from The University of Chicago; the University of California, Santa Barbara; the University of California, Irvine; and Argonne. The team crystallized the CdiA-CT toxin in complex with its CdiI immunity protein and EF-Tu, and solved the structure using diffraction data collected at the SBC-CAT 19-ID-D beamline at the APS. The structure shows that the three proteins bind to each other to form a trimer with the head of the immunity protein bound to a pocket on the C-terminal side of the toxin and EF-Tu bound to the N-terminal side. In the structure, the trimers then associate with each other to form a dimer (Fig. 1).

Comparison of the data to known structures revealed that the toxin is structurally related to a family of ribonucleases that preferentially act on transfer RNA (tRNA). This is consistent with the involvement of EF-Tu, which binds to tRNAs tightly and delivers them to the ribosome during protein synthesis. The team found that expression of the toxin inside *E. coli* cells led to the preferential cleavage of several specific tRNAs. To show that this activity is relevant to the CDI mechanism, the researchers confirmed that these same tRNAs are cleaved in target bacteria when subjected to attack by toxin-deploying neighbors. In a neat internal control, target bacteria that express the immunity protein were shown to be protected from tRNA cleavage, confirming the specificity of the toxic ribonuclease activity.

Although the sequences were not similar between the toxin and its ribonuclease relatives, the investigators were able to use known structures to predict active-site residues. Mutation of these confirmed that arginine 200 and histidine 248 are critical to the tRNA cleavage activity of the toxin and inhibition of target bacteria.

Finally, the essential role of EF-Tu in toxin activity was confirmed with *in vitro* ribonuclease assays, but with a twist. When they added just purified toxin and EF-Tu with tRNA substrate, there was no cleavage activity! Going back to their results from a finding they had made in a previous study, there was a suggestion that another translation factor called EF-Ts might also be involved. Indeed, once EF-Ts was included in the reaction, the tRNA substrate was efficiently cleaved.

What's the next step? The team says they would like to determine whether other CDI toxins require EF-Tu and EF-Ts in the same manner as the NC101 toxin. Genetic evidence indicates that there are at least four other CDI toxins that require EF-Tu. Remarkably, these other toxins do not share significant sequence identity with the NC101 toxin and they cleave other subsets of tRNA substrates. These observations suggest that inter-bacterial competition systems commonly exploit EF-Tu to promote toxin activity. Hopefully, detailed structural analyses will reveal how these sequence-diverse toxins all trick EF-Tu into doing their bidding.

— Sandy Field

See: Karolina Michalska[1], Grant C. Gucinski[2], Fernando Garza-Sánchez[2], Parker M. Johnson[5], Lucy M. Stols[1], William H. Eschenfeldt[1], Gyorgy Babnigg[1], David A. Low[2], Celia W. Goulding[3], Andrzej Joachimiak[1,4]**, and Christopher S. Hayes[2]*, "Structure of a novel antibacterial toxin that exploits elongation factor Tu to cleave specific transfer RNAs," Nucleic Acids Res. **45**(17), 10306 (2017).
DOI: 10.1093/nar/gkx700
Author affiliations: [1]Argonne National Laboratory, [2]University of California, Santa Barbara, [3]University of California, Irvine, [4]The University of Chicago
Correspondence:
* chayes@lifesci.ucsb.edu,
** andrzejj@anl.gov

This research was funded by National Institutes of Health (NIH) GM094585, GM115586 to A.J., GM117373 to C.W.G., D.A.L., C.S.H.. SBC-CAT is operated by UChicago Argonne, LLC, for the U.S. Department of Energy (DOE) Office of Biological and Environmental Research under Contract No. DE-AC02-6CH11357. This research used resources of the Advanced Photon Source, a U.S. DOE Office of Science user facility operated for the DOE Office of Science by Argonne National Laboratory under Contract No. DE-AC02-06CH11357.

19-ID-D • SBC-CAT • Life sciences • Macromolecular crystallography, multi-wavelength anomalous dispersion, subatomic (<0.85 Å) resolution, large unit cell crystallography, single-wavelength anomalous dispersion • 6.5-19.5 keV • On-site, remote, mail-in • Accepting general users •

Pink-Beam Serial Crystallography for Microcrystal MX

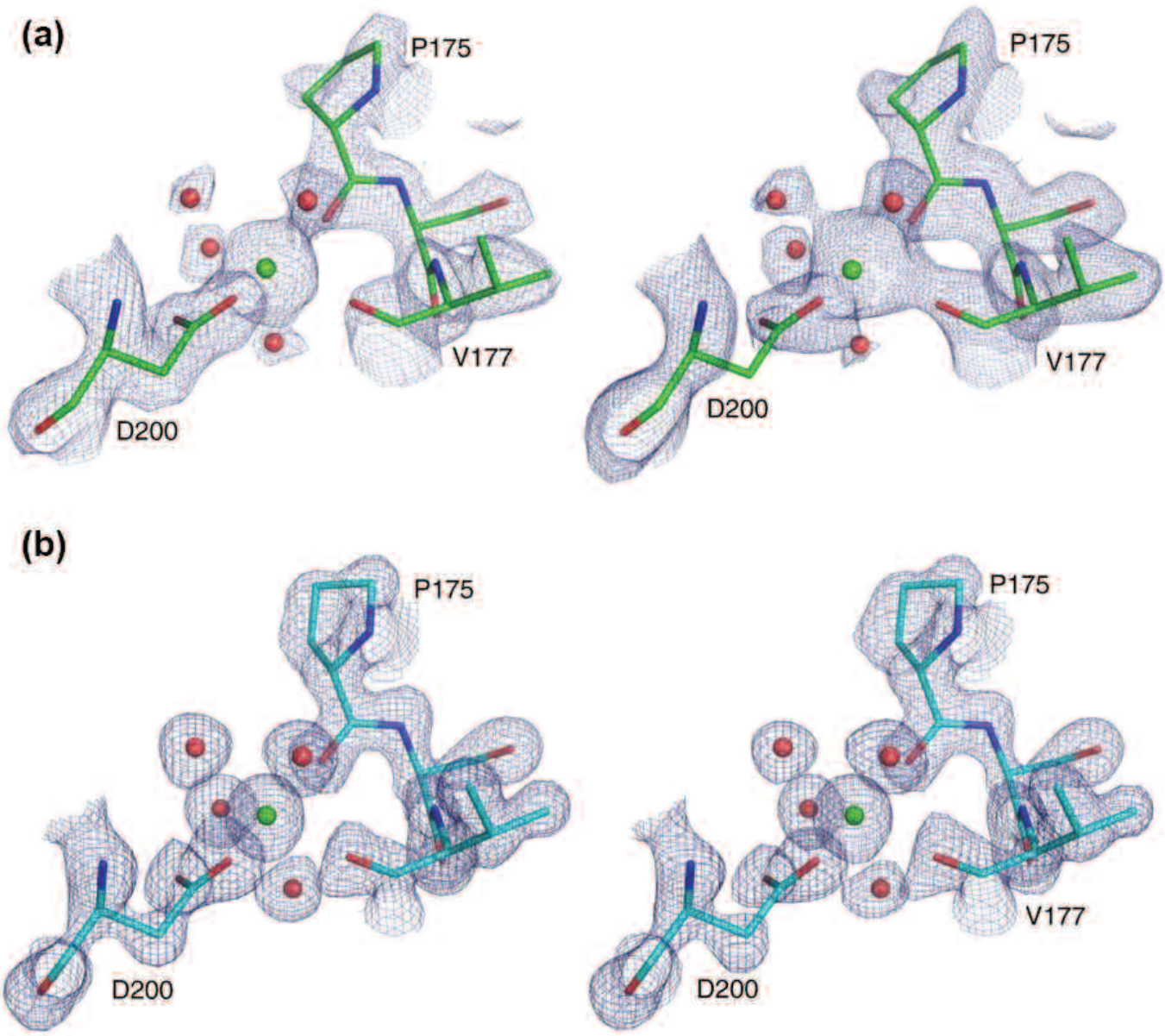

Fig. 1. Comparison of electron density maps from proteinase K structures obtained from different diffraction methods showing the calcium binding site with the coordinating water molecules. (a) Structure obtained from our single shot pink-beam serial crystallography experiment. (b) Proteinase K structure from conventional single crystal rotation photographs (PDB ID: 2PRK). The blue grid represents $2mF_o$-DF_c maps (left side) and $2mF_o$-DF_c simulated annealing composite omit maps (right side) both at a contour level of 1.5σ, respectively. From A. Meents et al., Nat. Commun. **8,** 1281 (2017).

14-ID-B • BioCARS • Life sciences, materials science, physics, chemistry • Time-resolved crystallography, time-resolved x-ray scattering, Laue crystallography, wide-angle x-ray scattering, biohazards at the BSL2/3 level, macromolecular crystallography • 7-19 keV • On site • Accepting general users •

Pink-beam serial x-ray microcrystallography represents a methodological improvement that allows for analysis of protein microcrystals and permits collection of time-resolved data of enzyme and other irreversible reactions at room temperature with microcrystals. Together, these important advances open the door for obtaining data that have thus far remained inaccessible. In order to develop and validate pink-beam crystallography for microcrystals, researchers compared structures of the well-known proteins proteinase K and phycocyanin generated utilizing pink-beam serial ,microcrystallography carried out at the APS, with those generated via standard monochromatic serial diffraction method. The data show that the pink-beam serial microcrystallography methodology yields highly detailed electron density maps with minimal background noise, reinforcing the applicability of this technique for learning more about proteins that may otherwise be ineligible for crystallographic study.

To solve the three-dimensional structure of a protein, an x-ray beam is passed through a crystal that is formed from purified protein, resulting in a diffraction pattern. This pattern, analogous to molecular shadows cast by atoms, is then used to develop an electron density map. The protein's amino acid subunits, along with supporting ions can then be modeled to fit the experimentally obtained pattern of density, resulting in a three-dimensional structure. Traditionally, x-ray crystallography has relied on collection of multiple images from a single large crystal using a monochromatic beam. Large crystals are technically difficult to obtain, and exposure to x-rays damages the specimen, limiting the number of snapshots that can be collected from a single crystal. To limit this damage, data collection is often carried out at extremely cold cryogenic temperatures.

A polychromatic or "pink" beam has about 100 times more flux (i.e., photons on the sample) than a standard monochromatic beam. While polychromatic nature of the beam reduces the number of snapshots needed for obtaining a three-dimensional structure as compared to monochromatic data collection, high flux permits very short x-ray exposure times. Because such short exposures are possible, pink beam crystallography is ideally suited for studies of biological molecules in action in real time at room temperature. It has been extensively used for such time-resolved studies of biological macromolecules. However, prior to this work large crystals were used and little was known about how the technique could be used to glean structural information from a large number of microcrystals, where each crystal is exposed only once in serial microcrystallography approach. One particular advantage of using serial crystallography approach in conjunction with the reduced exposures is the possibility to conduct time-resolved studies of irreversible reactions which require fresh sample after each exposure. Further, microcrystals are better suited to experiments where a protein activating ligand is soaked into the crystal because of smaller diffusion times.

In the current study, an international collaboration of researchers working at BioCARS beamline 14-ID-B validated pink-beam serial microcrystallography by comparing the structures of two model proteins built using the new method with structures gleaned from other methods (Fig. 1). The authors found that a high level of detail was obtained from room-temperature microcrystals. Experimental design optimized for reducing the background levels in the diffraction patterns was critical for the experiment success. The low level of background that was achieved suggests that even smaller crystals may be examined using this method. Importantly, the number of microcrystals needed to obtain a complete dataset was reduced to between 50 and 200, a significant improvement from the several thousand required using serial monochromatic crystallography approaches.

This work paves the way for rapid assessment of proteins that crystalize as microcrystals, and makes time-resolved analysis of irreversible reactions possible. These advances drastically increase the capabilities of researchers to obtain protein structures, accelerating knowledge important for human health.

— Emma Nichols

See: A. Meents[1]*, M.O. Wiedorn[1,2], V. Srajer[3,] R. Henning[3], I. Sarrou[1], J. Bergtholdt[1], M. Barthelmess[1], P.Y.A. Reinke[4], D. Dierksmeyer[1], A. Tolstikova[2], S. Schaible[1], M. Messerschmidt[5], C.M. Ogata[7], D.J. Kissick[6], M.H. Taft[4], D.J. Manstein[4], J. Lieske[1], D. Oberthuer[1], R.F. Fischetti[6], and H.N. Chapman[1,2,7], "Pink-beam serial crystallography," Nat. Commun. **8**, 1281 (2017).
DOI: 10.1038/s41467-017-01417-3
Author affiliatons: [1]Deutsches Elektronen Synchrotron (DESY), [2]University of Hamburg, [3]The University of Chicago, [4]Institut für Biophysikalische Chemie, [5]National Science Foundation BioXFEL Science and Technology Center, [6]Argonne National Laboratory, [7]Centre for Ultrafast Imaging
Correspondence:
* alke.meents@desy.de

This work was funded as part of the European Cluster of Advanced Laser Light Sources project, which has received funding from the European Union's Horizon 2020 research and innovation program under Grant Agreement No. 654220. This work was further supported by the European Research Council under the European Union Seventh Framework Program (FP/2007-2013)/ERC Grant Agreement No. 609920, "X-probe" funded by the European Union's 2020 Research and Innovation Program under the Marie Skłodowska-Curie Grant Agreement 637295, BMBF project 05K14CHA "Sync-FELMed", and the Virtual Institutes VI-403 and VI-419 of the Helmholtz Association. Use of BioCARS was supported by the National Institute of General Medical Sciences of the National Institutes of Health under grant number R24GM111072. The time-resolved setup at BioCARS was funded in part through a collaboration with Philip Anfinrud (NIH/NIDDK). This research used resources of the Advanced Photon Source, a U.S. Department of Energy (DOE) Office of Science user facility operated for the DOE Office of Science by Argonne National Laboratory under Contract No. DE-AC02-06CH11357.

How Anticancer Drugs Enter Cells

Nucleosides, which are precursors of nucleic acids, are involved in many biochemical processes in cells, especially in the storage and transfer of genetic information. Concentrative nucleoside transporters (CNTs) play an important role in transporting nucleosides and nucleoside-derived drugs into cells. Although scientific advances have recognized the elevator model as the mechanism of this transport process, scientists have only identified the structures of the two end states of the transporter that exist at the start and end of the transport cycle; the more detailed structural changes involved throughout the entire cycle have remained somewhat of a mystery. Researchers set out to further investigate the transport cycle utilizing data collected at the APS and characterized most of the structural changes, including novel intermediate-state conformations, that occur in the CNT throughout its transport cycle as it moves nucleosides and nucleoside analogs across the cell membrane. The results of this study could help scientists better understand the elevator model for transporting various molecules into cells, and could also help with discovery of new nucleoside-derived drugs such as anticancer and antiviral therapies.

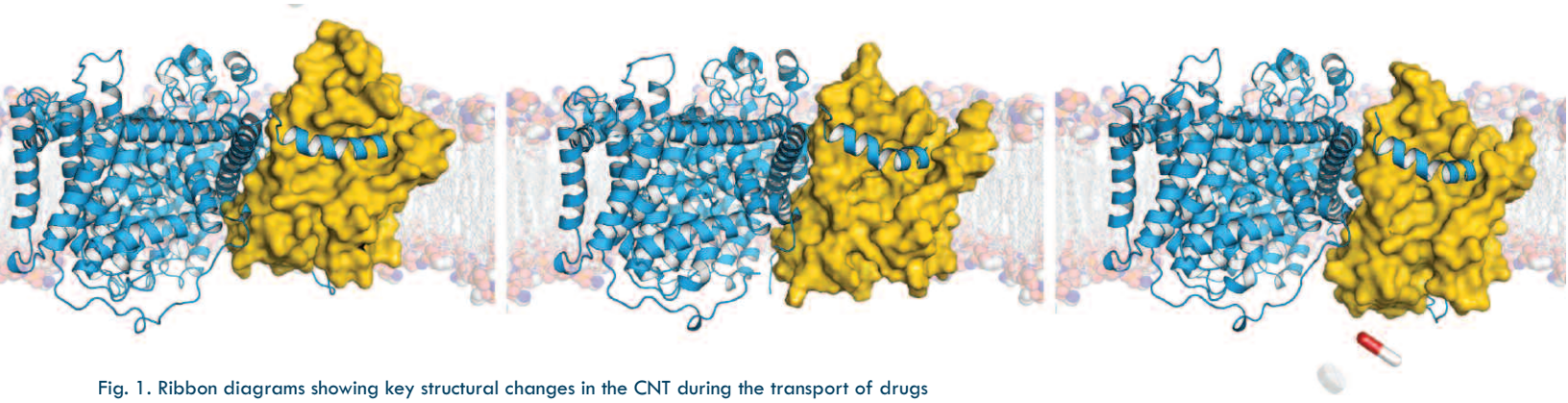

Fig. 1. Ribbon diagrams showing key structural changes in the CNT during the transport of drugs across the cell membrane, into the cell.

Nucleoside analogs represent an important class of compounds that are used clinically, as anticancer drugs and antiviral drugs, for example. These analogs are essentially modified nucleosides that have antitumor or antiviral properties because of their ability to block DNA synthesis. The CNT proteins are used to help nucleosides and their analogs enter cells. These transporters use an ion gradient as an energy source to transport nucleosides and nucleoside-derived drugs against their chemical gradients across cell membranes into cells.

The elevator model represents an emerging mechanism of the transport process, in which a region of the CNT known as the substrate-binding transport domain moves a large distance across the membrane. This mechanism has been characterized by a transition between two states, but the conformational path that leads to the transition has remained unknown. This is mostly because the available structural information has been limited to the two end states of the CNT that exist at the start and end of the transport cycle.

Using data collected at the SER-CAT 22-ID-D beamline and the NE-CAT 24-ID-C beamline, both at the APS, the researchers from Duke University Medical Center captured and visualized the movements of the CNT in a time-lapse manner, helping them to better understand how this transporter works. Although they had previously tried to capture alternate conformations of the CNT during transport, most of their approaches had failed. This study, however, was the first to provide a visualization of almost all stages of the elevator model. They determined the structures of nearly all the shapes of the CNT in motion, providing a trajectory of its conformational transitions in the elevator model (Fig. 1). These findings showed that multiple intermediate steps and state-dependent conformational changes occur within the transport domain as the CNT slowly moves its cargo like an elevator, stopping at different points across the cell membrane before reaching the inside of the cell.

The researchers were initially surprised when they identified these intermediate steps. It had traditionally been believed that the transition between the starting and ending states of the CNT was transient, and that the transport cycle did not involve intermediate states. However, the more the researchers analyzed the novel intermediate state structures, the more they realized that these intermediate conformational changes do occur and play important roles in the transport cycle. Their subsequent biochemical studies are consistent with their structural observation of the importance of the intermediate

"Anticancer" cont'd. on page 120

Light Can Make Things Happen

Light-oxygen-voltage (LOV) receptors are modular sensory proteins employed by many organisms to perceive light. The blue-light sensing apparatus is conserved among LOV proteins, but the downstream response to light can vary depending on how the initial signal is transmitted to an effector module. For example, these proteins are known to activate movements toward light, regulate stress responses, and control DNA binding. The modular arrangement of LOV receptors has worked well to adapt light responses to the different needs of various species and has attracted interest in the world of bioengineering for the possibilities surrounding the synthesis of light-sensitive proteins that perform functions useful to humans. As a case in point, various LOV-based systems now allow researchers to use blue light to deliberately control a number of intracellular processes, including cytoskeletal dynamics and the subcellular location of proteins of interest. Although researchers have uncovered the photochemical mechanism underlying the LOV receptor light response, there is still a gap in our understanding of how the initial signal is coupled to activation of the downstream function. New work on a homodimeric bacterial LOV called "YtvA," carried out at the APS, has shed some light on this problem. The findings improve our understanding of how LOV transmits a signal from light to the associated effector protein that controls the response and opens the door to the development of bioengineered proteins that are responsive to light.

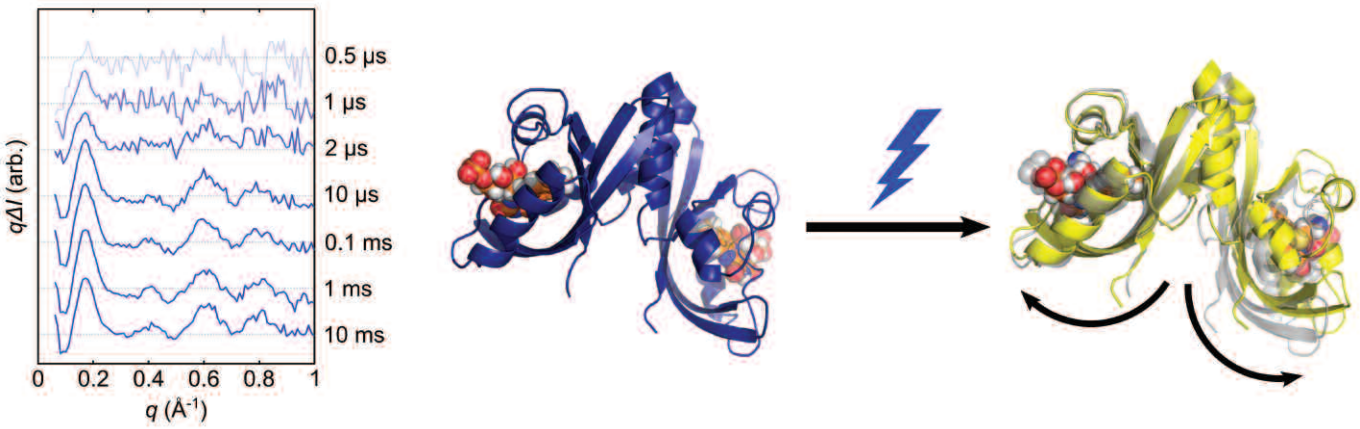

Fig. 1. X-ray solution scattering data and structural models of dark-to-light transition of YtvA. X-ray solution scattering data for YtvA between 0.5 µsec and 10 ms after a blue laser flash is shown next to a model of the dark-adapted (blue) and light-adapted (yellow) structures. The light-sensitive chromophore is shown as a space-filling molecular model.

The research team in this study was a collaboration between scientists at the University of Gothenburg (Sweden), Humboldt-Universität zu Berlin and Universität Bayreuth (Germany), the European Synchrotron Radiation Facility (France), the Paul Sherrer Institute (Switzerland), and The University of Chicago. The structure of the LOV domain from YtvA had been previously solved by x-ray crystallography, but the differences between the dark and light-activated structures of the protein were not large enough to conclusively point

"Light" cont'd. on page 120

"Anticancer" cont'd. from page 118
states. They now hope to capture a few more of these intermediate conformations to help map the entire conformational landscape of the transport cycle used by this transporter.

This more detailed understanding of the elevator model can help guide development of new anticancer and antiviral drugs that are more selective and more efficient. *— Nicola Parry*

See: Marscha Hirschi, Zachary Lee Johnson, and Seok-Yong Lee*, "Visualizing multistep elevator-like transitions of a nucleoside transporter," Nature **545**, 66 (4 May 2017).
DOI: 10.1038/nature22057
Author affiliation: Duke University Medical Center
Correspondence:
* seok-yong.lee@duke.edu

This work was supported by National Institutes of Health (NIH) R01 GM100984 (S.-Y.L.) and NIH R35 NS097241 (S.-Y.L.). Supporting institutions for the Southeast Regional Collaborative Access Team may be found at www.ser-cat.org/members.html. Northeastern Collaborative Access Team beamlines, which are funded by the National Institute of General Medical Sciences from the National Institutes of Health (P41 GM103403). The Pilatus 6M detector on 24-ID-C beam line is funded by a NIH-ORIP HEI grant (S10 RR029205). This research used resources of the Advanced Photon Source, a U.S. Department of Energy (DOE) Office of Science user facility operated for the DOE Office of Science by Argonne National Laboratory under Contract No. DE-AC02-06CH11357.

22-ID-D • SER-CAT • Life sciences • Macromolecular crystallography, multi-wavelength anomalous dispersion, single-wavelength anomalous dispersion, microbeam • 6-20 keV • On-site, remote • Accepting general users •

24-ID-C • NE-CAT • Life sciences • Macromolecular crystallography, microdiffraction, single-wavelength anomalous dispersion, single-crystal diffraction, microbeam, multi-wavelength anomalous dispersion, subatomic (<0.85 Å) resolution • 6.5-23 keV • On-site, remote • Accepting general users •

"Light" cont'd. from page 119
to a mechanism by which the structural changes would transmit a signal to the effector domain of the protein. Also, the structure was missing a helical domain that the team felt might be important to the activity of the LOV domain. They decided to do x-ray scattering experiments in solution with a form of the protein that contained that domain to see if they could observe structural changes that might provide more information.

They first performed x-ray solution scattering of the complete YtvA LOV domain in the transition between dark and light. The BioCARS 14-ID-B x-ray beamline at the APS was used to record results between 0.5 µsec and 10 ms after a brief blue laser flash, and the Swiss Light Source (SLS) was used to record the data at times greater than 100 ms. These resources provided the ability to record data at time scales compatible with the timing of the structural transition of the protein (Fig. 1). LOV is known to transform very quickly from a dark-adapted state through two photochemical intermediates before a bond is formed that stabilizes the state which transmits the downstream signal. X-ray solution scattering was able to capture this transition and provided data for comparison to molecular models of possible structural rearrangements.

Molecular dynamic simulations yielded approximately 50,000 possible dark- and light-state structures of the protein that were compared to the x-ray scattering data, thereby providing a clearer picture of the global structural changes that occur in the dark-to-light transition. The data showed that the two monomers of YtvA separate by about 3 Å in the dark-to-light transition (Fig. 1). The separation of the monomers occurs at the interface with the domain responsible for biochemical output, consistent with its role in signal transmission.

The helical domain, which was not present in the previous crystal structure, acts as a hinge allowing the monomers to move away from each other by about 6 degrees, levering the domains apart in a manner that suggests that this structural change is robust enough to be exploited for protein engineering projects.

The team has already extended this investigation to a blue-light-regulated histidine kinase using x-ray solution scattering recorded at the BioCARS beamline. Indeed, the solution x-ray scattering data provide a structural rationale for recent findings on a system for blue-light-regulated gene expression, thus facilitating the engineering of enhanced light-gated protein actuators. *— Sandy Field*

See: Oskar Berntsson[1,7], Ralph P. Diensthuber[2,7], Matthijs R. Panman[1], Alexander Björling[1], Ashley J. Hughes[1], Léocadie Henry[1], Stephan Niebling[1], Gemma Newby[3], Marianne Liebi[4], Andreas Menzel[4], Robert Henning[5], Irina Kosheleva[5], Andreas Möglich[2,6]*, and Sebastian Westenhoff[1,8]**, "Time-Resolved X-Ray Solution Scattering Reveals the Structural Photoactivation of a Light-Oxygen-Voltage Photoreceptor," Structure **25**, 933 (June 6, 2017).
DOI: 10.1016/j.str.2017.04.006
Author affiliations: [1]University of Gothenburg, [2]Humboldt-Universität zu Berlin, [3]European Synchrotron Radiation Facility, [4]Paul Scherrer Institut, [5]The University of Chicago, [6]Universität Bayreuth
Correspondence:
* andreas.moeglich@uni-bayreuth.de,
** westenho@chem.gu.se

S.W. acknowledges funding from the Swedish Foundation for International Cooperation in Research and Higher Education, the European Research Council, and the Foundation of Strategic Research, Sweden. A. Möglich acknowledges support from Deutsche Forschungsgemeinschaft through DFG grant MO2192/3-1 and a Sofja-Kovalevskaya Award by Alexander-von-Humboldt Foundation. Use of BioCARS was also supported by the NIGMS/NIH under grant number R24GM111072. The time-resolved setup at BioCARS was funded in part through a collaboration with Philip Anfinrud (NIH/NIDDK). This research used resources of the Advanced Photon Source, a U.S. DOE Office of Science user facility operated for the DOE Office of Science by Argonne National Laboratory under Contract No. DE-AC02- 06CH11357.

14-ID-B • BioCARS • Life sciences, materials science, physics, chemistry • Time-resolved crystallography, time-resolved x-ray scattering, Laue crystallography, wide-angle x-ray scattering, biohazards at the BSL2/3 level, macromolecular crystallography • 7-19 keV • On site • Accepting general users •

How Multiple Proteins Coordinate for the Controlled Release of Neurotransmitters

Communication between groups of neurons requires coordinated release of neurotransmitters by pre-synaptic neurons into the synaptic cleft, where they can be sensed by post-synaptic neurons. (A synapse is a structure that permits a neuron to pass an electrical or chemical signal to another neuron or to the target cell.) This process, called "synaptic transmission," takes place within milliseconds, and is initiated when an influx of calcium ions (Ca^{2+}) causes neurotransmitter-containing vesicles to fuse with the presynaptic neuronal membrane and release neurotransmitters into the synaptic cleft. To better understand the mechanism underlying the coordinated action of synaptic proteins known to regulate vesicle fusion, a research team from Stanford University crystalized a five-protein complex containing the neuronal SNARE complex (consisting of syntaxin, SNAP-25, and synaptobrevin), complexin, and synaptotagmin-1. The x-ray diffraction pattern collected at the APS allowed the researchers to determine the protein complex structure and identify intermolecular interactions that underpin cooperative activity. Knowledge of the molecular mechanisms of neurotransmitter release may be a first step to better understand how the process is altered in certain neurodegenerative diseases.

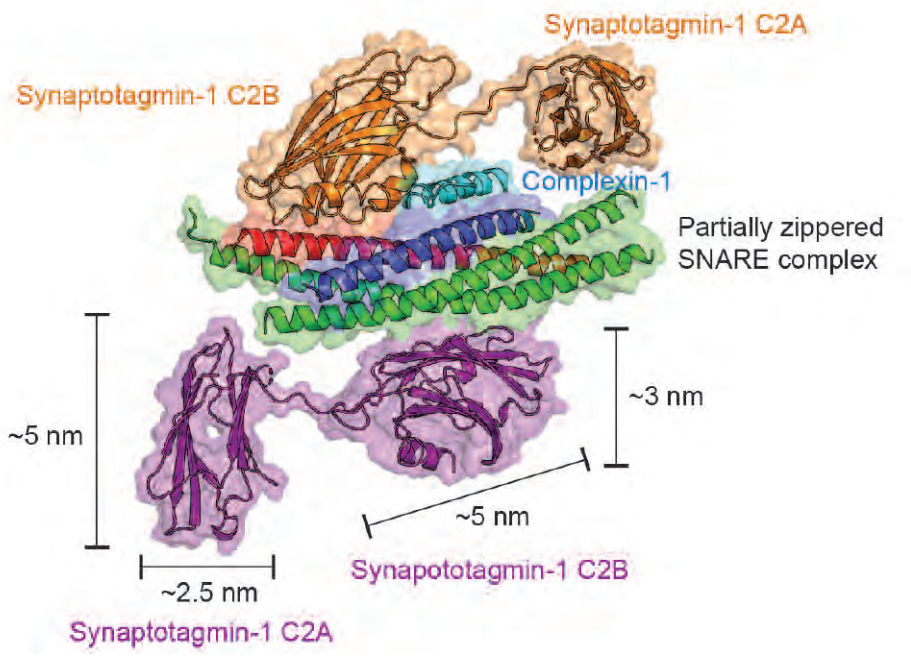

Fig. 1. Diagram of the SNARE-complexin-synaptotagmin-1 crystal structure. One synaptotagmin-1 molecule (orange) interacts with both the SNARE complex (red, green, and blue helices) and complexin (cyan) via the tripartite interface (the region of synaptotagmin-1 C2AB in contact with the top portion of SNARE). A second synaptotagmin-1 molecule (purple) interacts with the same SNARE complex through the previously identified primary interface.

In order for neurotransmitters to relay an electrical signal from one neuron to another, they must first be released into the synaptic space. This process relies on fusion of synaptic vesicles, bubble-like structures inside cells that contain various chemicals, with the cell membrane of the pre-synaptic neuron. Once this fusion takes place, the synaptic vesicle empties its contents (that is, neurotransmitter molecules) outside of the cell where the released neurotransmitter molecules can be detected by other, post-synaptic neurons. Five proteins are known to be critical for neurotransmitter release (Fig. 1). The neuronal SNARE complex, which is composed of three proteins (syntaxin, synaptobrevin, SNAP-25), serves to dock synaptic vesicles on the inside of the neuron's cell membrane so that they are poised for fusion. The synaptotagmin-1 protein interacts with SNAREs, and serves to sense the influx of Ca^{2+} that signals the need for synchronous fusion. Finally, the complexin protein assists in this process.

Prior to the current work, the importance of these synaptic proteins was known; however, the way that the proteins work together to tightly regulate neurotransmitter release remained un-

"Release" cont'd. on page 123

Breaking Up an Insulin Duo to Watch It Reunite

Insulin is essential to human life; type 1 diabetes, a disease characterized by an inability to make insulin, is fatal without daily injections of the hormone. When unneeded, insulin joins up with other copies of itself to form hexamers (structural subunits that are stored in the pancreas and are composed of six subunits of similar shape), which are inactive. When blood glucose rises, the insulin bundles break apart, releasing the hormone in its active monomeric form, allowing the protein to do its job of ushering glucose out of the bloodstream into the cells where the sugar can be consumed for energy. The molecular details for how insulin breaks apart and comes together have been difficult to assess. To better understand how insulin associates with itself, a team of researchers performed time-resolved x-ray solution scattering (TRXSS) and static small-angle x-ray scattering (SAXS) measurements at the APS. Taken together, the data revealed five new transient species in a dynamic process from insulin dimer to insulin monomer, highlighting a new role for TRXSS in the study of structural dynamics in non-photoactive proteins. *Cont'd. on the next page*

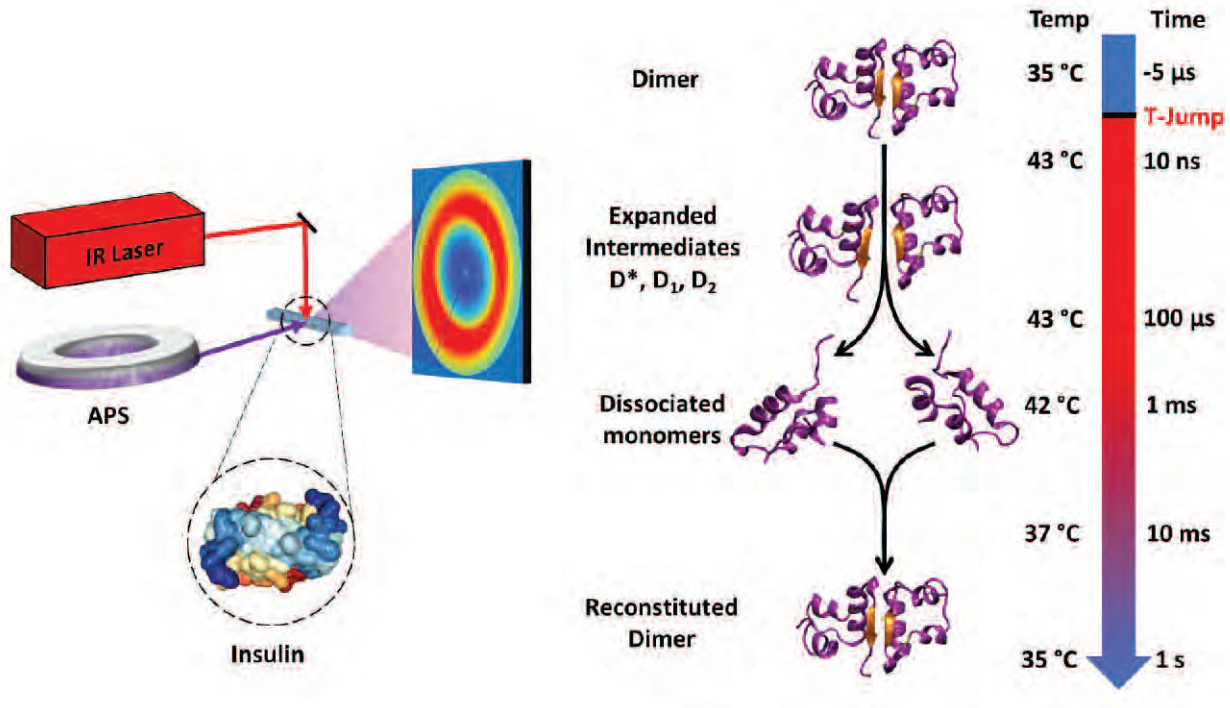

Fig. 1. Left: TRXSS T-jump instrument at BioCARS. Right: Dynamics of insulin dissociation/association revealed by TRXSS. The time delays and corresponding temperature are shown on the arrow.

5-ID-B,C,D • DND-CAT • Materials science, polymer science • Powder diffraction, x-ray standing waves, x-ray optics development/techniques, small-angle x-ray scattering, surface diffraction, x-ray reflectivity, wide-angle x-ray scattering • 6-17.5 keV • On-site • Accepting general users •

14-ID-B • BioCARS • Life sciences, materials science, physics, chemistry • Time-resolved crystallography, time-resolved x-ray scattering, Laue crystallography, wide-angle x-ray scattering, biohazards at the BSL2/3 level, macromolecular crystallography • 7-19 keV • On site • Accepting general users •

To study the association dynamics, the scientists from Northwestern University, The University of Chicago, and Argonne first needed a strategy for rapidly breaking apart the insulin dimers, assessing association, ironically, by the reverse process of disassociation. Previous studies demonstrated that the association and dissociation of insulin is temperature dependent. Therefore, the researchers decided to use laser-induced temperature jumps to rapidly split insulin dimers into monomers, and then use TRXSS at the BioCARS Beamline 14-ID-B at the APS (Fig. 1) to observe the aftermath. The TRXSS signal includes two components: the SAXS region, which reports on tertiary structure, and the wide-angle (wide-angle x-ray scattering, or WAXS) region, which tells the story of secondary structure. For each TRXSS experiment, the researchers shone a laser on a solution of insulin dimers, raising the sample's temperature by 8° C in nanoseconds. Then, the researchers waited increasing intervals of time, from 10 nsec to 100 msec, capturing snapshots of the protein structures along the way as the dimer split apart.

Overall, the researchers identified five distinguishable transient species during the dissociation process. In the early moments after heating up the insulin, the researchers, utilizing the DND-CAT 5-ID-B,C,D beamline at the APS, detected a loss in SAXS intensity, labeling this expanded structure as a "hot" dimer with weakened hydrogen bonds. Next, the dimer proceeded through two additional states, D1 and D2, at 310 nsec and 900 nsec, respectively. These states had even less SAXS intensity, and a complete absence of WAXS features, indicating that secondary structure was being maintained. D1's defining characteristic was an increase in protein mass, attributed to a flood of water into the dimer due to its expansion, while D2 showed an even more expanded conformation. At 240 msecs after the temperature jump, another state emerged, 2M, this one characterized by the appearance of WAXS features, indicating that the protein secondary structure was undergoing changes (Fig. 1).

By comparing the 2M TRXSS data to steady state WAXS data, the researchers assigned 2M to the dissociated state, meaning the dimer had become monomers. The agreement of the data further indicated that the WAXS features could be attributed to the loss of the intermolecular beta sheet that defines the border between insulin molecules in the dimer. The final intermediate, 2M′, is the beginning of the association of insulin monomers to the dimeric state, characterized by a decay in WAXS features as the molecules rearrange themselves to secondary structures that are similar to those found in the dimeric state.

In addition to the information, the scientists gathered about the complexity of insulin association dynamics, the method of using a laser-induced temperature jumps and TRXSS to study the dynamics of non-photoactive proteins are novel, and could be applied to the study of other molecules.

— Erika Gebel Berg

See: Dolev Rimmerman[1], Denis Leshchev[1], Darren J. Hsu[1], Jiyun Hong[1], Irina Kosheleva[2], and Lin X. Chen[1,3]*, "Direct Observation of Insulin Association Dynamics with Time-Resolved X-ray Scattering," J. Phys. Chem. Lett. **8**, 4413 (2017).
DOI: 10.1021/acs.jpclett.7b01720
Author affiliations: [1]Northwestern University, [2]The University of Chicago, [3]Argonne National Laboratory
Correspondence:
* l-chen@northwestern.edu, lchen@anl.gov

This work was supported by the National Institute of Health, under contract no. R01-GM115761. Use of BioCARS was supported by the National Institute of General Medical Sciences of the National Institutes of Health under grant number R24GM111072. Time-resolved setup at Sector 14 was funded in part through a collaboration with Philip Anfinrud (NIH/NIDDK). We acknowledge Robert W. Henning (BioCARS) for his assistance in performing the TRXSS experiments. We also acknowledge Guy Macha (BioCARS) for his assistance in designing the sample holder. DND-CAT is supported by Northwestern University, E.I. DuPont de Nemours & Co., and The Dow Chemical Company. Data were collected using an instrument funded by the National Science Foundation under Award Number 0960140. This research used resources of the Advanced Photon Source, a U.S. DOE Office of Science user facility operated for the DOE Office of Science by Argonne National Laboratory under Contract No. DE-AC02-06CH11357.

"Release" cont'd. from page 121
clear. To understand the interactions between the proteins, the researchers purified the neuronal SNARE complex, complexin, and the C2AB fragment of synaptotagmin-1, assembled the complex, and then crystalized the complex in order to observe the molecular interactions that allow for cooperation between the proteins. The 1.85-Å crystal structure of the complex determined at the NE-CAT 24-ID-C beamline revealed a tripartite interface between synaptotagmin-1 and both SNARE and complexin (Fig. 1). This interaction was previously unknown, and disruption of the interaction with mutations to amino acids within the interface impaired synchronous release of neurotransmitter by neurons.

Using these data, the researchers proposed a model in which the tripartite interface between the neuronal SNARE complex, complexin, and synaptotagmin-1 locks the primed complex into a state of low fusion probability until synaptotagmin-1 is triggered by Ca^{2+} influx so that the synaptic proteins can initiate fusion. This degree of cooperation would support the synchronous release of neurotransmitters on the required sub-millisecond timescale. Remaining questions are centered on how the complex is situated between the synaptic vesicle and plasma membrane, the nature of changes in protein interactions, and activities upon calcium triggering. *— Emma Nichols*

See: Qiangjun Zhou, Peng Zhou, Austin L. Wang, Dick Wu, Minglei Zhao‡, Thomas C. Südhof, and Axel T. Brunger*, "The primed SNARE–complexin–synaptotagmin complex for neuronal exocytosis," Nature **548**, 420 (24 August 2017).
DOI: 10.1038/nature23484
Author affiliation: Stanford University
‡Present address: The University of Chicago,
Correspondence:
* brunger@stanford.edu

The authors thank the National Institutes of Health (NIH) for support (R37 MH63105 to A.T.B.; P50 MH086403 to T.C.S.). The Northeastern Collaborative Access Team (NECAT) beamlines are funded by the National Institute of General Medical Sciences (NIGMS) from the NIH (P41 GM103403). The Pilatus 6M detector at the 24-ID-C beam line is funded by an NIH-ORIP HEI grant (S10 RR029205).

How RNA Polymerase "Melts" Double-Stranded DNA to Initiate Gene Expression

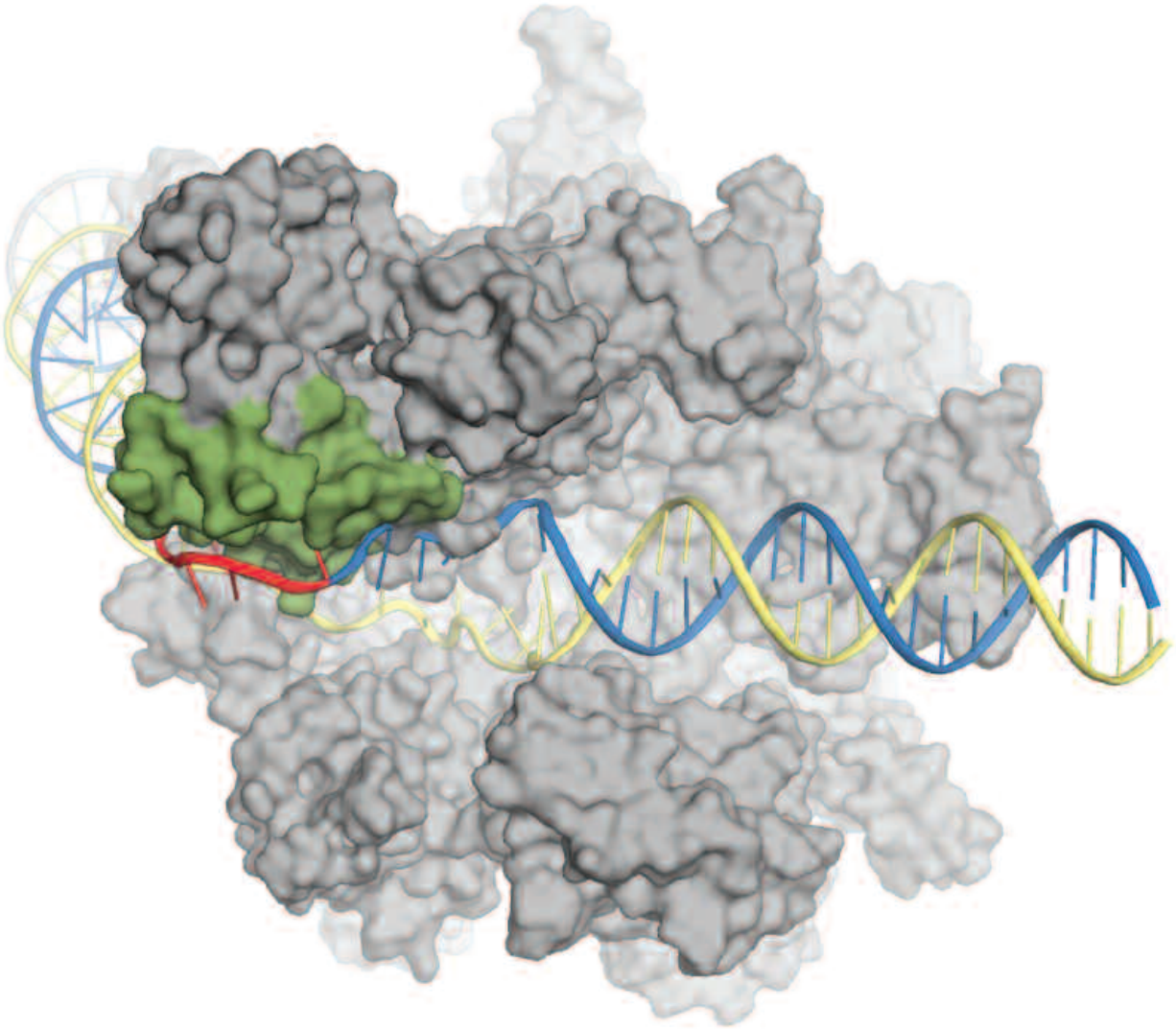

RNA polymerase (RNAP) is a large cellular macromolecule responsible for finding and transcribing genes so that they can be translated into the functional proteins that enable cellular life. In all organisms, RNAP is able to respond to cellular signals so that it can transcribe the right gene at the right time. Prior to this study, little was known about how bacterial RNAP is able to search through vast regions of DNA to actually find the right gene promoter. Once a promoter is located, RNAP "melts" the double-stranded DNA and initiates RNA transcription. To better understand RNAP dynamics during transcription initiation, researchers used x-ray diffraction data collected at the APS to solve the structure of a late-initiation bacterial RNAP intermediate to a resolution of 2.6 Å. This structure, together with complementary biochemical techniques, illuminates the mechanism by which RNAP locates specific gene promoters and how the motions of flexible parts of RNAP involved in the initiation of gene expression can occur without external energy sources.

RNAP is a complex molecule that carries out the transcription of genes so that they can be translated into functional proteins that sustain the activities of a given cell. RNAP has many distinct structural features, among them a "clamp domain" that has long been assumed to function by separating DNA strands while in the "open" position and then closing around the DNA strand to be transcribed (the template strand) so that the RNAP can transcribe large genes without falling off. Data produced in this work by researchers from The Rockefeller University, Saint Louis University School of Medicine, Helmholtz Centre for Infection Research (Germany), the Institute of Pharmaceutical Sciences (Switzerland), and the University of Wisconsin-Madison, however, support a different model that better dovetails with the energetic requirements of transcription initiation. Instead, the RNAP clamp closes around a promoter to initiate melting of the two DNA strands, then opens so that the template strand can be loaded into the active site cleft of the RNAP. Once the template strand is in place, the clamp closes once more to further melt the promoter so that transcription can begin. Remarkably, each of these significant structural changes occurs without the input of external energy.

To study the dynamics of RNAP during transcription initiation, well-characterized molecules were used to bias the RNAP clamp in the open or closed position, and then the efficiency of promoter recognition and melting in real time was measured using a fluorescence-based assay. This assay showed that only the closed form of RNAP is able to identify the starting potion of the gene embedded within the promoter, the -10 element.

To better understand the movement of single-stranded template DNA into the open cleft of RNAP a 2.6-Å crystal structure of RNAP in the late stages of promoter melting was obtained at the NE-CAT 24-ID-E and analyzed (Fig. 1). The structure showed how duplex DNA can rotate around its axis within the active site cleft of the enzyme to allow spontaneous DNA unwinding and loading of the DNA template strand into the active site cleft, so that the promoter sequence can be read by the enzyme. Together, these results build an understanding of how RNAP is able to recognize and initiate transcription at specific promoters, and therefore a mechanism underlying the tight control of gene expression.

— Emma Nichols

Fig. 1. Modeled structure of RNAP in complex with a gene promoter (-10 element is shown in red) within DNA (blue and yellow strands). The RNAP clamp domain (part of the clamp recognizing -10 element is shown in green) is shown in the open position, and the template strand (yellow) is loaded into the enzyme's cleft through electrostatic interactions.

See: Andrey Feklistov[1]*, Brian Bae[1], Jesse Hauver[1], Agnieszka Lass-Napiorkowska[2], Markus Kalesse[3], Florian Glaus[4], Karl-Heinz Altmann[4], Tomasz Heyduk[2], Robert Landick[5], and Seth A. Darst[1], " RNA polymerase motions during promoter melting," Science **356**, 863 (2017). DOI: 10.1126/science.aam7858
Author affiliations: [1]The Rockefeller University, [2]Saint Louis University School of Medicine, [3]Helmholtz Centre for Infection Research, [4]Institute of Pharmaceutical Sciences, [5]University of Wisconsin–Madison
Correspondence:
* afeklistov@rockefeller.edu

This work was supported by National Institutes of Health grants R01 GM38660 to R.L. and R35 GM118130 to S.A.D. and FP7 grant 260872 to K.-H. A. NE-CAT beamlines are funded by the National Institute of General Medical Sciences from the National Institutes of Health (P41 GM103403). Foundation under Award Number 0960140. This research used resources of the Advanced Photon Source, a U.S. Department of Energy (DOE) Office of Science user facility operated for the DOE Office of Science by Argonne National Laboratory under Contract No. DE-AC02- 06CH11357.

24-ID-E • NE-CAT • Life sciences • Macromolecular crystallography, microbeam, microdiffraction, single-wavelength anomalous dispersion, single-crystal diffraction • 12.68 keV • On-site, remote • Accepting general users •

A Potential New Treatment Approach to Help Fight Parasites

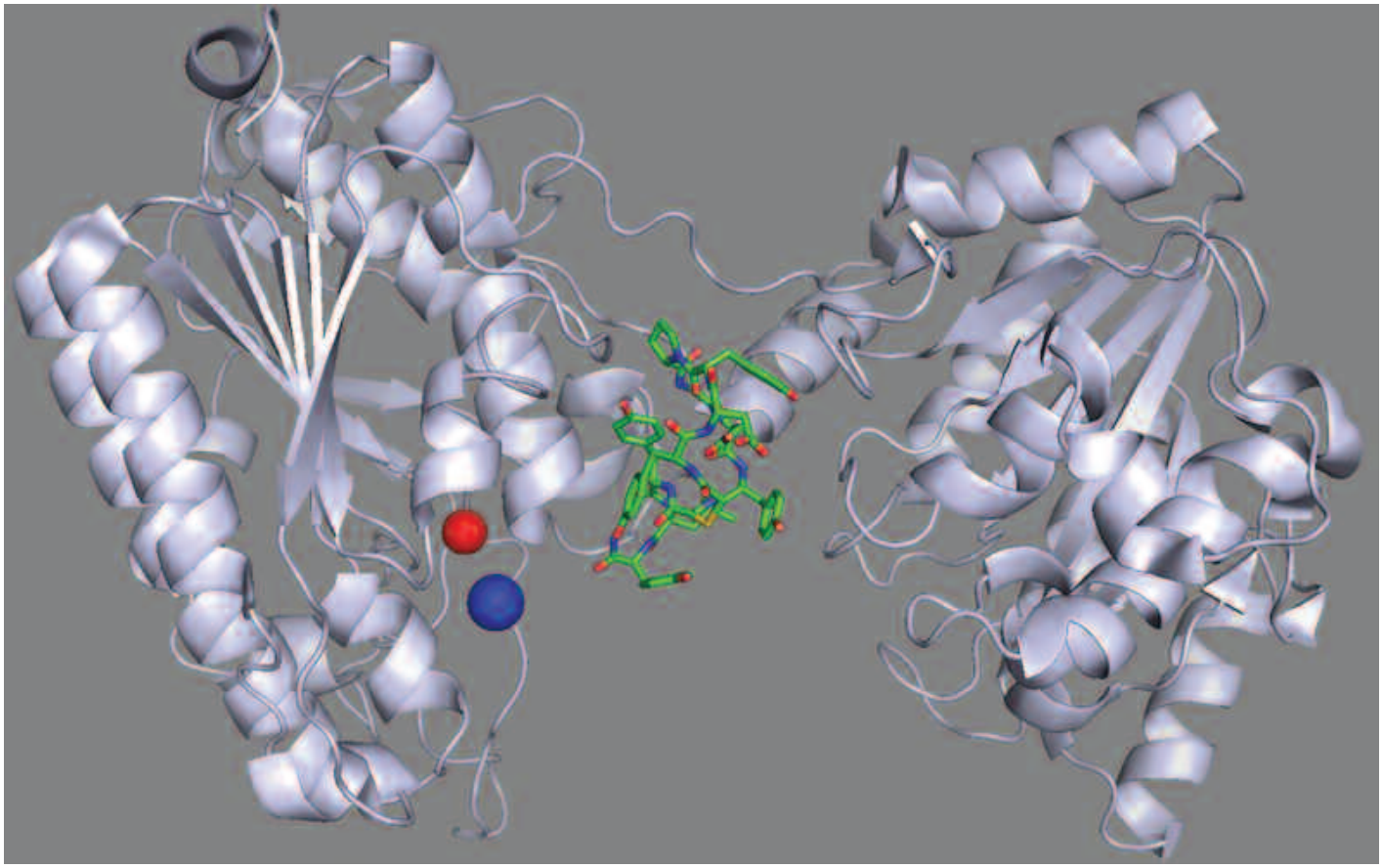

Fig. 1. The binding interaction between the parasite enzyme target (shown as a ribbon) and the cyclic peptide (shown in sticks) as revealed in this molecular structure.

River blindness is a devastating, neglected tropical disease that causes suffering to millions of people worldwide, especially in African countries, where it is endemic. The disease is caused by the parasitic roundworm (or nematode) *Onchocerca volvulus*, and is transmitted to humans by the bites of blackflies that carry the parasite. The enzyme cofactor-independent phosphoglycerate mutase (iPGM) is critical for survival of some pathogens, including the *Onchocerca volvulus*. However, although iPGM is recognized as a drug target in this setting, studies have failed to identify any compound that targets the iPGM enzyme, and use of traditional small molecules in particular has failed to be a useful approach. Researchers therefore set out to test a vast ensemble of these cyclic peptides, and identified one that bound tightly to the enzyme. Utilizing x-ray diffraction data collected at APS, they characterized the molecular details of the interaction between this cyclic peptide and iPGM that effectively blocks the enzyme from functioning. The results of this study could eventually help scientists better treat diseases such as river blindness. They could also help guide discovery of new agents that can be used against targets for which conventional small-molecule drugs have failed.

Although doctors currently use ivermectin to treat river blindness, this drug mostly targets early-stage worm larvae, and is ineffective against the adult worm. So, researchers have continued to search for more effective treatments for this disease.

Some years ago, iPGM was identified as a potential new drug target in roundworms. This enzyme is found in various pathogenic organisms, including in *Onchocerca volvulus*, and is required for their survival. The enzyme plays a key role in cellular energy metabolism, driving reactions in the pathways of glycolysis and gluconeogenesis. And, although these processes also occur in humans, they rely on different enzymes. As such, iPGM became a particularly appealing therapeutic target to help fight diseases such as river blindness, because a drug that would target iPGM would potentially kill the roundworm without negatively affecting the human.

Small-molecule drugs are often employed as enzyme inhibitors because they bind to the pocket-shaped active site of most enzymes and block their activity. But the iPGM active site is somewhat unique in that it forms transiently during catalysis. This short-lived nature of its accessibility has made it difficult for researchers to find a small-molecule drug to target the enzyme.

With this in mind, an international group of researchers from the University of Tokyo (Japan), the National Institutes of Health, New England Biolabs, the National Institute of Standards and Technology, and the University of Kansas set out to identify a compound that could disable iPGM.

The group considered a different class of molecules called cyclic peptides. Because these have a larger surface area than do small molecules, the researchers thought they might more easily bind to the enzyme and block its activity. During their study, the researchers produced a collection of more than one trillion cyclic peptides, using resin-bound iPGM enzyme to enrich for those with the highest affinity interaction. They found one in particular that bound very tightly to iPGM and prevented its activity.

Using x-ray diffraction data collected at the IMCA-CAT beamline 17-ID-B at the APS, the team investigated the molecular aspects of the iPGM-cyclic peptide arrangement. They determined its co-crystal structure, showing in detail how the cyclic peptide binds to the parasitic enzyme (Fig. 1) to prevent it from functioning. This molecular blueprint will help guide efforts to incorporate drug-like properties into the cyclic peptide structure, while avoiding disruptions of key interactions necessary for its binding to the enzyme.

Although this cyclic peptide molecule needs to be further refined before it can become a drug, the results of this study have the potential to positively impact the devastating burden of river blindness. More generally, the findings will also help guide development of new forms of molecular modalities based on cyclic peptides that can be directed against a broad class of targets not well-addressed by traditional small-molecule drugs. *— Nicola Parry*

See: Hao Yu[1], Patricia Dranchak[2], Zhiru Li[3], Ryan MacArthur[2], Matthew S. Munson[4], Nurjahan Mehzabeen[5], Nathan J. Baird[1‡], Kevin P. Battalie[6], David Ross[4], Scott Lovell[5], Clotilde K.S. Carlow[3], Hiroaki Suga[1*], and James Inglese[2**], "Macrocycle peptides delineate locked-open inhibition mechanism for microorganism phosphoglycerate mutases," Nat. Commun. **8**, 14932 (3 April 2017). DOI: 10.1038/ncomms14932

Author affiliations: [1]University of Tokyo, [2]National Institutes of Health, [3]New England Biolabs, [4]National Institute of Standards and Technology, [5]University of Kansas, [6]IMCA-CAT ‡Present address: University of the Sciences

Correspondence:

* hsuga@chem.s.u-tokyo.ac.jp,

** jinglese@mail.nih.gov

This research was supported in part (Z1ATR000247-01) by the Intramural Research Program of the National Center for Advancing Translational Sciences, National Institutes of Health (NIH) (J.I.), and in part by the AMED Basic Science and Platform Technology Program for Innovative Biological Medicine (JST-CREST Molecular Technologies) to H.S. Use of the IMCA-CAT beamline 17-ID was supported by the companies of the Industrial Macromolecular Crystallography Association through a contract with Hauptman-Woodward Medical Research Institute. This research used resources of the Advanced Photon Source, a U.S. Department of Energy (DOE) Office of Science user facility operated for the U.S. DOE Office of Science by Argonne National Laboratory under Contract No. DE-AC02-06CH11357.

17-ID-B • IMCA-CAT • Life sciences • Macromolecular crystallography, multi-wavelength anomalous dispersion, microbeam, single-wavelength anomalous dispersion, large unit cell crystallography • Subatomic (<0.85 Å) resolution • 6-20 keV • On-site, remote • Accepting general users •

Identifying the First Selective HAT Inhibitor

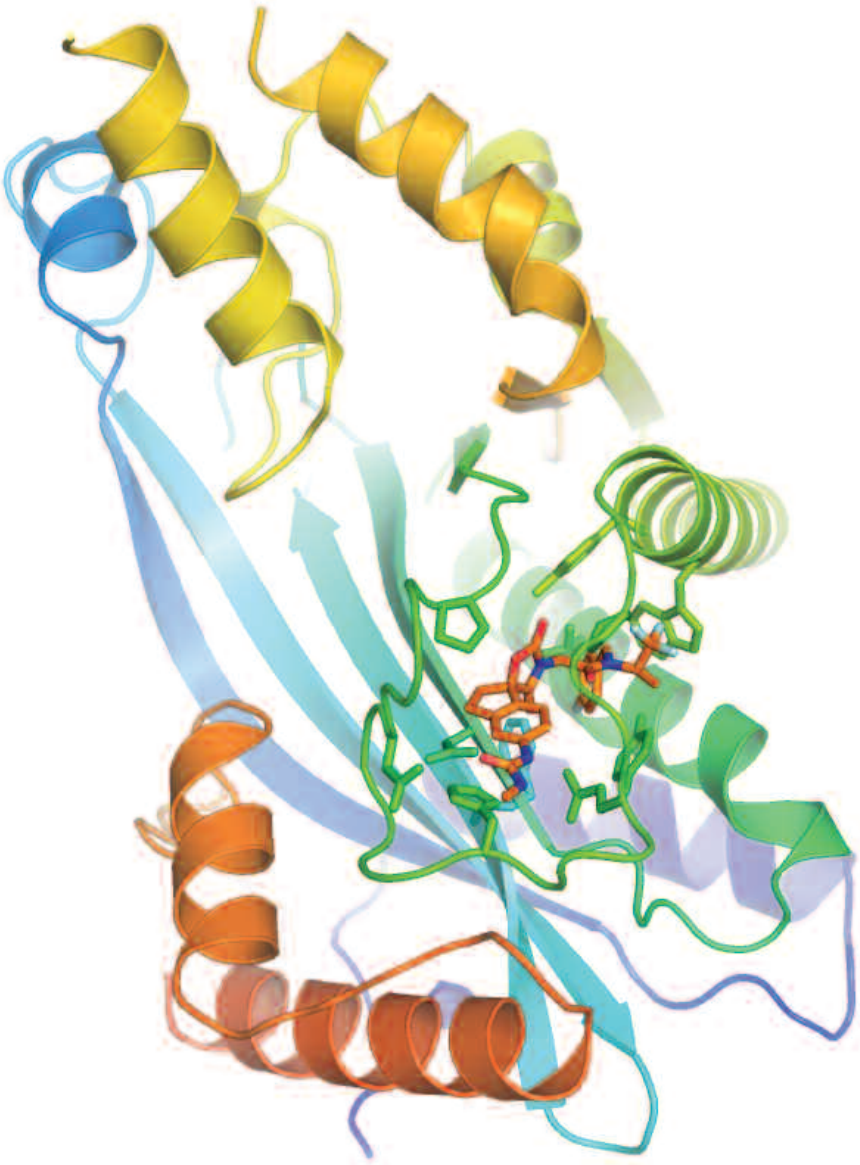

Fig. 1. The structure of Δp300 HAT domain with A-485. The protein is shown in ribbon representation with key interacting residues shown in sticks. A-485 shown in orange sticks binds in the active site and inserts into the L1 loop.

17-ID-B • IMCA-CAT • Life sciences • Macromolecular crystallography, multi-wavelength anomalous dispersion, microbeam, single-wavelength anomalous dispersion, large unit cell crystallography • Subatomic (<0.85 Å) resolution • 6-20 keV • On-site, remote • Accepting general users •

The human genome contains about 19,000 genes that are organized and tightly condensed within our cells by histone proteins that wrap up the chromosomes and make genes available when needed. This process is regulated by the addition and removal of epigenetic "tags" on these histone proteins that can make a gene more available for transcription or can silence it. If this process goes awry, disease can occur. For example, dysregulation of one of these epigenetic tags, acetylation, has been shown to be important for the development and progression of cancer. This process is reversible and regulated by enzymes that put the acetyl group on and take it back off again, histone acetyltransferases and histone deacetylases, or HATs and HDACs. This makes them an attractive target for therapy. In fact, HDAC inhibitors have already made it to the clinic and are being used to treat epilepsy, depression, and some cancers. HAT inhibitors have been more difficult to develop but a recent collaboration between pharmaceutical researchers working at the APS has made an important first step toward bringing them to the clinic.

This major drug discovery effort involved a team of researchers from both AbbVie, Inc. and Acylin Therapeutics. The first task for the team was identifying possible candidates that might inhibit members of the p300/CBP family of HAT enzymes that they wanted to target. They started with in silico modeling by docking 800,000 potential inhibitor molecules to p300 and then moved to the lab to test 1,300 of them that were commercially available. This led to two positive hits and one of these was optimized to improve its activity and stability, and to reduce the impact of unwanted sites that might be metabolically active and could potentially lead to reduced in vivo exposure. The resulting compound, called A-485, is 1000 times more potent than previously identified p300 inhibitors and has a slow off rate from the enzyme, suggesting it could be an effective HAT inhibitor. It is also quite specific for p300/CBP and does not inhibit other HAT subfamilies, a good sign that the therapy would not have off-target effects.

The next step was to determine how A-485 binds to p300. The team crystallized the catalytically active domain of p300 in a co-crystal with A-485 and determined the structure at a resolution of 1.95Å using data collected at the APS IMCA-CAT beamline 17-ID-B (Fig. 1). They were able to confirm how the inhibitor works by comparing this structure to the structures of p300 bound to its substrates. This showed that A-485 blocks acetyl-coenzyme A binding but not the binding of the peptide substrate. Comparison to other HAT family members also showed why A-485 is specific for the p300/CBP subfamily, the loop that binds A-485 is absent in other HAT subfamilies so they would not be predicted to bind to A-485 very well.

The identification of A-485 as a strong and specific inhibitor of p300/CBP was followed by experiments to determine whether it works the same way in cells. The first test was to see if it could inhibit p300/CBP activity in cells in culture. The team showed that A-485 inhibited histone acetylation by p300/CBP but did not inhibit other HATs in prostate cancer cells, confirming the selectivity of A-485. Further testing in 124 additional cancer cell lines showed that A-485 was effective in blocking the growth of many hematological malignancies and androgen receptor-positive prostate cancer cells but was not as effective at blocking the proliferation of melanoma, breast cancer, or lung cancer cells.

Interestingly, although A-485 blocked HAT activity in androgen receptor-negative prostate cancer cells, it was not sufficient to block the growth of those cells. This suggested to the team that HAT inhibition is not generally antiproliferative but must be applied in cases where HAT dysregulation is a driver of the cancer. This finding was supported by experiments in androgen receptor-positive prostate cancer cells in which A-485 was able to inhibit the transcriptional activity of the androgen receptor and expression of the MYC oncogene, both important drivers of prostate cancer progression. These results led the team to test A-485 in a mouse model of castration-resistant prostate cancer. Mice who were given A-485 had a 54% inhibition of tumor growth, reduced MYC activity, and reduced androgen receptor transcriptional activity, confirming the results from cultured cells. The researchers concluded from these results that A-485 is a potent, selective inhibitor of HAT and that there is likely to be a benefit from future evaluation of the clinical utility of HAT inhibitors in multiple human diseases.

— Sandy Field

See: Loren M. Lasko[1], Clarissa G. Jakob[1], Rohinton P. Edalji[1], Wei Qiu[1], Debra Montgomery[1], Enrico L. Digiammarino[1], T. Matt Hansen[1], Roberto M. Risi[1], Robin Frey[1], Vlasios Manaves[1], Bailin Shaw[1], Mikkel Algire[1], Paul Hessler[1], Lloyd T. Lam[1], Tamar Uziel[1], Emily Faivre[1], Debra Ferguson[1], Fritz G. Buchanan[1], Ruth L. Martin[1], Maricel Torrent[1], Gary G. Chiang[1,2], Kannan Karukurichi[3], J. William Langston[4], Brian T. Weinert[5], Chunaram Choudhary[5], Peter de Vries[6], John H. Van Drie[7], David McElligott[8], Ed Kesicki[3], Ronen Marmorstein[9], Chaohong Sun[1], Philip A. Cole[10], Saul H. Rosenberg[1], Michael R. Michaelides[1], Albert Lai[1]**, Kenneth D. Bromberg[1]*, "Discovery of a selective catalytic p300/CBP inhibitor that targets lineage-specific tumours," Nature **550**, 128 (5 October 2017).
DOI: 10.1038/nature24028
Author affiliations: [1]AbbVie, [2]eFFECTOR Therapeutics, [3]Petra Pharma Corporation, [4]Faraday Pharmaceuticals, [5]University of Copenhagen, [6]Cascadian Therapeutics, Inc., [7]Van Drie Research, [8]Accelerator Corporation, [9]University of Pennsylvania, [10]Johns Hopkins University
Correspondence:
* kenneth.bromberg@abbvie.com,
** Albert.Lai@abbvie.com

C.C. is supported by the Hallas Møller Investigator award from the Novo Nordisk Foundation (NNF14OC0008541). The Novo Nordisk Foundation Center for Protein Research is supported financially by the Novo Nordisk Foundation (Grant agreement NNF14CC0001). P.A.C. was supported by the National Institutes of Health (NIH) and the FAMRI foundation. R.M. is supported by the NIH. Use of the IMCA-CAT beamline at the Advanced Photon Source was supported by the companies of the Industrial Macromolecular Crystallography Association through a contract with Hauptman-Woodward Medical Research Institute. This research used resources of the Advanced Photon Source, a U.S. DOE Office of Science user facility operated for the DOE Office of Science by Argonne National Laboratory under Contract No. DE-AC02-06CH11357.

Insight into the Evolution of Photosynthesis

Photosynthesis is one of the most important biochemical pathways in the world. Responsible for the conversion of the Sun's energy into the chemical energy required for growth, photosynthesis is carried out by plants, as well as by green algae and cyanobacteria. Embedded within the cellular membranes of these organisms are specialized membrane proteins called reaction centers (RC). While high-resolution structures of the Photosystem I and II (PSI, PSII) RCs found in plants and cyanobacteria, as well as those RCs found in purple bacteria and Chloroflexi have been obtained, work carried out by researchers utilizing high-brightness APS x-rays resulted in the first-ever structure of the RC present within anoxogenic phototrophic bacteria, organisms most like those present on early Earth. This information illuminates a mode of energy capture and electron transfer unique to anoxogenic phototrophic bacteria and reveals a symmetric reaction center that has retained characteristics of the RC present in the common ancestor of all photosynthetic organisms, thus providing a glimpse into the biochemical underpinnings of the ancestral RC that fueled over 3.5 billion years of evolution and shaped the atmosphere of our planet.

Photosynthesis was responsible for driving the atmospheric changes on Earth that permitted evolution of multicellular life, and remains a critically important process for sustaining life on Earth. Within the RC proteins of photosynthetic organisms, the energy from light photons is used to separate an electron from a donor molecule (e.g., abstraction of an electron from water by chlorophyll in green plants leads to release of oxygen gas), and this electron is then transferred through a chain of cofactors, a process that provides energy to drive the metabolism of high-energy molecules (e.g., glucose) that can be used by the cell for energy.

Even though photosynthetic organisms are evolutionarily divergent, for example, plants and purple bacteria have evolved to occupy physically and biochemically distinct niches, the RCs of all photosynthetic organisms share a similar overall structural organization: two core subunits, each of which is comprised of five transmembrane helices, encircle and support the activity of the electron transport (ET) chain cofactors. Though the identity of the cofactors can vary between desperate organisms, their function is retained: to transfer the electron from the initial receptor molecule to the terminal acceptor, generating energy for metabolism at each step.

Using x-ray light from two DOE Office of Science user facilities, the SBC-CAT 19-ID-D beamline at the APS; and beamline 8.2.1 at the Lawrence Berkeley National Laboratory Advanced Light Source, the team visualized the *Heliobacterium modesticaldum* RC for the first time at near-atomic, 2.2-Å resolution. Prior to this study, the only photosynthetic RC proteins for which high-resolution structures were available were heterodimeric, meaning that each of the two core RC subunits are structurally distinct. When these researchers, from Arizona State University, the Deutsches Elektronen-Synchrotron (DESY), The Pennsylvania State University, and the Biodesign Institute solved the structure of the HbRC, they observed that the core subunits are homodimeric, or identical, and therefore more closely resemble the ancestral RC that existed prior to the genetic duplication and divergence event that let to the heterodimers present in other RCs. Furthermore, the atomic-level resolution to which the structure was solved permitted researchers to identify four previously unidentified cofactors unique to the HbRC and to confirm the absence of a tightly bound menaquinone cofactor in the *H. modesticaldum* ET chain, a significant divergence from other RCs and a former subject of controversy in the field.

In addition to providing an explanation for the differences in ET rates between HbET and PSI ET systems observed through collection of biophysical data, information from the HbRC structure set the stage for future studies of possible charge separation mechanisms. *— Emma Nichols*

See: Christopher Gisriel[1], Iosifina Sarrou[2], Bryan Ferlez[3], John H. Golbeck[3], Kevin E. Redding[1], and Raimund Fromme[1,4]*, "Structure of a symmetric photosynthetic reaction center–photosystem," Science **357**, 1021 (2017). DOI: 10.1126/science.aan5611
Author affiliations: [1]Arizona State University, [2]Deutsches Elektronen-Synchrotron (DESY), [3]The Pennsylvania State University, [4]Biodesign Institute
Correspondence:
* raimund.fromme@asu.edu

This work was funded by the Division of Chemical Sciences, Geosciences, and Biosciences, U.S. Department of Energy (DOE) Office of Science-Basic Energy Sciences through Grant DE-SC0010575 to K.E.R., R.F., and J.H.G.. The Advanced Light Source is a DOE Scientific User Facility supported by the Director, Office of Science-Basic Energy Sciences and operated for the DOE Office of Science by Lawrence Berkeley National Laboratory. SBC-CAT is funded by the DOE Office of Science, Office of Biological and Environmental Research. This research used resources of the Advanced Photon Source, a U.S. DOE Office of Science user facility operated for the DOE Office of Science by Argonne National Laboratory under Contract No. DE-AC02-06CH11357.

Environmental, Geological & Planetary Science

Water Loss in Rocks Might Trigger Earthquakes

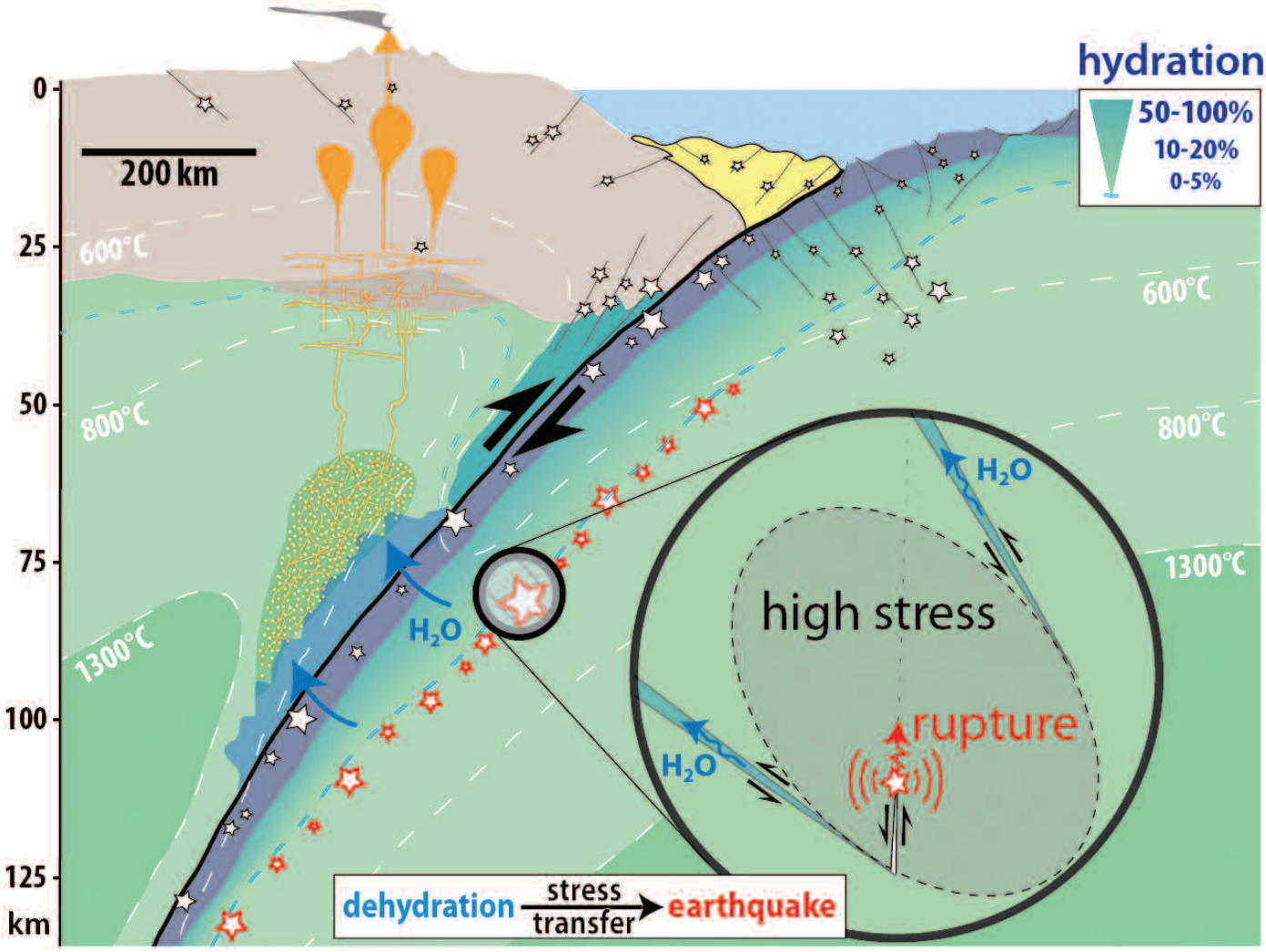

Fig. 1. This diagram shows a subduction zone, where an oceanic plate bends underneath another plate. As the rock is dragged down, the temperature and pressure reach a point where water-removing reactions occur in hydrous minerals. According to a new model, this dehydration causes a stress transfer to the surrounding non-hydrous minerals, which rupture as a result. This can explain intermediate-depth earthquakes that occur 30 to 300 km beneath the surface. Credit: Thomas P. Ferrand

Many earthquakes occur under the ocean at subduction zones, where two lithospheric plates meet and one is forced to sink beneath the other. Some of these quakes occur many kilometers below the surface, in rock that is assumed to be too "soft" to allow fracturing. To help explain the existence of these intermediate-depth earthquakes, a new study has placed rock samples under high pressure and high temperature, mimicking the relevant geological conditions. With synchrotron light from the APS, a team of researchers tracked the stress and mineralogical transformations within the rocks. Their observations revealed that rock fracturing occurred as water was "squeezed" out of the rock. The connection to dehydration suggests that intermediate-depth earthquakes arise due to a sudden transfer of stress between different types of minerals in the rock.

Roughly two-thirds of earthquakes occur within a few tens of kilometers of the Earth's surface. These shallow quakes arise when brittle slabs of rock undergo a critical mechanical stress. At this frictional limit, a rupture nucleates, and sliding occurs along a fault surface. However, this mechanism cannot explain the other third of earthquakes that erupt at deeper levels, where the pressure goes above 1 GPa (roughly 10,000 atm). Under these conditions, the rock is no longer thought to be brittle, so some other process must be causing the rock structures to fail.

Different theories have been put forth to explain deep earthquakes. One hypothesis places the blame on water in the rocks. At a subduction zone, water is dragged down with the lithosphere, allowing the formation of hydrous (water-carrying) minerals. But as the lithosphere is pulled down deeper, the pressure and temperature become high enough for dehydration reactions that remove water from the water-carrying minerals. This released fluid would presumably generate extra pressure that could crack the rock. However, previous experiments have not shown a connection between dehydration and seismic activity.

The new experiment by researchers from Ecole Normale Supérieure (PSL Research University, France); Université de Lille (France); Université Pierre et Marie Curie (France); Ruhr Universität Bochum (Germany); The University of Chicago; and the University of California, Riverside, takes a different approach to dehydration and its role in earthquake triggering. As opposed to previous work, the team looked at samples composed of both hydrous and non-hydrous minerals. In particular, the studied mixtures of olivine and antigorite. Olivine is a magnesium iron silicate that constitutes most of the upper mantle, while antigorite is the most common hydrous phase in subduction zones. The researchers synthetically formed different samples with varying concentrations of antigorite relative to olivine.

To study dehydration effects, the team placed each sample in a multi-anvil apparatus at the GSECARS 13-BM-D x-ray beamline at the APS. At fixed pressures of 1 GPa and 3.5 GPa, the team raised the temperature from roughly 700 K to over 1000 K, while measuring both the x-ray diffraction and the acoustic activity from the samples. The diffraction data offered a measure of the internal stress, as well as the mineralogical composition. The acoustic emissions, on the other hand, were signatures of sudden rock deformations, which correspond to dynamic ruptures that resemble "micro-earthquakes" within the samples.

The x-ray diffraction measurements revealed that the antigorite underwent dehydration reactions starting at around 873 K. Depending on the antigorite concentration, this temperature also coincided with several acoustic emissions, implying a connection between dehydration and earthquakes. However, the researchers showed that the underlying cause is not fluid overpressure, as previous models suggested. Instead, the team formulated a new model in which subduction zone rock contains clusters of both olivine and antigorite grains that "share" the high-pressure load, like multiple columns supporting a heavy ceiling. When the antigorite dehydrates, it becomes soft, meaning its load suddenly shifts to the olivine columns. This stress transfer causes the olivine framework to fracture in multiple spots as a chain reaction.

The stress transfer model suggests that earthquakes only occur where the concentration of antigorite is within a specific range. In this sense, the antigorite is like the trigger to an elastically-loaded olivine "bomb." Too little antigorite, and the olivine doesn't "ignite." Too much antigorite, and the olivine "explosion" is too weak. The researchers are currently validating their stress transfer model using real-world seismic data. *— Michael Schirber*

See: Thomas P. Ferrand[1]*, Nadège Hilairet[2], Sarah Incel[1], Damien Deldicque[1], Loïc Labrousse[3], Julien Gasc[1], Joerg Renner[4], Yanbin Wang[5], Harry W. Green II[6], and Alexandre Schubnel[1], "Dehydration-driven stress transfer triggers intermediate-depth earthquakes," Nat. Commun. **8**, 15247 (15 May 2017).
DOI: 10.1038/ncomms15247
Author affiliations: [1]Ecole Normale Supérieure (PSL Research University), [2]Université de Lille, [3]Université Pierre et Marie Curie, [4]Ruhr Universität Bochum, [5]The University of Chicago, [6]University of California, Riverside
Correspondence:
* ferrand@geologie.ens.fr

This research was funded by L'Agence Nationale de la Recherche (project "DELF" ANR12-JS06-0003 to A.S.), the LABoratoire d'EXcellence MATISSE (UPMC—Sorbonne Universités). GeoSoilEnviroCARS is supported by the National Science Foundation–Earth Sciences (EAR-1128799) and U.S. Department of Energy (DOE)–Geosciences (DE-FG02-94ER14466). This research used resources of the Advanced Photon Source, a U.S. DOE Office of Science user facility operated for the DOE Office of Science by Argonne National Laboratory under Contract No. DE-AC02-06CH11357.

13-BM-D • GSECARS • Geoscience, environmental science • Tomography, high-pressure diamond anvil cell, high-pressure multi-anvil press • 4.5-80 keV • On-site • Accepting general users •

An Earth-bound Amino Acid that May Be Common in Outer Space

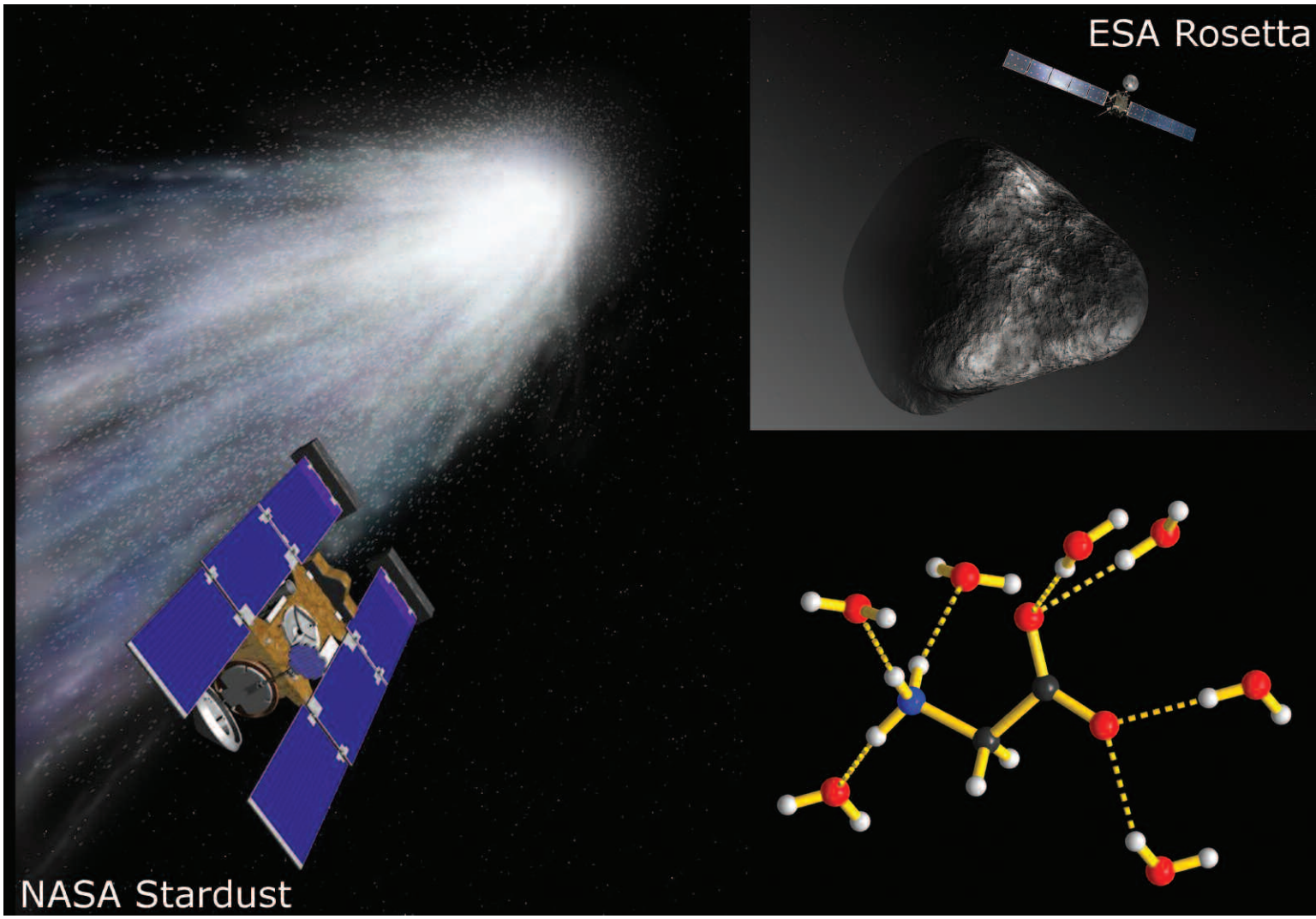

Fig. 1. Left-hand side depicts the Stardust spacecraft flyby of comet Wild 2 in January 2004, collecting dust samples from the surrounding coma. In January 2006, a capsule from Stardust returned to Earth, leading to the first discovery of glycine in a comet. Upper-right panel depicts the European Space Agency's Rosetta mission to comet 67P/Churyumov–Gerasimenko, where glycine was detected via onboard spectrometry. Lower-right panel illustrates glycine dihydrate—a water/glycine co-crystal held together by hydrogen bonds. The central glycine molecule, composed of nitrogen (blue), carbon (gray), oxygen (red), and hydrogen (white), is shown connected (the yellow dashed lines) to seven peripheral water molecules.

17-BM-B • XSD • Chemistry, materials science • Powder diffraction, pair distribution function • 27-51 keV • On-site • Accepting general users •

Of the many amino acids essential for life, glycine has both the fewest number of atoms and the greatest known number of polymorphs (unique structural forms). Although scientists have long recognized that glycine displays multiple polymorphs, the exact structure of several of these forms has remained a mystery. Now a research team has uncovered the precise molecular arrangement of one of these mysterious structural phases, which they have dubbed "glycine dihydrate," or GDH. The researchers deduced the structure of GDH by applying computational analysis to powder x-ray diffraction measurements collected at the APS. These results constitute the first structural description of a hydrated (i.e., water-based) form of glycine. Deciphering the structure of GDH has important ramifications for understanding the behavior of glycine in water-based solutions, including how it crystallizes when frozen or when grown from solution. The discovery also benefits planetary science since glycine has been detected in comets and meteorites, and GDH is its most likely polymorph within these celestial bodies.

All amino acids have two molecules in common, the functional groups amine ($-NH_2$) and carboxyl (-COOH). What differentiates one amino acid from another is the accompanying side chain. Glycine is considered the simplest amino acid since its side chain consists of just a single atom of hydrogen. The various polymorphs of glycine are due to variations in the three-dimensional arrangements of its molecules, which change according to temperature and pressure.

In 1939, scientists used x-ray crystallography to decipher the first known glycine structure, called the alpha-phase. From the early 1960s onward, additional glycine polymorphs were found, all labeled using Greek letters (for instance, the beta, gamma, and delta phases).

This research, by a team from Argonne, the University of Nevada Las Vegas, Stony Brook University, and New York University focuses on the most recently-discovered glycine phase, detected in 2001, which was observed at low temperatures in an aqueous solution frozen with liquid nitrogen. Though known to be distinct from other glycine forms, its exact structure was unknown. In 2012, a research group at Novosibirsk State University (Russia) investigated this polymorph (which they called the "X-phase"). Though the researchers collected x-ray powder diffraction data of the X-phase, they were unable to establish its precise structure.

The journey toward a complete structural description of the X-phase began with an alternative method of sample preparation. In previous experiments, a glycine-bearing solution was rapidly cooled either by pouring it over a frigid surface or into liquid nitrogen. For the current research, an alternative technique called flash cooling was used: An aqueous solution containing glycine was encapsulated in a tiny glass capillary (0.7 mm in diameter) that was suddenly exposed to a stream of liquid nitrogen. This technique instantly froze the glycine/water mixture, transforming it from a transparent liquid to a cloudy solid.

High-resolution x-ray measurements, gathered at XSD beamline 17-BM-B of the APS, provided the necessary experimental data for determining the X-phase structure. A solution containing 20% glycine was frozen via flash cooling at a temperature of 173 K (-100° C). The x-ray measurements indicated only the presence of water ice at this temperature. As the sample temperature was raised to 208 K (-65° C), x-ray data indicated the emergence of glycine's X-phase.

The entire x-ray data set was subsequently analyzed using sophisticated computational software such as USPEX. The analysis indicated that the X-phase is a hydrated form of glycine (now called glycine dihydrate), existing as a co-crystal of water and glycine connected via intermolecular hydrogen bonding. The lower-right inset in Fig. 1 shows how each glycine molecule forms hydrogen bonds with seven peripheral water molecules. This arrangement effectively isolates the glycine molecules from one another, allowing little interaction between them. Although other amino acids have hydrated polymorphs, only glycine dihydrate exhibits such negligible interaction between its neighboring amino acid molecules.

The left side of Fig. 1 pays homage to NASA's Stardust mission that returned a cometary dust sample gathered near comet Wild 2, marking the first direct confirmation of glycine in outer space. The Rosetta mission to comet 67P (upper-right inset) also detected glycine. Evidence is accumulating that the essential ingredients of life, including water and glycine, were transported to Earth via comets and asteroids. Given the frigid conditions of these celestial bodies, GDH is the most likely structural phase of any glycine present. In more general terms, deciphering glycine's hydrated phase is important for understanding the phase evolution and stability of this key amino acid. *— Philip Koth*

See: Wenqian Xu[1], Qiang Zhu[2,3], and Chunhua Tony Hu[4]*, "The Structure of Glycine Dihydrate: Implications for the Crystallization of Glycine from Solution and Its Structure in Outer Space," Angew. Chem. Int. Ed. **56**, 2030 (2017). DOI: 10.1002/anie.201610977
Author affiliations: [1]Argonne National Laboratory, [2]University of Nevada Las Vegas, [3]Stony Brook University, [4]New York University
Correspondence:
* chunhua.hu@nyu.edu

Work at UNLV is supported by the National Nuclear Security Administration under the Stewardship Science Academic Alliances program through the U.S. Department of Energy (DOE) Cooperative Agreement DE-NA0001982. Work at NYU is supported by the Materials Research Science and Engineering Center (MRSEC) program of the National Science Foundation (NSF) under Awards Number DMR-0820341 and DMR-1420073. Calculations were performed on XSEDE facilities and on the cluster of the Center for Functional Nanomaterials, Brookhaven National Laboratory under Contract No. DE-AC02-98CH10086 supported by the U.S. Department of Energy (DOE)-Basic Energy Sciences. This research used resources of the Advanced Photon Source, a U.S. DOE Office of Science user facility operated for the DOE Office of Science by Argonne National Laboratory under Contract No. DE-AC02-06CH11357.

The Cause of Seismic Anisotropy in the Lowermost Mantle

Discovering the cause of seismic anisotropy in the lowermost layer of the Earth's mantle is difficult due to the problem of replicating the extreme pressures and temperatures found there. Utilizing the APS and realistic pressure-temperature conditions, researchers discovered that deformation of the mineral-phase silicate post-perovskite is the main cause for the abnormal seismic behaviors. The (001) texture produces a shear wave radial anisotropy of ~ 3.7%, which corresponds to seismic observations beneath the circum-Pacific rim. Robust mineral physics results illuminate our understanding of the deformation mechanism and seismic anisotropy in the lowermost mantle. *Cont'd. on the next page*

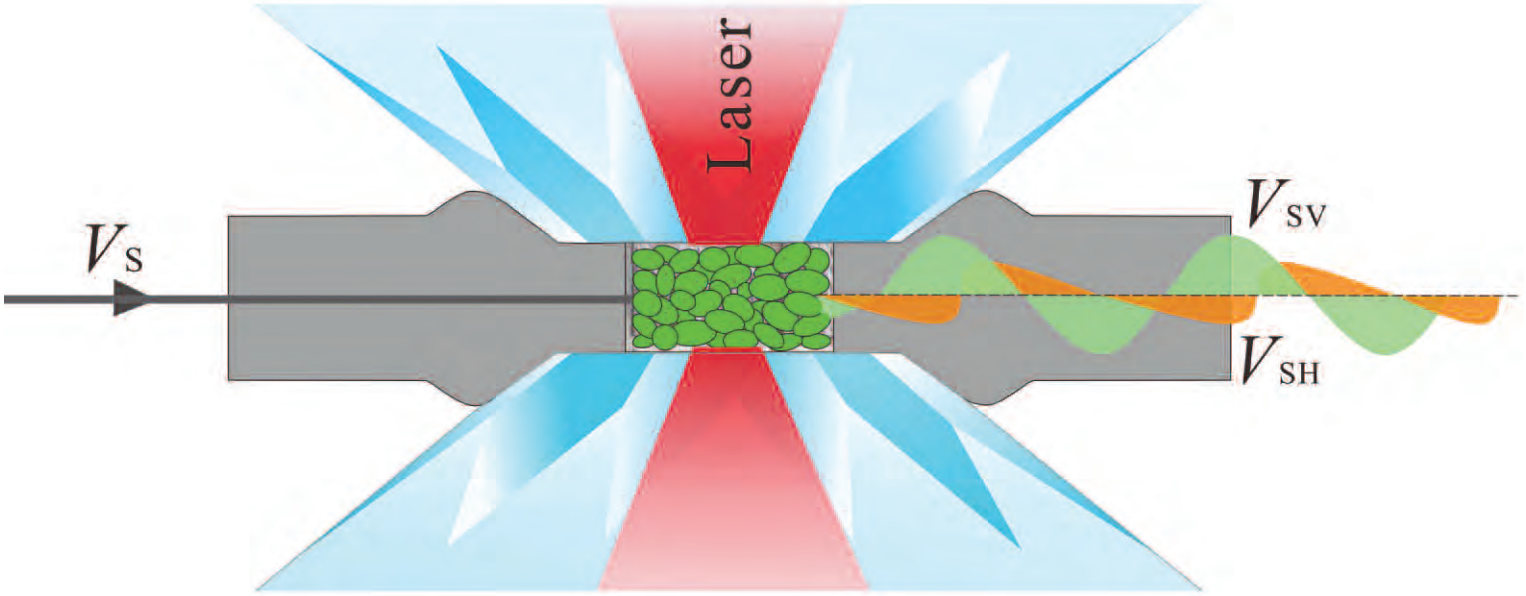

Fig. 1. Sketch of crystallographic preferred orientation of post-perovskite occurring at the pressure-temperature conditions of the lowermost mantle, observed in diamond anvil cell by synchrotron radial x-ray diffraction (left). This behavior produces a fast VSH and the radial anisotropy of 3.7% (right) if the shear wave passes through the sample.

The lowermost 200-450 km of Earth's mantle, called the D′′ layer, is different from the rest of the mantle. This boundary layer exhibits complex shear wave anisotropy; shear waves emanating from earthquakes travel through the material at slightly different speeds depending on their direction of polarization. Although the source of this seismic anisotropy has been under debate, one explanation has been the texturing, or crystallographic preferred orientation (CPO), primarily of silicate post-perovskite (pPv). In addition, three-dimensional geophysical models predicted that the anisotropy seismic velocity is from deformation due to dislocation slip in the minerals. In a series of seismic studies in the circum-Pacific rim, shear wave radial anisotropy was shown to be 1-3% with horizontally polarized shear waves (VSH) travelling faster than vertically polarized shear waves (VSV).

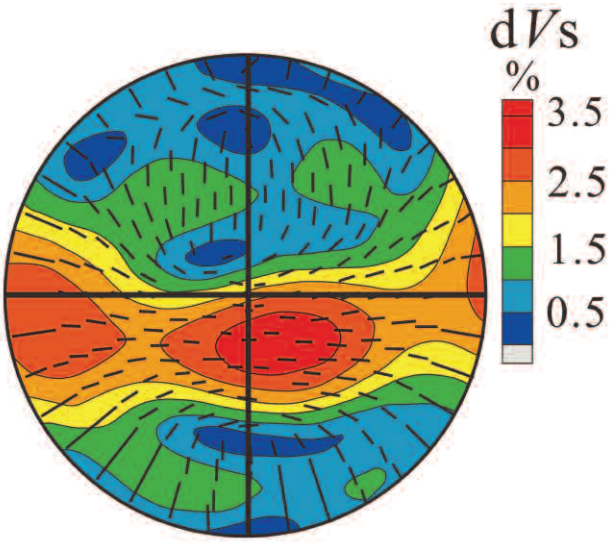

To better understand the unusual seismic features of the D′′ layer, researchers must understand the CPO and deformation of deep mantle mineral phases at the pressures and temperatures of the lowermost mantle. However, since silicate post-perovskite is only stable at extremely high pressures (>125 GPa) and temperatures (>2000 K), replicating these conditions in the laboratory is challenging. Studies of analog minerals, which are stable at lower mantle pressures but at room temperatures, likely do not have the same slip systems and may not replicate the CPO of pPv in the lowermost mantle.

Advancing our understanding of the seismic anisotropy of the D′′ layer required developing a unique system. To make these advances, researchers from the China University of Geosciences; The University of Texas at Austin; the University of Liverpool (UK); the University of Science and Technology of China; the University of California, Berkeley; and The University of Chicago first synthesized pPv. Then they performed deformation experiments on the pPv by applying stress conditions to the sample to reproduce the textures found under the pressure and temperature conditions relevant to the D′′ layer. Their unique approach used synchrotron radial x-ray diffraction at the GSECARS beamline 13-ID-C,D at the APS in a membrane-driven, laser-heated diamond anvil cell where pressures/temperatures from 135 GPa and 2500 K to 154 GPa and 3000 K, respectively, were applied.

The researchers found the (001) intrinsic texture of the pPv in the D′′ layer; the deformation mechanism was slip on the (001)[100] and (001)[010] or on (001)<110>. This deformation slip produces a fast, horizontal polarization. The shear wave radial anisotropy was 3.7%, which is consistent with seismic observations of the region beneath the circum-Pacific rim (Fig. 1).

Recent geodynamic modeling shows that subducting slabs sink to the lowermost mantle where an iron-bearing pPv phase becomes stable. Dislocation slip in this phase is the main cause of the seismic anisotropy of the D′′ layer. Grain-grain interactions between these stronger pPv crystals and other weaker mineral grains, which are deformed together, likely also affect the CPO. These combined affects can explain the source of shear wave anisotropy in the D′′ layer beneath the circum-Pacific rim. This knowledge can illuminate the geodynamic processes that take place deep within our planet.

— Dana Desonie

See: Xiang Wu[1]*, Jung-Fu Lin[2]**, Pamela Kaercher[3], Zhu Mao[4], Jin Liu[2], Hans-Rudolf Wenk[5], and Vitali B. Prakapenka[6], "Seismic anisotropy of the D′′ layer induced by (001) deformation of post-perovskite," Nat. Commun. **8**, 14669 (8 April 2017).
DOI: 10.1038/ncomms14669
Author affiliations: [1]China University of Geosciences, [2]The University of Texas at Austin, [3]University of Liverpool, [4]University of Science and Technology of China, [5]University of California, Berkeley, [6]The University of Chicago
Correspondence:
* wuxiang@cug.edu.cn,
** afu@jsg.utexas.edu

X.W. acknowledges financial support from the National Science Foundation (NSF) of China (U1232204 and 41473056). J.F.L. acknowledges financial support from the U.S. National Science Foundation and Center for High Pressure Science and Technology Advanced Research. GSECARS operations are supported by NSF-Earth Sciences (EAR-1128799) and U.S. Department of Energy (DOE) Geosciences (DE-FG02-94ER14466). H.R.W. is appreciative for support from NSF EAR-1343908, CSEDI 1067513 and CDAC. This research used resources of the Advanced Photon Source, a U.S. DOE Office of Science user facility operated for the DOE Office of Science by Argonne National Laboratory under Contract No. DE-AC02-06CH11357.

13-ID-C,D • GSECARS • Geoscience, environmental science • Microdiffraction, x-ray standing waves, x-ray absorption fine structure, resonant inelastic x-ray scattering, x-ray emission spectroscopy, high-pressure diamond anvil cell, high-pressure multi-anvil press • 4.9-45 keV, 10-75 keV • On-site • Accepting general users •

Teasing Out Iron's Structural Subtleties

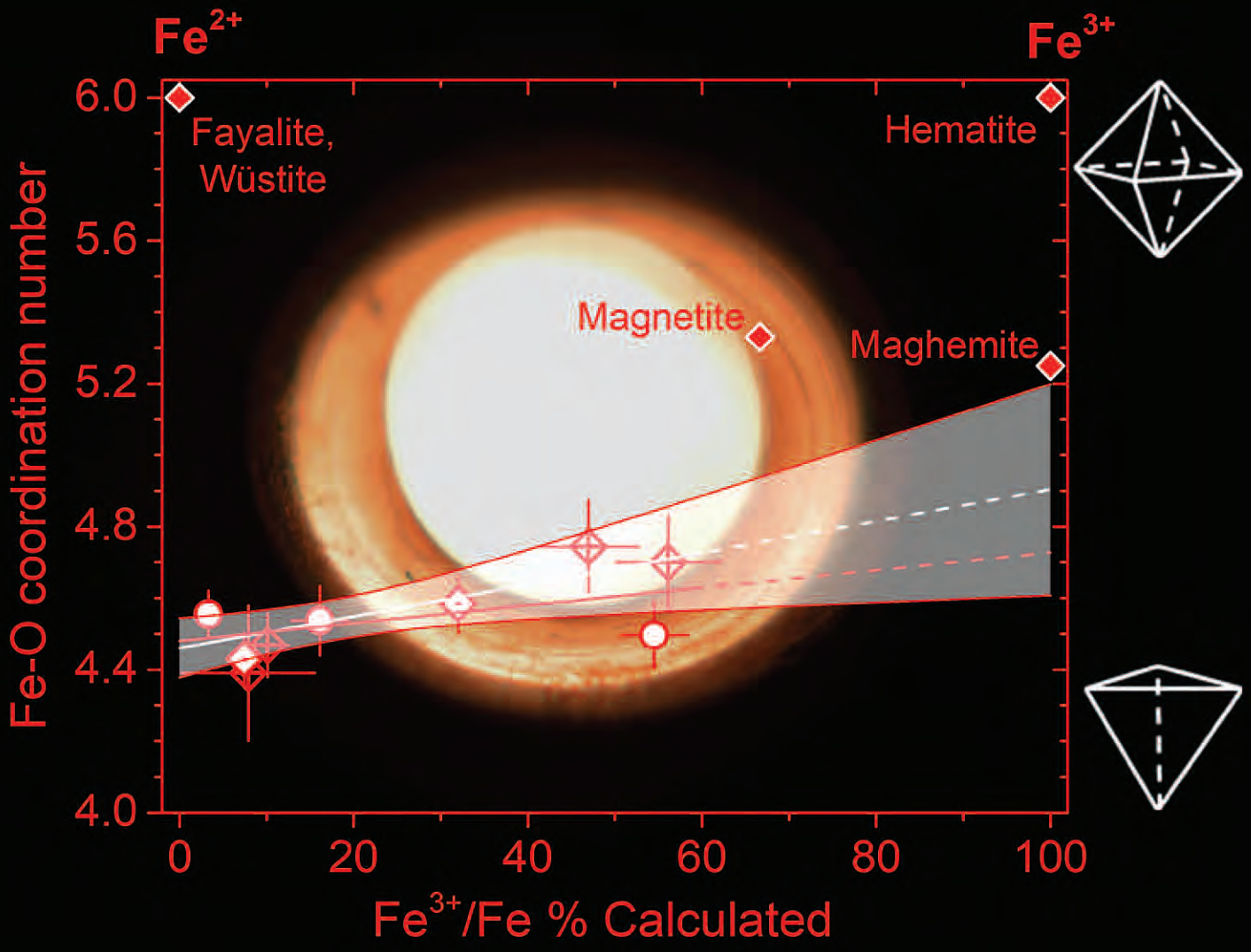

Fig. 1. Two aspects of the results. The background shows a levitating melt droplet surrounded by light reflected from the levitator nozzle. The graph in the foreground shows the experimental results from three campaigns: as the iron oxidation state increases, due to an increase in oxygen fugacity, the number of oxygen ions around the melt's iron cations (the coordination number) does not increase appreciably. Common mantle minerals, including crystalline fayalite and hematite, are shown for perspective. The two white polyhedra on the right indicate the ideal geometrical arrangements of iron and oxygen at different coordination numbers.

The behavior of iron at high temperatures and pressures plays an important part in our understanding of Earth's interior. Scientists must quantify how iron's physical and chemical characteristics are both affected by and affect the environment within Earth's mantle and core to make sense of the reactions undergone by molten, subsurface magmas. Researchers using high-brightness x-rays at the APS monitored the behavior of a model iron silicate melt to investigate how its structure and oxidation state change as a function of the amount of oxygen present. These new results — using melts based on fayalite (Fe_2SiO_4), the iron-rich end-member of the olivine solid-solution series — reveal contrasting behavior between this melt and more silicic magmas, including basaltic melts. They show that the iron in the iron-rich melt bonds differently with oxygen ions than in its crystalline counterpart. Additionally, they show that iron-rich melts may not retain their oxidation state during rapid cooling.

The multinational team of researchers from Materials Development, Inc., Argonne, Stony Brook University, University College London, and the University of Tennessee Space Institute investigated the structure of molten fayalite as a function of temperature and oxygen fugacity. Oxygen fugacity is effectively a measure of the amount of oxygen present in the surrounding gas. The team chose fayalite because it is a volcanic mineral whose relatively simple melt structure can be characterized using x-ray diffraction. The iron in fayalitic melts can take multiple oxidation states, depending on its environment, and can bond with varying amounts of oxygen ions. The team found that lowering the oxygen fugacity of the environment caused a change in the oxidation state of the iron cations, increasing the numbers of Fe^{2+} ions and decreasing the numbers of Fe^{3+} ions.

The team used a combination of techniques to measure the number of oxygen ions bonded to the iron cations in the fayalitic melts (the number of bonded oxygen ions per iron cation is called the "coordination number"). To make these measurements, they placed the melt samples inside an aerodynamic levitation furnace and heated the samples using a CO_2 laser. Aerodynamic levitation utilizes gas pressure to suspend materials for measurements in a manner that removes issues of sample contamination. To monitor the structure, the team used high-energy x-ray diffraction at the XSD 6-ID-D x-ray beamline at the APS, and iron K-edge x-ray absorption near-edge structure (XANES) spectroscopy at the XSD 20-BM-B beamline. Figure 1 shows a graph plotting the average coordination number as a function of the iron oxidation state. (The background of Fig. 1 shows a levitating melt droplet. See the caption for additional details.) Also, Fig. 1 plots the coordination number for common iron oxide mantle minerals, many of which are minerals that result when the fayalitic melt cools and crystallizes. The graph indicates the coordination number of the cooled and crystallized minerals are all larger than the measurements made by the team for the fayalitic melts.

Based on these measurements — showing a slightly lower coordination number for Fe^{2+} than Fe^{3+} — the team concluded that Fe^{2+} is less efficient than alkali cations at stabilizing the tetrahedral form of Fe^{3+}. Furthermore, the team concluded that the combined effect of oxidation state change and small coordination number change is unlikely to strongly affect dynamic properties such as the liquid viscosity, in contrast to what occurs with alkali-rich silicate melts. The iron-rich melts therefore remain fluid over a wide range of oxidation states, temperatures, and pressures. As such, they will tend to accelerate composition changes of magmas as well as crystallization into intrusive rock formations.

By comparing results from XANES and Mössbauer spectroscopies, the team concluded that oxidation state is not always preserved in iron-rich melts during rapid cooling, unlike what happens with basaltic and more silicic magmas. This lack of preservation of oxidation state adds an additional level of difficulty when inferring the oxygen fugacity of a melt's source in the case of ancient rocks derived from hot, fluid melts, such as the komatiites produced between 4 to 2.5 billion years ago. In addition to the geochemical results, the team's experimental setup demonstrated the power of combining multiple techniques — specifically the x-ray diffraction and XANES spectroscopy used in conjunction with the laser-heated aerodynamic levitation — to probe more subtle details of the structure-oxidation state relationship in high temperature melts than have previously been measured. *— Mary Alexandra Agner*

See: O.L.G. Alderman[1,2]*, L. Lazareva[3], M.C. Wilding[4], C.J. Benmore[2], S.M. Heald[2], C.E. Johnson[5], J.A. Johnson[5], H.-Y. Hah[5], S. Sendelbach[1], A. Tamalonis[1], L.B. Skinner[2,3], J.B. Parise[3], and J.K.R. Weber[1,2], "Local structural variation with oxygen fugacity in Fe_2SiO_{4+x} fayalitic iron silicate melts," Geochim. Cosmochim. Acta **203**, 15 (2017). DOI: 10.1016/j.gca.2016.12.038
Author affiliations: [1]Materials Development, Inc., [2]Argonne National Laboratory, [3]Stony Brook University, [4]University College London, [5]University of Tennessee Space Institute
Correspondence:
* o.alderman@gmail.com

This work was supported by the U.S. Department of Energy (DOE) under grant number SBIR DE-SC0007564 (O.L.G.A., A.T., S.S., R.W.) and the U.S. DOE Office of Science-Basic Energy Sciences (BES), grant BES DE-FG02-09ER46650 (L.B.S., L.L., and J.B.P.). We acknowledge support from the Center for Laser Applications and the University of Tennessee Space Institute (C.E.J., J.A.J., H.-Y.H.). This research used resources of the Advanced Photon Source, a U.S. DOE Office of Science user facility operated for the DOE Office of Science by Argonne National Laboratory under Contract No. DE-AC02-06CH11357.

6-ID-D • XSD • Physics, materials science • magnetic x-ray scattering, high-energy x-ray diffraction, powder diffraction, pair distribution function • 50-100 keV, 70-130 keV • On-site • Accepting general users •

20-BM-B • XSD • Materials science, environmental science, chemistry • X-ray absorption fine structure, microfluorescence (hard x-ray) • 2.7-32 keV, 2.7-35 keV • On-site • Accepting general users •

How Oxygen Infiltrates Uranium Dioxide

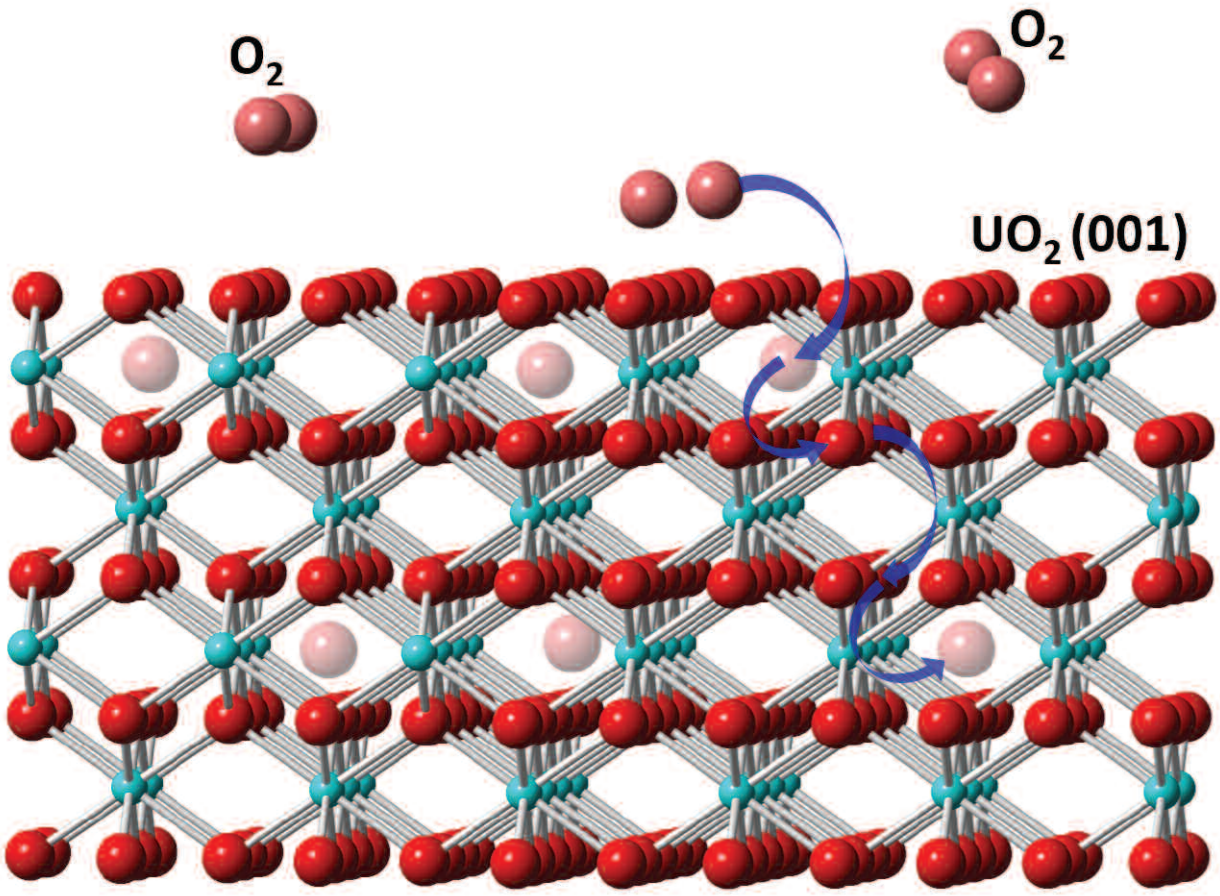

Fig. 1. Oxygen atoms penetrate the lattice of uranium dioxide through its (001) surface. They occupy interstitial sites in alternate layers, as their presence in one layer of the structure disfavors their presence in adjacent layers. Red spheres are O, cyan spheres are U, and blue arrows show a possible mechanism for O diffusion from gas phase to interstitial sites.

13-ID-C,D • GSECARS • Geoscience, environmental science • Microdiffraction, x-ray standing waves, x-ray absorption fine structure, resonant inelastic x-ray scattering, x-ray emission spectroscopy, high-pressure diamond anvil cell, high-pressure multi-anvil press • 4.9-45 keV, 10-75 keV • On-site • Accepting general users •

13-BM-C • GSECARS • Geoscience • Environmental science • Surface diffraction, high-pressure diamond anvil cell, single-crystal diffraction • 15-15 keV, 28.6-28.6 keV • On-site • Accepting general users •

Uranium dioxide, UO_2, is the main component of typical fuel rods for nuclear reactors. It is also an end-product of many remediation processes for contaminated environments, as it contains uranium in a largely insoluble form. Researchers carrying out studies at the APS have confirmed that UO_2 undergoes oxidation in an unusual way that leads to a layered disruption of the lattice and the transformation of uranium into much more soluble oxidation states. The findings are important for understanding the chemical and physical integrity of fuel rods and the effectiveness of bioremediation programs.

Oxygen atoms absorbed by UO_2 can occupy the empty center of the mineral's face-centered cubic structure up to a stoichiometry of $UO_{2.25}$ with only modest distortion of the lattice. However, in work performed at APS three years ago, researchers from The University of Chicago, Pacific Northwest National Laboratory (PNNL), and the Stanford Synchrotron Radiation Lightsource demonstrated that oxygen atoms absorbed through the (111) surface of UO_2, diffused through the lattice in a highly non-uniform way, entering every third layer beneath the exposed surface.

To see whether this distinctly nonclassical mode of diffusion is a property of the lattice in general or a peculiarity of the (111) surface, the same researchers have now examined oxygen absorption through the (001) surface of UO_2 (Fig. 1).They prepared samples by polishing the (001) surface under oxygen-free conditions, then exposed them to dry oxygen gas at 1 atm pressure for periods of 0, 1, 2, 6, 10, and 21 days. After the chosen exposure period, the samples were wrapped in Kapton® film to block photochemical changes and sealed in cells that allowed them to undergo crystal truncation rod (CTR) x-ray diffraction studies.

Using intense synchrotron x-rays from the APS and highly sensitive detectors at the GSECARS 13-ID-C and 13-BM-C beamlines, CTR measured weak diffraction features arising from interfaces; these features lie between the much stronger conventional Bragg peaks generated by the bulk structure of a crystal. In this case, the CTR analysis revealed the locations of uranium atoms that are displaced as oxygen atoms infiltrate the lattice. The appearance of oscillations in data collected in both specular and off-specular geometry after oxygen exposure indicates that the oxidized layers share the lateral atomic arrangement of bulk UO_2.

To infer lattice structures from the data, the team used a differential evolution software package coupled to a model that divided the lattice into thin slabs parallel to the surface, each slab being half the depth of the unit cell. Best-fit analysis showed that the slabs in the UO_2 lattice contracted in the perpendicular direction as oxygen atoms penetrated more deeply. After 21 days of exposure, the top 19 layers had experienced extensive contraction relative to the bulk, with the top 8 layers showing a pattern in which every other layer was more strongly contracted than its neighbors.

In their previous study of the (111) surface, the researchers found a three-layer periodicity, and developed a model in which oxygen atoms fill up one-quarter of the interstitial sites in every third layer, causing lattice contraction by altering the oxidation state of the uranium atoms. The extra oxygen atoms capture electrons from as far away as 6 Å, compared to the lattice parameter of about 5.5 Å, so that the presence of oxygens in one layer of the lattice tends to exclude them from neighboring layers. (X-ray photoelectron spectroscopy of exposed samples at the DOE's PNNL confirmed that a significant fraction of uranium atoms changed from the U(IV) oxidation state to the U(V) and U(VI) states.) That same model, the researchers find, explains equally well the results from the new study, because the placement of the added oxygen atoms manifests itself as a two-layer periodicity with respect to the alignment of the (001) surface relative to the bulk lattice.

The periodic structure caused by oxygen infiltration is characteristic of UO_2 in bulk, the researchers conclude, with the phase of the oscillatory oxidation front set by the surface. Previous work on oxygen absorption has been done at high temperatures, around 1000° C, so is relevant for the stability of fuel rods in a reactor but not for the long-term fate of UO_2 resulting from bioremediation. The new research should help researchers predict the behavior of uranium minerals, especially the release of soluble U(VI) ions, under ambient condition in the natural environment. *— David Lindley*

See: Joanne E. Stubbs[1]*, Craig A. Biwer[1‡], Anne M. Chaka[2], Eugene S. Ilton[2], Yingge Du[2], John R. Bargar[3], and Peter J. Eng[1], "Oxidative Corrosion of the UO_2 (001) Surface by Nonclassical Diffusion," Langmuir **33**, 13189 (2017).
DOI: 10.1021/acs.langmuir.7b02800
Author affiliations: [1]The University of Chicago, [2]Pacific Northwest National Laboratory, [3]Stanford Synchrotron Radiation Lightsource ‡Present address: University of Michigan
Correspondence:
* stubbs@cars.uchicago.edu

Support was provided by DOE-Biological and Environmental Research (BER), Subsurface Biogeochemical Research, through the SLAC SFA program. The Stanford Synchrotron Radiation Lightsource, SLAC National Accelerator Laboratory, is supported by the DOE Office of Science-Basic Energy Sciences under Contract No. DE-AC02-76SF00515). A.M.C. and E.S.I. were supported by the Geosciences Research Program at PNNL, DOE Office of Science-Basic Energy Sciences, Division of Chemical Sciences, Geosciences and Biosciences. XPS data were collected in the Radiochemistry Annex at the Environmental Molecular Sciences Laboratory, a national scientific user facility sponsored by DOE-BER and located at PNNL. PNNL is a multiprogram national laboratory operated for DOE by Battelle. GSECARS is supported by the National Science Foundation−Earth Sciences (EAR-1634415) and the U.S. Department of Energy (DOE)−GeoSciences (DE-FG02-94ER14466). This research used resources of the Advanced Photon Source, a U.S. DOE Office of Science user facility operated for the DOE Office of Science by Argonne National Laboratory under Contract No. DE-AC02-06CH11357.

Data

X-ray Availability and Reliability

In fiscal year 2017*, the APS x-ray source continued to function as a highly reliable delivery system for synchrotron x-ray beams for research. Several factors support the overall growth in both the APS user community and the number of experiments carried out by that community. But there is a direct correlation between the number of x-ray hours available to users; the success of the APS experiment program; and the physicists, engineers, and technicians responsible for achieving and maintaining optimum x-ray source performance. Below are definitions of important measures for the delivery of x-ray beam to users (latest data shown graphically).

APS storage ring reliability (MTBF), fiscal years 1999-2017

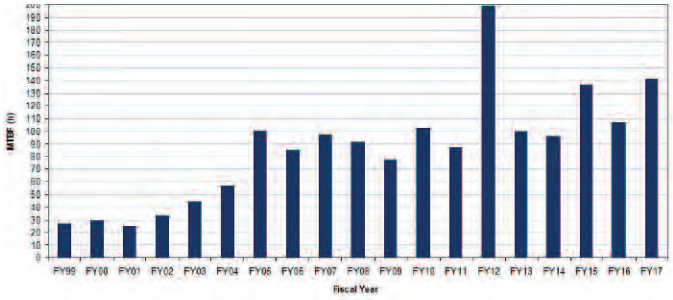

Storage Ring Reliability: A measure of the mean time between beam losses (faults), or MTBF, calculated by taking the delivered beam and dividing by the total number of faults. The APS targets, and routinely exceeds, 70 h MTBF. A fault is defined as complete unavailability of beam either via beam loss or removal of shutter permit not related to weather. A fault also occurs when beam has decayed to the point where stability and orbit can no longer be considered reliable. At the APS, this threshold is 50 mA.

X-ray Availability: The number of hours that the beam is available to the users divided by the number of hours of scheduled beam delivery prior to the beginning of a run. The specific definition of available beam is that the APS main control room has granted permission to the users to open their shutters, *and* there is more than 50-mA stored beam in the storage ring.

* While the highlights in, and title of, this report cover calendar year 2017, data on accelerator performance and user statistics are measured on the basis of fiscal years.

APS x-ray availability, fiscal years 1999-2017

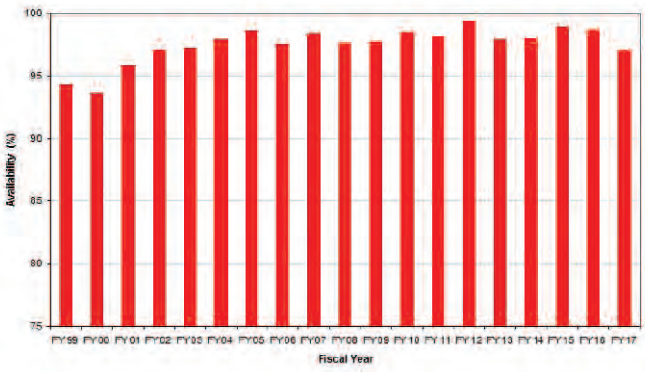

APS funding levels, fiscal years 2006-2017

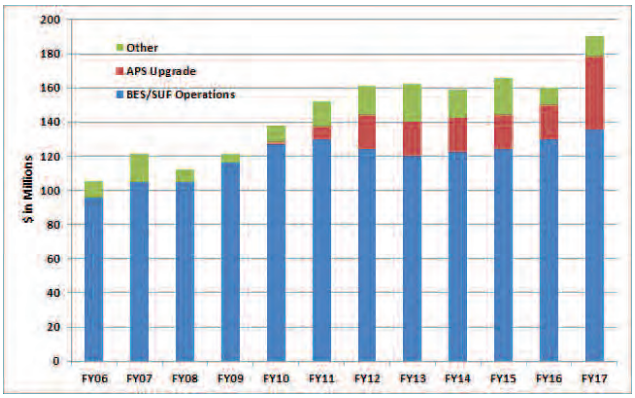

APS staffing levels, fiscal years 2006-2016

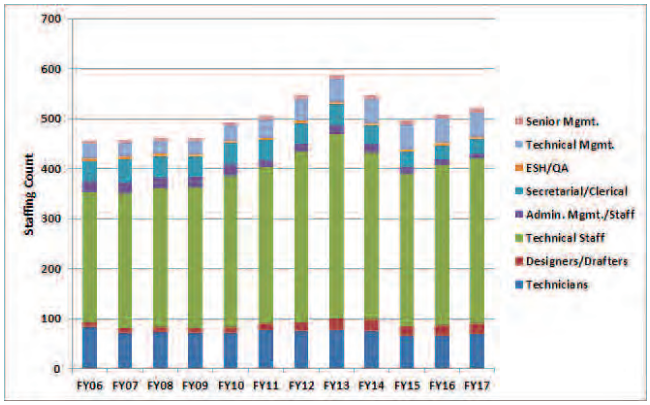

Number of APS publications, calendar years 1998-2016, recorded as of 8.18

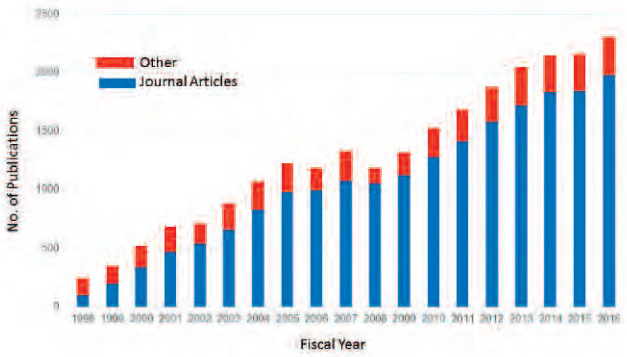

For lists of APS publications see http://www.aps.anl.gov/Science/Publications/

Deposits in Protein Data Bank from research at world-wide light sources, calendar years 1998-2017 (of 18.8.10)

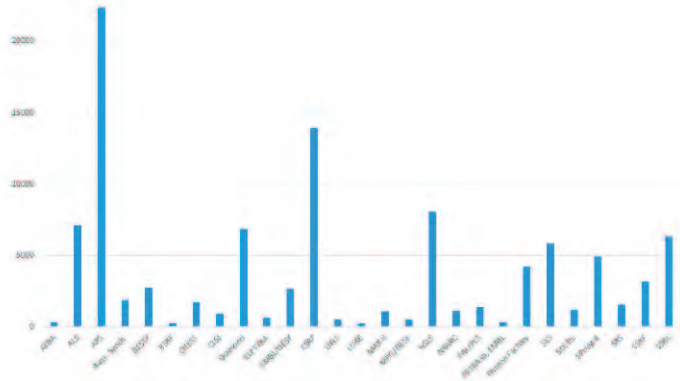

Nanoscience

Nanoscale 3-D Strain Imaging with a Simplified Coherent Diffraction Technique

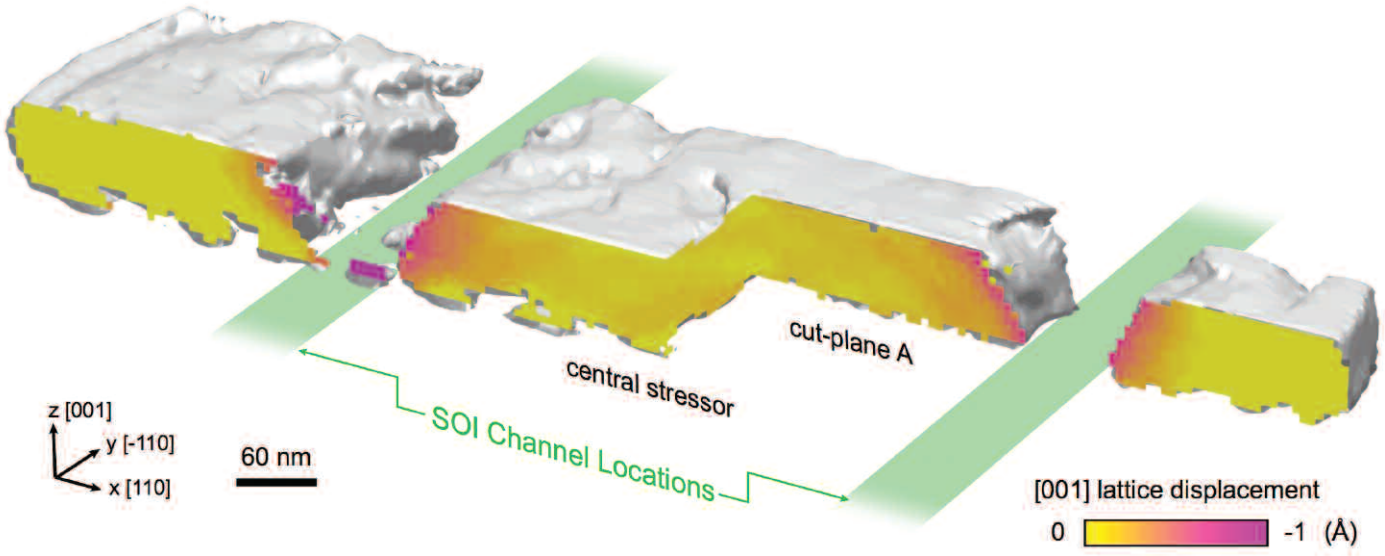

Fig. 1. A cutaway view depicting the displacement of the crystalline lattice within the prototype semiconductor device. The lattice displacements were revealed via three-dimensional Bragg projection ptychography. The device structure spans a total of 460 nm and consists of periodically-embedded silicon-germanium (SiGe) crystals. Note that the greatest lattice displacements occur near the edges. The two large gaps are due to a pair of silicon-on-insulator (SOI) channels, each measuring 60 nm in width.

26-ID-C • CNM/XSD • Physics, materials science • Nanodiffraction, nano-imaging, coherent x-ray scattering • 6-12 keV • On-site • Accepting general users •

Retrieving phase information from hard (high-energy) x-ray diffraction patterns is one way to improve sample imaging. One such phase-retrieval technique uses multiple overlapping diffraction patterns derived from a coherent x-ray beam. Using this scheme, highly detailed three-dimensional (3-D) images of a sample's nanostructure have been obtained, along with additional information such as variations in the local strain field. However, phase-retrieval techniques face certain limitations, such as the need to rotate the sample. In this study, researchers implemented a new phase-retrieval technique called 3-D Bragg projection ptychography (3DBPP). A major advantage of this method is that the sample remains fixed. Utilizing a specially tailored micro-electronic prototype device, the researchers used the 3DBPP technique to create a nanoscale 3-D reconstruction of the device's lattice distortions, thereby revealing its internal strains. Employing the highly intense and coherent x-rays of the APS was essential to the experiment. The comparative simplicity of 3DBPP, coupled with its powerful 3-D imaging and strain field capabilities, is expected to find application in a wide variety of experimental settings for improved 3-D x-ray microscopy of crystalline materials.

An x-ray beam interacting with a crystalline structure forms a diffraction pattern containing diverse fringes. X-ray detectors only capture part of the information in a diffraction pattern since they register only the intensity (brightness) of the diffracted x-rays and not their phase. Coherent x-rays (the type used in this study) are in-phase, meaning that the crests and valleys of the sinusoidal waves are in sync when they arrive at the sample. After diffraction from an object, however, the x-rays are perturbed and form a distinctive pattern in intensity and phase that encodes structural information about the sample. Determining how the phases of the diffracted x-rays have been shifted from their original phase is known as the "phase problem."

It was only in the 1930s that a solution to the phase problem was devised, albeit for the optical microscope. Solving the phase problem for x-ray diffraction awaited the development of several key technologies, including x-ray mirrors and diffraction gratings; highly sensitive electronic x-ray detectors; powerful computers and algorithms for x-ray data processing; and coherent x-rays produced by synchrotron facilities like the APS.

Scientists have applied these technological advances to successfully resolve the x-ray phase problem from progressively complicated samples by gleaning information from multiple overlapping diffraction patterns. This process is known as ptychography, which exploits the presence of spatial overlap in the coherent x-ray diffraction patterns to form high-resolution 3-D images. Using these techniques, nanoscale imaging of crystalline lattices and their distortions has been achieved at length scales smaller than the size of the beam.

In relation to crystalline diffraction, current ptychography methods are hindered by the need for multiple x-ray beam diffraction angles, which is usually achieved by rotating the sample. In contrast, the 3DBPP technique relies solely on a "raster" approach: the beam moves laterally across the sample in a step-by-step process. The orientation of the beam (measuring a mere 46 nanometers across in this study) remains fixed relative to the sample.

Sweeping the x-ray beam across the sample yields overlapping diffraction patterns. 3DBPP utilizes back projection of the two-dimensional (2-D) structural information contained in each of these diffraction patterns. Taken together, the back projections of hundreds of 2-D diffraction patterns are used to produce a 3-D image that is sensitive to lattice strain in the crystal. 3DBPP takes advantage of this fact and integrates it into phase retrieval so that both the phase problem and the 3-D structure are solved from a fixed-angle measurement.

Researchers from Argonne National Laboratory, Aix-Marseille University (France), the IBM T.J. Watson Research Center, and the IBM Semiconductor Research and Development Center tested the 3DBPP technique on a prototype semiconductor device featuring lithographically-patterned silicon-germanium (SiGe) crystals. The x-ray diffraction data were gathered at the XSD/CNM 26-ID-C Hard X-ray Nanoprobe beamline at the APS. Figure 1 shows a cutaway view of the tiny semiconductor device, revealing its morphology and internal lattice displacement, which indicates the sample's strain field.

The researchers behind this study anticipate that their 3DBPP technique will prove applicable to a variety of synchrotron beamline configurations, such as beamlines with distinct x-ray focusing setups including x-ray mirrors, diffraction gratings, or pinholes. The researchers also anticipate that 3DBPP will open up new opportunities to image materials structure in environments difficult to access with any other method, such as materials synthesis chambers, and the active regions buried deep within electronic devices.

— William Atkins and Philip Koth

See: S.O. Hruszkewycz[1]*, M. Allain[2], M.V. Holt[1], C.E. Murray[3], J.R. Holt[4], P.H. Fuoss[1], and V. Chamard[2], "High-resolution three-dimensional structural microscopy by single-angle Bragg ptychography," Nat. Mater. **16**, 244 (February 2017). DOI: 10.1038/NMAT4798
Author affiliations: [1]Argonne National Laboratory, [2]Aix-Marseille University, [3]IBM T.J. Watson Research Center, [4]IBM Semiconductor Research and Development Center
Correspondence: * shrus@anl.gov

3DBPP simulations and experimental measurements were supported by the U.S. Department of Energy (DOE) Office of Science-Basic Energy Sciences, Materials Science and Engineering Division. Design of the 3DBPP phase retrieval algorithm was partially funded by the French ANR under project number ANR-11-BS10-0005 and the French OPTITEC cluster. Use of the Center for Nanoscale Materials and the Advanced Photon Source were supported by the U.S. DOE Office of Science-Basic Energy Sciences, under Contract No. DE-AC02-06CH11357.

Observing the Growth of Voids in Oxidizing Iron Nanoparticles

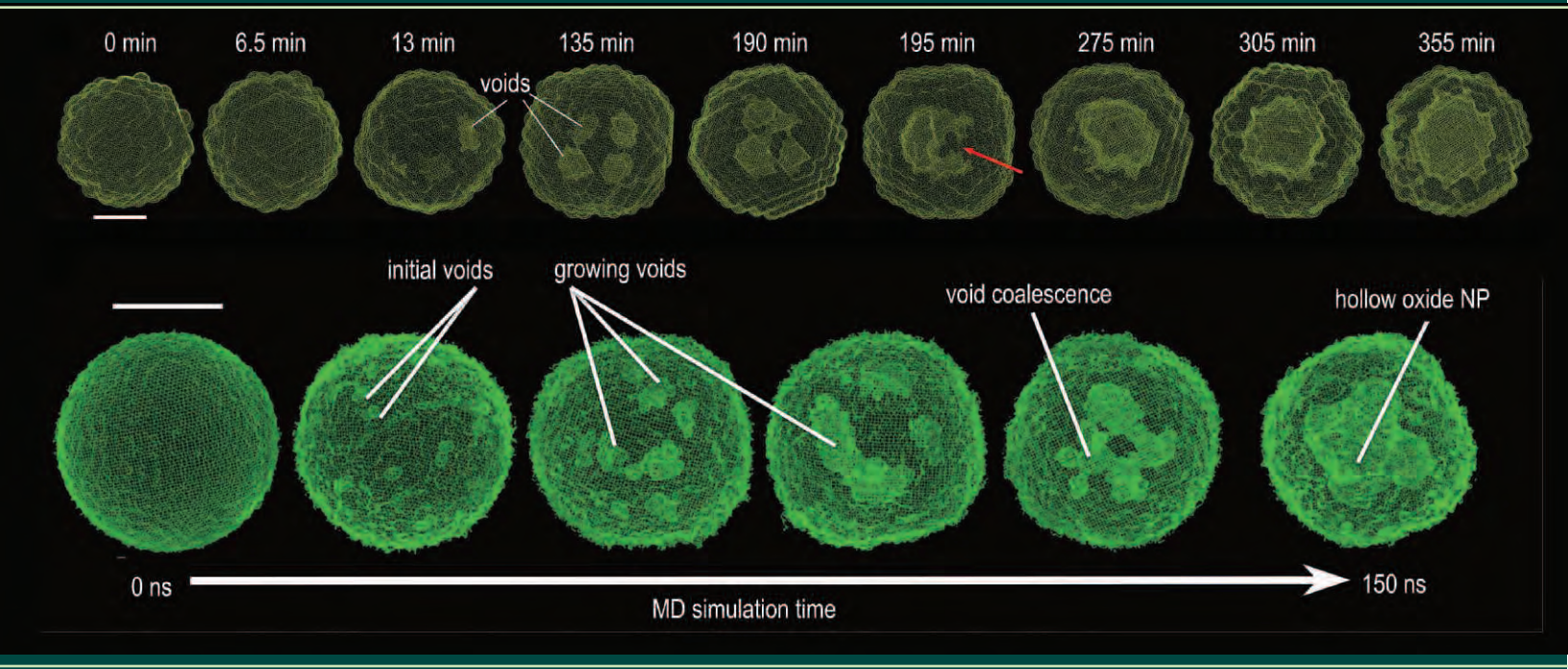

Fig. 1. Top row: iron nanoparticle evolution over a span of 6 h. Bottom row: a sequence of iron nanoparticle evolution based upon a MD simulation. The scale bars represent 5 nm.

Anyone who has had a rusting vehicle has suffered the effects of iron oxidation. Iron nanoparticles can also "rust" to form an iron oxide compound, but unlike a rusting vehicle, the oxidation of iron nanoparticles is not necessarily a bad thing because this class of nanoparticles has important technological applications. To better understand this oxidation process, researchers used small- and wide-angle x-ray scattering (SAXS/WAXS) at the APS to observe the gradual transformation of solid iron particles into hollow iron-oxide shells. The experiments revealed the step-by-step geometrical transformation of iron nanoparticles due to oxidation, which involved the appearance and growth of numerous voids within the nanoparticles until the voids merged to form a hollow shell of iron oxide. Understanding this complex process offers hope for controlling the properties of these nanoshells. For instance, controlling the oxidation process will allow manipulation of nanoparticle porosity, nanoshell crystallinity, and their iron-to-oxygen ratio. The ability to manipulate the properties of iron oxide nanoshells may lead to improvements in catalytic processes, electric batteries, and clean-fuel technologies.

For this study, the researchers from Temple University and Argonne employed highly uniform iron nanoparticles of ~ 10 nm in diameter evenly dispersed as colloids in solution. The colloidal nanoparticles quickly developed an iron oxide coating 2-3-nm thick, which prevented additional oxidation. As the solution temperature rose, iron and oxygen atoms were able to diffuse across the iron oxide coating (the Kirkendall process). Characterizing the iron/oxygen diffusion through the nanoparticles was a major goal of this research.

Previous transmission electron microscopy studies had gleaned limited information about the oxidation of iron nanoparticles. To gain much greater insight into the oxidative process, the researchers used APS synchrotron x-rays at XSD beamline 12-ID-B to fully penetrate the dense colloid and three-dimensionally image large numbers of nanoparticles during oxidation. The SAXS technique proved especially adept at following the real-time oxidation of the colloidal nanoparticles.

SAXS patterns of the colloidal nanoparticles were recorded every 30 sec while the colloidal temperature was periodically raised as a means of altering the oxidation dynamics. Structural computer programs were employed to interpret the scattering data and determined the best-fit three-dimensional structures. The top row of Fig. 1 shows nanoparticle evolution over a span of 6 h.

During the first minutes of the experiment, the temperature was raised to 100° C, which significantly increased nanoparticle oxygen uptake. The top row in Fig. 1 shows a nanoparticle (at 6.5 min into the experiment) that remained solid but increased in size due to the outward diffusion of iron. At 13 min the first voids appeared at the interface between the iron core and the outer iron oxide layer. The voids continued to grow as iron migrated outward. After about 3 h, the first voids began to coalesce, with the colloid temperature raised to 140° C. A few minutes later, the merged voids formed a crescent shape. The crescent's small opening allowed iron to continue to escape from the nanoparticle's core.

At the 4-h mark, the temperature was elevated to 180° C. An image from around this time (275 min) shows a completely hollow interior. At this point all the iron had diffused out to react with oxygen, leaving a hollow shell of iron oxide. The last two images show the hollow nanoparticle as it crystallizes due to the elevated temperature.

The bottom row of Fig. 1 shows a sequence of iron nanoparticle evolution based on a molecular dynamics (MD) simulation. Comparison of the SAXS data to the MD simulation shows a close correspondence between them.

The WAXS study showed that after 265 min, the amorphous iron oxide nanoshells began to crystallize along with an increase of temperature. This crystallization process was associated with a significant increase in oxygen uptake by the nanoparticles.

The experimental results contradict the existing core-void-shell model, which envisions iron diffusion traveling through thin filaments that run from the nanoparticle's core to its shell. The results also suggest several approaches to tuning the properties of metal nanoparticles. More broadly, the researchers anticipate that the complementary x-ray experiments and MD simulations will prove applicable to addressing issues in a wide variety of material and chemical systems.

— Philip Koth

See: Yugang Sun[1]*, Xiaobing Zuo[2]**, Subramanian K.R.S. Sankaranarayanan[2]***, Sheng Peng[2], Badri Narayanan[2], and Ganesh Kamath[2], "Quantitative 3D evolution of colloidal nanoparticle oxidation in solution," Science **356**, 303 (21 April 2017).
DOI: 10.1126/science.aaf6792
Author affiliations: [1]Temple University, [2]Argonne National Laboratory
Correspondence: * ygsun@temple.edu, ** zuox@anl.gov, *** ssankaranarayanan@anl.gov

Y.S. thanks Temple University for startup support. Use of the Center for Nanoscale Materials, a U.S. Department of Energy (DOE) Office of Science user facility, was supported by the DOE Office of Science-Basic Energy Sciences under Contract no. DE-AC02-06CH11357. This research used resources of the National Energy Research Scientific Computing Center, which is supported by the U.S. DOE Office of Science under Contract no. DE-AC02-05CH11231. An award of computer time was provided by the Innovative and Novel Computational Impact on Theory and Experiment (INCITE) program. This research used resources of the Argonne Leadership Computing Facility at Argonne National Laboratory, which is supported by the U.S. DOE Office of Science under Contract no. DE-AC02-06CH11357. This research used resources of the Advanced Photon Source, a U.S. DOE Office of Science user facility operated for the U.S. DOE Office of Science by Argonne National Laboratory under Contract No. DE-AC02-06CH11357.

12-ID-B • XSD • Chemistry, materials science, life sciences, polymer science, physics • Small-angle x-ray scattering, grazing incidence small-angle scattering, wide-angle x-ray scattering, grazing incidence diffraction • 7.9-14 keV • On-site • Accepting general users •

How a Virus Earned Its Nanorod-synthesizing Stripes

Being able to synthesize nanomaterials with controllable dimensions remains an important challenge in nanotechnology. Toward that end, some research teams have looked at utilizing naturally occurring biomaterials, such as viruses, as templates to reliably produce predictable nanostructures on a large scale. Thus far, the majority of studies in this area have focused on just two viruses: the M13 bacteriophage and the tobacco mosaic virus (TMV). Taking advantage of the multiple functionalities afforded by these viruses' protein coats, such as polar, hydrophilic, charged, acidic, and basic chemical groups, researchers have been able to create an array of nanostructures by coating these viruses with noble metals, bimetallic materials, and semiconductors. However, these viruses are just two in a vast multitude of virus species on the planet. In an effort to expand the biodiversity of virus templates, a team of researchers tested the potential of the barley stripe mosaic virus (BSMV) to produce metallic nanomaterials. Coating this virus with the noble metal palladium (Pd), the researchers found that BSMV could readily template the production of high-quality nanorods. A variety of synchrotron x-ray experiments carried out at the APS allowed the researchers to characterize both the mineralization process and the structures of particles as they developed. The findings showcase the potential of BSMV for nanomaterial synthesis.

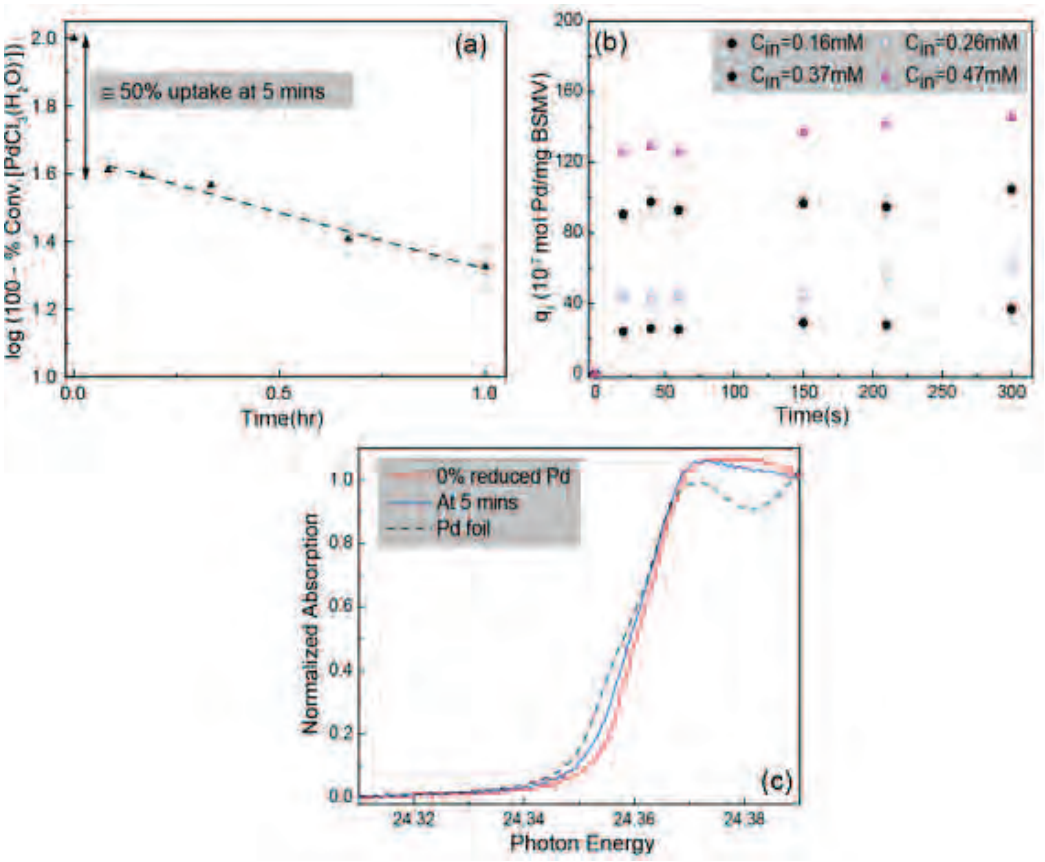

Fig. 1. Changes in Pd during mineralization on BSMV. (a) First order kinetic model fit to $[PdCl_3(H_2O)^-]$ uptake on BSMV (b) Uptake of $PdCl_3(H_2O)^-$ at early times obtained by UV-Vis absorbance experiments at 256 nm. (c) XANES spectra of Pd references and spectrum at five minutes after incubation. Experiments were performed at six different $Pd^{(2+)}$ concentrations (three of them are shown here).

9-ID-B,C • XSD • Chemistry, materials science, life sciences • Nanoimaging, microfluorescence (hard x-ray), coherent x-ray scattering (hard x-ray), ultra-small-angle x-ray scattering • 4.5-30 keV • On-site • Accepting general users •

10-ID-B • MR-CAT • Materials science, environmental science, chemistry • X-ray absorption fine structure, time-resolved x-ray absorption fine structure, microfluorescence (hard x-ray) • 4.3-27 keV, 4.8-32 keV, 15-65 keV • On-site • Accepting general users •

To determine this virus' suitability as a biotemplate, the researchers from Purdue University started by adding a solution containing BSMV to a continuous stirred-tank reactor containing a Na_2PdCl_4 solution. After a 20-min incubation, transmission microscopy images showed the formation of nanorods on the viral coat. The BSMV was coated with palladium nanoparticles, which had an initial diameter of 1 to 2 nm. After recoating the BSMV several times, the diameter of the Pd-coated BSMV increased to about 57 nm.

Sampling the reaction materials periodically during the incubation process, the researchers used UV-vis spectroscopy and x-ray absorption spectroscopy to characterize the biomineralization process (Fig. 1). Their findings showed that Pd from the Na_2PdCl_4 solution adsorbed to the viruses within seconds after combination, a process driven by both electrostatic and covalent bonds between the precursor Pd ions and the functional groups on the viral coat. The total absorption capacity of BSMV proved to be more than double that of TMV under the same reaction conditions.

After several minutes, the adsorbed Pd ions then underwent a reduction reaction, a process, which lasted up to several hours. Further coatings repeated this process, sequentially thickening the diameter of the nanorods (Fig. 2).

Further investigation by the Purdue team and Argonne colleagues utilizing x-ray absorption spectroscopy (XAS) and small- (SAXS) and ultra-small-angle x-ray scattering (USAXS) at the XSD 9-ID-B,C and MR-CAT 10-ID-B beamlines at the APS (SAXS/USAXS at 9-ID-B,C and *in situ* XAS at 10-ID-B) showed that these particles displayed a core-shell morphology and were uniform and monodisperse, with quality as high as those synthesized using TMV as a biotemplate. Because the x-ray imaging techniques allowed the researchers to follow growth from the primary Pd nanoparticles through their growth to final size, the researchers note that to their knowledge, this study is the first to comprehensively and simultaneously analyze all size levels in a rod-like mineralized virus.

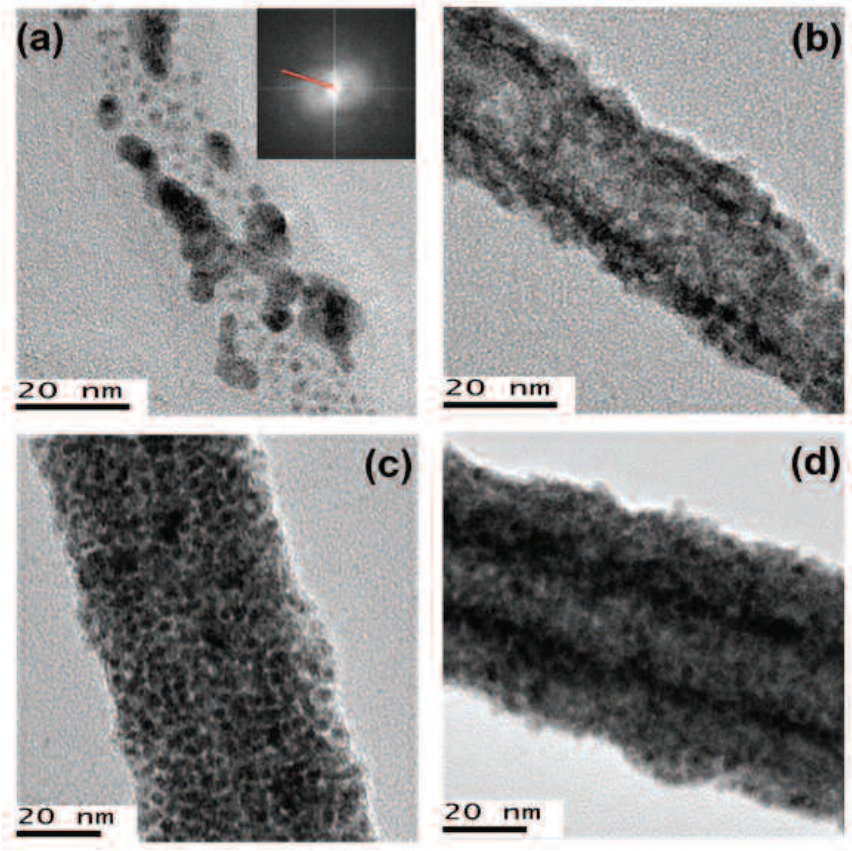

Fig. 2. TEM images of single BSMV-Pd after incubation of 0.02 mg/mL of BSMV in 7.5×10^{-2} mM of Na_2PdCl_4. BSMV-Pd collected after (a) one coating cycle. Inset in shows the Fourier transform of a high-resolution TEM (HRTEM) image of Pd particles after one coating. Spacing 0.22 nm corresponding to d(111) of $Pd^{(0)}$ was observed (b) two coating cycles (c) BSMV-Pd collected after five coating cycles and (d) six coating cycles.

They add that in total, these findings expand the biotemplate toolbox for synthesizing new materials and comparatively studying biomineralization processes between templates. The unique active surface of these particles left on the viral coat could serve in a variety of applications, the researchers say, such as catalysis, battery electrodes, and further electroless deposition. In addition, this work shows that the native amino acid and functional groups on BSMV offer the potential of new kinds of mineralization possibilities not yet realized with current biotemplate offerings.

Future research might be able to expand the products of these synthesis reactions by genetic engineering of the virus, metallization with other metals, and exploring selective inner channel mineralization to produce superfine nanowires. *— Christen Brownlee*

See: Oluwamayowa O. Adigun[1], Erin Lynn Retzlaff-Roberts[1], Gloria Novikova[1], Longfei Wang[1], Bong-Suk Kim[1], Jan Ilavsky[2], Jeffrey T. Miller[1], L. Sue Loesch-Fries[1], and Michael T. Harris[1]*, "BSMV as a Biotemplate for Palladium Nanomaterial Synthesis," Langmuir **33**, 1716 (2017).
DOI: 10.1021/acs.langmuir.6b03341
Author affiliations: [1]Purdue University, [2]Argonne National Laboratory
Correspondence:
* mtharris@purdue.edu

MR-CAT operations are supported by the U.S. Department of Energy (DOE) and the MR-CAT member institutions. Zhenwei Wu, Evan Wegener, and Guanghui Zhang are acknowledged for their assistance with XAS experiments. This research used resources of the Advanced Photon Source, a U.S. DOE Office of Science user facility operated for the U.S. DOE Office of Science by Argonne National Laboratory under Contract No. DE-AC02-06CH11357.

Shedding Light on Nanoscale Energy Dissipation

Zinc oxide (ZnO) nanostructures have attracted significant attention in recent years for their remarkable semiconducting and piezoelectric (the ability to accumulate electrical charge in response to mechanical stress) properties. Together, these features have formed the basis for their use in electromechanically coupled sensors and transducers, with further potential in photodetectors, optical communications, photovoltaic devices, piezoelectric devices, and nanoelectromechanical systems. They are also being explored for applications including nanogenerators, actuators, and sensing devices due to the intricate and poorly understood interactions between strain fields, charge distribution, and mechanical deformation modes in ZnO. To explore these phenomena, researchers carried out two complementary studies using laser-pumped x-ray Bragg coherent diffractive imaging (BCDI) on ZnO nanocrystals. In the first study, bare ZnO crystals were excited with ultraviolet laser light, and in the second, nanorods composed of a ZnO core wrapped with a Ni shell were excited with infrared laser light. Both studies exploited the high-brightness coherent x-ray pulses from the APS timed with the laser pulses to image the mechanical dynamics of the ZnO crystals and nanorods by BCDI . These ultrafast imaging methods, combined with computer modeling, revealed complex deformations in ZnO's crystal structure in response to stimulation from short laser pulses. These deformations temporally affect the charge distribution in these nanostructures, which could have significant implications for developing new materials for power generation and other applications that use ZnO nanostructures.

In the first study, researchers from Argonne and the European Synchrotron Radiation Facility assessed the temporal response of isolated ZnO nanocrystals to optical excitation. Working at the XSD 7-ID-B,C,D x-ray beamline at the APS, the scientists used an ultraviolet laser to excite these particles with a series of picosecond optical pulses, as illustrated in Fig. 1(a). Between these pulses, the researchers probed the nanocrystals with x-ray flashes and ultrafast x-ray BCDI to image them at high resolution in three dimensions. The resulting images in Fig. 1(b) show the evolution of strain within a bare ZnO crystal along the axial and radial directions. Acoustic phonons, which are the collective motions of groups of atoms, are observed to propagate along the axis of the nanocrystal, as evinced by the pocket of strain (region in red) propagating along its length. The images were then utilized to develop a computer simulation with finite element modeling (FEM). The simulations were performed using the high-performance computing cluster (Carbon) at Argonne's Center for Nanoscale Materials (CNM).

Together, these results revealed a variety of mechanical deformations taking place upon laser excitation. Some of these deformations were "homogenous," reaching across the entire crystal at the same length scales — these include breathing modes, in which the crystal expands and contracts uniformly. Others were "inhomogenous," in which some atoms of the crystal are moving closer together and others are moving farther apart — these include axial, radial, and torsional deformation modes, each with unique frequencies.

Each of these modes significantly affected the charge distribution inside these nanocrystals, some with consequences that could influence applications using these materials. For example, their FEM studies showed that one inhomogenous torsional mode yields an electric potential gradient across the crystal that's 50% higher than that resulting from typical flexural mode that's currently used in piezoelectric ZnO-based nanoscale power-generation devices. This effect, the researchers add, could be exploited to achieve higher efficiency nanoscale power generators. Developing a better understanding of this behavior could also aid in tailoring and design of mechanical, optical, and piezoelectric responses of materials for the next generation of sensors, actuators, and energy harvesting devices of broad interest to technology and industry.

In their second study, the researchers selectively excited the Ni in ZnO core/Ni shell nanoparticles with short laser pulses, subsequently probing how the ZnO core's structure changes with time. These experiments revealed a complex interplay of induced radial, axial, and shear deformations of the ZnO crystal structure. To help elucidate the source of these deformations, the researchers transferred the experimental images obtained from the BCDI data directly into a computer model. The FEM studies performed on CNM's supercomputer Carbon indicated structural deformation of the ZnO core followed deformation of the Ni shell after it became heated by the laser pulse and thermally expanded, causing surface and interfacial shearing of the underlying ZnO. Figure 1(c) shows the dominant vibrational modes of the ZnO core. This structural deformation could be used to remotely affect electric current flow through these core/shell nanoparticles.

Gaining a better understanding of this behavior, the authors say, could help researchers design better devices with metal-semiconductor interfaces and core-shell nanoparticles, such as optoelectronic, catalysis, and sensors. In addition, they add, the ultrafast three-

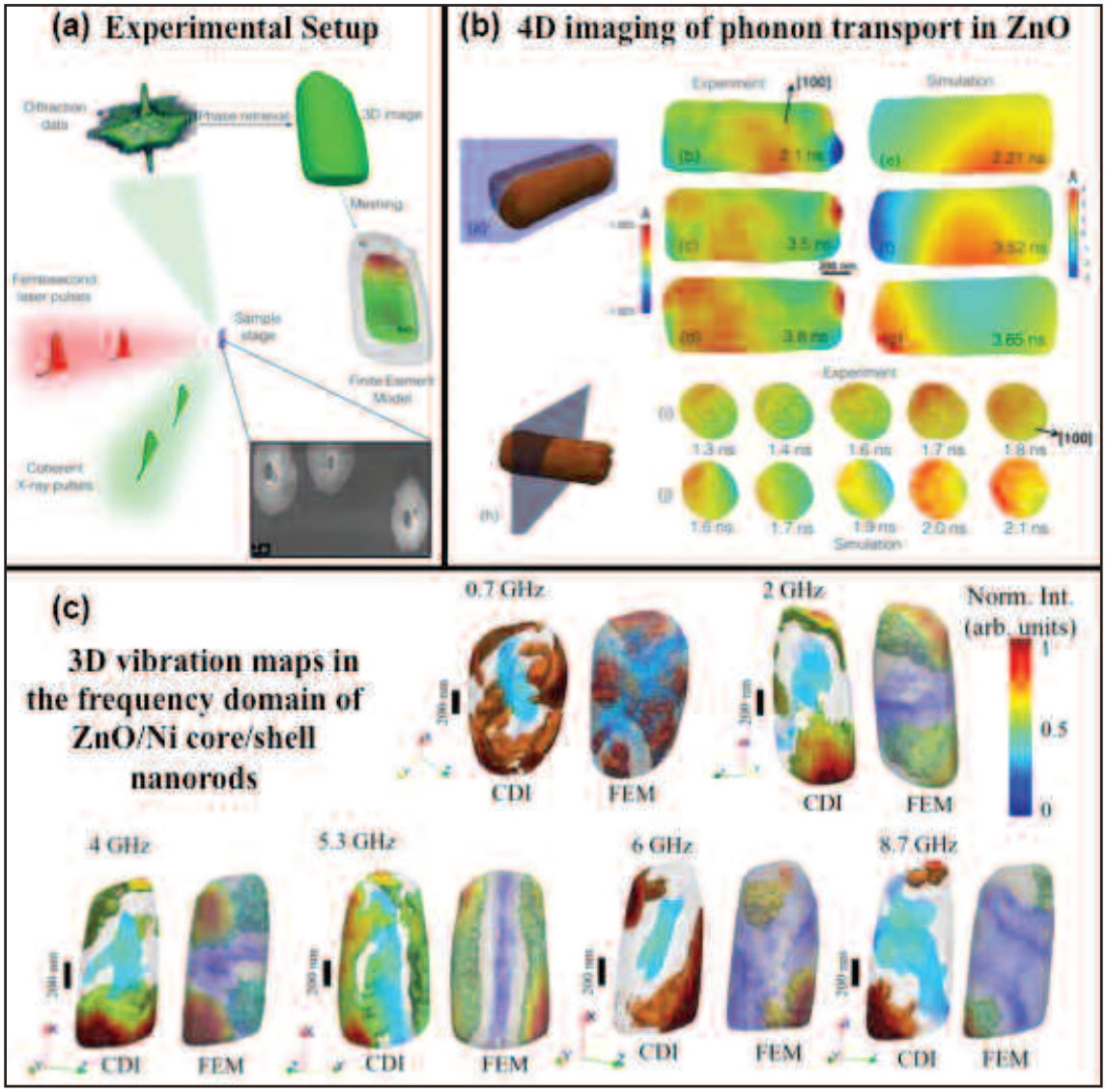

Fig. 1. Integrating information from x-ray imaging and materials modeling provides insight into how energy is dissipated at the nanoscale in sub-nanosecond timescales. (a) Schematic of the experimental setup, in which scientists used an ultraviolet laser to excite ZnO nanocrystals with a series of picosecond optical pulses (b) Three-dimensional images of the evolving strain field in bare ZnO. After stimulation with the laser, acoustic phonons, or collective motions of groups of atoms, propagate along the axis of the nanocrystal. (c) Frequency domain response of the ZnO core in a ZnO/Ni core/shell structure from experiment and modeling. Regions in red are portions of the crystal with the greatest vibrational amplitude at the given frequency, while regions in blue are portions of the crystal with the least vibrational amplitude at that frequency.

dimensional imaging used here could shed light on the dynamic behavior of other types of semiconductor nanocrystals. *— Christen Brownlee*

See: Mathew J. Cherukara[1], Kiran Sasikumar[1], Wonsuk Cha[1], Badri Narayanan[1], Steven J. Leake[2], Eric M. Dufresne[1], Tom Peterka[1], Ian McNulty[1], Haidan Wen[1], Subramanian K.R.S. Sankaranarayanan[1]**, and Ross J. Harder[1]*, "Ultrafast Three-Dimensional X-ray Imaging of Deformation Modes in ZnO Nanocrystals," Nano Lett. **17**, 1102 (2017).
DOI: 10.1021/acs.nanolett.6b04652
Author affiliations: [1]Argonne National Laboratory, [2]The European Synchrotron Radiation Facility
Correspondence:
* rharder@aps.anl.gov,
** ssankaranarayanan@anl.gov

This material is based upon work supported by Laboratory Directed Research and Development (LDRD) funding from Argonne National Laboratory, provided by the Director, Office of Science, of the U.S. Department of Energy (DOE) under Contract No. DE-AC02-06CH11357. This work was supported by Argonne LDRD 2015-149-R1 (Integrated Imaging, Modeling, and Analysis of Ultrafast Energy Transport in Nanomaterials) and Argonne LDRD 2018-019-N0 (A.I C.D.I: Atomistically Informed Coherent Diffraction Imaging). Work at the APS and the CNM, both Office of Science user facilities, was supported by the U.S. DOE Office of Science-Basic Energy Sciences under Contract No. DE-AC02- 06CH11357.

Nanocrystals Melt in the Glare of Light

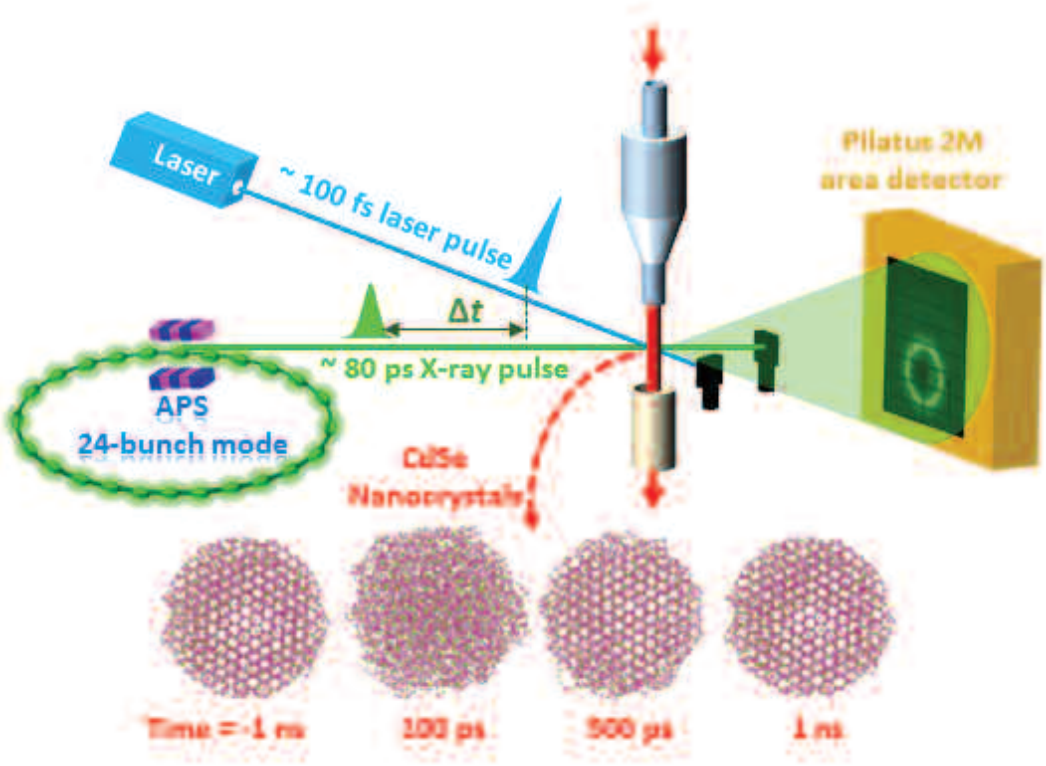

Fig. 1. The APS, operating in 24-bunch mode, produces a train of 80-ps x-ray pulses that are directed to a liquid jet containing CdSe nanocrystals. A synchronized 100-fs laser, operating at 400 nm, was overlapped with the region of the jet that the x-rays probed. Both the laser intensity and time delay between laser pulse and x-ray probe were varied. The diffraction from the nanocrystals in solution was monitored on a 2-MP gated x-ray detector, revealing peak positions and amplitudes. Snapshots of crystalline CdSe nanocrystals, disordered, and recrystallized particles are shown for indicated laser-to-x-ray time delays. Image Credit: Xiaoyi Zhang and Matthew S. Kirschner

11-ID-D • XSD • Chemistry, environmental science, materials science • Time-resolved x-ray absorption fine structure, time-resolved x-ray scattering • 6-25 keV • On-site • Accepting general users •

Nano-sized particles of semiconductor material offer unique optical properties that make them valued for many applications including fluorescent bio-labels, light-emitting diodes, lasers, and solar cells. The size of these nanocrystals determines the wavelengths at which they absorb or emit light. Researchers have generally assumed that the atomic structure of nanocrystals doesn't budge even when the particles are strongly excited. However, experiments performed at the APS have shown that nanocrystals can expand and partially melt under strong excitation. This melting may explain observed deleterious changes in the performance of nanocrystals. The results suggest that designs of nanocrystals may need to be adapted for applications requiring high-energy inputs, such as lasers and concentrated solar energy.

Nanocrystals are generally synthesized in large quantities within solutions containing inorganic precursors and organic molecules. This scalable wet chemical fabrication is what distinguishes nanocrystals from quantum dots, which have some similar properties but are typically made using physical methods. The advantage of shrinking semiconductor materials down to nanoscales is that this allows researchers to control their electronic properties and their photo-response. When a photon is absorbed by a nanocrystal, it forms an electron-hole pair. In most cases, the number of excitations is only a few per nanocrystal, but for lasing and other high-input applications, each nanocrystal may contain numerous excitations at a time. Although some of this energy is re-emitted as light, some of it is converted into heat. Researchers from Northwestern University and Argonne National Laboratory investigated how this heating can affect the physical and optical properties of nanocrystals.

The team looked specifically at cadmium-selenide (CdSe) nanocrystals, created with resources at Argonne's Center for Nanoscale Materials (CNM) and sprayed as a jet through the cross-hairs of a blue laser and an x-ray beamline. The researchers used femtosecond pulses from the laser to excite the nanocrystals. After a controlled time delay, they employed time-resolved x-ray diffraction utilizing 11.7-keV x-ray pulses from the XSD beamline 11-ID-D at the APS to study the excited particles. The x-ray diffraction pattern was captured with a gated array detector increased measurement sensitivity.

By controlling the intensity of the laser pulses, the researchers varied the average number of excitations per nanocrystal from less than one to a few hundred. At the low end, the handful of excitations resulted in a small amount of heating, which was detected through a shift in the peaks of the diffraction pattern. For higher numbers of excitations, these diffraction peaks showed a decrease in their height—a signature that part of the crystal had melted. Surprisingly, melting occurred in nanocrystals containing as few as 15 excitations. Both the thermal expansion and melting may be a concern for a wide range of nanocrystal applications.

The researchers could also explore recrystallization by extending the time delay between the laser and x-ray pulses. They found that most of the nanocrystals had completely re-solidified within 1 nsec after melting. They also showed that the final crystalline structure (post-melting) was the same as it was initially (pre-excitation). This observation implies that the melting occurs predominantly in the outer shell of the nanocrystal, leaving a crystal core that dictates the structure as the particle re-solidifies.

To explore the possible effects of heating and melting, the researchers performed molecular dynamics simulations, which showed that the electronic band gap becomes smaller as the temperature goes up. Such a change in band gap would cause a redshift in the wavelength at which a nanocrystal interacts with light. The simulations also suggest that melting may explain previous observations of a loss in optical gain for nanocrystals experiencing high excitation rates. To avoid such deleterious effects, chemists and engineers may want to look for ways to raise the melting point of a nanocrystal, such as coating each particle with a shell made of a different material.

— Michael Schirber

See: Matthew S. Kirschner[1], Daniel C. Hannah[1], Benjamin T. Diroll[2], Xiaoyi Zhang[2], Michael J. Wagner[1], Dugan Hayes[2], Angela Y. Chang[1], Clare E. Rowland[1], Clotilde M. Lethiec[1], George C. Schatz[1], Lin X. Chen[1,2], and Richard D. Schaller[1,2]*, "Transient Melting and Recrystallization of Semiconductor Nanocrystals under Multiple Electron−Hole Pair Excitation," Nano Lett. **17**, 5314 (2017).
DOI: 10.1021/acs.nanolett.7b01705
Author affiliations: [1]Northwestern University, [2]Argonne National Laboratory
Correspondence: * schaller@anl.gov; schaller@northwestern.edu

We acknowledge support from the Ultrafast Initiative of the U.S. Department of Energy (DOE Office of Science-Basic Energy Sciences, through Argonne National Laboratory under Contract No. DE-AC02-06CH11357. D.K.H. is supported by the Joseph J. Katz Postdoctoral Fellowship at Argonne. Use of the Center for Nanoscale Materials, an Office of Science user facility, was supported by the U.S. DOE Office of Science-Basic Energy Sciences, under Contract No. DE-AC02-06CH11357. This research used resources of the Advanced Photon Source, a U.S. DOE Office of Science user facility operated for the DOE Office of Science by Argonne National Laboratory under Contract No. DE-AC02-06CH11357.

A New Way to Make Nanocrystals

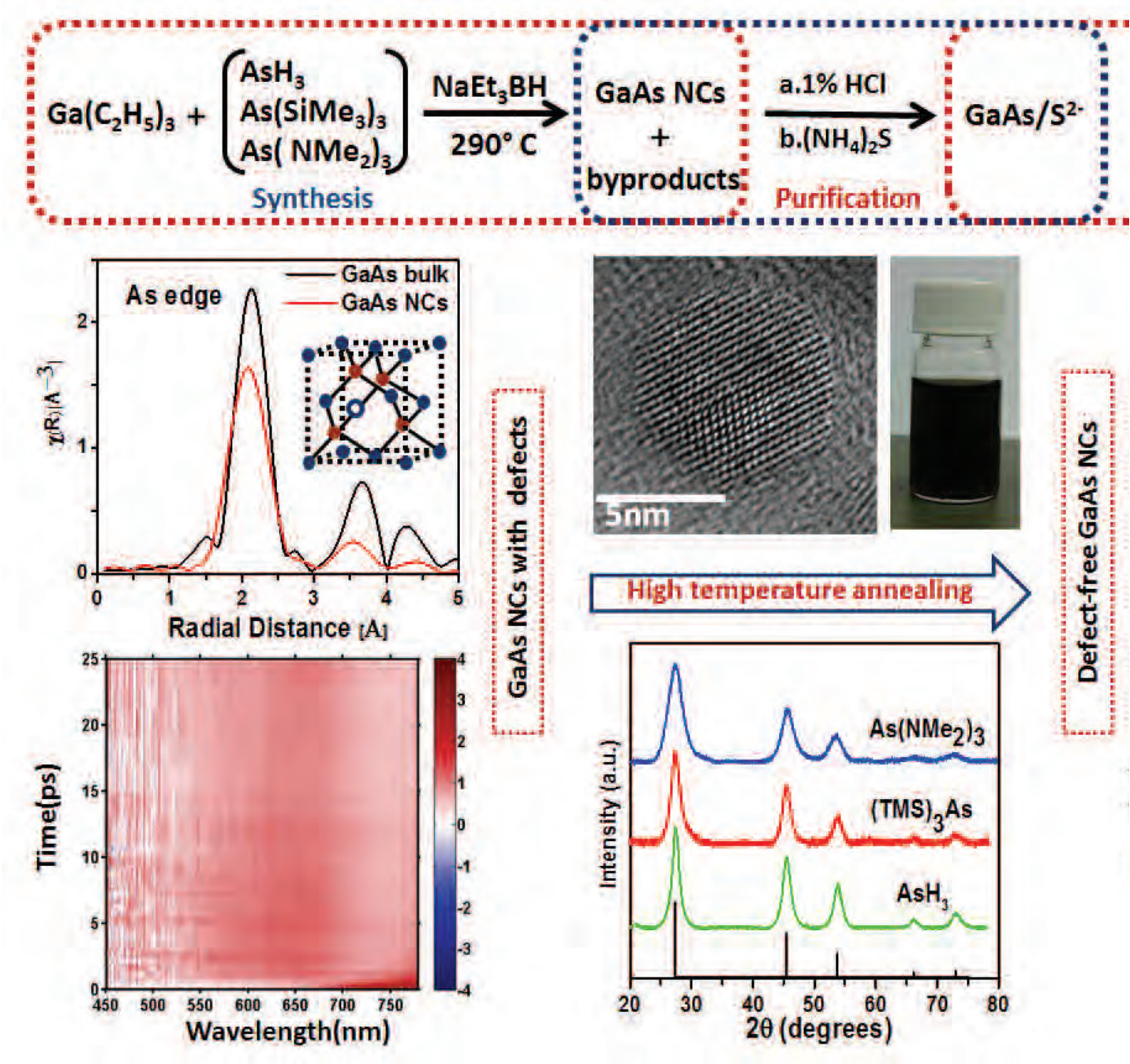

Fig. 1. GaAs nanocrystals can be synthesized by reacting triethylgallium with arsenic precursors (top). EXAFS studies of GaAs before annealing (center left) show different results for powder (black) versus nanocrystals (red), though the measurements change after annealing (center right). The optical properties also change from before (bottom left) to after (bottom right) annealing. The nanocrystals in a TEM image (center). All three precursors produce nanocrystals with similar x-ray diffraction patterns (bottom center).

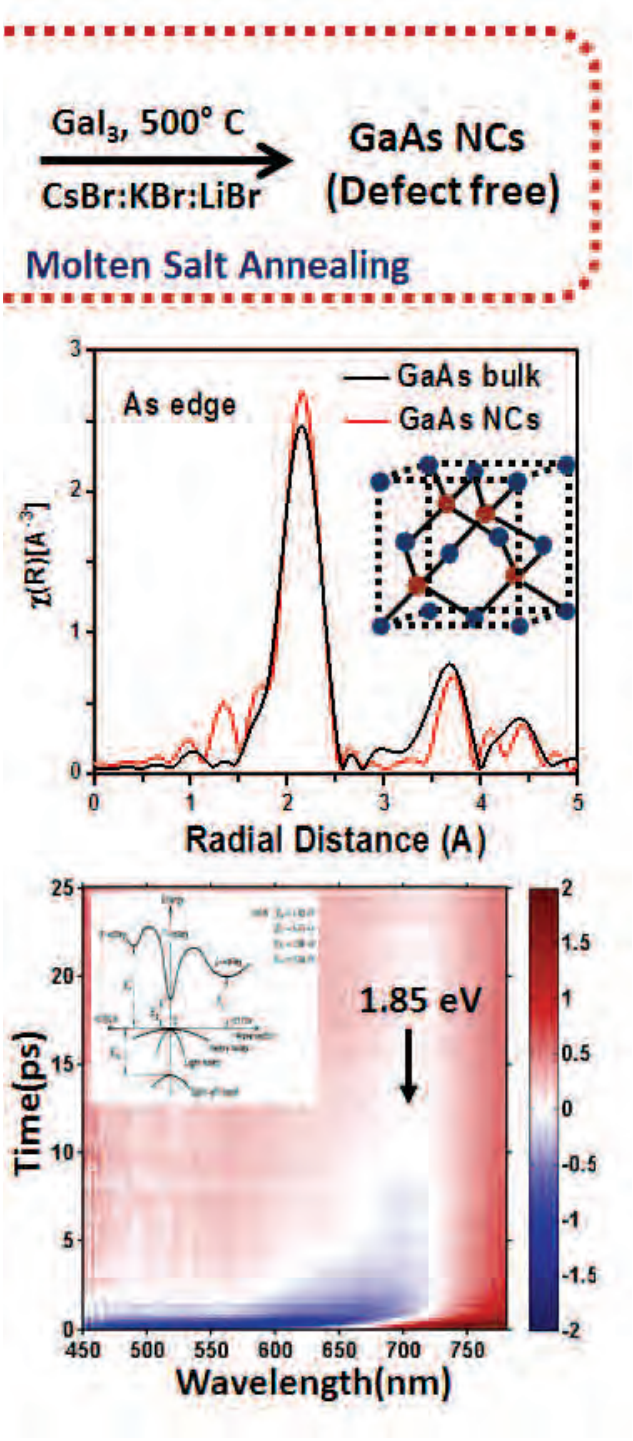

The semiconductor gallium arsenide (GaAs) is widely used in optoelectronic devices. Its electrical and optical properties make for highly efficient solar cells, lasers, light-emitting diodes, and transistors. If GaAs could be made into nanocrystals, it could improve solar cells further, as well as providing nanometer-scale light sources for molecular imaging and other applications. Unfortunately, GaAs nanocrystals do not exhibit the same properties as the other semiconductors do at the nanoscale. Now researchers using the APS and Argonne Center for Nanoscale Materials (CNM) have come up with methods for making GaAs nanocrystals that work as expected at the nanoscale.

Bulk GaAs is usually produced with techniques such as metal-organic chemical vapor deposition or molecular beam epitaxy, which deposit gaseous forms of the materials on a substrate at temperatures above 600° C, producing high-quality thin films. Nanocrystals, on the other hand, are often made through colloidal synthesis, where the materials react together in a solution at temperatures below 350° C. While the colloidal process results in good-quality nanocrystals for materials such as cadmium selenide or indium phosphide, GaAs nanocrystals made this way have poor optical properties.

The researchers from The University of Chicago and Northwestern University compared a fine powder of bulk GaAs with GaAs nanocrystals, using extended x-ray absorption fine structure (EXAFS) analysis conducted at XSD beamlines 20-ID-B,C and 20-BM-B at the APS (Fig.1). The x-ray absorption differed between the two materials, revealing that while the arsenic atoms in the powder were surrounded by four gallium atoms each, the arsenic in the nanocrystals had some empty spaces around them. Other measurement techniques, including Raman, electron paramagnetic resonance spectroscopy and transient absorption spectroscopy accomplished at CNM, filled out the picture, showing that the nanocrystals had a different electronic structure than the powdered form. The researchers concluded that the gallium vacancies in the nanocrystals were to blame for the poor performance.

It is the high temperature in the synthesis of bulk GaAs that allows defects to be annealed out, so the researchers developed a process that allowed the nanocrystals to reach higher temperatures. They synthesized GaAs nanocrystals by reacting the gallium and arsenic precursors in the presence of sodium triethylborohydride, also known as superhydride, which was essential for balancing the reactivity of the two precursors and led to spherical GaAs nanocrystals without any impurities. To anneal the nanocrystals as well, the team dispersed them in molten inorganic salts. The salt allowed them to heat up the mixture to 500° C,while maintaining their size and preventing the nanocrystals from fusing together. The researchers also added gallium iodide to the mix, providing a source of gallium atoms to fill in the vacancies.

The synthesis entailed reacting triethylgallium with 1 of 3 different arsenic precursors, including arsine gas. All three precursors produced similar nanocrystals, which performed as well as the bulk material. Small-angle x-ray scattering conducted at the XSD 12-ID-B beamline at the APS, along with transmission electron microscopy (TEM) measurements, allowed them to measure the size distribution of the nanocrystals and confirm that they were not clumping together.

It should be possible, the researchers say, to alter the surface chemistry of the crystals to achieve certain electrical or optical properties. They also plan to experiment with different elements to make other

"A New Way" cont'd. on page 157

Catching the Drift of Nanoparticles

Understanding how nanoparticles diffuse in materials such as polymers and surfactant solutions is important in a variety of areas. Pharmaceutical companies that want to use tiny capsules to deliver drugs need to know how fast they pass through bodily fluids such as mucus. The dispersion of particles can affect the properties of all sorts of materials — even something as simple as how carbon black nanoparticles behave in rubber can affect an automobile tire's performance. And understanding the motion of nanoparticles can give researchers insight into the microstructure, and hence the mechanical properties, of such complex fluids, which differ from simple liquids because of that structure. Now scientists using the APS have measured how the relative sizes of the microstructure and nanoparticles relate to the particles' motion. The findings fit a theory that says nanoparticles can move not only when the cages break but also when thermal motion temporarily opens holes to slip through. Knowing this alternative mechanism should allow researchers to better predict the behavior of nanoparticles in complex fluids, and perhaps make alterations to either the nanoparticles or the solution to better control the behavior of the particles and the properties of the material. *Cont'd. on the next page*

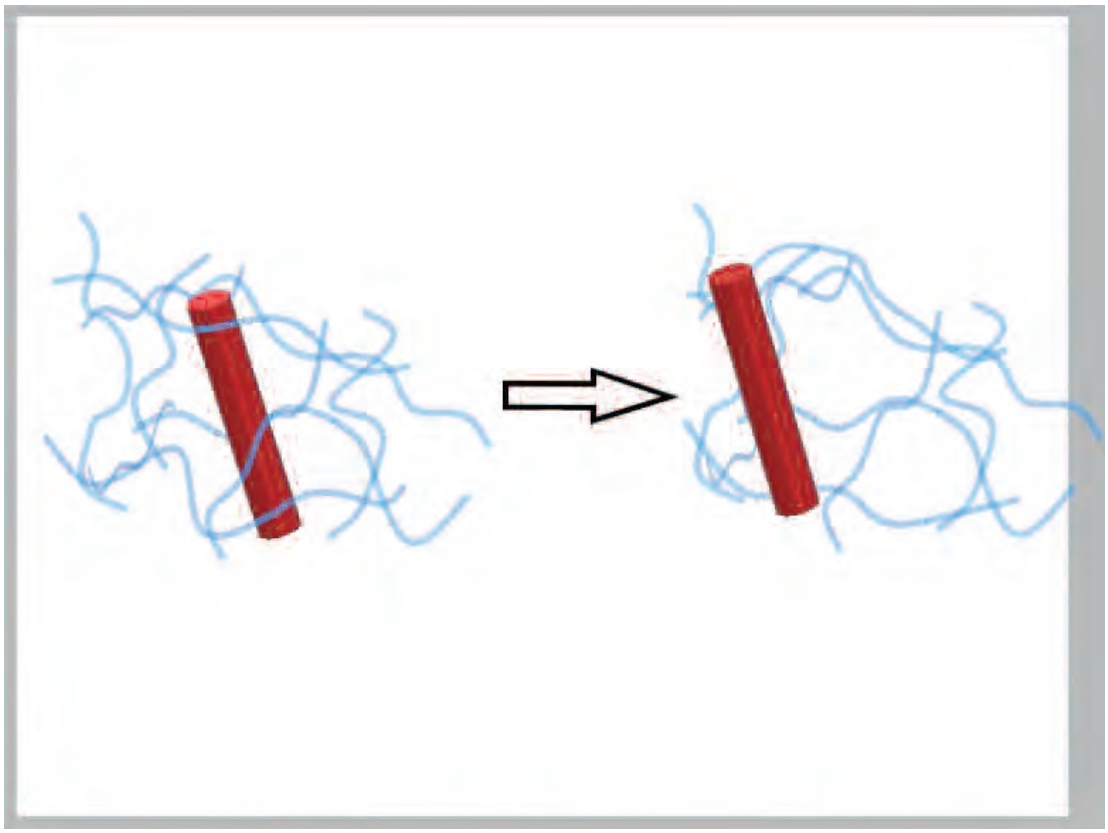

The researchers from Argonne, the Federal University of Parana (Brazil), and Johns Hopkins University created a complex fluid by mixing a surfactant (cetylpyridinium chloride) with a salt (sodium salicylate) in water. Surfactants have both hydrophilic and hydrophobic ends, so in solution they assemble into forms that hide the hydrophobic tails and expose the hydrophilic heads. In this case, the molecules organize into long tubes, known as wormlike micelles, which become entangled with each other, forming a mesh. The amount of salt controls the flexibility of the tubes and hence the fluid's viscosity. They also fabricated gold nanorods, roughly 8 nm in radius and 47 nm long.

If the nanoparticles were much smaller than the mesh, they would be able to diffuse freely. But when they're larger than the spaces in the mesh, they get caught in tiny cages. Eventually, random thermal motion causes the cage to fall apart and the particle breaks free, only to get stuck in another cage for a time. The researchers wanted to understand how the relative sizes of the mesh and particles affect the time it takes the rods to diffuse, so they varied the space between the micelles by varying the surfactant concentration.

Scientists can measure the flow properties of a substance on the macroscopic scale. The results, along with the size of the particle and the temperature of the system, allows them to predict the diffusion rate through a relation known as the generalized Stokes-Einstein equation.

Using the XSD 8-ID-I beamline at the APS, the researchers performed x-ray photon correlation spectroscopy to measure the movement of nanoparticles through the solution as they increased the concentration of the micelles. At low concentrations, when the mesh spacing was much larger than the rod, the nanoparticles moved freely, as if the solution were not very viscous. As they increased the concentration of surfactant and shrank the mesh, the particles moved more slowly. Over a few microseconds, the motion matched the prediction of the equation.

But when the researchers watched for a few seconds, they saw the rods moving much more freely than the equation predicted even as the nanoparticles became larger than the mesh. In other words, on the microscopic scale, the solution remained effectively much less viscous than at the macroscopic. Only when the particle size reached several times the mesh spacing did the microscopic and macroscopic viscosities match.

— Neil Savage

< Fig. 1. A nanorod (red) is trapped in a cage formed by an entangled mesh of wormlike micelles (blue lines) when its length is similar to the length scale of the micelles (left). Thermal motion allows the rod to escape from the cage on a time scale determined by temperature and relative size.

See: Jonghun Lee[1], Aline Greinlankovski[1,2], Suresh Narayanan[1], and Robert L. Leheny[3]*, "Nanorod Mobility within Entangled Wormlike Micelle Solutions," Macromol. **50**, 406 (2017). DOI: 10.1021/acs.macromol.6b02091
Author affiliations: [1]Argonne National Laboratory, [2]Federal University of Parana, [3]Johns Hopkins University
Correspondence: * leheny@jhu.edu

J.L. acknowledges the support from the Argonne Laboratory Directed Research and Development program. A.G.I. acknowledges a scholarship from CAPES/PDSE (BEX 3193/14-4). R.L.L. thanks the Argonne National Laboratory X-ray Science Division Visiting Scientist Program for support. The authors also acknowledge the Brazilian funding agency CNPq (Grant 477467/2010-5) and the National Science Foundation (NSF DMR-1207117 and DMR-1610875). This research used resources of the Advanced Light Source, which is a DOE Office of Science user facility under contract no. DE-AC02-05CH11231. This research used resources of the Advanced Photon Source, a U.S. Department of Energy (DOE) Office of Science user facility operated for the DOE Office of Science by Argonne National Laboratory under Contract No. DE-AC02-06CH11357.

8-ID-I • XSD • Polymer science, materials science, physics • X-ray photon correlation spectroscopy, intensity fluctuation spectroscopy, small-angle x-ray scattering • 6-12.5 keV, 10.9--10.9 keV, 7.35 keV • On-site • Accepting general users •

"A New Way" cont'd. from page 155
nanocrystals, such as indium gallium arsenide or indium gallium phosphide, opening a wider range of properties they could potentially achieve.

— Neil Savage

See: Vishwas Srivastava[1], Wenyong Liu[1], Eric M. Janke[1], Vladislav Kamysbayev[1], Alexander S. Filatov[1], Cheng-Jun Sun[2], Byeongdu Lee[2], Tijana Rajh[2], Richard D. Schaller[2,3], and Dmitri V. Talapin[1,2]*, "Understanding and Curing Structural Defects in Colloidal GaAs Nanocrystals," Nano Lett. **17**, 2094 (2017).
DOI: 10.1021/acs.nanolett.7b00481
Author affiliations: [1]The University of Chicago, [2]Argonne National Laboratory, [3]Northwestern University
Correspondence:
* dvtalapin@uchicago.edu

This work was supported by the Department of Defense Air Force Office of Scientific Research under grant number FA9550-14-1-0367, Office of Naval Research under grant number N00014-13-1-0490, National Science Foundation under Awards DMR-1310398 and DMR-1611371, and by the II–VI Foundation. Sector 20 facilities at the Advanced Photon Source, and research at these facilities, are supported by the U.S. Department of Energy (DOE) Office of Science-Basic Energy Sciences, the Canadian Light Source and its funding partners, and the Advanced Photon Source. Use of the CNM and the APS, Office of Science user facilities operated for the U.S. DOE Office of Science by Argonne National Laboratory, was supported by the U.S. DOE under Contract No. DE-AC02-06CH11357.

12-ID-B • XSD • Chemistry, materials science, life sciences, polymer science, physics • Small-angle x-ray scattering, grazing incidence small-angle scattering, wide-angle x-ray scattering, grazing incidence diffraction • 7.9-14 keV • On-site • Accepting general users •

20-BM-B • XSD • Materials science, environmental science, chemistry • X-ray absorption fine structure, microfluorescence (hard x-ray) • 2.7-32 keV, 2.7-35 keV • On-site • Accepting general users •

20-ID-B,C • XSD • Materials science, environmental science, chemistry • X-ray absorption fine structure, x-ray Raman scattering, micro x-ray absorption fine structure, microfluorescence (hard x-ray), x-ray emission spectroscopy • 4.3-27 keV, 7-52 keV • On-site • Accepting general users •

Diverse Nanocrystals Form Stable Colloids in Molten Salts

Colloids typically consist of two disparate substances that form a homogeneous mix. In this study, researchers created a wide range of previously-unknown colloids consisting of many distinct combinations of nanocrystals and salts homogeneously dispersed in molten salts that reached temperatures as high as 350° C (662° F). The stability and other characteristics of these colloids were explored using several techniques, including x-ray scattering experiments carried out at the APS. In addition to creating entirely new colloids, the researchers also uncovered the chemical nature of the mechanism responsible for their stability, which is unlike the mechanisms known to underlie most colloidal stability. These findings may have several beneficial applications, such as creating new possibilities in nanocrystal synthetic chemistry, improving the post-treatment of unconventional solvents at high temperatures, and improving the heat storage and conductivity properties of molten salts. Additionally, the colloid-formation mechanism uncovered by this study may prove applicable to other classes of colloidal solutions, for example in colloids where the solvent consists of a liquid metal. *Cont'd. on the next page*

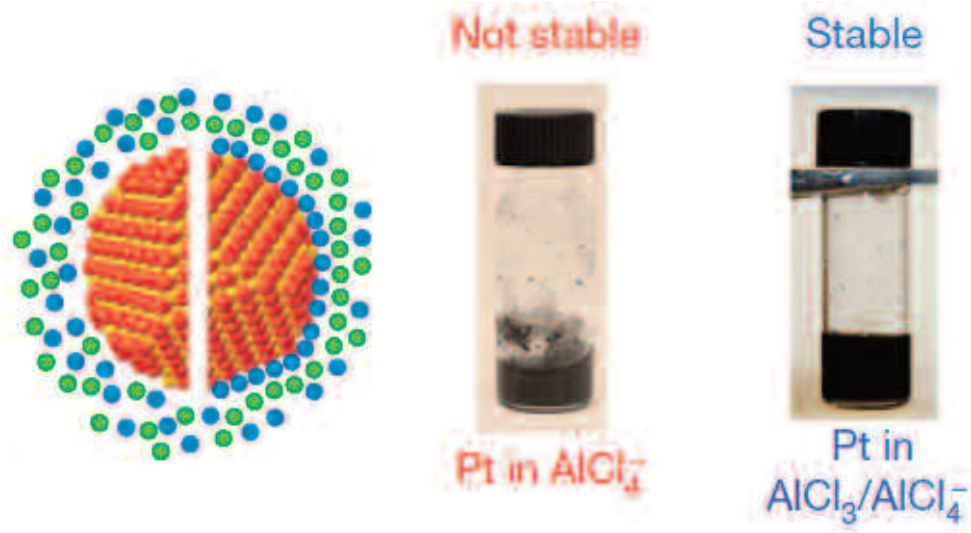

Fig. 1. Left image: Illustration depicting the origin of stability within molten-salt-based colloids. The right half of the image shows a portion of a nanocrystal (colored red) surrounded by the ions of a molten salt (green and blue spheres). Chemical affinity between certain ions in the molten salt and the nanocrystal form a layer (the blue spheres) on the nanocrystal's surface. This layer keeps the nanocrystals from clumping. The left half of the image shows a lack of chemical affinity between a nanocrystal and salt ions, resulting in no protective layer and nanocrystal clumping. Right image: Comparison of stable and unstable colloids. Both vials contain platinum nanocrystals suspended within the same type of chlorine-based molten salt ($AlCl_3$/NaCl/KCl). The difference between the two solutions is the proportion of aluminum chloride (Al-Cl) ions. The vial at right has formed a stable colloid. It features a combination of highly stable $AlCl_4$ ions and less stable (more reactive) $AlCl_3$ ions, the latter of which form a protective layer around the platinum nanocrystals which keeps them apart. In contrast, the vial on the left has only the highly stable $AlCl_4$ ions and cannot form a protective nanocrystal layer, which in turn leads to particle clumping. Adapted from H. Zhang et al., Nature **542**, 328 (16 February 2017).

A colloid is only viable if its constituent particles stay apart from one another. This is oftentimes difficult to achieve because fine particles mixed into a solvent tend to clump together. This tendency to aggregate is due to the attractive force between the particles known as the "van der Waals force." Conventional colloids overcome this clumping tendency in one of two of ways. First, some particles can be electrostatically charged so that they repel one another; however, this technique is only viable for certain types of solvents. Alternatively, stable colloids are sometimes achieved by coating the particles prior to dispersal in the solvent. The coating consists of molecules that form brush-like appendages at each particle's surface that repel similarly-coated particles.

For the types of colloids produced for this study, neither of these mechanisms could be counted on to achieve stability. For instance, the high temperatures required by many of the molten-salt solvents would disintegrate the conventional coatings used for stabilization. In spite of these limitations, the researchers from The University of Chicago, the University of Massachusetts Medical School, and Argonne succeeded in creating a wide variety of stabile colloids based upon molten salts. A chief aim of this study was to uncover the mechanism responsible for the colloids' stability.

The nanocrystals used in this research included pure metals (platinum and palladium), magnetic materials (iron oxide), semiconductor quantum dots, and so-called "upconverting nanoparticles," which convert a pair of lower-energy photons into a single higher-energy photon. The nanocrystals were dispersed into a range of molten salts, including halide, nitrate, and thiocyanate compounds. Halide salts incorporate one or more of the five halogen elements: chlorine, iodine, bromine, fluorine, and astatine. Nitrate salts contain nitrogen bonded to oxygen, while thiocyanates contain sulfur, carbon, and nitrogen.

Small-angle x-ray scattering (SAXS) experiments were performed at XSD beamline 12-ID-B of the APS on a colloid consisting of platinum (Pt) nanocrystals dispersed within a mixture of molten chloride salts consisting of aluminum chloride, sodium chloride, and potassium chloride ($AlCl_3$/NaCl/KCl). The SAXS x-ray pattern of the chloride salts with dispersed Pt nanocrystals was compared to the SAXS pattern of a known colloid containing identical Pt nanoparticles dispersed in an organic solvent. The two patterns were quite similar, indicating that the Pt/chloride salt solution had successfully formed a colloid.

The researchers relied on a combination of experimental data and molecular dynamics simulations to find the underlying mechanism producing the molten salt colloids. They found that the stability of the colloids was directly related to the chemical affinity between ions in the molten salt and the surfaces of the nanocrystals. Figure 1 (left) illustrates how the presence of ion affinity for nanocrystals determines colloidal stability. In some cases, colloidal stability could be seen visually (Fig. 2, right).

Certain types of molten salts failed to support the formation of colloids altogether. For instance, the researchers were unable to get any combination of molten nitrate salts and nanocrystals to form a colloid.

Looking ahead, the researchers note that the ability to use a variety of diverse nanocrystals (such as nanocrystalline semiconductors) in molten salts may find application to several energy-related technologies. The researchers also note that using liquid metals in place of molten inorganic salts could result in composite metals of superior stiffness and durability.

— Philip Koth

See: Hao Zhang[1], Kinjal Dasbiswas[1], Nicholas B. Ludwig[1], Gang Han[2], Byeongdu Lee[3], Suri Vaikuntanathan[1], amd Dmitri V. Talapin[1,3]*, "Stable colloids in molten inorganic salts," Nature **542**, 328 (16 February 2017). DOI: 10.1038/nature21041

Author affiliations: [1]The University of Chicago, [2]University of Massachusetts Medical School, [3]Argonne National Laboratory

Correspondence:

* dvtalapin@uchicago.edu

This work was supported by the National Science Foundation (NSF; DMR-1611371), Air Force Office of Scientific Research (AFOSR; FA9550-14-1-0367), Department of Defense Office of Naval Research (grant number N00014-13-1-0490), and by the II-VI Foundation. G.H. acknowledges support from the National Institutes of Health (R01 MH103133) and the Human Frontier Science Program (RGY-0090/2014). N.B.L acknowledges support from the University of Chicago Research Computing Center. The work used facilities supported by the NSF Materials Research Science and Engineering Center (DMR-14-20703). This work was performed, in part, at the Center for Nanoscale Materials, a U.S. Department of Energy (DOE) Office of Science User Facility, and supported by the U.S. DOE Office of Science, under Contract No. DE-AC02-06CH11357. This research used resources of the Advanced Photon Source, a U.S. DOE Office of Science user facility operated for the DOE Office of Science by Argonne National Laboratory under Contract No. DE-AC02-06CH11357.

12-ID-B • XSD • Chemistry, materials science, life sciences, polymer science, physics • Small-angle x-ray scattering, grazing incidence small-angle scattering, wide-angle x-ray scattering, grazing incidence diffraction • 7.9-14 keV • On-site • Ac

Single-Crystal Carbon Nanothreads Made under Uniaxial Pressure

Under pressure, coal turns into diamond when heated. But what if that pressure is slightly higher in one direction? By pushing on benzene molecules with pressure thousands of times that of the atmosphere more slowly than before, researchers working at the APS produced long nanothreads of single-crystal carbon that are hundreds of microns in length, providing new insights into structure-function relationships in a material that might have the highest known specific strength to date. Previous reports of carbon nanothreads demonstrate the highest known specific strength, but they are also flexible, unaffected by defects, and highly resilient. Both crystallinity and length scale of a material affect many materials properties, including mechanical, electrical, and optical, so understanding structure-function relationships is crucial to materials design. Control over crystallinity via stress gives researchers a new way to fine-tune properties of functional materials.

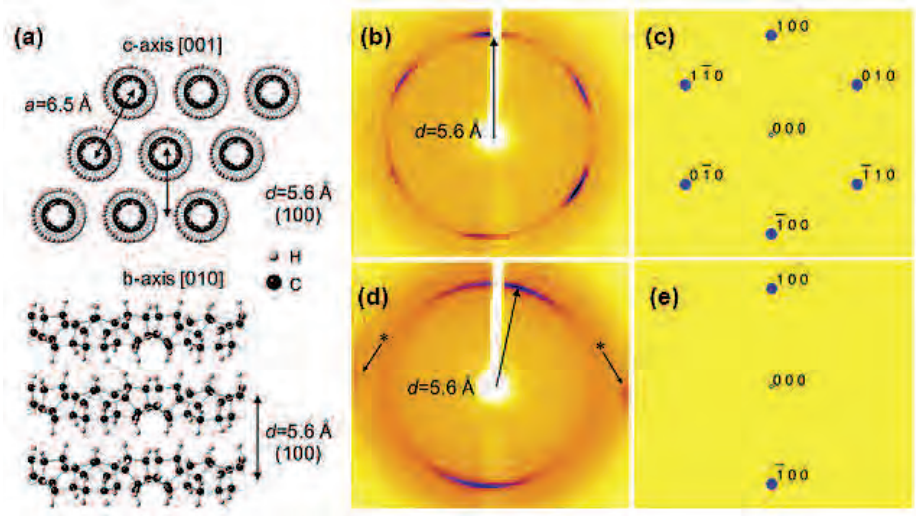

Fig. 1. Predicted and observed nanothread crystal diffraction patterns. (a) A polytwistane crystal structure is one of two possibilities for nanothread packing. It is viewed down the hexagonal c-axis, along which nanothreads are parallel, and as a side view down the b-axis. (b) X-ray diffraction for a nanothread crystal synthesized at Oak Ridge National Laboratory from polycrystalline benzene shows a hexagonal pattern that matches (c) predicted for the c-axis of the polytwistane crystal. (d) Diffraction after 90° rotation of the nanothread crystal, along the b-axis, matches the pattern predicted in (e). From X. Li et al., J. Am. Chem. Soc. **139**, 16343 (2017). © 2017 American Chemical Society

16-ID-B • HP-CAT • Materials science, geoscience, chemistry, physics • Microdiffraction, single-crystal diffraction, high-pressure diamond anvil cell • 18-60 keV • On-site • Accepting general users •

Carbon nanothreads have been previously made from benzene through this kind of "mechanochemical" synthesis, but none have created single crystals. Instead, methods that applied pressure slowly and equally from all directions made polycrystalline carbon nanothreads with many small crystals oriented in different directions. This is expected, as most carbon-based solids are polycrystalline or amorphous, with a few exceptions found in diamond, graphite, and some fullerenes and polymers.

But the researchers from Argonne, The Pennsylvania State University, the Carnegie Institute of Washington, Cornell University, Oak Ridge National Laboratory, and the European Spallation Source found that slowly applying pressure to benzene along one axis causes molecules to fall in line as they form new carbon-carbon bonds. The effect was so robust, oriented crystals even formed when benzene was prepared as a polycrystalline mixture. This synthesis could be a general route to achieving long-range crystallinity in carbon-based functional materials.

Placed in either a Paris-Edinburgh press or a diamond anvil cell, liquid benzene was compressed with pressures up to 23 GPa at room temperature. The pressure was ramped up slowly over the course of 8 h, at first 2-3 GPa/h, then less than 1 GPa/h. Pressure was released at the same slow rate to recover stable nanothread samples for optical microscopy.

Polarization analysis under a microscope showed thin flakes of material tens to hundreds of microns in each direction with parallel striations. Because neighboring threads have slightly different crystal alignments, strong birefringence, or changes in the absorption of polarized light, was observed as cross-polarizers were rotated. Much like graphene, small sections could be exfoliated off of the larger sample, creating bundles of several nanothreads.

"Nanothreads" cont'd. on page 162

Bridging the Gap in Dual Metal Nanowires

Catalysts are a cornerstone of industrial chemistry, efficiently transforming feedstocks into chemicals that permeate the modern world. Discovery of new catalysts with improved catalytic activity and chemical selectivity drive increases in productivity, efficiency, and cost-savings. An emerging class of nanoscale catalysts supported by metal-organic frameworks (MOFs) provides a new route to improving catalyst selectivity due to the well-defined atomic structure of the catalyst. To resolve the atomic structure of nanocatalysts made using atomic layer deposition (ALD) on MOFs, researchers combined complementary structural and computational analyses to build the complete picture of catalytic Ni-Hydroxo clusters on a zirconia-based MOF. Critical structural tools for this research included x-ray scattering and spectroscopy measurements at the APS. They discovered a heterobimetallic nanowire structure formed within the MOF, offering a new general approach for the construction of nanowires with specific structures using ALD on MOFs.

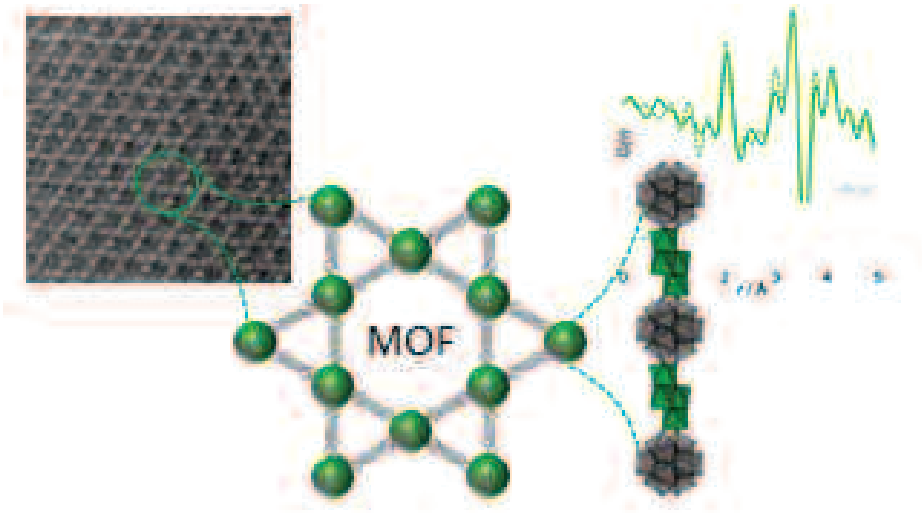

Fig. 1. A scanning transmission electron micrograph (left) of a zirconium-based metal-organic framework (MOF, center), NU-1000, containing Zr6-based nodes (grey clusters) with hexagonal and triangular pores shown. The MOF was functionalized with nickel-hydroxo clusters (green clusters, right) to generate heterobimetallic nanowires (right). A representative differential pair distribution function (green line, upper right) is shown, derived from x-ray total scattering experiments at beamline 11-ID-B of the APS and helped resolve the structure of the nanowires.

10-ID-B • MR-CAT • Materials science, environmental science, chemistry • X-ray absorption fine structure, time-resolved x-ray absorption fine structure, microfluorescence (hard x-ray) • 4.3-27 keV, 4.8-32 keV, 15-65 keV • On-site • Accepting general users •

11-ID-B • XSD • Chemistry, environmental science, materials science • Pair distribution function, high-energy x-ray diffraction • 58.66 keV, 86.7 keV • On-site • Accepting general users •

17-BM-B • XSD • Chemistry, materials science • Powder diffraction, pair distribution function • 27-51 keV • On-site • Accepting general users •

20-BM-B • XSD • Materials science, environmental science, chemistry • X-ray absorption fine structure, microfluorescence (hard x-ray) • 2.7-32 keV, 2.7-35 keV • On-site • Accepting general users •

MOFs are structurally regular, with an open crystalline lattice defining a regular network of internal pores with high surface area of well-defined surface chemistry. Atomic layer deposition of catalysts onto MOFs can produce well-defined structures with intriguing catalytic function; but local disorder within the structure makes it difficult to resolve the structure of emerging MOF-based catalysts, hindering efforts to understand, and improve, their reactivity.

The team from the Inorganometallic Catalyst Design Center, an Energy Frontier Research Center funded by the U.S. Department of Energy involving partners from Argonne, the University of Minnesota, the Pacific Northwest National Laboratory (PNNL), and Northwestern University focused on NU-1000, a zirconium-based MOF with large pores, strong zirconium-oxygen bonds, and high chemical and thermal stability. Using a two-step ALD process, the researchers deposited catalytic nickel clusters onto the MOF, replacing hydroxyl groups. To work out the details of deposition, the researchers analyzed the catalyst's structure via multiple complementary methods.

As a first step, the researchers performed synchrotron x-ray scattering on NU-1000 before and after nickel functionalization: powder x-ray diffraction on XSD beamline 17-BM-B and total scattering data for pair distribution function (PDF) analysis on XSD beamline 11-ID-B, both at the APS (Fig. 1). Based on the relatively broad diffraction data of

"Bridging" cont'd. on page 162

"Nanothreads" cont'd. from page 160

While phase I benzene was observed in the Paris-Edinburgh press, a mixture of phase I and phase II benzene was prepared in the diamond anvil cell, as was pure phase II. To study the reaction of this polycrystalline starting material that remarkably leads to long-range order, *in situ* synchrotron x-ray diffraction (XRD) experiments were performed on the diamond anvil cell samples at the HP-CAT beamline 16-ID-B at the APS.

In samples made by every method, XRD revealed 6-fold arcs, indicating a hexagonal structure expected for benzene-derived carbon materials (Fig. 1). Because x-rays were parallel to the compression axis, these data also showed that the *c*-axis of nanothreads, which runs along their length, is aligned with the direction that pressure is applied. The stress imposed on just one axis by high pressure, or uniaxial stress, selects the direction along which the crystallization reaction proceeds.

Density functional theory and simulations based on lattice parameters from the XRD patterns allowed the team to narrow the possible thread structures to just two: polytwistane and tube.

The consistency with which crystallization was guided by uniaxial stress — regardless of the type of opposed-anvil apparatus or initial benzene structure — indicates this method could be generalized to create many carbon-based solids. The researchers have already expanded this work to carbon nitride made from pyridine. Furthermore, the researchers suggest that stress could be applied in a stepwise fashion from different directions to guide complex patterns of crystallization, potentially unlocking new materials properties. *— Amanda Grennell*

See: Xiang Li[1], Maria Baldini[2], Tao Wang[1], Bo Chen[3], En-shi Xu[1‡], Brian Vermilyea[1], Vincent H. Crespi[1], Roald Hoffmann[3], Jamie J. Molaison[4], Christopher A. Tulk[4], Malcolm Guthrie[5], Stanislav Sinogeikin[2], and John V. Badding[1]*, "Mechanochemical Synthesis of Carbon Nanothread Single Crystals," J. Am. Chem. Soc. **139**, 16343 (2017). DOI: 10.1021/jacs.7b09311
Author affiliations: [1]The Pennsylvania State University, [2]Carnegie Institution of Washington, [3]Cornell University, [4]Oak Ridge National Laboratory, [5]European Spallation Source ‡Present address: George Washington University
Correspondence:
* jbadding@chem.psu.edu

Work was supported as part of the Energy Frontier Research in Extreme Environments (EFree) Center, an Energy Frontier Research Center funded by the U.S. Department of Energy (DOE) Office of Science under award number DE-SC0001057. Sample synthesis was performed at the Spallation Neutrons and Pressure beamline at the Spallation Neutron Source, a DOE Office of Science user facility operated by the Oak Ridge National Laboratory. HP-CAT operations are supported by DOE-NNSA under Award No. DE-NA0001974, with partial instrumentation funding by the National Science Foundation. This research used resources of the Advanced Photon Source, a U.S. DOE Office of Science user facility operated for the DOE Office of Science by Argonne National Laboratory under Contract No. DE-AC02-06CH11357.

"Bridging" cont'd. from page 161

functionalized NU-1000, the researchers concluded it had increased distortions compared to NU-1000. The diffraction data provided a low-resolution map of where the nickel was deposited, indicating localization within the small pores of the NU-1000 framework, while the PDF data provided precise information on the Ni-O and Ni…Ni atom distances. Next, the team performed x-ray absorption spectroscopy (XANES and EXAFS), collecting transmission geometry XAS measurements at the MR-CAT 10-ID-B and the XSD 20-BM-B beamlines, also at the APS. These data demonstrated that on average, the nickel atoms were 6-coordinated (NiO_6) with a slightly distorted octahedral geometry.

Using structural information from the x-ray data, the researchers were able to distinguish the computational models that best matched the experimental observations. Adjacent zirconia nodes appeared to be bridged by the nickel clusters, creating bimetallic nanowires. The tight binding and separation between clusters may be key to catalytic function, and appears to mitigate deactivation of the catalyst during the hydrogenation of light olefins.

The researchers suggest it may be possible to dissolve the MOF to isolate the nanowires and develop a novel approach to nanowire synthesis. Because ALD can work with a variety of chemicals, such an approach may produce a rich menagerie of bimetallic nanowires. *— Erika Gebel Berg*

See: Ana E. Platero-Prats[1], Aaron B. League[2], Varinia Bernales[2], Jingyun Ye[2], Leighanne C. Gallington[1], Aleksei Vjunov[3], Neil M. Schweitzer[4], Zhanyong Li[4], Jian Zheng[3], B. Layla Mehdi[3], Andrew J. Stevens[3], Alice Dohnalkova[3], Mahalingam Balasubramanian[1], Omar K. Farha[4,6], Joseph T. Hupp[4], Nigel D. Browning[3,5], John L. Fulton[3], Donald M. Camaioni[3], Johannes A. Lercher[3,7], Donald G. Truhlar[2], Laura Gagliardi[2], Christopher J. Cramer[2], and Karena W. Chapman[1]*, "Bridging Zirconia Nodes within a Metal−Organic Framework via Catalytic Ni-Hydroxo Clusters to Form Heterobimetallic Nanowires," J. Am. Chem. Soc. **139**, 10410 (2017). DOI: 10.1021/jacs.7b04997
Author affiliations: [1]Argonne National Laboratory, [2]University of Minnesota,[3]Pacific Northwest National Laboratory, [4]Northwestern University, [5]University of Washington, [6]King Abdulaziz University, [7]Technische Universität München
Correspondence:
* chapmank@aps.anl.gov

This work was supported as part of the Inorganometallic Catalysis Design Center, an Energy Frontier Research Center funded by the U.S. Department of Energy (DOE) Office of Science-Basic Energy Sciences, under Award No. DE-SC0012702. A.E.P.P. acknowledges a Beatriu de Pinós fellowship (BP-DGR 2014) from the Ministry of Economy and Knowledge from the Catalan Government. STEM experiments were supported by the Chemical Imaging Initiative (CII) Laboratory Directed Research and Development Program at PNNL, which is a multiprogram national laboratory operated by Battelle for the U.S. DOE under Contract DE-AC05-76RL01830. The STEM work was performed using the Environmental Molecular Sciences Laboratory, a national scientific user facility sponsored by the DOE Office of Biological and Environmental Research and located at MR-CAT operations are supported by the DOE and the MR-CAT member institutions. This research used resources of the Advanced Photon Source, an Office of Science user facility operated for the U.S. DOE Office of Science by Argonne National Laboratory, and was supported by the U.S. DOE under Contract No. DE-AC02-06CH11357, and by the Canadian Light Source and its funding partners.

Novel Accelerator & X-ray Techniques & Instrumentation

Spotting Crystals and Non-Crystals in One Shot

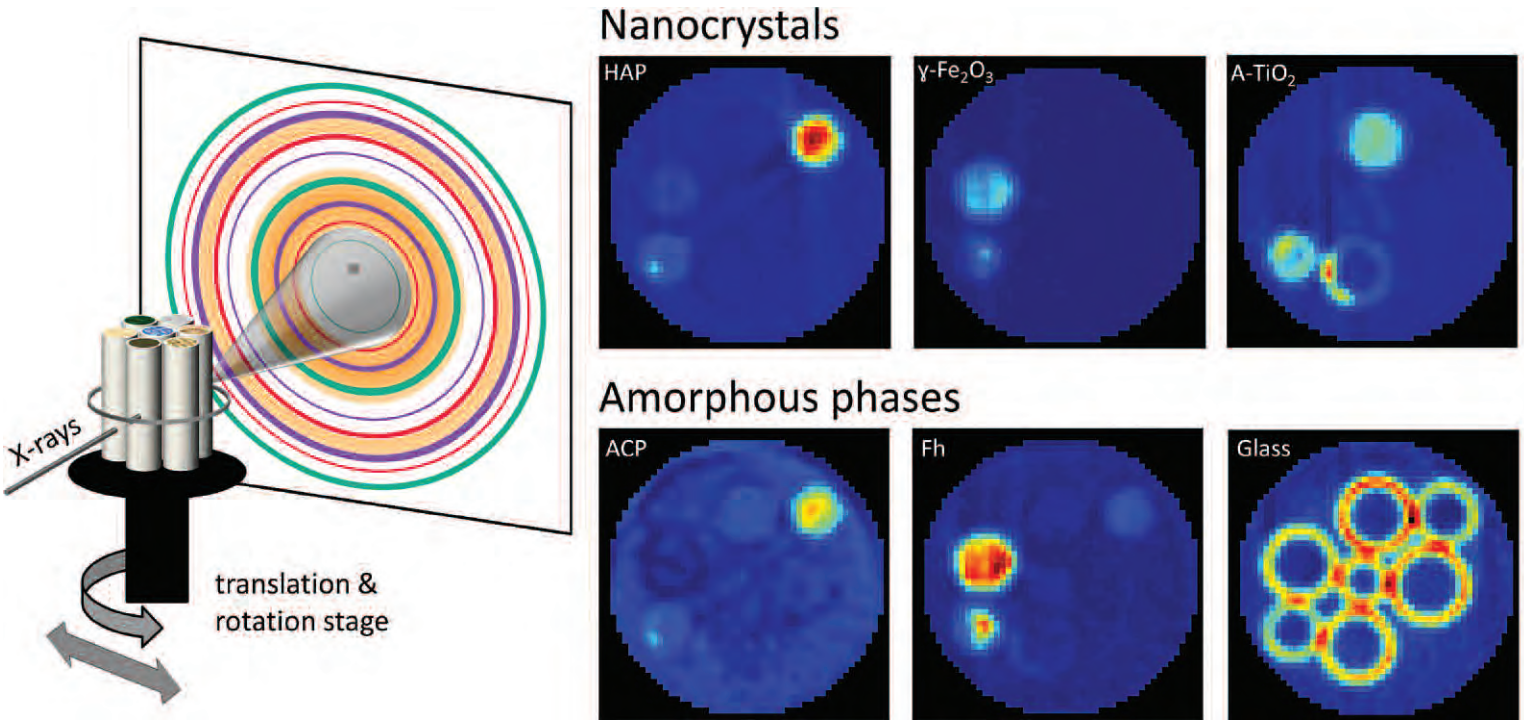

Fig. 1. Researchers employed diffraction scattering computed tomography to map out crystalline and amorphous phases in a material. In the experiments, the sample was exposed to a beam of x-rays at the APS and the diffraction signal was recorded (diagram on left). By translating and rotating the sample, the researchers were able to identify the location of four different crystalline phases (right, top row) and four different amorphous phases (right, bottom row). Credit: Henrik Birkedal, adapted from J. Appl. Cryst. **50**, 192 (2017). © 2017 International Union of Crystallography

Many biological tissues and electronic devices contain a hodgepodge of components that are both crystalline and amorphous (without defined shape). X-ray diffraction techniques can pinpoint the crystals, but they are often blind to the disordered arrangements in the surrounding amorphous substances. A new synchrotron x-ray research method based on diffraction scattering computed tomography (DSCT) is able to measure both crystalline and amorphous phases simultaneously. In experiments performed at the APS, researchers produced a spatially-resolved map of a multi-component object consisting of four different crystals and four different amorphous materials. Having a full picture like this of an object, such as a bone or a fuel cell, could help understand how it works or — as the case may be — how it fails.

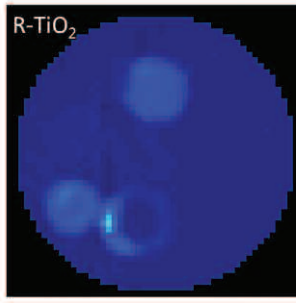

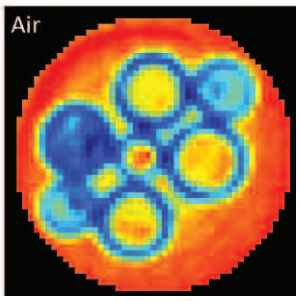

The idea of DSCT has been around for a long time, but the technique only became widely applicable within the last decade. Several groups around the world are using DSCT to study complex materials like biominerals, batteries, catalysts, and cements. The method is similar in principle to the computed tomography that hospitals use to make detailed maps of a patient's head or internal organs. To create a CT scan, multiple images of the target object are taken from different angles. The various components within the target, such as bone and muscle, are identified by the way they absorb x-ray light. DSCT also creates a map from multiple images, but it utilizes diffraction rather than absorption as its signal. Diffraction is the angle-dependent scattering of x-rays passing through a material. Diffraction imaging is often used to identify crystalline components within an object, as the ordered structure of a crystal produces sharp diffraction peaks that act as a kind of chemical fingerprint. However, diffraction is less well-suited for picking out amorphous components, which tend to produce a less well-defined diffraction signal.

To capture the full range of components in a material, a team of researchers from Aarhus University (Denmark), Northwestern University, and Argonne have developed a new method for analyzing DSCT data. Instead of using only the sharp diffraction peaks from the crystalline phases, the researchers also extract the broad diffraction patterns that characterize amorphous phases. To demonstrate the method, the team constructed a target sample with seven capillary tubes. Each tube contained different materials, some of which were crystalline (e.g., anatase and hydroxyapatite) while others were amorphous (e.g., air and ferrihydrite). The sample was exposed to a focused x-ray beam at XSD beamline 1-ID-B,C,E at the APS, and the diffraction signal was recorded over an angular range of roughly 13° using four detectors. To minimize absorption, the researchers employed high-energy (42.7 keV) x-rays, which are only available at APS and a few other synchrotron light sources in the world.

Utilizing translation and rotation stages, the team took over 3000 diffraction images of the sample at different positions and from different angles. The resulting map revealed the telltale peaks of the four crystalline phases at their corresponding locations within the sample (Fig. 1). Once a particular crystal component was identified, the researchers used the widths of the diffraction peaks to infer the size and shape of the crystals. This analysis technique, which is called "Rietveld refinement," generates a model that fits the various diffraction peaks, while also accounting for the background between the peaks. In previous studies, this background was ignored, but in this case, it was reanalyzed to investigate the non-crystalline materials in the sample. By comparing the background to standardized data on amorphous materials, the team was able to identify the four amorphous phases that had been placed in the sample.

The team plans to use their DSCT method to study bone and other biological materials, which are notoriously difficult to analyze due to the wide variety of components that they contain. In particular, the researchers want to apply a load to bone samples and observe how much of the weight different parts of the bone carry. Studies like this should help in relating structure — i.e., where crystalline and amorphous phases are located — to function.

— Michael Schirber

See: Mie Elholm Birkbak[1], Ida Gjerlevsen Nielsen[1], Simon Frølich[1], Stuart R. Stock[2], Peter Kenesei[3], Jonathan D. Almer[3], and Henrik Birkedal[1]*, "Concurrent determination of nanocrystal shape and amorphous phases in complex materials by diffraction scattering computed tomography," J. Appl. Cryst. **50**, 192 (2017).
DOI: 10.1107/S1600576716019543
Author affiliations:
[1]Aarhus University, [2]Northwestern University, [3]Argonne National Laboratory
Correspondence:
* hbirkedal@chem.au.dk

Support from the Human Frontiers Science Program, the Danish Research Councils for Independent Research in the form an Elite-Forsk Travel Scholarship to SF, and the Danish Agency for Science, Technology and Innovation (DANSCATT) is gratefully acknowledged. This research used resources of the Advanced Photon Source, a U.S. Department of Energy (DOE) Office of Science User Facility operated for the DOE Office of Science by Argonne National Laboratory under contract No. DE-AC02-06CH11357.

1-ID-B,C,E • XSD • Materials science, physics, chemistry • High-energy x-ray diffraction, tomography, small-angle x-ray scattering, fluorescence spectroscopy, pair distribution function, phase contrast imaging • 41-136 keV, 45-116 keV • On-site • Accepting general users •

Achieving Better Resolution for X-ray Microscopy with a Multilayer Laue Lens

As the versatility and power of x-ray synchrotron facilities have continued to grow, so has the demand for ever more sensitive and higher-resolution x-ray imaging at the nanoscale. However, achieving the Abbe diffraction limit to resolution has proven far more elusive with hard x-rays than with visible light, because the properties of x-rays demand different approaches to fabricating optics. One promising avenue is the multilayer Laue lens (MLL), which can focus hard x-rays to very small dimensions at a theoretical limit below 1 nm. But MLLs are also challenging to fabricate with a suitable numerical aperture (NA) because of stresses that build up and lead to cracking in their layered microstructures. Researchers from Fraunhofer IWS Dresden (Germany), the Leibniz-Institut für Polymerforschung Dresden e.V. (Germany), and Argonne reported on the fabrication and testing of a three-material MLL with a 50-μm thickness and an efficiency of almost 40%.

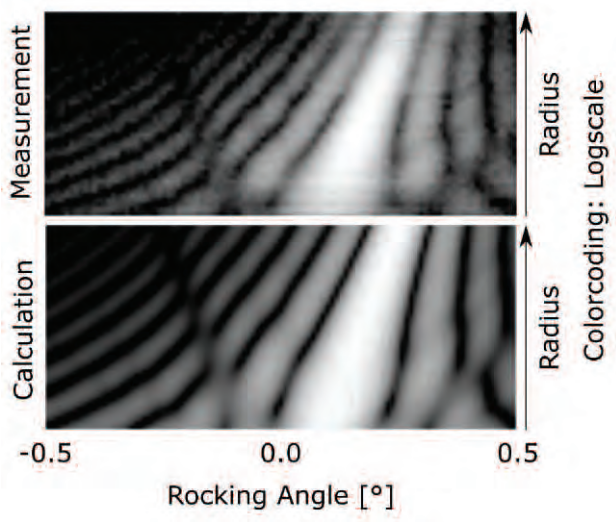

Fig. 1. A comparison between calculation and actual measurement of the MLL in log-scale.

Multilayer Laue lenses are essentially based on one-dimensional Fresnel zone plate optics, consisting of deposited nanoscale layers of alternating absorbing (often tungsten) and spacer (usually silicon) materials, sometimes with additional transition layers between them. The MLL is built up from hundreds to thousands of such layer pairs with increasingly smaller width. The choice and combination of materials directly affect the inherent stresses of the MLL and thus the achievable thickness of the multilayer stack. In the current work, the research team used magnetron sputtering deposition of molybdenum (absorber) and silicon (spacer) layers with carbon as a transition layer, arranged in a Mo/C/Si/C structure for each period. Diffraction efficiency measurements were conducted at the XSD 1-BM-B,C beamline of the APS, employing an x-ray energy of 12 keV.

The experimenters found that this particular MLL structure offers some notable strengths. Because high resolution requires a large numerical aperture of the lens, which in a MLL is equivalent to the total stack thickness, a thicker multilayer stack means a larger NA and therefore higher resolution. The three-material, four-layer structure allowed the manufacture of a 50-μm-thick stack equivalent to 6000 Fresnel zones, totaling 12,000 individual layers. Compared to a typical two-material system, the use of three different materials allows a lower stress multilayer stack because the relative layer thicknesses among the different materials can be controlled. This allows the fabrication of structures with larger thicknesses and therefore potentially larger NA.

This MLL displayed a high degree of mechanical stability and low stress, enabling it to achieve a total diffraction efficiency of 39.8% (focused) and 39.9% (defocused). These measurements are much higher than the previously achieved efficiencies of 14% with a flat lens and 27% with a wedged lens, with close agreement between the experimental data and the efficiencies of a bilayer Mo/Si MLL calculated with coupled-wave theory. Although the current MLL was flat, the investigators calculate that a wedged MLL with the same material system could achieve approximately 70% efficiency at the given x-ray energy. Also, the stability demonstrated by this example shows that far thicker three-material multilayer stacks can be reasonably fabricated.

The work opens new possibilities for high-efficiency, large-aperture multilayer Laue lenses with large working distances, which will greatly expand the resolution and capabilities of hard x-ray microscopy at the nanoscale.

— Mark Wolverton

See: A. Kubec[1]*, J. Maser[2], P. Formánek[3], V. Franke[1], S. Braun[1], P. Gawlitza[1], A. Leson[1], and A. Macrander[2], "Fabrication and efficiency measurement of a Mo/C/Si/C three material system multilayer Laue lens," Appl. Phys. Lett. **110**, 111905 (2017).
DOI: 10.1063/1.4978610
Author affiliations: [1]Fraunhofer IWS Dresden, [2]Argonne National Laboratory, [3]Leibniz-Institut für Polymerforschung Dresden e.V.
Correspondence:
* adam.kubec@iws.fraunhofer.de

This work was supported by the U.S. Department of Energy (DOE)-Basic Energy Sciences, under Contract No. DE-AC-02-06CH11357 and used resources of the Advanced Photon Source, a U.S. DOE Office of Science user facility operated for the U.S. DOE Office of Science by Argonne National Laboratory under Contract No. DE-AC02-06CH11357.

Mapping Elemental Composition and Surface Topography with Synchrotron X-ray Scanning-Tunneling Microscopy

What if you could identify elements atom by atom as your eyes scanned across any material? Researchers recently showcased their ability to do just that by imaging cobalt nanoclusters with a combination of scanning-tunneling microscopy and synchrotron x-ray absorption spectroscopy at the APS. Their work can be extended to map any element with near-atomic resolution and investigate quantum effects within nanomaterials one particle at a time.

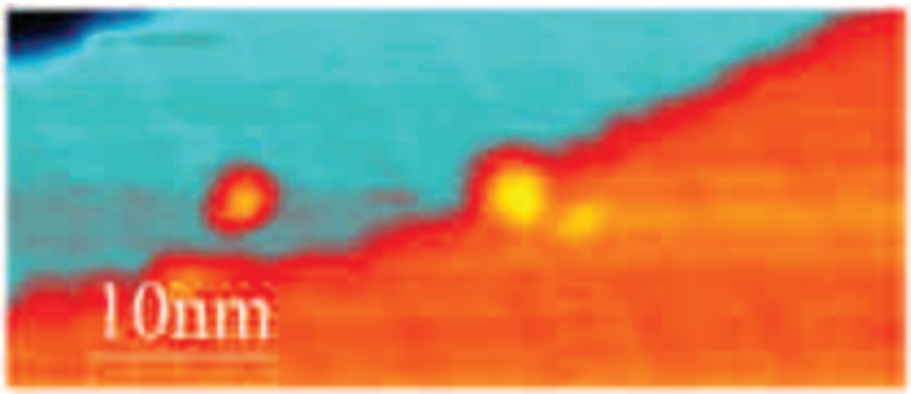

Fig. 1. Elemental mapping of a gold surface (cyan) with cobalt clusters on top (red), measured with the SX-STM. The cluster is about 4 nm wide.

Since seminal work on scanning tunneling microscopy (STM) won the Nobel Prize in 1986, the technique has revealed the shape of increasingly tiny bits of matter. When an atomically sharp tip is brought within a nanometer of a sample, electrons can hop, or tunnel, from the sample to the tip, creating a small current. Due to the nature of tunneling, the closer the tip is to the sample, the higher the current is. Measuring current as the tip scans across the surface generates a topographical map.

Researchers from Ohio University and Argonne found, if the sample is simultaneously scanned and bombarded with x-rays of the right energy, the STM current is sensitive to both sample topography and element identity. Tuning x-ray energy for specific elements would therefore allow elemental mapping on a very small scale. This technique could reveal key nuances of structure-function relationships in nanoscale materials.

The team started with a special nanofabricated tip sheltered from the high-energy x-ray beam focused on the junction between the tip and the sample. Evaporation of cobalt onto a gold substrate created nanoclusters of cobalt about two atomic layers thick. The team placed their sample and tip in the synchrotron x-ray STM (SX-STM) system at the CNM/XSD beamline 26-ID-C at the APS.

The presence of cobalt was confirmed by tuning the x-ray energy to the cobalt K-edge, which is the binding energy of core electrons in the K shell. The energy of these x-rays is just enough to ionize electrons from cobalt atoms. With the STM tip placed 400 nm away, much farther than usual, the researchers saw an increase in current through the tip once x-ray energies reached the K-edge of cobalt. Because the current jump occurred precisely at an x-ray energy associated only with cobalt, the team was confident that cobalt existed on the substrate.

Once they brought the STM tip within about 5 Å of the sample, contributions to tip current came from multiple new sources. Primarily, electrons that just barely pushed above the Fermi level of cobalt were now able to tunnel to the tip. This “tunnel current” could be separated from the current arising from completely ionized electrons. Both currents were monitored as x-ray energies varied from just below the cobalt K-edge to well after it.

The STM current in the absence of x-ray absorption was also monitored by chopping the x-ray beam at 3000 Hz. Thus, the topography of the sample was collected nearly simultaneously with the x-ray induced tip currents. Scanning across the surface revealed clusters of cobalt several nanometers wide.

While the tip was directed in a straight line across the sample and held at a constant height, the team observed the tip approach cobalt clusters. As it approached, the x-ray induced tunnel current jumped up, but only when x-ray energy was greater than the K-edge energy. The tunnel current continued to increase as it approached the top of the cluster, while the current coming from the gold substrate did not change.

The behavior of the tunnel current

“Mapping” cont’d. on page 169

Making X-ray Transition-Edge Sensors Sharper

From detecting x-rays from outer space to elemental mapping at the nanoscale, transition-edge sensors (TES) are essential tools for scientific discovery. These devices measure the electrical resistance of superconducting materials close to their transition temperature, a regime in which small changes in temperature result in large changes in resistance. The energy of an x-ray photon absorbed by a TES is thus converted to heat and the resulting change in resistance is proportional to x-ray energy. While bismuth (Bi) excels as an x-ray absorbing component for TES devices, the energy spectrum generated by these devices suffers from an unexpected non-Gaussian line shape, specifically a low-energy tail, which limits the device's ability to detect and map trace elements. However, by electroplating the bismuth film rather than preparing it via evaporation, researchers have recently eliminated this low-energy tail. Using high energy x-ray diffraction at the APS, these researchers found order-of-magnitude larger grain sizes in the electroplated bismuth, resulting in trapping of thermal energy in the absorber, and thus the desired spectral line shape.

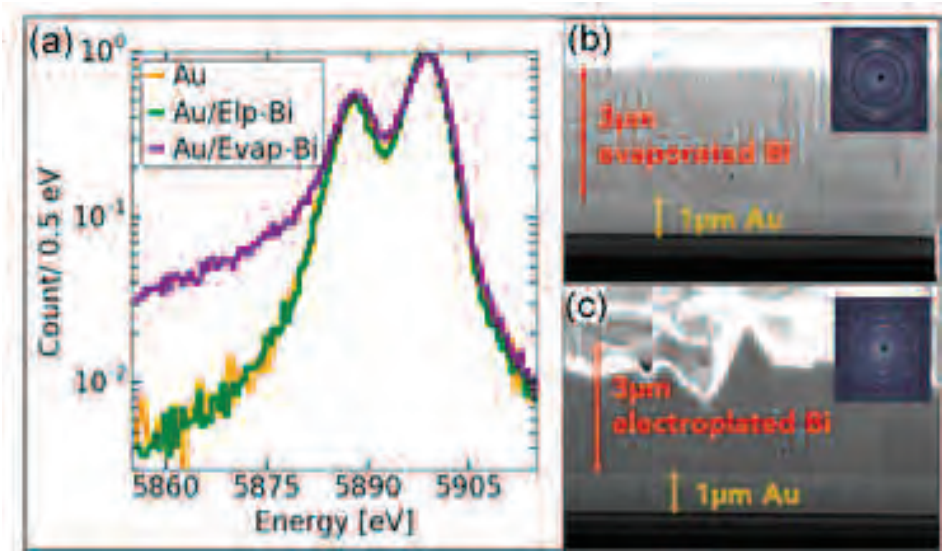

Fig. 1. (a) Comparison of the Mn Kα spectrum measured by the three TES devices, normalized at the peak maxima. A low-energy tail is observed only in the Au/evaporated-Bi absorber devices (b) Scanning electron micrograph of the Au/evaporated-Bi absorber. Inset: X-ray diffraction pattern of electroplated-Bi. (c) Scanning electron micrograph of the Au/electroplated-Bi absorber cross-sections. Inset: X-ray diffraction pattern of electroplated-Bi.

1-ID-B,C,E • XSD • Materials science, physics, chemistry • High-energy x-ray diffraction, tomography, small-angle x-ray scattering, fluorescence spectroscopy, pair distribution function, phase contrast imaging • 41-136 keV, 45-116 keV • On-site • Accepting general users •

To isolate the effect of bismuth morphology, the team of researchers from Argonne National Laboratory, Northwestern University, the National Institute of Standards and Technology, and the University of Colorado compared three TES devices prepared in near-identical fashion on the same die. In each device, the absorber was deposited onto a 1-μm-thick film of gold, which was connected to a Mo/Cu superconductor through a copper bank. This ensured thermal coupling between the absorber and the superconductor was identical. The bismuth film was either electroplated (elp-Bi) or evaporated (evap-Bi) into a 3-μm-thick film onto the gold. On the third device, no bismuth was added, and the gold acted alone as an x-ray absorber.

The non-Gaussian nature of the spectrum generated by the conventionally prepared Au/evap-Bi TES is shown in Fig. 1a (purple). Instead of two overlapping Gaussians expected from the Kα lines of the Mn x-ray source, a significant tail is seen on the low-energy (LE) side of the spectrum, causing a simple Gaussian fit to fail. This LE tail is not observed in the Au/elp-Bi (green) nor in the Au-only

Cont'd. on the next page

devices (yellow), and a Gaussian function models both line shapes well.

Turning to morphology, the team examined focused-ion beam cross-sections of Bi films in a scanning electron microscope. Figure 1 shows the striking difference in morphology they immediately found; the evap-Bi (b) is made of narrow column-like grains, whereas the elp-Bi (c) contains much larger, irregularly shaped grains. The grain size was measured using high-energy x-ray diffraction (XRD) at the XSD 1-ID-B,C,E beamline of the APS. The resulting diffraction patterns are shown in the insets of Figs. 1b and 1c. While these diffraction patterns are both dominated by the same monoclinic crystal structure of Bi, substantial differences in the patterns, such as intense spots observed only in elp-Bi, reflect differences in grain size and shape. The grains sizes were measured to be 30 nm in evap-Bi and over 700 nm in elp-Bi.

This order-of-magnitude difference in grain size is the key the researchers needed to explain the LE tail. LE tail indicates that not all of the x-ray energy absorbed by the Bi film is registered by the TES. Additionally, the percentage of the total signal observed in the LE tail was found to be proportional to x-ray energy. Several energy-loss mechanisms were eliminated by the researchers as either being inconsistent with this energy dependence or unlikely in this TES architecture. But the smaller, and therefore more numerous, grains of evap-Bi present a new loss mechanism: the trapping of heat carriers at grain boundaries.

After absorption and thermalization of an x-ray, its energy is carried to the TES as heat. But in evap-Bi, heat transfer within the Bi layer itself is hindered significantly by smaller grains. The dependence of LE tail signal on x-ray energy is consistent with this loss mechanism; higher energy x-rays create larger secondary electron clouds, which would interact with more grain boundaries, result in more loss and bigger LE tails. Furthermore, electronic measurements show that elp-Bi is a semimetal but evap-Bi is a semiconductor, supporting the idea that more trapping occurs in evap-Bi.

With the LE tail eliminated, weak signals in x-ray spectra are more likely to be resolved with simple Gaussian fits. TES devices with electroplated bismuth will have lower detection levels and be better able to identify elements and chemical states within highly complex mixtures. This development, when combined with advances in the nanofocusing capabilities of the upgraded APS, will prove to be especially exciting for chemical state mapping of elaborate materials at the nanoscale. *— Amanda Grennell*

See: Daikang Yan[1,2], Ralu Divan[1], Lisa M. Gades[1], Peter Kenesei[1], Timothy J. Madden[1], Antonino Miceli[1]*, Jun-Sang Park[1], Umeshkumar M. Patel[1], Orlando Quaranta[1,2], Hemant Sharma[1], Douglas A. Bennett[3], William B. Doriese[3], Joseph W. Fowler[3], Johnathon D. Gard[3,4], James P. Hays-Wehle[3], Kelsey M. Morgan[3,4], Daniel R. Schmidt[3], Daniel S. Swetz[3], and Joel N. Ullom[3,4], "Eliminating the non-Gaussian spectral response of X-ray absorbers for transition-edge sensors," Appl. Phys. Lett. **111**, 192602 (2017).
DOI: 0.1063/1.5001198
Author affiliations: [1]Argonne National Laboratory, [2]Northwestern University, [3]National Institute of Standards and Technology, [4]University of Colorado
Correspondence: * amiceli@anl.gov

This work was supported by the Accelerator and Detector R&D program in the Basic Energy Sciences Scientific User Facilities Division at the U.S. Department of Energy (DOE) Office of Science. This research used resources of the Advanced Photon Source and Center for Nanoscale Materials, U.S. DOE Office of Science User Facilities operated for the DOE Office of Science by Argonne National Laboratory under Contract No. DE-AC02-06CH11357.

"Mapping" cont'd. from page 167
demonstrates that imaging based on signals from one element is possible; as long as x-rays are tuned to core level electron binding energies unique to one element, the tunnel current reflects the distance from atoms of only that element. For cobalt nanoclusters, elemental mapping across a large area is demonstrated by Fig. 1.

The ability to map element composition and topography with nanoscale resolution is a powerful tool against particle-to-particle variation common in nanomaterials. In bulk measurements of nanomaterials such variation averages out, leading to fuzzy associations between structure and function.

Due to quantum confinement effects, just one layer of atoms could change a nanomaterial function substantially. Pinpointing the effect of structure at the atomic level is key to design of functional nanomaterials. With molecular and single-atom resolution on the horizon, researchers could use SX-STM to map any material on an atom-by-atom basis.

Although the unique capabilities of the SX-STM technique provide already today a rare view into the nanoworld, it is expected that the machine upgrade of the APS will lead to even new insights by enabling higher scanning speeds and enhancements in chemical sensitivity by providing a much higher photon flux in the future.

— Amanda Grennell

See: Heath Kersell[1,2], Nozomi Shirato[1], Marvin Cummings[1], Hao Chang[1,2], Dean Miller[1], Daniel Rosenmann[1], Saw-Wai Hla[1,2], and Volker Rose[1]*, "Detecting element specific electrons from a single cobalt nanocluster with synchrotron x-ray scanning tunneling microscopy," Appl. Phys. Lett. **111**, 103102 (2017).
DOI: 10.1063/1.4990818
Author affiliations: [1]Argonne National Laboratory, [2]Ohio University
Correspondence: * vrose@anl.gov

This work was funded by the U.S. Department of Energy (DOE) Office of Science Early Career Research Program through the Division of Scientific User Facilities-Basic Energy Sciences through Grant No. SC70705. H.K. and S.W.H. acknowledge the support of the U.S. DOE Office of Science-Basic Energy Sciences, under Contract No. DE-FG02-02ER46012 for the SX-STM spectroscopic data analysis. Use of the Advanced Photon Source and the Center for Nanoscale Materials was supported by the U.S. DOE Office of Science-Basic Energy Sciences, under Contract No. DE-AC02-06CH11357.

26-ID-C • CNM/XSD • Physics, materials science • Nanodiffraction, nano-imaging, coherent x-ray scattering, synchrotron X-ray Scanning Tunneling Microscopy • 6-12 keV • On-site • Accepting general users •

An Energy-Resolution Record for Resonant Inelastic X-ray Scattering

Resonant inelastic x-ray scattering (RIXS) is a powerful technique for studying electronic excitations in a wide variety of new and complex materials, offering momentum- and energy-resolution and potentially even analysis of scattered polarization. Since its inception in the 1990s, the development of RIXS instrumentation and scientific subjects have benefited from a closely intertwined evolution; improvements in energy resolution and throughput, spurred by specific scientific cases, have in turn made new subjects of study feasible. In the continued quest for substantially improved energy resolution, a novel prototype RIXS flat-crystal spectrometer was tested at XSD beamline 27-ID-B at the APS. The spectrometer established a new record resolution for RIXS below 10 meV, together with a promise to do even better soon.

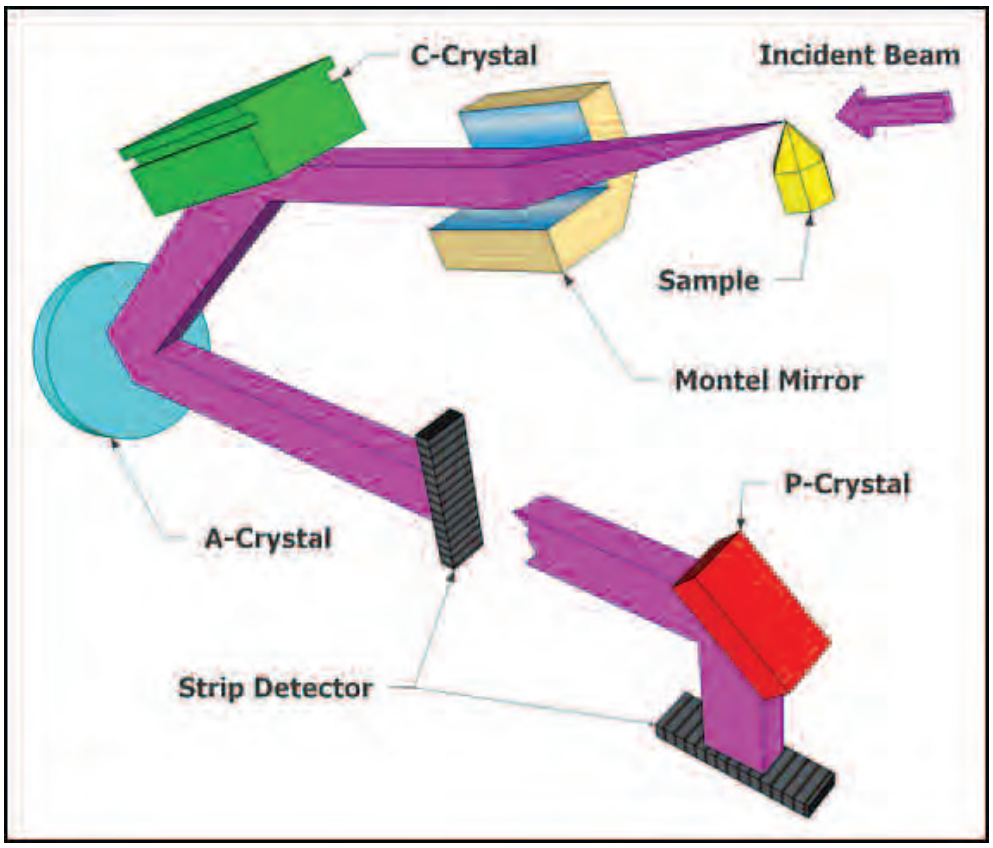

Fig. 1. Schematic rendering of the new flat-crystal RIXS spectrometer.

Early RIXS work was aimed at the study of charge transfer excitations in transition metal oxides (TMO), including the high-T_c superconducting cuprates, where electronic excitations could be observed at a few eV. As the understanding of strongly correlated electron systems progressed, orbital degrees of freedom came into focus: in many Mott insulators, transitions between the active *d*-orbitals, the "*dd* excitations," were hot topics and could reliably be observed with the then state-of-the-art resolution of 100-200 meV. Magnetism and magnetic ordering are central questions in the study of correlated electron systems. For example, the layered perovskite Iridates showing strikingly similar magnetic exchange interactions as the cuprates, implying that unconventional superconductivity might be found here, to the intriguing assertion that magnetic properties of honeycomb Iridates might point to a quantum spin liquid as ground state of this material, the spectrum of novel, exotic properties uncovered or anticipated promise a treasure trove of scientific discoveries. In the late 2000s, RIXS was established as a probe of magnetic excitations. However, spectral features associated with magnetic excitations ("magnons") lie at a fraction of an

eV or even in the sub-10-meV regime. A significant advance in energy resolution is needed to attack such subjects with RIXS. The new spectrometer at APS beamline 27-ID-B (Fig. 1) uses a multi-layer-based collimating mirror and successive flat-crystal optics. With flat crystals one can largely avoid figure errors and strain, which often are the limiting factor for traditional curved crystal spectrometers. Furthermore, the additional variable of crystal asymmetry allows tailoring the angular acceptance and degree of beam collimation of a flat crystal, and ultimately the resolution and efficiency of the assembly. Lastly, but very importantly, flat crystal assemblies provide the opportunity to include polarization analysis of the scattered beam efficiently and without loss of energy resolution.

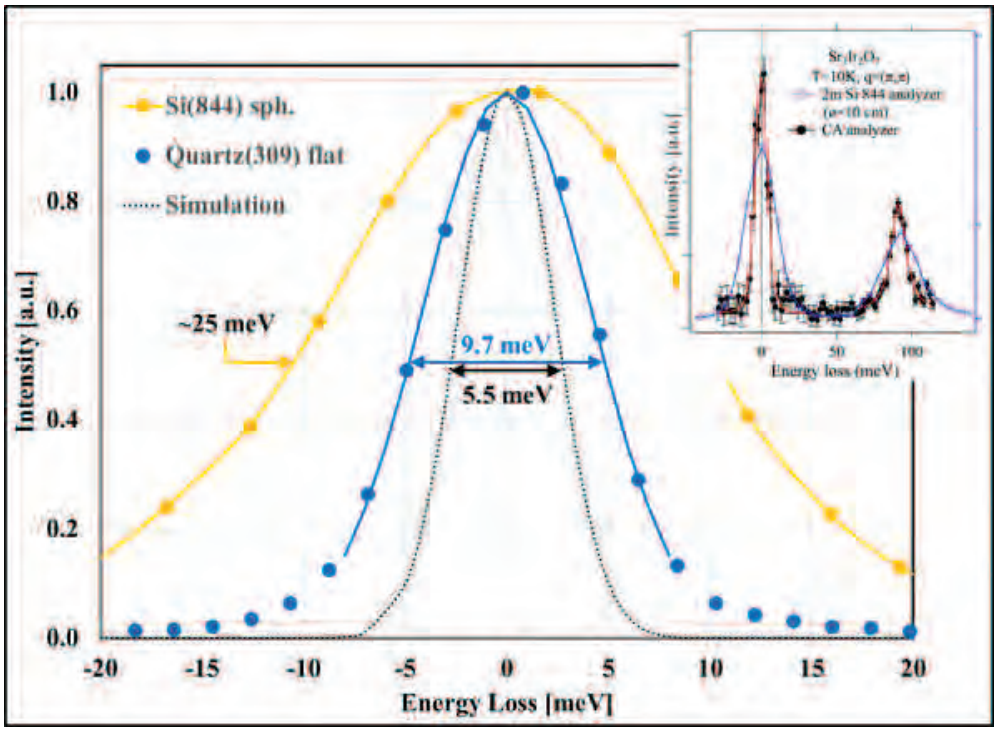

Fig. 2. Elastic lines recorded with a traditional curved-crystal spectrometer, using a Si 844 spherical analyzer (yellow), and the new flat-crystal ("CA-analyzer") instrument (blue). The dashed curve is a simulation of the latter when used with a matching monochromator. The inset shows a magnon spectrum measured with the same two instruments. Sharpening of spectral features is clearly visible for the case with higher resolution.

While polarization is necessary to attain a complete picture of the physics in an inelastic scattering event, routine polarization measurements have not been accomplished thus far in any RIXS measurement with better than a few hundred meV of resolution. The problem with flat crystals, however, is their minuscule solid angle x-ray acceptance. With the advent of advanced multilayer mirrors, collimators can now be devised that offer an acceptance comparable to curved analyzers, while collimating to a degree palatable for flat crystals.

The prototype spectrometer tested at beamline 27-ID was designed for measurements at the iridum L_3 absorption edge (11.215 keV). Scattered x-rays emanating from the sample are collected by a parabolic Ru/C Montel mirror. The pre-collimated exit beam is further collimated by the highly asymmetric Si(111) C-crystal. A near-backscattering Quartz(309) A-crystal followed by a position-sensitive detector performs the high-resolution spectral analysis. For polarization analysis, a Si(444) P-crystal with a Bragg angle of close to 45º is inserted in the setup as necessary.

In a first set of demonstrations this instrument has achieved an overall energy resolution of 9.7 meV, a new record for any hard x-ray RIXS measurement. Furthermore, in the present case, the overall resolution was limited by the available high-resolution monochromator. Given an intrinsic analyzer resolution of only 3.9 meV, using a monochromator with matching band pass would result in an overall resolution of 5.5 meV. Such a monochromator is currently under development.

Elastic lines recorded from Scotch tape are shown in Fig. 2. Here the yellow trace is characteristic for a state-of-the-art curved-crystal spectrometer using a Si(844) spherical analyzer, while the blue trace was measured on the new flat-crystal ("CA-analyzer") instrument, showing an improvement by a factor of 2.5 over the curved analyzer. The dashed trace is a simulation for the new instrument in combination with a matching monochromator. In the inset, a magnon spectrum from $SR_3Ir_2O_7$ is shown, measured by the same two instruments. Dramatic sharpening of features and new spectral structures are clearly visible in the spectrum with higher resolution, measured by the CA-analyzer instrument.

The flat crystal spectrometer design can easily be expanded for other absorption edge energies of scientific interest, by choosing an appropriate combination of crystals and multilayer mirror.

See: Jungho Kim[1], D. Casa[1], Ayman Said[1], Richard Krakora[1], B.J. Kim[2,3,4], Elina Kasman[1], Xianrong Huang[1], and T. Gog[1]*, "Quartz-based flat-crystal resonant inelastic x-ray scattering spectrometer with sub-10 meV energy resolution," Sci. Rep. **8**, 1958 (2018). DOI: 10.1038/s41598-018-20396-z
Author affiliations: [1]Argonne National Laboratory, [2]Pohang University of Science and Technology, [3]Institute for Basic Science, [4]Max Planck Institute for Solid State Research
Correspondence: * gog@anl.gov

This research used resources of the Advanced Photon Source, a U.S. Department of Energy (DOE) Office of Science user facility operated for the DOE Office of Science by Argonne National Laboratory under Contract No. DE-AC02-06CH11357.

27-ID-B • XSD • Physics • Resonant inelastic x-ray scattering • 5-14 keV, 5-30 keV • On-site • Accepting general users •

A Polished Approach to Imaging Integrated Circuits

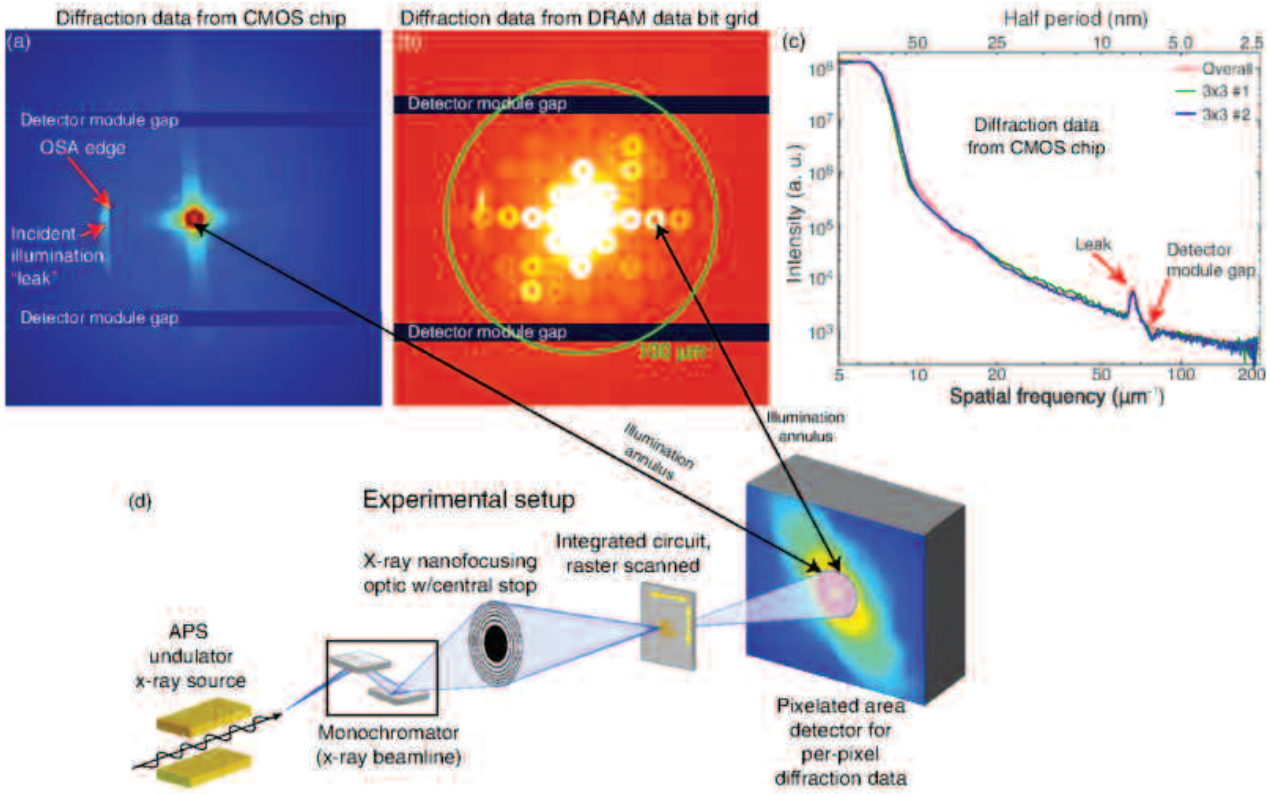

Fig. 1. (d) shows a schematic of the experiment where 10-keV x rays were produced by an undulator at the APS, monochromatized using Bragg diffraction from a pair of silicon crystals, and focused by a Fresnel zone plate with a central stop at a 100-nm-radius spot. The integrated circuit was scanned across this spot while coherent diffraction patterns were collected on a pixel array detector extending to an angle well beyond the numerical aperture of the Fresnel zone plate. (a) and (b) are the average diffraction patterns from a CMOS chip and a region of regularly spaced bit cells in a DRAM chip; one can see gaps between active pixel modules in the detector as well as a slight amount of illumination leakage caused by slight misalignment of an order sorting aperture placed between the zone plate optic and the specimen (not shown). The azimuthal average power spectrum of the CMOS chip is shown in (c), both from the average of all illuminated pixels and from two examples of 3×3 illumination spots, such as might overlap upon one specimen feature during continuous scanning. These power spectra suggest that there is measurable signal at spatial frequencies of about 100 μm^{-1}, corresponding to half-period feature sizes of 5 nm or smaller. This is corroborated in (b) where the annular illumination pupil function is replicated over many diffraction orders from the underlying data-bit array periodicity. From J. Deng et al., Phys. Rev. B **95,** 104111 (2017)

21-ID-D • LS-CAT • Life sciences • Macromolecular crystallography • 6.5-20 keV • On-site, remote, mail-in • Accepting general users •

Modern integrated circuits (ICs) — groups of connected electronic base circuits arranged on small, flat pieces of semiconductor materials—incorporate a variety of different materials. Examining the as-manufactured structures of these complex devices can help explain departures from their intended performance as well as aid in adjusting designs to create even better devices. However, the tools that have been used to probe ICs in the past have critical drawbacks. For example, transmission electron microscopy allows resolution at the atomic level on sufficiently thin structures, but the etching required for this thinning comes with a substantial risk of IC breakage or alteration of electronic properties. Transmission x-ray microscopy allows examination of whole, unetched ICs, but presently lacks the required resolution for the finest linewidth chips. One alternative is x-ray ptychography, in which a lens focuses an x-ray beam onto a small spot through which the sample is scanned, producing diffraction patterns that are processed into images using a computer. This technique has been used in the past to produce images with a resolution between 20 nm and 40 nm on highly thinned ICs. In a new study, a team of researchers used the APS to perform x-ray ptychography on two different types of ICs. Their results show that it is possible to achieve sub-20-nm resolution with only slight thinning from mechanical polishing.

The researchers from Northwestern University; Argonne; the University of Southern California, Los Angeles; the University of Southern California, Marina del Rey; and Intel Corporation started by developing a theoretical model that they used to calculate the required x-ray photon exposure to penetrate a silicon wafer. Their results suggested that a 10-keV beam should accomplish this goal without substantial IC thinning.

Using this insight, and working at the LS-CAT 21-ID-D x-ray beamline at the APS, the researchers used a focused x-ray beam with a 100-nm radius for ptychographic imaging of a complementary metal-oxide semiconductor chip with eight copper interconnect layers on a 300-μm-thick silicon wafer. After acquiring the resulting diffraction patterns, they obtained images using a reconstruction algorithm with massively parallel computing for rapid data processing (Fig. 1).

When the researchers performed this scan on a chip that underwent no further processing beyond removal from its IC package, the resulting image easily showed details of the circuit layers. However, it also showed an overlay of contrast "stripes" along with fringes from features at a different plane than the one that was reconstructed.

Working under the assumption that these artifacts were due to scratches on the silicon surface, which changed the thickness of the wafer in discrete areas, the researchers mechanically polished the wafer, taking off 60 μm of this substrate in the process. When they imaged this IC again, the stripes were gone, revealing a range of wider and finer features in the circuit layer. Although the IC was only 240 μm after polishing, compared to its original thickness of 300 μm, enough silicon remained for it to be robust in handling and avoid problems with heat transfer that come with additional thinning.

In a second set of experiments, the researchers scanned an 8-Gb dynamic random-access memory chip composed of six different metal and dielectric layers. Using mechanical polishing, the researchers removed the top few layers to expose all the layers locally in one array. Scanning this array resulted in images with a spatial resolution better than 20 nm.

The researchers note that because x-ray ptychography has no optics-imposed resolution limits and uses small wavelengths, increases in photon exposure could lead to imaging with even lower resolution. Thus, they say, additional study could lead to ICs being imaged with resolutions better than 10 nm while still maintaining their ability to function in electrical tests.

— Christen Brownlee

See: Junjing Deng[1], Young Pyo Hong[1], Si Chen[2], Youssef S.G. Nashed[2], Tom Peterka[2], Anthony J.F. Levi[3], John Damoulakis[4], Sayan Saha[5], Travis Eiles[5], Chris Jacobsen[1,2]*, "Nanoscale x-ray imaging of circuit features without wafer etching," Phys. Rev. B **95**, 104111 (2017).
DOI: 10.1103/PhysRevB.95.104111
Author affiliations: [1]Northwestern University, [2]Argonne National Laboratory, [3]University of Southern California, Los Angeles, [4]University of Southern California, Marina del Rey, [5]Intel Corporation
Correspondence:
* c-jacobsen@northwestern.edu

We thank C. Roehrig for help with the Pilatus 300K detector configuration and K. Brister, J. VonOsinski, and M. Bolbat for assistance in using the LS-CAT beamline. Argonne's work was supported under U.S. Department of Energy (DOE) Contract No. DE-AC02-06CH11357. The work of J.D. and C.J. on x-ray ptychography was partly supported by a National Institutes of Health (NIH) Grant No. R01 GM104530. The BioNanoprobe instrument was funded by ARRA: NIH/NCRR High End Instrumentation Grant No. S10 RR029272-01, and the Pilautus 3 detector was funded by a supplement to NIH Grant No. R01 GM038784. This research used resources of the Advanced Photon Source, a U.S. Department of Energy (DOE) Office of Science user facility operated for the DOE Office of Science by Argonne National Laboratory under Contract No. DE-AC02-06CH11357.

Real-Time Data Analysis and Experimental Steering at the APS Using Large-Scale Computing

Instrumentation improvements have greatly increased the amount and rate of data collected at APS beamlines but also pose tremendous analysis challenges. For instance, data generation rates in full-field imaging experiments can reach 2000 projections (16 Gb) per second, which with traditional techniques might require hours to analyze after an experiment has completed. New techniques developed at Argonne allow these vast data to be processed as they are collected, enabling dynamic studies in which the results of computational analysis are used to drive changes to instrument configuration as an experiment proceeds.

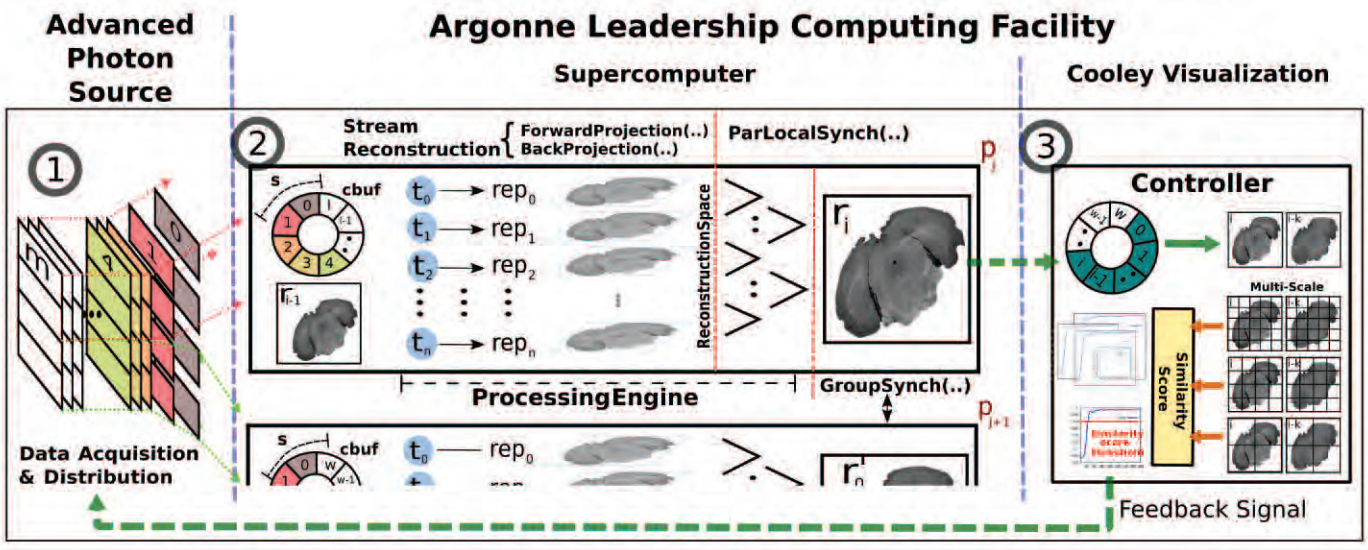

Fig. 1. Real-time tomographic reconstruction workflow. The system consists of three components: (1) Data acquisition component collects and streams experimental data; (2) data analysis component utilizes tens of thousands of cores at ALCF Supercomputers to perform data analysis; and (3) Controller component makes decisions according to reconstruction results and sends signals to data acquisition process for experimental steering.

Traditional beamline data analysis pipelines run only after data acquisition is completed, and on small, often local computers. The resulting long delay between data collection and analysis prevents real-time experimental decision making, compromising researcher productivity. These problems will become yet more serious with next-generation photon sources such as the APS upgrade, where beam intensity and resulting data sizes and computational demands will increase by orders of magnitude.

To address these issues, and to be ready to translate the improvements in synchrotron capabilities from APS upgrade to improvements of similar scale in scientific productivity, scientists from the Argonne Data Science and Learning Division, the Argonne Leadership Computing Facility (ALCF), and the APS have applied innovative data acquisition, transfer, and parallelization techniques to stream data to a remote supercomputer and process them live on thousands of cores [1,2]. The live analysis of data, while the data acquisition is in progress, provides real-time feedback during the experiment. The developed software system consists of three main components: data acquisition and transfer, data analysis, and control feedback (Fig. 1). The data acquisition and transfer component interacts with the instrument control system, such as the Experimental Physics and Industrial Control System, and monitors data acquisition. Once the beamline scan engine starts collecting data, this layer streams data (after doing a basic sanity check) from the memory of the data acquisition machine to the memory of the data analysis processes. The data analysis is performed using Trace, a high- performance implementation of map-reduce processing that performs a highly optimized parallel analysis of large data sets using large-scale compute resources. Trace provides the necessary infrastructure to process the streaming data in a real-time fashion; namely, setting up the frequency of analysis operations, processing partial data and resolving data dependencies using replication (Figs. 2, 3). After processing each data chunk, the results are streamed to the control feedback that further analyzes the results and interacts with the data acquisition process to manage the instrument control system and steer the experiment to its desired conditions. The control feedback

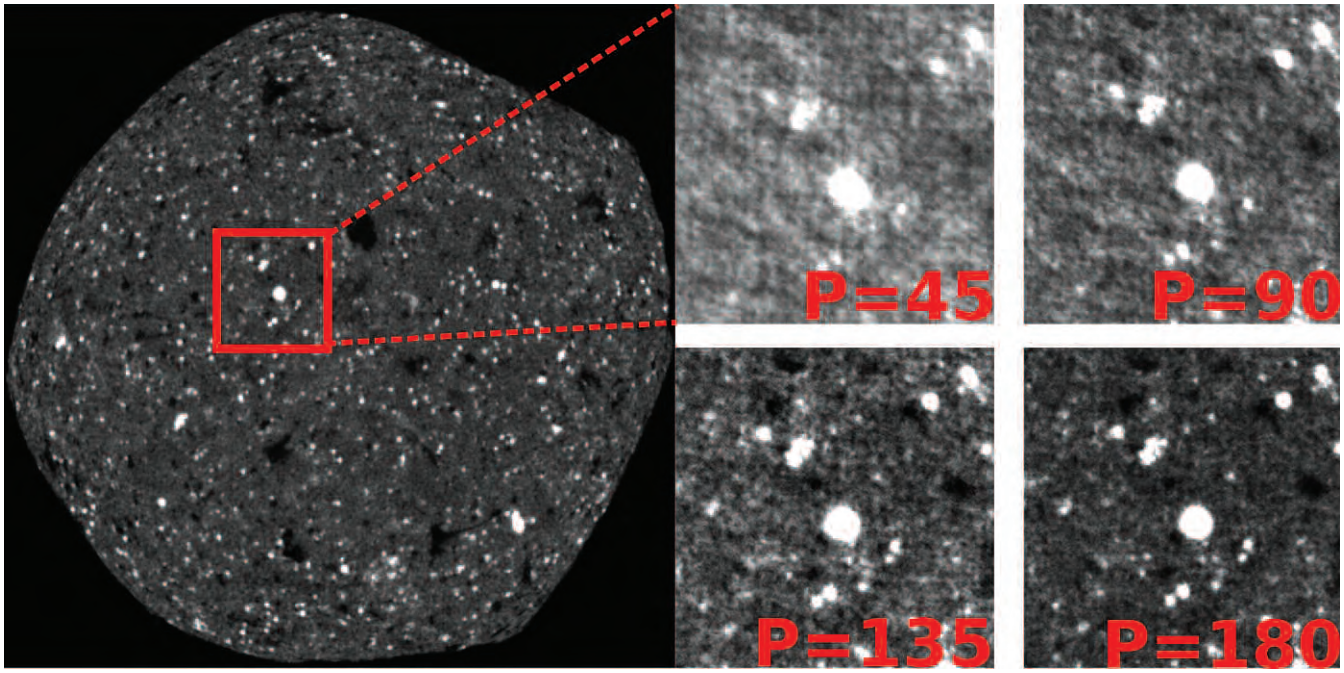

Fig. 2. Real-time reconstruction of a shale sample. The finale reconstructed sample is shows in left figure. Right figures show reconstructions only after 45, 90, 145 and 180 projections.

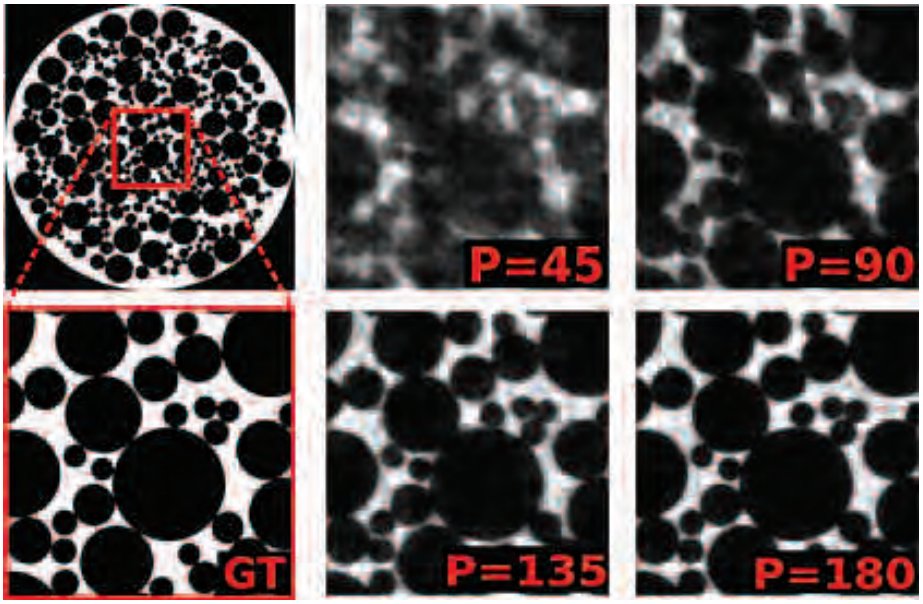

Fig. 3. Real-time reconstruction of a phantom sample. Left two figures show the ground truth. Right four figures show reconstructions only after 45, 90, 145 and 180 projections.

component makes decisions according to constraints specified by beamline scientist, such as adjusting data acquisition to capture region of interest, detecting dynamic features and changing scanning pattern, or minimizing data acquisition and dose exposure using image quality thresholds.

The system has been deployed for testing at beamlines 2-BM-A,B and 32-ID-B,C of the APS using ALCF computing resources where three-dimensional iterative tomographic image reconstruction algorithms are implemented and executed using Trace. The control feedback is programmed to stop the data acquisition when the image quality exceeds a predefined threshold; therefore, the experiment is gracefully ended with minimum data acquisition time and dose exposure. Experimental results show that this system can process as high as 204 projections per second using 1200 cores. Moreover, given more resources, the system can process higher number of projections per second as it shows a strong scaling efficiency of 68-98%. The system also reduces the data acquisition time of full field imaging experiments by 22-44% while meeting the desired reconstructed image quality.

Contact: Tekin Bicer (bicer@anl.gov), Rajkumar Kettimuthu (kettimut@mcs.anl.gov), Doga Gursoy (dgursoy@anl.gov), Vincent De Andrade (vdeandrade@aps.anl.gov), Francesco De Carlo (decarlo@aps.anl.gov), William Scullin (wscullin@alcf.anl.gov), all Argonne National Laboratory; Bin Ren (bren@wm.edu) College of William and Mary; Mert Hidayetoglu (hidayet2@illinois.edu) University of Illinois at Urbana Champaign; Ian T. Foster (foster@anl.gov) Argonne National Laboratory and The University of Chicago

References

[1] T. Bicer, D. Gursoy, R. Kettimuthu, I. T. Foster, B. Ren, V. De Andrade and F. De Carlo, "Real-Time Data Analysis and Autonomous Steering of Synchrotron Light Source Experiments", in Proceedings of the International eScience Conference (eScience'17), Auckland, New Zealand, Oct. 2017

[2] T. Bicer, D. Gursoy , V. De Andrade, R. Kettimuthu, W. Scullin, F. De Carlo, I. T. Foster, "Trace: A High-Throughput Tomographic Reconstruction Engine for Large-Scale Datasets", Special Issue on High-Throughput X-Ray Imaging and Algorithms, *Advanced Structural and Chemical Imaging*, 2017

Real-time Beamline Data Analysis Utilizing High-Performance Computing

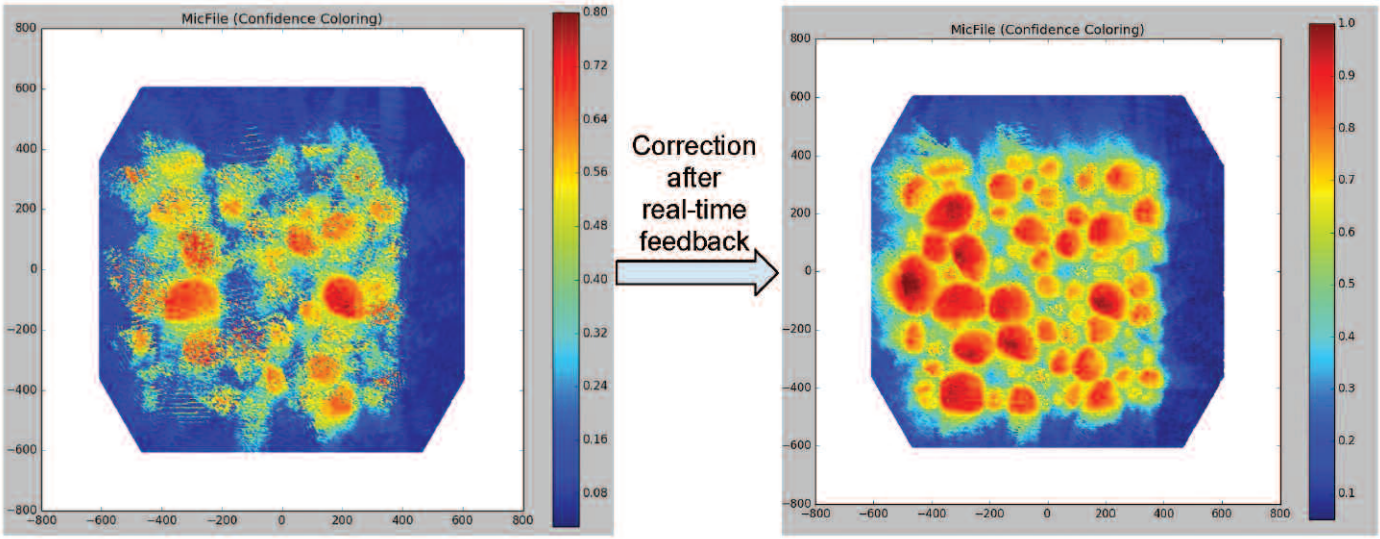

Fig. 1. Example of an experiment where real-time feedback improved the quality of acquired data. Confidence indicates quality of reconstruction, higher is better.

As data collection rates continue to accelerate at the APS, it is increasingly difficult for data analysis to keep up. Experimental practice is greatly facilitated when results are obtained quickly enough to be able to steer the experimental procedure in real time. All of this will become an even more pressing problem upon completion of the APS Upgrade Project, since data collection rates will increase for some beamlines by as much as a factor of 1000. Until fairly recently, computer speeds increased significantly each year, meaning that if a program was not fast enough, this could be solved by purchasing a newer computer. At present, computer clock speeds are not increasing, which means that computation speeds can only be increased by faster algorithms or by developing efficient parallel processing adaptations, which distribute computing tasks across multiple computer (CPU) cores. The expected scaling due to source and detector advances will require high-performance computing (HPC), utilizing supercomputers with hundreds of thousands of CPU cores. Argonne and the Department of Energy (DOE) complex are particularly rich in HPC computing, with many of the world's fastest supercomputers. The XSD Computational X-ray Science Group has been exploring HPC applications for photon sciences with four examples described here.

The MIDAS system for analysis of high-energy diffraction microscopy (www.aps.anl.gov/Science/Scientific-Software/MIDAS) has greatly facilitated this technique, which interrogates the strain state and orientation of individual crystalline grains that determine the strength and crack resistance of metals and ceramics, and can be used to see how materials are changed by physical means such as repeated external strain and/or heating. While this type of analysis formerly took months of computing on a single workstation, MIDAS has been incorporated into a data processing workflow where data files are sent, as they are collected, to a National Energy Research Scientific Computing Center (NERSC) supercomputer, located at the DOE's Lawrence Berkeley National Laboratory (LBNL), which offers rapid access for experimental data analysis. A run with circa 2000 CPU cores is usually initiated within seconds of data collection and is completed within 5-10 min (depending on experimental complexity). This allows the investigator to get real-time feedback. As an example, Fig. 1 shows an experiment where real-time feedback allowed the investigator to make improvements in the setup, resulting in higher quality data. The map on the left of the figure is the original reconstruction and the map on the right is the reconstruction after experimental changes.

The APS-led Monitoring, Optimization, Navigation, and Analysis (MONA) project is piloting HPC integration into the data collection process for real-time steering of experimental conditions, with collaboration from the National Synchrotron Light Source II at the DOE's Brookhaven National Laboratory, and the Center for Advanced Mathematics for Energy Research Application at LBNL. Incorporating data analysis into the experimental process allows users to ensure that the experiment they are conducting actually addresses the hypothesis they intend to test. They can also see and correct experimental artifacts in real time. The MONA team

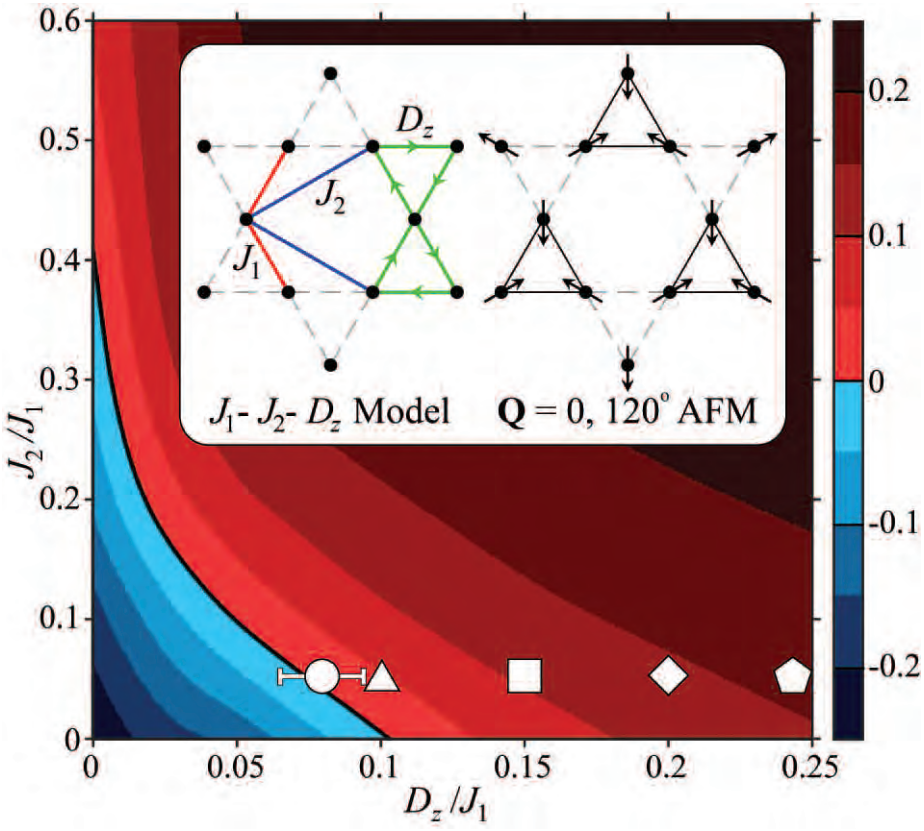

Fig. 2. Phase diagram of the Heisenberg J1-J2-Dz model from ANL studies. Blue region shows magnetic spin distortion, whereas red region shows 120-degree antiferromagnetic order. Inset shows the structure of the Kagome lattice. White geometric symbols in the lower part indicate various known Kagome compounds, most famous of them being herbertsmithite, depicted as a circle in the magnetic transition region.

successfully demonstrated an operational real-time streaming data processing pipeline for real-time reconstruction and visualization of a specimen at XSD beamline 2-BM-A,B at the APS utilizing remote HPC resources. One of the key goals is to adapt to changes faster than a human can react, for example, by identifying and "zooming" in on a region of interest before a transformation occurs or with minimal sample dose.

Crystallographic analysis is being revolutionized by XSD beamlines such as 11-ID-B, 11-ID-C and 17-BM-B, where a full dataset can be collected in fractions of a second, in comparison to hours on a lab instrument. As an example of a study that such instruments allow, a 2015 paper by Yang et al. shows >2000 powder diffraction datasets on battery material α-MnO_2, collected as a function of heating and cooling cycles. Recent work by O'Donnell et al. that incorporated HPC functionality into the GSAS-II crystallographic analysis package, allowed completion of analysis computations on all 2191 datasets in 300 sec, while the equivalent computation on just one dataset requires ~ 35 sec.

Theoretical studies in the field of frustrated quantum magnetism within CXS are also made possible by HPC. A novel state-of-the-art numerical scheme, implemented using Argonne's PETSc scalable computational library and performed on NERSC's Edison supercomputer at LBNL, diagonalizes square matrices with dimensions exceeding 9.6 billion (reduced from half a trillion using group symmetry), to provide ground states in Kagome lattice compounds. The work brings further insight into an exotic state called a quantum spin liquid that was first proposed by physicist Phil Anderson in 1973, as well as greater understanding of gapless spin excitations found in herbertsmithite, an experimentally studied Kagome mineral. Results from these computations are shown in Fig. 2.

Contact: Brian Toby (toby@anl.gov)

Researchers:

MIDAS: Hemant Sharma, Peter Kenesei, Jun-Sang Park, Jonathan Almer (all Argonne)

MONA: Tekin Bicer (Argonne), Daniel Allan, Thomas Caswell, Julien Lhermitte, Maksim Rakitin (all Brookhaven National Laboratory), Francesco De Carlo, Barbara Frosik, Arthur Glowacki, Pete Jemian, Nicholas Schwarz, Xianghui Xiao, William Scullin (all Argonne), Harinarayan Krishnan, Dinesh Kumar, James Sethian, Ronald Pandolfi, Dilworth Parkinson (all Lawrence Berkeley National Laboratory), Doga Gürsoy (Argonne and Northwestern University)

GSAS-II: Brian Toby, Robert Von Dreele, Maria Chan (Argonne), Jackson O'Donnell (The University of Chicago)

Quantum magnetism: Michel van Veenendaal, Tsezár Szeman (both Argonne and Northern Illinois University)

The APS Data Management System

Data are essential to the scientific discoveries enabled by experiments performed at the APS. At present, the APS collects an estimated 4 PB – 6 PB of raw experimental data per year. Data volumes and rates continue to quickly increase due to beamline advances, such as improved detectors, high-throughput instrumentation, and multi-modal instruments that can acquire several measurements in a single experiment. This trend is expected to continue in the future and will be accelerated by the improved source and instruments planned as part of the APS Upgrade Project. As a result, successful management of data is of particular importance to the current and future scientific productivity of the APS.

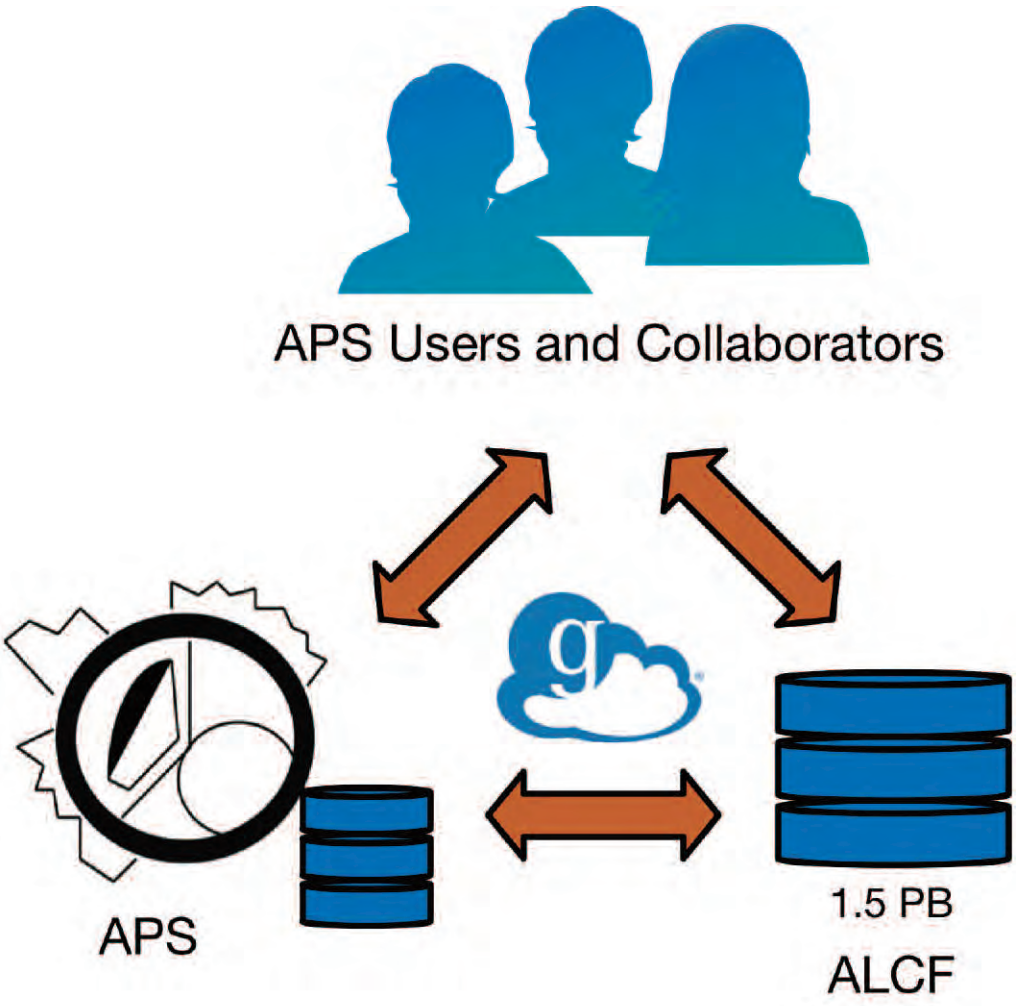

Historically, the task of managing and distributing data at the APS has been left to individual user groups and beamline staff. This process usually consisted of manually copying large amounts of data to removable hard drives, which users either carry or ship to their home institutions, and beamline staff collect on office shelves. Data were rarely cataloged, and when thry were, paper logbooks were the most popular method. This process was very tedious, often prone to errors and inconsistencies, and cannot scale along with current and anticipated data sizes. In order to cope with current and future data rates and volumes, the APS is adopting more automated, electronic, and consistent approaches to managing data.

At the end of 2016, the APS, through collaboration with the Argonne Leadership Computing Facility (ALCF), made a Data Direct Networks S2A9900 1.5-PB storage system available for APS experiments. Managed by the APS, this system is housed in an Argonne Computing, Environment, & Life Sciences (CELS) Division data center located in Argonne Building 369. It is connected to the APS via multiple dedicated 10-Gbps network links, which may be increased if needed (Fig. 1). This system is now being utilized by more than 20 beamlines operated by either XSD or collaborative access teams. Since its deployment, the amount of data stored on the system has grown to over 1 PB (Fig. 2).

To best use this storage capability, the APS Data Management System contains a set of software tools that integrate with beamline data workflows.

< Fig. 1. Pictorial diagram of storage available for the APS and logical connections. A storage system housed in a CELS data center in Building 369 provides 1.5 PB of storage space for the APS. APS Data Management System tools are currently deployed on over 20 APS beamlines to automate the transfer, organization, and distribution of data on this system. APS users and collaborators can access data from off-site using Globus Online.

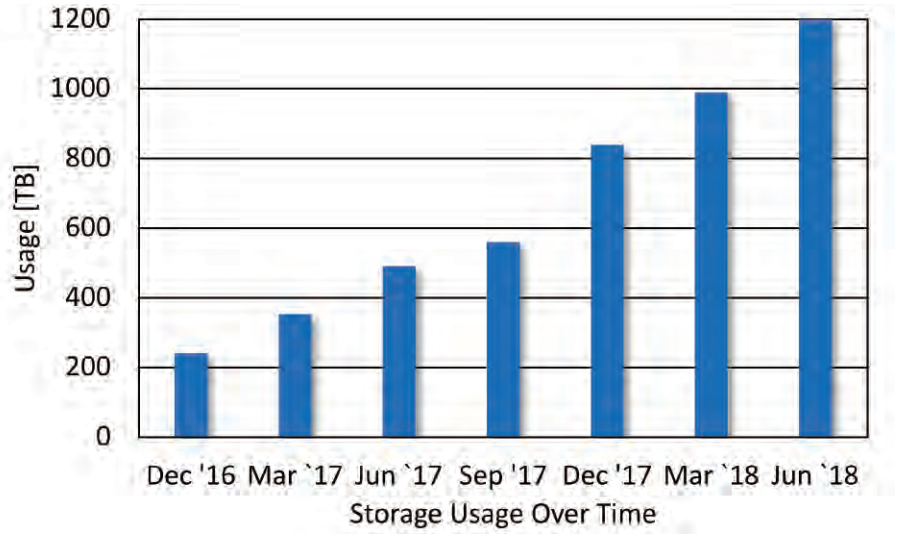

Fig. 2. Amount of data stored using the APS Data Management System since December 2016. Over this period, APS beamlines have stored approximately 1 PB of experimental data.

Beamline data acquisition systems are monitored for the generation of new files that feed the data workflow. Data files are automatically copied from acquisition systems to the 1.5-PB storage system. A metadata catalog tracks user and experiment information along with information such as file checksums. Access permissions are set based on user information from the APS proposal and safety databases. A processing service supports user-defined data workflows and automated data processing tasks. Experimenters and staff at the APS may interact with the system via a web portal, graphical user interface, command line tools, and/or an application programming interface. Users can download data at their home institutions using the Globus Online data transfer tool.

As the current system is quickly reaching capacity, the APS is in the process of procuring a larger, next-generation Data Direct Networks GS14KX data storage system. This next generation system will have enough storage to support the current needs of the facility and is expandable to store up to 20 PB of data as the need arises. It is anticipated that this system will be online by the end of 2018.

The APS Data Management System will continue to be deployed at more beamlines in the coming years. Based on feedback, these resources will be improved with new features and capabilities. The APS is now better equipped to realize the data management tasks critically needed to deal with the deluge of data the APS will continue to produce. *— Nicholas Schwarz*

Contact: Sinisa Veseli (sveseli@anl.gov), Collin Schmitz (caschmitz@anl.gov), Dariusz Jarosz (djarosz@anl.gov), Roger Sersted (rs1@anl.gov), Dave Wallis (wallis@anl.gov), and Nicholas Schwarz (nschwarz@anl.gov)

Acknowledgements: Many helped to make this work possible: Jon Almer, Francesco De Carlo, Barbara Frosik, Arthur Glowacki, Doga Gursoy, Peter Kenesei, Faisal Khan, Wenjun Liu, Suresh Narayanan, Jun-Sang Park, Jon Tischler, Stefan Vogt, and Ruqing Xu (XSD); Brian Pruitt, Brian Robinson, Giampiero Sciutto, Ken Sidorowicz, and Dave Wallis (Argonne APS Engineering Support Division - AES); William Allcock and Mike Papka (CELS/ALCF); and Rachana Ananthakrishnan and Ian Foster (Globus Services). Work at the APS is supported and maintained by the XSD Scientific Software Engineering & Data Management Group, the AES Information Technolog Group, and many XSD beamline staff, with funding from U.S. Department of Energy Office of Science under Contract No. DE-AC02-06CH11357.

The APS Modular Deposition System

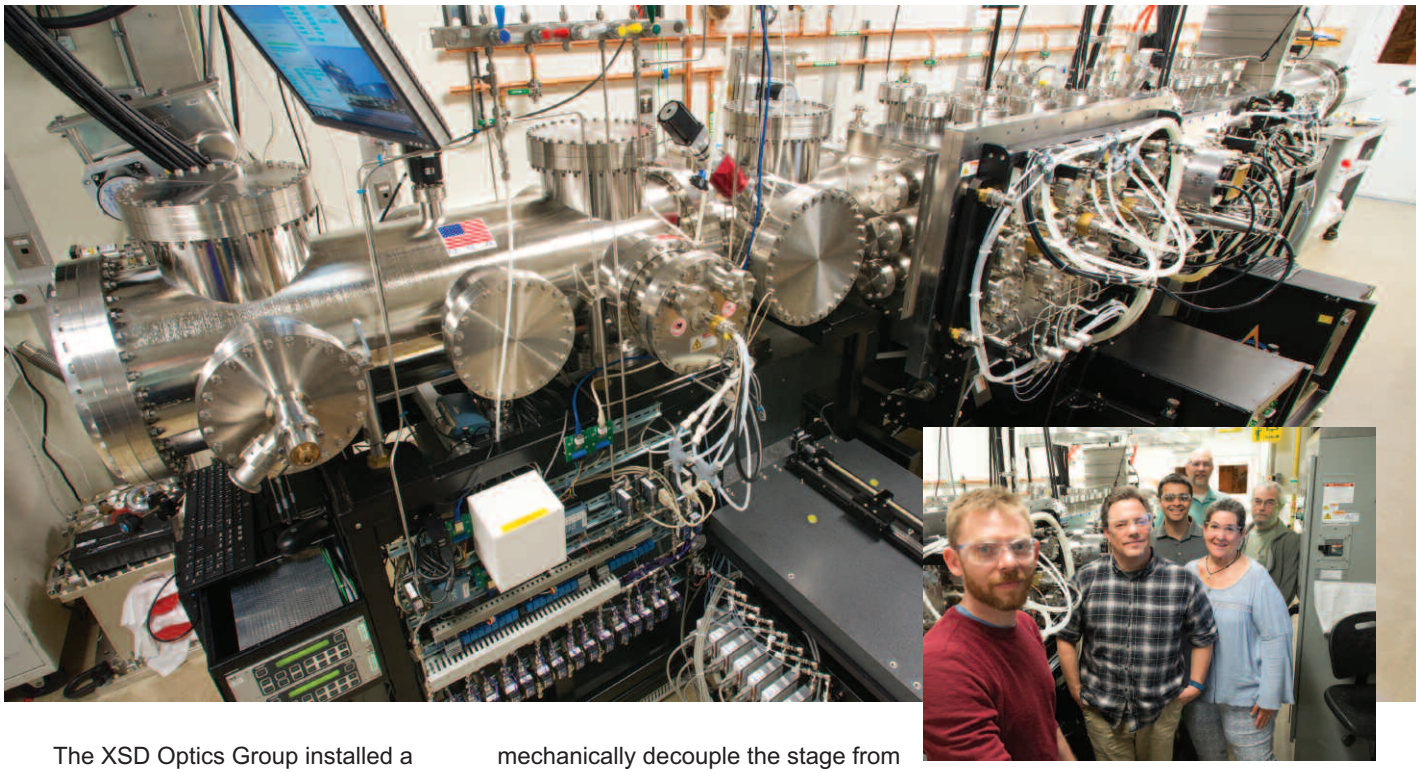

Fig. 1. Main photo: the MDS. Inset photo: A few of the many people who contributed to the project are (starting from left) Ray Conley, Jon Montgomery, Sunil Bean, Scott Izzo, Patricia Gunkelman, and Tim Mooney.

The XSD Optics Group installed a highly specialized multilayer fabrication system in order to meet the increasingly challenging specifications for x-ray optics required by APS beamlines.

This Modular Deposition System (MDS, Fig. 1) utilizes a linear geometry where substrates travel within a central region that contains the process modules (magnetron sputtering sources or other instruments) with a landing zone on one end and a load-lock region on the other. Multilayer structures are fabricated by raster-scanning the substrate across sequentially activated fixed-rate deposition sources, and layer thickness is thus a function of substrate velocity and deposition flux intensity. Multilayer structures may be depth-graded or laterally-graded to suit specific energy bandwidth or beam steering requirements.

The MDS is built around a 4.7-m-long, ultra-high vacuum (UHV), direct-drive linear motor servo scanner designed with dual voice-coils, sinusoidal commutation, and 5-nm position resolution, which provides velocity stability better than 99.9975%. The scanner stage is temperature-controlled and rests on a granite support structure that is nested within the frame in order to mechanically decouple the stage from the UHV enclosure and pumping systems. Mirror and multilayer substrate dimensions up to 1200 x 150 x 100 mm can be accommodated; however, most optics are significantly smaller. Eight sputtering cathodes currently installed aim horizontally towards the scanner. Three large-area cathodes, optimized for low-pressure deposition and reduced deposition rate drift, are dedicated for large-area reflective multilayer deposition. Five smaller cathodes are utilized for single-layer coatings or material system and process development. A flexible gas mixing and delivery system allows precision reactive sputtering of many conductive, semi-insulating, or ferromagnetic materials at pressures below 0.2 mTorr in order to produce multilayer structures with minimal interlayer roughness.

The design revolves around modularity and adaptability, where sources, metrology, or other instrumentation are easily changed or upgraded to adapt to future requirements. For example, a metrology and ion-beam figuring module are being added to the instrument that will provide the APS with the unique ability to explore new concepts such as combining *in situ* surface metrology with sub-aperture figure correction methods.

Additionally, provisions within the instrument for a dynamically-actuated shaped aperture will be used to explore methods to produce thickness gradients along both axes for three-dimensional multilayer deposition — possibly opening up new optical geometries, and allowing for higher efficiency and a reduced number of reflecting surfaces. Machine capabilities are being brought online in phases, with multilayer deposition as the first priority. Other features related to metrology and figuring, and the dynamic aperture, will be brought online later as they are developed.

Contact: Ray Conley (rconley@aps.anl.gov)

This research used resources of the Advanced Photon Source, a U.S. Department of Energy (DOE) Office of Science user facility operated for the U.S. DOE Office of Science by Argonne National Laboratory under Contract No. DE-AC02-06CH11357.

Access to Beam Time at the Advanced Photon Source

Five types of proposals are used at the APS: general user, partner or project user, CAT member, CAT staff, and APS staff. All beam time at the APS must be requested each cycle through the web-based Beam Time Request System. Each beam-time request (BTR) must be associated with one of the proposals mentioned above.

General-user proposals and BTRs

Proposals are peer reviewed and scored by a General User Proposal Review Panel, and time is allocated on the basis of scores and feasibility. A new BTR must be submitted each cycle; or each cycle, allocation is competitive. Proposals expire in two years or when the number of shifts recommended in the peer review has been utilized, whichever comes first.

Partner- or project-user proposals and BTRs

Proposals are peer reviewed by a General User Proposal Review Panel and reviewed further by a subcommittee of the APS Scientific Advisory Committee and by APS senior management. Although a new BTR must be submitted each cycle, a specific amount of beam time is guaranteed for up to three years.

CAT-member proposals

Proposals from CAT members are typically much shorter and are reviewed by processes developed by individual CATs. Allocation/scheduling is determined by the CAT management.

CAT- and APS staff-member proposals and BTRs

These proposals are also very short and are reviewed through processes developed by either the CAT or the APS. Each CAT/beamline determines how beam time is allocated/scheduled. Collaborative access team and/or APS staff may submit general user proposals, in which case the rules for general user proposals and BTRs are followed.

In addition to the above, the APS has developed an industrial measurement access mode (MAM) program to provide a way for industrial users to gain rapid access for one-time measurements to investigate specific problems. A MAM proposal expires after one visit.

The APS User Information page (www.aps.anl.gov/Users-Information) provides access to comprehensive information for prospective and current APS users.

Typical APS Machine Parameters

Linac

Output energy	375 MeV
Maximum energy	500 MeV
Output beam charge	0.3–3 nC
Normalized emittance	5–20 mm-mrad
Frequency	2.856 GHz
Modulator pulse rep rate	30 Hz
Gun rep rate (1–6 pulses, 33.3 ms apart every 0.5 s)	2–12 Hz
Beam pulse length	8–15 ns
Bunch length	1–10 ps FWHM

Particle Accumulator Ring

Nominal energy	375 MeV
Maximum energy	450 MeV
Circumference	30.66 m
Cycle time	500 ms or 1000 ms
Fundamental radio frequency (RF1)	9.77 MHz
12th harmonic RF frequency (RF12)	117.3 MHz
RMS bunch length (after compression)	0.34 ns

Injector Synchrotron (Booster)

Nominal extraction energy	7.0 GeV
Injection energy	375 MeV
Circumference	368.0 m
Lattice structure	10 FODO cells/ quadrant
Ramping rep rate	2 Hz or 1 Hz
Natural emittance	69 nm-rad (actual)
	92 nm-rad (nominal)
Radio frequency	351.930 MHz

Storage Ring System

Nominal energy	7.0 GeV
Circumference	1104 m
Number of sectors	40
Length available for insertion device	5.0 m
Nominal circulating current, multibunch	100 mA
Natural emittance	2.5 nm-rad
RMS momentum spread	0.096%
Effective emittance	3.1 nm-rad
Vertical emittance	0.040 nm-rad
Coupling (operating)	1.5%
Revolution frequency	271.555 kHz
Radio frequency	351.935 MHz
Operating number of bunches	24 to 324
RMS bunch lengths	33 ps to 25 ps
RMS bunch length of 16 mA in hybrid mode	50 ps

APS Source Parameters

Undulator A (29 insertion devices [IDs])

Period: 3.30 cm
Length: 2.1 m in sectors 16, 21, 23, 24, 34; 2.3 m in Sector 6; 2.4 m in others
Minimum gap: 10.5 mm
B_{max}/K_{max}: 0.892 T/2.75 (effective; at minimum gap)
Tuning range: 3.0–13.0 keV (1st harmonic)
3.0–45.0 keV (1st–5th harmonic)
On-axis brilliance at 7 keV (ph/s/mrad^2/mm^2/0.1%bw):
4.1 x 10^{19} (2.4 m), 4.0 x 10^{19} (2.3 m), 3.3 x 10^{19} (2.1 m)
Source size and divergence at 8 keV:
Σ_x: 276 μm Σ_y: 11 μm
$\Sigma_{x'}$: 12.7 μrad (2.4 m), 12.8 μrad (2.3 m), 12.9 μrad (2.1 m)
$\Sigma_{y'}$: 6.7 μrad (2.4 m), 6.8 μrad (2.3 m), 7.1 μrad (2.1 m)

2.30-cm Undulator (2 IDs in sectors 11, 14)

Period: 2.30 cm Length: 2.4 m
Minimum gap: 10.5 mm
B_{max}/K_{max}: 0.558 T/1.20 (effective; at minimum gap)
Tuning range: 11.8–20.0 keV (1st harmonic)
11.8–70.0 keV (1st-5th harmonic, non-contiguous)
On-axis brilliance at 12 keV (ph/s/mrad^2/mm^2/0.1%bw): 6.9 x 10^{19}
Source size and divergence at 12 keV:
Σ_x: 276 μm Σ_y: 11 μm
$\Sigma_{x'}$: 12.3 μrad $\Sigma_{y'}$: 5.9 μrad

2.70-cm Undulator (5 IDs in sectors 3, 12, 14, 35)

Period: 2.70 cm
Length: 2.1 m in Sector 12; 2.4 m in sectors 3, 14, and 35
Minimum gap: 10.5 mm
B_{max}/K_{max}: 0.698 T/1.76 (effective; at minimum gap)
Tuning range: 6.7–16.0 keV (1st harmonic)
6.7–60.0 keV (1st-5th harmonic, non-contiguous)
On-axis brilliance at 8.5 keV (ph/s/mrad^2/mm^2/0.1%bw):
5.7 x 10^{19} (2.4 m), 4.7 x 10^{19} (2.1 m)
Source size and divergence at 8 keV:
Σ_x: 276 μm Σ_y: 11 μm
$\Sigma_{x'}$: 12.7 μrad (2.4 m), 12.9 μrad (2.1 m)
$\Sigma_{y'}$: 6.7 μrad (2.4 m), 7.1 μrad (2.1 m)

3.00-cm Undulator (9 IDs in sectors 12, 13, 16, 21, 23, 27, 34, 35)

Period: 3.00 cm
Length: 2.1 m in sectors 12, 13, 16, 21, 23, 34; 2.4 m in sectors 27 and 35
Minimum gap: 10.5 mm
B_{max}/K_{max}: 0.787 T/2.20 (effective; at minimum gap)
Tuning range: 4.6–14.5 keV (1st harmonic)
4.6–50.0 keV (1st-5th harmonic)
On-axis brilliance at 8 keV (ph/s/mrad^2/mm^2/0.1%bw):
4.8 x 10^{19} (2.4 m), 3.9 x 10^{19} (2.1 m)
Source size and divergence at 8 keV:
Σ_x: 276 μm Σ_y: 11 μm
$\Sigma_{x'}$: 12.7 μrad (2.4 m), 12.9 μrad (2.1 m)
$\Sigma_{y'}$: 6.7 μrad (2.4 m), 7.1 μrad (2.1 m)

3.50-cm SmCo Undulator (Sector 4)

Period: 3.50 cm Length: 2.4 m
Minimum gap: 9.75 mm
B_{max}/K_{max}: 0.918 T/3.00 (effective; at minimum gap)
Tuning range: 2.4–12.5 keV (1st harmonic)
2.4–42.0 keV (1st-5th harmonic)
On-axis brilliance at 7 keV (ph/s/mrad^2/mm^2/0.1%bw): 3.7 x 10^{19}
Source size and divergence at 8 keV:
Σ_x: 276 μm Σ_y: 11 μm
$\Sigma_{x'}$: 12.7 μrad $\Sigma_{y'}$: 6.7 μrad

3.60-cm Undulator (Sector 13)

Period: 3.60 cm
Length: 2.1 m
Minimum gap: 11.0 mm
B_{max}/K_{max}: 0.936 T/3.15 (effective; at minimum gap)
Tuning range: 2.2–11.8 keV (1st harmonic)
2.2–40.0 keV (1st-5th harmonic)
On-axis brilliance at 6.5 keV (ph/s/mrad^2/mm^2/0.1%bw): 2.8 x 10^{19}
Source size and divergence at 8 keV:
Σ_x: 276 μm Σ_y: 11 μm
$\Sigma_{x'}$: 12.9 μrad $\Sigma_{y'}$: 7.1 μrad

1.72-cm Undulator (Sector 30)

Period: 1.72 cm
Length: 4.8 m (2 x 2.4 m)
Minimum gap: 10.6 mm
B_{max}/K_{max}: 0.330 T/0.53 (effective; at minimum gap)
Tuning range: 23.7–26.3 keV (1st harmonic)
On-axis brilliance at 23.7 keV (ph/s/mrad^2/mm^2/0.1%bw): 1.0 x 10^{20}
Source size and divergence at 23.7 keV:
Σ_x: 276 μm Σ_y: 11 μm
$\Sigma_{x'}$: 11.6 μrad $\Sigma_{y'}$: 4.3 μrad

1.80-cm Undulator (Sector 32)

Period: 1.80 cm
Length: 2.4 m
Minimum gap: 11.0 mm
B_{max}/K_{max}: 0.244 T/0.41 (effective; at minimum gap)
Tuning range: 23.8 - 25.3 keV (1st harmonic)
71.4 - 75.9 keV (3rd harmonic)
On-axis brilliance at 23.8 keV (ph/s/mrad^2/mm^2/0.1%bw): 2.8 x 10^{19}
Source size and divergence at 23.8 keV:
Σ_x: 276 um Σ_y: 11 um
$\Sigma_{x'}$: 11.9 urad $\Sigma_{y'}$: 4.9 urad

IEX 12.5-cm Quasi-Periodic Polarizing Undulator (Sector 29)

Period: 12.5 cm
Length: 4.8 m
Circular polarization mode:
Max. currents: horizontal coils 34.4 A, vertical coils 20.7 A
K_{max}: 2.73 (effective; at max. currents)
B_{max}: 0.27 T (peak; at max. currents)
Tuning range: 0.44–3.5 keV (1st harmonic)
On-axis brilliance at 1.8 keV (ph/s/mrad^2/mm^2/0.1%bw): 1.4 x 10^{19}
Linear horizontal polarization mode:
Max. current: vertical coils 47.6 A
K_{max}: 5.39 (effective; at max. current
B_{max}: 0.54 T (peak; at max. current)
Tuning range: 0.24–3.5 keV (1st harmonic)
0.24–11.0 keV (1st–5th harmonic)
On-axis brilliance at 2.1 keV (ph/s/mrad^2/mm^2/0.1%bw): 1.1 x 10^{19}
Linear vertical polarization mode:
Max. current: horizontal coils 50.3 A
K_{max}: 3.86 (effective; at max. current)
B_{max}: 0.37 T (peak; at max. current)
Tuning range: 0.44–3.5 keV (1st harmonic)
0.44–11.0 keV (1st–5th harmonic)
On-axis brilliance at 2.1 keV (ph/s/mrad^2/mm^2/0.1%bw): 1.1 x 10^{19}
Fast polarization switching not required
Source size and divergence at 2 keV:
Σ_x: 276 μm Σ_y: 13 μm
$\Sigma_{x'}$: 13.9 μrad $\Sigma_{y'}$: 8.8 μrad

12.8-cm Circularly Polarizing Undulator (Sector 4)

Period: 12.8 cm
Length: 2.1 m
Circular polarization mode:
Max. currents: horizontal coils 1.34 kA, vertical coils 0.40 kA
K_{max}: 2.85 (effective; at max. currents)
B_{max}: 0.30 T (peak; at max. currents)
Tuning range: 0.4–3.0 keV (1st harmonic)
On-axis brilliance at 1.8 keV (ph/s/mrad^2/mm^2/0.1%bw): 3.1 x 10^{18}
Linear horizontal polarization mode:
Max. current: vertical coils 0.40 kA
K_{max}: 2.85 (effective; at max. current)
B_{max}: 0.30 T (peak; at max. current)
Tuning range: 0.72–3.0 keV (1st harmonic)
0.72–10.0 keV (1st–5th harmonic)
On-axis brilliance at 2.1 keV (ph/s/mrad^2/mm^2/0.1%bw): 2.3 x 10^{18}
Linear vertical polarization mode:
Max. current: horizontal coils 1.60 kA
K_{max}: 3.23 (effective; at max. current)
B_{max}: 0.34 T (peak; at max. current)
Tuning range: 0.58–3.0 keV (1st harmonic)
0.58–10.0 keV (1st–5th harmonic)
On-axis brilliance at 2.1 keV (ph/s/mrad^2/mm^2/0.1%bw): 2.3 x 10^{18}
Switching frequency (limited by storage ring operation): 0–0.5 Hz
Switching rise time: 50 ms
Source size and divergence at 2 keV:
Σ_x: 276 μm Σ_y: 12 μm
$\Sigma_{x'}$: 16.7 μrad $\Sigma_{y'}$: 12.7 μrad

1.80-cm Superconducting Undulator (2 IDs in Sectors 1, 6)

Period: 1.80 cm
Length: 1.1 m
Gap: 9.5 mm (fixed)
Max. current: 450 A
B_{max}/K_{max}: 0.962/1.61 (effective; at maximum current)
Tuning range: 11.2–24.7 keV (1st harmonic)
11.2–150.0 keV (1st-13th harmonic, non-contiguous)
On-axis brilliance at 13 keV (ph/s/mrad^2/mm^2/0.1%bw): 3.2 x 10^{19}
Source size and divergence at 13keV:
Σ_x: 276 μm Σ_y: 11 μm
$\Sigma_{x'}$: 13.2 μrad $\Sigma_{y'}$: 7.5 μrad

APS Bending Magnet

Critical energy: 19.51 keV
Energy range: 1–100 keV
On-axis brilliance at 16 keV (ph/s/mrad^2/mm^2/0.1%bw): 5.4 x 10^{15}
On-axis angular flux density at 16 keV (ph/s/mrad^2/0.1%bw): 9.6 x 10^{13}
Horizontal angular flux density at 6 keV (ph/s/mradh/0.1%bw): 1.6 x 10^{13}
Source size and divergence at the critical energy:
Σ_x: 92 μm Σ_y: 31 μm
$\Sigma_{x'}$: 6 μrad $\Sigma_{y'}$: 47 μrad

Acknowledgments

***APS Science 2016* Editorial Board:**

Mark A. Beno (ANL-PSC), John Byrd (ANL-ASD), John P. Connolly (ANL-AES), Robert Fischetti (ANL-XSD), Robert O. Hettel (ANL-PSC), Jonathan C. Lang (ANL-XSD), Dennis M. Mills, (ANL-PSC), George Srajer (ANL-PSC), Stephen K. Streiffer (ANL-PSC), Stefan Vogt (ANL-XSD)

Unless otherwise noted, the research highlights in this report were written by:

Mary Alexandra Agner (marymary@alum.mit.edu)
William Arthur Atkins (waarc@grics.net)
Erika Gebel Berg (erikagebel@gmail.com)
David Bradley (david@sciencebase.com)
Christen Brownlee (christenbrownlee@gmail.com)
Vic Comello (ANL-CPA - retired, vcomello@anl.gov)
Dana Desonie (desonie@cox.net)
Sandy Field (sfield@fieldscientific.com)
Amanda Grennell (amanda.jnb@gmail.com)
Joseph E. Harmon ANL-BIS - (harmon@anl.gov)
Emma Nichols (emma@nascentmc.com)
Philip Koth (philkoth@comcast.net)
Kim Krieger (mskrieger@gmail.com)
David Lindley (dxlindley@gmail.com)
Tien Nguyen (tmnguyen5@gmail.com)
Chris Palmer (crpalmer2009@gmail.com)
Nicola Parry (nicola@parrymedicalwriting.com)
Neil Savage (neil@stefan.com)
Michael Schirber (mschirber@gmail.com)
Mark Wolverton (exetermw@earthlink.net)

Photography: Wes P. Agresta, Mark L. Lopez (both ANL-CPA)
Aerial photograph of the APS: John Hill (Tigerhill Studio, http://www.tigerhillstudio.com)
Publications, contracts, rights and permissions, circulation: Jessie L. Skwarek (ANL-PSC)
Printing oversight: Gary R. Weidner (ANL-CPA)
Editorial, project coordination, design, photography: Richard B. Fenner (ANL-PSC)

Our thanks to the corresponding authors and others who assisted in the preparation of the research highlights, to the users and APS personnel who wrote articles for the report, and our apologies to anyone inadvertently left off this list. To all: your contributions are appreciated.

U.S. DEPARTMENT OF
ENERGY

Office of Science

Advanced Photon Source
Argonne National Laboratory
9700 S. Cass Ave.
Argonne, IL 60439 USA
www.anl.gov • www.aps.anl.gov